Environmental Assessment of the Alaskan Continental Shelf

Annual Reports of Principal Investigators for the year ending March 1981

Volume VII: Hazards

US DEPARTMENT OF COMMERCE
National Oceanic & Atmospheric Administration
National Ocean Service
Office of Oceanography & Marine Services

US DEPARTMENT OF THE INTERIOR
Minerals Management Service

Environmental Assessment of the Alaskan Continental Shelf

Annual Reports of Principal Investigators for the year ending March 1981

Volume VII: Hazards

US DEPARTMENT OF COMMERCE
National Oceanic & Atmospheric Administration
National Ocean Service
Office of Oceanography & Marine Services

US DEPARTMENT OF THE INTERIOR
Minerals Management Service

Annual Reports of Principal Investigators

1981

The facts, conclusions and issues appearing in these reports are based on interim results of an Alaskan environmental studies program managed by the Outer Continental Shelf Environmental Assessment Program (OCSEAP) of the National Oceanic and Atmospheric Administration (NOAA), U.S. Department of Commerce, and primarily funded by the Bureau of Land Management (BLM), U.S. Department of Interior, through interagency agreement.

DISCLAIMER

Volume 7
HAZARDS

Annual Report

A SEISMOTECTONIC ANALYSIS OF THE SEISMIC AND VOLCANIC HAZARDS IN THE PRIBILOF ISLANDS - EASTERN ALEUTIAN ISLANDS REGION OF THE BERING SEA

Contract: NOAA 03-50-022-70

Research Unit: 16

1 April 1980 through 31 March 1981

Principal Investigators

Dr. John N. Davies
Dr. Klaus H. Jacob

Lamont-Doherty Geological Observatory
of Columbia University in the City of New York
Palisades, New York 10964

TABLE OF CONTENTS

I. SUMMARY

<u>Objectives</u>. Through work carried out under this project we attempt to assess the volcanic and earthquake hazards that exist in the Eastern Aleutian Islands and Pribilof Islands region of the southeast Bering Sea and the western Gulf of Alaska. This assessment is made in the context of exploration for and possible future development of petroleum resources on the continental shelves which constitute most of the region. The present work focuses on the collection and analysis of new seismic data obtained from a seismic network jointly funded under this NOAA project and a companion project supported by D.O.E. During the past two years, however, we have also analyzed historical data which have led to an increased estimate for the seismic potential of the Shumagin Gap and a region near Unalaska Island. Through the companion D.O.E. and several smaller projects other geophysical, geodetic, and geologic and seismic engineering data are available to this study and the results relevant to hazards assessment are reported here to NOAA.

<u>The Specific Objectives of the Current Work are</u>: (1) to monitor seismic activity in the Shumagin Islands and Dutch Harbor regions of the Eastern Aleutian Island Arc and western Alaska Peninsula regions, and of the pribilof Islands region of the southeast Bering Sea; (2) to relate this seismic activity to particular faults or fault zones, where possible; (3) to monitor seismically the eruptive activity of three volcanoes: Pavlof, Akutan and Makushin; (4) to evaluate these seismic and volcanic activities for their potential hazards to exploration for and development of petroleum resources on the continental shelves within the study area. An important aspect of seismic hazard assessments is that they require a long-term continuous and reliable data base.

<u>Major Conclusions and Implications</u>. The addition of new historical data and information on repeat times strengthens the conclusion that the Aleutian arc segment near the Shumagin Islands and the tip of the Alaska Peninsula is likely to be the site of one or more great ($M \geq 7.75$) or large ($M \geq 7$) earthquakes and related aftershock sequences within the next several years or a few decades.

Such events have a high potential for producing destructive tsunamis and inducing hazardous submarine mudflows. At the present time this "seismic gap" is relatively quiescent, and we note occasional, moderate-sized earthquakes (m_b 5 to 6.5) associated with the unusually high stress drops (600 to 800 bars) and above-average levels of groundmotion. These events occur near the down-dip end (depths of about 40 km) of the inferred zone of contact between the North American and Pacific plates. They are located directly beneath fore-arc basins which have potential for petroleum exploration. Minor, probably shallow crustal activity appears to be associated with the Sanak Basin on the Pacific Side, and the southwesternmost portions of Bristol Bay, near the Black Hills (Alaska Peninsula) on the Bering-Sea side of the studied arc segment. The extent of rupture zones of past earthquakes appear to have been controlled by transverse structural features. This seismicity (especially in Sanak Basin) may be along a transverse feature that will control the extent of rupture of a future great earthquake in the Shumagin Gap. Other minor, shallow crustal seismicity in the overriding (North American) plate is apparently related to volcanic or magmetic activity. The Dutch Harbor region appears to be characterized by moderate seismicity typical of most portions of the former 1957 rupture zone, although data coverage was incomplete during this reporting period. Analysis of teleseismic data and tsunami arrival times lead us to the tentative conclusion that there is a seismic gap in the Dutch Harbor region. Some events were recorded in the southeast Bering Sea with a single seismic station located on St. Paul, in the Pribilof Islands. The distance range inferred from seismic travel times would indicate that some of these events are associated with the St. George Basin. The single-station limitation does not, however, allow any definite correlation with specific tectonic structures. Analysis of historic and teleseismic data for the St. George region reveals that large earthquakes have occurred there (I_{MM} = X, 1836; M = 7.2, 1925), and suggests that for a randomly selected site within the region there is an 11% probability for strong ground motion in excess of 0.2g and a 3% probability to exceed 0.5g.

II. INTRODUCTION

General Nature and Scope of Study. The present NOAA funded study "A Seismotectonic Analysis of the Seismic and Volcanic Hazards in the Pribilof Islands - Eastern Aleutian Islands Region of the Bering Sea" is an amplification of the hazards aspects of a previously existing and concurrent seismotectonic study of the Aleutian arc, funded by D.O.E. The D.O.E. study is very broad in scope and as such includes hazards analysis, but at a low level of priority. NOAA funds are used to accelerate hazards analysis by providing (1) additional staff, (2) equipment for data collection for projects specifically or primarily directed toward hazards anal;ysis, and (3) logistic support to maintain the extensive network of seismic stations and fieldwork required by the combined studies. The general goal of the present study is to monitor seismic and volcanic activity over a long time span and to evaluate this activity in terms of the hazard it implies for the exploration for and possible development of petroleum resources within the study area. The evaluation of this seismic and volcanic data requires the broad seismotectonic framework which is provided by the D.O.E. study.

Specific Objectives. The specific objectives of the past year have been (1) to continue to monitor the seismic activity in the Sand Point, Dutch Harbor and St. Paul areas, (2) to attempt to relate activity to specific faults, (3) to significantly increase the strong motion recording capability to improve estimates of strong ground motion, (4) to monitor the activity of Pavlof, Akutan and Makushin Volcanoes, and (5) to begin to evaluate the data (where it is sufficient) in terms of its hazards implications.

Relevance to Problems of Petroleum Development. The relevance of this work to petroleum development is straightforward: The basic problem is to design structures that will sithstand expected earthquakes, associated tsunamis, and volcanic activity within an acceptable level of risk. This design problem requires, as inputs, knowledge of the probable space-time distribution of large earthquakes, the acceleration vs. distances relations for those earthquakes and the distance to which various volcanic eruptions can be expected to be destructive. Prediction of the space-time distribution of large earthquakes requires a comprehensive understanding of the seismotectonic setting, nowledge of the distribution of preexisting faults and the longest possible record of previous seismic activity. Determination of acceleration vs. distance relations requires actual measurements of accelerations within the region over as broad a range of distance and magnitude as possible. Specification of the minimum safe distance from a given volcano requires knowledge of the type of eruption to be expected and the frequency of eruption. The data being collected are essential to each of the above prerequisites to the inputs for the problem of designing safe and economical structures.

III. CURRENT STATE OF KNOWLEDGE

Shumagin Islands Seismic Gap. Our present understanding of the seismic regime in the Shumagin Islands region is based on the concepts of plate tectonics (Isacks et al., 1968) and seismic gaps (Kelleher, 1970; Sykes, 1971; McCann et al., 1978). The Aleutian Island arc, of which the Shumagin Islands region is a part, is a convergent plate boundary between the Pacific and North American (Alaskan) plates. Along this plate boundary most of the seismic energy is released during great earthquakes ($M \geq 7.8$) (Kanamori, 1977). The aftershock zones of these great earthquakes do not overlap, which suggests that the area left between recent aftershock zones, the seismic gaps, are the most likel sites of the next great earthquake. Other things being equal, the longer the time since the occurrence of a great earthquake in a given gap, the higher is the probability that the gap will be the site of the next great earthquake.

Davies et al. (1976) discussed the historic record of earthquakes in the Shumagin Gap and assessed various methods for estimating the occurrence time of the next great earthquake there. Unfortunately, the error limits on all such estimates are so large as to make them inpractical as predictions. We reported in last years' annual reoprt the results of the D.O.E. funded geodetic tilt measurements. While still preliminary, they suggest that the Shumagin Islands region is tilting trenchward at .4 to 4 microradians per year. This tilt rate, if substantiated, would be consistent with that observed in Japan for interseismic periods (Scholz, 1974); i.e., the period between great earthquakes during which strain energy is accumulating. This suggests that such an earthquake was not imminent (due within a few months) at the time of the last measurement (June, 1978).

Davies and House (1979) have compared the Benioff zone seismicity beneath the Shumagin Islands with that beneath other regions of the Aleutian arc and with some other subduction zones. This comparison suggests that the future fault plane of a great earthquake in the Shumagin Gap will be in the main thrust zone (MTZ), the shallowl;y dipping portion of the Benioff zone above 40 km depth. Below, we interpret most of the shallow seismicity (less than 80 km depth) as being the result of an edge effect of stress accumulation around the future fault plane. This is consistent with Mogi's (1969) observations of a "doughnut" pattern of seismicity around future fault planes in Japan.

The high stress levels implied by this ("our") interpretation have been observed in two studies. Archambeau (1977) computed the stress drop for several earthquakes in the Shumagin Islands region using Ms/Mb ratios. The high, kilobar stress drops that he obtained have been questioned by some seismologists. House and Boatwright (1980) obtained a maximum stress drop of 600-900 bars for the April 1974 Shumagin Islands earthquake. Additionally, we have recorded two more earthquakes (M_b = 5.5 and 6.5) near the Shumagin Islands. Both of these events were located at the lower edge of the MTZ and triggered the strong-motion instrument at Sand Point. Unfortunately, these records are not suitable to the stress-drop analysis of House and Boatwright (1980). The strong motion accelerograph at Simeonof Island was not triggered by this event. Finally, we report below the analysis of several events by Mori that also show relatively high stress-drops within the Shumagin Gap. The occurrence of these events is consistent with the Mogi "doughnut" pattern described above and strenghthens our conclusion that high stresses are accumulating in this region.

The high stress level observed in the main thrust zone probably implies relatively high stress in the upper crust. This stress will most likely be relieved along pre-existing faults. We are only just now beginning to acquire enough shallow seismicity data to identify active surface faults. If segmentation of the upper plate exists, there would be linear zones transverse to the arc that would have a high risk for large strike-slip or normal faulting earthquakes. We have also observed terraces (see the geologic results reported last year) that are evidence for episodic uplift. It may be that a study of uplifted terraces would allow us to define boundaries for crustal blocks. These boundaries, too, would be zones of high risk for fault motion during large earthquakes.

Sykes (1980), Davies et al. (1981), and House et al. (1981) have reported new historical data and new analysis of the teleseismic data for the Shumagin and Unalaska regions. They conclude that the Shumagin region is a seismic gap with a high potential for a very great ($M_w \geq 8.7$) earthquake or a series of very large (M_w = 7.5) earthquakes. Although the record is not as clear for the Unalaska region a possibility exists that a similar seismic gap with high seismic potential exists there as well.

Pribilof Islands Region. We continue to record earthquakes at the St. Paul seismic station whose hypocenters are probably located in the St. George Basin. This basin is fault bounded (Marlow et al., 1977) and these faults may extend northwesterly between St. Geroge and St. Paul Island (Hopkins, 1976). We cannot determine the association, if any, of the earthquakes to these or other faults until we have more than one seismic station in the Pribilof Islands.

We report here an analysis of the historic and teleseismic data for the St. George Basin region. It shows that large earthquakes have occurred in this region: I_{MM} = X on St. George Island in 1836, and an M_b = 7.2 quake in the basin itself in 1925. Using the teleseismic data for a recent 22 year period, we estimate an 11% probability for strong ground motion to exceed 0.2g at a randomly selected site within the St. George region and a 3% probability to exceed 0.5g.

IV. STUDY AREA

In the combined D.O.E.-NOAA program, by far the strongest concentration of effort has been in the Shumagin Islands region. Within the OCSEAP program this region is classified as part of the western Gulf of Alaska. The specific area referred to as the Shumagin Islands region extends from SW of the Semidi Islands to Sanak Island. Within this area is the 13 station Shumagin network and the 12 station network on Pavlof Volcano, the latter supported primarily by D.O.E. This area it also identical with the Shumagin Islands seismic gap.

The Dutch Harbor area, also within the western Gulf of Alaska, receives the second highest level of effort. This area includes the NOAA funded stations on Akutan and Makushin Volcanoes.

Lastly we operate a three station network on St. Paul Island, one of the Pribilof Islands. This network is in the Bering Sea region according to the OCSEAP classifications.

V. SOURCES, METHODS, AND RATIONALE OF DATA COLLECTION

Seismic Data. Our primary emphasis in data collection is the operation of local, high gain, telemetered networks of short period seismic stations. These local networks allow the precise location of smaller magnitude earthquakes that is necessary for the timely and accurate delineation of tectonic features such as activity faults, segmentation of the subducted slab and patterns of volcanic activity. Precise locations are also critical for the evaluation of strong-motion records. The principal regional network is located in the Shumagin Islands. It consists of 15 remote (single component, vertical except CNB which is a 3-component station) stations and one 3-component station at the recording center, Sand Point.

Within this network we also operate a dense, 12 station network around Pavlof Volcano. The main purpose of this D.O.E. funded network is to provide data with which to study the geothermal potential of Pavlof Volcano. This network, in conjunction with the regional Shumagin Islands network, may also provide data that would allow us to study the relationship between variations in local volcanic activity and changes in the regional stress field as infered from seismic activity. Several studies have suggested that such volcanic activity may be useful in predicting great earthquakes (Kimura, 1976; Nakamura et al., 1977; McCann, 1978).

At Dutch Harbor we record three local components and four remote stations (including Akutan and Makushin Volcanoes). The local components are intended to complement the long period seismograph there and the remote stations are intended to monitor volcanic activity on Akutan and Makushin volcanoes as well as provide improved locations of local earthquakes that trigger the strong motion instrument at Dutch.

At St. Paul, in the Pribilof Islands, we operate three, short period, vertical seismometers. This network monitors activity in the St. George Basin and also complements the long period seismograph there.

Other sources of seismic data are the long period seismographs that we operate under D.O.E. funding at Sand Point, Dutch Harbor, and St. Paul, the broad band data that we discuss below in the hazard analysis section under "Results" and the World Wide Standard Seismograph Network.

Strong Motion Accelerographs. For the past few years (primarily under D.O.E. funding) L-DGO has operated Kinemetrics SMA-1 accelerographs at Dutch Harbor, Sand Point and Simeonof Island. Recently, under USGS funding, we have added eight more SMA-1's, all located at remote seismic stations. We have also taken over operation of the USGS instrument at Cold Bay. The purpose of these instruments is to collect acceleration data with which to construct acceleration vs. distance relations that are essential to the safe engineering design of large structures wuch as drilling rigs, pipelines, and holding tanks.

Tilt Measurements. Under D.O.E. and NSF funding we annually reoccupy several 1 km level lines in the Shumagin Islands. These tilt measurements provide important data regarding the accumulation of stress in the Shumagin Seismic Gap.

Geologic Investigations. Since June 1978 L-DGO geologists have carried out a reconnaissance of faults and terraces in the Shumagin Islands region. They have mapped several minor new faults and tentatively identified several terraces. The identification and evaluation of faults is essential to the assessment of the activity level of faults within the study area. The ages, heights and distribution of terraces can provide extremely important data regarding past episodes of rapid uplift, perhaps during previous great earthquakes. These terraces may help to define block boundaries that may be particularly prone to relative motion during future earthquakes.

VI. RESULTS, VII. DISCUSSION, IX. NEED FOR FURTHER STUDY

A. Seismic and Volcanic Risk in the St. George Basin and Adjacent Aleutian Arc (J. Davies)

SEISMICITY

Historic Record

Data. The earthquake record prior to the development of sensitive seismographs in the late 1890's and early 1900's relies on observations of the effects of earthquakes on people and objects. For southern Alaska, the Aleutians in particular, these observations are most complete during the period of the Russian occupancy, generally from about 1740 to 1870. Earthquakes for this period have been catalogued by Davis and Echols (1962), Coffman and vonHake (1973), and Kisslinger et al. (manuscript in preparation); these references will be abbreviated 1, 2, and 3, respectively.

Pribilof Islands. The historic record of earthquakes in the Pribilof Islands region is summarized in Table 1. Because the epicenters and maximum intensities of these events are so poorly known it is not possible to compare the occurrence rate for this period, 1815-1861, to that computed below from the teleseismic record for the period 1957-1978. Significant, is the observation that the 1836 earthquake caused damage rated at Modified-Mercalli Intensity X on the Pribilof Islands themselves. This event, those of 1847 and 1954, which were felt with intensity (M.M.) V-VI, and those of 1925, 1942, 1958, and 1959 with magnitudes of 7.2, 6.75, 6.38, and 6.50, respectively (Table 2) demonstrate that large earthquakes have occurred in the St. George region, the Pribilof Islands in particular, and must be expected in the future. This expectation is quantified in the section below on the teleseismic record.

Teleseismic Record

Data. The teleseismically located earthquakes compiled in Table 2 are derived from four sources: (1) ISC (International Seismological Center), (2) PDE (Preliminary Determination of Epicenters, published by the USGS and archived by NOAA), (3) relocations by Tobin and Sykes (1966), and (4) relocations by Sykes (1971). These events are mapped in Figure 1. We restrict this analysis to events in the crustal material containing the St. George Basin; therefore, deep events (depth greater than 110 km, shown by dashed circles in Figure 1) are excluded. From their locations (Figure 1) it can be seen that these deep events occur within the northernmost limb of the downgoing slab of Pacific lithosphere.

Interspersed with the epicenters of the deep events are those of about 30 events, the depths of which are unknown. Since we would like to account for these events in our analysis we observe that in the same area there are 7 shallow events and 13 deep events. We will assume that the same ratio of shallow-to-deep events holds for 30 events mentioned above.

To the northwest of this band of interspersed epicenters of deep and shallow events there are 19 additional events with unknown depths. We assume from their locations that these are shallow and, for purposes of identification assign them the depth 1.11 km (Tables 2 and 3).

In Figure 1 epicenters appear to be concentrated in the immediate region of the St. George Basin. A second concentration is centered in the southwest corner of the search area; these events are in the vicinity of the Umnak Plateau and the Bering Canyon. Lastly, a few outliers occur in the northeast part of the area. We further restrict the analysis by reducing the geographic area to the immediate St. George Basin region as shown in Figure 2 and the time interval to the 22 year period 1957-1978 as shown in Figure 3B. The resultant data set (Table 3) is the basis for the analysis that follows.

Frequency of Occurrence for Events in Various Magnitude Ranges

This calculation is summarized in Table 4. From Table 3 we have 14 events for which both the magnitude and depth are known or inferred. Also, there are 10 events of unknown depth whose magnitudes are known. We assume that every third one of these (in order of decreasing magnitude) is shallow and for identification assign them a depth of 2.22. This results in a total of 18 events with known magnitudes that are known or inferred to be shallow. The magnitudes of these events and the number at each magnitude are listed in columns 2 and 3, respectively. In addition to these 18 events there are 6 for which only the depth is known (or inferred) and 14 for which the depth is unknown. The epicenters of the latter 14 are above the northern limb of the downgoing slab, so some of them are probably deep. We assume that the same ratio of shallow-to-deep events holds for these 14 as held for the 20 (7 shallow, 13 deep) enumerated above from the data set in Table 2. Therefore, we infer that 4.9 of these 14 were shallow. Adding these 4.9 to the 6 known to be shallow we obtain an additional 10.9 shallow events for which to account that have unknown magnitudes. Thus, the total number of shallow events that occurred in the limited St. George basin region during the years 1957 through 1978 is 28.9. We assume that these additional 10.9 events are distributed by magnitude the same as the 18 for which magnitudes are known; therefore, since 28.9 is 1.606 times 18 we multiply the n in column 3 of Table 4 by r = 1.606 to obtain the nr listed in column 4. Thus, nr is the estimated number of events at each magnitude for the specified region and time interval. We next obtain the cummulative number at successively smaller magnitudes, N, by summing the nr down column and listing the partial sums in column 5. That is:

$$N_j = \sum_{i=1}^{j} (nr)_i$$

Thus N_j is the number of events larger than or equal to M_j where j is the row number. The last column is simply the logarithm (base 10) of the corresponding entry in the previous one. This is computed for the b-value plot shown in Figure 4.

The b-value is the absolute value of the slope of the well-known relation

$$\log N_j = a - bM_j. \tag{1}$$

We expect a b-value of about 1.0 which is the slope of the reference line plotted in Figure 4. The shape of the curve in this plot is controlled by the numbers of events actually observed at each magnitude listed in Table 4, column 3. The shallow slope above magnitude 4.2 indicates that M = 4.2 is about the detection threshold for this data set. The increase in slope toward higher magnitude implies that more events with $M > 5.0$ were observed than would usually be the case for this region and interval. We note that the slope in the magnitude range $4.2 \leq M \leq 5.0$ is very close to 1.0. To determine the value of "a" in (1) it is best to use the values of M_j and N_j corresponding to the lowest magnitude above the detection threshold; viz., M = 4.2 and N = 24.09. This maximizes the number of observations used and hence minimizes the importance of observing or not observing any given event. Using the above values we obtain

$$a = \log (24.09) + 4.2 = 5.58184 \tag{2}$$

where we have assumed b = 1.0.

Using (1) and (2) we can compute the number of events expected within any magnitude range from

$$N (M_i,M_j) = N_i - N_j; \; M_i < M_j. \tag{3}$$

We next assume that $N (M_i,M_j)$ is the expected value for the St. George basin region for any 22 year interval and that the number of events per unit time is distributed according to the Poisson function. We can then write (Hald, 1948, p. 732) the probability for the occurrence of one or more events in a given range $M_i \leq M \leq M_j$ and time interval τ = t years ÷ 22 is given by

$$P_{ij} \text{ (one or more)} = 1 - P_{ij} \text{ (none)} = 1 - e^{-N (M_i,M_j)\tau} \tag{4}$$

Using (1) through (4) and t = 40 years we find:

j	M_j	N_j	$N(M_{j-1}, M_j)$	$P_{j-1,j}$ (one or more)
1	4	38.18	----	----
2	5	3.818	34.36	1.0000
3	6	.3818	3.436	0.9981
4	7	.03818	.3436	0.4646
5	8	.003818	.03436	0.0606

The probability for the occurrence of an event of a certain size is not directly of interest: what is of more interest is the joint probability that the event will occur and that it will cause damage. We will reduce the problem to the exceedence of two specific accelerations; viz., 0.2 and 0.5g. The conditional probability that given an event of a certain size it will cause accelerations greater than or equal to α is

$$P\,(ij|\alpha) = \frac{\pi r_{ij}^2(\alpha)}{A} \tag{5}$$

where $r_{ij}(\alpha)$ is the radius from the site of interest within which the event must occur if the acceleration is to reach α, and A = 80,770 km^2 is the total area of the limited St. George Basin region as outlined in Figure 3. Therefore, the joint probability that an event of a certain size will occur and it will be close enough to exceed an acceleration of α is given by

$$P\,(ij \text{ and } \alpha) = P_{ij} \text{ (one or more) } P\,(ij\,|\alpha). \tag{6}$$

Finally, the total (or marginal) probability that α will be exceeded is the sum of the probabilities of each of the possible cases, neglecting terms of order $(P\,(ij \text{ and } \alpha))^2$ and higher: i.e.,

$$P(\alpha) = \sum_{j=2}^{5} P_{j-1,j}\,(\text{one or more})\; P(j-1,j\,|\,\alpha) \qquad (7)$$

where, as above, j=1 corresponds to M = 4.0, 2 to 5.0, etc.

The radii, $r_{ij}(\alpha)$ are scaled from the plot of acceleration-vs.-distance given in Figure 5. Most of the data in this figure were compiled by Page et al. (1972) for the western U.S. The larger symbols represent data collected at Sand Point, in the Shumagin Islands. The Aleutian data show systematically higher accelerations at a given distance than do those of the western U.S. Therefore these data are used to determine the intercepts of the lines labeled 4.5, 5.5, etc., in Figure 5, while the western U.S. data are used to determine the slopes. The line labeled 4.5 is used to specify the acceleration-vs.-distance relation for earthquakes in the magnitude range $4.0 \leq M \leq 5.0$, that labeled 5.5 for the range $5.0 \leq M \leq 6.0$, etc. Thus, for example, the radius from a given site within which an earthquake in the range $6.0 \leq M \leq 7.0$ must occur if the acceleration is to exceed 0.5g is 30 km. From (5) the conditional probability that should such an earthquake occur in the St. George Basin region it will be close enough to a given site to cause an acceleration greater than 0.5g is

$$P(3,4\,|\,0.5) = \frac{\pi\, 30^2}{80{,}770} = 0.035 \qquad (8)$$

Calculation of the probabilities for the ground acceleration to exceed 0.2 or 0.5 in 40 years for a site within the St. George Basin region is summarized in Table 5. The values in this table are determined using (1) through (7) and the relations plotted in Figure 5. These calculations indicate for the limited St. George Basin region in a 40 year period the probability to exceed 0.2g is about 11% and that to exceed 0.5g is about 3%.

Local Record

Data. A Geospace HS-10/1B seismometer was installed in the Seismic Cottage (near the National Weather Service Observatory) on St. Paul Island during October 1975. This instrument is recorded on a Helicorder with a magnification at 5 Hz of about 17,500. The magnification of the St. Paul seismograph is limited by the surf noise propagated by the alluvium on which the Seismic Cottage is located.

In an attempt to determine the azimuth of the events recorded by this station, two remote station were installed on St. Paul Island in July 1980. None of the local events recorded since then have been impulsive enough so that arrival times could be read with any confidence. Therefore, all of the data discussed in this section were recorded by the local, short period, vertical seismograph at St. Paul Island.

Table 6 gives arrival times, distances (from S-P times) and magnitudes for events detected at St. Paul (SNP) which might have occurred in the St. George Basin, without azimuths only the distance can be specified. Magnitudes were calculated using Richter's (1958, p. 342) local scale and a correction determined by comparing the SNP magnitudes for the larger events to those listed in the PDE. Some larger ($M \approx 5$) events in the Aleutian arc between the Fox Islands and the Alaska Peninsula were included for this analysis.

Comparison of Seismic Rate

Figure 6 is a plot of magnitude vs. distance which shows that the magnitude threshold at about 450 km is approximately 4.0. In other words, an earthquake in the southern St. George Basin must have a magnitude greater than or equal to 4.0 to be detected at SNP. Therefore, in comparing seismicity rates the analysis must be restricted to events of 4.0 and larger.

There are only 3 such events listed in Table 6, all between $M = 4$ and $M = 5$. Thus, in the nomenclature of the previous section, $N(M_4,M_5) = 3$ which can be extrapolated (assuming a b-value of 1.0) to: $N(M_5,M_6) = 0.3$, $N(M_6,M_7) = 0.03$, and $N(M_7,M_8) = 0.003$. Using (4) from that section and the above $N(M_{j-1,j})$, the $P_{j-1,j}$ (one or more) for $j=2$ through 5 are 1.00, 0.98, 0.32, and 0.04, respectively. These are the probabilities that an earthquake in the respective range of magnitudes will occur within 40 years. The comparable probabilities computed from the teleseismic data are 1.00, 0.998, 0.46, and 0.06. Thus, the local data over a 3 1/6 year span indicate the same order of activity as do the teleseismic data over a 22 year span.

VOLCANIC ACTIVITY

Pribilofs. Mushketov and Orlov (1893, p. 198) report "a submarine earthquake and eruption" northeast of St. George in 1815. Barth (1956) references Landgrebe (1855) for the statement that "flames have been seen to rise from the sea northeast of the Pribilof Islands". It is likely that both of these reports are based on a report from Kotzebue around 1821 to 1828 which we have not been able to find. Barth (1956, p. 154) concludes "However, in spite of these assertions any present volcanic activity must be regarded as doubtful". Hopkins (1976) similarly concludes "The volcanic hazard is small on and near St. Paul Island and negligible elsewhere". He also states "The numerous isolated shocks in the vicinity of the Pribilof Islands are probably [emphasis ours] mostly ancient, eroded, volcanic centers... appropriate paleontological or radiometric methods [should be] used to establish their age". We conclude that volcanic activity is unlikely but suggest that Hopkins' advice be followed if any structures are to be built on or near St. Paul and St. George.

Makushin Bay. In 1878 the village of Makushin was destroyed by an earthquake (Mushketov-Orlov, 1893, p. 468). The earthquake and associated tsunami have been reported as part of a crater-forming event at Okmok Volcano (Hantke, 1951). Apparently the village was destroyed by the tsunami that swept along the north shore of Unalaska Island. Note that Makushin Bay is also exposed to Bogoslof Volcano at a distance roughly equal to that of Okmok.

Scotch Cap. The 1978 eruption of Westdahl deposited 1 m of ash on the U.S. Coast Guard light station at Scotch Cap. The ash damaged the light and forced the evacuation of the site, meltwater floods washed out the road to Cape Sarichef.

Other Volcanic Activity. Table 7 is a summary of reports of volcanic activity (Hickman, unpublished files) in the eastern Aleutian arc from Okmok Volcano on Umnak Island to Pavlof Volcano on the Alaska Peninsula. Of the 16 volcanoes listed, 8 are rated as having a high potential for eruption (4,5 on a scale of 0-5; see footnote 1, Table 7): Okmok, Bogoslof, Makushin, Akutan, Pogromni, Westdahl, Shishaldin, and Pavlof. Isanotski is given a moderate potential (3) and the remaining seven are rated at a low to negligible potential (2-0).

For the purpose of siting a pipeline terminal/tanker facility those volcanoes with a high potential for eruption should be regarded as likely to produce the following hazards:

(1) lavaflows, mudslides, floods, incandescent bombs, and nuee ardent on the flanks and in valleys around the volcano.

(2) ash and sand clouds capable of depositing up to a meter of material several tens of km downwind from the volcano and a few centimeters of material at 100 to 150 km. The fine particles will produce a plume in which planes should not fly 100 to 200 km wide and 200 to 500 km long. This phase may persist for hours to days.

(3) local tsunamis to distances of 100 to 150 km.

(4) several hours to 10's of hours of radio interference during the eruption.

B. Contributions to Seismic Exposure Mapping for the Gulf of Alaska (K. Jacob)

Under separate contract Woodward-Clyde Consultants is presently preparing for OCSEAP a seismic exposure map for large portions of the Gulf of Alaska. L-DGO has provided to this project a considerable amount of historic and instrumental seismic data and associated interpretations (see Tables 8 and 9). These data form an essential portion of the input base for this exposure map. An important innovation for hazards mapping under this program is the incorporation of the seismic gap concept (Morgot and Shah, 1979) in which L-DGO has been spearheading research both in Alaska and on a global scale for more than a decade. The following L-DGO contributions, many of the more recent ones supported by the OCSEAP program, provided the data or interpretational base essential for defining many of the details of the seismic exposure map.

History of Large Earthquakes, Seismic Gaps, and Arc Segmentation. One of the dominating sources for seismic hazards is the occurrence of great thrust-zone earthquakes in subduction zones. Sykes (1971) relocated the aftershocks of most large and great earthquakes that occurred since 1900 along the Alaska-Aleutian plate boundary, and thereby delineated for the first time the considerable size of these rupture zones. Sykes introduced in this early study the concept of seismic gaps and pointed out for this region possible gaps located near Sitka, Yakutat-Yakataga, and a then questionable gap near the Shumagin Islands. This work has been recently extended in scope and time to include the early period of Russian ownership of Alaska (mid-1700) using original historic sources. The results of these studies are summarized by Davies et al. (1981), Sykes et al. (1980), and Kisslinger et al. (manuscript in preparation). These studies enables us to establish the history of large earthquakes ($M > 7.0$) and in some cases estimates of earthquake size (area, length, moment, magnitude), and approximate recurrence times, thereby providing the data necessary to apply Markov-process modeling (Patwardhan et al., 1980) for the occurence of large earthquakes above a certain minimum magnitude, as used by Woodward-Clyde for the OCSEAP hazards mapping project in the Gulf of Alaska.

Through the studies of Davies et al. (1981) the advanced state in the earthquake cycle of the Shumagin gap has been demonstrated which raises considerably the seismic risk parameters in this gap and its vicinity for the immediately forthcoming exposure period. Similarly the studies of McCann et al. (1980) and Perez and Jacob (1980b) thoroughly discussed the earthquake history and tectonics of the Yakataga seismic gap and they derived from this data the present seismic potential of this gap as defined in its slightly diminished extent after occurrence of the 1979 St. Elias earthquake (Perez and Jacob, 1980a). A consequence of the tectonic analysis by Perez and Jacob (1980b) for hazards mapping is the possibility for large (but rare) shallow thrusting events seaward of the Pamplona zone-Icy Bay lineament. Such shallow thrusting may extend as much as 200 km offshore from Yakutat (and beneath a presently active lease area), up to the NW striking shelf-edge structure, where the latter terminates the Yakutat Block-Fairweather Ground against the abyssal Pacific ocean plate.

In deviation from practice for earlier hazards maps for the Gulf of Alaska region, we urged (Jacob, written communication, 1981) to include a zone of normal faulting earthquakes near and seaward of the Aleutian trench and to derive its statistical properties from global data contained in Chapple and Forsyth (1979). Although not instrumentally verified for the Aleutian arc for events with magnitudes above $m_b = 6.5$, such rare normal-faulting events can globally attain great size ($M_w \approx 8$).

A refinement for the 1957 rupture zone by House et al. (1981) has little effect on the currently prepared Gulf of Alaska hazards map because it lies just off its western edge. For a future westward extension of such a map covering future lease areas in the continental shelfs of the eastern Aleutian and Beringian Sea margins the results of the study by House et al. (1981) should be considered, however, since it suggests a possible seismic gap near Unalaska Island. This island is the site of a presently important harbor (Dutch Harbor) and of possible future tanker or pipeline terminal facilities.

Tsunami Run-Up Heights. The seismic hazards mapping project for OCSEAP as presently conceived does not provide a systematic compilation of tsunami wave run-up heights on Pacific and Beringian coastal shore lines. Many of the above quoted studies, but in particular those of Davies et al. (1981), House et al. (1981), Sykes et al. (1980), Kisslinger et al. (in preparation), and McCann et al. (1980) cite the sources for, and compile or discuss data on observed tsunami heights for many of the coastlines of concern. The results indicate that maximum run-up on exposed Pacific shore lines appears to have locally reached 30 m in height (or more).

Configuration of Dipping Seismic Zone. The network data from the Shumagin Islands seismic network have provided a tight constraint on the locus of the main thrust zone for shallow depths (< 40 km) and of the dipping seismic (Benioff) zone beneath the island arc to depths of about 250 km. First compilations by Davies and House (1979), Jacob et al. (1977), and Davies et al. (1981) have now been refined by Reyners and Coles (1981) to show the double-planed nature of the Benioff zone. This refined hypocentral data set of the subduction zone seismicity has been used to define the contorted geometry of the main thrust zone between the 1938 rupture, the Shumagin gap, and the 1946 rupture zone, and of the smooth geometry of the dipping Benioff zone in this arc segment. Because of attenuation of ground motion with distance, the accurate location of potential sources is essential for accurate estimations of ground shaking at any given site on the hazards map.

Recurrence Time Modifications. There is an ongoing discussion whether and how the actual recurrence time (holding time) within a certain arc segment is being prolonged or foreshortened from the long-term average recurrence time as a function of size and/or stress drop of the last (previous) great thrust earthquake and/or the size/stress drop of the next (future) great thrust earthquake. While one approach is to use statistics of holding times based on the available historic data, Sykes and Quittmeyer (1981) have attempted a deterministic analysis of the existing data on great earthquakes. For a deterministic approach the following two hypothetical end-member models can be postulated: (1) the holding time to the next event is independent of the magnitude/stress drop of the previous event, but magnitude/stress drop of the next event increases with increasing holding time; and (2) the holding time to the next event is controlled by the magnitude/stress drop of the previous great thrust earthquake such that this holding time is longer for a larger preceding event. The magnitude of the next (future) great event is, however, independent of the preceeding holding time.

In their analysis of available Alaskan and other global subduction zone earthquakes Sykes and Quittmeyer (1981) find: (1) a weak positive correlation of stress drop with size (magnitude, moment) of great earthquakes; and (2) a preference of the historic data to conform to hypothesis 2, i.e., the holding time to the next event tends to increase with size or stress drop of the previous event while the size of the next event is indeterminate, i.e., independent of the preceding holding time.

We recommend that this finding be incorporated in future estimates of the holding times for rupture zones or gap segments within the region of the Gulf of Alaska hazards map; such details may modify the outcome of the Markov-modeling for the occurrence of great earthquakes, and thus, the time-dependent seismic hazards quantities to be mapped.

Strong Motion Data. The scarcity of Alaskan strong motion records prevails despite a moderate recent increase in strong motion recording sites, the density of which is still too low to firmly guarantee records from events below a certain minimum magnitude (m_b < 6.5). A total of five strong-motion records from our strong-motion station at Sand Point (SAN), Shumagin Islands, have been forwarded in 1981 to Woodward-Clyde for digitization and incorporation of the data into attenuation versus distance analysis.

C. A Possible Seismic Gap near Unalaska (L. House)

In addition to the Shumagin Gap, which has received the bulk of study during efforts to evaluate seismic risk in the eastern Aleutians, another nearby area of comparable dimensions (about 80 km by 200 km) may also pose significant seismic and tsunamic risks. This area, which we term the "possible Unalaska Gap" lies along the interface between the North American and Pacific plates in the eastern Aleutians between about 163°W and 167°W. From a study of both seismic and tsunami information, it seems that the area of the Unalaska Gap may not have broken in an earthquake since perhaps the period 1900-1903. If this interpretation is correct, the possible Unalaska Gap could, if it ruptured during a single event, produce an earthquake as large as magnitude 8. The remainder of this section discusses the observations pertinent to the conclusion stated above.

A great earthquake (M_w = 9.1, Kanamori, 1977a) broke a 1200 km long segment of the Alaska-Aleutian plate margin in 1957 (Mogi, 1968; Kelleher, 1970; Sykes, 1971). Aftershocks of this event were located between 180°W and about 164°W. Closer study of the distribution of these aftershocks, however, (see Figure 7) reveals that those in the easternmost 200 km segment (the Unalaska segment) occurred only in a narrow zone. Compared to the other 1000 km of the aftershock zone (the main segment), those aftershocks within the Unalaska segment occurred at the northern edge of the width of aftershocks within the main segment. The lack of aftershocks within much of the width of the Unalaska segment suggests that this segment may not have ruptured in 1957.

The distribution of seismic activity before the 1957 main shock supports such a suggestion. Earthquakes within the 1957 aftershock zone that occurred in the 11 years preceeding the main shock (see Figure 8) cluster in two significant locations. One is located near the western edge of the entire aftershock zone, at about 180°W. The other is located at about 168°W, near the western edge of the Unalaska segment. These precursory clusters of events could represent a preparatory process at the margins of the impending rupture zone. As such, they lend additional support for the idea that rupture during the main shock may not have extended into the Unalaska segment.

The strongest evidence bearing on the question of rupture within the Unalaska segment comes from tide gauge recordings of the tsunami generated by the 1957 main shock. Tide gauges along the west coast of North and South America recorded the tsunami. Six of the recordings show especially good arrivals. These six tsunami travel times constrain the eastern extent of the tsunami source. As Figure 9 shows, the six individual estimates (2 coincide in the figure) all fall within about 50 km of the eastern edge of the main segment of the aftershock zone. The Unalaska segment stretches between the main aftershock segment at the west and the 1946 aftershock zone at the east.

The combined foreshock, aftershock, and tsunami information provide strong evidence that the Unalaska segment behaved quite differently from the rest of the aftershock zone of the 1957 earthquake. Although we cannot rule out aseismic slip within the Unalaska segment, aseismic slip does not seem to play a significant role in taking up convergent motion in the Aleutians (Kanamori, 1977b). In addition, a conservative approach to hazards assessment in the eastern Aleutians would assume that the Unalaska segment did not slip in 1957 and therefore could represent an area of high seismic potential. Thus, we term the area the possible Unalaska Gap.

Unfortunately, currently available information cannot further elucidate the behavior of the Unalaska segment in 1957. Additional information, such as crustal uplift, felt reports, and possibly study of surface waves of the 1957 main shock, would be needed to confirm or deny the existence of the possible Unalaska Gap.

D. <u>Fine Structure of the Dipping Seismic Zone in the Shumagin Islands (K. Coles)</u>

A careful analysis of microearthquake data from the Shumagin array has increased our knowledge of the local crustal structure and possible state of stress of the convergent plate boundary. The results summarized below are presented in detail by Reyners and Coles (1980, and submitted to J. Geophys. Res.). The horizontally-layered velocity model used to locate hypocenters is necessarily an approximation of the structure variations one might expect at a converging plate boundary. To obtain a sample of hypocenters free of velocity model errors we used only those events for which the epicentral distance to the nearest station is less than or equal to twice the hypocentral depth. This procedure improves hypocentral depth control, as arrivals to the closest stations are interpreted as direct arrivals, the travel times of which are less prone to errors (due to an inadequate crustal structure model) than critically refracted arrivals, which may arrive first if the ratio of epicentral distance to hypocentral depth is large.

A depth section of well-determined hypocenters satisfying the above condition and occurring during the one and a half year period from July 1978 to December 1979 is shown in Figure 10. The section is oriented at N30°W, perpendicular to the strike of the arc; it has a width of 400 km and is centered on the Shumagin array. The dipping seismic zone shown in Figure 10 appears double-planed. The upper plane dips 32° from 45 to 100 km depth, where it exhibits a knee-like bend below the volcanic front. The lower plane begins at about 65 km depth, where it is separated from the upper plane by some 25 km, and converges with the upper plane at about 125 km depth. This lower plane appears to be real, and not related to lateral segmentation of the subducted plate, since the microearthquakes comprising it are evenly spread along the strike of the arc. This is illustrated in Figure 11, which shows the lower plane hypocenters in map view. Indeed, the clear separation of the two planes of the dipping seismic zone evident in the 400 km-wide section shown in Figure 10 attests to the uniformity of the subducted Pacific plate along the strike of the arc in the region of the Shumagin array.

Double-planed seismic zones have recently been found in other areas of subduction, including the Kurile Islands (Veith, 1974), the Centarl Aleutian Islands (Engdahl and Scholz, 1977) and northeastern Japan (Hasegawa et al., 1978a,b), and the northern Mariana Islands (Samowitz and Forsyth, 1979). Various explanations have been proposed for such zones, including elastic unbending of the subducted slab (Engdahl and Scholz, 1977), phase changes in the slab (Veith, 1974) and sagging of the slab under its own weight (Sleep, 1979). Composite fault-plane solutions for subsets of the microearthquake activity which give consistent focal mechanisms are shown in Figure 12, together with a depth section showing the subsets themselves. Solution C in Figure 12 shows a down dip tension axis in the upper plane of the double seismic zone, rather than the down-dip compression that would be consistent with a simple unbending model (Engdahl and Scholz, 1977). Solutions D and E, from the lower plane of the double-planed dipping seismic zone, have no simple explanation in terms of down-dip stresses. It may be that, because the plate interface is currently locked at shallower depths, slab pull is overprinting unbending stresses; such an interpretation is consistent with the currently high seismic potential inferred for the region (Davies et al., 1981).

The composite fault-plane solution for the concentrated activity shallower than 45 km (solution A in Figure 12) indicates thrust faulting. As can be seen in Figure 12A, the P axis of this composite fault-plane solution is near-horizontal, and its azimuth (330°) is very similar to the azimuth of plate convergence predicted by the RM2 model of Minster and Jordan (1978) for the region of the Shumagin array (329°). In addition, one nodal plane of the solution is subparallel to the dipping zone defined by the 25-45 km deep activity. Landward of this activity, microearthquakes in the overlying North American plate show a strike-slip mechanism (see Figure 12B), with the P-axis again near-horizontal and oriented in the direction of plate convergence. This result is consistent with the interpretation that the plate interface in the region of the Shumagin Islands is currently locked, with stresses due to plate convergence being transmitted to the overlying plate.

E. Stress Drops for Earthquakes in the Eastern Aleutians (J. Mori)

Estimates of stress drops of earthquakes are important because the ground acceleration produced by an earthquake of a given moment is dependent upon the stress drop (Hanks and Johnson, 1976). Also if one can assume high stress drop earthquakes are an indicator of a high level of regional stress, the location of these earthquakes should help in identifying areas under high tectonic stress, and thus likely sites of great earthquakes in the near future.

Last year we reported source parameters for four earthquakes in the Eastern Aleutians. Using the methods described in last year's report, we estimated the stress drop for 11 more moderate earthquakes in the same region (Figure13). The data used were short-period WWSSN film chips and records from a broadband instrument located in Palisades, New York. One factor which was not taken into account last year was attenuation. More recently we assumed that anelastic attenuation was represented in frequency domain by

$$Q(w) = \exp\left[-wt^* + \frac{iwt^*}{2}\left(\ln \frac{w}{w'} - 2\right)\right]$$

where w is the angular frequency, w' is the Nyquist frequency, and t* is a measure of the enrgy loss per cycle (Carpenter, 1966). Then one can form an inverse Q operator, transform it into time domain, and apply it to the data to take out the effects of attenuation. Figure14 shows the plots of velocity and velocity convolved with the inverse Q operator. The t* used in this study was taken to be 0.6 for all the events. Published values of t* range from 0.1 to 1.0 (Der and McElfresh, 1975; Anderson and Hart, 1978; Sommerville et al., 1976). A differentt* could change the absolute value of stress drop by a factor of 2 or 3, but it would not change the relative values obtained for the earthquakes in this study.

The dynamic stress drops calculated for the 15 events are tabulated in Table 10. Despite the scatter in the data, there are significant differences in the dynamic stress drops among these earthquakes. The scatter in the results could partly be due to local conditions at the site and receiver. The shallow earthquakes occur in areas which are probably more complex structurally. This may account for the more complex pulse shapes of the shallow events. No corrections were made for structures at the source, such as the dipping slab which could significantly offset shape and amplitude of the waveform.

Figure 15 is a plot of dynamic stress drop versus depth. Lines connect points which represent stations used in analyzing the same event. Although this data set is too small to represent a fair statistical sampling, we believe it indicates that differences in stress drop occur as a function of location. At depths of 100-200 km where no great earthquakes are known to occur the stress drops of these moderate earthquakes fall in the range of 20-70 bars. The very shallow normal-faulting earthquakes near the trench seem to have in the average somewhat higher dynamic stress drops than the Benioff zone events. Whether this high stress is a local feature of this particular arc segment or occurs consistently along the entire arc is not known at this stage of the study.

The earthquakes within the main thrust zone (depth 15 to 50 km) show the greatest variation in dynamic stress drop, ranging from 10 to 300 bars. Figure 16 shows the dynamic stress drops of the main thrust zone earthquakes as a function of location along the arc. There are low stress drop events throughout the region punctuated by two high stress drop events: one located in the Shumagin Gap (Davies et al., 1981) and one located on the edge of the Unalaska Gap (Davies et al., 1981). Although these high stress drop events seem to be associated with seismic gaps, the low stress drop events indicate that the Shumagin gap is not uniformly under such high stress. Instead the close proximity of low and high stress drop earthquakes reflect the inhomogeneity of the stress field. If one assumes that the dynamic frictional stress is the same for all these earthquakes, another consequence of varying dynamic stress drop is that it implies differences in material strength, since failure is occurring at different tectonic stresses.

In terms of strong motion studies the two high stress drop events are important because whether they are high stress drop or high rupture velocity earthquakes, the slope of their velocity pulses, i.e. acceleration, is large. So a model of a large earthquake in this region should include subevents which initially produce large accelerations.

F. Pavlof Volcano and Wind Directions at Cold Bay in Relation to Hazardous Ash-Fall (S. McNutt)

Pavlof Volcano erupted in November 1980 for the first time in several years. A summary of the major features of the eruption is given in the Section XI.D. Seismic activity as of late April 1981 remains at a high level on the order of 100-200 very small volcanic earthquakes per day with infrequent explosions. The data from 10 stations surrounding Pavlof (see Figure 17) are now recorded on high quality analog and digital tape recorders, as well as one station (either PN6, PN7, or PVV) displayed on a helicorder. This new high quality data will permit us to locate the events, as well as determine source and propagation effects related to volcanism (During the 1980 field season two stations, PN1 and PN5, were removed so that the hardware could be used to repair other sites. This is not expected to lower the overall quality of our data set).

We wish to stress the contrast and variability in seismic precursors to eruptions mentioned in paragraph 3 of Section XI.D. Seismology is one of the best and most reliable means of determining the eruptive state of a volcano (Decker, 1973; Shimozuru, 1971; Minikami, 1960, 1969). Nevertheless, the variability in both seismic and eruptive behavior at any one volcano, as demonstrated at Pavlof during its last 5 eruptions (1973-1980) shows that seismic data must be carefully examined and interpreted, often over a short period of time, if it is to be useful for forecasting eruptions. Continued seismic monitoring of the volcano over a period of many years is necessary to statistically evaluate and eventually understand the relationships between volcano seismicity and eruptions.

Figure 18 shows the results of a study of wind patterns at Cold Bay, Alaska, approximately 35 km southwest of Pavlof. Wind-blown ash is the most widespread volcanic hazard; generally both particle size and thickness of deposits decrease with increasing distance from the vent. Obviously, the locations of ash deposition depend on the prevailing winds at the time of the eruption. Figure 18 is a polar histogram which shows average wind direction and speed for the period January 1974-January 1981. The data is taken from the monthly Climatological Data for Alaska Bulletins published by NOAA. Each datum is a vector sum of wind directions and speeds divided by the number of observations during a period of one month. Note that the instruments recording wind speed and direction are near the ground, whereas most volcanic vents are at a height of 2000-3000 meters. Winds in Alaska are highly variable both in space and in time; since eruption columns often rise many kilometers, it is quite possible that ash will be blown several directions simultaneously at different elevations. Despite these limitations Figure 18 gives a representative picture of the wind directions in the vicinity of Pavlof. It is unfortunate that so few weather stations exist in the Alaska Peninsula-Aleutian Islands region. We infer from Figure 18 that most winds blow from the Pacific Ocean towards the Bering Sea; if this is true throughout the region then the north shores of the Alaska Peninsula and the Aleutian Islands would be the sites most likely to suffer the effects of ash fall during a volcanic eruption. Designs for buildings or other facilities near active volcanoes should take the possibility of heavy ash fall into account.

VIII. CONCLUSIONS

A. Seismic and Volcanic Risk in the St. George Basin and Adjacent Aleutian Arc

Pribilof Islands and the St. George Basin. This region has produced earthquakes of M = 7.2 (1925) and I_{MM} = X (1836). The St. George Basin is a graben bounded by growth faults, one of which shows a scarp of about 1 m. It is likely that the larger events occur along these boundary faults. The maximum magnitude expected is about M_w = 8.0. The probability that a randomly selected site within the St. George Basin region will experience strong ground shaking in excess of 0.2g acceleration within 40 years is about 11%; for 0.5g it is about 3%. These values are based on 22 years of the teleseismic record of earthquakes in the St. George region, excluding Benioff zone events of the Aleutian arc. It is not possible to accurately quantify the rate of seismicity using the historic record or that obtained for a recent 3 year period from the St. Paul seismic station. Nevertheless, both of these data sets indicate activity of the same order as calculated from the teleseismic record. The probability of volcanic activity in the Pribilofs is very low. The possibility of recent submarine eruptions exists.

Aleutian Arc from Umnak to Pavlof Bay on the Alaska Peninsula. The seismic potential of this region has been described by Sykes (1980), Davies et al. (1981), and House et al. (1981). Of principal concern are the Shumagin Gap (162-159°W) and the possible Unalaska Gap (167-164°W). Both of these regions have a relatively high potential to produce a very great earthquake (M_w > 8.7) or a series of very large earthquakes (M_w > 7.8). The risk is greatest on the south side of the arc where there is the possibility of very strong ground motion (≈1 g) and local tsunami heights of ≈30m. The seismic risk of the southeasternmost St. George basin is higher than estimated above for the whole basin as a result of the potential for these very large or great earthquakes.

Within the Aleutian arc from Okmok to Pavlof are 8 volcanoes that have a high potential for eruption with localized effects described in the last section. These effects along with the seismic risk are discussed for specific sites below:

- Bering Canyon. There is a suggestion in the epicenter map shown in Figure 1 of a tendency for earthquakes to occur beneath the Bering Canyon. It is possible that the canyon may be an active structure, although it is not possible to conclude this on the basis of the poorly located events mapped in Figure 1. The Umnak Plateau region is seismically active; hence, increasing the probability for slumps along the walls of the Bering Canyon and edge of the Bering Shelf.
- Makushin Bay. Makushin Volcano is close enough so that significant ash-fall could occur here. Also the bay opens toward both Okmok and Bogoslof Volcanoes exposing it to the risk of a local tsunami. If the Unalaska Gap ruptures strong ground motion will occur here.
- Dutch Harbor. Makushin Volcano or one of the cones north of Wide Bay could deposit a significant amount of ash here, small amounts might originate from Akutan. A local tsunami from Akutan is possible. If the Unalaska Gap ruptures strong ground motion and a weak tsuani (1-3m) will occur here.
- Ikatan or Morzhovoi Bay. Moderate ash-fall from Shishaldin is possible. If either the Unalaska Gap or the Shumagin Gap ruptures strong ground motion and a large tsunami (≈10-30 m) will occur here. Ikatan Bay would be more sheltered from the Unalaska event and more exposed to the Shumagin event and vice-versa for Morzhovoi Bay.
- Cold Bay. Small amounts of ash are possible from Shishaldin or Pavlof Volcanoes. Strong ground motion will occur if the Shumagin Gap ruptures, depending on the exact rupture area this bay may be somewhat sheltered from the tsunami.
- Pavlof Bay. Heavy ash-fall is possible from Pavlof Volcano, as is a local tsunami. Strong ground motion and a large tsunami are possible if the Shumagin Gap ruptures. The Pavlof Islands may moderate the tsunami height within the bay.

B. Contributions to Seismic Exposure Mapping for the Gulf of Alaska

The seismic exposure map for the Gulf of Alaska under development by Woodward-Clyde Consultants includes a number of innovations, most notably the semi-Markov modeling of seismic gaps. The conclusions to be drawn from this map, as for any seismic risk map, depend critically upon the fundamental seismotectonic models on which it is based. L-DGO scientists have contributed important data and/or interpretations to the understanding of the following elements of the seismotectonics of the Gulf of Alaska: (1) the history of large earthquakes, seismic gaps and arc-segmentation, particularly in relation to the Shumagn, Unalaska, and Yakataga seismic gaps; (2) the formal recognition of the risk posed by normal faulting earthquakes near and seaward of the trench; (3) an improved compilation of tsunami run-up heights; (4) refined constraints on the locus, geometry, and faulting patterns in and around the main thrust zone; (5) the relation between the recurrence time and the size and/or stress drop of the previous great earthquake; and (6) the acquisition and interpretation of strong-motion data.

C. A Possible Seismic Gap Near Unalaska

Seismic and tsunamic information support the interpretation of the region between about 163°W and 167°W as a possible seismic gap. Although we cannot rule out aseismic slip, a conservative assessment of the hazard in this region would assume that it did not slip during the 1957 Andreanof-Fox Islands earthquake and therefore could represent an area of high seismic potential.

D. Fine Structure of the Dipping Seismic Zone in the Shumagin Islands

A cross-section of hypocenters selected to minimize errors due to the velocity model reveals a double-planed seismic zone. The upper plane dips at 32° from 45 to 100 km depth; the lower plane begins at about 65 km depth, where it is 25 km below the upper one, and converges with the upper plane at about 125 km depth. Composite fault-plane solutions suggest down-dip tension in the upper plane and a complicated stress pattern in the lower one that may be related to the high seismic potential of the gap. Composite solutions for events in the overlying North American plate suggest strike slip mechanisms, with the P-axis near horizontal and in the direction of plate convergence. These results are consistent with the interpretation that the main thrust zone of the Shumagin Gap is locked.

E. Stress Drops for Earthquakes in the Eastern Aleutians

There is a difference in stress drops of earthquakes in this region. This difference is important in identifying areas which may be underhigh tectonic stress and thus likely sites of large or great earthquakes in the near future. The breaking of high stress asperities may also be a part of the rupture process in all earthquakes, so the distribution of high and low stress drop events is important in predicting strong ground motion from earthquakes of all sizes.

F. Wind Directions at Cold Bay in Relation to Hazardous Ash-Fall

There may be a larger risk of wind-borne ash fall on the northern shores of the Aleutian Islands and Alaska Peninsula than the southern.

X. SUMMARY OF FOURTH QUARTER OPERATIONS (January-March 1981) AND STATUS OF TECHNICAL WORK

A. Field Work and Status of Remote Station and Recording Centers (D. Johnson)

1. Network Status, Spring 1981

There are now three networks operated by L-DGO in the eastern Aleutian arc-Pribilof Islands region (Figure 19): the Pribilof Network, recorded at St. Paul (SNP); the Unalaska Network, recorded at Dutch Harbor (DUT); and the Shumagin Network, recorded at Sand Point (SAN). The Pribilof and Unalaska Networks have been established largely with the support of the NOAA/BLM OCSEA Program for the purpose of seismic hazards evaluation. The Shumagin Network and its subarray on Pavlof Volcano was established largely with support from the DOE and some initial equipment from the USGS. The original purpose of the Shumagin Network was to provide data for tectonic studies with some geothermal studies being added when the Pavlof subarray was installed. The data from all of these networks can, of course, be used for both hazards and tectonic studies; indeed, there is a synergistic benefit in carrying out these studies simultaneously.

The Pribilof Network (Figure 20) consists of two remote stations and the local station at St. Paul. The sensors at the local station (SNP) consist of a short- and a long-period vertical seismometer. The two remote stations, which were installed during the summer of 1980 are short-period vertical stations.

The Unalaska Network (Figure 21 consists of three remote seismic stations, one repeater station and the local station at Dutch Harbor. The sensors at the local station (DUT) consist of three orthogonal short-period seismometers, a long-period vertical seismometer and an orthogonal set of strong-motion accelerometers. The seismometers at the remote stations are all short-period vertical instruments. One of the remote stations (SDK) was installed during the summer of 1980.

The Shumagin Network (Figure 22) consists of 13 remote stations plus 8 stations in the Pavlof Volcano subarray, three repeater only stations and the local station at Sand Point (SAN). Each remote station has a single, short-period vertical seismometer except Chernabura (CNB) which was converted to a three-component station during the 1980 summer season. Within the region of the Shumagin Network there are now nine strong-motion accelerographs (see Figure 22 and the discussion below), six of which are co-located with remote stations of the network. Sensors local to the recording center at Sand Point (SAN) consist of orthogonal sets of short- and long-period seismometer, and strong-motion accelerometers.

The three component station at Chernabura was established following a decision to begin a program of upgrading a subset of the network by adding horizontal seismometers. The horizontal components yield important information that is not obtainable from a single, vertical component regarding the arrival times of the shear and converted waves (see section by Coles); these arrival times can strongly constrain the location of the hypocenters of earthquakes within the network and provide an almost unique data set for interpreting first-order velocity discontinuities below the net. The location and nature of these discontinuities are important elements of a seismotectonic analysis of the subduction process in the Shumagin region.

Six new strong-motion accelerographs were installed last summer (1980), bringing the total in the region to nine (plus one at DUT). These are all Kinemetrics lg SMA-1's. Five of them (see Figure 22) are connected to the telemetry system so that a trigger signal allows us to know the exact time at which the SMA began recording a given earthquake. Most of the support for these instruments came from a USGS contract. This system has already recorded one $m_b = 5.2$ event just SW of Nagai (NGI); we hope to retreive the records in June 1981.

Helicopter support was provided by the NOAA/BLM OCSEA Program. This support would cost about $100,000 from a private contractor and is vital to the maintenance of the number of stations in the Shumagin and Unalaska Networks. Maintenance of the remote stations requires about 30 days for a five person crew. The central recording stations require about two weeks of maintenance, three times per year by a two man crew.

2. Improvements made at the Central Recording Stations

Universal time receivers for the standard time broadcast via the GOES satellite were installed at all three of the recording centers during 1980. These receivers provide a local time source automatically synchronized to Coordinated Universal Time to within a few milliseconds. This obviates the need to maintain time corrections for the data collected at a particular site and, more importantly, eliminates the need to collect time-correction information (like the date) from the local station operators, removing the seemingly inevitable confusion between local and CUT time. A separate, local clock (TS250, e.g.) is maintained at each recording center in case the receiver or the satellite fail.

Intermediate period seismographs were installed at Sand Point and Dutch Harbor during 1980. Two three-component sets of Baby-Benioff seismometers (1 Hz natural frequency) were provided by L-DGO to the Alaska-Aleutian project; one set each was installed in the vaults at SAN and DUT. The signals from these instruments are conditioned by two-channel filter-amplifier-VCO units newly built by the L-DGO seismology group. OLne channel provides a standard short-period output (am and fm) and the other, an intermediate period (IP) output (am and fm). The IP output is designed to cover the range 20 to .25 sec and to be intermediate in gain between the short period and strong motion systems (see Figure 23). The IP system is intended to provide data critical to the stress-drop and waveform studies described above by J. Mori. The amplitude-modulated (am) outputs can be recorded on the Develocorder, a Helicorder or the digital event recording system, whereas the frequency-modulated (fm) outputs are mixed onto the analog event recording ystem.

Event-detecting, analog recording systems were installed at both Sand Point and Dutch Harbor. The event-detector consists of one to eight analog signal-detector modules and a logic unit which is based on a programmable-read-only-memory (PROM) chip. The signal-detectors switch to an "on" state whenever the short-term average (STA) of the signal exceeds the long-term average (LTA) by a selectable level between 3 and 24 db. The PROM can be programmed so that any logical combination of states of the signal-detectors can cause the event-detectopr to declare an event and switch on the recording systems (Figure 24). Two analog recording systems, each consisting of two four-channel TEAC audio tape recorders have been installed, one each at SAN and DUT. One of the TEACs operates in a continuous-loop mode to provide a twenty second pre-event "memory", and the other in a standard, reel-to-reel mode to record the data. Frequency-modulated tones from the remote and local sensors are mixed onto the four channels along with an IRIG time code and a frequency-compensation tone (see Figure 25). Eight to ten signals can be mixed onto three of the channels and five can be mixed with the 1000 Hz time code, so that a total of about 32 signals can be recorded. In addition to the tones from the seismic stations, 409 Hz tones from the SMA trigger units are also recorded. Whenever one of these tones is detected the tape recorder is always turned on, so that the on- and off-times of the SMA's can be determined. The magnetic tapes are demodulated, digitized and processed at L-DGO (see discussion under Playback below).

A digital magnetic tape recording system was installed at SAN in December 1980. This L-DGO designed system is similar to one L-DGO has been operating in the Caribbean for two years. It has the capability to digitize up to 32 analog seismic signals, with 12 bit resolution, at a rate of 100 samples per second. It has a maximum pre-event capacity of 512 channel-seconds (i.e., 16 seconds for 32 channels). The station operator can vary a number of operating characteristics:

a) which channels are active (i.e. being digitized);

b) the pre-event time;

c) the post-event time;

d) the A/D gain (1,2,4, or 10x)

e) the D/A gain (the system has two selectable D/A outputs).

At present, events are detected by the analog event detecting system, which sends an event signal to the recording system. It is anticipated that a digital event detecting system will be on-line in 1981.

An uninterruptible power-supply (UPS) system was installed at SAN in December 1980. A battery-backup system provides 4 to 8 hours of uninterrupted power for the entire station should the town power system fail. A propane powered alternator will be installed in the summer of 1981. It is designed to automatically start after about 80% of the battery capacity has been used and to run for about one week without refueling. A UPS with battery-powered back-up is planned for Dutch Harbor (summer or fall, 1981).

The Dutch Harbor recording station and vault were relocated from the old site adjacent to the airport to a concrete bunker on Standard Oil Hill. The old site suffered from proximity to a powerful radio transmitter and the propsect that it would be demolished in the near future because it is too close to the landing strip. We have negotiated a reasonable annual lease with the native corporation for use of the new building and power. Last summer's field party at Dutch Harbor spent about two weeks refurbishing (insulating, wiring, etc.) the bunker and relocating the equipment there.

B. Switch to a New Data Analysis System (J. Peterson)

The L-DGO version of the USGS-PDP 11/70 seismic data analysis system is about 75 percent operational. The hardware and most of the software is now installed. Software development to establish a data base management system to handle the large libraries of digital seismograms has been the primary emphasis this year. A great deal of effort has been expended to modify many programs into a coherent and flexible group for routine data processing. This has been complicated by having different data sources and different networks utilizing this system. We can now digitize the demodulated output from the TEAC tape recorders and "pick" the arrival times on a digital seismogram displayed on a fast graphics terminal; the arrival times can then automatically become input to a hypocenter location program and the resultant epicenter be plotted on a map. We also have the added capabilities of performing historic data searches of the Global Digital Seismograph Network. Even mopre important than the improved speed and convenience that this system offers is the potential for far more sophisticated waveform analysis. It will be possible, for example, to write programs to analyze converted phases by examining the particle motion recorded by three-component stations, or to make routine estimates of the stress-drop from the shape of the first cycle of the P-wave.

Another advantage of digitizing the seismograms from magnetic tape (or better, digitizing the seismic output) is that during large events, large excursions on the recorder don't overlap onto adjacent channels obscuring information that may otherwise have been available. An example of the sort of improvement that is possible is shown in Figure 26 (a and b). Significant projects still underway are the creation and maintainence of a station data base, a phase data base and bulletin catalog program. Brief descriptions of the programs and data flow charts follow. Program authors are "in-house" except where noted.

I. Routine Data Processing Programs

CONVERSN - converts earthquake summary file from standard to NOAA format.

DMUX - creates demultiplexed data files from multiplexed files.

DPLTWT - plots weighted regressions on s-p vs. distance and travel time vs. distance for origin time and depth. Gives focal mechanism and map.

DVCH - adds recording device/channel codes to phase data for keying magnitude constants.

ETOI - converts hypoellipse phase data to hypoinverse phase data.

FOOLSGOLD - brings in an event from digital tape in multiplexed form.

HBEAM - earthquake location routine for regional events, outside network, less than teleseismic (SLU).

HFASTPONG - fast earthquake location and plotting routine (SLU).

HNEWPING - interactive display and pick of phase data, period/amplitude and duration (SLU-LDGO).

HPLANEWAVE- teleseism location routine.

HPLT - plots maps, cross-sections and space-time plots.

HYINV - hypoinverse standard hypocenter location routine calculates magnitudes (USGS).

IFAZ - interactive phase data input program.

PUNT - creates hard copy of demultiplexed data.

SECTONM - converts P amplitude in seconds to true ground motion in nanometers.

STPLOT - plot multiplexed data on versatec.

TAR - tape archive system (UNIX).

TDUMP - plot large sections of multiplexed data on versatec.

TICOR - time correction program.

TRACE - plot multiplexed data on T4014.

TRD1 - 11/34 program to list files on digital tape.

71TOS - converts earthquake summary file from hypo71 format to standard format.

II. ISC Geographic Region/NOAA Seismic Region File Search Programs

RESTORE - 11/34, creates data files

SELECT - 11/34, selects hypocenters

PARE - 11/34, compares and selects from duplicate hypocenters

HPLT - as above

SELECT - 11/70 version

III. Network Dat Tape Programs (CIRES)

NDTSUM - reads GDSN tape, produces summary

RETRV - retrieves data

PANG - prepares multiplexed data (LDGO)

HNEWPING - as above (SLU-LDGO)

We estimate the time necessary for routine data processing will be cut in half once the software is fully operational and timesharing is established among the networks. There is a finite (1 year of data) amount of analog to digital conversion which covers the time period of the introduction of the event detector system and digital recording system.

C. Data Collection and Submission (J. Hauptman)

Sand Point Data Submission

The last submission of hypocentral data was made in October 1980. It contained 47 events from January, February, and March 1980. Although epicentral data through July 1980 has been processed, it has not been submitted due to lack of magnitude assignments.

A total system magnification routine is being worked out so magnitude determination can be consistantly applied to all epicentral locations both past and future. The routine requires the formulation of the following:

1. Total instrument configuration as a function of time (i.e. seismometer, damping pad, amplifier VCO, discriminator, recordingdevice);
2. Sensor (seismometer damping pad and lifier amp.) sensitivity at 1 Hz;
3. Sensor response as a function of frequency normalized to 1 Hz;
4. Recorder sensitivity (i.e. telemetry plus develocorder or helicorder) at 1 Hz; and
5. Recorder response as a function of frequency normalized to 1 Hz.

A computer program still under development will convert P amplitudes and periods, which are measured in seconds and stored in the standard phase data file, into true ground motion in nanometers. This ground motion will then be converted into a local body wave magnitude M_b. Duration magnitude will also be computed from the coda lengths picked from the records.

We are also converting the method of recording earthquakes from using a develocorder and analog tapes to a digital recording system with digital event detection. Computer programs must also be constructed and/or refined so that processing this new data can be made simple and routine.

There exists a suite of analog recordings for which conversion to digital-multiplexed data is necessary. It is this analog to digital conversion along with develocorder films that will be the source of epicentral data until the digital system is fully installed and operative.

Data Submitted During Report Period

Quarter	Date Submitted	Scheduled
4Q79	21 May 1980	
1Q80	24 Oct 1980	
2Q80	completed (not submitted no mag)	July 1981
3Q80	in progress	July 1981
4Q80		Sept 1981
1Q81		Nov. 1981
2Q81		Mar. 1982

St. Paul Data Collection

Lamont's seismic station on St. Paul Island, in the Pribilofs, which monitors the seismicity of the SE Bering Sea vicinity consists of one long period and one short period vertical seismometer. On July 19, 1980, the station was expanded to receive two short period vertical seismometers from remote sites (Rush Hill, RHH; Polivina Hill, PLH) on the island (Figure 20). Their respective signals are radio telemetered to the central recording site at the National Weather Service Observatory, where they are recorded on helicorder drums along with the original St. Paul station.

These two stations were installed in order to increase the number and certainty of earthquakes recorded in this region as well as developing the ability to locate these earthquakes.

The records have been carefully scanned and except for an isolated missing record or records with high levels of cultural noise (surf, wind, etc.) a complete data set exists for the entire period covered by this report.

Tables 11 through 14 list date, time, amplitude, period and S-P interval where these criteria exist for the original St. Paul station and the two new remote stations.

Precise locations of earthquakes was not possible with the data collected. However, a number of events detected could fall within the proper distance range for sources in the St. George basin or various locations along the Aleutian Island arc. The approximate distances were obtained by applying the Jeffrey-Bullen travel time table (1958) to the S-P interval (where applicable) and assuming a surface focus (0 depth). Several events on the tables have been located in the PDE (Preliminary Determination of Epicenters) published by the National Earthquake Service of NOAA. In summary, 55 events were recorded on the 3 short period instruments. Two events had S-P intervals of 5 and 6 seconds, which corresponds to distances of about 40 and 48 km, respectively. These events may have occurred in the Saint Paul Island vicinity. 18 events had S-P intervals between 45 and 120 seconds (360-960 km). These events could have occurred along the Aleueian arc between Kodiak Island and the Near Islands. Only one event had an S-P of 15 seconds which would correspond to a distance of about 120 km which is consistent with the Saint George Basin as a source area. S-P intervals could not be determined for 54 events.

Dutch Harbor Data Collection

The recording site at Dutch Harbor consists of an event detecting system using two four-channel TEAC tape recorders. Short period vertical seismic signals from stations at Akutan Volcano (AKA), Makushin Volcano (MAK) and a newly installed station at Sedanka Island (SDK installed, July 1980) as well as long intermediate, and short period local Dutch Harbor stations and a satellite clock are mixed and recorded on a continuous tape loop on the first recorder. The event detection is based on a comparison of short term average (STA) and long term average (LTA) of signal noise. For each station when the STA exceeds the LTA for a given station a signal is sent to a control unit. If this occurs for two stations simultaneously an event is detected and the second or main recorder switches on and records the contents of the tape loop. These analog tapes are to be digitized for processing on a computer.

Also operating are two helicorders, one long period vertical and one short period vertical. After scanning these records for earthquakes, Tables 15 and 16 were constructed listing dates, times, amplitudes, periods and S-P intervals where applicable for all events recorded. Regional locations and magnitudes for events located by the PDE are cross-referenced in the tables.

In summary, 87 events were recorded on the short period instrument. 29 events had S-P intervals of $\leq$ 25 sec; corresponding to distances within 200 km of Dutch Harbor. 31 events had S-P > 25 secs; corresponding to distances of greater than 200 km. S-P intervals could not be determined for 27 events.

XI.A. REFERENCES

Anderson, D.L., and R.S. Hart, 1978. Attenuation models of the earth, Phys. Earth Planet. Int., 16, 289-306.

Archambeau, C.B., 1977. Earthquake predictions based on tectonic stress determinations, Eos Trans. AGU, 57(4), p. 290, abstract.

Barth, T.F., 1956. Geology and petrology of the Pribilof Islands, Alaska, U.S. Geol. Surv. Bull. 1028-F, 101-160.

Carpenter, E.W., 1966. Absorption of elastic waves - An operator for constant Q mechanisms, United Kingdom Atomic Energy Authority, Report D-43/66.

Chapple, W.M., and D.W. Forsyth, 1979. Earthquakes and bending of plates at trenches, J. Geophys. Res., 84(B12), 6729-6749.

Coffman, J.L., and C.A. von Hake (editors), 1973. Earthquake History of the United States, Publ. 41-1, U.S. Dept. of Commerce/NOAA, U.S. Gov't. Printing Office, Washington, D.C.

Davies, J.N., L. House, K.H. Jacob, R. Bilham, V.F. Cormier, and J. Kienle, 1976. A seismotectonic study of the seismic and volcanic hazard in the Pribilof Islands - Eastern Aleutian Islands region of the Bering Sea, NOAA Annual Report, 1 April 1975 - 31 March 1976.

Davies, J.N., and K.H. Jacob, 1979. A seismotectonic analysis of the seismic and volcanic hazards in the Pribilof Islands - Eastern Aleutian Islands region of the Bering Sea, NOAA Annual Report, Research Unit 16, 1 April 1978 - 31 March 1979.

Davies, J.N., and L. House, 1979. Aleutian subduction zone seismicity, volcano-trench separation, and their relation to great thrust-type earthquakes, J. Geophys. Res., 84, 4583-4591.

Davies, J., L. Sykes, L. House, and K. Jacob, 1981. Shumagin seismic gap, Alaska Peninsula: History of great earthquakes, tectonic setting, and evidence for high seismic potential, J. Geophys. Res., 86(B5), 3821-3856.

Davis, T.N., and C. Echols, 1962. A Table of Alaskan Earthquakes, 1788-1961, Geophysical Institute, Univ. of Alaska, Fairbanks, Alaska, Geophys. Rep. No. 8.

Decker, R.W., 1973. State-of-the-art in volcano forecasting, Bull. Volcano., 37(3), 372-394.

Der, Z.A., and T.W. McElfresh, 1975. Attenuation of short period P and S waves in the United States, Geophys. J., 40, 85-106.

Engdahl, E.R., and C.H. Scholz, 1977. A double Benioff zone beneath the central Aleutians: An unbending of the lithosphere, Geophys. Res. Lett., 4(10), 473-476.

Gutenberg, B., 1956. Great earthquakes 1896-1903, Trans. Amer. Geophys. Union, 37(5), 608-614.

Hald, A., 1948. Statistical Theory with Engineering Applications, John Wiley & Sons, New York, 783p.

Hanks, T.C., and D.A. Johnson, 1976. Geophysical assessment of peak accelerations, Bull. Seismol. Soc. Amer., 66, 959-968.

Hantke, G., 1951. Review of volcanic activity 1941-47 (in German), Bull. Volcan., 11, 161- .

Hasegawa, A., N. Umino, and A. Takgai, 1978a. Double-planed structure of the deep seismic zone in the northeastern Japan arc, Tectonophysics, 47, 43-58.

Hasegawa, A., N. Umino, and A. Takagi, 1978b. Double-planed deep seismic zone and upper mantle structure in the northeastern Japan arc, Geophys. J. Roy. astr. Soc., 54, 281-296.

Hopkins, D.M., 1976. Fault history of the Pribilof Islands and its relevance to bottom stability in the St. George Basin, in Environmental Assessment of the Alaska Continental Shelf, Principal Investigators Annual Reports April 1975 - March 1976, NOAA/BLM OCSEAP, Geology Volume 13, 41-68.

House, L., and J. Boatwright, 1980. Investigation of two high stress-drop earthquakes in the Shumagin Seismic Gap, Alaska, J. Geophys. Res., 85, 7151-7165.

House, L., L.R. Sykes, J.N. Davies, and K.H. Jacob, 1981. Identification of a possible seismic gap near Unalaska Island, Eastern Aleutians, Alaska, in Earthquake Prediction - An International Review, Maurice Ewing Series 4, edited by D.W. Simpson and P.G. Richards, 81-92, AGU, Washington, D.C.

Isacks, B., J. Oliver, and L.R. Sykes, 1968. Seismology and the new global tectonics, J. Geophys. Res., 73(18), 5855-5899.

Jacob, K.H., K. Nakamura, and J.N. Davies, 1977. Trench-volcano gap along the Alaska-Aleutian arc: Facts, and speculations on the role of terrigenous sediments for subduction, in Island Arcs, Deep Sea Trenches, and Back-Arc Regions, Maurice Ewing Series 1, edited by M. Talwani and W.C. Pitman III, 259-272, AGU, Washington, D.C.

Jeffries, H., and K.E. Bullen, 1958. Seismological Tables, British Assoc. Adv. Sci., London.

Kanamori, H., 1977a. The energy release in great earthquakes, J. Geophys. Res., 82(20), 2981-2988.

Kanamori, H., 1977b. Seismic and aseismic slip along subduction zones and their tectonic implications, in Island Arcs, Deep Sea Trenches, and Back-Arc Basins, Maurice Ewing Series 1, edited by M. Talwani and W.C. Pitman III, 163-174, AGU, Washington, D.C.

Kelleher, J.A., 1970. Space-time seismicity of the Alaska-Aleutian seismic zone, J. Geophys. Res., 75, 5745-5756.

Kimura, M., 1976. Major magnetic activity as a key to predicting large earthquakes along the sagams trough, Japan, Nature, 260, 5547, 131-133.

Landgrebe, G., 1855. Naturgeschichte der Vulkane, Gotha.

Marlow, M.S., D.W. Scholl, and A. Cooper, 1977. St. George Basin, Bering Sea Shelf: A collapsed Mesozoic margin, in Island Arcs, Deep Sea Trenches, and Back-Arc Basins, Maurice Ewing Series 1, edited by M. Talwani and W.C. Pitman III, 211-220, AGU, Washington, D.C.

McCann, W.R., S.P. Nishenko, L.R. Sykes, and J. Krause, 1980. Seismic gaps and plate tectonics: Seismic potential for major plate boundaries, Pure Appl. Geophys., 117, 1082-1147.

McCann, W.R., O.J. Perez, and L.R. Sykes, 1980. Yakataga seismic gap, southern Alaska: Seismic history, and earthquake potential, Science, 207, 1309-1314.

Minikami, T., 1960. Fundamental research for predicting volcanic eruptions (Part I), Bull. Earthq. Res. Inst., 38(4), 497-544.

Minikami, T., S. Hiraga, T. Miyazaki, and S. Utibori, 1969. Fundamental research for predicting volcanic eruptions (Part II), Bull. Earthq. Res. Inst., 47, 893-950.

Minster, J.B., and T.H. Jordan, 1978. Present-day plate motions, J. Geophys. Res., 83, 5331-5354.

Mogi, K., 1968. Development of aftershock areas of great earthquakes, Bull. Earthq. Res. Inst, Univ. of Tokyo, 46, 175-203.

Mogi, K., 1969. Some features of recent seismic activity in and near Japan, 2, Activity before and after great earthquakes, Bull. Earthq. Res., Inst. of Tokyo Univ., 47, 395-417.

Mortgat, C.P., and H.C. Shah, 1979. A Bayesian model for seismic hazard mapping, Seis. Soc. Amer. Bull., 69(4), 1237-1251.

Mushketov, I., and A. Orlov, 1893. Catalog of earthquakes of the Russian Empire, Contr. Russian Geog. Soc., in general geography, 26, 582p.

Nakamura, K., K.H. Jacob, and J.N. Davies, 1977. Volcanoes as possible indicators of tectonic stress orientation - Aleutians and Alaska, in Stres in the Earth, edited by Max Wyss, PAGEOPH, 115, 87-112.

Orth, D.J., 1967. Dictionary of Alaska Place Names, U.S. Geol. Surv. Prof. Paper 567, 1084p.

Page, R.A., D.M. Boore, W.B. Joyner, and H.W. Coultner, 1972. Ground motion values for use in the seismic design of the Trans-Alaska Pipeline System, U.S. Geol. Surv. Circular 672.

Patwardhan, A.S., R.B. Kulkarni, and D. Tocher, 1980. A semi-Morkov model for characterizing recurrence of great earthquakes, Seis. Soc. Amer. Bull., 70(1), 323-347.

Perez, O.J., and K.H. Jacob, 1980a. Tectonic model and seismic potential of the eastern Gulf of Alaska and Yakataga seismic gap, J. Geophys. Res., 85, 7132-7150.

Perez, O.J., and K.H. Jacob, 1980b. St. Elias, Alaska earthquake of February 28, 1979: Tectonic setting and precursory seismic pattern, Bull. Seismol. Soc. Amer., 70, 1595-1606.

Reyners, M., and K. Coles, 1980. Fine structure of the dipping seismic zone in the Shumagin Islands, Alaska, abstract, Eos Trans. Amer. Geophys. Union, 61, 1045.

Reyners, M., and K. Coles, 1981. Fine structure of the dipping seismic zone and subduction mechanics in the Shumagin Islands, Alaska, submitted to J. Geophys. Res.

Richter, C.F., 1958. Elementary Seismology, W.H. Freeman and Co., San Francisco, Calif., 768p.

Samowitz, I., and D. Forsyth, 1979. Double seismic zone beneath the Marianas, abstract, Eos Trans. Amer. Geophys. Union, 60, 958.

Scholz, C.H., 1974. Postearthquake dilatancy recovery, Geology, 2, 551-554.

Shimozuru, D., 1971. A seismological approach to the prediction of volcanic eruptions, in The Surveillance and Prediction of Volcanic Activity, UNESCO Earth Science Mono. #8, 19-45, Paris.

Sleep, N.H., 1979. The double seismic zone in downgoing slabs and the viscosity of the mesosphere, J. Geophys. Res., 84, 4565-4571.

Sommerville, P.G., R.A. Wiggins, and R.M. Ellis, 1976. Time domain determination of earthquake fault parameters from short period P waves, Bull. Seismol. Soc. Amer., 66, 1459-1484.

Sykes, L.R., 1971. Aftershock zones of great earthquakes, seismicity gaps, earthquake prediction for Alaska and the Aleutians, J. Geophys. Res., 76(36), 8021-8041.

Sykes, L.R., J.B. Kisslinger, L. House, J.N. Davies, and K.H. Jacob, 1980. Rupture zones of great earthquakes, Alaska-Aleutian arc, 1784-1980, Science, 210, 1343-1345.

Sykes, L.R., and R.C. Quittmeyer, 1981. Repeat times of great earthquakes along simple plate boundaries, in Earthquake Prediction - An International Review, Maurice Ewing Series 4, edited by D.W. Simpson and P.G. Richards, 217-247, AGU, Washington, D.C.

Sykes, L.R., J.B. Kisslinger, L. House, J. Davies, and K.H. Jacob, 1981. Rupture zones and repeat times of great earthquakes along the Alaska-Aleutian arc, 1784-1980, in Earthquake Prediction - An International Review, Maurice Ewing Series 4, edited by D.W. Simpson and P.G. Richards, 73-80, AGU, Washington, D.C.

Tarr, R.S., and L. Martin, 1912. The earthquake at Yakutat Bay, Alaska, in September 1899, U.S. Geol. Surv. Prof. Paper 69.

Thatcher, W., and G. Plafker, 1977. Int. Union Geod. Geophys. IASPEI/IAVCEI Assem., abstract, 54.

Tobin, D.G., and L.R. Sykes, 1966. Relationship of hypocenters of earthquakes to the geology of Alaska, J. Geophys. Res., 71, 1659-1667.

Veith, K.F., 1974. The relationship of island arc seismicity to plate tectonics, abstract, Eos Trans. Amer. Geophys. Union, 55, 349.

Waldron, H., 1961. Geologic reconnaissance of Frosty Peak Volcano and vicinity, Alaska, U.S. Geol. Surv. Bull. 1028-T.

XI.B. Papers Published, Submitted, and In Preparation

Papers Published

(1) McCann, W.R., O.J. Perez, and L.R. Sykes, 1980. Yakataga seismic gap, southern Alaska: Seismic history and earthquake potential, Science, 207, 1309-1314.

(2) Perez, O.J., and K.H. Jacob, 1980. Tectonic model and seismic potential of the eastern Gulf of Alaska and Yakataga seismic gap, J. Geophys. Res., 85, 7132-7150.

(3) Perez, O.J., and K.H. Jacob, 1980. St. Elias, Alaska earthquake of February 28, 1979: Tectonic setting and precursory seismic pattern, Bull. Seismol. Soc. Amer., 70, 1595-1606.

(4) House, L., and J. Boatwright, 1980. Investigation of two high stress-drop earthquakes in the Shumagin seismic gap, Alaska, J. Geophys. Res., 85, 7151-7165.

(5) Boatwright, J., 1980. Preliminary body wave analysis of the St. Elias, Alaska earthquake of February 28, 1979, Bull. Seismol. Soc. Amer., 70, 419-436.

(6) Sykes, L.R., J.B. Kisslinger, L. House, J.N. Davies, and K.H. Jacob, 1980. Rupture zones of great earthquakes, Alaska-Aleutian arc, 1784-1980, Science, 210, 1343-1345.

(7) Davies, J., L. Sykes, L. House, and K. Jacob, 1981. Shumagin seismic gap, Alaska Peninsula: History of great earthquakes, tectonic setting, and evidence for high seismic potential, J. Geophys. Res., 86, 3821-3856.

(8) House, L., L.R. Sykes, J.N. Davies, and K.H. Jacob, 1981. Identification of a possible seismic gap near Unalaska Island, Eastern Aleutians, Alaska, in Earthquake Prediction - An International Review, Maurice Ewing Series 4, edited by D.W. Simpson and P.G. Richards, AGU, Washington, D.C., 81-92.

(9) Sykes, L.R., J.B. Kisslinger, L. House, J. Davies, and K.H. Jacob, 1981. Rupture zones and repeat times of great earthquakes along the Alaska-Aleutian arc, 1784-1980, in Earthquake Prediction - An International Review, Maurice Ewing Series 4, edited by D.W. Simpson and P.G. Richards, AGU, Washington, D.C., 73-80.

(10) Sykes, L.R., and R.C. Quittmeyer, 1981. Repeat times of great earthquakes along simple plate boundaries, in Earthquake Prediction - An International Review, Maurice Ewing Series 4, edited by D.W. Simpson and P.G. Richards, AGU, Washington, D.C., 217-247.

Papers Submitted

(1) McNutt, S.R., and R.J. Beavan, 1981. Volcanic earthquakes at Pavlof Volcano, Alaska, correlated with the solid earth tide, submitted to Nature.

(2) Reyners, M., and K. Coles, 1981. Fine structure of the dipping seismic zone and subduction mechanics in the Shumagin Islands, Alaska, submitted to J. Geophys. Res.

Papers in Preparation

(1) McNutt, S.R., in preparation. Short term patterns of seismicity at Pavlof Volcano and the solid earth tides, IAVCEI Sympsoium on Arc Volcanism.

(2) House, L., and K.H. Jacob, in preparation. Earthquake focal mechanisms and tectonics of the eastern Aleutian arc.

(3) Kisslinger, J., J. Davies, L. Sykes, L. House, and K. Jacob, in preparation. Historical earthquakes of Alaska and the Aleutian Islands: A compilation of original references, some newly translated.

(4) Mori, J., in preparation. Stress drops of moderate earthquakes in the Eastern Aleutians.

(5) Harlow, D.H., S.R. McNutt, and P.L. Ward, in preparation. Seismicity at Fuego, Pacaya, Izalco, and San Cristobal Volcanoes, Central America.

CRUSTAL DEFORMATION AND STRESS PATTERNS RESULTING FROM THE SHALLOWLY DIPPING SUBDUCTION ZONE IN THE GULF OF ALASKA

K. H. Jacob (both at: Lamont-Doherty Geological Observatory of Columbia University, Palisades, NY 10964)
O. J. Perez (also at FUNVISIS, Venezuela, and Dept. of Geol. Sci. of Columbia Univ.)

Based on well-constrained new and published fault plane solutions, we infer the crustal deformations and stress patterns of the gently dipping interface between the N. American and Pacific plates in the Gulf of Alaska, and within the overriding plate in central Alaska, south of the Arctic circle. The gently NW dipping portion of the subduction zone between the Aleutian trench and the Shelikof Strait/Cook Inlet trough is dominated by subhorizontal (dip < 15°) detachment faulting (thrusting) and occasional upward imbrication through the accretionary prism. Nowhere is the downdip width of this major thrust or subhorizontal detachment less than 200 km wide; its maximum width may exceed 400 km NE of Anchorage. The overriding crust appears at places 35 ±10 km thick and generally tapers towards the trench. Beneath Kodiak and offshore the Kenai Peninsula two distinct groups of high-stress drop earthquakes show normal faulting at depths near 35 km and 25 km, respectively (from pP and sP depth phases). These events appear to be associated with bending stresses either at the top of the downward bending Pacific slab, or at the bottom of an upward bending, leading edge of the overriding plate. North of the Cook Inlet/Chugach Mountain region northerly directed compressional stresses developed by friction between the N. American and Pacific plates and transmitted through the overriding plate, are relieved mostly on strike slip faults, except near Mt. McKinley where southward thrusting of the northern forelands beneath the Alaskan Range may occur. North of the Kaltag fault and near the Seward Peninsula a tensional crustal regime dominates indicated by at least one normal faulting solution and Quaternary alkaline volcanism.

1. 1981 Spring AGU Meeting

2. JACOB 021138

3. Klaus H. Jacob
   Lamont-Doherty Geol. Obs.
   Palisades, NY 10964

4. T (Tectonophysics)

5. Special Session:
   Large Scale Thin-Skin Tectonics

6. O (Oral)

7. 0%

8. a) Ms. Pat Damuth
      Purchasing Dept.
      Lamont-Doherty Geol. Obs
      Palisades, NY 10964

   b) not applicable

   c) not applicable

9. C (Contributed)

AN APPARENT DOUBLE SEISMIC ZONE IN THE EASTERN ALEUTIANS

L. S. House (Lamont-Doherty Geol. Obs. & Dept. of Geol. Sci. of Columbia Univ., Palisades, NY 10964)

K. H. Jacob (Lamont-Doherty Geol. Obs. of Columbia Univ., Palisades, NY 10964)

Well-located earthquakes of $m_b > 5.5$ and in the eastern Aleutians form an apparent double zone of activity at depths between 100 and 200 km. Events in the upper zone occurred west of Unimak Pass (165°W). Focal mechanisms of these two events have compressional (P) axes aligned down-dip in the seismic zone. The two events in the lower zone are located to the east of Unimak Pass; their focal mechanisms have down-dip tensional (T) axes. Epicenters of these events span a segment of the Aleutian arc that includes part of the aftershock zone of the 1957 great earthquake and the Shumagin seismic gap. Since the detailed geometry of the downgoing plate is not known, the apparent double seismic zone could result from a tear in the plate. Such a phenomenon fails to reconcile, however, the reversal of focal mechanisms between upper and lower zones. The distribution of inferred stresses (down-dip P in the upper zone, down-dip T in the lower) is similar to that of a double seismic zone identified beneath north Honshu, Japan. In the area of the Aleutians where we find down-dip tensional events, Reyners and Coles (1980) identify a double seismic zone beneath the Shumagin seismic network at depths between 50 and 120 km. They also find down-dip tension for events at depths between 130 and 170 km but cannot resolve a double zone for this depth range. Combining these observations we infer that activity in the eastern Aleutians may represent a true double zone that is modified along strike by processes that alter the stresses in the downgoing slab on either side of Unimak Pass. Such processes might include the coupling between the North American and Pacific plate at shallow (crustal) depths, the recent history of great earthquakes along the interface between the plates, and the buoyancy of the downgoing slab.

1. Spring Meeting, AGU, 1981

2. HOUS026666

3. Leigh House
   Lamont-Doherty Geol. Obs.
   Palisades, NY 10964

4. S (seismology)

5. none

6. O (oral)

7. 15%, Spring Meeting, 1977

8. Ms. Pat Damuth
   Purchasing Dept.
   Lamont-Doherty Geol. Obs.
   Palisades, NY 10964

   student rate applicable

9. C (contributed)

SHORT TERM PATTERNS OF SEISMICITY AT PAVLOF VOLCANO AND THE SOLID EARTH TIDES

Steve McNutt
Lamont-Doherty Geological Observatory of Columbia University and
Department of Geological Sciences, Palisades, New York 10964

Pavlof Volcano is a 2,715 m high stratovolcano located near the end of the Alaska Peninsula at 55°25'N, 161°54'W. A single short-period seismometer has been operated 7 km to the southeast of the summit of the volcano since July 1973. Continuous helicorder records for an eruption sequence beginning 27 October 1974 and ending 13 January 1975 show four types of seismic signals: high-frequency tremors, volcanic earthquakes (B-type, Minakami (1960)), explosion earthquakes, and harmonic tremors. B-type earthquakes are the most numerous, followed by explosions, high-frequency tremors, and harmonic tremors.

The 1974/75 eruption sequence consisted of three episodes of explosive activity: from October 29-November 19, November 25-December 16, and December 25-January 6. Reported observations indicate an eruption cloud of steam and ash to approximately 6 km, and minor fountaining of incandescent material.

Seismicity is divided into four periods on the basis of explosive activity: non-eruptive (background), pre-eruptive, eruptive, and post-eruptive. Seismicity is highest during pre-eruptive periods, followed by eruptive, post-eruptive, and background periods. Calculation of the slope of the frequency-magnitude relation for each period shows values ranging from 1.9 to 2.6, with no clear correlation based on seismicity episodes.

Harmonic tremor is observed mainly during pre-eruptive and post-eruptive periods, and to a lesser extent during eruptive periods. Very narrow, evenly spaced peaks in the spectra of the tremor suggest the presence of a resonating body, possibly magma in a conduit vibrating in organ pipe-like modes.

During pre- and post-eruptive periods, B-type earthquakes occur in pronounced daily swarms. Histograms of the number of events during each two-hour interval were compared with the horizontal components of the stress rate computed for the solid-earth tides as a function of azimuth. Linear regression between the number of B-type earthquakes per two hours and the tidal stress rate for periods of 3-4 days immediately before and after explosive activity shows statistically significant and distinct correlations for the pre- and post-eruptive periods. Before the explosions, swarms of B-type earthquakes correlate with the times of maximum rate of change of tidal stress going from compression to extension. After the explosions, the swarms correlate with maximum rate of change of stress in the opposite sense; that is, from extension to compression. Tidal stresses may modulate the magmatically induced inflation and deflation of the volcano, thus triggering the swarms of B-type earthquakes. This result suggests that eruptive activity of Pavlof Volcano responds to small changes in ambient stress of the order of 10^{-2} bars.

Minakami, T., 1960. Fundamental research for predicting volcanic eruptions (I) - Earthquakes and crustal deformations originating from volcanic activities. Bull. Earthquake Res. Inst., Univ. Tokyo, 38: 497-544.

NANOEARTHQUAKE SWARMS IN GUATEMALA OBSERVED PRIOR TO THE FEBRUARY 4, 1976 EARTHQUAKE

S. McNutt (Lamont-Doherty Geological Observatory and Department of Geological Sciences of Columbia University, Palisades, NY 10964)
D. Harlow (U.S. Geological Survey Menlo Park, California 94025)

A network of six seismograph stations in the vicinity of Guatemala City began continuous operation in February 1975. Swarms of nanoearthquakes (events with $M<1$) were recorded by one or more stations between March and May 1975. Examination of the records and histograms of the number of events per hour indicated that, although the swarms are recorded during the same time period at two or more stations, the events originate from discrete regions within 5 km of each station. The largest swarms, on May 7, and 8, 1975, consisted of separate swarms of several hundred events each, recorded simultaneously over a period of 4 hours at 3 different stations. Microearthquake locations indicate that faults near each of the stations are seismically active, suggesting that these faults are the sources of the nanoearthquake swarms. These faults underwent extensive secondary rupturing during and after the Guatemalan earthquake of February 4, 1976. Smaller swarms were observed on some records available at two stations prior to 1975, but the swarm appear to cease after the February 4 earthquake.

We speculate that the simultaneous occurrence of nanoearthquake swarms over a wide area many months prior to the 1976 Guatemalan earthquake may represent a precursory phenomenon.

1. Spring Meeting
2. MCNU202573
3. S. McNutt
   Lamont-Doherty Geol. Ob:
   Palisades, NY 10964
4. Seismology
5. Earthquake Prediction
6. 0
7. 0%
8. Ms. Pat Damuth
   Purchasing Dept.
   Lamont-Doherty Geol. Ob:
   Palisades, NY 10964
9. C

GEOLOGIC AND GEODETIC STUDIES IN THE SHUMAGIN SEISMIC GAP

M. A. Winslow
T. C. Ray
R. J. Beavan (all at: Lamont-Doherty Geological Observatory of Columbia University, Palisades, New York 10964
(Sponsor: Klaus H. Jacob)

Seismologic investigations in the Shumagin Islands of southwest Alaska suggest that a major earthquake is likely to rupture the seismic gap within the next one to two decades. Geodetic and geologic evidence indicate vertical motions and tilting in the region which appear to vary in magnitude and polarity among the islands and localities on the peninsula. Uplifted marine terraces ranging in age from 9540 to 460 years B.P. are locally developed and some are widespread, covering several km^2. Of 80 terrace sites which were sampled, 14 have a clear marine - non-marine transition. The maximum uplift rate, from a terrace on Andronica Island, is 2.2 cm/yr over a period of 460 years. Most other inferred uplifts are less than 0.8 cm/yr. Their magnitudes are similar to those observed in the Gulf of Alaska. With minor exceptions, uplift rates decrease from the Alaska Peninsula toward the trench axis. The oldest dated terraces (up to 9500 yrs BP) are from the Inner Shumagin Islands, decreasing in height and age both toward the Peninsula and toward the trench.

One precision levelling line has been monitored yearly since 1972. Additional 1 km long level lines have been established between 1977 and 1980. The 1972-1978 results for one line on Unga Island revealed a consistent downward tilt of the trenchward end (SE) of less than 0.5 microradians per year. In 1979 and 1980, the trenchward end began to tilt upward relative to the north end, which may represent crustal deformation precursory to a large earthquake. Levelling results from a line nearest the trench indicate a similar trend to the inferred precursory tilt on Unga Island.

1. Fall Meeting 1980 AGU

2. 021138JACOB (Sponsor)

3. M. Winslow
   214 Seismology
   Lamont-Doherty Geol. Obs.
   Palisades, NY 10964

4. Tectonophysics

5. None

6. P

7. 0%

8. Purchasing
   Lamont-Doherty Geol. Obs.
   Palisades, NY 10964

9. C

EFFECTIVE STRESS DROPS OF MODERATE EARTHQUAKES IN THE EASTERN ALEUTIANS

J. Mori (Dept. Geol. Sci. and Lamont-Doherty Geological Observatory of Columbia University, Palisades, NY 10964)

Estimates of the effective stress drop are calculated for 11 earthquakes of limited magnitude range (m_b = 5.1-6.1) but diverse tectonic settings in the eastern Aleutians. Effective stress drop represents the difference between initial stress and dynamic frictional stress. Digitization of the P arrivals from short period WWSSN records are deconvolved for instrument response and band passed filtered to obtain velocity and displacement seismograms. The effective stress is then proportional to the initial slope of the velocity plot.

Although a large scatter exists in the results, the following trends in the stress measurements can be recognized: intermediate depth earthquakes (100-150 km) have effective stress drop of 50-100 bars; normal-faulting events close to the trench have effective stress drops of 100-300 bars; shallow (10-40 km) earthquakes along the main thrust zone have varying stress drops of 50-500 bars, with the two high stress drop earthquakes located in areas which are relatively inactive seismically.

1. Spring Meeting, 1980
2. 049825 MORI
3. Lamont-Doherty Geol. Observ. Palisades, New York 10964
4. S (Seismology)
5. None
6. O
7. 0%
8. Alma Kesner
   Purchasing Department
   Lamont-Doherty Geol. Observ.
   Palisades, New York 10964
9. C

FINE STRUCTURE OF THE DIPPING SEISMIC ZONE IN THE SHUMAGIN ISLANDS, ALASKA

M. Reyners (Lamont-Doherty Geological Observatory of Columbia University, Palisades, New York 10964)

K. Coles (Lamont-Doherty Geological Observatory and Department of Geological Sciences of Columbia University, Palisades, New York 10964)

Microearthquake data from a permanent, telemetered network has been used to elucidate the structure and tectonics of the subduction zone in the Shumagin Islands, Alaska. The shallow microseismicity is characterized by intense activity near the top of the subducted Pacific plate in the 25-45 km depth range. A composite fault-plane solution for this activity indicates thrust faulting with a near-horizontal P axis oriented approximately in the direction of plate convergence and with one nodal plane parallel to the plate interface. Landward of this intense activity, microearthquakes in the overlying North American plate show a strike-slip mechanism, with the P axis again near-horizontal and oriented approximately in the direction of convergence. The dipping seismic zone in the Shumagin Islands region appears to be double-planed. The upper plane dips at about 30° from 25 to 100 km depth, where it exhibits a knee-like bend below the volcanic front. The lower plane begins at about 75 km depth, where it is separated from the upper plane by some 25 km, and converges with the upper plane at about 120 km depth. This lower plane appears to be real, and not related to lateral segmentation of the subducted plate, since the microearthquakes comprising it are evenly spread along the strike of the arc.

1. Fall Meeting, 1980

2. REYN201474

3. Dr. Martin Reyners
   Lamont-Doherty Geol. Obs.
   Palisades, NY 10964

4. S

5. ----

6. 0

7. 0%

8. (Mrs.) P. Damuth
   Purchasing Dept.
   Lamont-Doherty Geol. Obs.
   Palisades, NY 10964

9. C

The period of time since the last great earthquake within the gap, 77 years, is approaching the longest possible recurrence intervals for the Shumagin gap (113 years) and for the adjacent area of the 1938 earthquake (91 years). Thus, both spatial and temporal seismicity information indicate that the Shumagin gap is likely to be well advanced into the earthquake cycle.

SEISMICITY IN AND NEAR THE SHUMAGIN SEISMIC GAP, ALASKA: INDICATION OF AN ADVANCED STAGE OF EARTHQUAKE PREPARATION?

L. House*, J.N. Davies, L.R. Sykes*, K.H. Jacob

Lamont-Doherty Geological Observatory of Columbia University
Palisades, New York 10964

(*Also with the Department of Geological Sciences, Columbia University)

The Shumagin seismic gap is a 200 km long segment of the Alaska-Aleutian plate boundary that is located between the aftershock zone of the 1946 tsunamigenic earthquake ($M_s = 7.4$) to the west and the zone of shallow (depth less than 50 km) aftershocks of the 1938 earthquake ($M_w = 9.2$) to the east. The Shumagin Gap may have broken during one or more of several large earthquakes between 1900 and 1903 although their locations are uncertain. The Shumagin gap, therefore, has not experienced a great earthquake for at least 77 years. Previous quiescent periods lasted 59 (1788-1847), 56 (1847-1903?) or as long as 113 (1847-1980) years.

The locations of moderate size ($m_b = 5.0$) and larger earthquakes from 1965 to 1979 in the vicinity of the gap define a pattern similar to the "doughnut" described by Mogi. During this time only one of these earthquakes occurred in the interior of the gap. In contrast a large number of events align subparallel to the strike of the arc at what we infer to be the northern edge of the gap. Of these, the larger events with magnitudes about 6, occurred at depths of 40-50 km. Smaller numbers of events form elongated clusters that nearly coincide with the western and southern edges of the gap.

Events located by the Shumagin Islands Network since its installation in 1973 show a distribution similar to that revealed by teleseismic observations over the past 15 years. The local network locations provide greater detail, however, and suggest that relatively high seismic activity within the 40-45 km depth range represents the deepest extent (and hence northern edge) of the plate interface or main thrust zone. The remaining shallow portion of the main thrust zone is currently aseismic. Seismicity within the overriding plate, scattered throughout a region above and landward of the main thrust zone, represents a sizeable fraction of all activity located by the network. We infer from this pattern of seismicity that the main thrust zone within the Shumagin gap is highly coupled or "locked". Seismicity within the overriding plate may result from the "locking" of the main thrust zone. Two earthquakes located at the down-dip edge of the main thrust zone at depths of about 40 km had high stress drops ($\Delta\sigma$= 600-800 bars). Although open to other interpretations, this result may indicate that considerable stresses have accumulated within the Shumagin Gap.

EVIDENCE FOR A POSSIBLE SEISMIC GAP NEAR UNALASKA ISLAND IN THE EASTERN ALEUTIANS, ALASKA

L. House
L.R. Sykes (both at: Lamont-Doherty Geological Observatory and Dept. of Geol. Sci., Columbia University, Palisades, New York 10964)
J.N. Davies
K.H. Jacob (both at: Lamont-Doherty Geological Observatory of Columbia University, Palisades, New York 10964)

The aftershock zone of the Aleutian Islands earthquake of 1957 (magnitude, Mw = 9.1) stretched along the North American-Pacific plate boundary from 180°W to 163°W. The eastern 200 km of this aftershock zone, located southeast of Unalaska Island, experienced only six moderate size (m_b = 6) or larger aftershocks, all located along the northern (arcward) edge. Within this 200 km long segment the rest of the width of the plate interface (the main thrust zone) lacked known aftershock activity and has experienced only two earthquakes (m_b = 5) of magnitude 5 and larger since 1957. In the three years before the 1957 main shock, two clusters of seismicity occurred within the future aftershock zone: one at the western end, near 180°W, the other at 168°W. Arrival times of the 1957 tsunami at tide gauges along western North and South America indicate a source area whose eastern end was located at about 167°W rather than at the eastern end of the aftershock zone, 200 km further east (163°W).

These observations strongly suggest that this 200 km long segment near Unalaska Island either did not rupture during the 1957 earthquake or at least did not break in the same manner as the rest of the 1957 aftershock zone. We cannot rule out the possibility that this segment slips aseismically. Since almost all other segments of the convergent margin in Alaska undergo episodic seismic deformation we infer that this 200 km long Unalaska portion does also. If it were to rupture during a single earthquake, this possible gap is large enough to produce an earthquake of magnitude 8 or larger.

1. Spring Meeting, 1980

2. AGU

3. Corresponding Address:

   Leigh House
   Lamont-Doherty Geol. Observ.
   Palisades, New York 10964

4. S (Seismology)

5. None

6. Oral

7. 5% at Fall, 1979 Meeting

8a. Alma Kesner
    Purchasing Department
    Lamont-Doherty Geol. Observ.
    Palisades, New York 10964

b. Not Necessary

c. Student Rate Applicable

9. C

PRELIMINARY CALCULATIONS OF MT. ST. HELENS b-VALUES

S. McNutt (Dept. Geol. Sci. and Lamont-Doherty Geol. Obs. of Columbia Univ., Palisades, NY 10964)

Amplitude b-values were calculated for subsets of the Mt. St. Helens earthquake sequence for the time period March 20 to May 18, 1980. The first calculation was made using data from station SHW, located 6.5 km west of the summit of Mt. St. Helens. All other calculations were made using station CPW, located 100 km northwest of the volcano. Maximum peak to peak amplitudes were measured to the nearest 1/2 mm on paper helicorder records.

Two distinct event types were recorded on station CPW; high frequency events (> 5 Hz) with P to S amplitude ratio of approximately 1:4, and low frequency events ($\sim$ 1.4 Hz) with P to S amplitude ratio of approximately 1:2. Calculations of b-values were made separately for each event type.

A b-value of approximately .6 was found for the initial earthquake sequence from March 21-24 as recorded at SHW. This value is quite low and is characteristic of tectonic rather than volcanic processes. Plots of b-values for later data sets from CPW show changes in slope for different time periods. Each plot shows one or more breaks in slope, indicating that more than one physical mechanism is acting. Each plot suggests the co-existence of a characteristic tectonic and volcanic b-value. B-values for high frequency events range from .4 to 2.4, while those for low frequency events range from .4 to 4.0.

1. PNAGU Meeting, 1979
2. MCNU202573
3. Corresponding Address:

Mr. Stephen R. McNutt
Lamont-Doherty Geol. Obs
Palisades, NY 10964

4. V
5. None
6. None
7. 0%
8. Mrs. Alma Kesner
Purchasing Department
Lamont-Doherty Geol. Obs.
Palisades, NY 10964

Pacific Northwest Meeting

The Twenty-Sixth Annual Meeting of Pacific Northwest AGU was held in Bend, Oregon, September 17–18, 1979, attracting 101 papers and approximately 400 participants. A special symposium on volcanism included five topical sessions: Large Explosive Eruptions, Volatiles in Volcanism, Rates of Magma Supply and Ages of Volcanic Systems, Magma Mixing, and Glacier-Volcano Interactions. Prior to and following formal sessions, field trips were taken to Columbia River Basalt-Clarno and John Day formations (Swanson, Wright, Robinson); Medicine Lake Highlands (Donnelly-Nolan, Eichelberger, Heiken, Fink); Newberry Volcano (Macleod, Chitwood, Sherrod); High Cascades (Ed Taylor); Christmas Lake Valley (Heiken, Fisher); Brothers Fault Zone-Harney Basin (Walker, Nolf). Session summaries follow.

Volcanology

The general volcanology session included 10 oral presentations and one poster presentation. Both geophysical and geological papers were included in this session.

Two volcano-seismology papers opened the session, presenting very different views of apparent correlations of seismic events with tides. McNutt recognized four types of seismic events at Pavlov Volcano, Alaska, during eruptive activity in 1974–1975: A-type microearthquakes, B-type tremors, harmonic tremor, and explosive quakes with an air phase. Of these, he found a correlation between B-type events and solid earth tides in the periods just before and after eruptions. He proposed that the events were triggered by tidal expansion and contraction of shallow magma conduits.

Lalla and Kienle reexamined a type of seismic activity at Augustine Volcano, Alaska, that was formerly interpreted as being tidally triggered (Mauk and Kienle, *Science*, *182*, 386, 1973). They observed that the events, whose maxima occurred at times of maximum oceanic tidal loading, only occurred when the regional air temperature fell below −7°C. They have identified the quakes as brittle rupture of coastal sea ice, which was visible on ERTS images recorded during one swarm. They contrasted these events with earthquake activity that occurred during several months prior to the 1976 eruption of Augustine.

Crumpler and Aubele reported their determinations of total magnetic fields across several undissected maars in the Mt. Taylor volcanic field. They observed positive magnetic anomalies of up to 1000 gammas of the inner crater slopes of most and attribute this to the presence of a ring dike. Ken Wohletz pointed out that a ring dike is present at the Zuni Salt Lake Crater, a similar maar.

Fink analyzed the surface structure of the Little Glass Mountain obsidian flow and suggested that most features could be attributed to compression during flow, facturing during cooling and gravity instability due to the presence of a vesicular base beneath the nonvesicular obsidian core of the flow.

Several papers discussed aspects of Cascade volcanology. Stoiber, Hughes, and Carr identified linear segments in the Cascade volcanic chain, 110 to 240 km long. They suggest that the volcanos within the interiors of the segments are compositionally uniform (convergent in the sense of McBirney, in the Andesite Conference Guidebook) 1968, and that those at segment boundaries are compositionally divergent.

Volcanology-General Session

VOLCANIC EARTHQUAKES CORRELATED WITH EARTH TIDES AT PAVLOF VOLCANO

S. McNutt (Dept. Geol. Sci. and Lamont-Doherty Geological Observatory of Columbia University, Palisades, New York 10964)
(Sponsor: Klaus Jacob)

A single short-period seismometer has been operated 7 km to the southeast of the summit of Pavlof Volcano since October 1973. Continuous helicorder records from an eruption sequence beginning 29 October 1974 and ending 13 January 1975 show four types of seismic signals: microearthquakes (A-type), volcanic tremors (B-type), explosion quakes with distinct air phases, and harmonic tremors. Histograms of the number of events of each type that took place during each two-hour interval are compared with the horizontal component of the theoretical solid-earth tidal strain, calculated for an azimuth of 135° (subparallel to the direction of plate convergence). For 3–4 days immediately before and after swarms of explosion quakes, a strong positive correlation is observed between B-type earthquake swarms and semi-diurnal tidal peaks. Before the explosions occur, swarms of B-type quakes correlate with the maximum tensional (high tide) peak, and after the explosions stop, swarms correlate with the maximum compressional (low tide) peak. This information strongly suggests that B-type earthquakes are caused by expansion and contraction, respectively, of shallow-depth magma conduits, and demonstrates that just before and just after eruptions the volcano is very sensitive and responsive to small changes in ambient stresses.

OBLIQUE SUBDUCTION AND RIFTING ALONG OCEAN-CONTINENT TRANSFORM BOUNDARIES

K.H. Jacob (Lamont-Doherty Geol. Observ. of Columbia Univ., Palisades, NY 10964)

Earthquakes, computed plate motions, bathymetric features, and other geologic and geophysical expressions of crustal deformation associated with the Queen Charlotte-Fairweather transform-fault system suggest a small component (~1 cm/y or less) of convergence across segments of this plate boundary. Most previous studies assumed at this boundary between the Pacific and North American plates pure dextral strike-slip motion with rates of 5 to 6 cm/y. The inferred small convergence appears to be taken up by slow subduction of Pacific lithosphere beneath the North American margin. In contrast to the inferred convergence on the seaward side of the transform boundary, there is weak evidence for rifting in the overriding continental plate on the NE trending Stikine alkaline volcanic belt. The observed stress and strain patterns are reminiscent of other ocean-continent plate boundaries of the transform type, such as in California, western Aleutians, the northern and southern boundary of the Caribbean plate, southern Chile, and the Burma-Andaman arc. These regions with over-all oblique slip across plate boundaries provide ample examples for simultaneous crustal extension (pull-apart basins, grabens, open rifting with and without alkali basalt volcanism) and crustal shortening (transverse thrust ranges, fold belts). The compressive features strike perpendicular to the azimuth of maximum principal stress, extensional features strike normal to that of minimum principal stress; both principal stress axes are horizontally oriented as expected for a strike-slip regime. Convergent features often dominate on the seaward side, extensional features on the landward side of the transform boundary. In cases where extension develops into mature rifting it can lead to conveyor-belt tectonics: the continental margin breaks into distinct terranes which are laterally transported away with the oceanic plate and are eventually accreted back to the continental side in regions with strong plate convergence.

1. Spring Meeting, 1980

2. AGU

3. K.H. Jacob
   Lamont-Doherty Geological Observ.
   Palisades, New York 10964

4. T (Tectonophysics)

5. Lithosphere
   or
   Crustal Processes (Tectonics)

6. O

7. 0%

8a. Alma Kesner
   Purchasing Dept.
   Lamont-Doherty Geol. Observ.
   Palisades, New York 10964

9. C

TRANSVERSE STRUCTURAL FEATURES, DISPLACED TERRANES AND THEIR RELATION TO RUPTURE ZONES OF GREAT EARTHQUAKES ALONG THE ALASKA-ALEUTIAN PLATE BOUNDARY

J.N. Davies
G. Bond (both at: Lamont-Doherty Geol. Observ. of Columbia Univ., Palisades, NY 10964)

Many workers have observed that the ends of aftershock zones of great-thrust-type earthquakes coincide with structural features transverse to the Aleutian Arc. Features transverse to the Aleutian arc have been associated with the trends of Shirshov and Bowers' Ridges and the edge of the Bering Shelf. Other transverse features have been postulated to cross the arc at both the western and eastern ends of Kodiak Island and through Prince William Sound. We propose that many of these transverse features represent structural boundaries between displaced terranes that have arrived at their present positions as a result of plate motions. We further propose that more subtle transverse features exist in the eastern Aleutian Islands-western Alaska Peninsula region. Here, these features represent extensional faulting of pre-Pliocene terranes that are continuous from the Alaska Peninsula through the Pribilof Islands region of the Bering Shelf. We suggest that most of these transverse features delimit adjacent portions of the overthrusting plate that are relatively mechanically independent. Thus, strain energy resulting from the underthrusting of the Pacific plate beneath these portions of the North American (Alaska-Aleutian) plate can be stored and released independently from one region to the next. Historically these independent regions, either singly or in various combinations, appear to correspond to the rupture zones of great thrust-type earthquakes along the Alaska-Aleutian plate boundary.

1. Spring Meeting, 1980
2. AGU
3. John N. Davies
   Lamont-Doherty Geol. Observ.
   Palisades, New York 10964
4. S (Seismology)
5. None
6. O
7. 0%
8. Alma Kesner
   Purchasing Department
   Lamont-Doherty Geol. Observ.
   Palisades, New York 10964
9. C

14 EOS, vol. 62, no. 2, January 13, 1981

XI.D. Eruption of Pavlof Volcano of 11-12 November, 1980

Pavlof Volcano, Alaska Peninsula, Alaska, U.S.A. (55.42°N, 161.90°W). All times are local (GMT − 10 h). An eruption from Pavlof November 11–12 ejected large lava fountains and ash clouds that reached 11 km altitude and may have produced lava flows.

A seismic station 10 km southwest of Pavlof registered a 2½ min burst of low-amplitude harmonic tremor beginning on November 5 at 1351. Emission of steam, ash, and some blocks from a vent high on the northeast flank started November 8 at 1047 and lasted about 5 min, without accompanying seismicity. A second burst of low-amplitude tremor occurred between 0536 and 0541 on November 9.

In contrast to the pattern observed before eruptions in 1973, 1974, 1975, and 1976, virtually no additional seismic activity was recorded until a group of seven low-frequency volcanic earthquakes occurred at about 2300 on November 10. After an explosion event appeared on seismic records at 0243 on November 11, 10 more low-frequency volcanic earthquakes were recorded between 0300 and 0400. Continuous harmonic tremor, of fairly low amplitude, began at 0608, but amplitude intensified around 0900.

Reeve Aleutian Airways pilot Everett Skinner saw rocks up to 1 m in diameter rising 10 to 30 m at 1315 on November 11. An observer in Cold Bay, 60 km to the West, noted an increase in activity about 1600. Skinner returned to the vicinity of Pavlof between 1630 and 1700, reporting lava fountaining from the summit, a black cloud hugging the volcano's upper north flank, and an eruption column reaching an estimated 6 km altitude. Between 1800 and 2000, various witnesses reported lava fountaining to a maximum height of 300 m and incandescent material moving down the north flank. A satellite image returned at 1958 shows a nearly circular plume, 15 km in diameter, north of the volcano. Activity was visible through the night from Cold Bay (see above) and the Sand Point area (50–65 km to the east northeast).

The next morning, at 0946, a satellite image revealed a plume 160 km long and almost as wide spreading north of Pavlof. Spectral analysis and weather balloon data indicate that the plume reached 8–9 km above sea level. Pilot reports on November 12 placed the top of the eruption cloud at 9 km at 1000, 6 km at 1100, and 11 km at 1400. The eruption clouds were described as varying from ash-rich to ash-poor. A helicopter crew from KENI television, Anchorage, videotaped pulses and bursts of lava fountaining, rising 150–300 m between 1600 and 1700. The fountains emerged from a preexisting vent high on the northeast flank, the only vent confirmed active during the eruption.

Very high amplitude harmonic tremor accompanied the eruption, reaching its strongest levels between 2000 on November 11 and 0700 on November 12. Tremor ceased at 1835 on November 12, at which time many B-type earthquakes began to be recorded.

By the morning of November 13, the eruption had ended. Several hundred B-type events per day were recorded November 14–15. Renewed high-amplitude tremor began November 15 at 1306, lasting until 1711. B-type earthquakes continued November 16–19, but fewer than 100/day were recorded.

Information contacts: S. McNutt and J. Davies, Lamont-Doherty Geological Observatory, Palisades, NY 10964.

Alison Till, U.S. Geological Survey, 1209 Orca St., Anchorage, AK 99501.

Jürgen Kienle, Geophysical Institute, University of Alaska, Fairbanks, AK 99701.

G. Roberts, Cold Bay Weather Station, Cold Bay, AK 99571.

Commander John Hair, Chief, Marine Environmental Branch, P.O. Box 3-5000 (MEP), Juneau, AK 99802.

XI.E. TABLES

TABLE 1

Earthquakes in the Pribilof Islands Region Located Without Seismographic Records

Year	Date	Location	Comments	References*
1815	----	NE of St. George	with eruption?	3
1826	April 2	Pribilof Island	"violent", identical with 1836?	2,3
1835	April 14	Pribilof Island	"severe", prob. identical with 1836	2,3
1836	April 2	Pribilof Island	Milne III, Rossi-Forel X	1,2,3
1836	August	Pribilof Island	weaker than April 2	2,3
1847	----	St. Paul	Rossi-Forel VI	3
1861	April 28	St. George	"light earthquake"	1,2,3
----	----	----	----	---
1954	May 16	St. George	Mod. Mercalli V	2

*see text

TABLE 2

All Events in the Greater St. George Basin Region for the Period 1925 through 1978

Date	HrMn	Sec	Lat		Long		Depth	Mag
250819	1207	27.30	55	14.40	167	41.40	.00	7.20
250905	1630	17.50	54	40.80	170	37.80	.00	.00
330427	1156	6.00	55	.00	166	.00	.00	.00
370718	101	12.00	55	.00	165	.00	.00	.00
410501	707	48.00	57	36.00	166	36.00	.00	.00
410806	615	4.00	55	30.00	163	.00	128.00	.00
410806	615	6.00	55	45.00	163	.00	150.00	6.75
410806	615	12.00	55	42.00	162	24.00	200.00	.00
410928	533	18.00	56	.00	164	.00	.00	.00
420610	108	.00	57	30.00	163	.00	.00	.00
440929	1908	14.00	57	30.00	169	.00	.00	.00
470525	1554	48.00	57	30.00	169	.00	.00	.00
511001	1011	40.00	55	.00	166	.00	.00	.00
550717	2158	23.00	54	24.00	168	18.00	.00	.00
570310	2034	.00	55	.00	165	.00	.00	.00
570312	449	30.00	55	.00	164	.00	.00	.00
570323	1029	10.00	54	30.00	165	30.00	.00	.00
570328	1251	45.00	55	.00	166	15.00	.00	.00
570521	1501	53.00	55	.00	164	.00	.00	.00
570531	1619	39.00	55	.00	169	.00	.00	.00
570609	2051	33.00	55	.00	167	30.00	.00	.00
580303	1618	23.	55	37.20	166	20.40	45.00	6.38*
590421	1242	50.00	56	.00	162	30.00	.00	.00
590512	0457	39.20	55	9.00	168	14.40	17.00	6.50*
600109	1749	7.00	55	30.00	165	.00	.00	.00
601030	2156	20.60	56	36.00	167	12.00	70.00	.00
610114	1639	9.00	55	30.00	165	.00	.00	5.75
610326	2010	31.70	55	42.60	164	.60	50.00	.00*
610326	2010	44.40	55	36.60	163	48.00	175.00	.00*
620408	2209	31.40	54	48.60	165	.60	25.00	.00
630508	850	54.00	55	30.00	163	48.00	.00	5.50
640311	459	45.60	54	42.00	169	54.00	33.00	4.20
640330	1921	51.00	55	30.00	168	6.00	30.00	4.30
640501	1557	28.90	56	4.80	167	36.00	33.00	4.30
640504	226	33.70	55	57.60	162	48.00	200.00	4.50
640827	310	19.40	54	6.00	167	24.00	33.00	4.30
640912	432	34.00	54	48.00	170	.00	33.00	4.00
650215	943	4.30	55	48.00	166	42.00	35.00	4.50
650325	2000	19.80	55	25.20	165	6.00	33.00	4.20
650406	1737	35.50	55	30.00	166	48.00	33.00	4.20
651022	1626	48.40	56	37.20	169	40.20	7.00	4.70
660717	103	4.00	56	29.40	167	2.40	40.00	4.80
661130	56	25.00	55	.00	167	.00	.00	4.20
670502	1756	33.00	57	.00	164	.00	.00	4.00
670703	932	35.30	54	37.20	166	.00	120.00	4.10
670806	1854	15.00	55	.00	168	.00	.00	4.10
670909	315	20.00	54	12.00	168	42.00	142.00	3.90
671130	937	12.00	56	.00	163	.00	.00	4.30
671213	1756	45.00	54	18.00	170	24.00	33.00	4.00
680114	1331	35.00	55	.00	164	.00	.00	4.00
680305	530	27.00	55	12.00	163	42.00	.00	4.00
680323	0	34.10	56	25.80	162	18.00	188.00	4.80
680530	1622	21.00	54	12.00	168	54.00	.00	4.50
690729	539	47.00	54	48.00	165	6.00	.00	3.50
690801	326	9.00	54	48.00	165	6.00	.00	3.50
690802	438	29.00	54	48.00	165	6.00	.00	3.40
690828	502	21.00	54	48.00	165	6.00	.00	3.40
691105	459	54.00	54	18.00	167	36.00	.00	3.50
691123	1815	20.00	55	42.00	166	.00	33.00	.00
691127	711	37.00	55	46.20	164	.00	33.00	.00
691129	1652	.00	54	18.00	167	36.00	.00	3.60
691130	421	2.00	56	24.00	166	48.00	.00	3.60
691207	13	13.00	54	30.00	171	.00	33.00	.00
691212	351	1.00	55	18.00	164	54.00	154.00	4.20
700126	833	49.00	57	18.00	163	.00	33.00	.00
700427	552	6.00	54	18.00	167	36.00	.00	3.40
700703	437	.00	57	6.00	164	.00	35.00	.00
701128	228	57.00	54	12.00	168	18.00	.00	3.50
701202	1814	50.50	55	54.60	163	58.20	221.00	4.70
701203	646	15.00	54	18.00	167	36.00	.00	3.30
701212	345	2.00	54	18.00	167	36.00	.00	3.50
701212	1517	21.00	54	18.00	167	36.00	.00	3.50
710805	1351	9.30	55	43.08	164	55.20	33.00	5.10
711231	844	47.20	54	51.06	164	23.22	33.00	4.50
720513	1309	26.10	54	54.06	166	36.66	.00	.00
730630	507	1.30	54	7.32	168	38.82	.00	.00
730820	2226	28.60	55	47.16	166	51.78	.00	4.40
740609	606	40.70	54	7.80	170	48.54	.00	.00
740724	1016	56.30	55	48.00	162	15.00	113.00	4.10
741019	54	44.60	54	37.62	165	10.80	.00	4.30
750129	1854	51.36	55	50.64	170	29.04	.00	.00
750210	220	58.49	54	59.94	169	36.78	.00	4.00
750311	1849	46.11	54	34.68	169	9.66	.00	4.50
751118	1303	47.16	57	30.66	170	25.08	33.00	.00
760930	143	27.30	56	28.08	162	32.94	75.00	.00
761023	825	31.88	55	2.64	165	55.32	188.40	4.70
761025	1124	7.76	57	8.82	165	56.58	33.00	4.60
770327	1841	57.90	57	34.80	169	57.00	33.00	4.20
780626	252	56.60	57	37.20	169	55.80	33.00	4.20
781207	16	49.20	54	40.20	165	36.00	127.00	4.60

*NB: '58 and '59 events added after analysis; both depths for '61 event inadvertently included in analysis.

TABLE 3

Shallow Events in the Limited St. George Basin Region for the Period 1957 through 1978

Date	HrMn	Sec	Lat		Long		Depth	Mag
570310	2034	.00	55	.00	165	.00	.00	.00
570312	449	30.00	55	.00	164	.00	.00	.00
570323	1029	10.00	54	30.00	165	30.00	.00	.00
570328	1251	45.00	55	.00	166	15.00	.00	.00
570521	1501	53.00	55	.00	164	.00	.00	.00
570609	2051	33.00	55	.00	167	30.00	.00	.00
600109	1749	7.00	55	30.00	165	.00	.00	.00
601030	2156	20.60	56	36.00	167	12.00	70.00	.00
610114	1639	9.00	55	30.00	165	.00	2.22	5.75
610326	2010	31.70	55	42.60	164	.60	50.00	.00
620408	2209	31.40	54	48.60	165	.60	25.00	.00
630508	850	54.00	55	30.00	163	48.00	.00	5.50
640330	1921	51.00	55	30.00	168	6.00	30.00	4.30
640501	1557	28.90	56	4.80	167	36.00	33.00	4.30
650215	943	4.30	55	48.00	166	42.00	35.00	4.50
650325	2000	19.80	55	25.20	165	6.00	33.00	4.20
650406	1737	35.50	55	30.00	166	48.00	33.00	4.20
651022	1626	48.40	56	37.20	169	40.20	7.00	4.70
660717	103	4.00	56	29.40	167	2.40	40.00	4.80
661130	56	25.00	55	.00	167	.00	1.11	4.20
671130	937	12.00	56	.00	163	.00	2.22	4.30
680114	1331	35.00	55	.00	164	.00	.00	4.00
680305	530	27.00	55	12.00	163	42.00	.00	4.00
690729	539	47.00	54	48.00	165	6.00	.00	3.50
690801	326	9.00	54	48.00	165	6.00	2.22	3.50
690802	438	29.00	54	48.00	165	6.00	2.22	3.40
690828	502	21.00	54	48.00	165	6.00	.00	3.40
691123	1815	20.00	55	42.00	166	.00	33.00	.00
691127	711	37.00	55	46.20	164	.00	33.00	.00
691130	421	2.00	56	24.00	166	48.00	1.11	3.60
710805	1351	9.30	55	43.08	164	55.20	33.00	5.10
711231	844	47.20	54	51.06	164	23.22	33.00	4.50
720513	1309	26.10	54	54.06	166	36.66	.00	.00
730820	2226	28.60	55	47.16	166	51.78	1.11	4.40
741019	54	44.60	54	37.62	165	10.80	.00	4.30
751118	1303	47.16	57	30.66	170	25.08	33.00	.00
770327	1841	57.90	57	34.80	169	57.00	33.00	4.20
780626	252	56.60	57	37.20	169	55.80	33.00	4.20

TABLE 4

Frequency of Occurrence by Magnitude

j	M	n	nr	N	log N
1	5.75	1	1.606	1.606	0.206
2	5.1	1	1.606	3.212	0.507
3	4.8	1	1.606	4.818	0.683
4	4.7	1	1.606	6.424	0.808
5	4.5	2	3.212	9.636	0.984
6	4.4	1	1.606	11.242	1.051
7	4.3	3	4.818	16.060	1.206
8	4.2	5	8.030	24.090	1.382
9	3.6	1	1.606	25.696	1.410
10	3.5	1	1.606	27.302	1.436
11	3.4	1	1.606	28.908	1.461
TOTALS		18	28.908		

TABLE 5

Probability for Acceleration to Exceed 0.2 or 0.5g in 40 Years for a Site Within the St. George Basin Region

j	M_j	$r_{j-1,j}(\alpha)$ (km)	$P_{j-1,j}$ {one or more}	$P\{j-1,j \mid \alpha\}$	$P\{j-1,j \text{ and } \alpha\}$
for α = 0.2g and t = 40 years:					
1	4.0	---	---	---	---
2	5.0	5	1.0000	0.00097	0.00097
3	6.0	20	0.9981	0.016	0.01597
4	7.0	60	0.4646	0.14	0.06504
5	8.0	100	0.0606	0.39	0.02363
				P(0.2) =	0.10561
for α = 0.5g and t = 40 years:					
1	4.0	---	---	---	---
2	5.0	2.5	1.0000	0.00024	0.00024
3	6.0	10	0.9981	0.0039	0.00389
4	7.0	30	0.4646	0.035	0.01626
5	8.0	50	0.0606	0.097	0.00588
				P(0.5) =	0.02627

TABLE 6

Events Detected at SNP in a Distance Range Such That Origin in St. George Basin is Possible

Time Interval: May 1977 - July 1980

Date	Time	Distance (deg.)	Distance (km)	Magnitude
77 05 20	12:50	0.58	64	2.2
77 07 20	21:19	1.34	149	2.7
77 07 21	12:56	2.17	240	3.8
77 08 11	01:54	2.45	272	3.8
77 09 25	17:21	0.77	85	2.1
77 11 30	00:15	0.92	102	2.0
78 03 07	02:56	0.77	85	4.1
78 07 13	13:26	2.17	241	4.5
78 07 24	14:52	0.16	68	3.0
78 08 09	01:51	3.88	431	4.0
78 08 24	09:01	2.27	252	3.6
78 09 24	16:43	0.79	88	3.0
78 11 28	17:42	1.01	112	2.5
79 04 29	14:16	0.38	42	1.8
80 02 08	13:38	0.69	77	2.5
80 03 22	10:31	2.08	231	3.5
08 07 23	17:13	0.46	51	1.6

TABLE 7

Reports of Volcanic Activity in the Eastern Aleutian Arc from Okmok Volcano, Umnak Island to Pavlof Volcano, Alaska Peninsula

Volcano	Report of Activity Earliest		Latest	Eruption[1] Potential	Number of Reports[2] A	E	Q	I	Remarks
Okmok	1805	-	1958	5	19	9	4	32	1878, Makushin Village destroyed
Bogoslof	1796	-	1926	5	14	12	1	27	1796,1883,1926: island-forming events
Makushin	1768	-	1980	5	22	7	2	31	two volcanoes active in 1768, Bishop Pt. mudflow 30m high at shore
Akutan	1790	-	1980	5	35	16	2	53	mud flow 1929, 1 km lava flow 1978
Akun	1828	-	1880	1	3	0	0	3	no historic eruiptions, deeply disected
Pogromni	1795	-	1965	4	9	7	1	17	
Westdahl	1826	-	1979	4	4	4	0	8	1m of ash fell on Scotch Cap forcing evacuation, damaging light, floods washed our road, 1978
Fisher	1826	-	1826	1	1	0	0	1	questionable report of eruption, 1826
Shishaldin	1775	-	1979	5	47	23	0	70	1978 Sept. 28, caused radio interference
Isanotski	1690	-	1845	3	6	4	1	11	1825: mudslides, ash to Pavlof Bay
Roundtop	none			0	0	0	0	0	no reports
Frosty	1768	-	1951	1	4	0	0	4	reports for Walrus & Morshova assigned to Frosty (3)
Amak	1700	-	1715	1	1	0	0	1	no activity since 1804 at latest
Emmons	1768	-	1953	1	4	0	0	4	reports for Medviednikof assigned to Emmons (4)
Pavlof	1790	-	1980	5	49	30	1	80	1914 eruption: 5 cm of sand on Unga
Pavlof's Sister	1762	-	1786	2	--	--	-	--	not active since major eruption in 1786

Footnotes for Table 7:

(1) Eruption Potential: scale 0-5

- 0 - no historic activity
- 1 - no historic eruptions, but smoke or steam reported
- 2 - last eruption in 1700's
- 3 - last eruption in 1800's
- 4 - last eruption in 1900's
- 5 - last eruption in 1900's and I > 25

(2) A = reports of activity
E = reports of activity including eruptions
Q = reports of eruptions with earthquakes
I = A + E + Q

Note that A includes E and E includes Q so that reports of earthquakes are added 3 times into the index, I, and reports of eruptions 2 times, whereas reports of activity (smoke, steam, etc.) are only counted once.

(3) Morzhovoi = Walrus (Orth, 1967) but Walrus Peak is nonvolcanic. Waldron (1961) thinks Morshova and Frosty are the same. We tentatively agree.

(4) Medvied = Bear; Medvednikova Zaliv = Bear Bay on Alaska Peninsula at 162°W (Orth, 1967). Since Emmons Volcano is at 162°W it seems possible that the old ($\leq$ 1850) reports for Medviednikof refer to Emmons. Note that Emmons received its present name $\sim$ 1940.

TABLE 8

List of Alaska Earthquakes Since 1788 Within the Gulf of Alaska Region

Date	LON°W[1]	M_w	State	Participating Source Regions	Comments
1788, July 22	161.5[2] - 152.5[2]	(9.0)[0]	3	SHU 100%; SEM 100%; PCK.1 100%	
1788, August 7	163.0[2] - 160.5[2]	[8.0][0]	1	UNI_{east} 50%; SHU_{west} 40%	
1844, April 20	154.5	[7.8]	1	PCK.1	
1847, April 16	160.5[2] - 156.5[2]	[8.5]	2	SHU_{east} 50%; SEM_{west} 80%	
1848, June 30	156.5	[7.8]	1	SEM	
1880, September 28	156.5	[>7.8]	1	SEM	
1899, July 14	166.5 - 160.0	(7.8)	1	SHU or SEM (UNI or UNA)	
1899, September 4	145.5 - 142[3,4]	8.2[5]	1	YAK_G 50%; PCK.3 50%	
1899, September 10	142 ± 3[6]	(7.8)	1	YAK_G ?	
1899, September 10	142 - 138[3,4]	8.2[5]	1	YAK_G 50%; YAK_T 50%	
1900, October 9	153[3,4]	8.1[5]	1	PCK.1 100%	Intensities drop below VIII to east, no reports to west.
1902, January 1	165 ± 9[6]	(7.8)	1	UNA ?	No felt reports[6]
1903, June 2	156[6] ± ?	8.3[8]	(2)[9]	(SEM and/or PCK.1)[9]	Not shallow, probably intermediate depth[6]; felt at Valdez[7]
1938, November 10	159 - 156[10]	8.2	1	SEM 100%	
1946, April 1	164.5 - 162[10]	[7.8]	1	UNI 100%	
1957, March 9	180 - 167 or 164.5	9.1	(3)[11]	(UNA 100%)	Probably did not rupture UNA
1958, July 9	140 - 137	8.2	1	FAIR	Consider removing from list purposes of computing P_{ij} and h_{ij} for areal sources.
1964, March 27	152 - 146.5	9.2	3	PCK.1,2,3	

TABLE 8 (con't.)

Footnotes:

[0]() consensus of operators; [] estimate by LDGO-group.

[1]Defined for sources normal to lines defined by the following modes: 74, 75, 80, 85, 86, 90, 95, 93, and 99, 98, 103.

[2]Estimate based on felt reports.

[3]With respect to segment 99-98-103.

[4]Limit of $I_{MM} \geq$ VIII; approximately the rupture zone.

[5]Thatcher and Plafker (1977).

[6]Gutenberg (1956), instrumental epicenter, not based on felt reports.

[7]Tarr and Martin (1912).

[8]Richter (1958), p. 714.

[9]Only if shallow, which it probably is not. Suggest removing from list.

[10]Sykes (1971), aftershock area.

[11]House (1981), probably did not rupture Unalaska zone, recommend removal from list.

TABLE 9

Initial Conditions for the Seismogenic Regions of the Gulf of Alaska:

Partial Input for the Markov Program

Prepared by J. Davies

Lamont-Doherty Geological Observatory of Columbia University
Palisades, New York 10964

June 1981

*Most likely options

REGION Name	Code	RANGE Longitude(W)	DATE	MAGNITUDE M_w	i	ELAPSED TIME (Years to 1 July 1981)
Unalaska	UNA	167.0-164.5	1957, March 9	9.1	3	24.31
or			1902, January 1	(7.8)	1	79.50*
or			1899, July 14	(7.8)	1	81.96
or			<~1845	(9.0)	(3)	>136 *
Unimak	UNI	164.5-161.9	1946, April 1	(7.8)	1	35.25
Shumagin	SHU	161.9-158.9	1903, June 2	8.3	2	78.08
or			1899, July 14	(7.8)	1	81.96*
or			1847, April 16	(8.5)	(2)	134.21*
Semidi	SEM	158.9-155.8	1938, November 10	8.2	1	42.64
Kodiak	PCK-1	155.8-152.1	1964, March 27	9.2	3	17.26
Cook Inlet	PCK-2	152.1-150.1	1964, March 27	9.2	3	17.26
Prince William Sound	PCK-3	150.1-146.5	1964, March 27	9.2	3	17.26
Yakataga	YAG	144.4-139.8	1899, September 4,10	8.3	1	81.81
Yakutat	YAT	139.8-136.0	<~1850	(8.0)	1	>131
Fairweather	FAIR	140 -137	1958, July 9	8.2	1	22.98
Sitka	SIT	137 -135	1972, July 30	(7.8)	1	8.92

TABLE 10

Event 1	6/20/69	Depth 7 km	m_b = 5.8
	DUG	83 bars	
	NDI	55 bars	
	PAL	50 bars	
	PTO	93 bars	
	SNG	105 bars	

Event 2	10/13/72	Depth 9 km	m_b = 6.0
	DUG	42 bars	
	GOL	58 bars	
	IST	161 bars	
	NDI	178 bars	
	PTO	115 bars	

Event 3	11/12/69	Depth 50 km	m_b = 5.5
	DUG	13 bars	
	GOL	6 bars	
	NDI	18 bars	
	TUL	7 bars	

Event 4	7/6/67	Depth 49 km	m_b = 5.9
	IST	44 bars	
	PAL	26 bars	
	PTO	47 bars	
	TRI	31 bars	

Event 5	5/29/73	Depth 50 km	m_b = 6.1
	DUG	163 bars	
	GOL	250 bars	
	LON	394 bars	
	NDI	256 bars	
	PTO	221 bars	
	SNG	109 bars	
	STU	286 bars	
	TUC	240 bars	

TABLE 10 (con't.)

Event 6	4/26/65	Depth 45 km	m_b = 5.8
	CAR	33 bars	
	IST	38 bars	
	NDI	42 bars	
	PTO	41 bars	
	TOL	47 bars	
	TRI	28 bars	
	TRN	36 bars	

Event 7	4/06/74	Depth 40 km	m_b = 6.0
	IST	96 bars	
	NDI	117 bars	
	PAL	109 bars	
	PTO	154 bars	
	SHK	212 bars	
	SNG	150 bars	
	TRN	179 bars	
	UME	102 bars	

Event 8	7/25/75	Depth 40 km	m_b = 5.6
	KTG	17 bars	
	MAT	47 bars	
	NDI	59 bars	
	SHK	50 bars	
	SNG	47 bars	
	TUC	25 bars	
	UME	30 bars	

Event 9	2/21/72	Depth 50 km	m_b = 5.7
	COL	14 bars	
	GSC	15 bars	
	NDI	25 bars	
	QUE	14 bars	
	SNG	38 bars	

Event 10	6/22/70	Depth 30 km	m_b = 5.5
	PTO	25 bars	
	STU	20 bars	
	TUC	13 bars	
	UME	26 bars	

TABLE 10 (con't.)

Event 11	4/05/71	Depth 150 km	$m_b = 5.8$
	KTG	76 bars	
	NDI	47 bars	
	SNG	68 bars	
	UME	60 bars	

Event 12	4/21/72	Depth 100 km	$m_b = 5.8$
	KTG	14 bars	
	NDI	12 bars	
	PTO	27 bars	

Event 13	9/04/71	Depth 115 km	$m_b = 5.7$
	DUG	21 bars	
	KIP	68 bars	
	KBS	49 bars	
	NDI	54 bars	
	PTO	83 bars	
	SNG	77 bars	
	UME	45 bars	

Event 14	6/10/68	Depth 170 km	$m_b = 5.5$
	DUG	26 bars	
	GOL	77 bars	
	LON	23 bars	
	QUE	17 bars	
	TUC	50 bars	

Event 15	11/25/71	Depth 136 km	$m_b = 5.5$
	GOL	44 bars	
	GSC	18 bars	
	KTG	47 bars	

TABLE 11

SAINT PAUL SHORT PERIOD EVENTS

April 1980 - March 1981

Date	Time	Amplitude (mm)	Period	S-P (sec)	Comments
4/03/80	06:35	1	1.0	--	Distant event
4/04/80	20:06	5	0	60	Fox Island 4.7
4/28/80	03:37	5	0	∿82	Alaska Peninsula 5.0
5/03/80	09:32	1	1.0	--	Near Island 5.7
5/14/80	11:52	3	.5	--	Time may be S. arrival?
5/30/80	18:22	1	1.0	--	Kuril Island 5.3
6/03/80	00:43	3	0	∿15	
6/07/80	22:41	10	?	--	Event?
6/09/80	20:13	2	.5	--	Time may be S. arrival?
6/10/80	23:18	2	.5	--	Sea of Skhotsk 5.2
6/11/80	08:21	3	1.0	--	Banda Sea 5.6
6/24/80	20:01	4	0	--	Event?
6/29/80	07:27	2	.5	--	Honshu 5.8
7/03/80	21:19	2	0	--	
7/05/80	15:20	4	.5	--	Andreanof Island 5.2
7/06/80	18:47	5	.5	∿ 2min.	Kodiak 5.2
7/08/80	04:50	2	0	--	
	23:30	2	.5	--	
7/16/80	20:08	4	.5	--	New Guinea 6.7
7/20/80	21:30	12	.75	--	Teleseism
7/22/80	07:18	4	1.0	--	New Hebrides 6.1
7/24/80	02:35	4	1.0	--	Unimak 4.7
7/29/80	19:12	2	1.0	--	
8/01/80	∿17:13	5	0	5??*	
8/02/80	∿07:07	19	0	∿45	Fox Island 5.4
8/03/80	∿07:00	18	.5	45	Fox Island 4.9
	∿18:18	4	0	--	
8/07/80	∿19:18	4	1.5	--	Central Alaska 5.1
8/14/80	∿10:37	2	0	--	
8/23/80	∿00:45	14	.5	∿ 2min.	Alaska Peninsula 5.3
	∿11:45	2	0	--	
8/24/80	∿20:00	2	.5	--	
9/06/80	∿19:30*	6	0	91	*No minute marks; times are approximate
9/19/80	∿08:50	1	1.0	--	
	∿09:30	1	.5	--	
	∿09:45	3	0	∿84	Andreanof Island 4.8
9/20/80	?	4	.5	66	
	?	12	.75	66	
10/14/80	09:21	7	.5	>60	
10/19/80	08:07	4	0	72	
10/20/80	15:51	1	--	--	Event could be Fox Is. 4.7
10/24/80	15:03	15	.75	--	

Saint Paul Short Period Events (Table 11 con't.)

Date	Time	Amplitude (mm)	Period	S-P (sec)	Comments
10/25/80	22:19	5	0	65	
11/04/80	20:29	5	1.0	--	Kamchatka 5.9??
11/21/80	14:57	47	0	72	Andreanof Island 5.7
12/03/80	13:20	5	0	60	
12/31/80	10:37	7	1.0	--	Kuril 6.2??
1981					
1/12/81	16:34	5	0	--	Fox Island 4.9
1/14/81	15:07	4	0	70	Fox Island 4.8
1/18/81	12:05	4	0	--	
1/20/81	06:22	5	1.0	--	Alaska Peninsula 4.7
1/30/81	08:54	38	.75	106	Rat Island 6.3
2/04/81	05:15	4	.75	--	Rat Island 5.3
3/22/81	10:43	2	0	--	
3/24/81	18:19	1	0	--	Event?
	18:22	18	.5	56	

TABLE 12

POLOVINA HILL SHORT PERIOD EVENTS

July 1980 - March 1981

*No minute marks; times are approximate.

Date	Time	Amplitude (mm)	Period	S-P (sec)	Comments
7/20/80	21:30	10	.5	--	Teleseism
7/22/80	07:18	4	1.0	--	New Hebrides 6.1
7/23/80	17:13	2	0	6	
7/24/80	02:35	4.5	1.5	47	Unimak 4.7
7/24/80	17:55	2	0	--	
7/26/80	16:21	2	.5	30??	
7/29/80	19:12	2	1.0	--	
8/01/80	∿17:13	5	0	5??*	
8/02/80	∿07:07	18	1.0	∿45	Fox Island 5.4
8/07/80	∿19:18	4	1.0	--	Central Alaska 5.1
8/14/80	∿10:37	2	.75	35??	
8/23/80	∿00:45	16	.5	∿ 2min.	Alaska Peninsula 5.3
8/24/80	∿20:00	2	1.0	--	
9/06/80	∿19:30	6	0	91?	
9/15/80	∿05:00	4	1.0	--	
9/19/80	∿08:50	1	1.0	--	
	∿09:30	1	1.0	--	
	∿09:45	5	0	∿84	Andreanof Island 4.8
10/14/80	09:21	6	0	>60	
10/20/80	15:51	1	--	--	Event could be Fox Island 4.7
10/24/80	15:03	12	1.0	--	
10/25/80	22:19	7	.5	∿65	
11/04/80	20:29	5	1.0	--	Kamchatka 5.9??
11/21/80	14:57	30	0	∿65	Andreanof Island 5.7
11/26/80	08:55	1	--	--	Fox Island 4.6??
12/03/80	13:20	5	.6	60?	
12/31/80	10:37	7	1.0	--	Fox Island 4.9
1981					
1/12/81	16:34	5	0	--	Fox Island 4.9
1/14/81	15:07	4	.5	∿70	Fox Island 4.8
1/18/81	12:05	4	0	--	
1/20/81	06:22	5	1.0	--	Alaska Peninsula 4.7
1/30/81	08:54	38	1.0	106	Rat Island 6.3
2/04/81	05:15	4	.75	--	Rat Island 5.3
3/22/81	10:43	2	0	--	
	10:44	2	0	--	
3/24/81	18:19	1	0	--	Event?
	18:22	16	1.0	53	

TABLE 13

RUSH HILL SHORT PERIOD EVENTS

July 1980 - March 1981

*No minute marks, time are approximate.

Date	Time	Amplitude (mm)	Period	S-P (sec)	Comments
7/20/80	21:30	12	.5	--	Teleseism
7/22/80	07:18	3	1.5		New Hebrides 6.1
7/23/80	17:13	1	1.0	--	See PLH
7/24/80	02:35	4	.75	48	Unimak 4.7
	17:55	2	0	72??	
8/01/80	∿17:13	10	0	5??*	
8/02/80	∿07:07	10	.5	∿45	Fox Island 5.4
8/07/80	∿19:18	5	1.0	--	Central Alaska 5.1
8/14/80	∿10:37	2	0	--	
8/22/80	∿20:00	5	0	--	
8/23/80	∿00:45	5	0	∿ 2min.	
	∿11:45	5	0	--	
8/24/80	∿20:00	2	1.0	--	
9/06/80	∿19:30	6	0	91?	
9/15/80	∿05:00	5	1.5	--	
9/19/80	∿08:50	2	1.0	--	
	∿09:30	3	1.0	--	
	∿09:45	10	0	∿84	Andreanof Island 4.8
10/14/80	09:21	4	.5	>60	
10/19/80	08:06	4	0	70	
10/24/80	15:02	13	.5	--	
10/25/80	22:19	4	.5	∿65??	
11/04/80	20:29	5	1.0	--	Kamchatka 5.9??
11/21/80	14:57	?	0	70	Andreanof Island 5.7
12/31/80	10:37	7	1.0	--	Kuril 6.2?
1981					
1/12/81	16:34	5	0	--	Fox Island 4.9
1/18/81	12:05	4	0	--	
1/20/81	06:22	5	1.0	--	Alaska Peninsula 4.7
1/30/81	08:54	31	.5	103	Rat Island 6.3
2/04/81	05:15	5	.75	--	Rat Island 5.3
3/22/81	10:43	5	0	--	
3/24/81	18:19	1	0	--	Event?
	18:22	15	.75	54	

TABLE 14

SAINT PAUL LONG PERIOD EVENTS

April 1980 - March 1981

Date	Time	Amplitude (mm)	Period	S-P (sec)	Comments
4/01/80	11:28				Surface waves
	17:05				Surface waves
4/03/80	20:43				Surface waves
	22:03				Surface waves
4/05/80	07:16				Surface waves
	16:25				Surface waves
	No records April 6 1980 - April 28 - 1980				
5/03/80	09:33	6		> 2min.	Near Island 5.7
5/04/80	19:08	5		--	Distant event
5/09/80	11/27				Surface waves
	14:18				Surface waves
5/14/80	11:49				Surface waves
6/18/80	09:26	8		--	
	10:57	6		--	Tonga Island 5.9
	17:22	10		9	Mindanao 5.8
6/19/80	07:15				Surface waves
	09:11				Surface waves
	16:16				Surface waves
6/23/80	20:52				Surface waves
6/25/80	23:39	8		9min.	
6/29/80	07:27	8		--	Honshu 5.8
6/30/80	18:07	--		--	Southeast Alaska 5.0
	18:58	9		--	Southeast Alaska 5.0
7/05/80	15:21	2		--	S. arrival, Andreanof Is. 5.2
7/06/80	18:49	6		--	S. arrival?, Kodiak 5.2
7/08/80	04:50	--		--	Mindanao 6.0
	23:30	62		--	
7/09/80	11:34				Surface waves
7/14/80	15:54				Surface waves
7/16/80	20:08	51		10min.	New Guinea 6.7

TABLE 15

DUTCH HARBOR SHORT PERIOD EVENTS

April 1980 - March 1981

Date	Time	Amplitude (mm)	Period	S-P (sec)	Comments
4/01/80	06:32	4	5	10	
	23:33	32	.5	2	
4/03/80	04:55	2	0	11	
	14:32	4	0	--	
	16:45	2	.5	--	Mindanao 5.7?
4/06/80	09:11	5	0	5.5	
4/09/80	10/14	8	.5	--	Peru 4.9?
4/10/80	06:47	2	0	14?	
	07:39	1	--	--	Distant event
	12:52	1	--	--	Distant event
	~19:26	40	0	15	Records with no dates could be 10th or 11th

No SP records 4/12/80 - 7/14/80

Intermediate period record start 7/14/80 but no events show
Back to short period 9/25/80

9/25/80	04:09	24	0	3	
	04:40	34	0	3	
	04:59	35	0	--	
	06:42	31	0	--	Fox Island 4.4
	07:49	19	0	4	
	12:21	5	0	5	
	19:27	14	0	--	
9/29/80	16:46	7	0	5.5	
9/30/80	12:06	5	0	--	Event?
	18:13	10	0	--	Event?
10/01/80	11:30	5	0	--	Event?
10/14/80	15:53	95	0	--	Fox Island 4.5
10/30/80	20:54	55	90		
11/01/80	04:49	20	0	<60	
11/02/80	21:17	20	0	30	
11/03/80	18:48	15	0	30	
11/04/80	06:55	15	0	10	
	18:28	18	0	~60	
	20:30	1	--	--	Kamchatka 5.9??
11/08/80	01:58	35	0	~30	
	10:33	16	0	--	
	14:01	10	0	~45	
	14:31	1	--	--	Event?
	22:45	1	--	--	Event?
11/09/80	06:42	58	0	~30	

Dutch Harbor Short Period Events (Table 15 con't.)

Date	Time	Amplitude (mm)	Period	S-P (sec)	Comments
11/09/80	15:18	12	0	30	
	17:44	62	0	30	
	17:53	37	0	~30	
11/11/80	14:33	25	0	30	
	18:19	32	0	<30	
11/12/80	03:42	60	0	60	
	05:46	27	0	--	Event?
11/13/80	19:55	14	0	--	Kamchatka 5.4?
	20:13	18	0	--	
11/14/80	13:33	7	0	--	Event?
11/15/80	09:38	6	0	--	Andreanof Island 4.4
	12:47	7	0	30	
	22:16	22	0	--	
11/60/80	11:42	8	0	15	
11/17/80	00:07	60	0	30	
	08:03	7	0	15	
11/18/80	02:39	18	0	~60	
	19:48	37	0	30	
11/21/80	14:57	60	0	~2½min.	Andreanof Island 5.7
11/22/80	07:57	20	0	15	
	09:57	30	0	15	
11/23/80	08:58	20	0	30	
	13:19	46	0	20	
	13:50	18	18	20	
11/25/80	15:53	7	0	30	
11/26/80	04:31	18	0	10	
	08:56	60	0	60	Fox Island 4.6
11/28/80	06:37	clipped	0	60	Unimak 4.7
11/29/80	10:19	45	0	60	Fox Island 4.5
12/01/80	19:55	30	0	--	
12/02/80	00:15	65	0	45	
	03:33	37	0	30	
12/03/80	13:20	60	0	45	
	13:33	22	0	10	
	17:09	11	0	30	
	22:20	5	0	10	
12/09/80	05:13	clipped	0	15	
	05:14	35	0	15	
12/11/80	02:05	45	0	~ 2	
12/13/80	18:33	70	0	~20	
12/15/80	05:49	1	--	--	
	08:24	1	--	--	Tonga 6.2??
	12:27	3	0	~ 9	
	13:24	11	0	~30	
	16:14	clipped	0	10	
	20:23	60	0	30	
12/16/80	02:53	1	--	--	
	03:01	clipped	0	21	
	08:59	20	0	11	
12/19/80	~19:11	10	0	28	
	23:25	27	.5	--	Volcanic event

TABLE 16

DUTCH HARBOR LONG PERIOD EVENTS

April 1980 - March 1981

Date	Time	Amplitude (mm)	Period	S-P (sec)	Comments
4/05/80	01:42	2	2.0	--	Unimak 4.9
4/13/80	02:10	3	1.0	--	Alaska Peninsula 5.4
	18:16	13	1.0	∿10min.	South of Fiji 6.5
5/03/80	09:33	6	3.5	--	Near island 5.7
5/14/80	11:37	5	5.0		Solomon Island 6.1??
5/25/80	16:41	3	3.0	--	
	20:02	2	---	--	
5/27/80	14:59				Surface waves
6/09/80	03:36	8	5.0	--	Amplitude and period measured on surface waves
6/08/80	09:29	6		--	
	11:00	5	---	--	Tonga 5.9?
	17:26	15	5.0	10min.	Mindanao 5.8
6/19/80	08:44	2	---	10min.	Kermadek Island 6.2
	16:03				Surface waves
6/23/80	20:26				Distant event?
6/25/80	23:29	2	3.0	∿10min?	
6/29/80	07:28	7.5	5.0	--	Honshu 5.8
7/08/80	04:50	6	5.0	∿ 9min.	Mindanao 6.0
7/09/80	∿21:07	18	4.0	10.5min?	P-P measured on surface waves Santa Cruz is 6.9

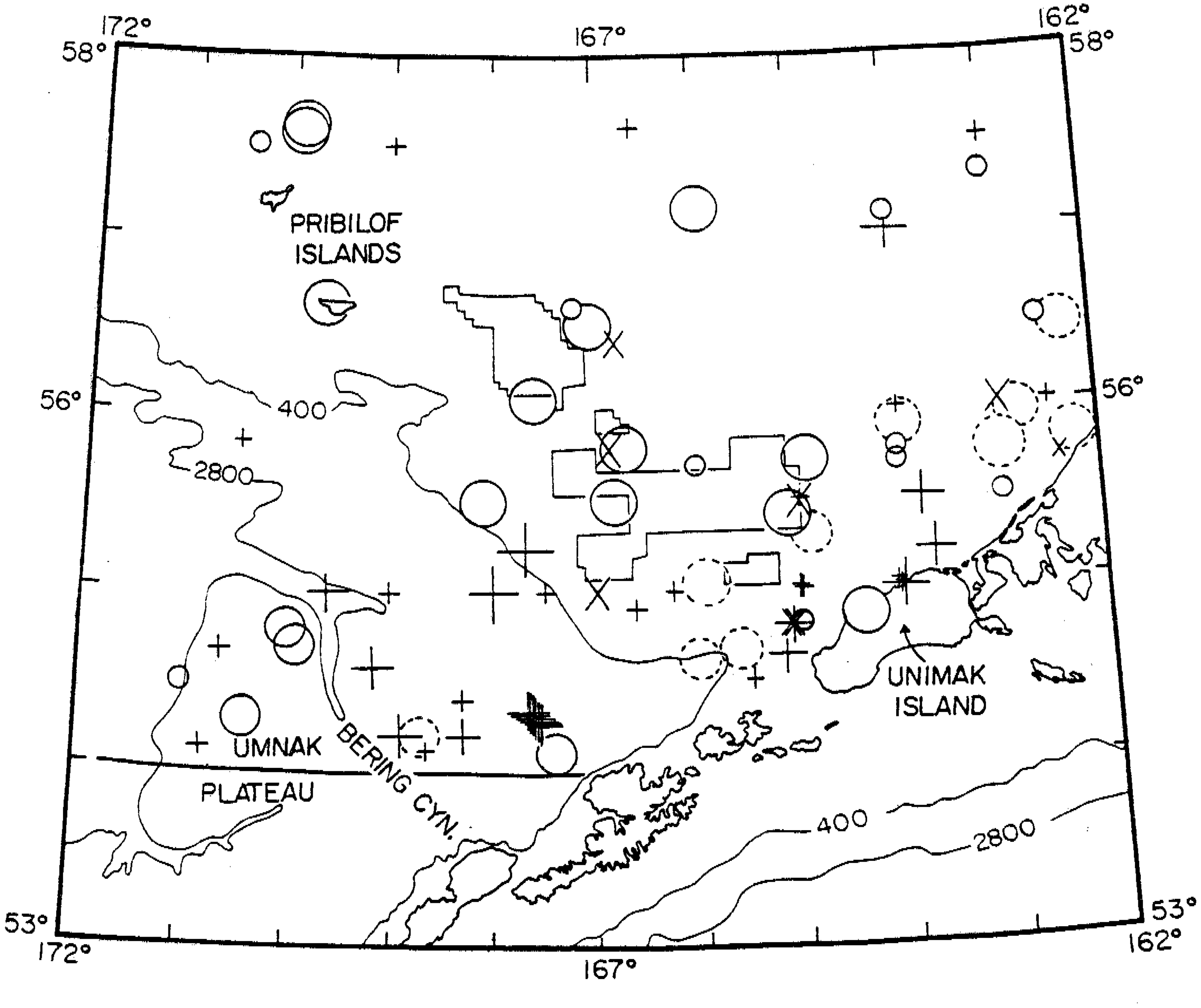

Figure 1. Earthquake epicenters, greater St. George Basin area, 1925 through 1978. Epicenter symbols are scaled by magnitude according to height (seconds) = 6.5 + 1.66 M; crosses represent events with unknown depth; x's those with depths inferred to be shallow; solid circles, those known to be shallow (Z ≤ 75 km); dashed circles, those known to be deep (Z ≥ 113 km). The greater St. George Basin area is bounded on the north, east, and west by the edges of the region shown; the southern boundary is the heavy line along 54°N to its intersection with the Aleutian arc and then along the northern edge of the arc. The potential lease areas are encompassed by the light rectangular boxes Isobaths are in meters.

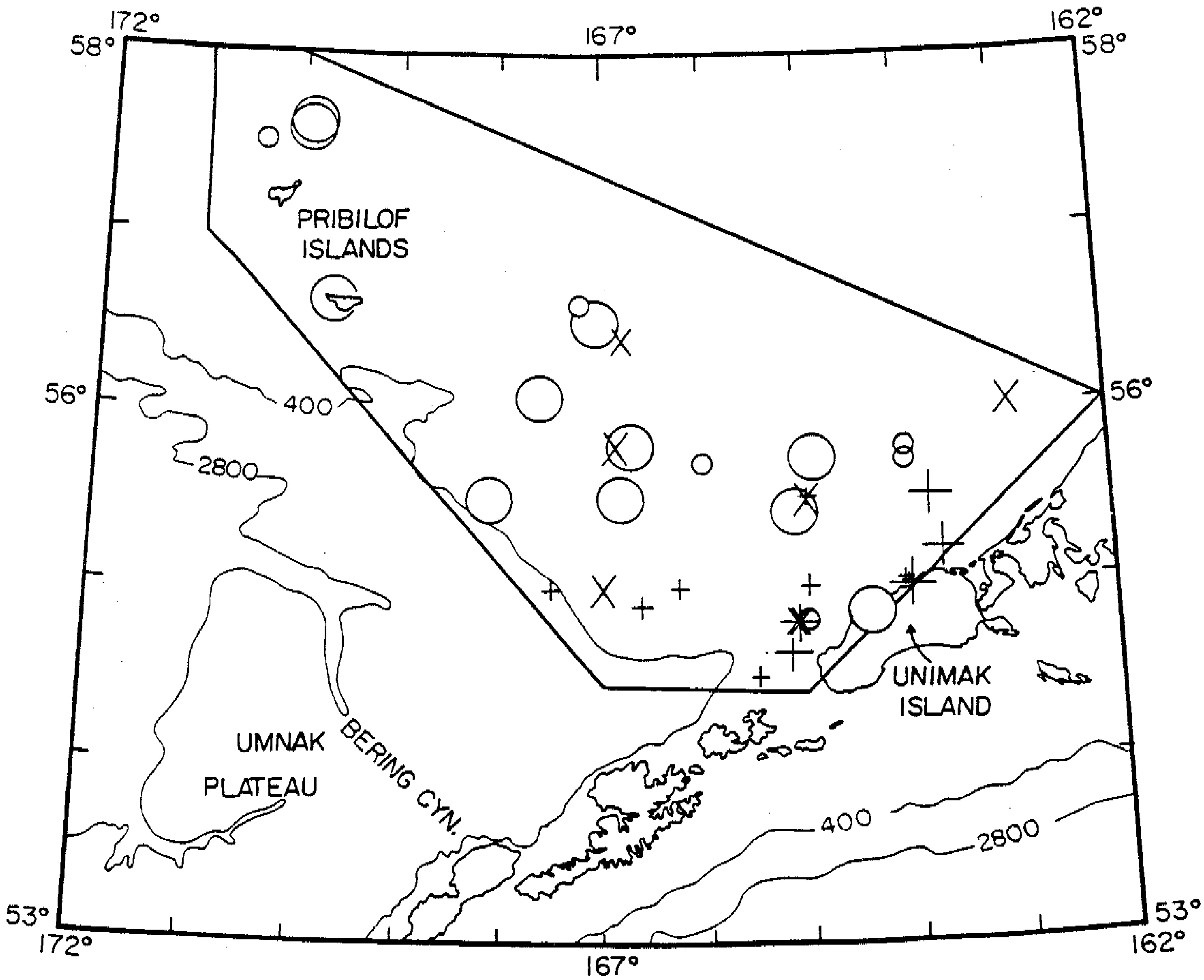

Figure 2. Epicenters of shallow (Z ≤ 70 km) earthquakes, limited St. George Basin area, 1957 through 1978. Symbols are as in Figure 2. The limited St. George Basin area is bounded approximately by the heavy line.

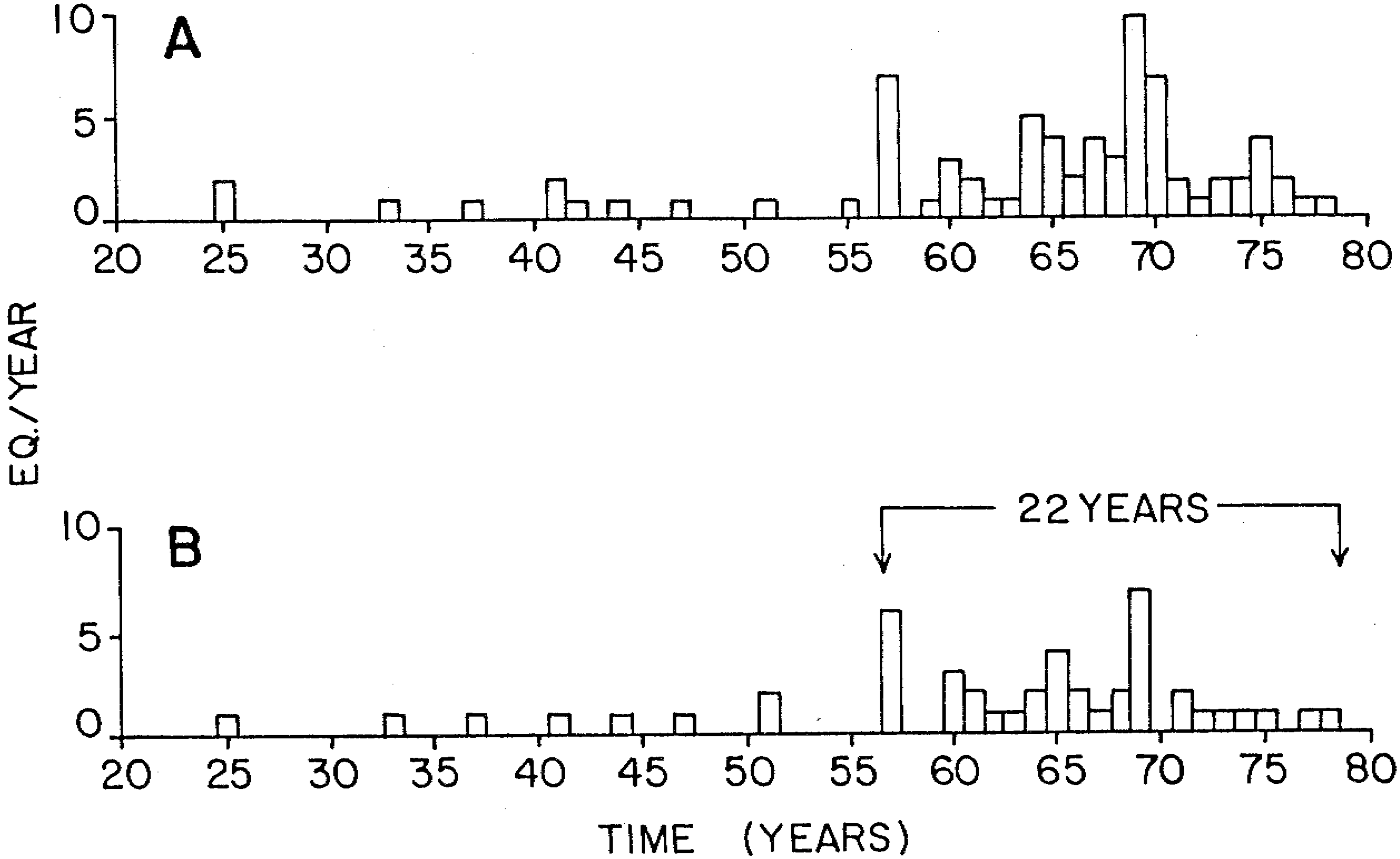

Figure 3. Earthquakes per year for (A) the greater and (B) the limited St. George Basin region. Origin time for this histogram is the year 1900. The 22 year time span indicated for 1957 through 1978 is the period used in the computation of the probabilities that accelerations of 0.2 and 0.5 g would be exceeded at a specific site. It is clear from this figure that the detection threshold was higher in previous years, hence the restriction to the last 22 years for the analysis.

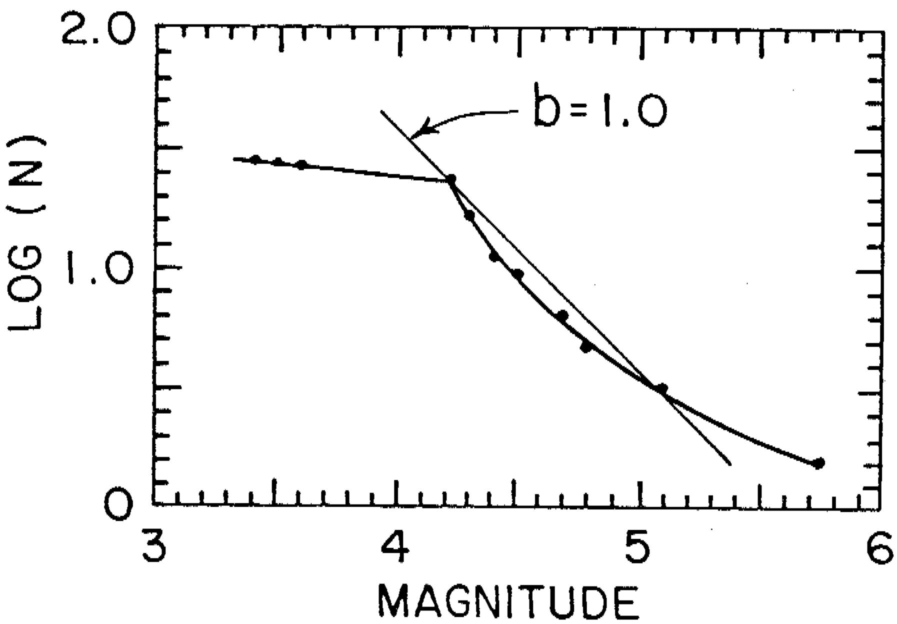

Figure 4. Logarithm cumulative number of earthquakes vs. magnitude for the limited St. George Basin region during the period 1957 through 1978. Light line labeled b = 1.0 is a plot of the relation log N = a - bM with a = 5.58184 and b = 1.0. The shallow slope of the heavy curve below M = 4.2 indicates that the data set is incomplete below this magnitude; i.e., M = 4.2 is the detection threshold for this region and period. The increasing slope near M = 5.0 suggests that more events of M $\geq$ 5 were observed than would usually be the case for this time inteval.

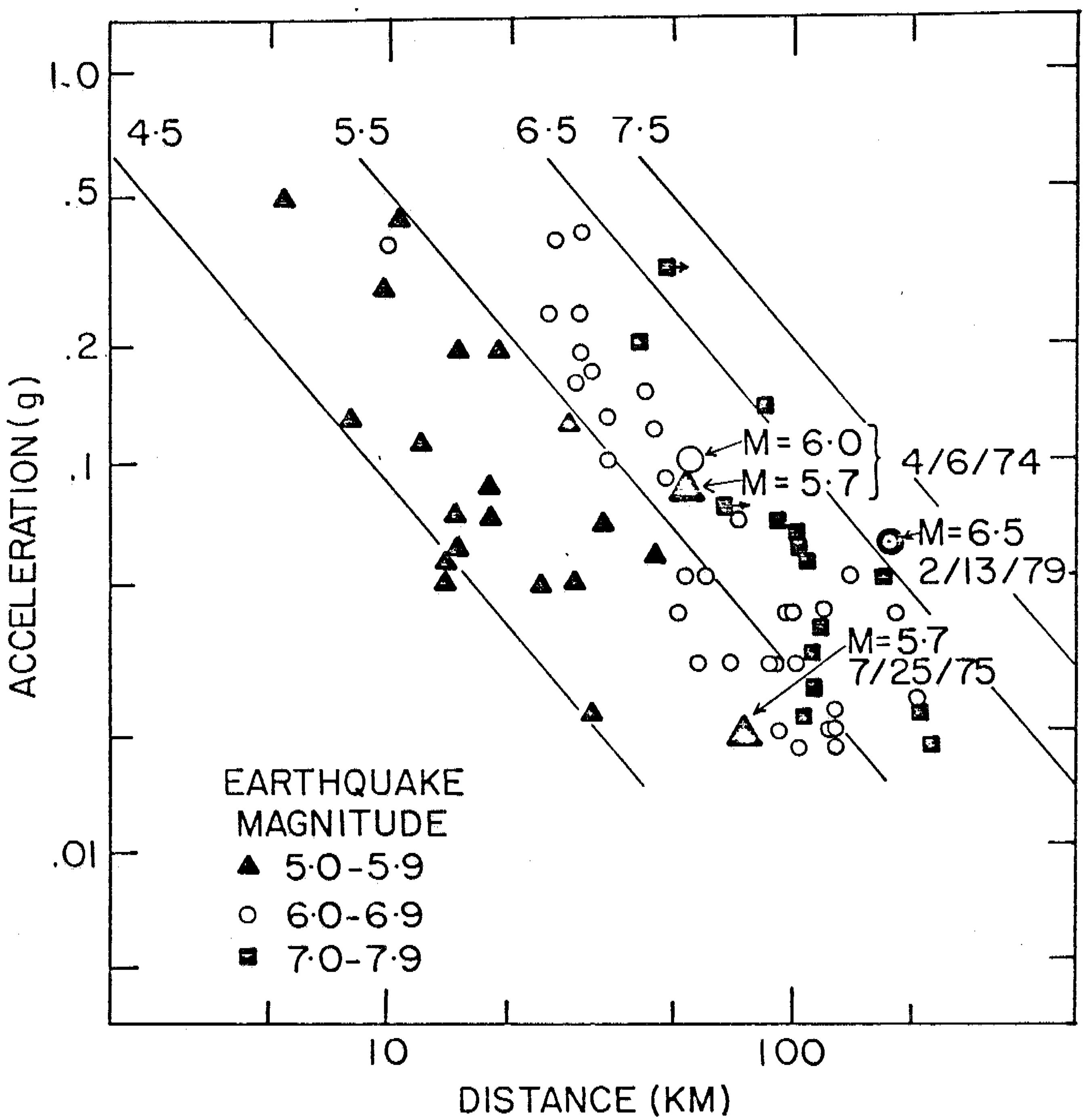

Figure 5. Peak acceleration vs. distance for some western U.S. earthquakes (small symbols, Page et al., 1972) and eastern Aleutian earthquakes (large symbols, Davies et al., 1979 and 1976; House and Boatwright, 1980). The lines labeled 4.5, 5.5, 6.5, and 7.5 are used to define the relationship between acceleration and distance for events in the magnitude ranges 4-5, 5-6, 6-7, and 7-8, respectively. The slopes of these lines are determined by the western U.S. data and the intercepts by the Aleutian data.

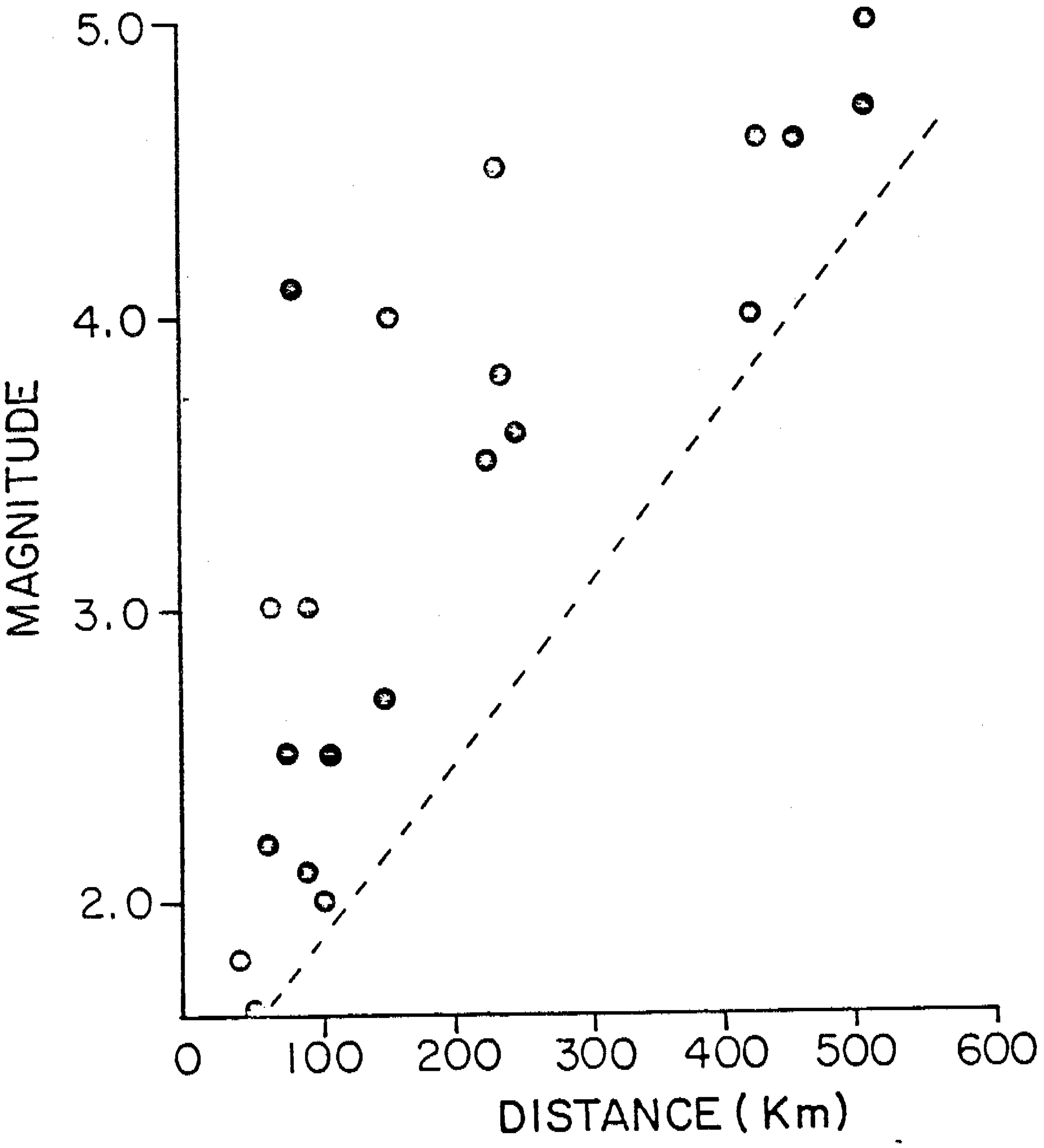

Figure 6. Detection threshold for St. Paul seismic station (SNP). Plotted is local magnitude (see text) vs. distance based on S-P time (the interval between the arrival of the P-wave and the S-wave). Since the southern end of the St. George basin is a little over 400 km from St. Paul Is., the smallest earthquake that can be detected over the whole basin by SNP is about M_L = 4.0.

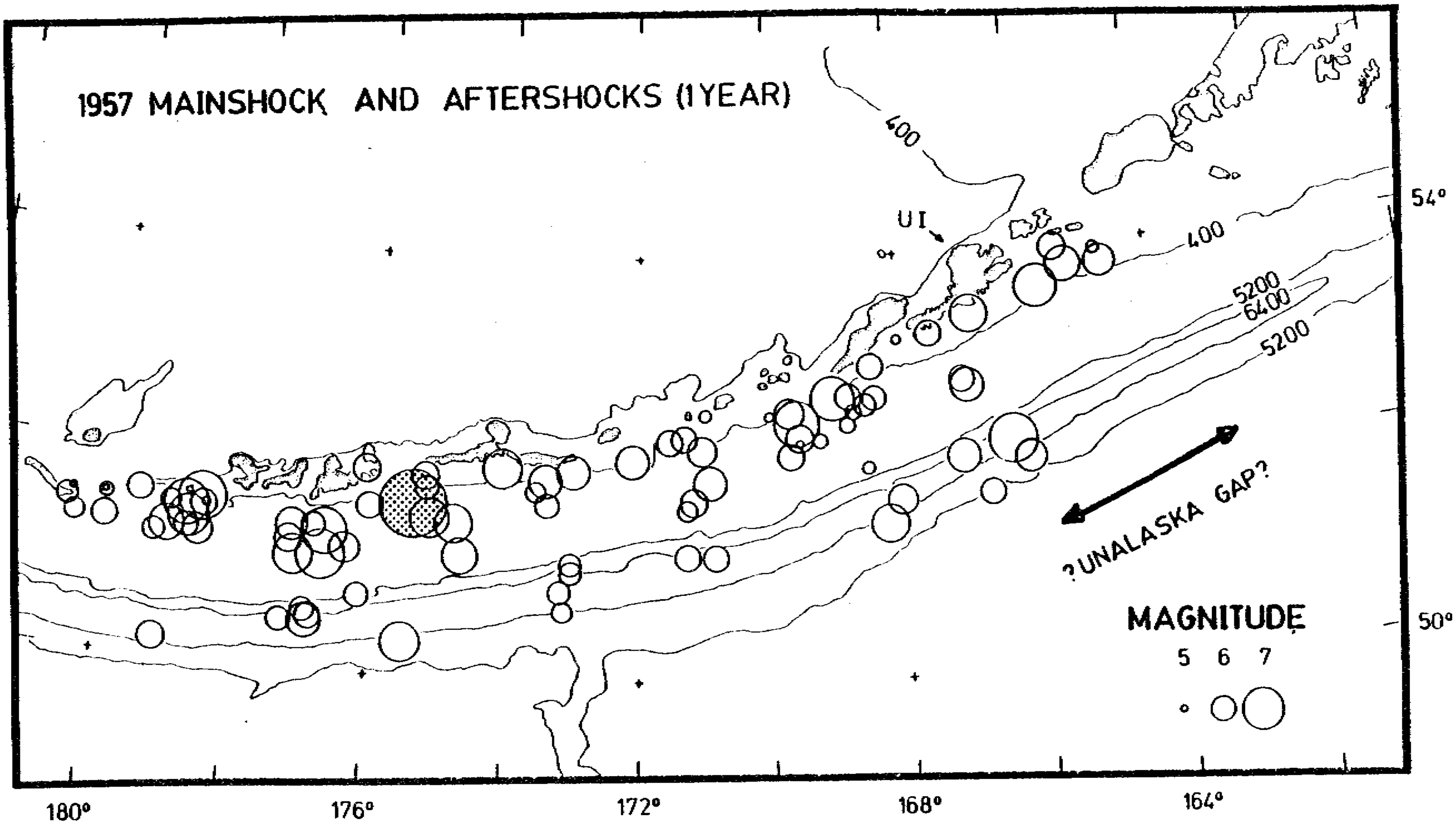

Figure 7. Detailed plot of the 1957 main shock and aftershocks over a period of 1 year. Aftershocks of March 1957 relocated by Sykes (1971) are supplemented by aftershocks located by the International Seismological Summary and the U.S. Coast and Geodetic Survey. Size of symbols is scaled to magnitude; only events assigned a magnitude of 5 or larger are plotted. The 1957 main shock is shaded and is plotted with a symbol size appropriate for its surface wave magnitude (M_S) of 8.2, rather than its M_W of 9.1. We infer that earthquakes located beneath the Aleutian Trench between the 5200 m contours are of normal faulting type although such mechanisms have actually been obtained for only two of the events (Stauder and Udias, 1963). Earthquakes at depths shallower than 80 km are included although none occurred that were deeper than 60 km. UI indicates the location of Unalaska Islands. Bathymetry is in meters.

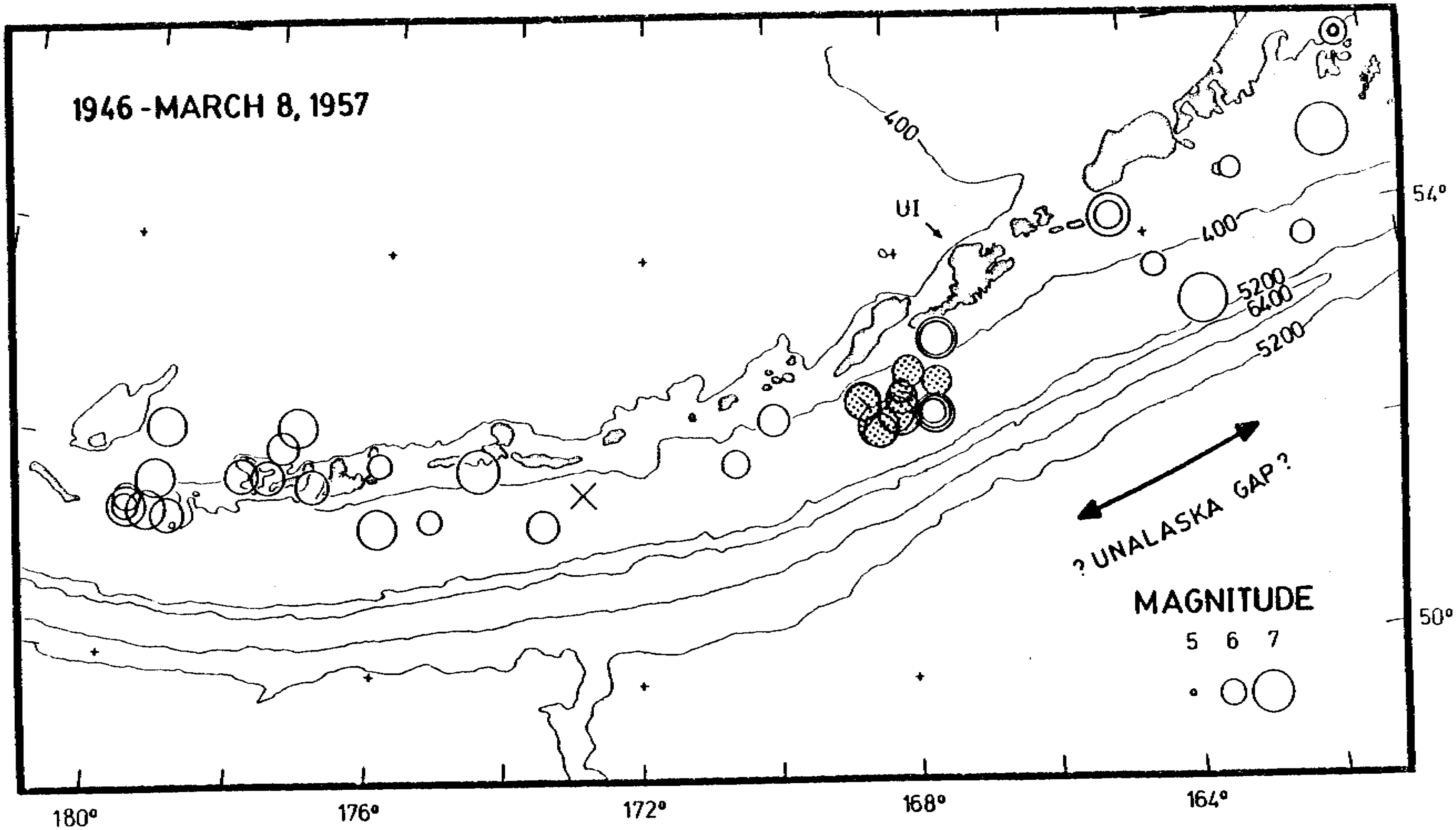

Figure 8. Plot similar to Figure , but of earthquakes from 1946 to just before the 1957 main shock. Earthquakes at depths shallower than 60 km are plotted as circles; those at depths of 60 to 80 km as X's. Note the clustering of epicenters near 180°W and near 168°W. Earthquakes that are part of a swarm that occurred in early January 1957 are shaded. Note also the location of the 1946 tsunamigenic earthquake, immediately to the left of the 5200 meter label.

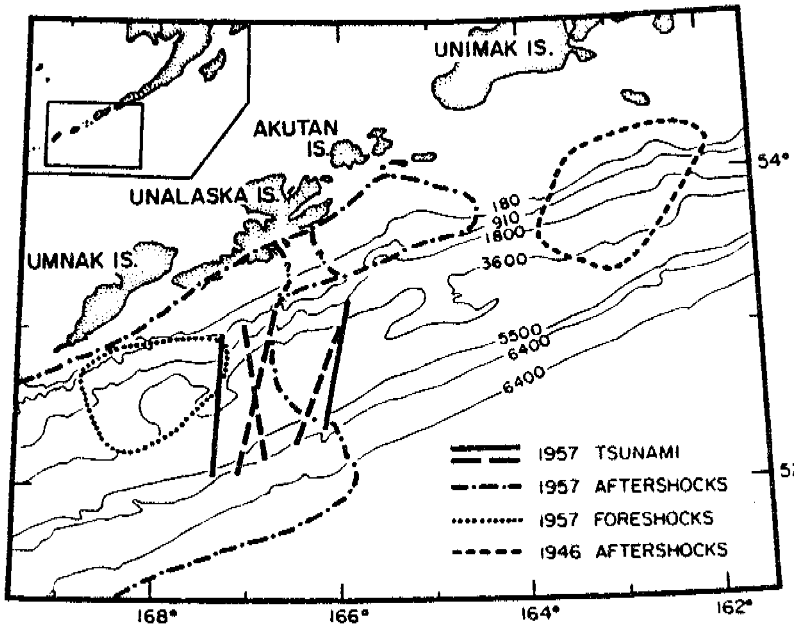

Figure 9. Detailed map and summary of information about the eastern portion of the aftershock zone of the 1957 earthquake. The eastern extent of the 1957 tsunami is indicated by a solid line for stations that the authors could reread arrival times and by a dashed line when the determination is based on published arrival times (see text for sources). Other lines enclose the aftershock zones of the 1957 and 1946 earthquakes, and a swarm that occurred 2 months before the 1957 main shock. Bathymetry is in meters.

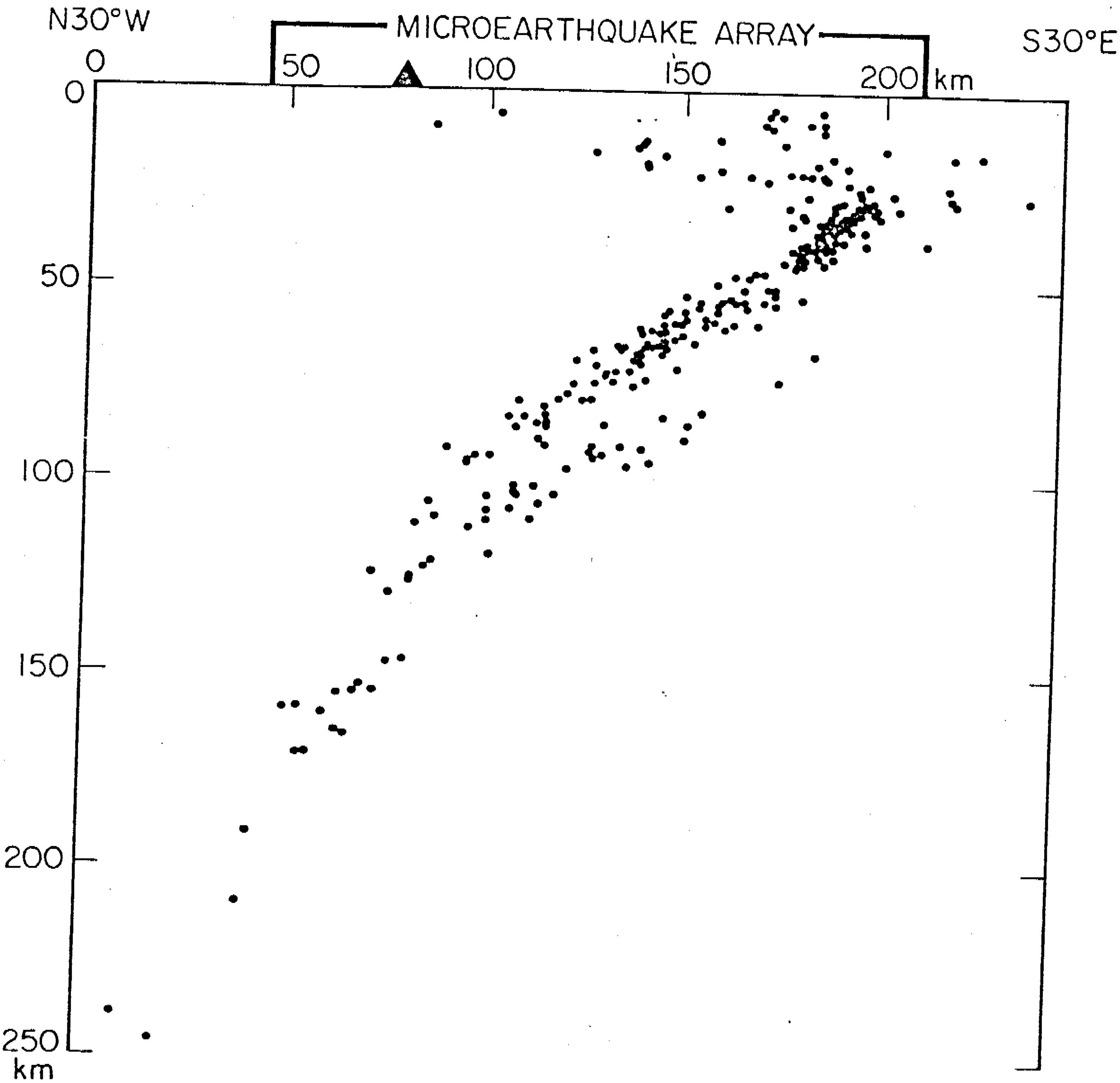

Figure 10. Depth section of well-determined hypocenters for the period July 1978 to December 1979. The section has a width of 400 km and is centered on the Shumagin Islands microearthquake array. The volcanic front is marked by the solid triangle.

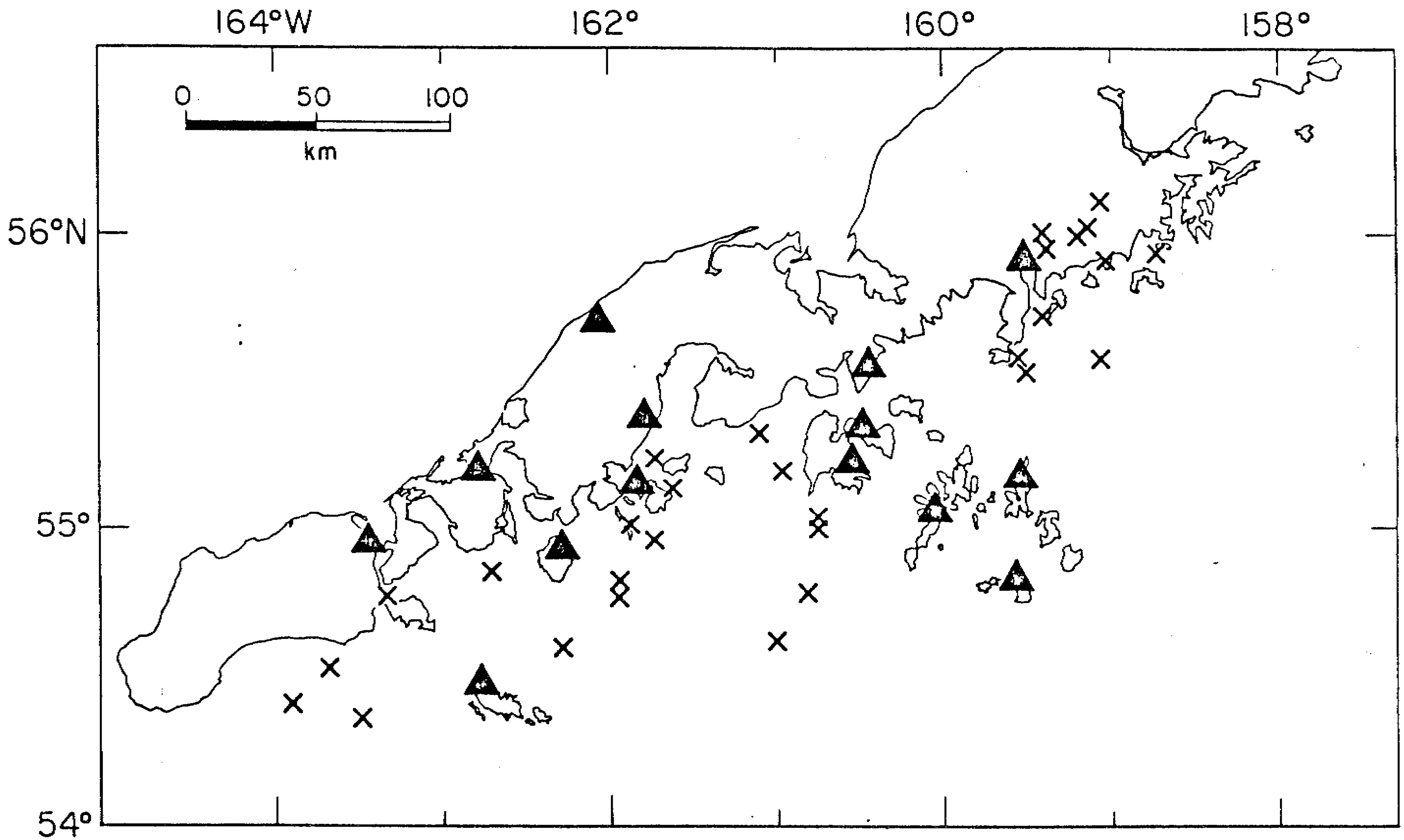

Figure 11. Epicenters of microearthquakes comprising the lower plane of the double-planed dipping seismic zone evident in Figure 10. The epicenters are shown by crosses, and the solid triangles represent seismograph stations.

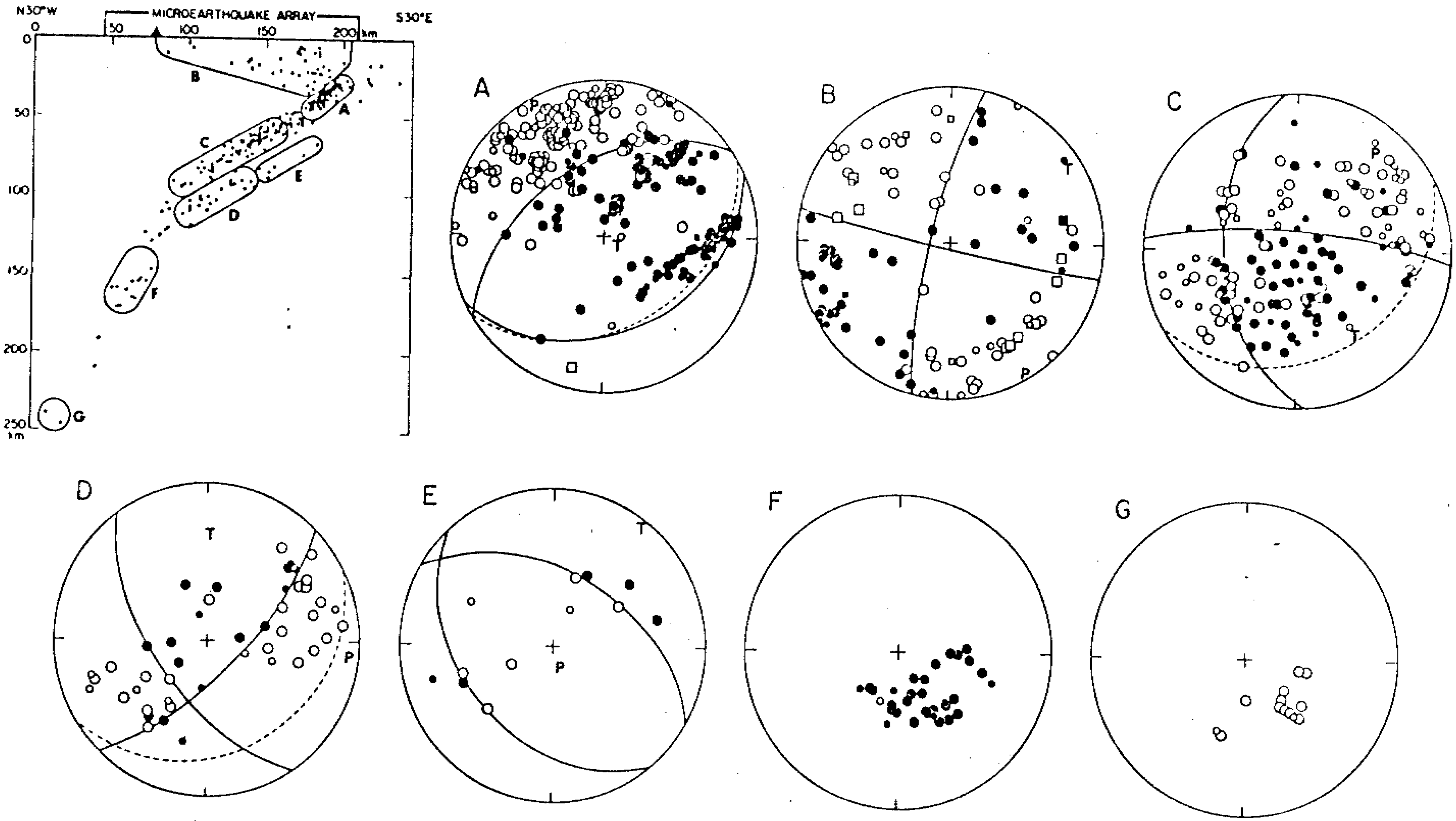

Figure 12 Subsets of microearthquakes for which composite fault-plane solutions have been determined (top left-hand diagram), together with the corresponding solutions. All stereograms are equal-area projections of the upper focal hemisphere. Open symbols represent dilatational, and solid symbols compressional P-wave first motions. Circles represent arrivals leaving the focus in an upward direction; squares are critically refracted arrivals projected from the lower hemisphere. Smaller symbols indicate less reliable readings, while P and T denote the axes of compression and tension respectively. Dashed curves indicate the approximate orientation of dipping planes of activity defined by the microearthquakes comprising the composite fault-plane solutions.

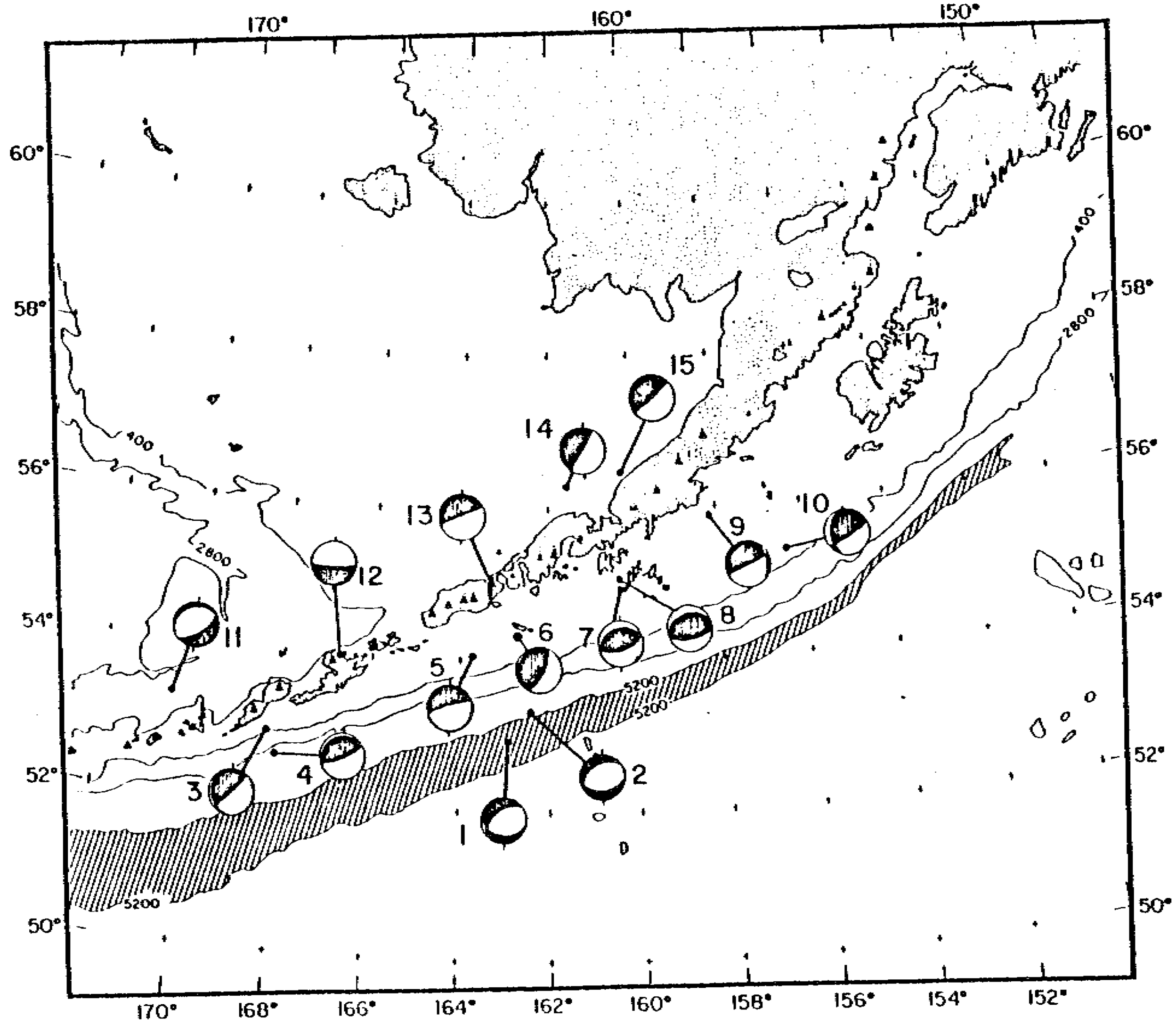

Figure 13 Focal mechanisms (Davies et al., 1980) (6) of earthquakes analyzed in this study.

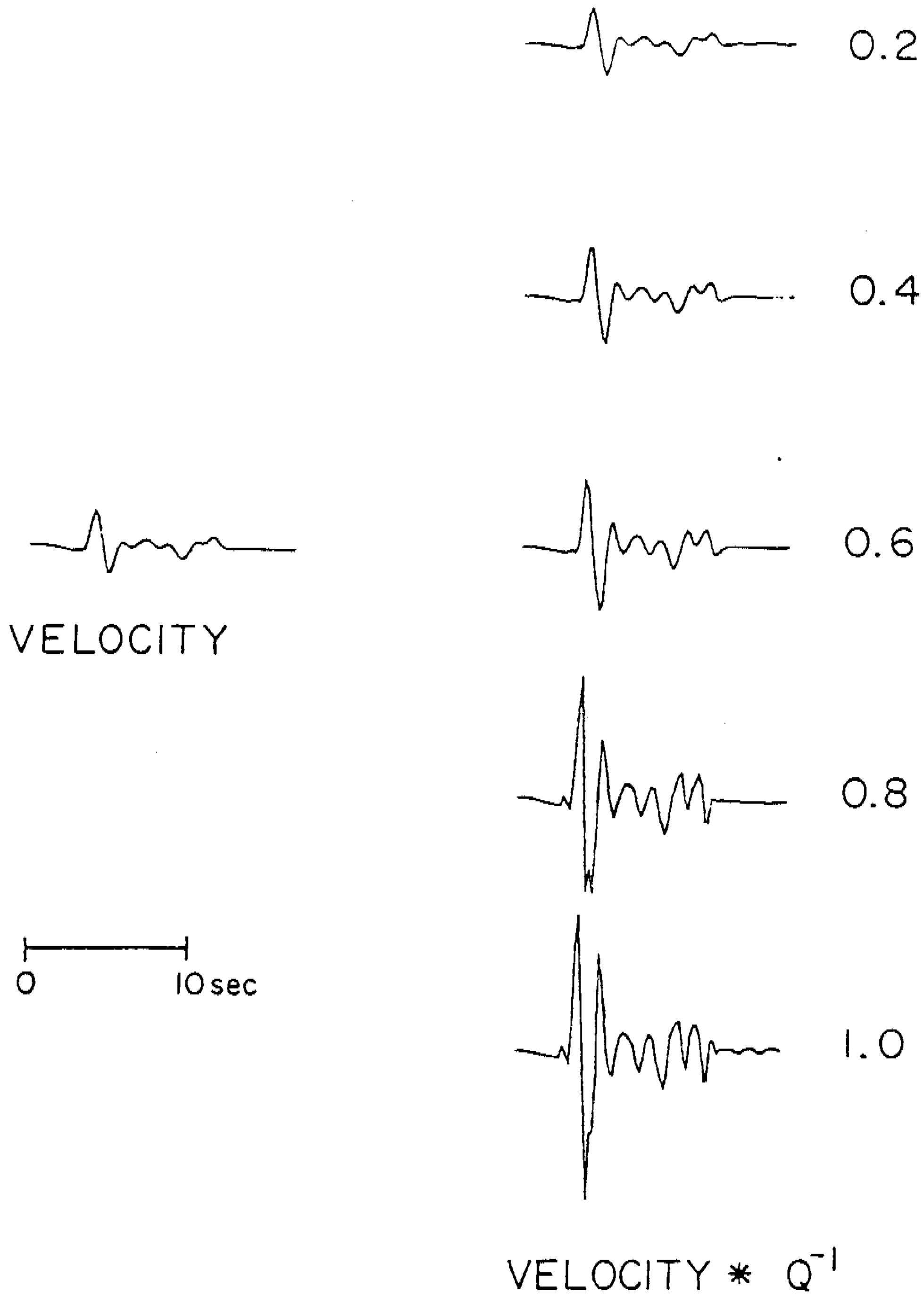

Figure 14. The effect of convolving a velocity pulse with an inverse Q operator for various values of t*. Frequencies above 5 herz are filtered out.

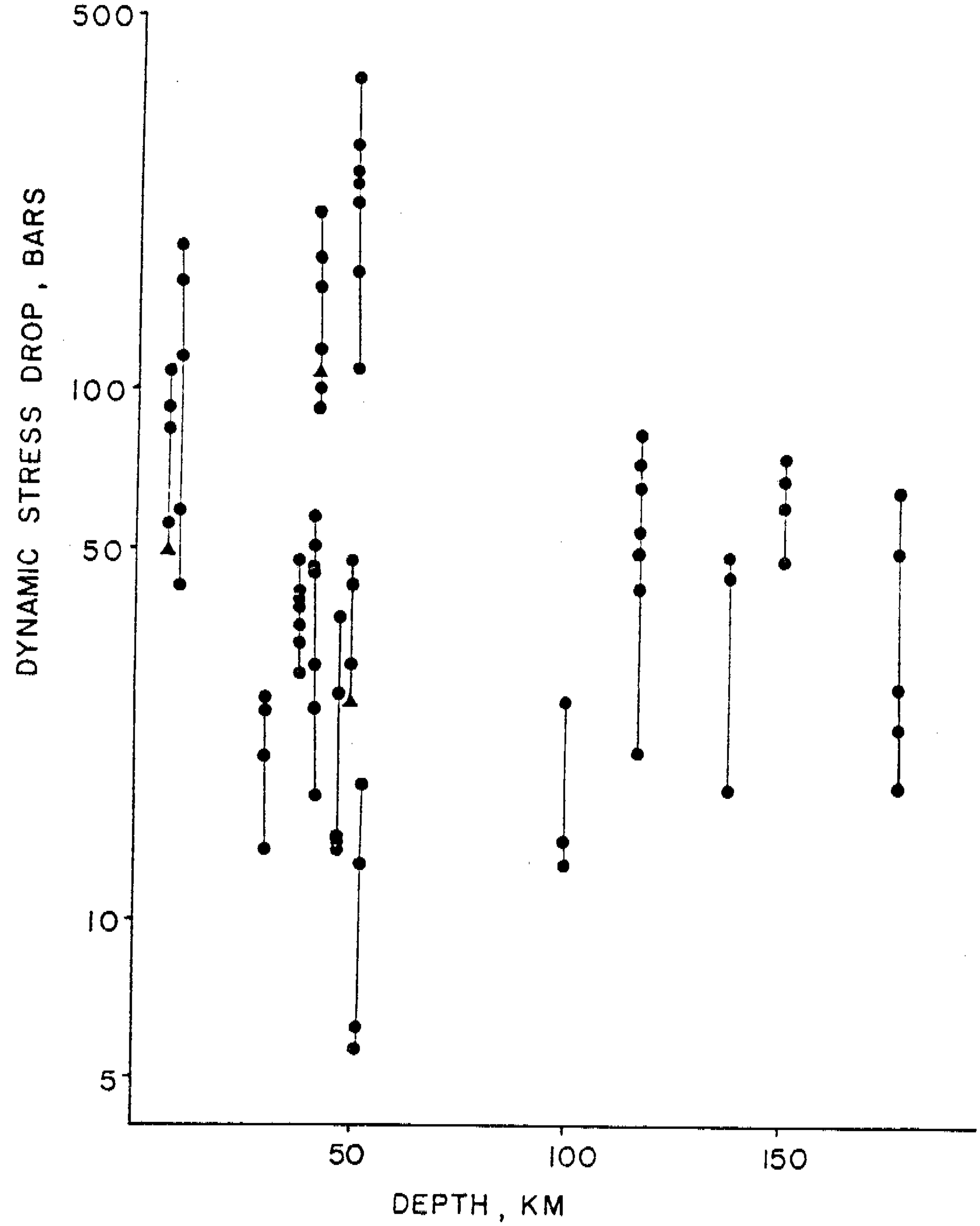

Figure 15 Plot of dynamic stress drop versus depth. Lines connect points which represent different stations used in analyzing the same event. Note the wide range of stress drops for the earthquakes at depths of 15-50 km.

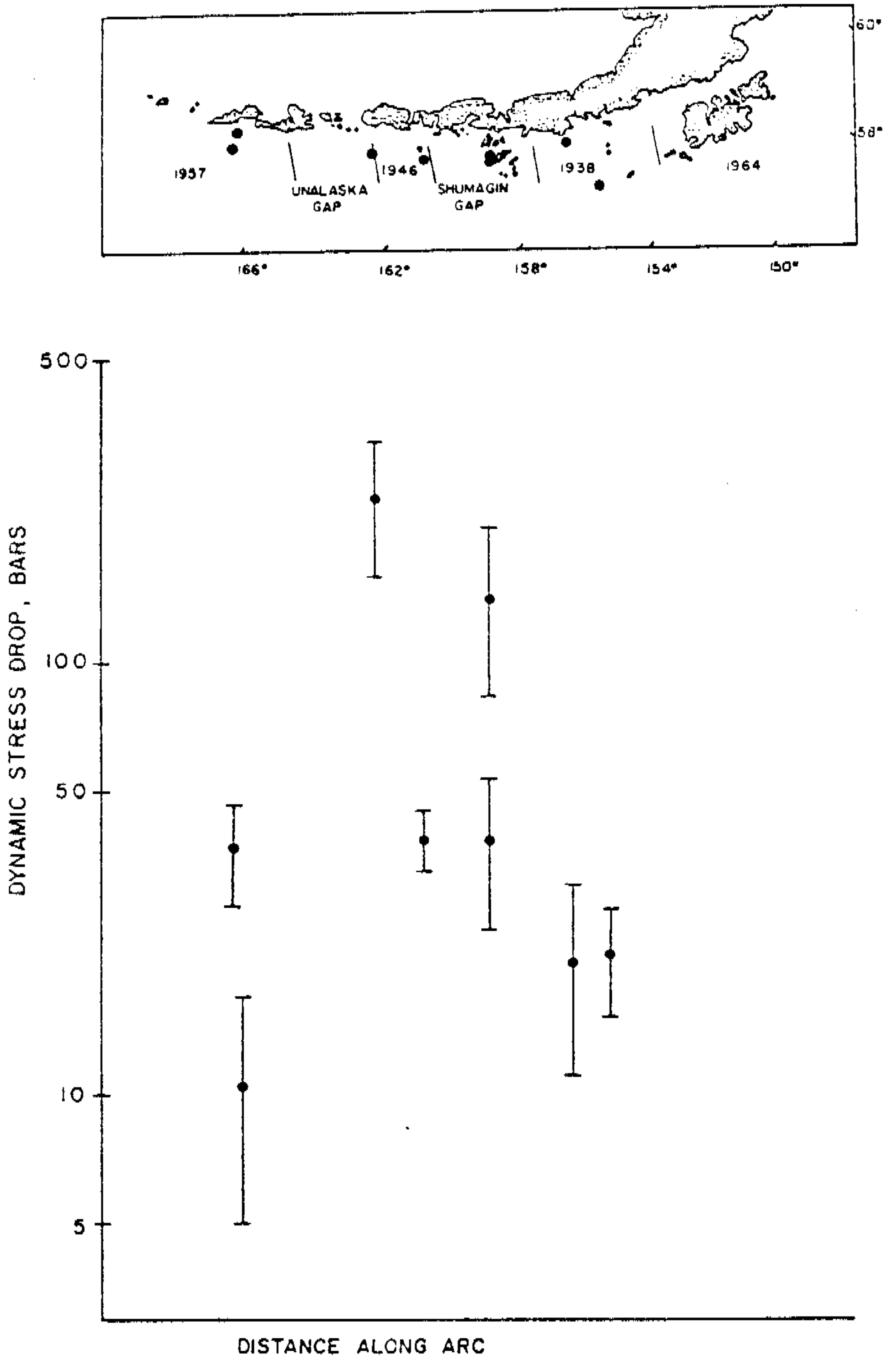

Figure 16. Dynamic stress drop plotted against longitude. Error bars are one standard deviation of the scatter among the different stations. High stress drop earthquakes are located within or at the edges of gaps.

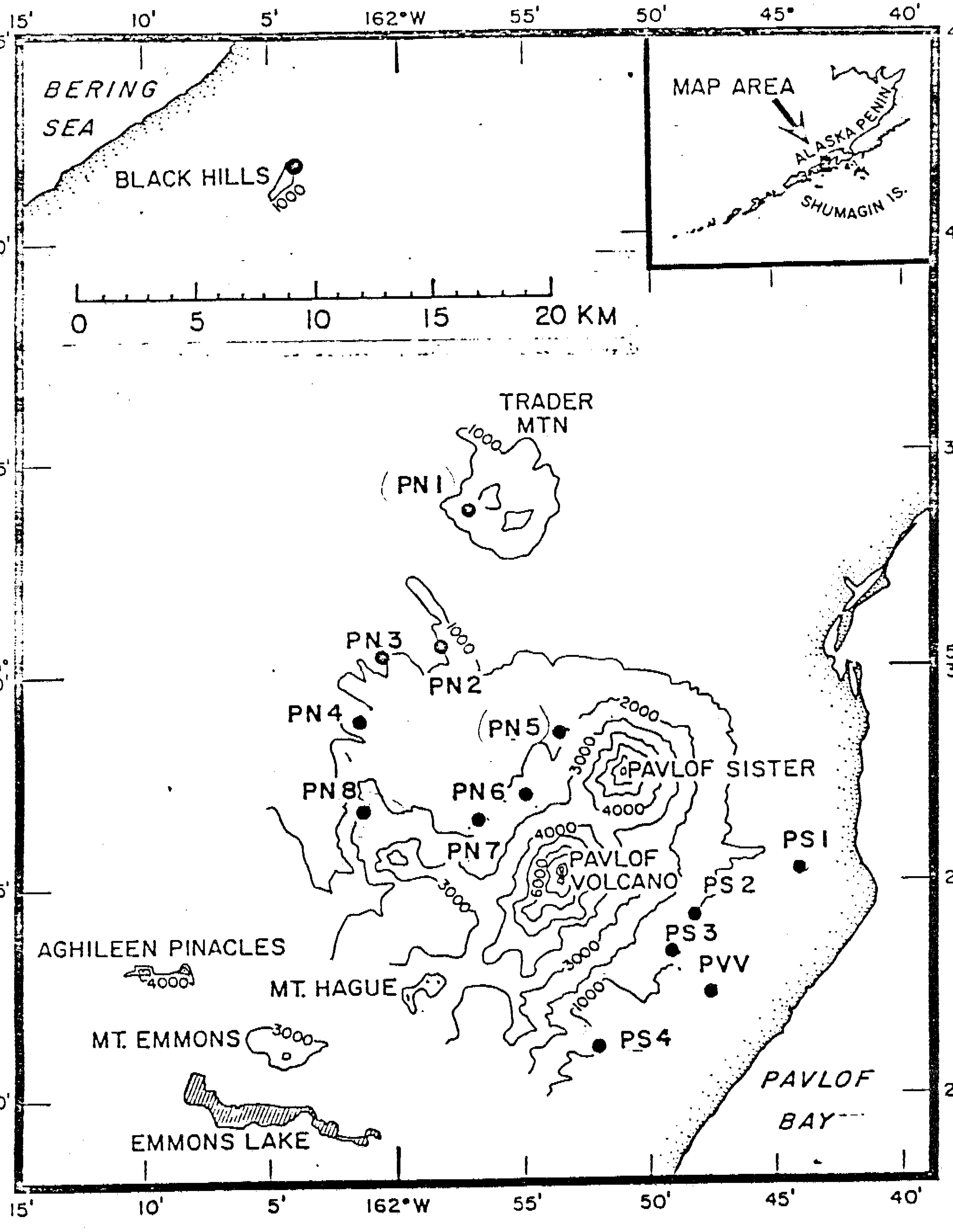

Figure 17. Locations of stations of the Pavlof seismograph array-

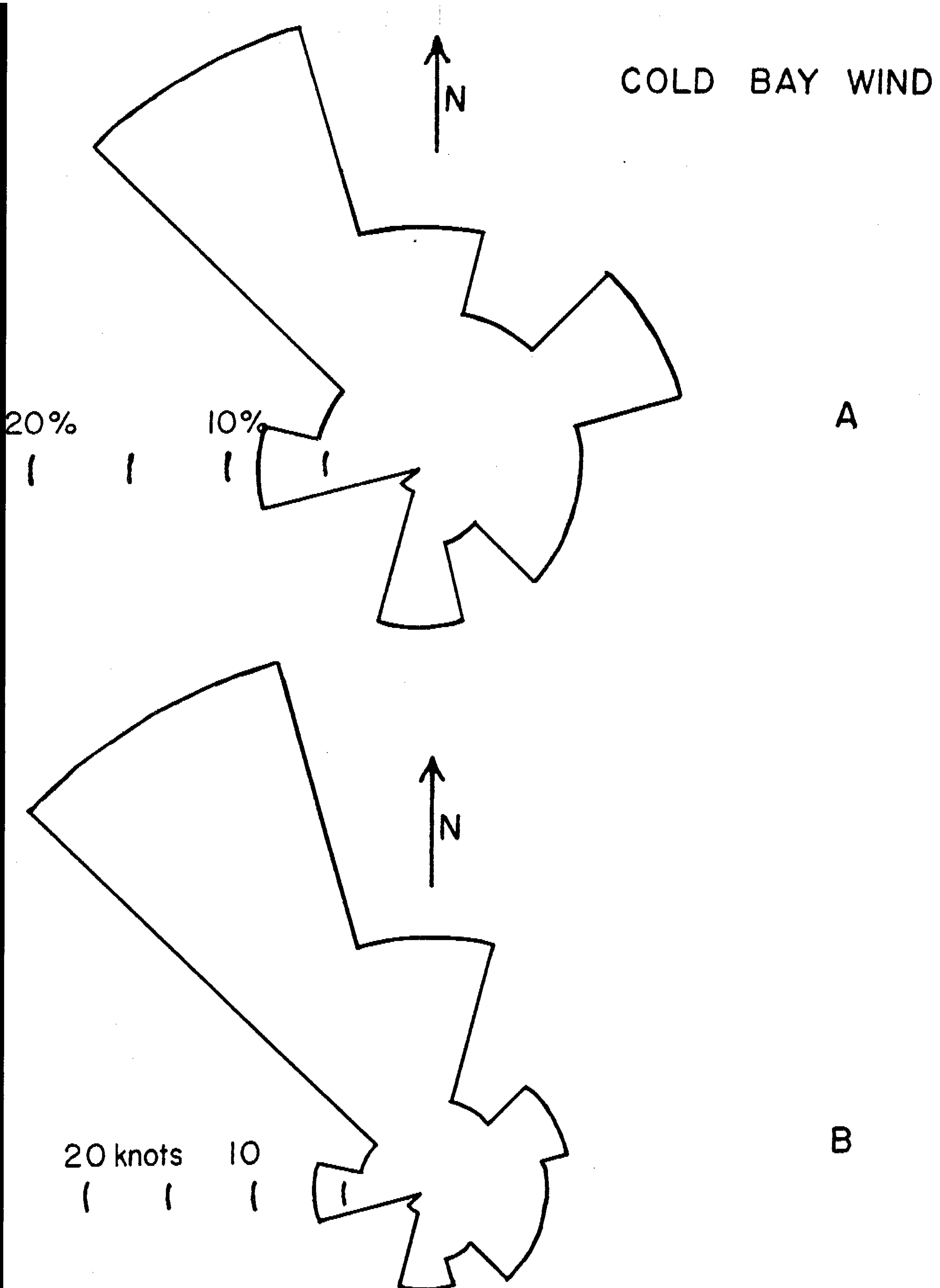

Figure 18. Polar histograms of Cold Bay Weather station wind direction and speed. A: percent of time wind blows in various directions. Each sector represents 30 degrees in azimuth. B: speed and direction, Distance away from center represents average wind speed for 30 degree sectors.

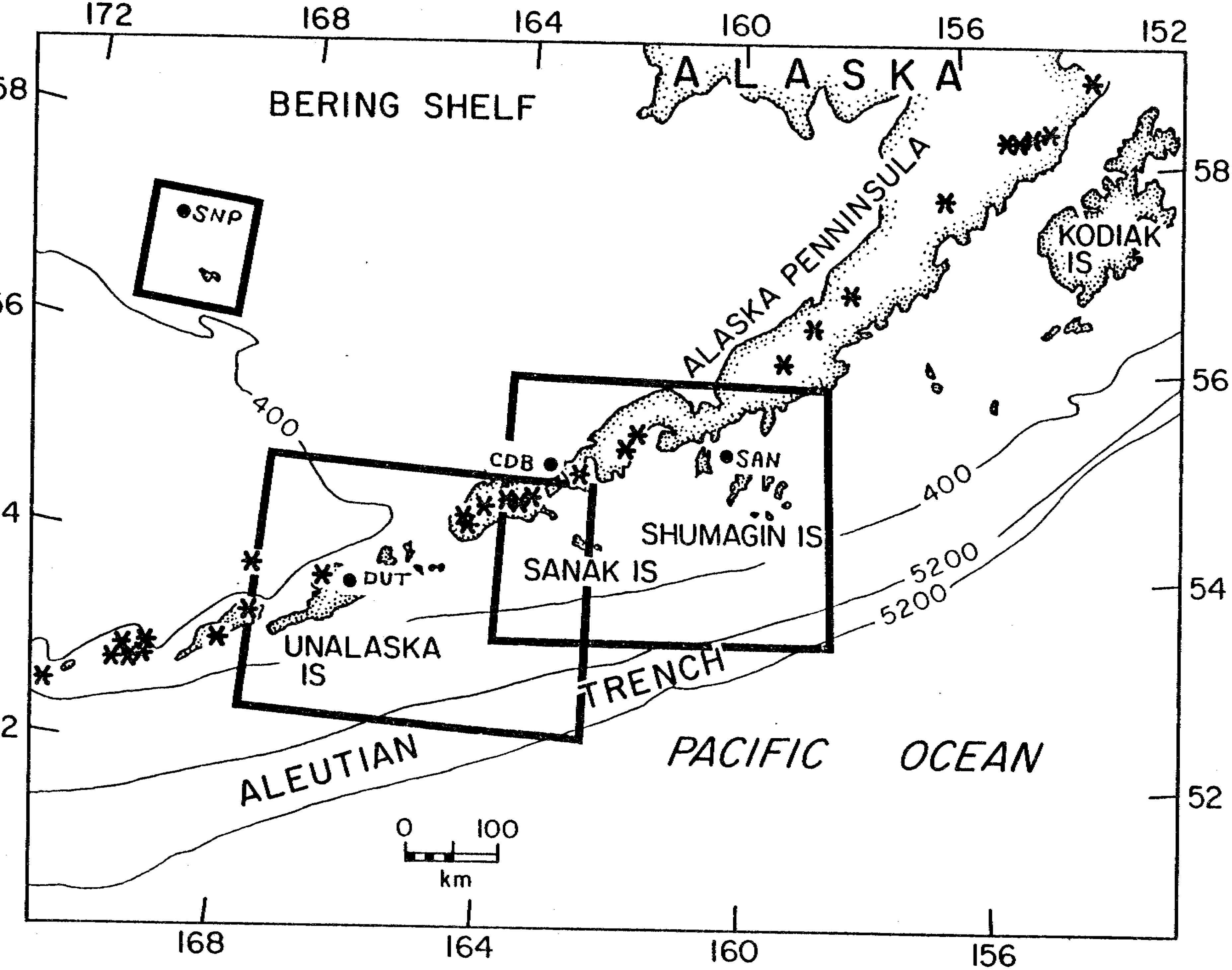

Figure 19. L-DGO Aleutian Networks-Location Map. Heavy boxes show approximate map areas for Figures 20-22, respectively.

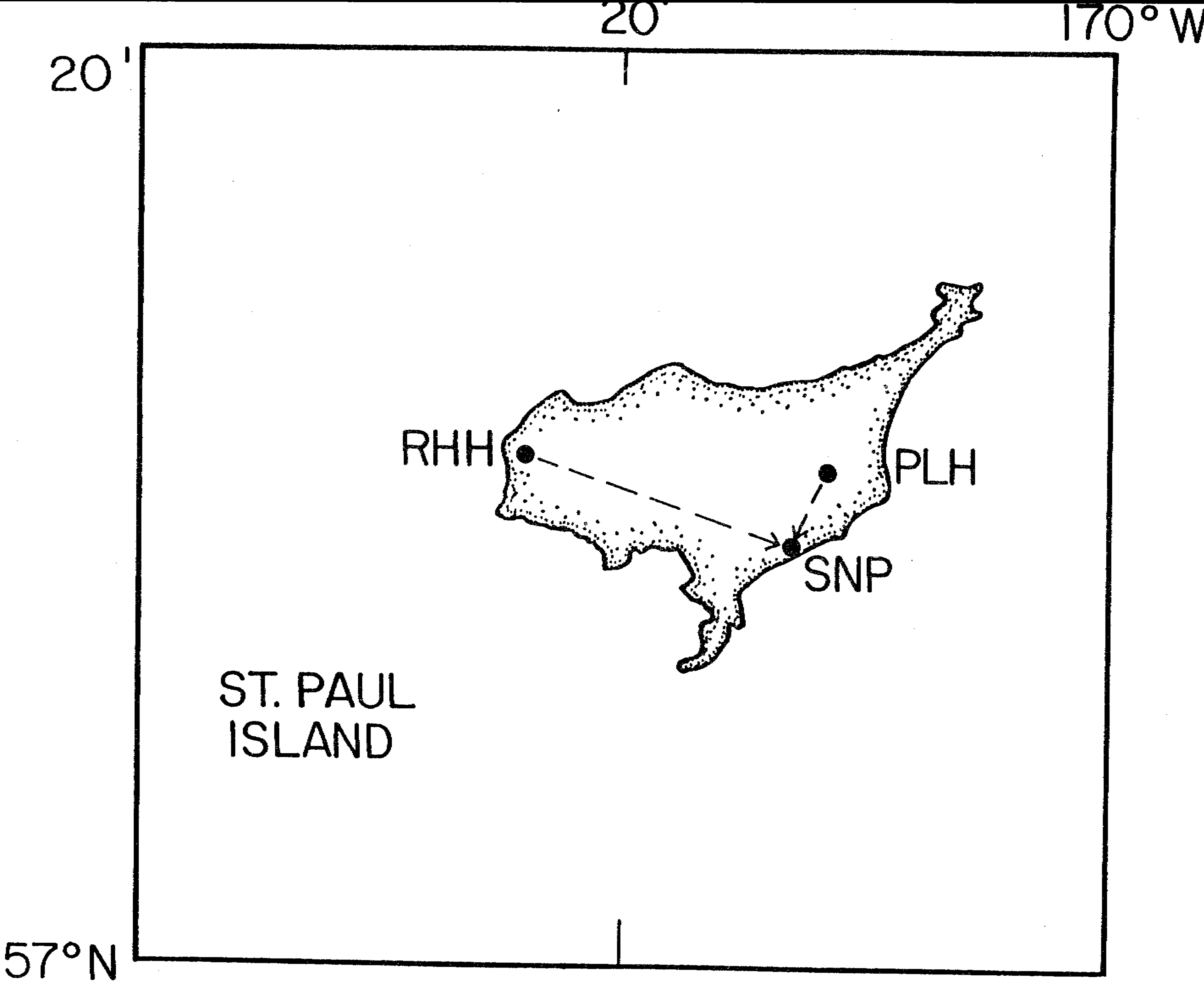

Figure 20. Pribilof Network. Remote stations RHH and PLH are telemetered to SNP where they and SNP are recorded on Helicorder

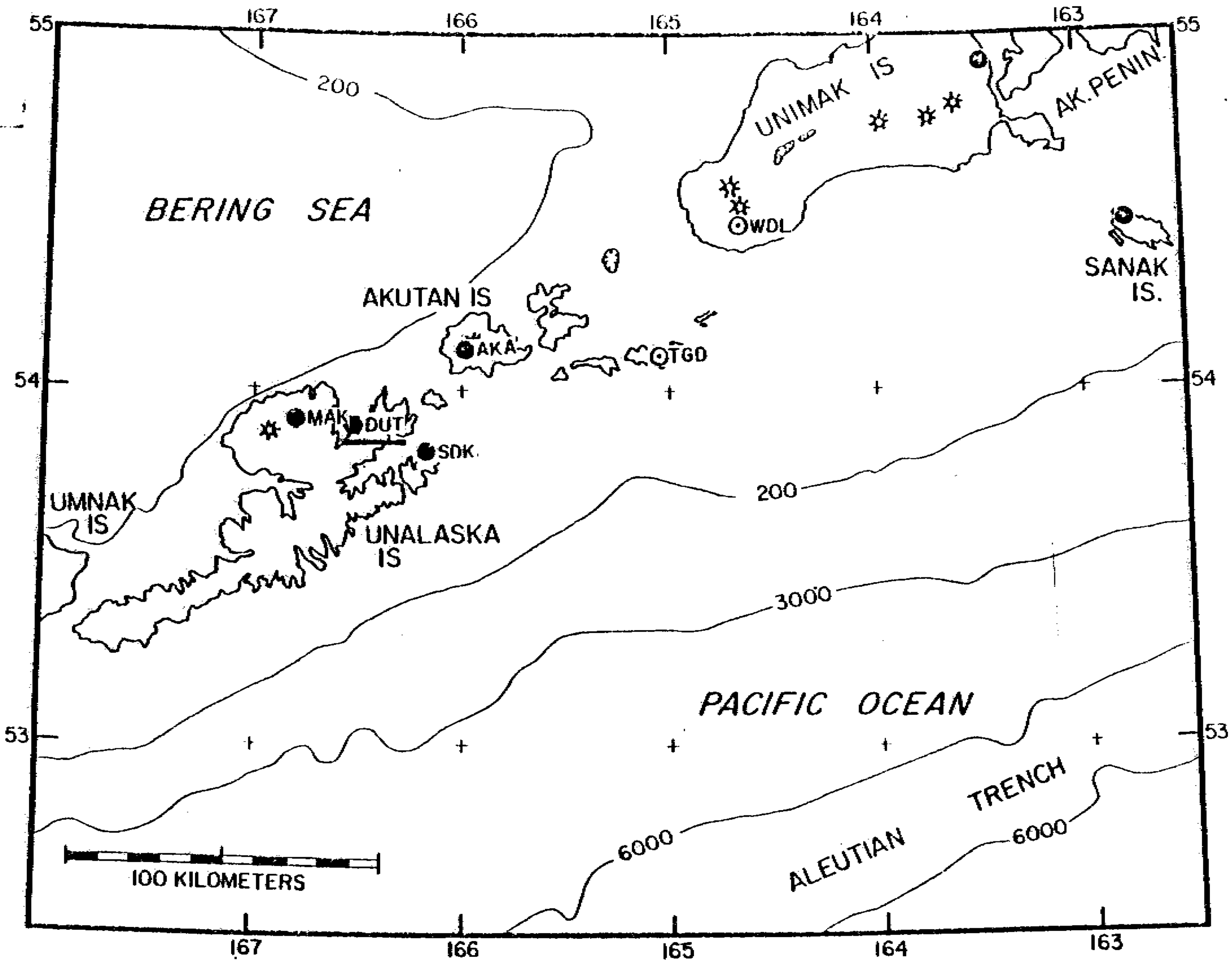

Figure 21. Unalaska Network (see Figure 23 for location). Remote stations (MAK, SDK, AKA) are shown by a filled circle, stations planned but not installed (TGD and WDL) due to weather and mechanical problems are shown by the circles enclosing a dot. The two filled circles in the upper right corner are the stations False Pass (FPS) and Sanak Island (SNK) of the Shumagin Network. The recording center for the Unalaska Network is in Dutch Harbor (DUT) shown by a filled hexagon. The sensor at each of the remote stations is a single, vertical seismometer of 1 Hz natural frequency. At DUT there are three orthogonal seismometers at 1 Hz, one vertical at 15 sec and a Kinemetrics SMA-1 strong-motion accelerograph (indicated by the heavy line under the designator code DUT). In addition to the usual short-period mode, the orthogonal set is also recorded in an intermediate period mode which is designed to span the band from 20 to .25 seconds period and to be intermediate in magnification between the short period and the strong-motion systems. All of the signals (except those of the SMA-1) are event-detected and recorded on analog magnetic tape. Two helicorder records are made to continuously monitor the system. The magnetic tapes are digitized and processed at L-DGO using the USGS PDP 11/70 data analysis sytem.

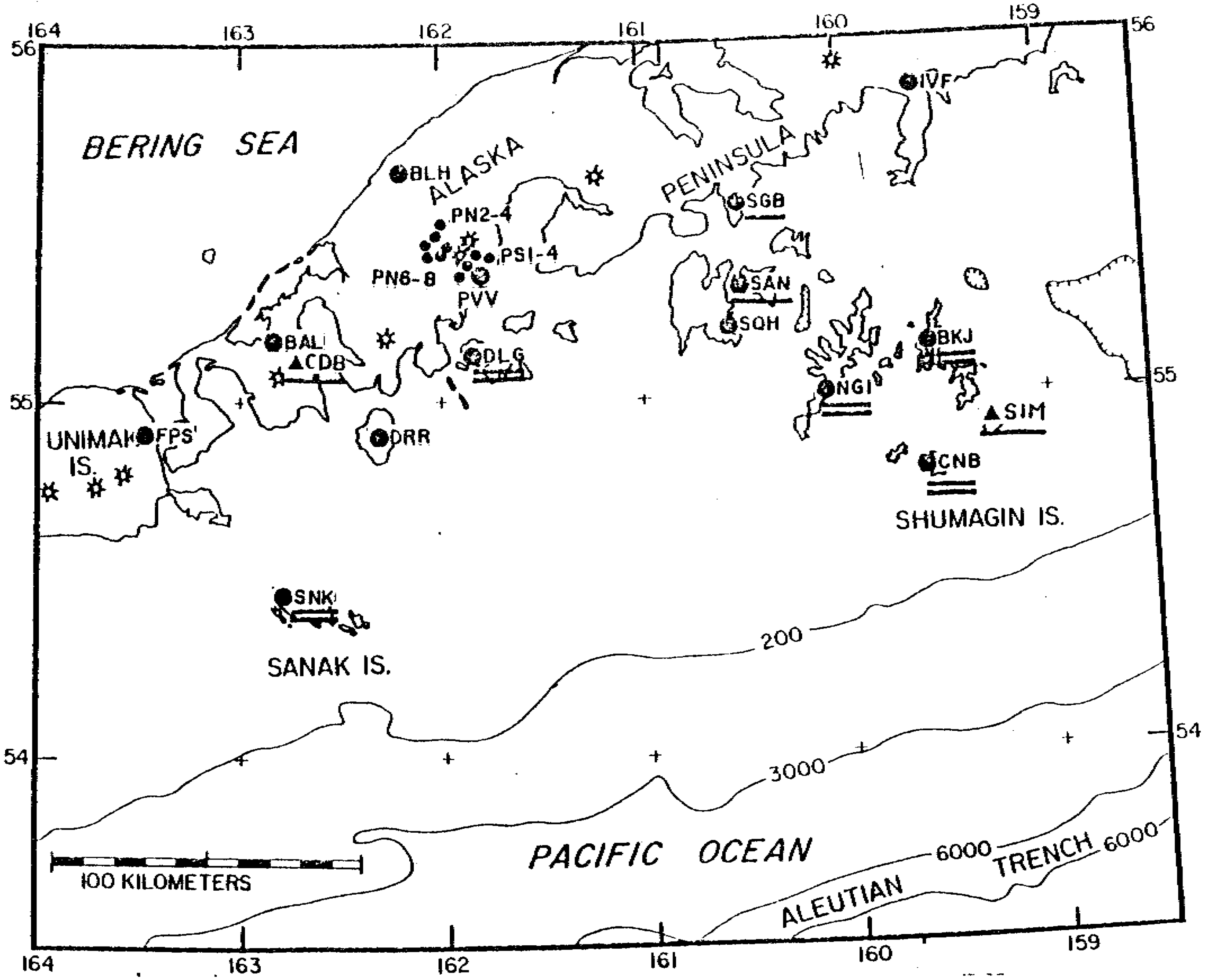

Figure 22. Shumagin Network (see Figure 23 for location). Remote stations with a single, vertical geophone are shown with filled circles. Stations with three orthogonal seismometers (CNB and SAN) are shown with a filled hexagon. Network stations with SMA-1 strong-motion accelerographs (SNK, NGI, DLG, SGB, BKJ, SAN, CNB) are indicated by the heavy line under the designator code. Those with double underlining transmit an SMA trigger signal: when one of these SMA's is triggered, a tone is sent via the VHF telemetry system to a detector at SAN which turns on the tape recorder. The triangles at SIM and CDB indicate SMA-1's unrelated to any network station. The SAN station has three orthogonal long period seismographs as well as the short and intermediate period system similar to that at DUF (see caption from Figure 25). Signals at SAN are recorded on an event detecting magnetic tape recorder, a Develocorder and 5 Helicorders; records from these devices are processed at L-DGO.

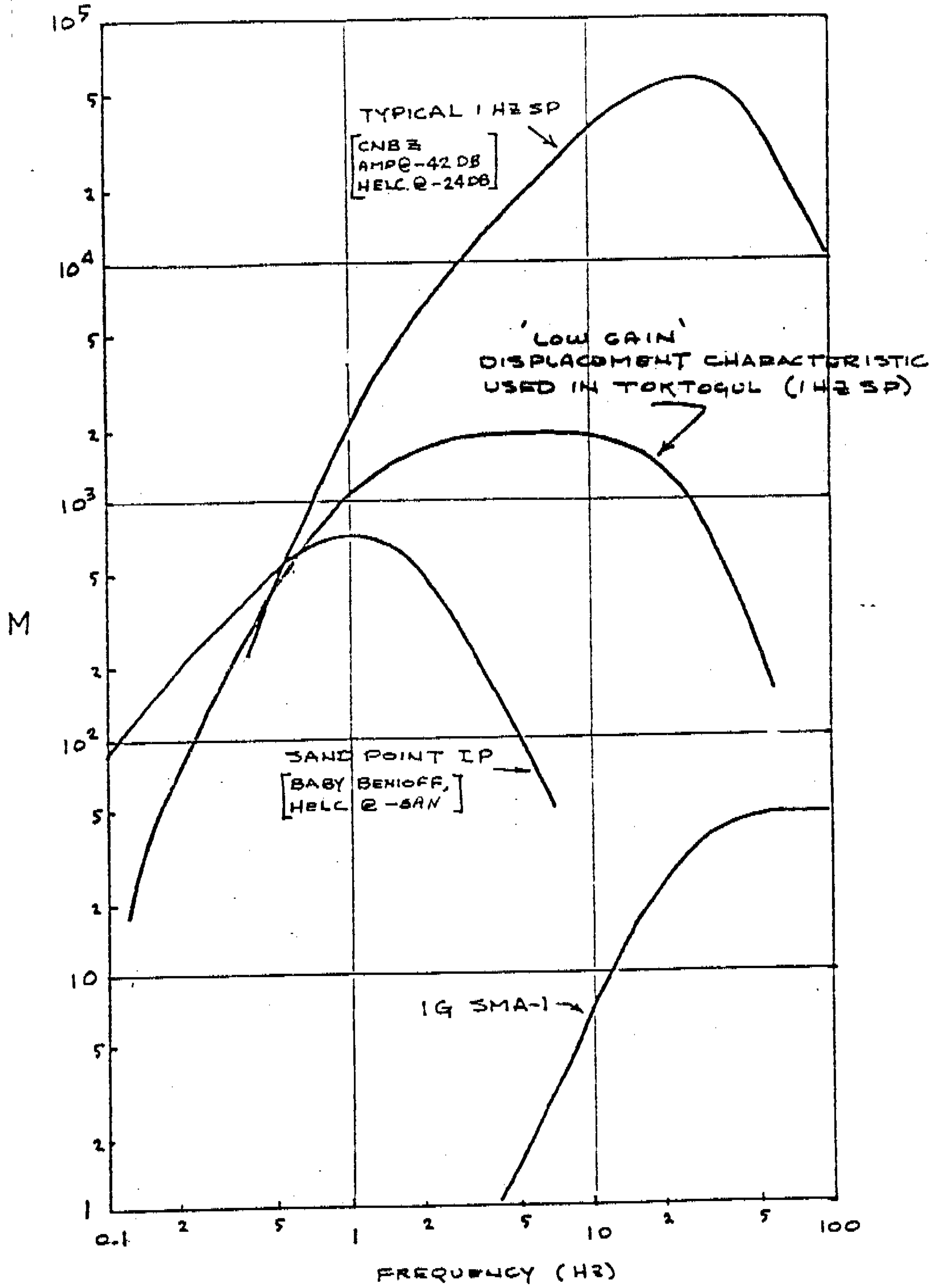

Figure 23. Comparison of the intermediate-period system to other seismographs. Response functions (magnification, M, vs. frequency) are shown for various seismographs: (1) the "typical 1 Hz sp" system is exemplified by the short-period station CNB (Figure 26) as recorded on a Helicorder; (2) the "low gain" system is not presently employed in the Alaska-Aleutian networks, is in use in the L-DGO Toktogul Network in the USSR; (3) the "Sand Point IP" system is the newly installed intermediate-period seismograph at SAN (and DUT; see Figures 25 and 26) as recorded on a Helicorder; (4) the "1G SMA-1" system is the Kinemetrics SMA-1 strong-motion accelerograph with sensitivity such that it will record on scale, accelerations up to 1g. Note that the IP system is intermediate in gain between the short-period system and the strong-motion system.

TRIGGER LOGIC FUNCTIONS

SAND POINT EVENT DETECTOR

1980 MARCH -

FUNCTION 1:	ANY ONE GROUP
FUNCTION 2:	ANY TWO GROUPS
FUNCTION 3:	ANY THREE GROUPS
FUNCTION 4:	ANY FOUR GROUPS
FUNCTION 5:	"STRONG EVENT"; ANY THREE GROUPS EXCEPT (F·G·H)
FUNCTION 6:	"WEAK EVENT"; ANY TWO CONTIGUOUS GROUPS, I.E.: A·B + A·C + B·C + D·E + D·F + D·G + D·H + F·G + G·H + F·H
FUNCTION 7:	SAME AS 6 EXCLUDING PAVLOF, I.E. F·G + G·H + F.H OMITTED
FUNCTION 8:	"GOOD STATION": SIGNAL DETECTOR A <u>OR</u> SIGNAL DETECTOR B <u>OR</u> ANY CONTIGUOUS GROUPS ON OTHER SIGNAL DETECTOR

<u>Figure 24a.</u> Table showing the eight (switch-selectable) logic functions stored in the PROM (programmable-read-only-memory) of the Sand Point event detector. The "groups" referred to in this table are sets of stations enclosed by the heavy lines in part (b) of this figure. For the event detector "group" means the signal detector representing a given group of stations; for example, in group F the signal from station SGB is input to signal detector F, that from NGI to G, and so on for the remaining groups of stations. If an event were to cause only signal-detectors F and G to switch "on" it would be recorded by the tape recorder only if one of logic functions 1, 2, 5, or 8 had been selected.

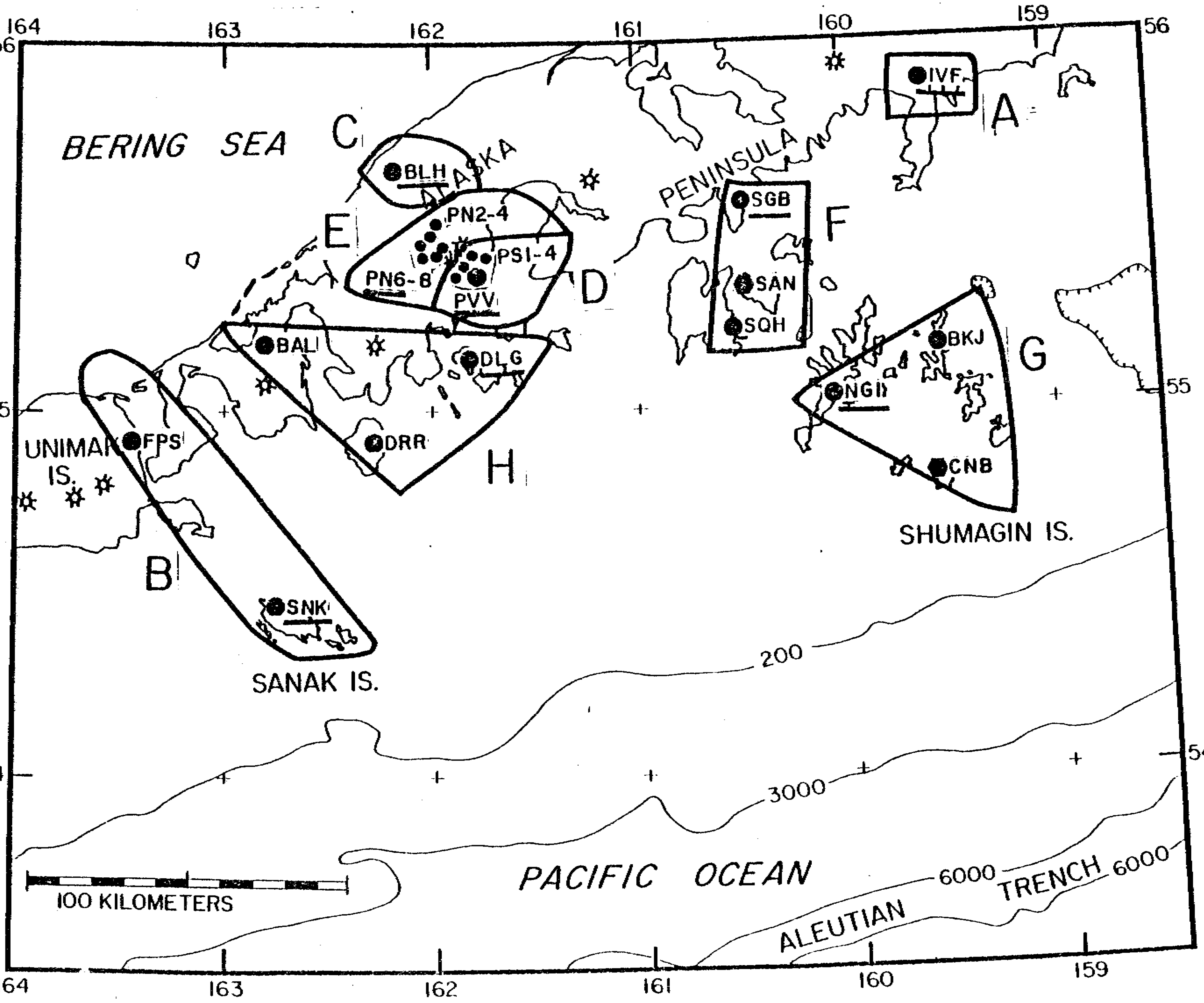

Figure 24b. Map showing the station groupings referred to in part (a). Within each group the signal fr[illegible] the underlined station is input to the signal-detector for that group.

SAND POINT RECORDING CENTER SEPTEMBER 1980

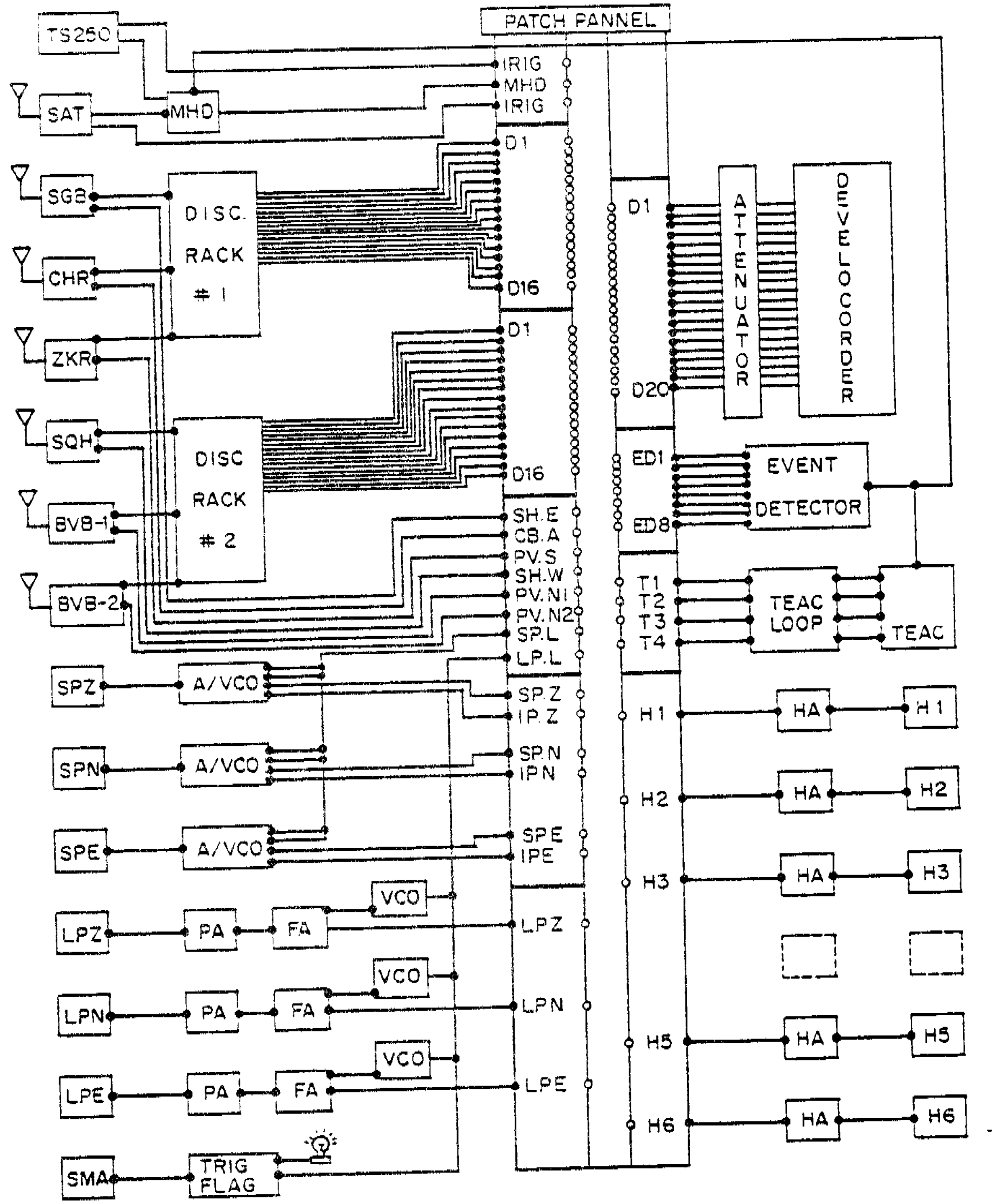

Figure 25. Block diagram for the Sand Point recording center, September 1980. Signal sources are arrayed down the far left of the diagram, signal conditioners are in the middle left, the patch panel in the center, and the recording devices on the right. Signal sources: Sprengnether TS250 chronometer; Kinemetrics satellite receiver for CUT; VHF receivers for subnetworks of the remote seismic stations - SGB (Shumagin-east subnet, SH.E), CHR (Cold Bay subnet, CB.A), ZKR (Pavlof-south subnet, PV.S), SQH (Shumagin-west subnet, SH.W), BVB-1 (Pavlof-north-1 subnet, PV.N1) and BVB-2 (Pavlof-north-2 subnet, PV.N2); SPZ, N and E, the local Baby Benioff, short-period seismometers; LPZ the local Sprengnether long-period vertical seismometer; LPN and E, the local Geotech long-period, horizontal seismometers; and Kinemetrics SMA-1 (1G) strong-motion accelerograph. Signal conditioners: L-DGO min.-hr.-day (MHD) board; discriminator racks 1 and 2; L-DGO two-channel amplifier-VCO units (A-VCO); L-DGO pre- and filter amplifiers (PA and FA) and modified Emtel 6202 VCO, for the long-period signals; and the L-DGO trigger-flag board. All of the signals are available on the patch panel where they can be routed to the event-detector and/or any recording device: Develocorder (18 data channels plus two for time); TEAC tape recorder (four channels, 32 seismic tones plus IRIG time code and tape-speed compensations tones); 5 Helicorders (one channel each, HA = Helicorder amplifier). Note that only the multiplexed output (SH.E through LP.L) are input to the TEAC system and that this system only records when the event-detector declares an event (see Figure 28).

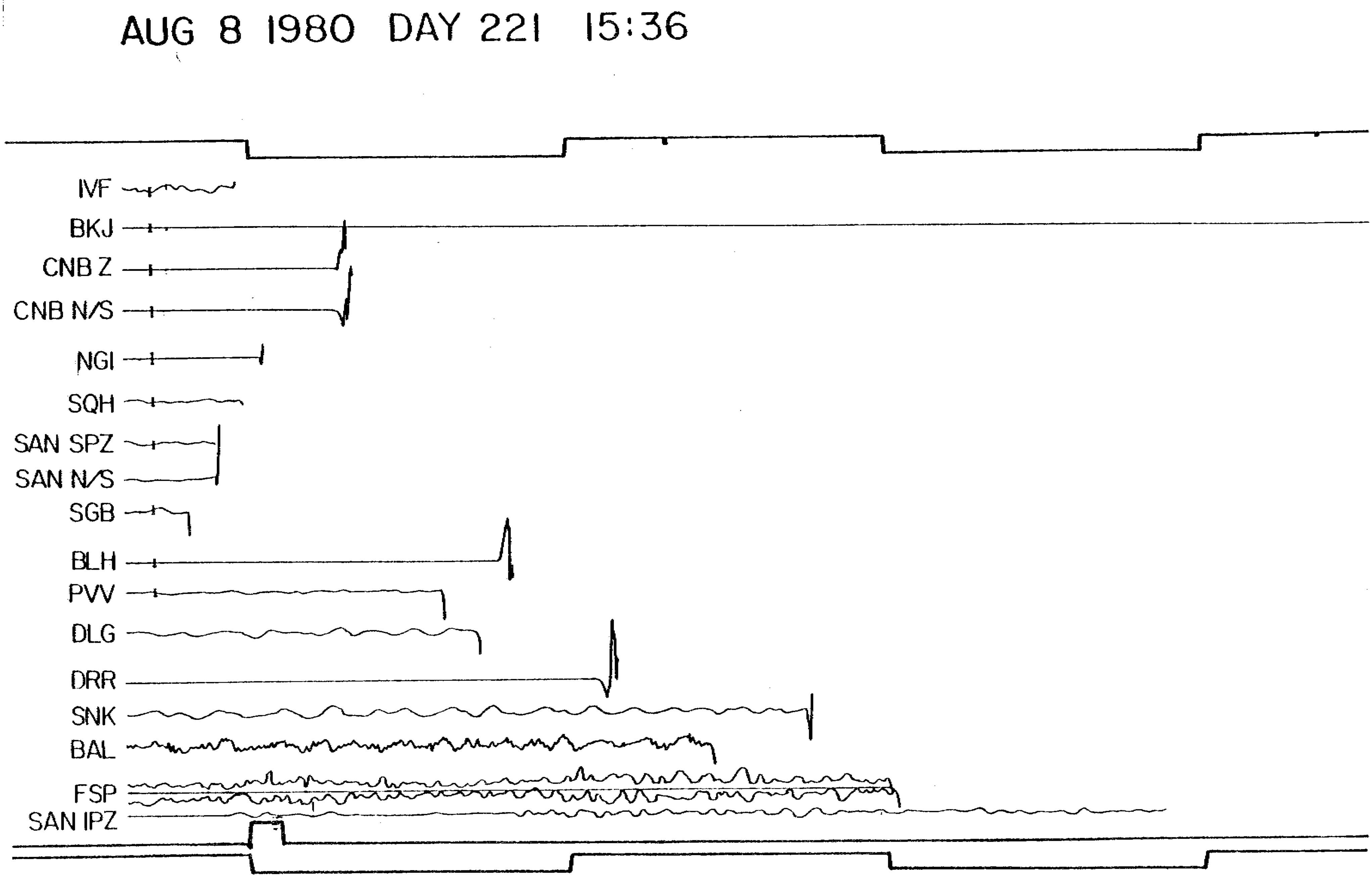

Figure 26a. Sample Develocorder record from 15:36 day 221, 1980. Tracings show the total amount of usable information from this event: the waveforms beyond the first few cycles of the P-wave are either clipped or obscured by the adjacent traces.

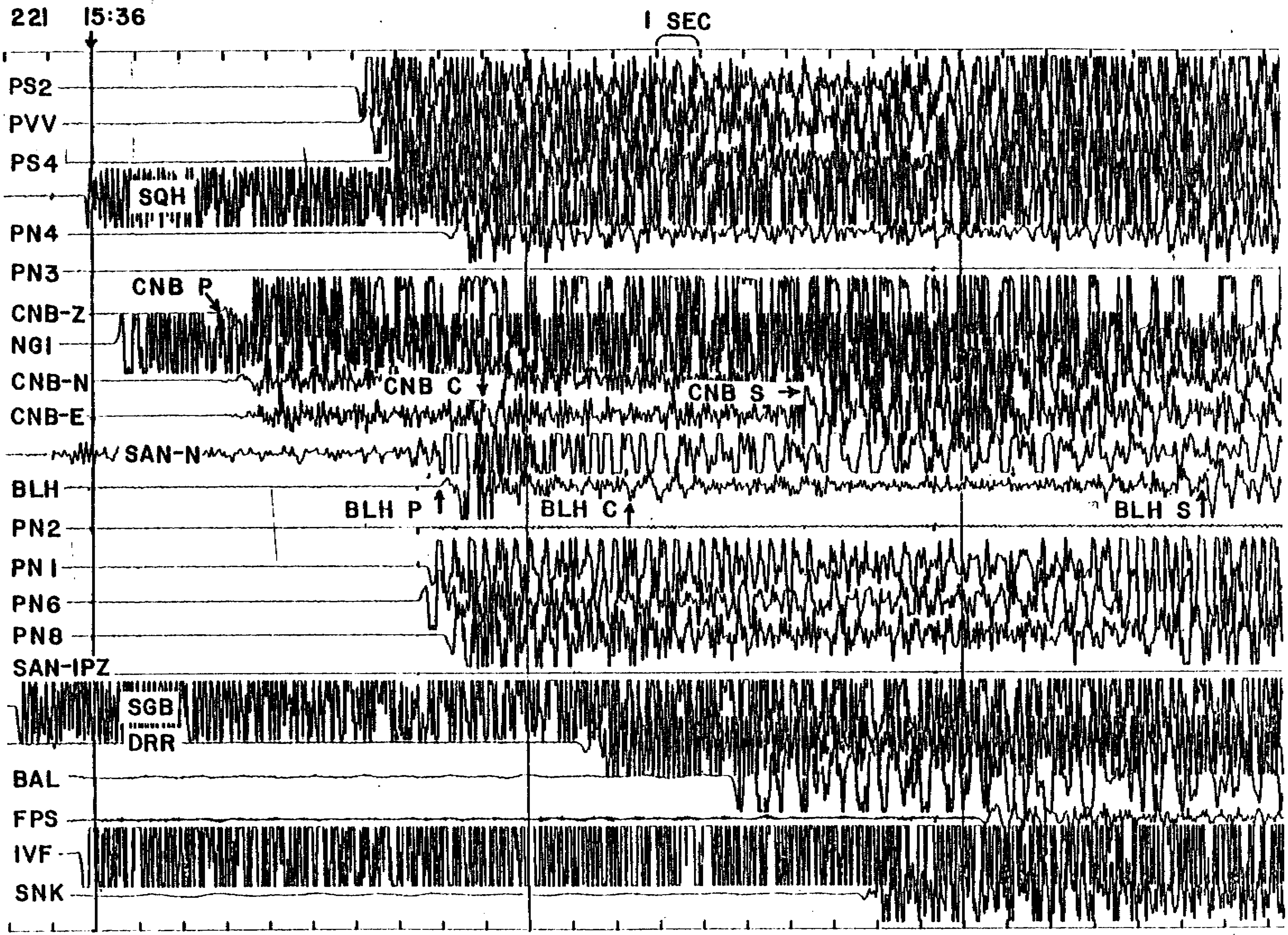

Figure 26b. Sample Versatec record from 15:36 day 221, 1980. This record was created by digitizing the demodulated TEAC tape and then plotting the digital data on a versatec plotter using the PDP 11/70. Note that many of the traces are unclipped and the whole waveform is available for analysis: for examples, note that the signals from CNB and BLH show clear P-, S- and converted (C) phases; these are labelled CNB P, CNB S, CNB C, BLH P, BLH S, and BLH C, respectively.

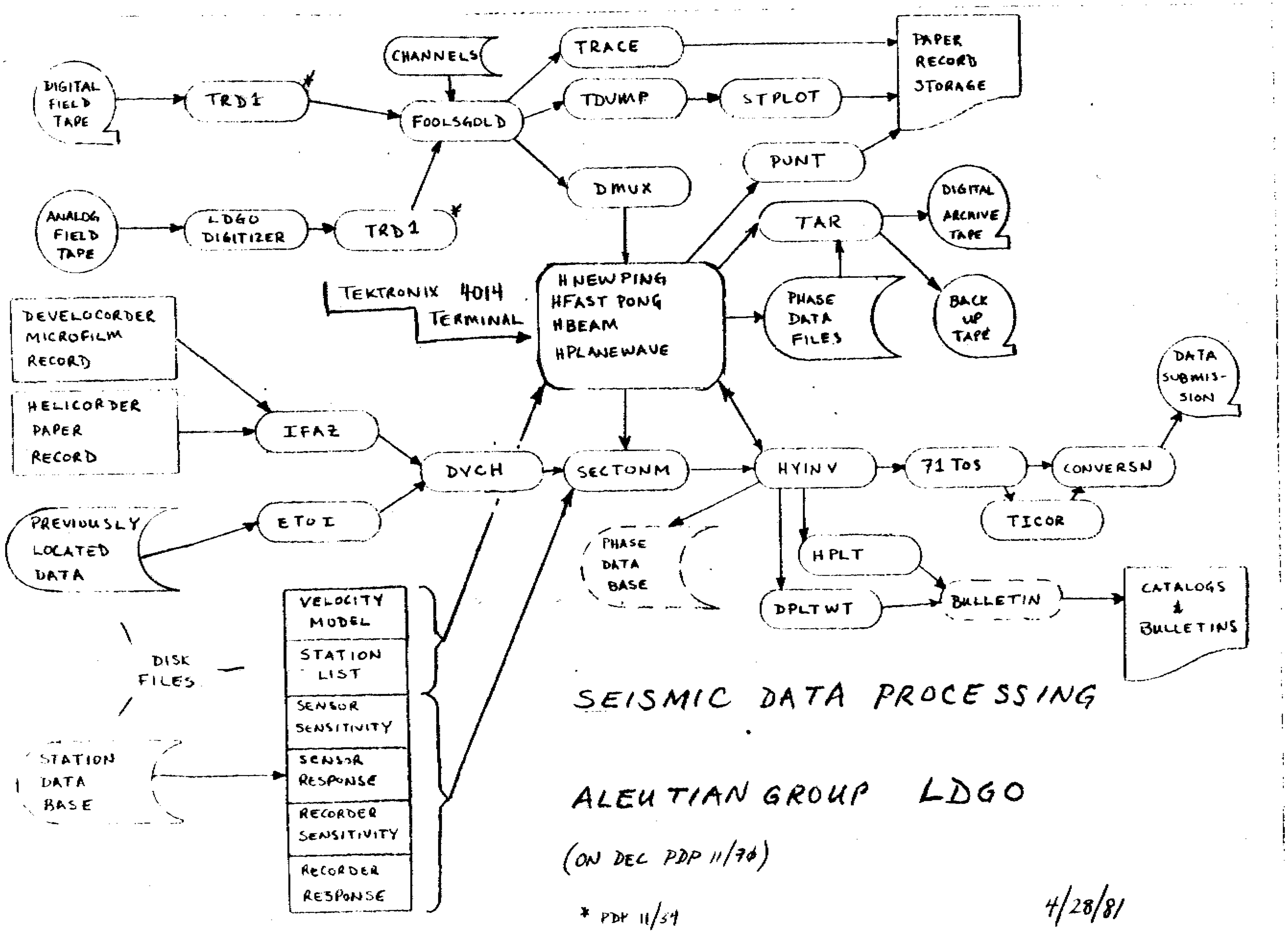

Figure 27. Data Flow Chart. See text for brief description of programs.

Annual Report
April 1980-March 1981
Research Unit #88
Number of Pages:

DYNAMICS OF NEAR-SHORE ICE

Principal Investigators: A. Kovacs and W.F. Weeks
Cold Regions Research and Engineering Laboratory

15 June 1981

I. SUMMARY OF OBJECTIVES, CONCLUSIONS, AND IMPLICATIONS

R.U. #88 investigates sea ice and ice induced gouges in the sea floor along the coasts of the Beaufort, Chukchi, and Bering Seas. New results reported during FY81 include further documentation of coastal ice pileup and over-ride events, studies of the block size distributions in first-year pressure ridges, investigations of additional laser profilometer observations on pressure ridges, radar studies of near-shore lakes on the North Slope that may serve as year-round sources of fresh water, and the preparation of a review paper on the physical environment of arctic Alaska as it relates to petroleum exploration and production.

II. INTRODUCTION

A. General Nature and Scope of Study

There are several principal thrusts to the present proposal. These are concerned with:

1. Studies of rubble piles and shore ice pile-ups along the coast of the Beaufort, Chukchi, and Northern Bering Seas.

2. Investigations of pressure ridge properties and ridge statistics in the Beaufort, Chukchi, and Northern Bering Seas.

3. Statistics of ice produced gouges on the sea floor of the Beaufort Sea.

4. Utilization of SLAR to study near-shore lakes along the Beaufort Coast.

B. The Specific Objectives of the Program are as Follows:

1. Obtain careful documentation of the locations and characteristics of rubble piles and shore ice pile-ups and ride-ups. Particular attention is to be paid to the geometry of these features (water depths, over-ride distances, pile-up heights, slope angles, etc.).

2. Obtain measurements via the use of laser profilometry of the distributions of sail heights and spacings of pressure ridges that occur over the Alaskan continental shelf.

3. By means of surface measurements study the relations between the thickness of ice blocks in pressure ridges and the height and geometry of the ridges.

4. By studies of the data on existing sea floor gouges collected by the U.S. Geological Survey, develop a statistical analysis that will allow probabilistic estimates to be made concerning safe burial depths for pipelines and blow-out-preventers.

5. Verify the interpertation of SLAR miagery to reveal if a given lake is or is not frozen to its bed at a specific time. Prepare maps showing the locations of these different types of lakes on the North Slope.

6. Prepare a summary document discussing the "Physical Environment of Arctic Alaska" as it affects exploration and production of oil and gas.

C. Relevance to Problems of Petroleum Development

The specific relevance of these programs to problems of petroleum development is as follows:

1. The potential for ice piling on or over-riding an offshore structure is recognized as one of the major dangers in arctic offshore operations. In Norton Sound the occurrence of large ice rubble features may constitute the "design ice force event." Therefore, any additional information on such phenomena and their magnitudes will be of great help in expanding both the existing data base and our knowledge of such threats to development.

2. In deeper water, encounters between pressure ridges and offshore structures may constitute the "ice force design event." Laser profilometery provides valuable information on pressure ridge heights and spacings that can be used to make quantitative assessments of the distribution of ice forces caused by ridges.

3. Statistical analysis of ice gouge characteristics are essential to making probabilistic estimates of safe burial depths for offshore pipelines and subsea christmas trees.

4. Studies of pressure ridge morphologies, block sizes, and ridge heights will contribute directly to improved estimates of ice forces on offshore structures.

5. As most North Slope lakes freeze to the bottom during the winter, sources of fresh water for coastal operations are hard to find. A rapid remote sensing method for identifying lakes that are not frozen would speed the location of adequate water sources.

6. The preparation of a summary of the status of present knowledge of the physical environment of arctic Alaska is very useful in identifying gaps in the knowledge.

III. CURRENT STATE OF KNOWLEDGE

The majority of the work on near-shore ice motions and ice properties relative to offshore development that is currently available in the non-proprietary literature has been produced by this project. A listing of these papers is given under results.

IV. STUDY AREAS

Areas of field study for this program include Norton Sound and the coastal areas of the Chukchi and Beaufort Seas.

V. RESULTS

Our results are documented in the following reports:

1. Published Reports:

    a) Kovacs, A. (1976) Grounded ice in the fast ice zone along the Beaufort Sea Coast of Alaska. *CRREL Report 76-32*, 10 pp.

    b) Kovacs, A. and Gow, A.J. (1976) Some characteristics of grounded floebergs near Prudhoe Bay Alaska. *CRREL Report 76-34*, 10 pp,; also available in *Arctic 29(3)*, 169-73 (1976).

    c) Weeks, W.F., Kovacs, A., Mock, S.H., Tucker, W.B., Hibler, W.D., and Gow, A.J. (1977) Studies of the movement of coastal sea ice

near Prudhoe Bay, Alaska. *Journal of Glaciology*, Vol. 19, No. 81, p. 533-46.

d) Kovacs, A. (1977) Sea ice thickness profiling and under-ice oil entrapment. *Offshore Technology Conference* Paper OCT 29-49.

e) Schwarz, J. and Weeks, W.F. (1977) Engineering properties of sea ice. *Journal of Glaciology*, Vol. 19, No. 81, p. 499-531.

f) Gow, A.J. and Weeks, W.F. (1977) The internal structure of fast ice near Narwhal Island, Beaufort Sea, Alaska. *CRREL Report 77-29*, 9 pp.

g) Sodhi, D.S. (1977) Ice arching and the drift of pack ice through restricted channels. *CRREL Report 77-18*, 14 pp.; also published by Sodhi, D.S. and Weeks, W.F. in Proceed. Part 2 IAHR Sympos. on Ice Problems, Lulea, Sweden, p. 415-32.

h) Kovacs, A. (1977) Iceberg thickness profiling. *In* "Conference on Port and Ocean Engineering under Arctic Conditions" Memorial University of Newfoundland, St. Johns.

i) Kovacs, A. (1978) Iceberg thickness and crack detection. *Iceberg Utilization* (A.A. Husseiny, ed.) Pergamon Press, p. 131-145.

j) Weeks, W.F. and Gow, A.J. (1978) Preferred crystal orientations in the fast ice along the margins of the Arctic Ocean. *CRREL Report 78-13*, 24 pp; also published in *Journ. Geophys. Res.*, *83(c10)*, p. 5105-21 (1978).

k) Weeks, W.F. (1978) Environmental hazards to offshore operations. *In* "Environmental Assessment of the Alaskan Continental Shelf; Interim Synthesis: Beaufort/Chukchi," NOAA/ERL Boulder, CO., p. 335-348.

l) Kovacs, A. (1978) Radar profile of a multiyear pressure ridge. *Arctic, 31(1)*.

m) Kovacs, A. and D.S. Sodhi (1979) Ice pile-up and ride-up on arctic and subarctic beaches, 5th Int. Conf. on Portland Ocean Engineering Under Arctic Conditions, Trondheim, Norway.

n) Tucker, W.B., Weeks, W.F., and Frank, M. (1979) Sea ice ridging over the Alaskan continental shelf. *Journal of Geophysical Research, 84 (C8)*, p. 4885-97; also published as *CRREL Report 79-8*, 24 pp.

o) Weller, G. and Weeks, W.F. (1979) Problems of offshore oil drilling in the Beaufort Sea. The *Northern Engineer 10(4)*, p. 4-11.

p) Weeks, W.F. and Gow, A.J. (1979) Crystal alignments in the fast ice of Arctic Alaska. *CRREL Report 79-22*, 21 pp.

q) Kovacs, A. and R.M. Morey (1979) Anisotropic properties of sea ice in the 50-150 MH_2 range. *Jl. Geophys. Res.*, Vol. 84, C9; also given at Int. Workshop on Remote Estimation Sea Ice Thickness, Memorial University of Newfoundland, St. Johns, Newfoundland.

r) Kovacs, A. (1979) Recent ice observations in the Alaskan Beaufort Sea federal-state lease area, *Northern Engineer*, Vol. 10, No. 3.

s) Tucker, W.B., Weeks, W.F., Kovacs, A., and Gow, A.J., (1980) Near-shore ice motion at Prudhoe Bay, Alaska. *In* "Sea Ice Processes and Models", R.S. Pritchard, Ed., Univ. of Washington Press, 261-272.

t) Weeks, W.F., Tucker, W.B., Frank, M., and Fungcharoen, S. (1980) Characterization of the surface roughness and floe geometry of the sea ice over the continental shelves of the Beaufort and Chukchi Seas. *In* "Sea Ice Processes and Models", R.S. Pritchard, ed., Univ. of Washington Press, 300-312.

u) Weeks, W.F. and Russer, J. (1980) Ice related environmental problems: Appendix VII. *In* "Environmental Exposure and Design Criteria for Offshore Oil and Gas Structures" Report of the Committee on Offshore Energy Technology of the Marine Board, Assembly of Engineering, National Research Council, Washington, DC, 167-185.

v) Kovacs. A., and D.S. Sodhi (1980) Shore ice pile-up and ride-up; field observations, models, theoretical analyses. *In* "The Seasonal Sea Ice Zone" *Cold Regions Science and Technology, (2)*, 209-88.

w) Kovacs, A. (1980) Some problems associated with radar sea ice profiling. *Cold Regions Research and Engineering Laboratory Technical Note*, 6 p.

x) Kovacs, A. (1980) Remote detection of water under ice covered lakes on the North Slope. *Arctic 31(4)*.

y) Weeks, W.F. (1980) The Seasonal Sea Ice Zone: An Overview. *In* "Workshop on Problems of the Seasonal Sea Ice Zone." *Cold Regions Science and Technology, (2)*, 1-35.

z) Kovacs, A. and R.M. Morey (1980) Investigations of sea ice anisotropy, electromagnetic properties, strength and under ice current orientations, U.S. Army Cold Regions Research and Engineering Laboratory, *CRREL Report 80-20*.

aa) Coon, M.D., Weeks, W.F. and 4 others (1981) Research in Sea Ice Mechanics. Marine Board, Assembly of Engineering, National Academy Press, 80 pp.

2. Reports currently in press.

a) Kovacs, A., R.M. Morey, D.F. Cundy, and G. Decoff (1981) Pooling of oil under sea ice, 6th Int. Conference on Port and Ocean Engineering under Arctic Conditions, University of Laval, Quebec, Canada.

b) Kovacs, A. and D.S. Sodhi (1981) Sea ice piling at Fairway Rock, Bering Strait, Alaska: Observations and Theoretical Analyses, 6th Int. Conference on Port and Ocean Engineering Under Arctic Conditions, University of Laval, Quebec, Canada.

c) Kovacs, A. (1981) Sea ice rubble formations off the northeast Bering Sea and Norton Sound Coasts of Alaska, 6th Int. Conference on Port and Ocean Engineering Under Arctic Conditions, University of Laval, Quebec, Canada.

d) Kovacs, A., D.S. Sodhi, and G.F.N. Cox (1981) Sea ice in the Bering Strait and the Fairway Rock icefoot, U.S. Army Cold Regions Research and Engineering Laboratory, CRREL Report (in draft form).

e) Tucker, W.B. III and J. W. Govoni (1981) Morphological investigations of first-year sea ice pressure ridges, *Cold Regions Science and Technology* (in press).

f) Weeks, W.F., Gow, A.J., and Schertler, R.J. (1981) Ground-truth observations on the radar return from ice-covered North Slope lakes. Cold Regions Research and Engineering Laboratory Report.

g) Weeks, W.F. and Sackinger, W. (1981) The physical environment of arctic Alaska. *In* "National Petroleum Council Report on Arctic Oil and Gas", National Petroleum Council, Washington, D.C.

h) Weeks, W.F. (1981) Sea ice: the potential of remote sensing. *Oceanus*.

3. Reports Currently in preparation

a) Gow, A.J., Weeks, W.F., Olhoeft, G., Kohnen, H. Shapiro, L., Onstott, R., Moore, R., Noguchi, Y., Aota, M., and Tabata, T. (1981). Interrelations between the internal structure and the physical properties of fast ice at Barrow, Alaska" (in preparation).

b) Weeks, W.F., Barnes, P. Rearic, D., and Reimnitz, E., (1981) Statistical aspects of ice gouging on the Alaskan shelf of the Beaufort Sea (in review).

c) Weeks, W. F. (1981) The mechanical properties of sea ice: a status report. *In* "Environmental Constraints and Offshore Petroleum Development" (L. Garrison and P. Teleki, eds) Marcel Dekker Inc. (in preparation).

VI. DISCUSSION

a) Kovacs successfully completed a field survey of rubble fields, ice pile-ups, and override features in Norton Sound and along the Chukchi and Beaufort Coasts during March and April 1981.

The 1980 observations of rubble pile formations in Norton Sound have been written up for presentation at POAC-81, see Results.

Continuation of field studies along the Norton Sound, Chukchi Sea, and Beaufort Sea coasts for March-April 1981 were in preparation.

A report on ice piling around Fairway Rock was completed for presentation at POAC-81, see Results.

b) Weeks successfully completed laser profilometery flights into the Bering, Chukchi, and Beaufort Seas during March 1981.

c) Tucker and Govoni successfully completed a series of measurements on pressure ridge characteristics which included approximately 60 pressure ridges along the Beaufort Coast north of Deadhorse in April 1981.

d) The report on sea ice gouging is currently in the final review stage. It will be submitted to *Journal of Geophysical Research* for publication.

e) The completion of the report on SLAR imagery from frozen North Slope lakes completes this particular study. No more work is contemplated in this subject area as the technique has now both been verified and shown to be useful.

VII. CONCLUSION

Field operations this season have been very successful. Data analysis and report writing are proceeding on schedule.

VIII. NEED FOR FURTHER STUDY

There is a great need to extend many of the observations made under this program so that improved time series can be obtained. There is also a need for improved and expanded studies in sea ice mechanics. Unfortunately, project funding levels are now at a level that does not allow for adequate field programs. Next fiscal year we plan to focus on completing the analysis of existing data.

IX. SUMMARY OF JAN-MAR QUARTER

Project personnel were primarily involved in data analysis, report writing and preparation for field studies. Weeks and Frank completed a series of laser profilometer flights and Kovacs and Cox started field work in Norton Sound.

Reporting Period	01-5-022-231
Contract No.	RU105
Research Unit No.	1 Apr 1980 - 31 Mar 1981
Number of Pages	18

ANNUAL REPORT

DELINEATION AND ENGINEERING CHARACTERISTICS OF PERMAFROST BENEATH THE BEAUFORT SEA

Principal Investigators:

P.V. Sellmann
K.G. Neave
E.J. Chamberlain

Associate Investigator:

A.J. Delaney

1 April 1981

Prepared for the BLM-NOAA Arctic Outer
Continental Shelf Environmental Assessment Program

UNITED STATES ARMY CORPS OF ENGINEERS
COLD REGIONS RESEARCH AND ENGINEERING LABORATORY
HANOVER, NEW HAMPSHIRE, U.S.A.

I. Summary

Velocity data derived from the study of industry seismic records from lease area #71 indicate that bonded permafrost is common. Its distribution will likely be as variable as it is to the east near Prudhoe Bay. Bonded permafrost should extend many kilometers offshore of the islands in the eastern part of the lease area. The velocity data for Harrison Bay suggest that bonded permafrost can be grouped into two categories. In the eastern part of the bay there is an orderly transition away from the shore, with the depth to bonded permafrost increasing and velocity decreasing with distance from shore until it is no longer apparent as high velocity material. In the western part of the bay it is less orderly, possibly reflecting the history of the original land surface. This western region may have been an extension of the low coastal plain characterized by the region north of Teshekpuk Lake, which could have contained deep thaw lakes.

Along some lines the high velocity material in Harrison Bay extends approximately 25 km offshore, as shown in the selected cross sections in Figures 1 and 2. The seismic velocities observed in the Harrison Bay region are shown in Figure 3. The low velocity peak is usually associated with thawed material and the higher velocities (>2.0 km/s) are representative of chemically or ice indurated material.

Additional seismic data from the Prudhoe Bay region indicate that ice-bonded permafrost can extend at least 15 km north of Reindeer Island.

Natural attenuation of the high frequency part of the seismic signals was frequently observed in the Harrison Bay region, and was interpreted to indicate that shallow gas may be common.

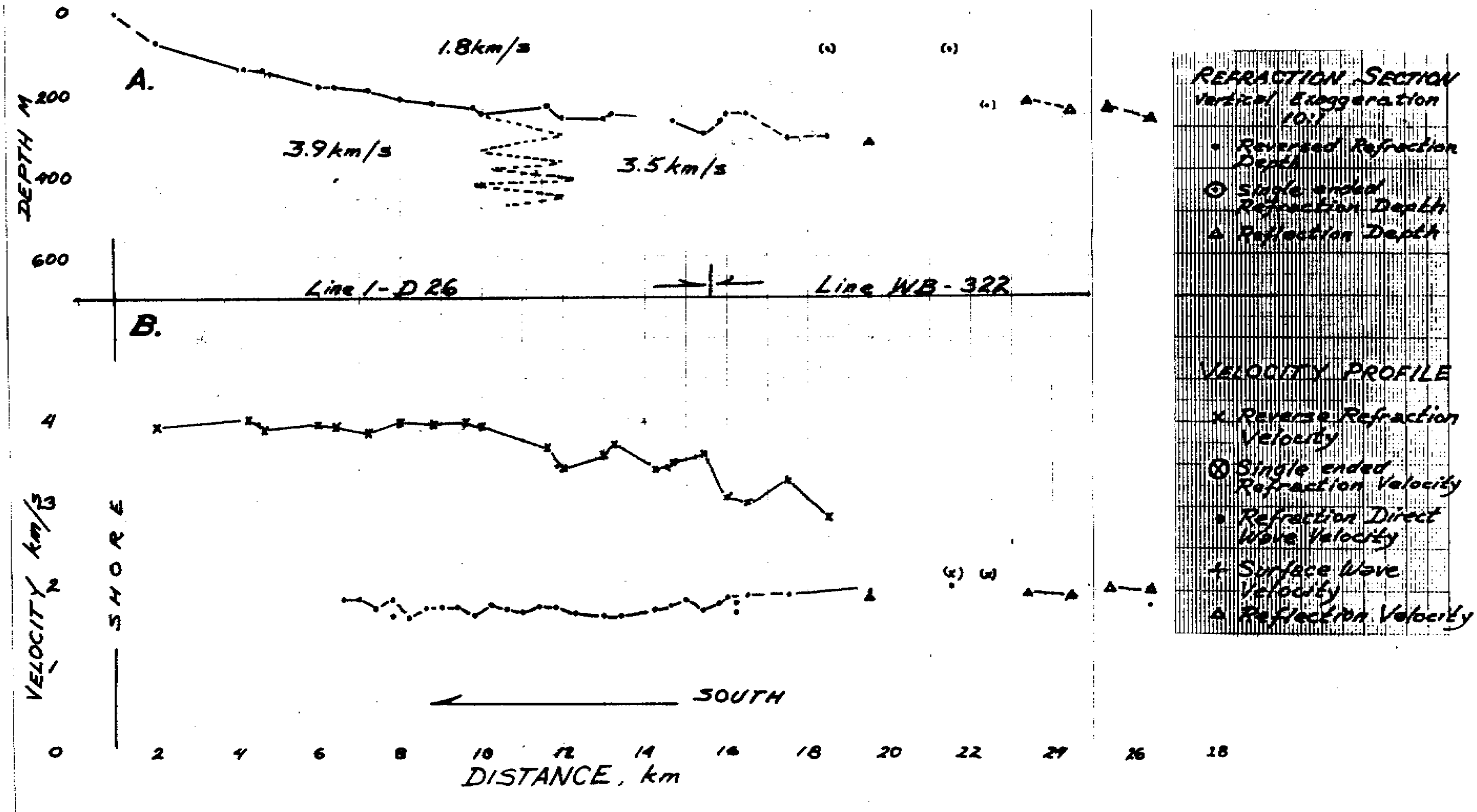

Figure 1. Velocity cross section from the eastern part of Harrison Bay. Shotline locations shown in Figure 4.

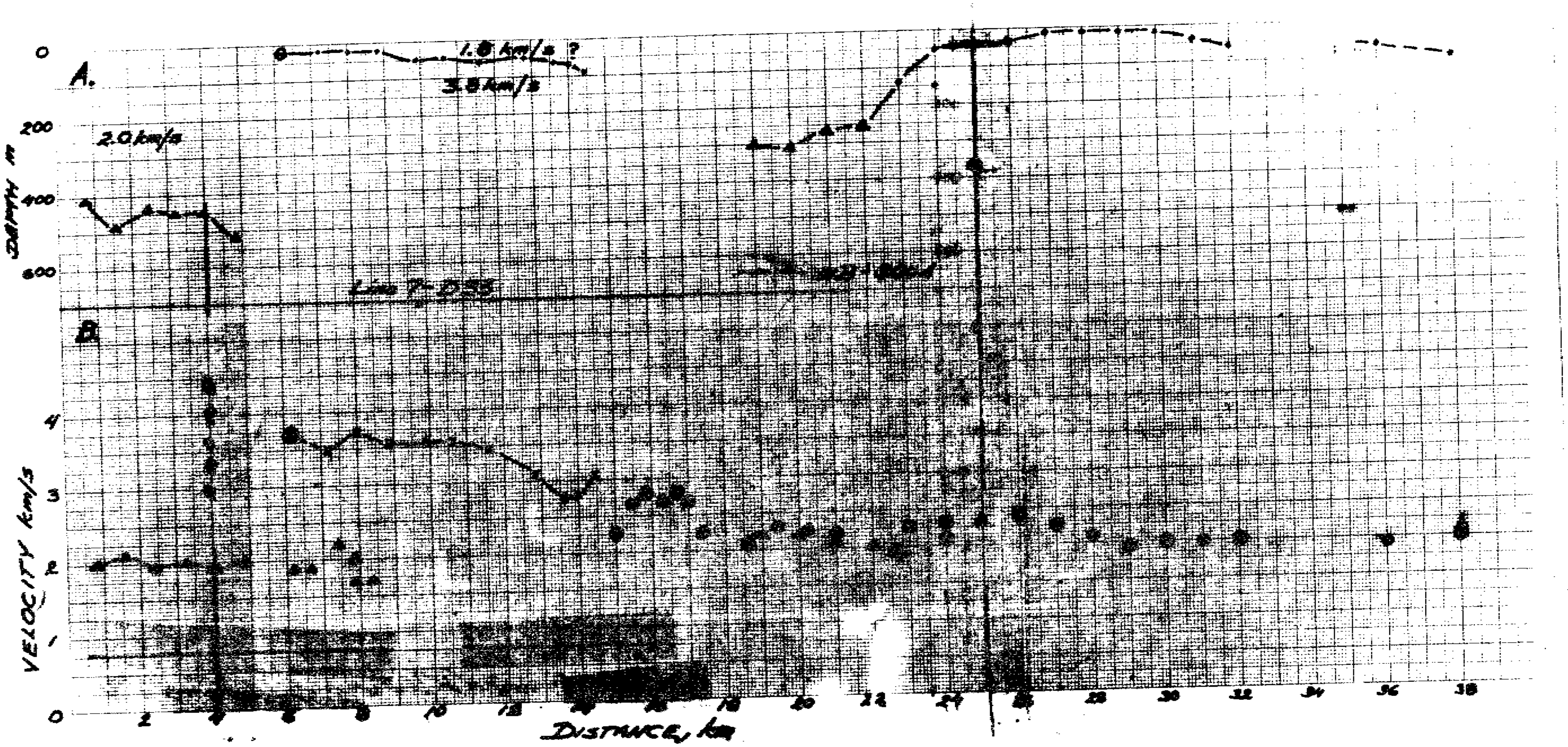

Figure 2. Velocity cross section from the western part of Harrison Bay, Shotline locations shown in Figure 4. Symbols are identified in Figure 1a.

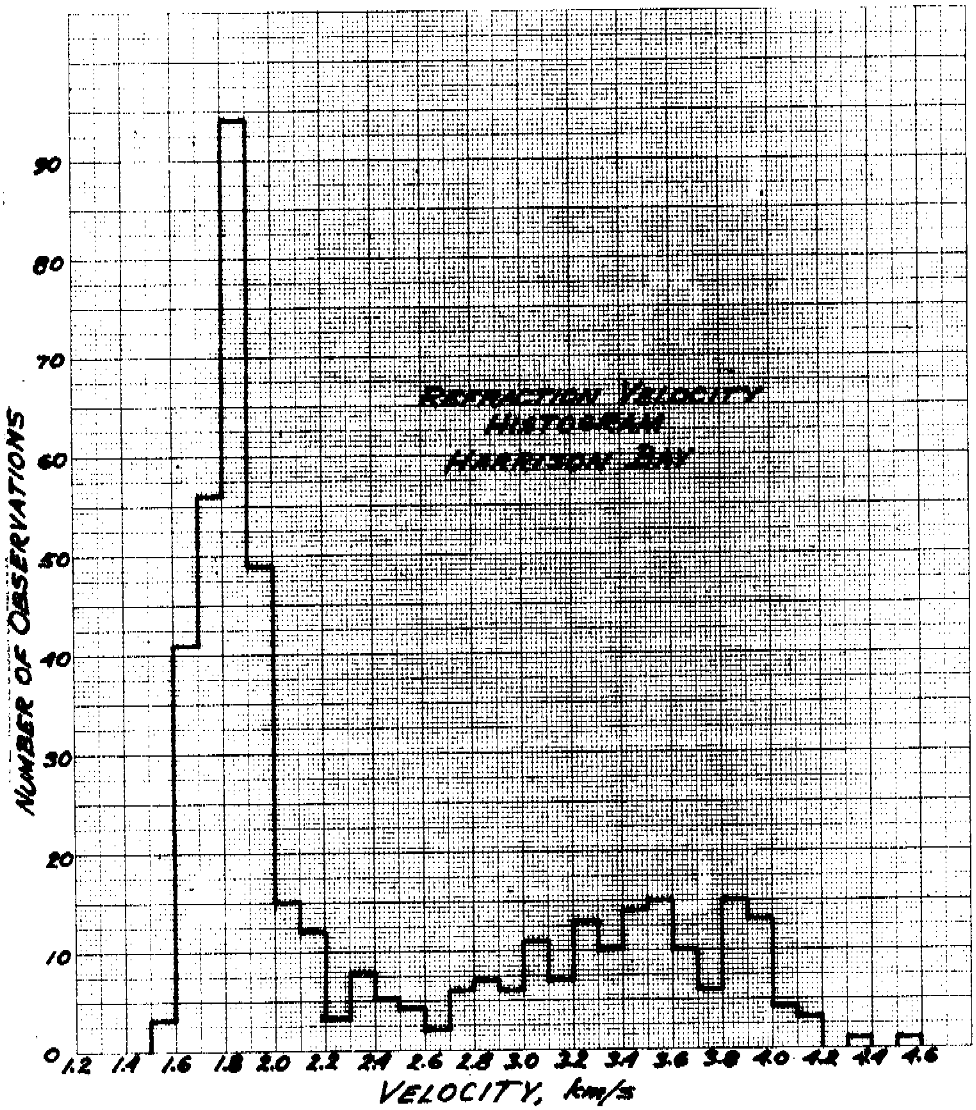

Figure 3. Velocity data from refraction analysis of Harrison Bay ice records and adjacent marine records. Lines are those shown clustered in Harrison Bay in Figure 4.

II. Introduction

The objectives of the 1981 CRREL subsea permafrost program were to obtain information on the distribution and properties of permafrost in the Beaufort Sea through study of seismic records, with emphasis on lease area #71. This investigation was based on interpretation of monitor seismic records from petroleum exploration programs. The first-return data used included data from the Naval Petroleum Reserve, Alaska (NPRA), speculative and nonproprietary data from Western Geophysical and Geophysical Services Inc., and data released by British Petroleum. Even though the emphasis was on the area around Harrison Bay, a limited amount of data from as far west as Point Barrow was examined. The distribution of the lines examined in the lease area is shown in Figure 4. Additional lines further to the west were examined and will be discussed in future reports. Most of the effort was expended on the lines clustered in Harrison Bay; the results are covered in this report. The composite represents more than 1700 km of seismic line. The bulk of the data in Figure 4, shown by solid lines, was received in February and therefore analysis of the longer offshore marine lines is only partially complete.

The data from inlets, shoreline transitions, and other shallow water coastal areas were from winter surveys conducted over the ice; all other deeper water data were from conventional open water marine surveys. Current ice survey data were not appropriate for this study, since vibrators were used as the energy source.

The information on permafrost distribution and properties of the offshore sediments was inferred from consideration of velocities and frequency

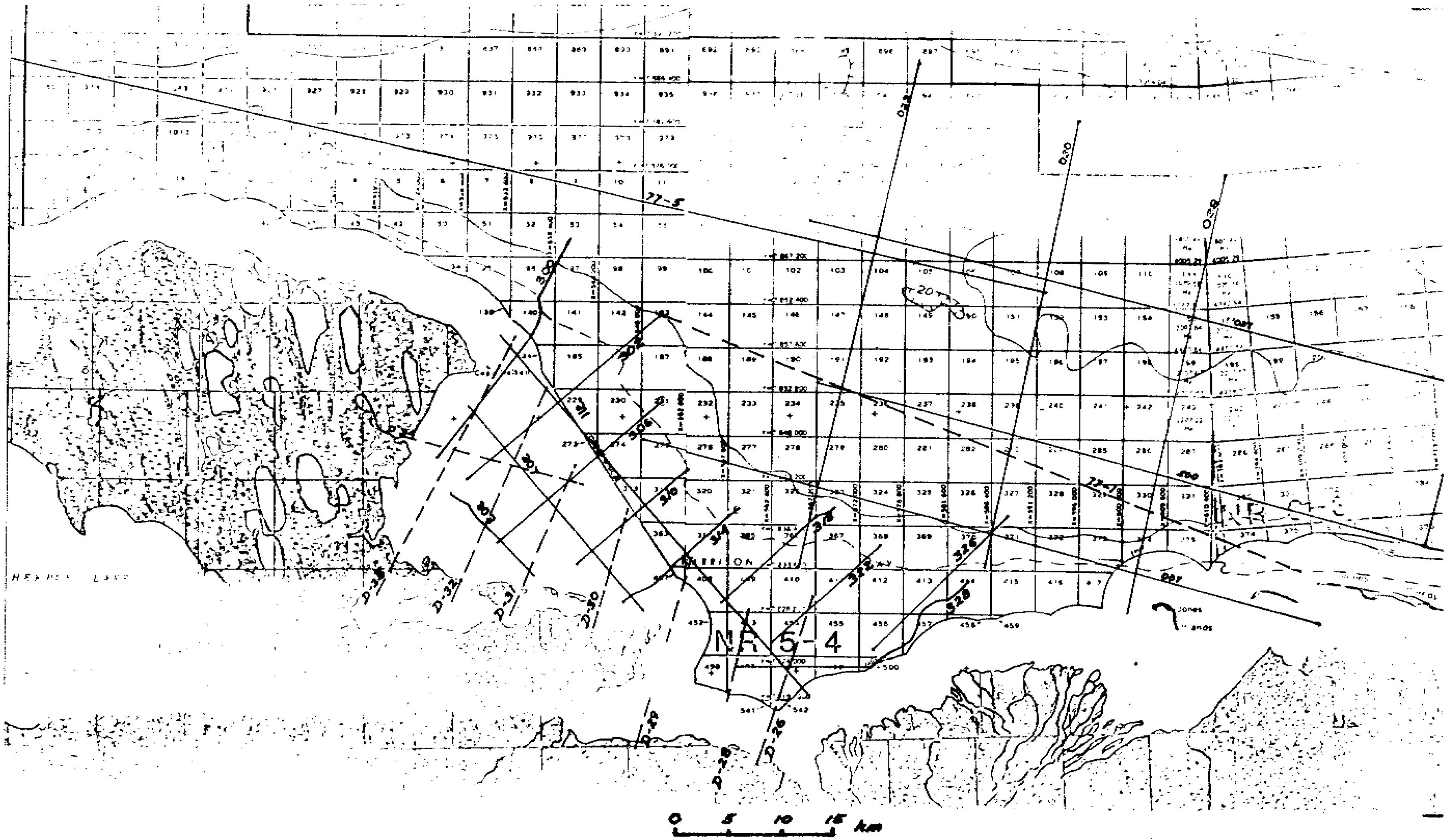

Figure 4. Index map of lines studies in Harrison Bay. Dashed lines are from an ice survey.

content (degree of attenuation of the return signals). Direct, refracted, reflected and surface wave data were obtained. Analysis included determination of velocity distribution and structure. Hyperbolic reflections were also examined to determine how they might be used to obtain sediment velocity data[1].

Record quality and signal characteristics also appeared to be an important qualitative means of determining variations in the properties of subsea materials. Factors considered include attenuation of high frequencies and identification of scattered or incoherent signals.

The data were used to construct velocity profiles, including velocity structure. Maps of near-surface velocities and zones where sediment properties are anomalous with respect to signal characteristics were also constructed.

III. Current State of Knowledge

Information on this region is based primarily on seismic studies. No drilling and sample analysis was done, although temperature data were obtained as part of Osterkamp and Harrison's program from shallow probe observations. The lack of core analysis has resulted in critical data gaps, particularly since results from the past program to the east cannot be extrapolated into this region because of contrasting geology and material types.

Topics for which no data have been acquired include 1) ground ice volume, 2) position of ice-bonded permafrost, 3) sediment type distribution, 4) strength properties, 5) index properties, 6) overconsolidation of

[1] Neave, K.G., P.V. Sellmann and A.J. Delaney (1981) Hyperbolic reflections on Beaufort Sea seismic records. CRREL Report 81-2, 16 p.

sediments, 7) gas distribution, and 8) deep temperature data.

At this time we have only a general idea about permafrost in the proposed lease area based on indirect observations. If the high velocity material observed offshore is bonded permafrost we can speculate about regional permafrost distribution in Harrison Bay as will be covered in this report.

IV. Study Area

Seismic records used for this year's study were selected from the shotlines shown in Figure 4.

V. Sources, Methods and Rationale of Data Collection

Velocity Study

The basis for this study is that noticeable changes in seismic velocities occur between frozen and unfrozen unconsolidated materials[2]. The contrast is often most apparent when the moisture content of the materials is near saturation. This fact and the existence of large amounts of seismic data from surveys conducted for petroleum exploration activities makes the study of the distribution of ice-bonded subsea permafrost by seismic techniques a reasonable approach. When records are available, and their quality and field recording parameters are appropriate, permafrost data can be extracted. The records can permit determination of direct wave velocities and refraction interpretation of the first returns for information on velocity structure. The velocity data can then provide the basis for predicting the distribution of ice-bonded permafrost and, when resolu-

---

2 Aptikaev, F.F. (1964) Temperature field effect on the distribution of seismic velocities in the permafrost zone. Akad. Nauk SSR, Sibirskoe otd-ie. Inst. Merzlotovedeniia. Teplovye protesessy v merzlykh porod.

tion is adequate, the depth to the top of the frozen sediments.

The offshore marine data used for this study were obtained by GSI with a 2350-m hydrophone array with a phone group spacing of 50 m, and multiple air guns for an energy source. The ice-shooting data were obtained with a 4800-m line on the ice surface, a group interval of 100 m, and explosive charges for the energy source.

The data are normally processed for petroleum exploration with emphasis on deep targets, commonly with first break suppression, increased gain with depth, and normal moveout corrections. These procedures tend to compromise the quality of the data from the near surface. In an attempt to obtain as much as possible from the records without costly processing, approximately the first 2 seconds of data were played back from the field tapes with expanded gain. They were printed in a wiggletrace or variable area format, without normal moveout corrections.

Resolution of Data

The resolution of this type of study is obviously not as great as can be obtained from a seismic investigation designed for the study of offshore permafrost. The resolution is variable and depends on a number of factors, including geophone spacing, signal frequency, and complexity of the subsurface. In general, the horizontal resolution of the data covered in this report, based on refraction interpretation of the compressional waves, should be a minimum of three phone spacings. This suggests that the minimum horizontal extent of a feature that can be detected is around 300 m for the ice-shooting data, and around 150 m for the marine survey data. The minimum vertical thickness of a detectable high-velocity layer is determined by the wavelength of the signal source, with resolution possible around 1/2 wavelength[3]. Therefore, the minimum vertical thickness of a detectable high-velocity layer is probably limited to about 50 m.

The resolution of the surface wave signal is also dependent on the wavelength involved. Ewing et al.[4] showed that a layer must be thicker than 0.6 wavelength in order to carry a signal which has no dispersion. Accordingly, the surface waves should be visible on the ice-shooting records where the surface thaw zone is approximately 25 m thick.

Natural Filtering (Attenuation)

The attenuation phenomenon is of considerable interest because strong attenuation has been associated with the presence of gas in the pores of sediments. A number of laboratory studies have shown that pore gas concentrations as low as a few percent by volume can cause an increase of attenuation up to two orders of magnitude over the water-saturated values. The high attenuation on Harrison Bay records could be explained by the presence of natural gas in the sediments. When natural gas occurs in shallow sediments, it can present a hazard to drilling or construction projects if adequate precautions are not used. If the natural gas is present at depths greater than 200 m in a permafrost environment, there is likely to be an associated hydrate phase which can also cause hazards to drilling operations.

The high frequency part of the signal was filtered on so many of the

---

[3] Sherwood, J.W.C. (1967) Refraction along imbedded high speed layer. In: Seismic Refraction Prospecting, Society of Exploration Geophysics, p. 138-151.

[4] Ewing, W.M., W.S. Jardetzky and F. Press (1967) Elastic waves in layered media. New York: McGraw-Hill, 380 p.

records that this phenomenon was examined. The areas in Harrison Bay where this occurred were mapped as shown in Figure 5. No formal attempt was made to determine the attenuation coefficients for comparison with existing data on marine sediments. This procedure would require frequency spectral analysis to establish relative amplitudes at the different frequencies. However, since this was not possible with the available records and equipment a simple qualitative procedure was used.

The records examined normally have a peak frequency of 30 to 40 Hz, and all records with peak frequencies lower than 15 Hz were classed as having been subject to considerable natural filtering and are those grouped in the attenuation zones in Figure 5.

In Harrison Bay the attenuated rays penetrate to a depth of 100-300 m and the reflected rays penetrate to 200-400 m as determined by standard refraction and reflection interpretation. As a result we describe the attenuation as a "shallow" anomaly.

Seismic Noise

The distribution of seismic noise was examined because many natural seismic sources appeared to be active close to the receiver array. Figure 6 shows a strong event which originated 50-75 ms after the shot and at a distance of about 1 km behind the boat. Signal characteristics of these events suggest that the energy source originated below the seabed.

These natural sources are of interest because they imply abundant storage of natural energy in the environment.

VI. and VII. Results and Discussion

Seismic Data Interpretation

The two cross sections (Figures 1 and 2) represent the two different

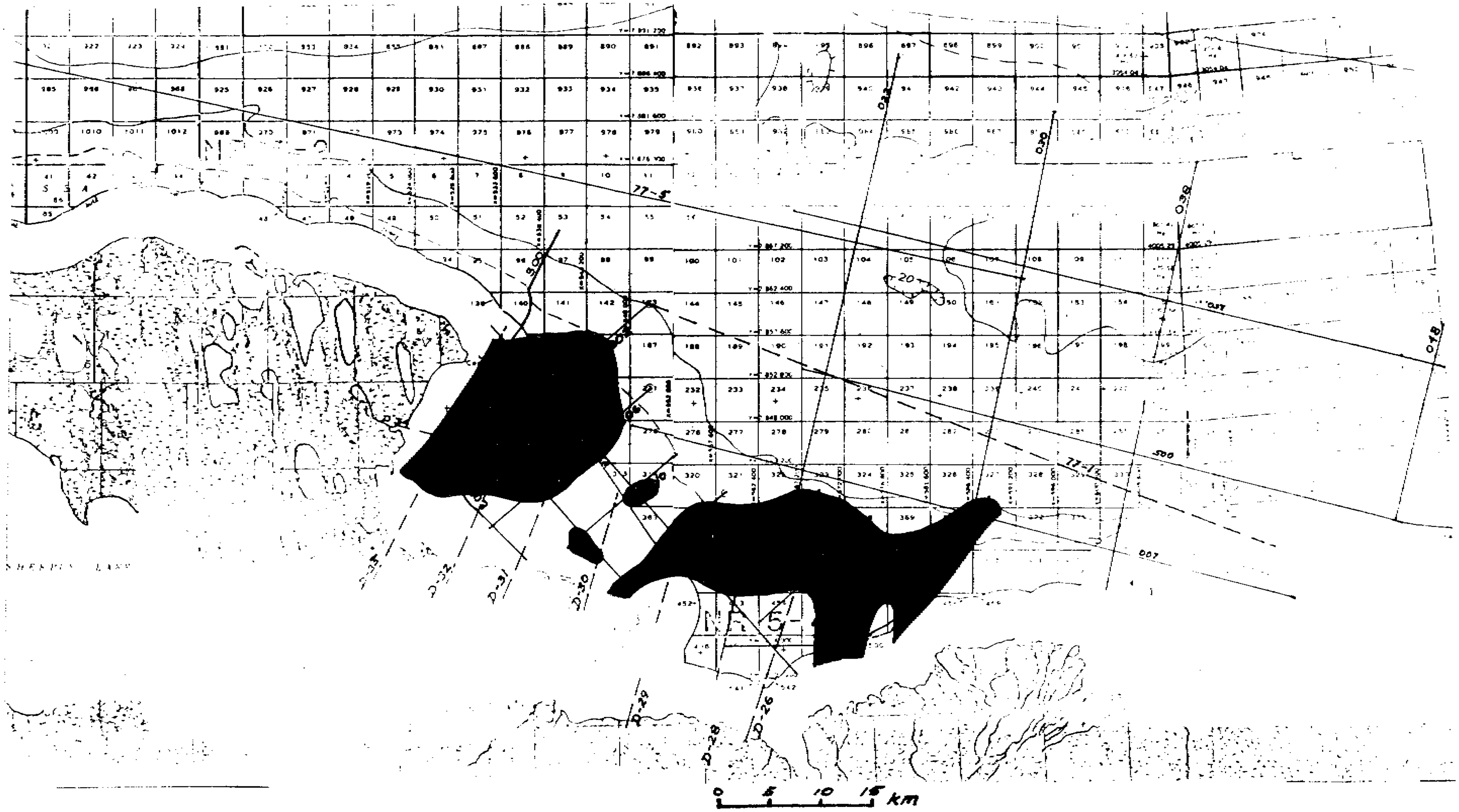

Figure 5. The high-frequency part of the seismic signals has been naturally filtered in the shaded zones. These zones have been interpreted to represent areas where "shallow" gas is likely to occur.

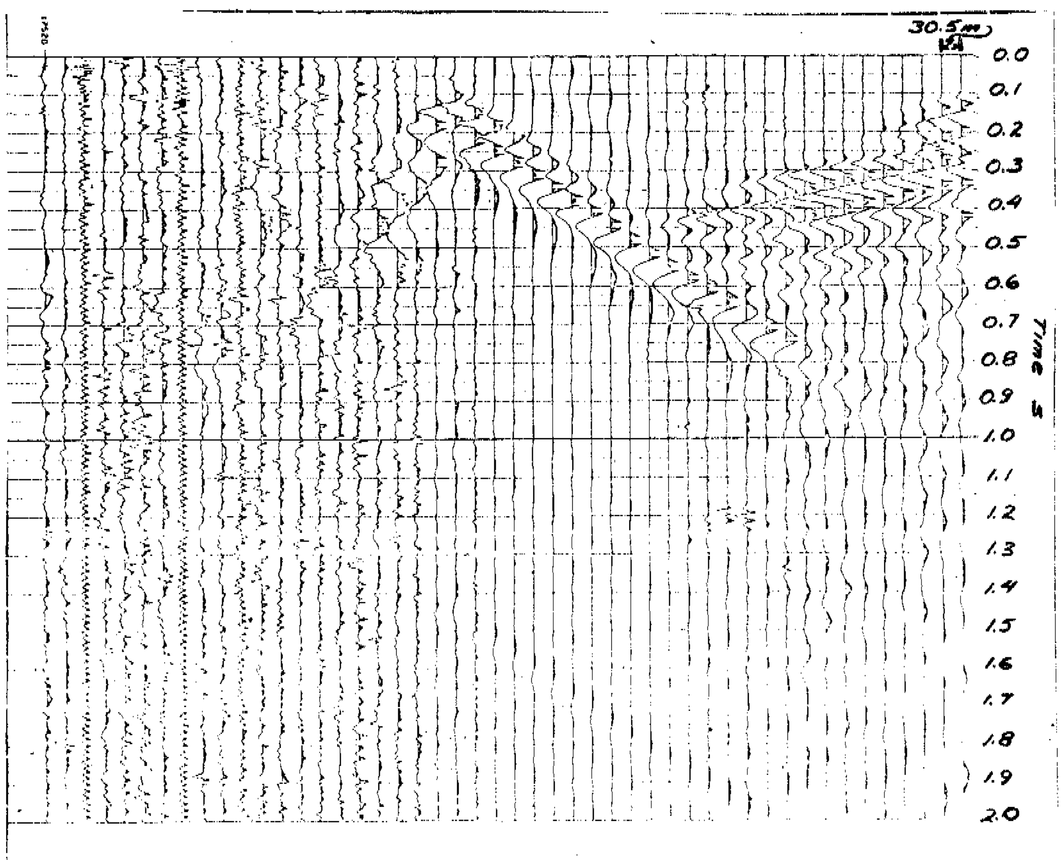

Figure 6. Natural seismic noise from a strong event observed in this region.

velocity regimes found in Harrison Bay. Both lines have a high velocity structure extending 25 km offshore. The eastern line (Figure 1a) shows a systematic thickening of the first layer (low velocity layer) with increasing distance from shore. The velocity of this upper layer (1.8 km/s) falls in the range that represents little or no ice-bonding of the sediments. The second layer has velocities of 3-4 km/s, values consistent with ice-bonded material. In addition, the lower layer velocity decreases with distance from shore (Figure 1b) suggesting that there has been partial melting of the second layer during progressive degradation and inundation of the permafrost. This combination of a thickening low velocity layer and a decrease in velocity of the second layer with distance from shore is a reasonable indicator that the lower unit represents bonded permafrost. The depth of this layer is greater than expected compared to observations near Prudhoe Bay, which should indicate different geology and permafrost degradation processes in this region.

The second set of profiles (Figure 2) illustrates the greater complexity encountered in the western half of Harrison Bay. Four separate velocity zones are encountered along this line. The first segment, including the onshore records and several offshore records, is anomalous because of the low velocities. A second segment near the shore has a shallow, high velocity refractor. The remaining offshore half of the line has two more distinct zones of material that may be partially bonded or represent a change in material type, one deep zone and one shallow zone.

Velocity cross sections like those discussed above were constructed for all the shotlines in Harrison Bay shown in Figure 4. These velocity data appear to provide some insight into the distribution of bonded permafrost when compiled on the map for this area (Figure 7). The velocity zone nearest shore indicates a two-layer situation. The deeper high velocity layer in this zone increases in depth and decreases in velocity with distance from shore, as indicated by a high velocity refractor. Continuing offshore, the next zone is characterized by a deep reflector, suggesting continuation of the high velocity structure (Figure 7).

The region beyond this zone lacks high velocities, making it difficult to determine if materials are ice-bonded. However, slight velocity increases and inversions may suggest that some ice-bonded sediment may exist. The high velocity materials are most common out to the 13-m isobath and are interpreted to represent ice-bonded permafrost.

Natural Filtering (Attenuation)

The mapped zones in Figure 5 represent areas where the dominant frequency of the reflected or refracted signals was reduced from approximately 30 Hz to less than 15 Hz. This phenomenon can best be explained by the presence of gas in the pores of the shallow sediments. As a result, the areas on the map have been interpreted as probable locations where free gas is trapped in the sediment somewhere in the depth range of 20–300 m. It can also be inferred that because there appears to be shallow gas above an ice-bonded layer a strong probability exists that there is gas in hydrate form within and below the ice-bonded layer.

Seismic Noise

The region in which seismic noise was observed on the records is shown in Figure 8. The distribution of the noise appears to correspond with both

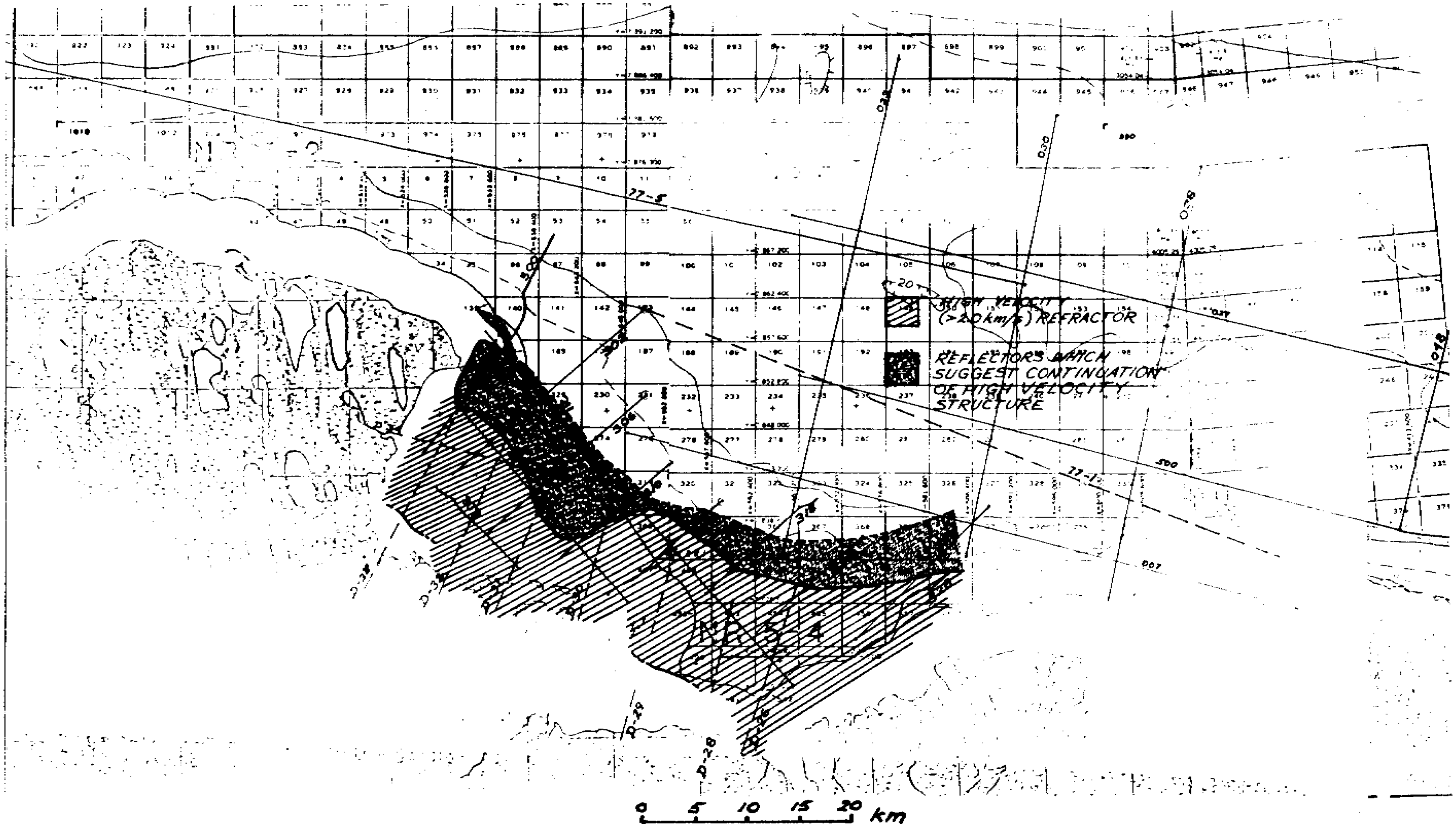

Figure 7. Distribution of high-velocity material in Harrison Bay, based on the shotlines clustered in the bay.

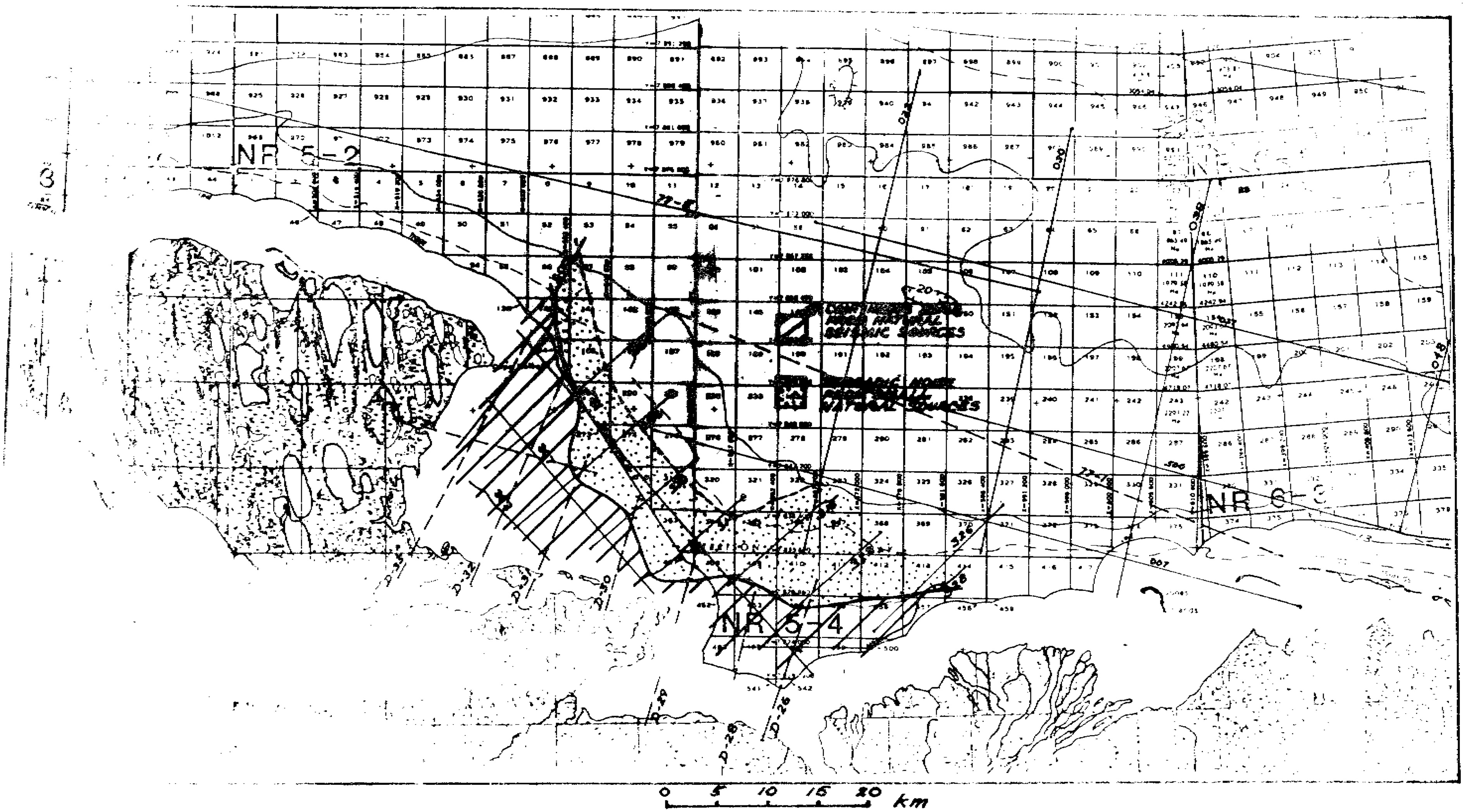

Figure 5. Distribution of natural seismic noise in Harrison Bay.

the location of high velocity material thought to be bonded permafrost and with areas in which shallow gas might occur. This suggests that the noise could be related to energy released during permafrost degradation. This energy might originate from expanding gas or dynamic adjustment of seabed material, including possible failure or settlement. A number of spurious sources of seismic energy have been considered and rejected, including surf and ice-generated energy. These alternatives were rejected because the geographic distribution of the noise does not appear to favor them.

VIII. Conclusions

The velocity profiles suggest that bonded permafrost is common in this region, with considerable variability, depending on the local geology. Distribution of permafrost similar to that observed near Prudhoe Bay should be anticipated in regions containing offshore islands. In these regions it is anticipated that bonded permafrost will extend many kilometers beyond the offshore islands and may be found at shallow depths (<10 m). In Harrison Bay the seismic data indicate that at least two distinct permafrost settings appear to exist. The offshore extent of the high velocity bonded permafrost in Harrison Bay appears to be at least 25 km from shore. This study also indicates that bonded permafrost may be modified to depths as great as 300 m in Harrison Bay.

The natural filtering of the high frequency part of the seismic record common in Harrison Bay can be interpreted as an indicator of free gas in the section above the frozen sediments. This could mean that gas hydrates occur at depth and may be the source of the free gas which was liberated as permafrost thawed.

The seismic noise observed in the nearshore area may be an indication of the thermal modification of this extensive zone of bonded permafrost now covered by the sea.

The most obvious lack of data for this region is due to the absence of control normally provided by drilling. This has greatly increased the amount of speculation required as part of our analysis of seismic data.

Annual Report Task D-9
Research Units 204 and 473
April, 1980 - March, 1981

OFFSHORE PERMAFROST STUDIES AND SHORELINE HISTORY AS AN AID TO PREDICTING OFFSHORE PERMAFROST CONDITIONS

Prepared by

D. M. Hopkins and P. A. Smith

U.S. Geological Survey
345 Middlefield Road
Menlo Park CA 94025

Table of Contents

INTRODUCTION

Research Units (R.U.) 473 and 204 combine attempts to delineate the distribution and characteristics of offshore permafrost, to identify possible sources of sand and gravel fill, and to determine the nature and rates of coastal processes in the arctic, using cores from offshore boreholes, observations of morphology of the coast, and observations and samples of material exposed in coastal bluffs. During 1980, our work has consisted chiefly of a continuing laboratory analysis of sediments and fossils recovered in offshore boreholes in the Joint Lease Sale area and field studies of the coast of the William O. Douglas Arctic Wildlife Range between the mouth of the Canning River and Demarcation Bay and of the coast of Chukchi Sea between Barrow and Peard Bay.

The borehole study utilizes cuttings and cores from offshore boreholes obtained by this and other OCSEAP projects through the shorefast ice during spring, 1976 and spring, 1977 and boreholes obtained through shorefast ice by the Conservation Division of the U.S. Geological Survey in spring, 1979. Results of geothermal and geotechnical studies of these boreholes have been published in the 1977-1980 Annual Reports of R.U. 105 and 204 and in the two volume report by Harding-Lawson Associates, "U.S.G.S. Geotechnical Investigation, Beaufort Sea, 1979" (U.S. Geological Survey Open File Report, 1979). Preliminary reports on paleontological and stratigraphic studies of samples from the offshore boreholes have been published in the 1977-1980 Annual Reports of R.U. 204. During 1981 work on offshore borehole samples consisted of identification and age assignments based on fossil foraminifera and ostracodes and development of a model for sea-level history based on these studies. The paleoclimatic and sea-level history provided by the borehole studies is combined with seismic and thermal information from other investigations (R.U. 105, 253, 271) to determine the thickness of and depth to permafrost and to map the sand- and gravel-filled paleovalleys of major rivers that formerly extended across the exposed Beaufort Sea shelf.

R.U. 473 involves study of the coasts of the northern Chukchi and the Beaufort Seas. The work involves excavation of sections in coastal bluffs and fluvial terraces near the coast and sampling of these exposures for microfossil analyses, geochronological studies, mollusk and bone identification, and grain-size analyses, as well as consideration of the nature and abundance of ice in the permafrost. Mollusk collections from modern beaches have also been made in an attempt to define the living fauna along the arctic coast of Alaska. During earlier years, driftwood lines along estuaries and bluffs were mapped to determine storm-surge limits, and sequential maps and air photos were analyzed to determine rates of coastal erosion and barrier-island migration. During 1980, fieldwork was concentrated along the coast of the William O. Douglas Arctic Wildlife Range from the mouth of the Canning River to the vicinity of Demarcation Bay and on the coast of the Chukchi Sea between Barrow and Peard Bay.

In the coastal study we have now examined about 60% of the arctic coast between Icy Cape on the Chukchi Sea and Demarcation Point on the Beaufort Sea.

SUMMARY OF FIELD ACTIVITIES

1) The coastline of the Beautfort Sea from the mouth of the Canning River to Beaufort Lagoon was examined during the months of July and August, 1980 by a five-member team consisting of: D. M. Hopkins (principal investigator), R. W. Hartz, R. E. Nelson and S. Pounder, all of the U.S. Geological Survey, and M. Sweeney of the University of Alaska.

2) The coastline of the northern Chukchi Sea from Point Barrow to Peard Bay was studied by Julie Brigham, U.S. Geological Survey and University of Colorado, and Terry Allen, University of Colorado, during July and August of 1980.

SUMMARY OF LABORATORY ACTIVITIES

1) Microfossils from 4 boreholes from the 1979 drilling program have been examined, summary charts and a tentative correlation chart comparing the boreholes have been drafted and appear as appendix A of this report.

2) Mollusks from modern beach and coastal bluffs at 14 locations have been identified. Subsamples from 5 locations have been sent to the Institute of Arctic and Alpine Research at the University of Colorado for amino-acid racemization studies.

3) Four samples from coastal exposures excavated during the summer of 1980 have been submitted for radiocarbon dating, further samples are ready for submission, pending earlier results.

4) Pollen samples from six sites visited during 1980 have been sent out for processing.

5) Five samples from a particularly interesting coastal bluff exposure informally named "Cookie's Bluff" have been washed, sieved, and picked for plant and insect remains.

6) Grain size analyses of 5 samples from "Cookie's Bluff" are in progress.

7) Radiocarbon dates from 5 locations have been received this year and are presented, along with a discussion of their significance, as appendix C of this report.

PROBLEMS ENCOUNTERED

1) A decision by the USGS to renovate the building housing our office necessitated moving our office shortly after returning from the field. This move resulted in a loss of about two months of time for analytical work.

2) A mid-year leave of six months by P. A. Smith and the resignation of R. W. Hartz after the end of the field season have also resulted in a delay in the processing of samples and the analysis of results.

Funds Expended: All

PAPERS IN PRINT

Herman, Y., and Hopkins, D. M., 1980, Arctic oceanic climate in late Cenozoic time: Science, v. 209, p. 557-562.

Hopkins, D. M., Smith, P. A., and Matthews, J. V., Jr., 1981, Dated wood from Alaska and the Yukon: implications for forest refugia in Beringia: Quaternary Research, v. 15, p. 217-249.

Miller, G. H., and Hopkins, D. M., 1980, Degradation of molluscan shell protein by lava-induced transient heat flow, Pribilof Islands, Alaska: implications for amino acid geochronology and radiocarbon dating, p. 445-451, _in_ Hare, P. E., Hoering, T. C., and King, K., Jr., eds., Biogeochemistry of amino acids: New York, John Wiley & Sons, 558 p.

PAPERS IN PRESS OR IN PREPARATION

Hamilton, T. D., and Hopkins, D. M., in preparation, Correlation of northern Alaskan glacial deposits: a provisional stratigraphic framework: U.S. Geological Survey Circular 822.

Hopkins, D. M., in preparation, Hard times in Beringia.

Hopkins, D. M., Matthews, J. V., Jr., Schweger, C. E., and Young, S. B., eds., in preparation, Paleoecology of Beringia: Academic Press.

Nelson, R. E., and Hopkins, D. M., in preparation, Late Quaternary glaciation and snowline history in the Grand Central River Valley, Seward Peninsula, Alaska.

Porter, L., and Hopkins, D. M., in preparation, Butchered caribou skulls, Pleistocene and Recent, from eastern Beringia: American Antiquity.

Swanson, S. E., Turner, D. L., Forbes, R. B., and Hopkins, D. M., 1981, Petrology and geochronology of Tertiary and Quaternary basalts from the Seward Peninsula, western Alaska: Geological Society of America, Program with Abstracts.

Taylor, A., Woo, G. S., Hopkins, D. M. Prager, E. M., and Wilson, A. C., in preparation, Electron microscopy of mammoth tissues: an overview: Science.

Weber, F. R., Hamilton, T. D., Hopkins, D. M., Repenning, C. A., and Haas, H., 1981, Canyon Creek: a late Pleistocene vertebrate locality in interior Alaska: Quaternary Research., v. 15.

RESULTS AND ACCOMPLISHMENTS

Fieldwork was completed for an inventory of on-land supplies of sand and gravel in coastal areas of the Arctic Wildlife Range between the Canning River and Beaufort Lagoon, but compilation is still in progress. Generally speaking, gravel is available beneath overburden less than 1 or 2 m thick in the broad, barren floodplains and the low terraces of the major streams. Upland areas away from river bars and low terraces between the Sadlerochit River and Beaufort Lagoon are underlain by ice-rich pebbly sand. Peat and silt overburden 1 to 3 m thick covers ice-rich pebbly sand up to 10 m thick in upland areas away from stream floodplains and terraces between the Sadlerochit River and Beaufort Lagoon.

Fieldwork in 1980 confirmed previous evidence that the area between Camden and Pokok Bays is undergoing active uplift. The presence in this area of upwarps and faults involving Tertiary marine sediments as young as 20 million years has long been known. Dinter and Grantz have shown that large continental-shelf areas of this segment of the coast have undergone Holocene deformation (deformation less than 10,000 years old), and Biswas' seismic network showed frequent small earthquakes on- and offshore. Our fieldwork established that shorelines about 120,000 and 80,000 years old have been uplifted at least several meters and probably much more.

A previously unrecognized soil type, the cryoturbated peat soil, was recognized in the course of 1980 fieldwork, and insight into time of inception and rate of formation was obtained from radiocarbon-dating. The soil type develops in flat and gently-sloping areas underlain by fine-grained sediments (silt or fine sand) with shallow permafrost. It consists of the following profile:

5-15 cm	Turf--root-bound silty or sandy peat, often dry.
5-45 cm	Silt or silty fine sand: wind-blown material from an unknown source--perhaps the basins of drained thaw lakes.
10-30 cm	Horizontally foliated peat.

Base of annually thawed active layer at 45-55 cm.

35-60 cm	Vertically foliated frozen peat grading down into

150 cm Disturbed frozen peat, predominantly vertically foliated, interspersed with masses and lenses of frozen silt and fine sand. Grades down into silt or fine sand containing clots of peat.

------------Parent material-------------

We interpret this profile to have evolved as follows:

(A) An initial exposed surface (a thinly vegetated upland landscape or bed of a drained lake) becomes colonized by Sphagnum and other mosses and peat accumulation begins.

(B) In early stages of peat accumulation, patterned ground (frost scars, peat rings) form as a result of frost-heaving. As peat continues to accumulate, some masses of silt and fine sand continue to migrate upward, but ultimately the peat forms a complete blanket. The vertical foliation results from expansion of the ground during summer following winter frost-cracking and filling of cracks with ice.

(C) Why peat changes from vertically to horizontally foliated at the frost-table is not yet clear.

D) Neither is it clear why there is consistently a layer of more or less clean silty fine sand at depths of a few centimeters below the surface.

A preliminary radiocarbon date on a cryoturbated peat soil on the shores of Camden Bay indicates that the deepest and presumably oldest peat is about 9,500 years. Dating of the lowest peat in a cryoturbated peat soil developed on the floor of a thaw lake drained in mid-Holocene time indicates that peat accumulation there began about 4,200 years ago, soon after the lake was drained. Figure 1, a copy of field notes and sketch of the upper half of

Figure 1. Example of cryoturbated peat soil location.

(Hp 55) = (Hp-49) Lewellen Map 807-1
Mt. Michelson D-2
Mon Notes - p. 808-1
Cooke's Bluff

12.5 ~~12~~ meter bluff just east of mouth of Carter Creek. Actually its a cut through a broad ridge sloping gently west toward Carter Creek and southward toward a minor drainage entering Carter Creek from right.

The bluffs here are a series of baidzherakhs extending down to beach level, implying presence of syngenetic ice. The sloping surfaces seem an unlikely site for former thaw lakes, & so we (Bob Nelson + I) doubt that ~~this is~~ the peaty deposits at surface are thaw-lake deposits.

These slumped bluffs were ~~clean~~ recently much fresher. Perhaps eroded during 1970 storm surge.

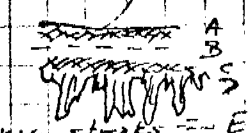

(A) 0.15 Root-bound sandy peat - turf

(B) 0.10 Grayish-yellow fine sand, organic streaks wind blown?

(C) 0.10 Horizontally stratified peaty silt. - base of active layer?

(D) 0.60 Vertically foliated peat + peaty silt.
80 Ahp 55A - Concentration of vertically-oriented twigs 45 cm below top of Unit - C14

(E) 1.4 Cryoturbated mixture of dk brown peat + light grey silt. Contact inclined toward ice-wedge trench.
80 Ahp 55B - Twigs from lowest part of vertical peat streamers (see opp. page)

80.57V Photos: Roll 22

"Cookie's Bluff", represents another location at which this cryoturbated peat soil is present. Samples for radiocarbon dating have been submitted.

Study of our field notes from previous years indicates that cryoturbated peat soils are present throughout the coastal areas of Beaufort Sea from Barrow to Beaufort Lagoon. They are probably present along the coast of Chukchi Sea, as well.

One implication of this developing study is that all of the land-derived organic detritus available to detritivores in Beaufort Sea lagoons must be younger than 9,500 years.

Micropaleontological results of study of 4 of the Harding-Lawson (1979) boreholes are summarized in appendix A. Preliminary results of field studies at Skull Cliff are given in appendix B. Appendix C represents a list of radiocarbon dates on arctic coastal plain samples obtained subsequent to our 1980 Annual Report and prior to March 31, 1981.

APPENDIX A

Preliminary results of foraminifera from boreholes HLA-10, -17, -18, and -19

by

Kristin McDougall

This report gives the result of microfossil analysis of 80 samples from boreholes HLA-10, -17, -18, and -19 drilled on the Beaufort Sea shelf during the winter of 1979 by the Harding Lawson Associates under contract to the U.S. Geological Survey. Location information for these boreholes may be obtained from the 1980 Annual Report for RU 204/473. The occurrence of benthic foraminifers and other microfossils are reported here. Ostracods have been sent to E. Brouwers, Denver, for further study. Interpretations based on benthic foraminifers are preliminary and may change as other boreholes are completed.

Short interpretations of the age and environment of each of the boreholes are given below, followed by Tables A-1 through A-4, which list species of benthic foraminifers identified at sampled intervals throughout each borehole. Figures A-1 through A-4 summarize the lithology, type, diversity, and abundance of key benthic foraminifers, along with an interpretation of the age and ecology represented at each interval. Figure A-5 represents a tentative correlation of the 4 boreholes.

BOREHOLE HLA-10

Age and environment: Foraminiferal assemblages in this borehole are indicative of the Holocene (samples 12.1 to 12.2 and 12.5 to 13.0 feet) and Sangamon (samples from 62.5 to 70.9 feet). The Holocene samples contain some reworked Sangamon specimens. These specimens are readily

Table A-1. Microfossil identifications in borehole HLA-10.

BOREHOLE 10 Mf 5726

SPECIES \ LOCATION DEPTH (m)	3.63-3.66	3.75-3.90	4.68-4.71	6.60-6.75	18.75 P.I.	18.90-19.05	21.21-21.27
Buccella sp.	<1						
Buccella frigida (Cushman)	11	2			2		8
Elphidium cf. E. asklundi Brotzen	<1						
Elphidium clavatum Cushman	35	14			52	21	25
Elphidium excavatum alba Feyling-Hanssen	20	50					3
Elphidium frigidum Cushman	1	1					
Elphidium incertum (Williamson)	13	10			18		
Elphidium orbiculare (Brady)	2	3			1		14
Elphidium sp.	12	13			1		11
Guttulina dawsoni Cushman and Ozawa	1	2			3	8	<1
Miliolinella chukchiensis Loeblich and Tappan	1	1			3	5	1
Polymorphina suboblongata (Cushman and Ozawa)	<1				6	2	<1
Polymorphina spp.	3	2				2	
Elphidium bartletti Cushman		1					1
Gordiospira arctica Cushman		1					
Cassidulina islandica Norvang					10		15
Laryngosigma hyalascidia Loeblich and Tappan					1		
Quinqueloculina seminulum (Linne)					5	7	
Astrononion gallowayi Loeblich and Tappan							<1
Cassidulina norcrossi Cushman							13
Discorbis baccata (Heron-Allen and Earland)							1
Entosolenia sp.							<1
Lagena gracillima (Sequenza)							1
Nonionella auricula Heron-Allen and Earland							<1
Pyrgo williamsoni (Silvestri)							<1
Triloculina trihedra Loeblich and Tappan							<1
Foram number	2133	4411	0	0	751	16	4012
Ostracod number	257	4601	4	4	9	44	84
Foram diversity	13	12	0	0	11	6	18

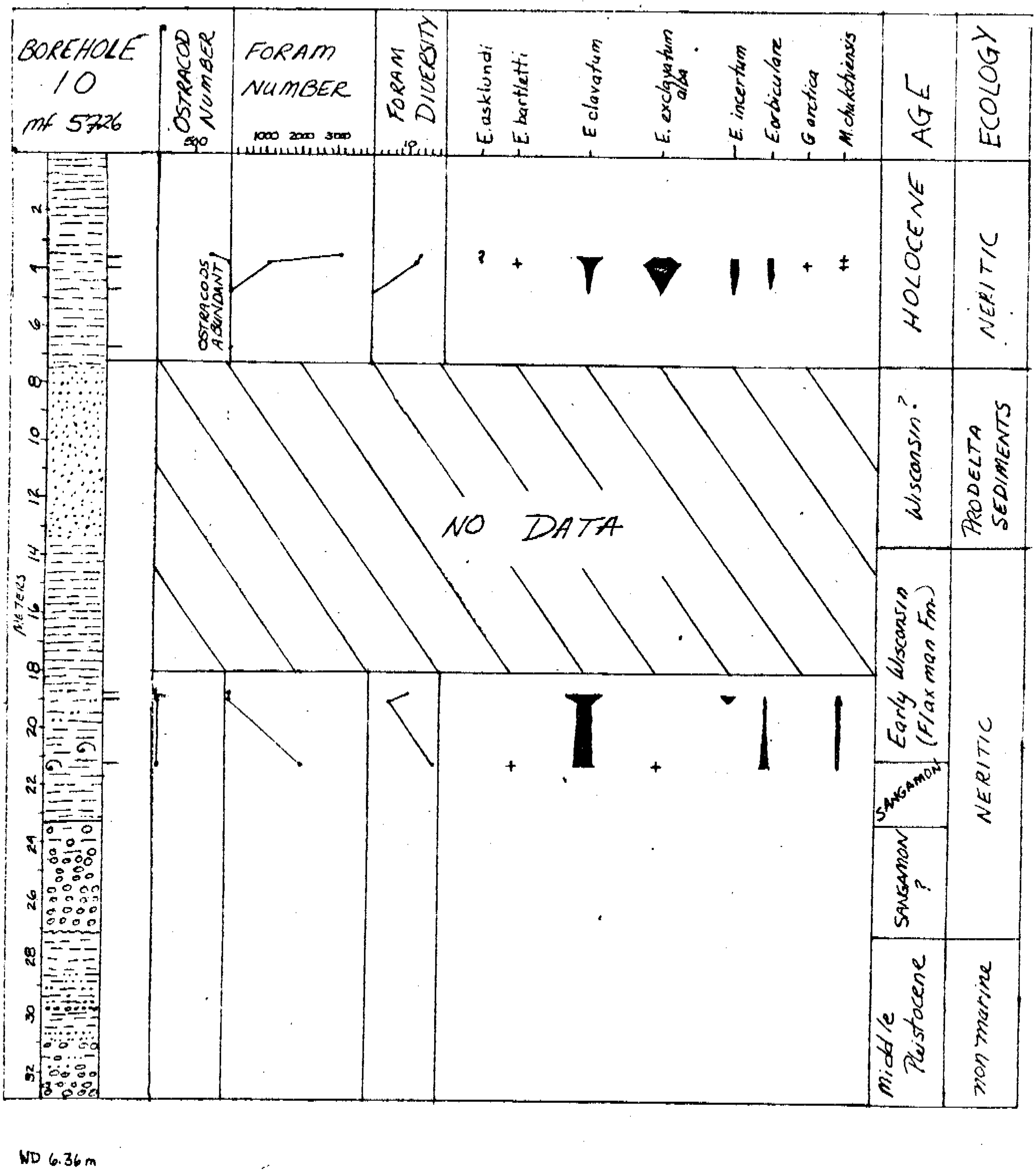

Figure A-1. Stratigraphy, paleontology and ecology of borehole HLA-10.

identified by the reddish color and worn appearance. The *in situ* faunas suggest deposition occurred in the inner neritic zone.

The abundant ostracods in samples 15.6 to 15.7 and 22.0 to 22.5 feet suggest this interval may be non-marine or an unusual marine environment which excludes benthic foraminifers.

The lower diversity and abundance in the Sangamon samples, 62.5 to 70.7 feet, is believed to be the result of shallow inner neritic (0-30 m) conditions rather than an indication of the Flaxman Formation.

BOREHOLE HLA-17

Age and environment: Benthic foraminifers present indicate that this borehole is no younger than Sangamon in age. The suspected middle Pleistocene age at the bottom of this hole cannot be verified yet. There is no indication of Holocene or Flaxman Formation.

These assemblages indicate middle neritic (30-100 m) depths. There are two intervals of decreased water depths or decreased salinities--13.5 to 17.5 feet and 37 to 52 feet. The first interval corresponds to the assumed pro-delta Canning River sediments. The latter interval corresponds to the latter part of the Sangamon transgression.

BOREHOLE HLA-18

Comments: Benthic foraminiferal assemblages in Mf 5625 (Borehole HLA-18) suggest that three interglacial and three glacial events including the middle Wisconsin warming and the early Wisconsin Flaxman faunas are present. Holocene assemblages are recognized from 0.0 to 1.8 m. These assemblages are characterized by the higher diversity, numerous reworked

Table A-2. Microfossil identifications in borehole HLA-17.

Borehole 17 Mf 5624

SPECIES \ LOCATION DEPTH (m)	0.6 nose	0.6-0.81	0.9-0.93	1.65	2.1-2.49	2.4-2.46	2.85	3.00	4.05	4.50	5.25	5.55	6.15	8.10	11.10	12.60	15.45-15.60	22.05	24.60	30.90
Buccella frigida (Cushman)	3	4	3	4	6	3	2	5	6	3	2	3	3	4	9	3	4	1	4	
Cassidulina islandica Norvang	11	15	11	11	6	16	6	7	16	15	15	8	12	12	5	15	16	10	22	<1
Cassidulina teretis Tappan	1	1	<1			<1	<1	<1			<1	<1		<1	<1	<1	7		8	
Discorbis baccata (Heron-Allen and Earland)	<1	1	2	<1	2	2	1	1	3	1	2	4	3	2	2		<1	1		<1
Elphidiella groenlandica (Cushman)	<1	1	<1		<1		<1	<1		<1				<1			<1		<1	<1
Elphidium bartletti Cushman	<1	1	<1		2	2	5	3		3	2	<1	2	<1				1		2
Elphidium clavatum Cushman	58	40	59	54	47	41	33	52	33	20	13	42	42	59	16	24	14	14	22	51
Elphidium excavatum alba Feyling-Hanssen	<1	1	<1	1	6	2	14	5				<1		1	2		<1	1	<1	2
Elphidium incertum (Williamson)	7	18	7	16	7	22	9	7	30	43	49	27	18	39	55	22	42		21	14
Elphidium orbiculare (Brady)	10	8	7	6	13	5	16	8	8	5	5	1	3	1	5	10	9	65	9	5
Glandulina laevigata d'Orbigny	3	1	2	2	2	1	5	2	1	3	<1	1	<1					4		
Guttulina austriaca d'Orbigny	2	2	2	2	2	1	2	3		4	6	3	3	2	<1	<1	1	1	1	
Miliolinella chukchiensis Loeblich and Tappan	<1	2	2	1		<1	<1	<1		<1	<1	1	3		<1		<1	1		2
Pyrgo williamsoni (Silvestri)	<1																			
Quinqueloculina arctica Cushman	<1	<1		<1	<1		<1	<1	<1					<1						
Quinqueloculina seminulum (Linne)	<1	<1		<1	1	1	1	1		<1	<1									2
Cyclogyra involvens (Reuss)		<1								<1	<1			<1						
Elphidium asklundi Brotzen		2	<1	<1		<1			<1		<1	<1		<1						13
Fissurina marginata (Montagu)		<1	<1	<1		<1	<1		<1						1	<1	<1			
Guttulina dawsoni Cushman and Ozawa		<1	<1		1	<1	<1	<1		<1	<1					<1		<1		3
Stainforthia concava (Hoeglund)		<1														<1			1	
Dentalina ittai Loeblich and Tappan			<1																	
Lagena gracillima (Sequenza)			<1																	
Largyngosigma williamsoni (Terquem)			<1																	
Pateoris haverinoides (Rhumbler)			1		1															
Triloculina trihedra Loeblich and Tappan				<1	2	2	<1		1	<1	1	2		1	<1	2				
Cassidulina norcrossi Cushman					<1															
Elphidium albiumbilicatum (Weiss)					1	5	2		6	1	1	4	<1	1	<1		3	<1	2	13
Gordiospira arctica Cushman					<1															
Lagena hexagona (Williamson)						<1														
Elphidium sp.							1	4					11				<1		<1	2
Lagena lineapunctata Heron-Allen and Earland								<1												
Guttulina sp.									<1						<	<1				
Bolivina sp.												<1		<1	<1				1	
Polymorphina sp.												<1						<1		
Fissurina sp.													<1		<1	<1	1			<1
Buccella sp.															2	20	<1		6	
Parafissurina himatiostoma Loeblich and Tappan															<1		<1			
Lagena sp.																	<1			
Reophax sp.																				<1

Table A-2 (cont.)

Borehole 17 Mf 5624

SPECIES \ LOCATION	0.6 nose	0.6-0.81	0.9-0.93	1.65	2.1-2.49	2.4-2.46	2.85	3.00	4.05	4.50	5.25	5.55	6.15	8.10	11.10	12.60	15.45-15.60	22.05	24.60	30.90
Foram number	2736	2848	3264	4928	3536	11232	6024	5424	2928	2520	3296	5360	1596	1264	3009	4000	4816	4320	8996	5264
Ostracod number	504	280	544	446	560	768	944	960	160	336	216	449	24	80	64	392	656	544	129	64
Foram diversity	16	20	20	15	19	19	20	18	13	16	17	17	15	17	17	14	18	13	14	16

Table A-3. Microfossil identifications in borehole HLA-18.

BOREHOLE 18
mf 5625

SPECIES \ DEPTH (m)	0.00	.75	1.20	1.65	1.80	2.25	3.30	3.90	4.29-4.44	6.48-6.63	6.90	7.95	@8.40	9.00-9.15	@9.30	10.95	@12.30	@13.65	@15.30	@16.80	19.65-20.10	21.15-21.60	22.65-23.10	24.15-24.60	25.65	27.60	33.40	36.60	39.60	42.75	54.60-55.05	63.75	75.45	@78.45	81.90	90.45-90.90
Gordiospira arctica Cushman																																				
Lagena laevis (Montagu)																															3				1	
Sigmomorphina sp.																															<1			<1		
Pyrgo williamsoni (Silvestri)																															<1					
Guttulina sp.																															<1			<1		
																																		<1		
Foram. Number	2488	209	7	23	22	0	0	100	58	294	0	0	47	7	3	43	0	216	1332	1960	3960	3768	10880	1876	5264	1394	5	513	3144	4472	687	0	0	1296	315	112
Ostracod Number	824	13	8	3	3	0	1	4	4	96	0	0	17	6	19	6	18	38	284	72	360	136	224	12	624	20	8	38	560	344	58	0	0	77	13	9
Foram Diversity	18	13	3	5	6	0	0	6	6	6	0	0	6	4	2	3	0	2	9	13	18	15	16	20	12	20	4	15	23	21	26	0	0	24	17	12

Table A-3 (cont.)

BOREHOLE 18 mf 5625 SPECIES / DEPTH (m)	0.0	.75	1.20	1.65	1.80	2.25	3.30	3.90	4.29-4.44	6.48-6.63	6.90	7.95	@8.40	9.00-9.15	@9.30	10.95	@12.30	@13.65	@15.30	@16.80	19.65-20.10	21.15-21.60	22.65-23.10	24.15-24.60	25.65	27.60	33.40	36.60	39.60	42.75	54.60-55.05	63.75	75.45	@78.45	81.90	90.45-90.90
Buccella frigida (Cushman)	4	<1			5														2	<1	2	2	2	2	6	6		4	10	8	6			16	5	2
Buccella inusitata Anderson	<1																								2	<1		1	<1	3	2			9		2
Cyclogyra involvens (Reuss)	<1																														<1				<1	
Elphidiella groenlandica (Cushman)	1	12		4				1													<1	6	<1	3	<1			<1	<1	1	2			2	1	3
Elphidium cf. E. asklundi Brotzen	<1	<1																				5														
Elphidium bartletti Cushman	2	3		4					2												<1	<1	4	6	12	<1		10	7	9	2			1	<1	
Elphidium clavatum Cushman	56	6	29	9	32			56	79	15			43	29	67	96		98	35	22	41	44	22	23		10		27	25	34	21			11	13	36
Elphidium excavatum alba Feyling-Hanssen	<1	61	43	43	36			27	10				2								2			<1		<1		<1	11	<1	2					
Elphidium incertum (Williamson)	8	1														2			<1	2	10	16	16	20	33	16		35		9	14			6	12	3
Elphidium nanum Vilks	1												11						5	11	3	<1	1	<1		1	20		3	2	2			2		
Elphidium orbiculare (Brady)	17	11	29	39	18			13	5	<1									5	8	12	13	13	18	30	21	20	13	10	17	14			21	20	9
Globulina sp.	<1																												<1							
Guttulina dawsoni Cushman and Ozawa	<1																		<1		<1		<1	<1					3		<1					
Guttulina glacialis (Cushman and Ozawa)	<1																			<1	1			1												
Guttulina lactea (Walker and Jacob)	<1	1						1		<1				14						<1		<1	<1		<1	<1		<1	2	1	7			9	8	2
Polymorphina suboblongata (Cushman and Ozawa)	2							2												1					<1											
Quinqueloculina seminulum (Linne)	4									5			6							<1	<1		<1		<1			<1	1	<1	2					35
Scutuloris tegminis Loeblich and Tappan	2	<1							2	79				43		2		2		<1	<1									<1	<1				2	<1
Dentalina pauperata d'Orbigny		1																						<1												
Elphidium albiumbilicatum (Weiss)		1											13									<1	2	2		2	40	<1	<1	1	<1					
Quinqueloculina arctica Cushman		2																			<1			<1		<1			1					<1	6	
Cassidulina norcrossi Cushman					5				2											1	12	10	4	10		31		<1	12	8					<1	<1
Cibicides lobatulus (Walker and Jacob)					5																															
Pateoris hauerinoides (Rhumbler)										<1																					1			2		
Milionella chukchiensis Loeblich and Tappan													23		33																					
Quinqueloculina stalkeri Loeblich and Tappan													2																							
Cassidulina islandica Norvang														14						3	13	1	27	9	2	7		2	5	4	18			16	18	4
Cassidulina crassa d'Orbigny																			<1		<1	<1														
Elphidium sp.																			<1			2								<1						
Triloculina trihedra Loeblich and Tappan																			<1																	
Stainforthia concava (Hoeglund)																				<1			3	1		4										
Dentalina ittai Loeblich and Tappan																					<1								<1	<1				<1		
Elphidium spp.																					<1		3	1	11	<1	20	3	2	<1	1			5	<1	
Glandulina laevigata d'Orbigny																						<1														
Fursenkoina schreibersiana (Czjzek)																							1						2							
Elphidium asklundi Brotzen																								<1	1			2	<1							
Fissurina marginata (Montagu)																								<1						<1	<1			<1	<1	<1
Guttulina austriaca d'Orbigny																								<1		<1								<1	<1	2
Dentalina frobisherensis Loeblich and Tappan																										<1										
Lagena gracillima (Seguenza)																										<1										
Lagena parri Loeblich and Tappan																										<1			<1		<1				<1	
Parafissurina lateralis (Cushman)																										<1										
Fissurina serrata (Schlumberger)																													<1	<1						
Nonion zaandamae (van Voorthuyen)																													2	1	<1			2		
Elphidium cf. E. frigidum Cushman																															1			<1		

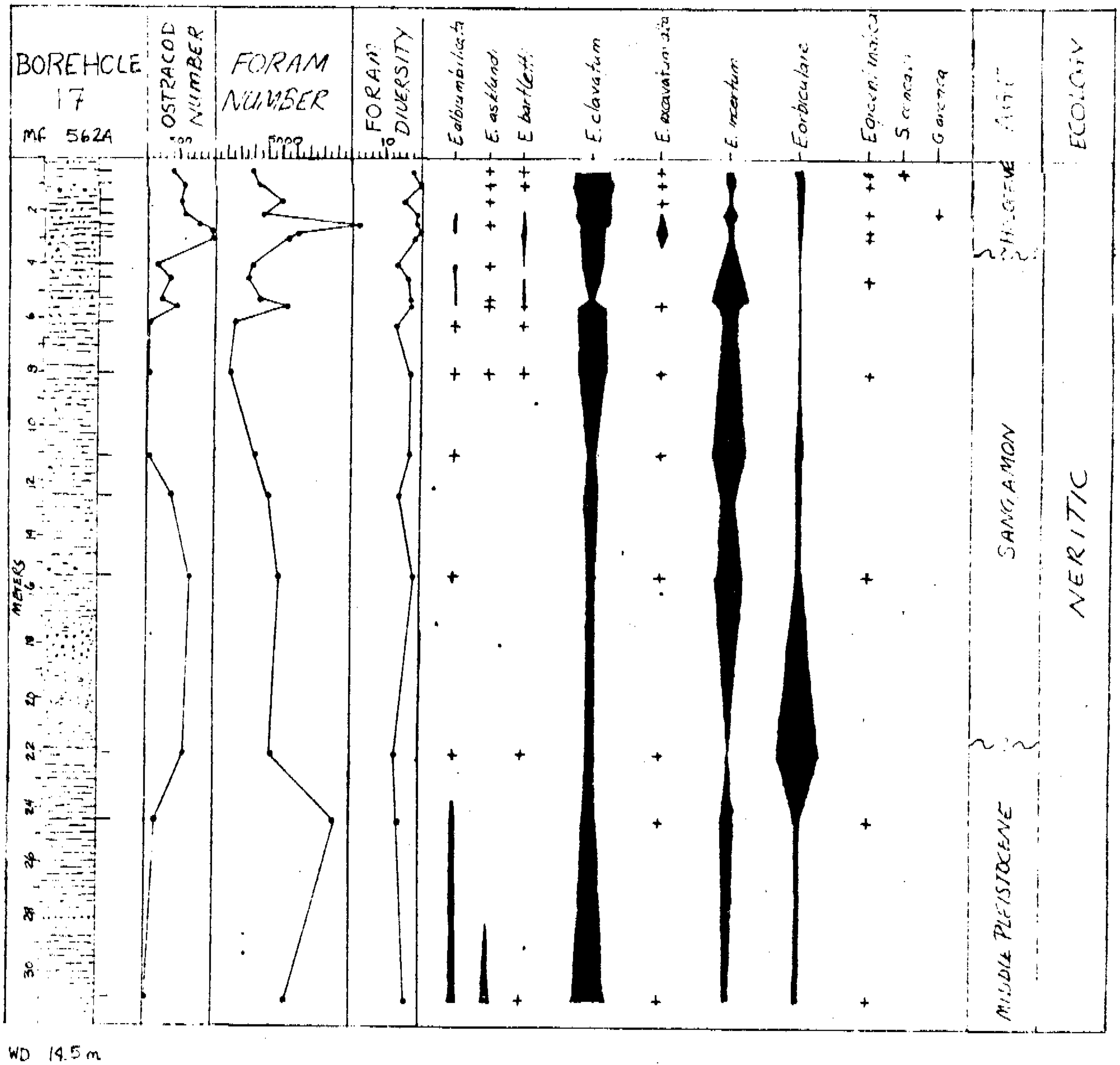

Figure A-2. Stratigraphy, paleontology, and ecology of borehole HLA-17.

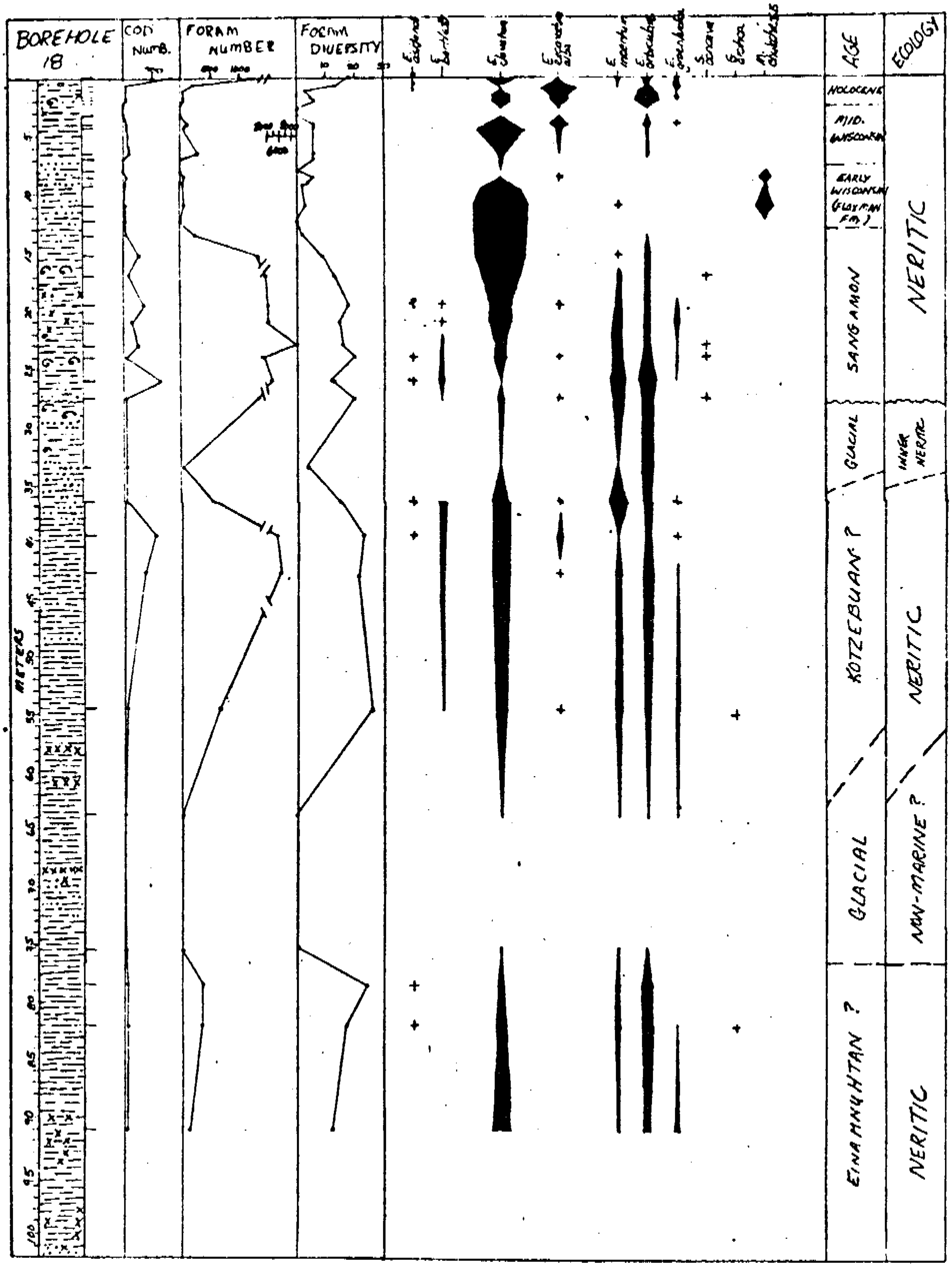

Figure A-3. Stratigraphy, paleontology, and ecology of borehole HLA-18.

older species, abundant specimens of *Elphidium excavatum alba* and, particularly in the youngest samples, the high foram. numbers. In the faunas between 3.9 and 6.6 m the diversity is still high, reworking is less common, the foram. number is moderate and *Elphidium excavatum alba* decreases in abundance whereas *Elphidium clavatum* increases. These characteristics are similar to the Holocene but suggest cooler, shallower waters. Samples at 2.25 and 3.3 m between the Holocene and middle Wisconsin assemblage are barren of benthic foraminifers.

Assemblages characteristic of the Flaxman Formation occur between 8.4 and 11 m. These assemblages have low foram. numbers, low diversity, and abundant *Elphidium clavatum*. *Elphidium asklundi* usually present in the Flaxman Formation is absent, probably because the water depth was greater and the salinity higher than in previously studied Flaxman samples. Samples barren of benthic foraminifers occur above (6.9 and 7.95 m) and below (12.3 m) the early Wisconsin Flaxman assemblages.

Sangamon assemblages occur between 15.1 and 27.6 m. These assemblages are characterized by high diversities and high foram. numbers. The abundance of species such as *Elphidiella groenlandica*, *Elphidium asklundi*, *Elphidium bartletti*, *Elphidium incertum*, and *Elphidium orbiculare*, and the decrease in the abundance of *Elphidium excavatum alba* are characteristic of the Sangamon.

Similar assemblages occur between 36-55 m and 78-91 m suggesting interglacial conditions. These intervals have been tentatively assigned to the transgressive units of Hopkins (1967):

Kotzebuan	36-55 m
Einahnutan	78-91 m

Non-marine or extremely shallow marine intervals separate each of the interglacial intervals. During the interglacial interval water depths appear to have been greater than the present depth (11.3 m). Depths were probably middle neritic (50-100 m).

BOREHOLE HLA-19

Age and environment: Benthic foraminiferal assemblages in Borehole 19 suggest the following interpretations:

Samples	.7- 4.4 feet	Holocene
	21.2-26.5 feet	Wisconsin?
	32.3-51.3 feet	early Wisconsin/late Sangamon
	71.5-96.5 feet	Sangamon

The Wisconsin? interval is believed to be a nearshore deposit into which specimens characteristic of the Flaxman Formation and deeper water are reworked. Flaxman assemblages occur below this and are identified by their low diversity and abundance, and characteristic species. Inner neritic depths are indicated for early Wisconsin/late Sangamon interval. Middle neritic to possibly outer neritic depths are suggested for the older Sangamon interval.

These interpretations may be modified with the completion of the ostracod work and as more boreholes are completed.

Table A-4. Microfossil identifications in borehole HLA-19.

BOREHOLE 19 Mf 5729

SPECIES \ LOCATION DEPTH (m)	0.21-0.30	0.45	1.32	6.15-6.60	7.89-7.95	9.69-9.72	10.65	11.70	13.95	15.33-15.39	21.45	22.86-22.92	27.60	28.95
Buccella frigida (Cushman)	12	9	11	2	7	<1		2			2	<1	4	7
Cassidulina teretis Tappan	<1			<1	<1	<1					<1		17	22
Discorbis baccata (Heron-Allen and Earland)	<1	1			<1								<1	2
Elphidium aff. E. asklundi Brotzen	<1													
Elphidium clavatum Cushman	19	21	7		2	13	96	1		33	17	38	17	7
Elphidium excavatum alba Feyling-Hanssen	18	13	16	36	26		3	<1			<1	<1	2	1
Elphidium orbiculare (Brady)	16	25	32	48	57	76	<1	82	100		38	60	24	32
Guttulina austriaca d'Orbigny	<1		<1	<1	<1	1		<1		33	<1	<1	2	<1
Guttulina dawsoni Cushman and Ozawa	2													
Guttulina sp.	<1													
Polymorphina spp.	<1	<1	<1	1	<1	<1				33				<1
Quinqueloculina stalkeri Loeblich and Tappan	<1													
Cassidulina islandica Norvang		4		1	1	<1		<1			6	<1	18	18
Elphidiella groenlandica (Cushman)		<1				<1					<1	<1	<1	
Elphidium albiumbilicatum (Weiss)				9	3	3		13						<1
Elphidium bartletti				2	<1								2	<1
Cibicides sp.					<1									
Elphidium asklundi Brotzen					<1	<1							1	8
Elphidium incertum (Williamson)						1					3		10	
Pateoris hauerinoides (Rhumbler)						1							<1	
Pyrgo williamsoni (Silvestri)						<1								
Stainforthia concava (Hoeglund)						<1					1			<1
Miliolinella chukchiensis Loeblich and Tappan											<1	<1	<1	<1
Triloculina trihedra Loeblich and Tappan											<1			
Dentalina ittai Loeblich and Tappan													<1	<1
Fissurina marginata (Montagu)													<1	<1
Lagena costata (Williamson)													<1	
Quinqueloculina aff. Q. seminulum (Linne)													<1	
Nodosaria sp.														<1
Foram number	2544	4592	2394	592	473	216	169	649	17	3	17408	8800	1808	2832
Ostracod number	128	160	298	86	188	5	21	554	5	10	256	912	140	48
Foram diversity	12	8	6	9	13	14	3	7	1	3	12	8	18	17

Figure A-4. Stratigraphy, paleontology, and ecology of borehole HLA-19.

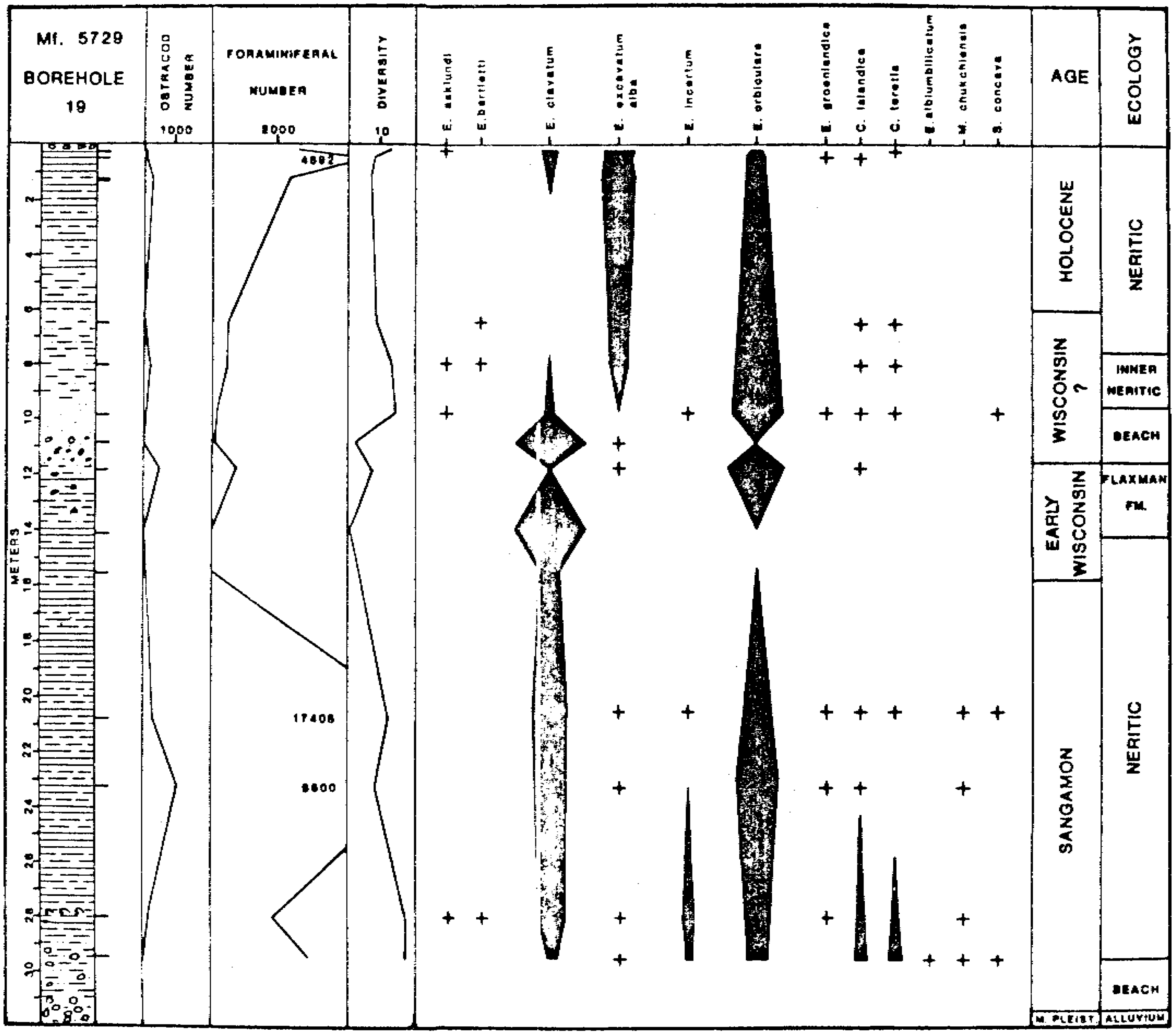

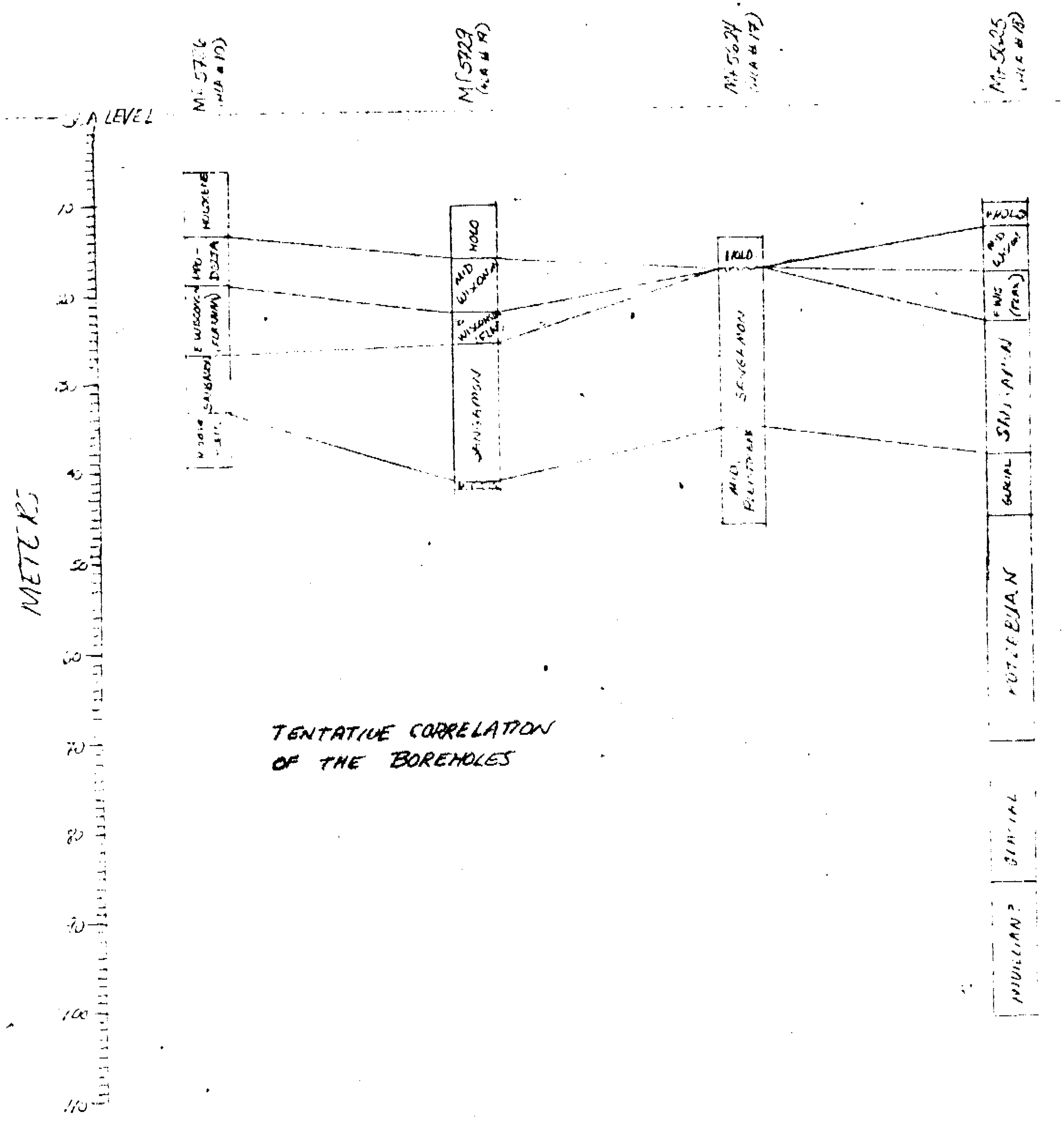

Figure A-5. Correlation of HLA boreholes.

APPENDIX B

Late Cenozoic stratigraphy of the Gubik Formation

by

Julie K. Brigham

INTRODUCTION

The Gubik Formation includes all of the unconsolidated deposits of late Tertiary and Quaternary age which veneer the bedrock platform of the Alaskan Arctic Coastal Plain. Recent information regarding these deposits has been derived from OCSEAP studies concerning coastal stability along the Chukchi and Beaufort Seas. In addition, these deposits have been used for predicting the spatial distribution of subsea permafrost (see Smith and others, 1980). Despite these and other related studies, the stratigraphy and sea level history of the Gubik Formation has never been properly documented. Early work by Schrader (1904), Leffingwell (1919), Meek (1923) and Smith and Mertie (1930) established the groundwork for later studies by O'Sullivan (1961), Black (1964) and McCulloch (1967); however, these regional studies grossly generalize the character of the stratigraphy. Recent studies (Sellmann and Brown, 1973; Williams and others, 1977; 1978; Williams, 1979; Hopkins, 1979, unpublished manuscript; Carter and others, 1979; Carter and Robinson, 1981) have been limited to investigations scattered across the Coastal Plain and the work verifies the complexity of the Gubik stratigraphy. The purpose of this study is to examine and describe in detail the stratigraphy of the Gubik Formation between two regions of the Coastal Plain, namely between Pt. Barrow and the Pt. Lay/Wainwright regions along the Chukchi Sea.

In the light of the rapidly increasing economic interests in the North Slope and Chukchi Sea regions, the reasons for studying the Gubik Formation are two-fold. First, reconnaissance work has indicated that the Gubik

Formation contains the stratigraphic information of Pleistocene tectonic movements. Often these deposits are found at altitudes in excess of known world eustatic sea levels, suggesting that significant uplift may have occurred across the coastal plain over the last 2-3.5 million years. Because periods of high (i.e., near present) sea level were infrequent throughout the Quaternary, the marine deposits and disjunct shorelines of the Gubik Formation form valuable markers for evaluating the long-term tectonic stability of the region.

Secondly, studies of the youngest shorelines provide information concerning long-term coastal stability and, in turn, long-term estimates of the sediment influx from the bluffs into the modern coastal environment complimenting other work of this nature in the region.

During July and August 1980, field research was initiated to investigate the stratigraphy of the Arctic Coastal Plain. Forty-eight stratigraphic sections were described and sampled from semi-continuous exposures along 80 km of the Chukchi Sea coast between Peard Bay and Pt. Barrow. Major lithologic units could be traced laterally between most sections resulting in the most comprehensive picture of the stratigraphy of the region compiled to date.

SUMMARY OF FIELD STUDIES

Lithostratigraphy and Relative Chronostratigraphy

Black (1964) first attempted to characterize the Gubik Formation by subdividing it into three units based upon textural and mineralogical changes. These units are still recognized in the literature as the Skull Cliff unit (oldest), the Meade River unit, and the Barrow unit (youngest). Black (1964) speculated that the oldest units were Illinoian and the younger units were Wisconsin in age. Although the lithologic motif he outlined grossly characterized portions of the Gubik, the stratigraphy is much more complex than his subdivision of the deposits would suggest. The problem which has plagued the interpretation of these deposits is the lack of a viable dating method. Classic stratigraphic methods cannot be uniquely applied due to the disjunct nature of adequate exposures and the physical similarity of deposits of widely different age.

Within recent years, the development of amino acid geochronology has provided Quaternary geologists with a reasonably reliable means of determining the relative and, theoretically, the absolute age of carbonate shells. The technique has been successfully applied as a stratigraphic tool to correlate and date raised marine deposits in many coastal areas of the United States and Canada (Mitterer, 1974, 1975; Wehmiller and others, 1977; Wehmiller and Belknap, 1978; Miller and others, 1977; Nelson, 1978; Kvenvolden and others, 1979; Brigham, 1980). A significant advantage of the technique is that it requires very little sample (40-50 mg) and at high latitudes has the potential of dating materials from 10,000 to 3,000,000 years old.

To differentiate and correlate the lithologic units of the Gubik Formation, amino acid analyses were completed by the author using the Amino Acid Geochronology Laboratory facilities at the University of Colorado, and more analyses are in progress. Based upon the extent of amino acid diagenesis in four species of marine molluscs (*Hiatella arctica*, *Mya truncata*, *Cardita crebricostata* and *Astarte borealis*), at least five depositional sequences of contrasting age can be differentiated in these deposits. Most of the coastal sediments exposed between Peard Bay and Pt. Barrow appear to be early to middle Pleistocene age. Theoretical age estimates, based upon the epimerization of isoleucine, suggest that the oldest deposits record marine transgression across the Coastal Plain more than 2.5 m.y. ago. Subsequent transgressions differentially eroded into the older deposits leaving a laterally discontinuous record of marine events. It is anticipated that the chronology and sea level history of these deposits will be synthesized by spring 1983.

Along at least 50 kilometers of the coastline examined, consolidated sandstones and clays of Cretaceous age outcrop at the base of the bluffs. Relief of the bedrock varies locally, but the Cretaceous beds are best exposed in the Skull Cliff region where they dip gently northward. They drop below the modern beach level near Nulavik and are not exposed further north. In many areas, the Cretaceous rocks are overlain by very massive, plastic, gray clay but fossiliferous, gravelly unconformaties are also common.

The part of the Gubik Formation overlying the gray clay varies widely in textural and structural character as well as age. As mentioned previously, a clear synthesis of the age relationships in these units is still in progress. The overlying marine sediments include coarse, sandy gravel, pebbly sand, fine sand, and clay, often interbedded. Unit thicknesses range from 0.5 to 50 cm or more. The marine part of the Gubik Formation is commonly capped by medium-fine sand, a few centimeters to a few meters thick, commonly containing organic stringers and lenses. These sediments appear to represent ancient thaw lake sediments. Basal peat in one section yielded a radiocarbon date of 11,175± 300 BP (Beta-1765).

Two major shorelines, at 6 m and 9 m a.s.l., were identified in the stratigraphy at the coast; driftwood in the highest and oldest of these beach deposits yielded an infinite radiocarbon date of >36,000 BP (Beta-1766). The absolute age of these features is not clear at present; however, evidence suggests that the 9 m shoreline represents the last interglacial (^{18}O stage 5e) while the younger 6 m shoreline may mark a mid-Wisconsin or late interglacial (5c?) sea level high associated with the deposition of the

Flaxman Formation east of Barrow. Reconstructions of the original position of the higher shoreline are possible assuming that the erosion of that feature was initiated 5,000 years ago when sea level reached its present position. Based upon an annual erosion rate of .3 m/yr, this accounts for probably a maximum of 1.5 km of shoreline retreat in 5,000 years.

Ice wedges, up to 3 m across, occur in several areas along the coast. Although permafrost binds all of the unconsolidated sediments interstitially, no lenses or thick horizontal masses of consolidated ground ice were seen in the deposits.

Possible Evidence for Pleistocene Tectonics

Information concerning the timing and magnitude of uplift over the Arctic Coastal Plain will best be attained by properly mapping and correlating disjunct beach ridges of similar age. L. D. Carter (U.S.G.S., personal communication, 1980) documents at least five marine shorelines east of Barrow near the Colville River based upon amino acid geochronology and stratigraphic data, but it is unclear how these features may correlate with the morphological shorelines in the western position of the coastal plain. Both O'Sullivan (1961) and Black (1964) attempted to correlate morphological shoreline features across the coastal plain; however, their results lack any adequate dating control.

Fieldwork during the 1981 field season will be concentrated southward along the Chukchi Sea coast between Pt. Lay and Wainwright. In this region, the widely separated beach ridges of the Coastal Plain appear to coalesce and intersect the present coastline. It is in this area that McCulloch (1967) suggested evidence for six transgressional episodes. Hence, this area may provide a key to linking appropriate shoreline fragments to make real assessments of the regional Pleistocene tectonic regime.

REFERENCES

Black, R. F., 1964, Gubik formation of Quaternary age in northern Alaska: U.S. Geological Survey Professional Paper 302-C, 91 p.

Brigham, J. K., 1980, Stratigraphy, amino acid geochronology and genesis of Quaternary sediments, Broughton Island, E. Baffin Island, Canada: Unpublished Masters Thesis, University of Colorado, Boulder CO, 199 p.

Carter, L. D., Marincovich, L., Brouwers, E., and Forester, R. M., 1979, Paleogeography of a Pleistocene coastline, Alaskan Arctic Coastal Plain: U.S. Geological Survey Circular 804-B, p. B39-B41.

Carter, L. D., and Robinson, S. W., 1981, Minimum age of marine deposits north of Teshekpuk Lake, Alaskan Arctic (in press).

Hopkins, D. M., 1967, Quaternary marine transgressions in Alaska, in Hopkins, D. M., ed., The Bering Land Bridge: Stanford University Press, p. 47-86.

_____1979, The Flaxman Formation of northern Alaska: record of Early Wisconsin shelf glaciation in the high Arctic?: XIV Pacific Science Congress, Khabarovsk, Abstracts, Add. Volume, p. 15-16.

Kvenvolden, K. A., Blunt, D. S., and Clifton, H. E., 1979, Amino acid racemization in Quaternary shell deposits at Willapa Bay, Washington: Geochimica et Cosmo. Acta, v. 43, p. 1505-1520.

Leffingwell, E. de K., 1919, The Canning River region, northern Alaska: U.S. Geological Survey Professional Paper 109, 251 p.

McCulloch, D. S., 1967, Quaternary geology of the Alaskan shore of the Chukchi Sea, in Hopkins, D. M., ed., The Bering Land Bridge: Stanford University Press, p. 91-120.

Meek, C. E., 1923, Notes of the stratigraphy and Pleistocene fauna from Peard Bay, Arctic Alaska: California University Department of Geological Sciences Bulletin, v. 14, p. 409-422.

Miller, G. H., Andrews, J. T., and Short, S. K., 1977, The last interglacial/glacial cycle, Clyde Foreland, Baffin Island, NWT: stratigraphy, biostratigraphy and chronology: Canadian Journal of Earth Sciences, v. 14, p. 2824-2857.

Mitterer, R. M., 1974, Pleistocene stratigraphy in southern Florida based on amino acid diagenesis in Fossil Merecenaria: Geology, v. 2, no. 1, p. 425-438.

_____1975, Ages and diagenetic temperatures of Pleistocene deposits in Florida based on isoleucine epimerization: Earth and Planetary Science Letters, v. 28, p. 275-282.

Nelson, A. R., 1978, Quaternary glacial and marine stratigraphy of the Qivitu Peninsula, northern Cumberland Peninsula, Baffin Island, Canada: Unpublished PhD thesis, University of Colorado, Boulder CO, 299 p.

O'Sullivan, J. B., 1961, Quaternary geology of the Arctic Coastal Plain, northern Alaska: PhD thesis, Iowa State University, 191 p.

Schrader, F. C., 1904, A reconnaissance of northern Alaska: U.S. Geological Survey Professional Paper No. 20, 139 p.

Sellmann, P. V., and Brown, J., 1973, Stratigraphy and diagenesis of perenially frozen sediments in the Barrow, Alaska region, in North American Contributions to 2nd International Conference on Permafrost, Yakutsk, USSR: Washington, D.C., National Academy of Sciences, p. 171-181.

Smith, P. A., Hartz, R. W., and Hopkins, D. M., 1980, Offshore permafrost studies and shoreline history as an aid to predicting offshore permafrost conditions: Annual Report Task D-9 to OCSEAP, 87 p.

Smith, P. S., and Mertie, J. B., Jr., 1930, Geology and mineral resources of northwestern Alaska: U.S. Geological Survey Bulletin 815, 351 p.

Wehmiller, J. F., and others, 1977, Correlation and chronology of Pacific coast marine terrace deposits of continental U.S. by fossil amino acid stereochemistry - technique, evaluation, relative ages, kinetic model ages and geological implications: U.S. Geological Survey Open File Report 77-680, 190 p.

Wehmiller, J. R., and Belknap, D. G., 1978, Alternative kinetic models for the interpretation of amino acid enantiomeric ratios in Pleistocene molluscs: examples from California, Washington and Florida: Quaternary Research, v. 1, no. 3, p. 330-348.

Williams, J. R., 1979, Stratigraphy of the Gubik Formation at Skull Cliff, northern Alaska: U.S. Geological Survey Circular 804-B, p. B31-B33.

Williams, J. R., Carter, L. D., and Yeend, W. E., 1978, Coastal plain deposits of NPRA: U.S. Geological Survey Circular 772-B, p. B20-B22.

Williams, J. R., Yeend, W. E., Carter, L. D., and Hamilton, T. D., 1977, Preliminary surficial deposits map of the National Petroleum Reserve - Alaska: U.S. Geological Survey Open File Report 77-862, 2 sheets, scale 1:500,000.

APPENDIX C

Radiocarbon dates from the Beaufort and Chukchi Sea coasts, 1980-1981

by

D. M. Hopkins and S. W. Robinson

We report here the results of radiocarbon dating of five samples from coastal areas of the Chukchi and Beaufort Seas as a contribution to the Outer Continental Shelf Environmental Assessment Program (OCSEAP) funded by the U.S. Bureau of Land Management and managed by the U.S. National Oceanographic and Atmospheric Administration. The report supplements information given in previous lists that described a total of 46 radiocarbon-dated speciments (Hopkins and Robinson, 1979; Hopkins and others, 1980). Locality data, stratigraphic notes, and some discussion are given in table 1.

Three of the dated samples (USGS-860, -861, and -862) were submitted as part of an attempt to settle questions raised by results of amino-acid analyses on shells from interglacial marine deposits exposed along the northern Alaskan coast. Comparison of amino-acid racemization ratios in fossil mollusks from western Alaska, northern Alaska, and Baffin Island indicated a discrepancy in correlation; deposits with similar amino-acid ratios were assigned ages of about 120,000 years in Alaska and about 10,000 years in the eastern Arctic (Brigham and others, 1980; Hopkins and Carter, 1980). The radiocarbon-dating results establish that the fossil shells from Pelukian deposits in northwestern Alaska are indeed much older than 10,000 years, even though a finite date of uncertain significance was obtained for sample USGS-860 (table 1).

The remaining two dated samples (USGS-882 and -883) were submitted as part of a larger effort to determine the history of dispersals of trees and large shrubs in Alaska during the last 35,000 years (Hopkins and others,

TABLE C-1

Radiocarbon age determinations from the Beaufort and Chukchi Sea coasts (1980-81)

Laboratory number (Field No.)	Location (Quadrangle)	Latitude N Longitude W	Material	Age Determination	Stratigraphic setting
USGS-860 (76ANr38d)	1.7 m above sea level in a 3.2 m bluff on west shore of Wainwright Inlet (Wainwright C-2)	70°37.1' 160°04.8'	Driftwood twigs	42,100 $\pm$ 1,400	Intended to date driftwood in an ancient barrier bar formed during the Pelukian (last interglacial) transgression. Finite age is surprising and needs to be confirmed.
USGS-861 (76ANr45)	1.8 m above sea level in a 10 m bluff on west shore of Wainwright Inlet (Wainwright C-2)	70°37.7' 160°01.6'	Driftwood twigs and wood fragments	>54,400	Dates driftwood in an ancient barrier bar formed during the Pelukian (last interglacial_ transgression.
USGS-862 (76Ahp139p)	16 m above sea level in a 22-m bluff near south end of Skull Cliff (Meade River D-4)	70°49.45' 158°06.06'	Driftwood log	>42,710	Dates driftwood in an ancient tidal delta exposed in a sea-cliff cut in the widespread marine terrace of middle Pleistocene age on the western Arctic coastal plain.
USGS-882 (Collected by H. J. Walker, Louisiana State Univ.)	3.6 m below surface in cutbank on west side of west channel of Colville River near head of the delta (Harrison Bay A-2).	70°13.3' 150°55.8'	Log of <u>Populus</u>	52,300 + 4,500 - 2,900	Indicates that an earlier age determination of 24,165 $\pm$ 1,410 (LSU-7345) on another segment of the same log should be regarded as a minimum age. Other wood samples from this same terrace have proven to be beyond the range of radiocarbon dating, and finite age for this specimen may reflect slight contamination since collection.
USGS-883 (78Ahp23A)	11 m below top of 14 m bluff on west bank of Ikpikpuk River several km above mouth of Titaluk Creek (Ikpikpuk C-4)	69°42.6' 154°53.0'	Peat	13,730 $\pm$ 110	Establishes age of leaves of <u>Populus balsamifera</u> on the western Arctic coastal plain and also helps to establish time when through-flowing drainage resumed through northern Alaska dune field.

1981), but they also illuminate the history of terrace formation and alluvial accumulation in northwestern Alaska and thus contribute to the location and assessment of sources of sand and gravel fill adjoining offshore leasing areas. A sample of Populus wood (collected by H. J. Walker, Louisiana State University, identified by Virginia Page, Stanford University) obtained from a gravel terrace that extends along the west bank of the lower Colville River had originally been dated as 24,165 $\pm$ 1410 years old (LSU-7345), but the date was suspect because other wood samples from the terrace yielded "more than" dates and suggested that the terrace was, in fact, formed during the last interglacial interval (Carter and Galloway, in press). A re-analysis of Walker's Populus log yielded a finite age of 52,300 $^{+4,500}_{-2,900}$ (USGS-882). In view of the infinite ages obtained for other logs from this terrace, however, it seems likely that the very slight radiocactivity detected is a result of contamination.

Leaves of Populus balsamifera (identified by Robert E. Nelson, U.S. Geological Survey) from the Ikpikpuk River are 13,730 $\pm$110 years old (USGS-883) and provide evidence that cottonwood trees persisted in Alaska throughout the last glacial period (Hopkins and others, 1981). The sample also helps to establish the time when dune activity in the northern Alaskan sand sea moderated enough and precipitation increased enough to permit through-flowing drainage to be re-established at the western end of the northern Alaska sand sea (Carter, 1981a, 1981b).

References Cited

Brigham, J. K., Hopkins, D. M., Carter, L. D., and Miller, G. H., 1980, Application of amino acid geochronology to deposits of the Arctic coastal plain, Alaska: preliminary results and implications: University of Colorado, Institute of Arctic and Alpine Research, 9th Arctic Workshop, Abstracts, p. 34-35.

Carter, L. D., 1981a, A Pleistocene sand sea on the Alaskan arctic coastal plain: Science, v. 211, p. 381-383.

_____ 1981b, Middle Wisconsinan through Holocene climate in the Ikpikpuk River region, Alaska: University of Colorado, Institute of Arctic and Alpine Research, 9th Arctic Workshop, Abstracts, p. 5-9.

Carter, L. D., and Galloway, J. P., in press, Terraces of the Colville River Delta region, Alaska: U.S. Geological Survey Circular (Accomplishments in Alaska, 1980).

Hopkins, D. M., and Carter, L. D., 1980, Application of amino acid geochronology to deposits of the Arctic coastal plain, Alaska: University of Colorado, Institute of Arctic and Alpine Research, 9th Arctic Workshop, Abstracts, p. 12-13.

Hopkins, D. M., and Robinson, S. W., 1979, Radiocarbon dates from the Beaufort and Chukchi Sea coasts: U.S. Geological Survey Circular 804-B (Accomplishments in Alaska, 1978), p. B44-B47.

Hopkins, D. M., Robinson, S. W., and Buckley, J., 1981, Radiocarbon dates from the Beaufort and Chukchi Sea coasts (1979-1980), in Smith, P. A., Hartz, R. W., and Hopkins, D. M., eds., Offshore permafrost studies and shoreline history as an aid to predicting offshore permafrost conditions: National Oceanographic and Atmospheric Administration, Environmental Assessment of the Alaskan Continental Shelf, Annual Reports, Principal Investigators, March, 1980, v. IV (Hazards), Appendix E, p. 203-220.

Hopkins, D. M., Smith, P. A., and Matthews, J. V., Jr., 1981, Dated wood from Alaska and the Yukon: implications for forest refugia in Beringia: Quaternary Research, v. 15, p. 217-249.

ANNUAL REPORT

Contract: NOAA 03-5-022-55
Research Unit: 251
Task Order: C1
Reporting Period: 01/01/80-12/31/80

SEISMIC AND VOLCANIC RISK STUDIES WESTERN GULF OF ALASKA

Principal Investigators
Hans Pulpan
Juergen Kienle

Geophysical Institute
University of Alaska
Fairbanks, Alaska 99701

TABLE OF CONTENTS

Figure 1 and Figure 26 were omitted from this report as copy provided was not of sufficient quality for reproduction.

I. SUMMARY

This report summarizes 1980 results of our ongoing study to evaluate seismic and volcanic risk to offshore petroleum-related development on the Cook Inlet and Alaska Peninsula/Kodiak/Semidi continental shelf. Historic earthquake and volcanic eruption data combined with earthquake data obtained from a high-gain regional network and a volcanic/geologic field study of the volcanoes of the eastern Aleutian arc provide the basis of this evaluation. The operation of the high gain seismic network is part of the program.

We report in detail on the:

(1) inter-plate seismicity associated with the underthrusting of the Pacific plate under the North American plate, a process which gives rise to great earthquakes ($M \geq 7.8$), and intra-plate shallow seismicity in the overriding plate,

(2) an attempt to relocate events outside our land-based network on the outer Kodiak shelf by combining land-based and ocean bottom seismometer data,

(3) the intra-plate seismicity and stress regime (from local mechanism studies) of the deeper portions of the subducting plate,

(4) identification of volcanic centers in Katmai and a preliminary evaluation of the volcanic hazards in that area.

II. INTRODUCTION

General Nature and Scope of Study

The present study attempts to develop the scientific and technical basis of assessing the hazards associated with petroleum related development on a portion of the Alaska Outer Continental Shelf subjected to a very high level of seismic and volcanic activity. In this respect the Alaskan shelf is unique among the United States Outer Continental Shelf areas. The study is a data gathering program in its attempt to obtain pertinent data from a large and remote area at a resolution not previously possible. It is a scientific program in its development of a better understanding of the fundamental processes underlying the seismic and volcanic activity. It is a technical program in its attempt to quantify the associated risk. The study is one of several in the Gulf of Alaska, addressing the hazard problems associated with a very active seismotectonic and volcanic regime.

Specific Objectives

The specific objectives over the past years have been:

(1) to monitor the seismic activity of Lower Cook Inlet, Shelikof Strait, Bristol Bay, and the offshore areas off Kodiak Island and off the Alaska Peninsula between Kodiak and the Semidi Islands;

(2) to delineate the potential seismic sources in the region based upon seismicity data;

(3) to obtain strong ground motion data;

(4) to perform in conjunction with other research units of the OCSEAP program a seismic risk analysis of the area;

(5) to assess the volcanic hazards and eruption potential of several Cook Inlet volcanoes and the Katmai group of volcanoes.

Relevance to Problems of Petroleum Development

Petroleum development will result in the erection of large temporary and permanent structures. The designs require knowledge of the space-time behavior of large, potentially damaging, earthquakes at a particular site and the level and nature of strong ground motion associated with these earthquakes.

With respect to volcanic hazards the potential range of lava flows, pyroclastic flows and mudflows, ash flows and glowing clouds, tephra falls, toxic fumes and gases needs to be known before a site can be selected for petroleum development. This requires identification of volcanoes likely to erupt, the determination of the probable eruptive style and the recurrence rate of eruptions.

III. CURRENT STATE OF KNOWLEDGE

A. Tectonic Setting

The tectonics of the Gulf of Alaska are dominated by the interaction of the North American and Pacific plates. Along the Queen Charlotte - Fairweather fault systems the two plates are slipping past one another along a right lateral transform fault system. Along the Aleutian volcanic arc and the Aleutian-Alaska Range, up to Mt. McKinley, the oceanic Pacific plate underthrusts the North American plate. The Aleutian trench-axis marks the initial down-bending of the Pacific plate and the arc of active volcanoes approximately traces the 100 km depth-contour of the subducted plate. The transition zone between these two distinct tectonic regimes lies between the Denali fault and Gulf of Alaska and contains a complicated system of thrust and strike slip faults. Lahr and Plafker (1980) have proposed a model where this part of the North American plate is divided into three subblocks, which are partially coupled to the Pacific plate. Our particular study area (Cook Inlet and western Gulf of Alaska) is dominated by the subduction process.

B. Seismicity and Seismic Source Zones

Subduction Zone: The most dominant source of earthquakes in our study area is the shallowly dipping interface between the underthrusting and overriding plates. The elastic strain accumulated along this zone by plate convergence is episodically released in the form of great (M_S>7.8) earthquakes. In our study area this occurred last during the 1964 Alaska earthquake. The aftershock activity indicates that the rupture surface of that earthquake reached a depth of approximately 50 km along the interface between the 2 plates.

Seismic activity at depths greater than 50 km is associated with stresses in the cold, brittle interior of the subducting plate, which is more steeply dipping than the shallow thrust zone and reaches a maximum depth of approximately 200 km behind the volcanic arc. Though this zone is seismically very active it has apparently not generated great earthquakes.

Faults: In our study area, four major fault systems have been mapped (Figure 1): the Castle Mountain fault (25), the Bruin Bay fault (26), the Border Ranges fault (23) and the Eagle River fault (24). A major unnamed fault separates the Mesozoic and the Cenozoic in southern Kodiak (near 8, Figure 1). The trace of the Castle Mountain fault cuts the grain of the arc system at an oblique angle of 20 degree and transects the volcano line just south of Mt. Spurr volcano. The relative motion along this fault is right lateral strike slip. Recent displacements have occurred along the Castle Mountain fault as indicated by offset Pleistocene glacial deposits and offset tectonic lineations (Evans et al., 1972). The Bruin Bay, Border Ranges and Eagle River faults are thrusts that follow essentially the trend of the arc structure. However, none of these faults have been active since late Mesozoic-early Tertiary time and the Bruin Bay fault is not offsetting any strata younger than 25 million years (Magoon et al., 1979).

Aside from the intense seismicity in the shallow thrust zone of the subducting Pacific Plate, shallow seismicity (hypocentral depth less than 50 km) in our area is diffuse and not preferentially associated with any of these major fault systems. Several shallow clusters of small magnitude events do, however, correlate with certain volcanoes in Cook Inlet and on the Alaska Peninsula. A persistent linear trend of seismic activity not correlated with a known fault occurs on Kodiak Island near Deadman Bay. Another area of persistent seismicity not correlated with any known faults lies east of Marmot Island.

On the Kodiak shelf area, between 150° and 154°W., the shallow thrust zone appears to be especially active (Pulpan and Kienle, 1979). This seismically active part of the shelf is also characterized by large sediment slides and strong structural deformation (Hampton et al., 1979). The concentration of seismic activity ends where the slides end and structural deformation decreases significantly. However, it has not yet been possible to correlate the seismicity with individually mapped faults.

In the lower Cook Inlet earthquakes cluster beneath Illiamna volcano. This activity occurs at intermediate depth (80-180 km) within the deeper portion of the subducting Pacific plate.

C. Volcanism

Our study area includes volcanoes of Cook Inlet and Katmai. Of the 5 principal Cook Inlet volcanoes we have in previous reports discussed hazards associated with Augustine Volcano (e.g., Kienle and Swanson, 1980) and Redoubt Volcano (Pulpan and Kienle, 1980; Riehle et al., 1981). Little new data is available from Iliamna Volcano since Juhle's (1955) reconnaissance geologic study. Mt. Spurr and Hayes Volcanoes to the north lie outside our study area.

Much of the previous work on the volanoes in Katmai National Park (Fig. 2) has concentrated around Mt. Katmai and specifically on the 1912 eruption that formed the Valley of 10,000 Smokes. Griggs (1922) and Fenner (1926, 1950) in their classic studies of the 1912 eruption identified several volcanic centers in the area including Mt. Katmai, Novarupta, Knife Peak (now renamed Mt. Griggs), Mt. Mageik, Mt. Martin, Mt. Trident and Mt. Peulik. Curtis (1968) also studied the 1912 eruption and made detailed examination of the tephra deposits. Hildreth (1980, 1981) and other U.S. Geologic Survey personnel have recently been reworking the petrology of the 1912 ejecta.

Few studies of the other volcanic centers in Katmai are available. Muller et al. (1954) reported on the volcanic activity in the Katmai area during the summer of 1953, including the 1953 eruption of Trident Volcano. Fumarole activity was noted on six other volcanoes: Steam issued from several vents on the side of a crater lake on Mt. Douglas; steam vents were observed at Kukak volcano, Mt. Griggs (Knife Peak), Novarupta, Mt. Mageik, and Mt. Martin. Snyder (1954) gave the first detailed report of the new activity at Trident Volcano. Ray (1967) studied the mineralogy and petrology of the lavas formed during the

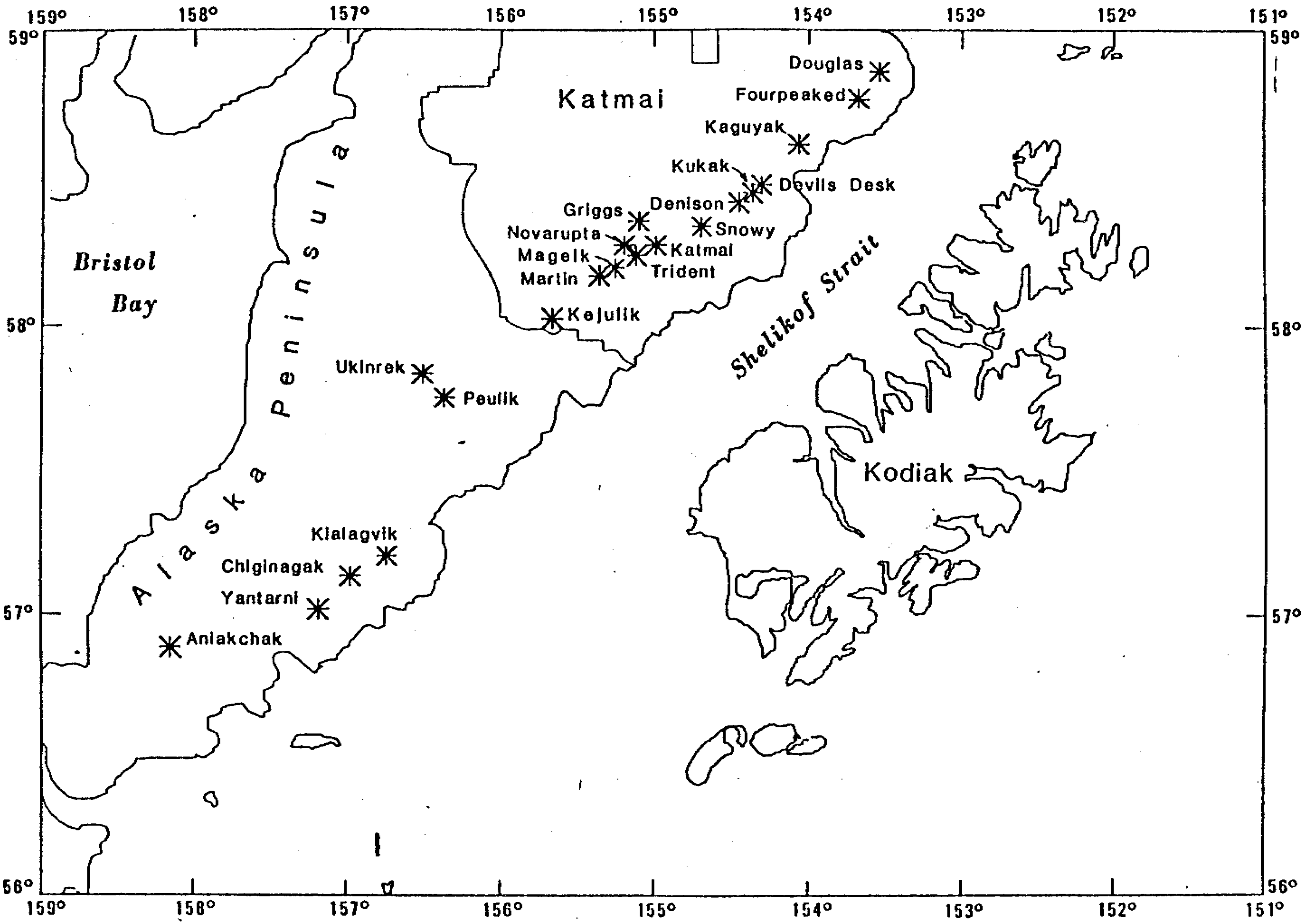

Figure 2. Volcanic centers on the northern Alaska Peninsula, including Katmai National Park.

1953-1963 eruptions of Trident Volcano. Keller and Reiser (1959) prepared a regional geologic map for the area from Cape Douglas to the Kejulik Mtns. and showed the distribution of volcanic rocks, but most of their effort was devoted to the Mesozoic and Tertiary sedimentary rocks. Keller and Reiser (1959) did however comment that Martin, Mageik, Novarupta, Knife, Kukak and Douglas Peaks were steaming with varying intensities and that Trident was steaming and extruding blocky lava. Ward and Matumoto (1967) published a summary of volcanic activity in Katmai National Monument from 1870 to 1965.

IV. STUDY AREA

The target areas for this study are the potential lease areas of the western Gulf of Alaska, in particular Cook Inlet, Shelikof Strait, the Kodiak Island shelf areas and Bristol Bay.

V. SOURCES, METHODS AND RATIONALE OF DATA COLLECTION

A. High Gain Seismic Network

A 29 station network of short-period, vertical-component seismographs operated under this contract is the prime data source for achieving the goal of the study. Data from the network permit the delineation of the seismic source zones, the study of short-term space-time behavior of seismicity, the determination of the mode of tectonic deformation (from fault plane solutions) and the study of seismicity patterns associated with volcanic activity.

Figure 3 shows the present layout of the system. All signals, with the exception of the Bristol Bay stations (BR1, BR2, BR3), are recorded at Homer on Develocorder film. Bristol Bay stations are recorded in King Salmon on digital magnetic tape, controlled by a seismic event

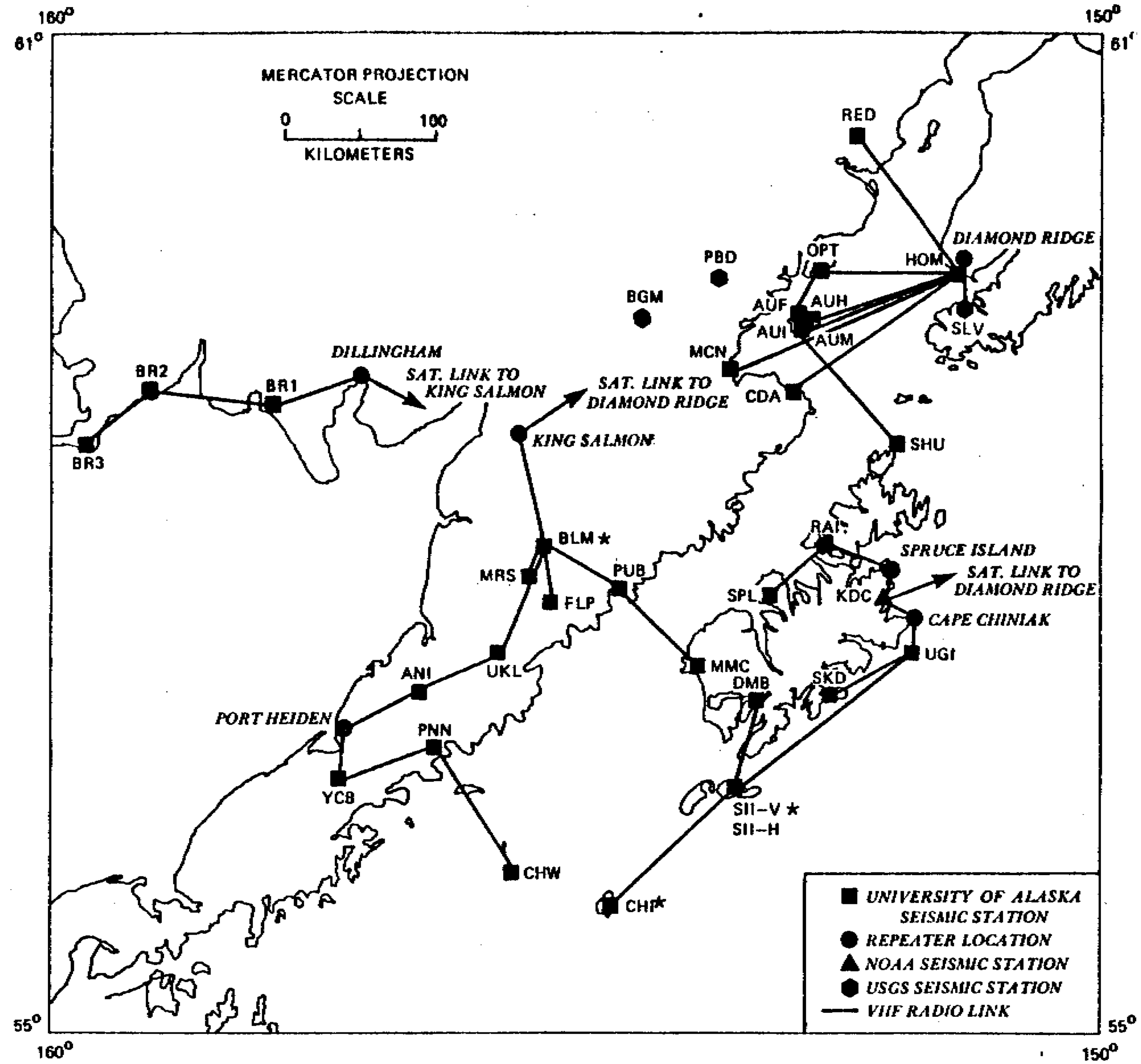

Figure 3. Current configuration of the seismic networks in Cook Inlet and Alaska Peninsula/Kodiak. Stations with asterisk (CHI, SII and BLM) also have strong motion instrumentation.

detection system. Some stations of the Alaska Peninsula network are also recorded with that system.

No major technical changes have been made during the report period, but we have continued our efforts to make the system even more resistent to the environment and hence technically more reliable. The system has performed well over the past year.

In addition to our own network we have also serviced and operated three stations originally installed by the USGS.

<u>Strong Motion Accelographs</u>

Over the recent years we have installed strong-motion accelerographs at certain locations of the high gain network. Kinemetrics SMA-1 instruments were deployed at sites PNN, BLM, SII, SKS and UGI. Originally these instruments were to be replaced by modified versions of ocean-bottom strong motion instruments developed by the University of Texas. Parts delivery problems at the University of Texas delayed the construction of nine of these units beyond the seismic station service window in 1980, and thus deployment of these instruments had to be delayed. During the 1981 service all Kinemetrics instruments were removed and 3 University of Texas packages were deployed at CHI, SII and BLM (see Figure 3).

The purpose of the strong-motion instruments is to obtain strong earthquake ground motion records associated with larger earthquakes (M_S>6). This type of data is needed to eventually derive a representative attenuation relationship, one of the critical parameters needed in seismic risk analysis.

<u>Volcanological Field Work</u>

Rock samples from several Cook Inlet and Alaska Peninsula volcanoes have been collected for later petrochemical laboratory analysis. Petrologic/geochemical analyses of the eruptive products of a given volcano provide information about its past eruptive style and the state of chemical evolution of its magmas. Highly evolved magmas (i.e., melts of high SiO_2 content) have a tendency to erupt more violently than less evolved magmas.

VII & VIII. RESULTS AND DISCUSSION

A. <u>Seismicity in the Cook Inlet and Alaska Peninsula/Kodiak Regions.</u>

Figures 4 through 23 are epicenter plots based on the short period seismic network data for the time period January through December 1980. The general seismicity does not greatly differ from that of the past years. The seismicity of the shallow thrust zone is quite different in the rupture zones of the 1938 and 1964 earthquakes. The boundary between the two zones runs transversely to the arc along a line from just southwest of the Trinity Islands to Wide Bay on the Alaska Peninsula (Pulpan and Kienle 1979). In the 1964 rupture zone seismic activity occurs over most of the width of the shallow thrust zone; there is an especially high level of seismicity in the shallowest part of the thrust zone near the southern corner of the 1964 rupture zone (offshore the southern tip of Kodiak Island). In the 1938 rupture zone seismic activity in the shallow thrust zone is at a much lower level. There is also an indication that the activity is more concentrated at the deeper arcward edge of the shallow thrust zone. The details of the feature are however difficult to resolve because of our particular station distribution. Relocation of events in the 1938 rupture zone using combined data from both the Lamont-Doherty Shumagin Island network and our own network might establish the existence of this feature more definitely. The difference in the overall seismicity in the shallow thrust zones of the 1964 and 1978 events also shows up in teleseismic earthquake locations (Davies et al., 1981).

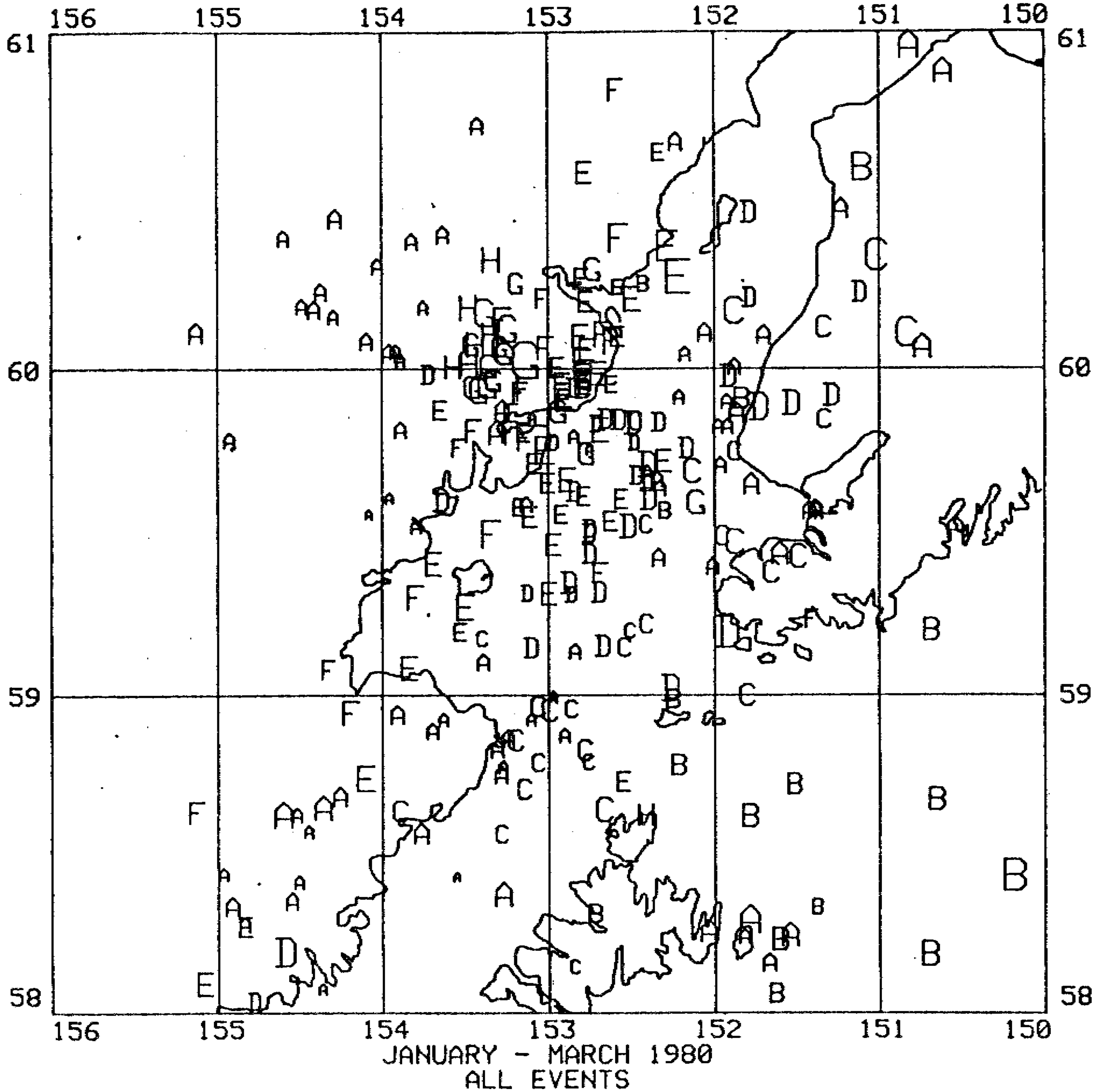

Figure 4. Cook Inlet epicenters.

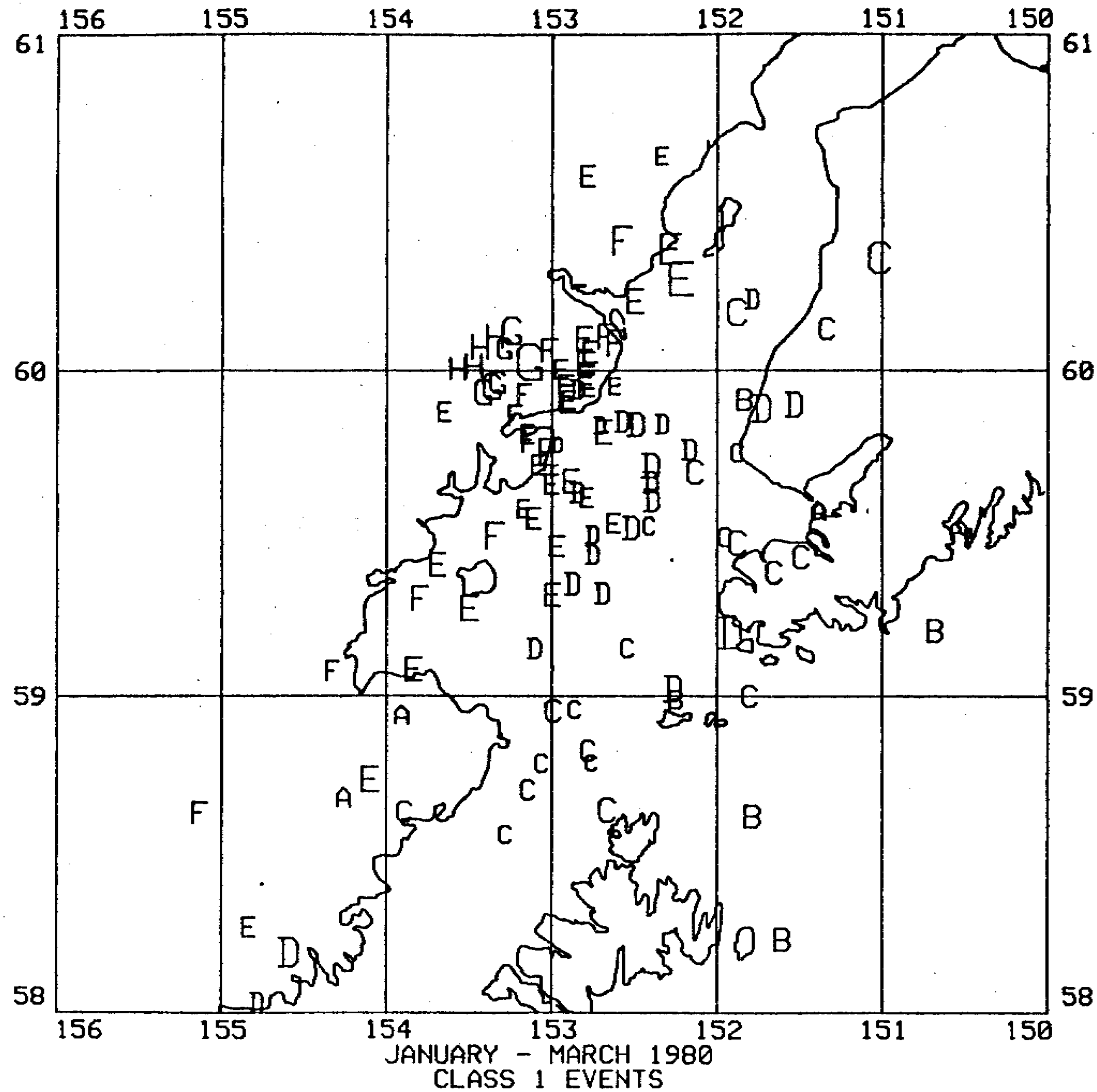

Figure 5. Cook Inlet epicenters.

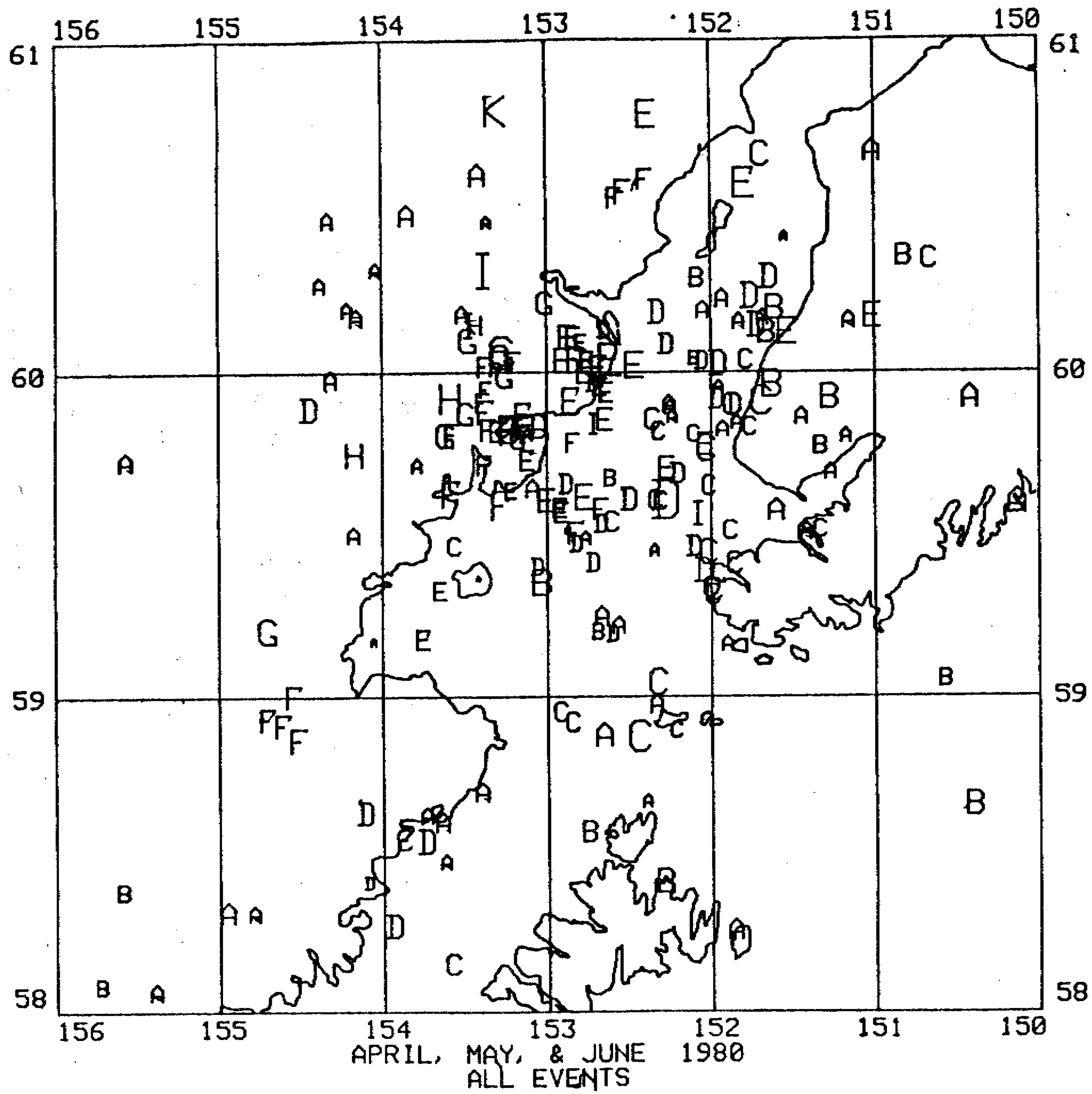

Figure 6. Cook Inlet epicenters.

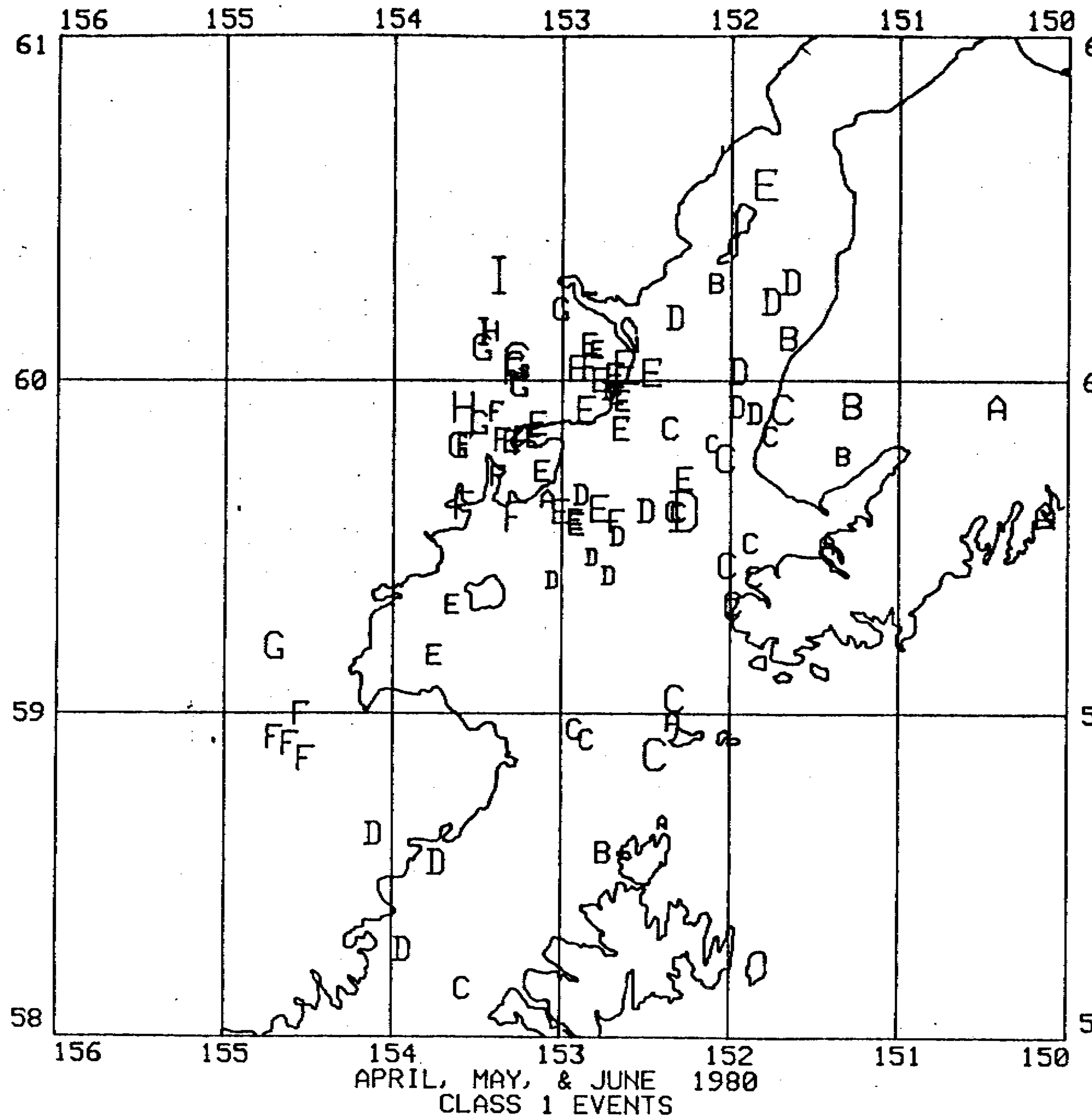

Figure 7. Cook Inlet epicenters.

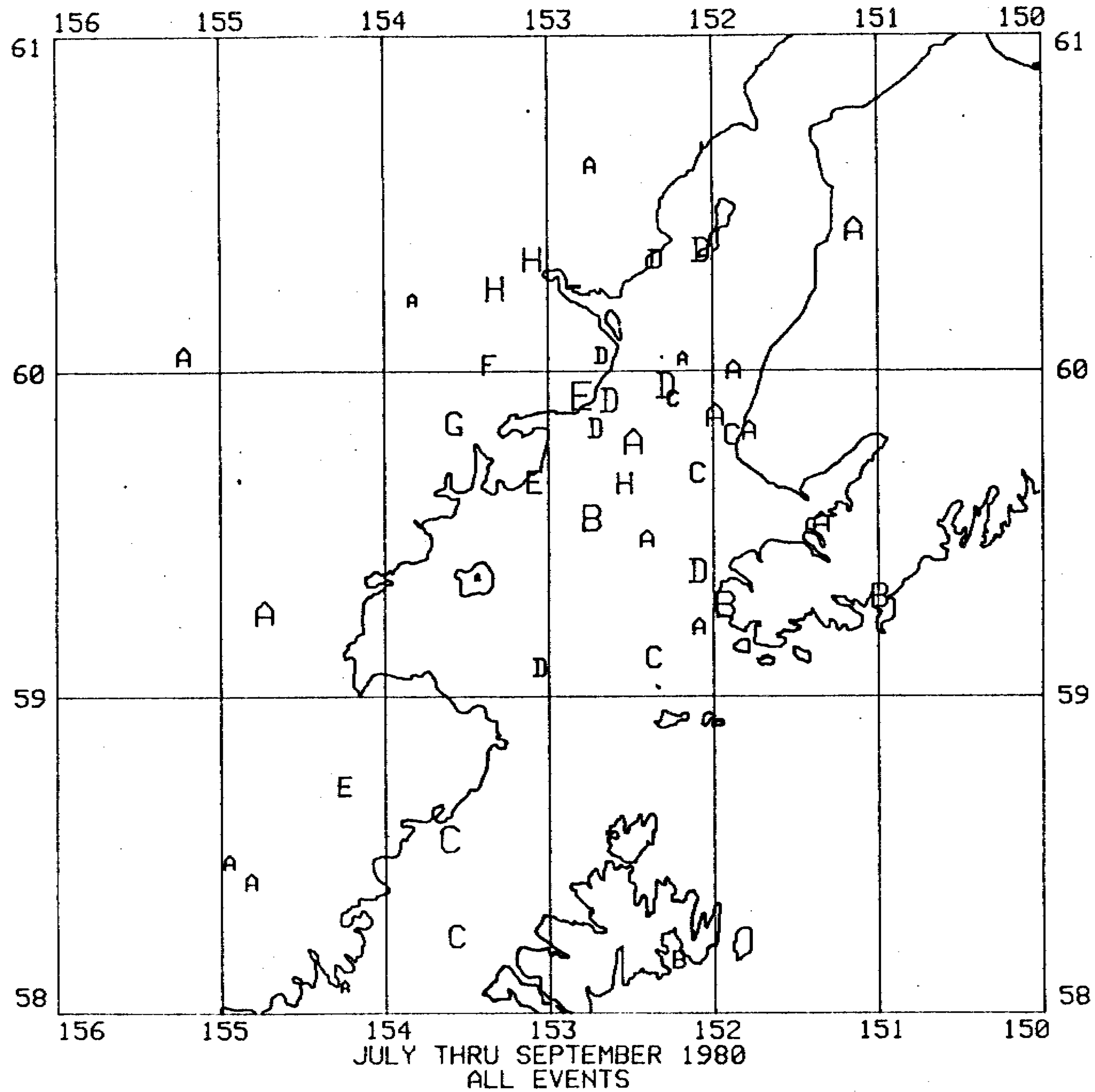

Figure 8. Cook Inlet epicenters.

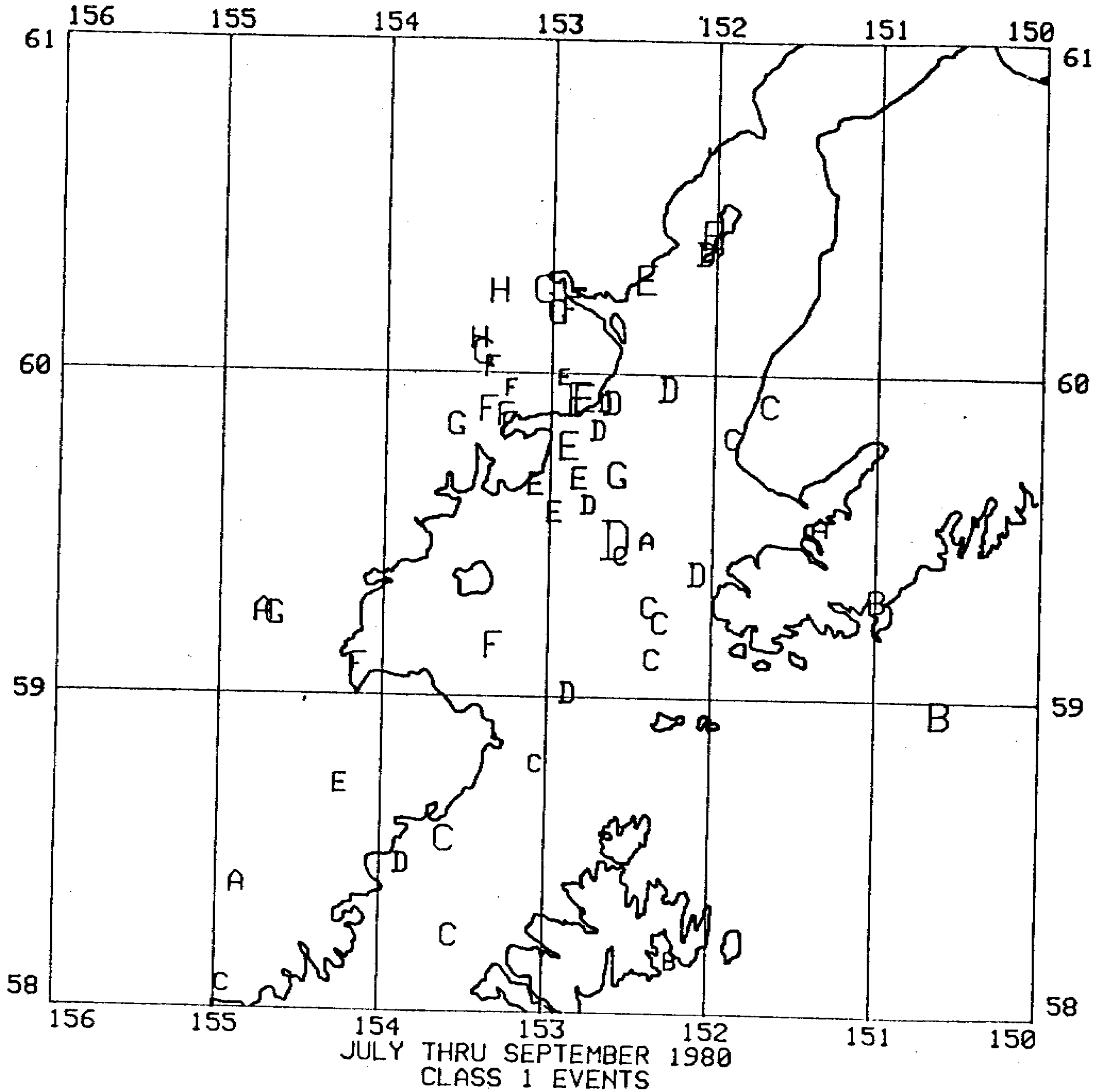

Figure 9. Cook Inlet epicenters.

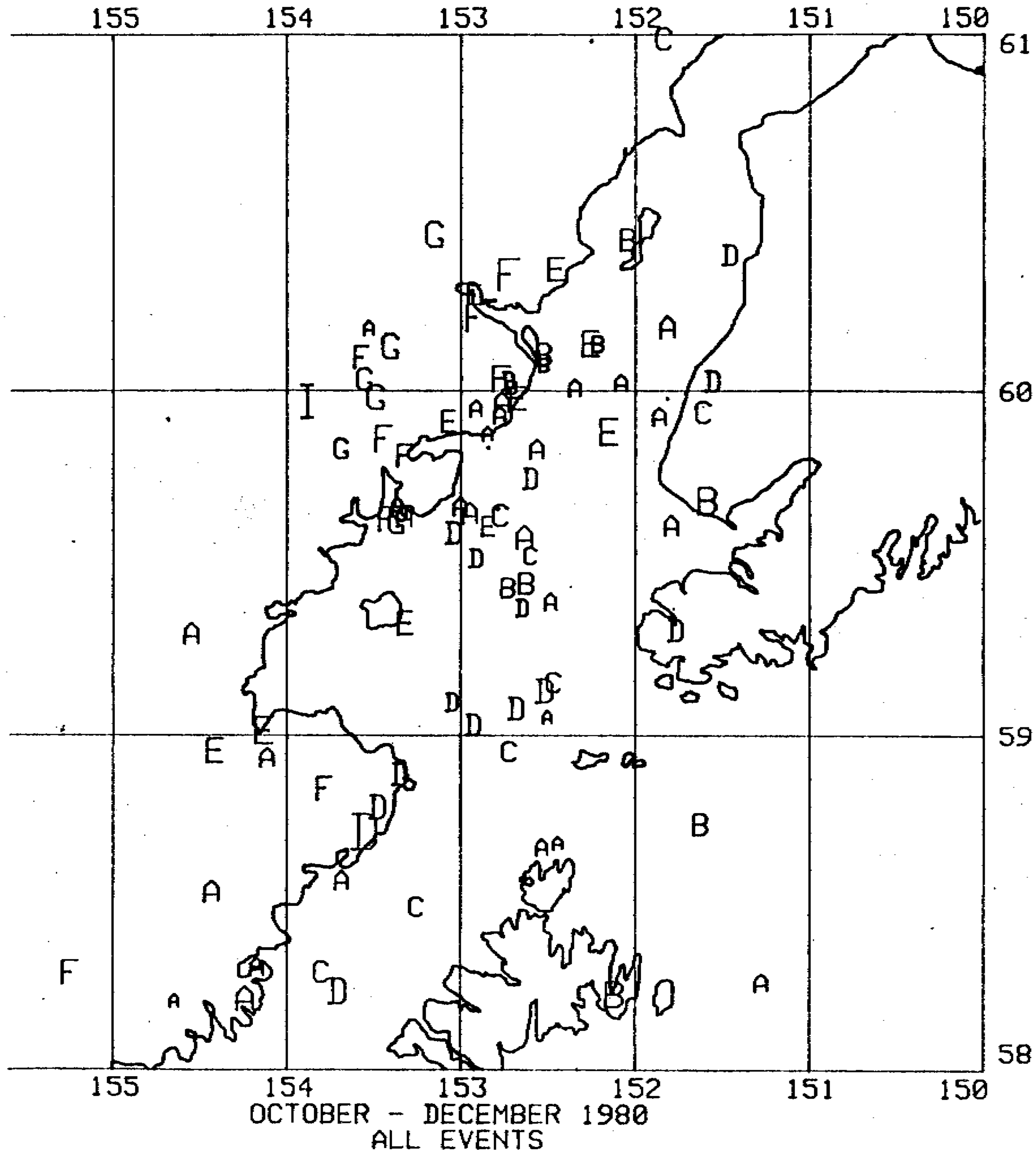

Figure 10. Cook Inlet epicenters.

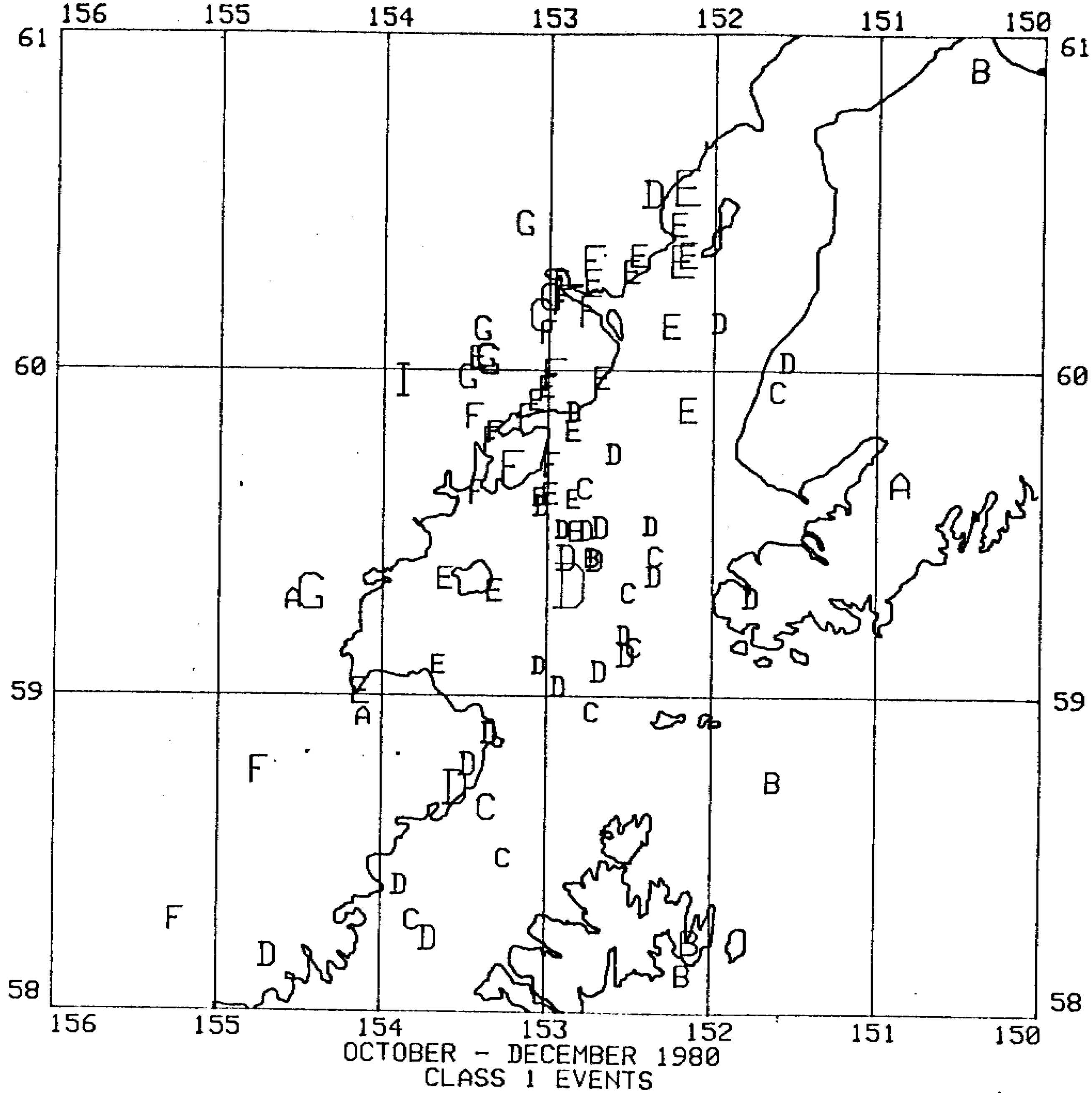

Figure 11. Cook Inlet epicenters.

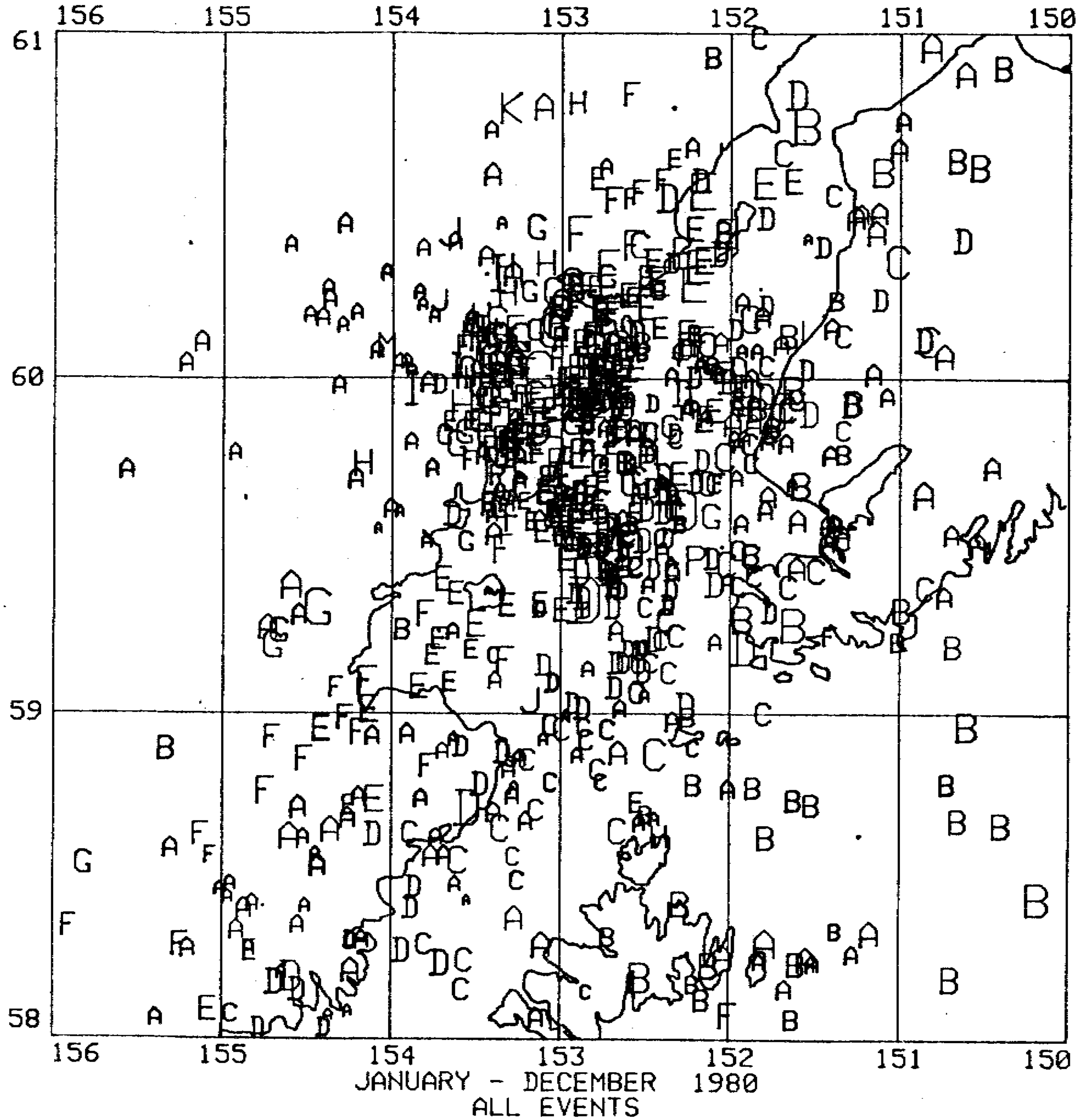

Figure 12. Cook Inlet epicenters.

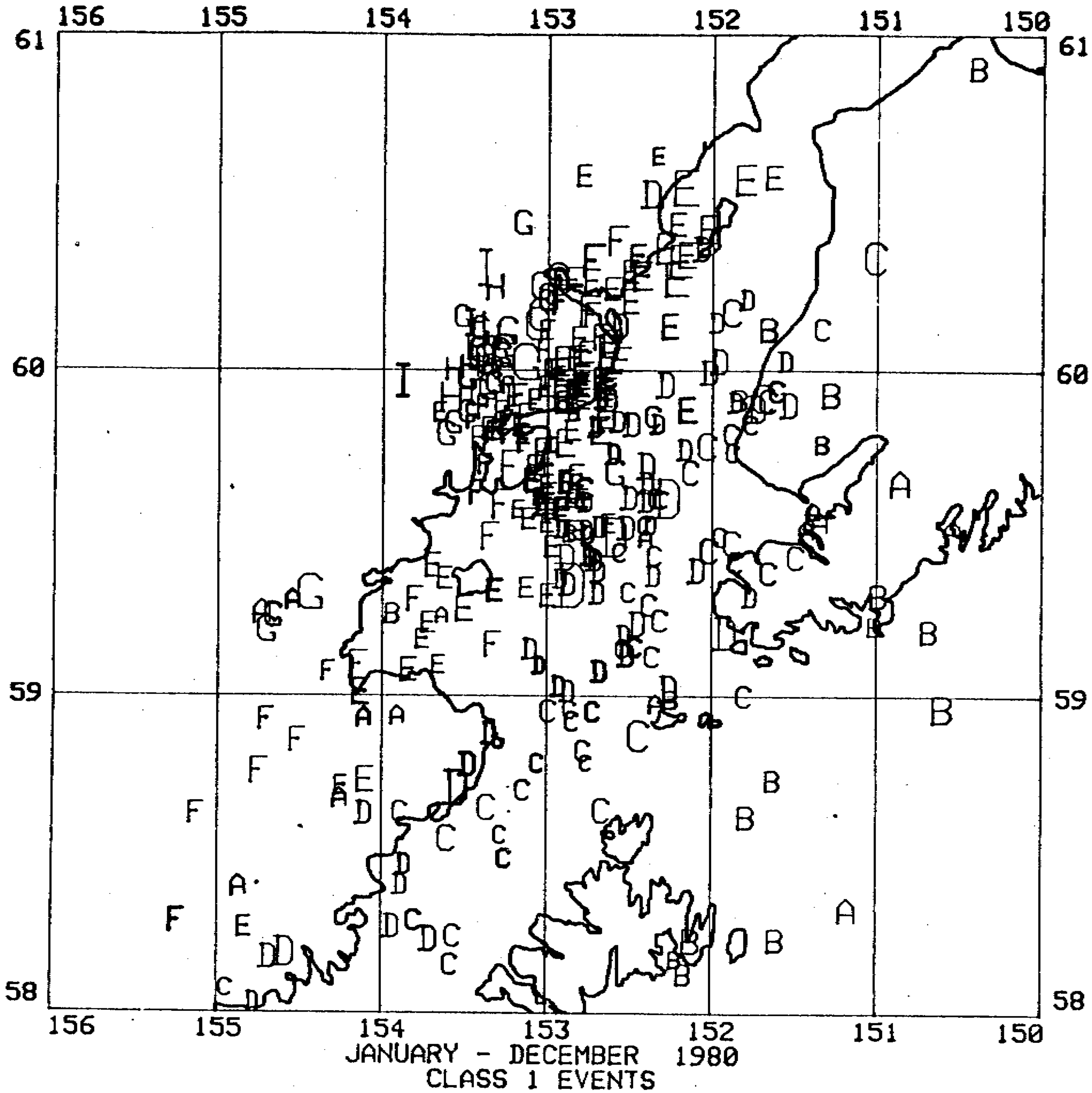

Figure 13. Cook Inlet epicenters.

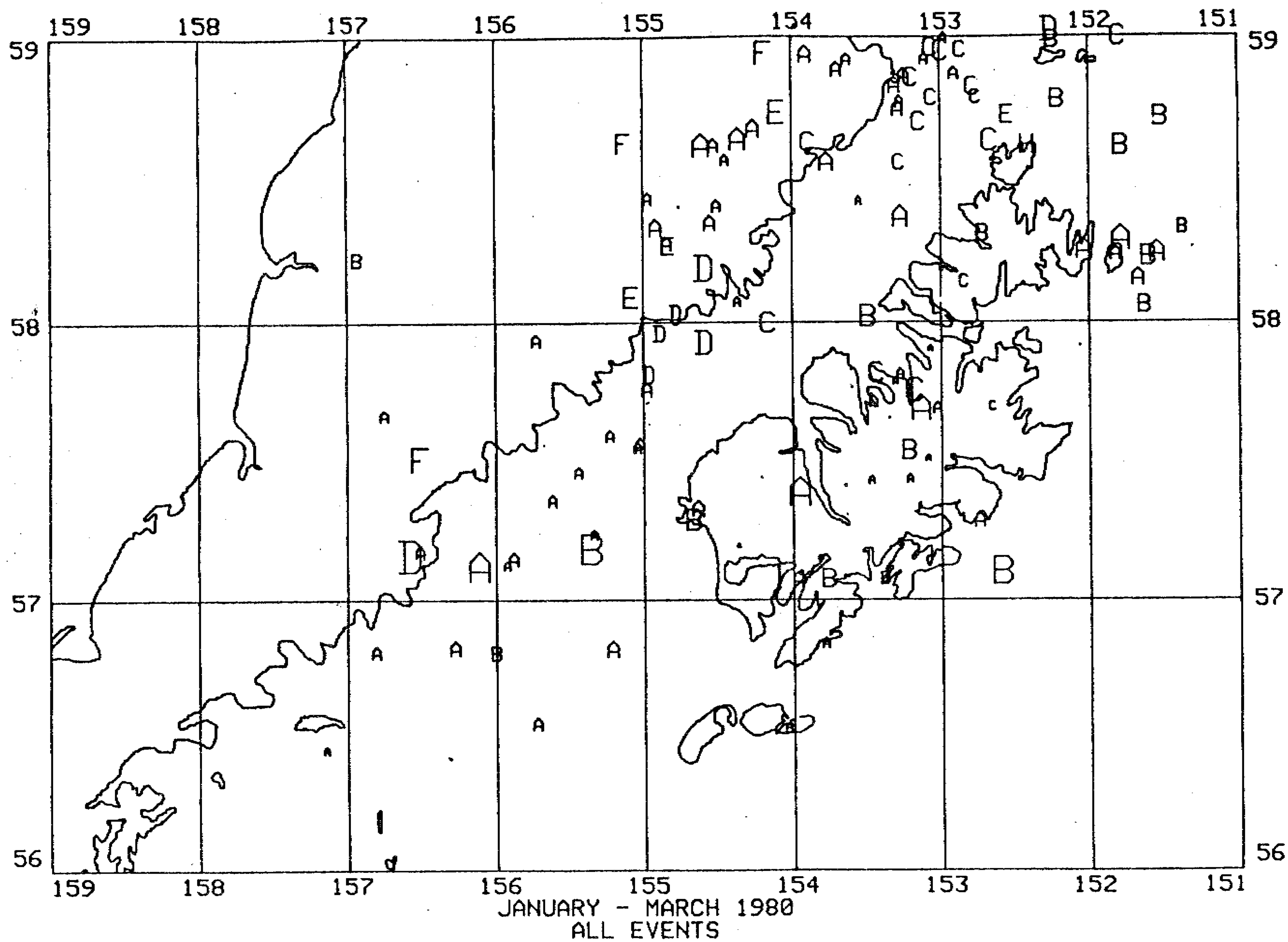

Figure 14. Alaska Peninsula/Kodiak epicenters.

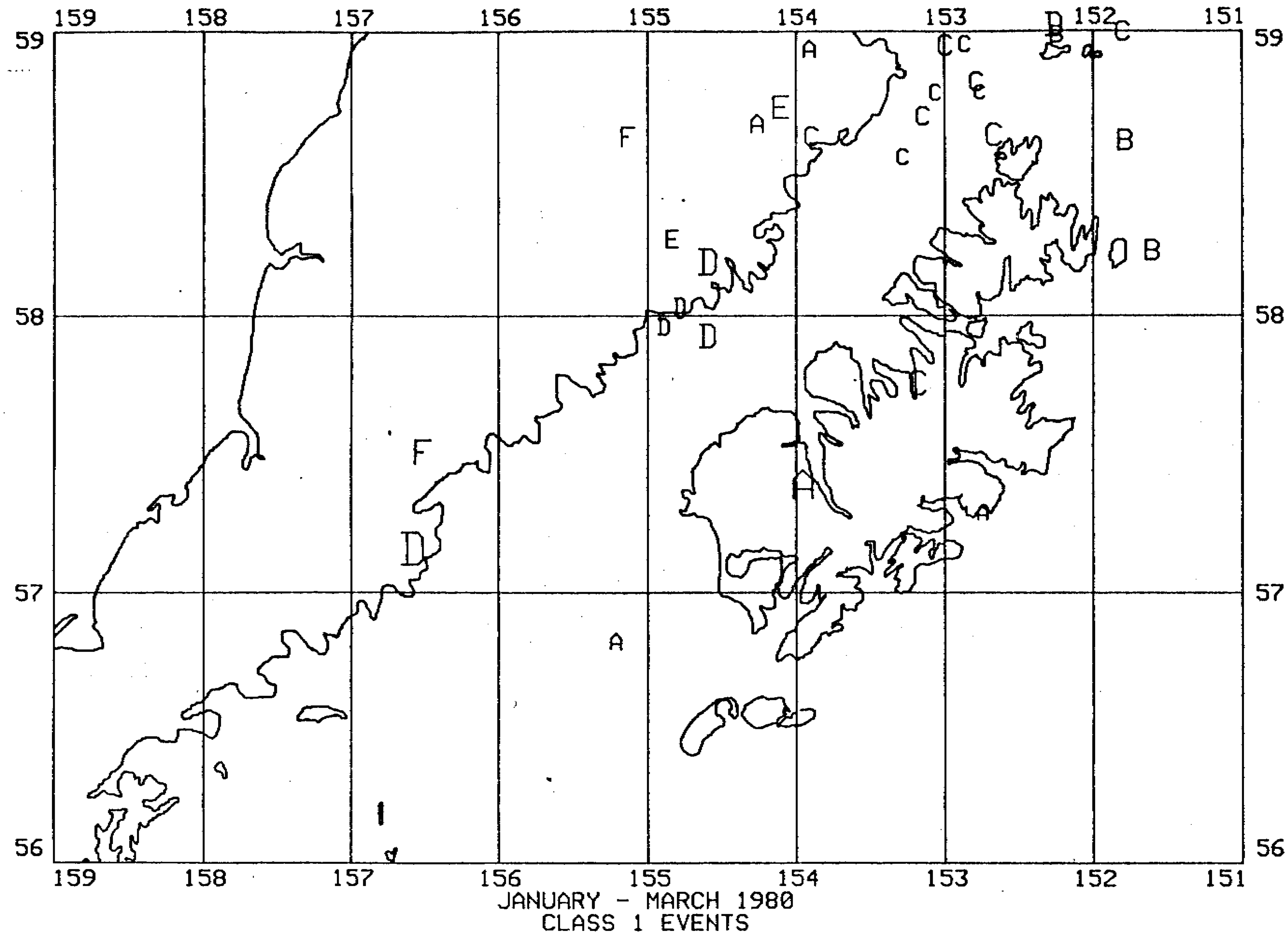

Figure 15. Alaska Peninsula/Kodiak epicenters.

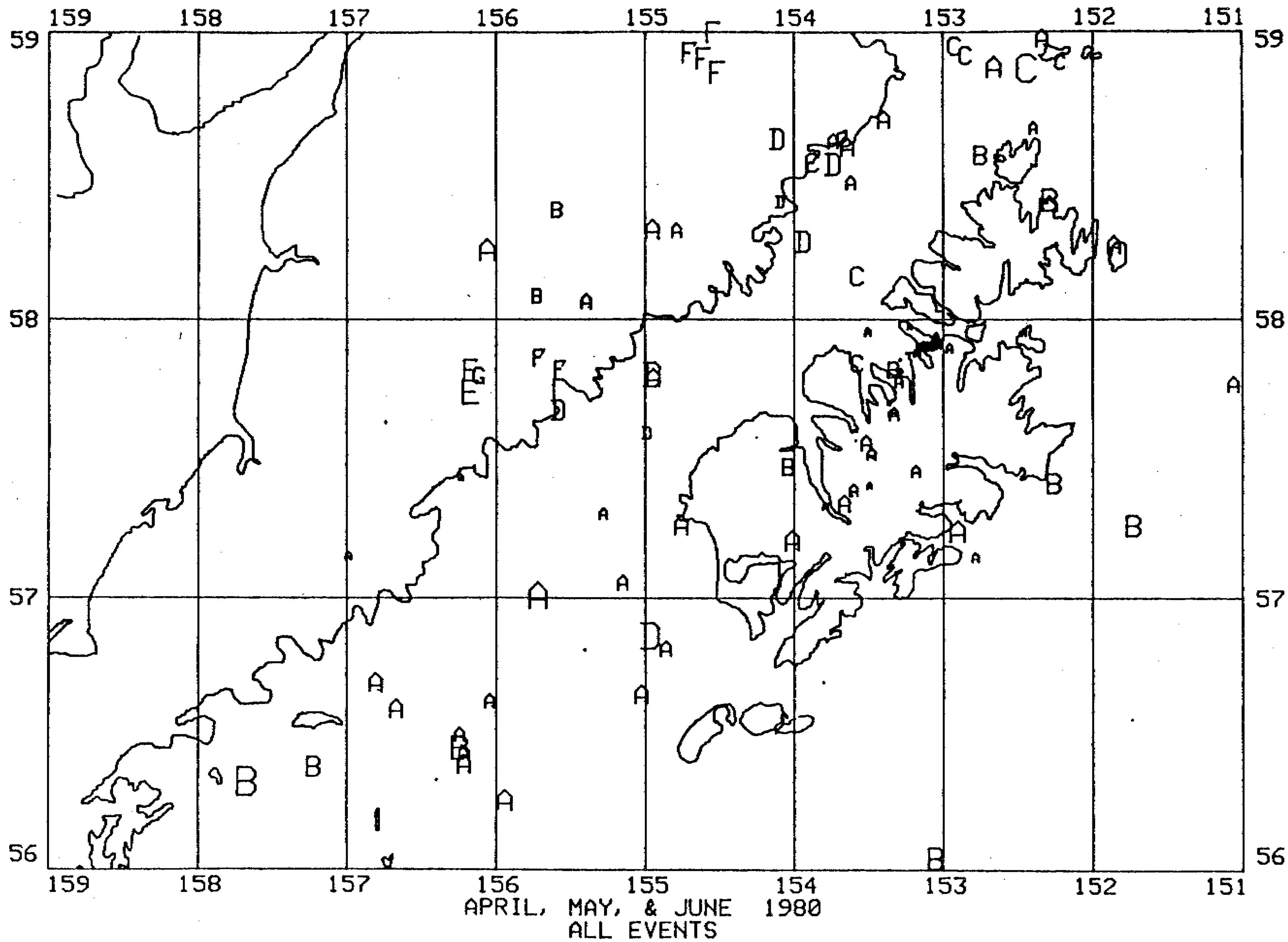

Figure 16. Alaska Peninsula/Kodiak epicenters.

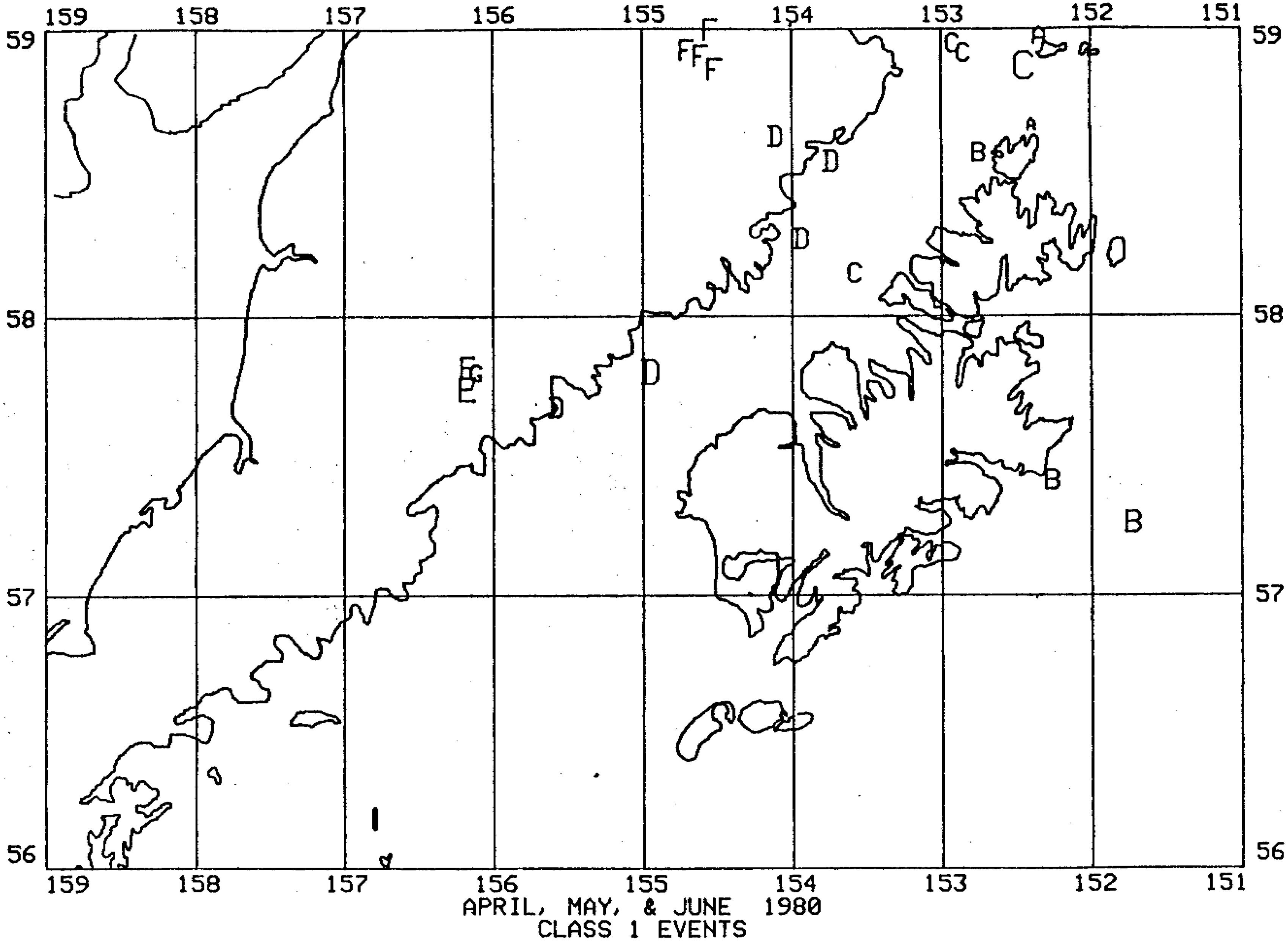

Figure 17. Alaska Peninsula/Kodiak epicenters.

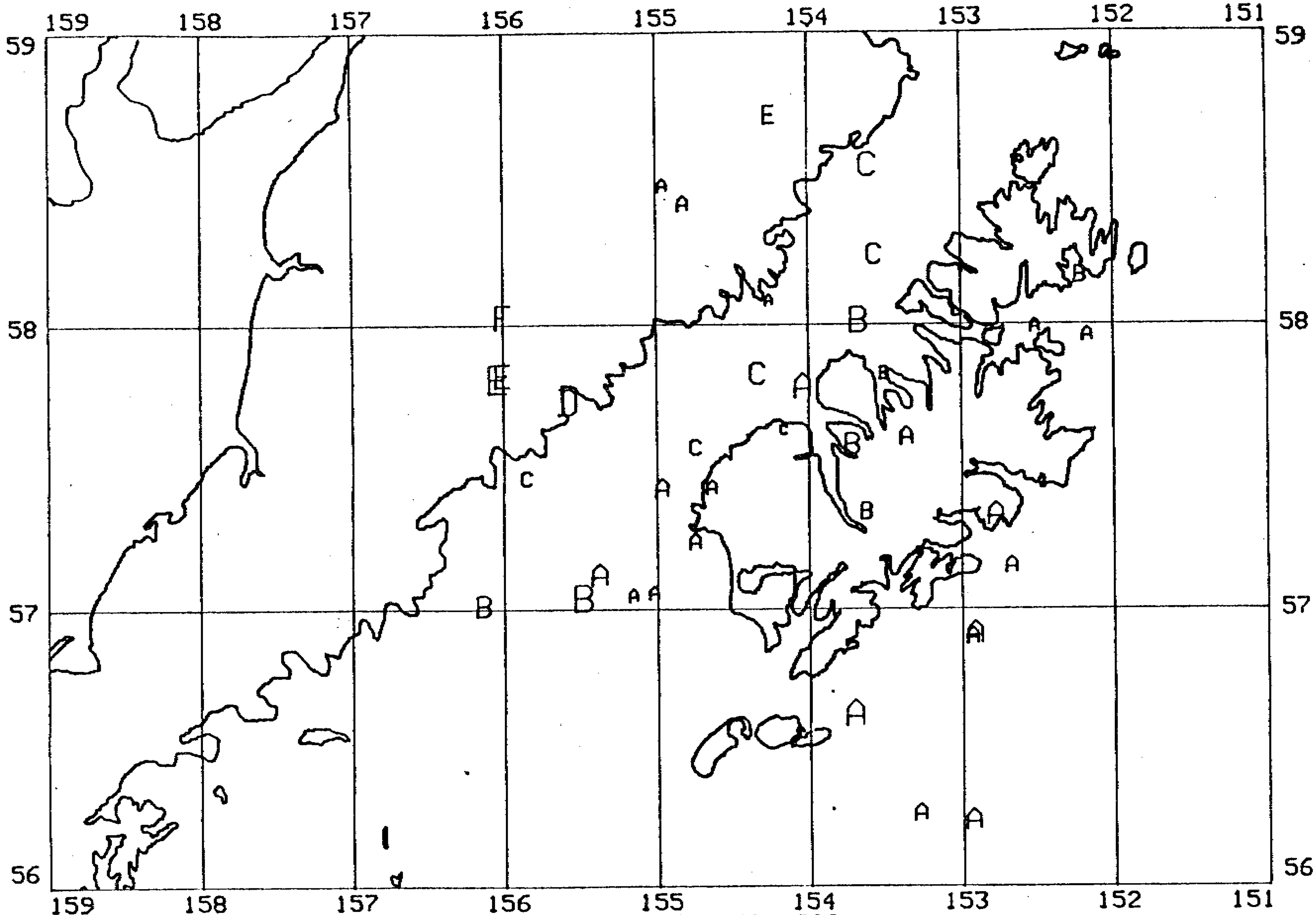

JULY THRU SEPTEMBER 1980
ALL EVENTS

Figure 18. Alaska Peninsula/Kodiak epicenters.

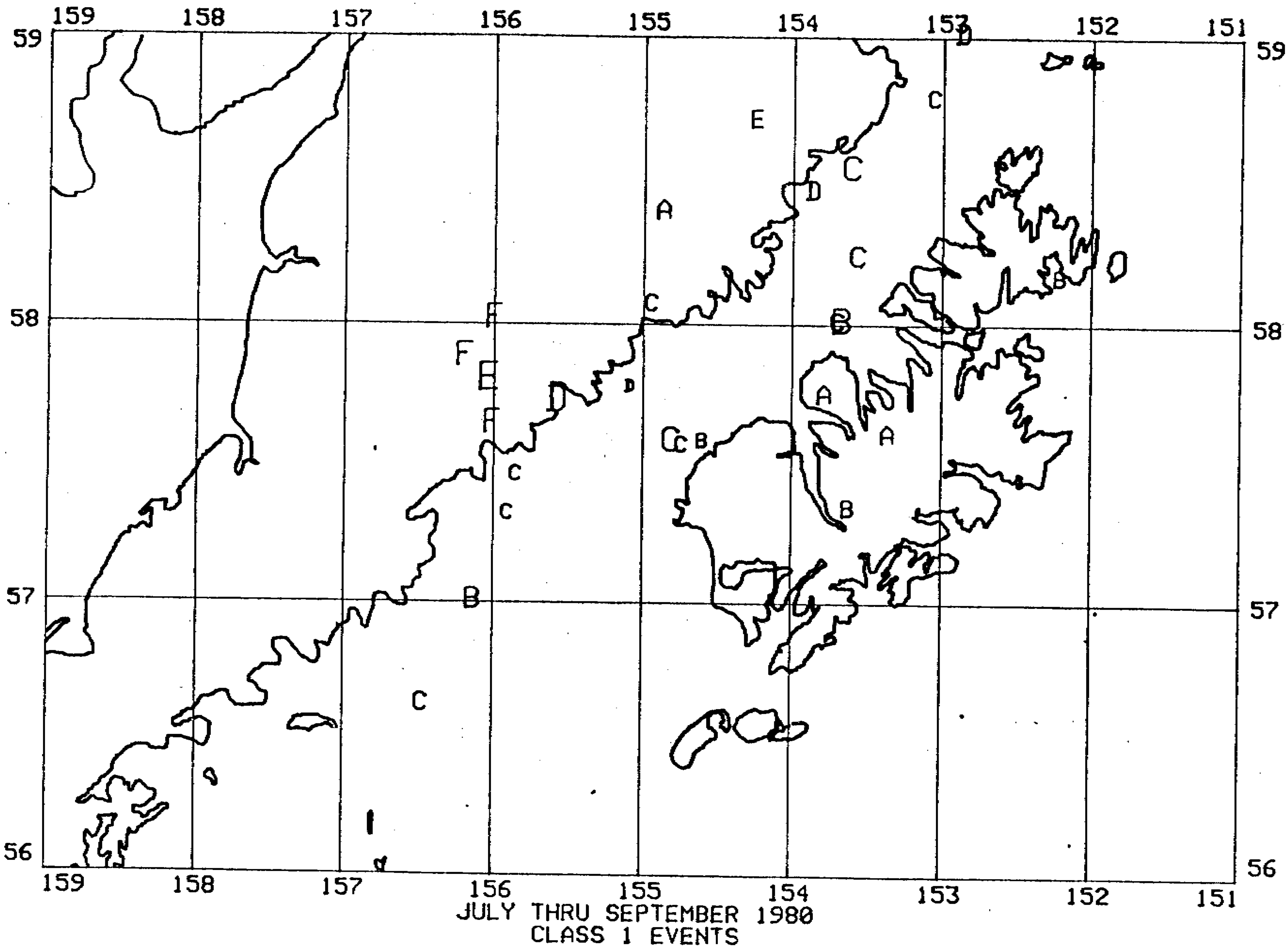

Figure 19. Alaska Peninsula/Kodiak epicenters.

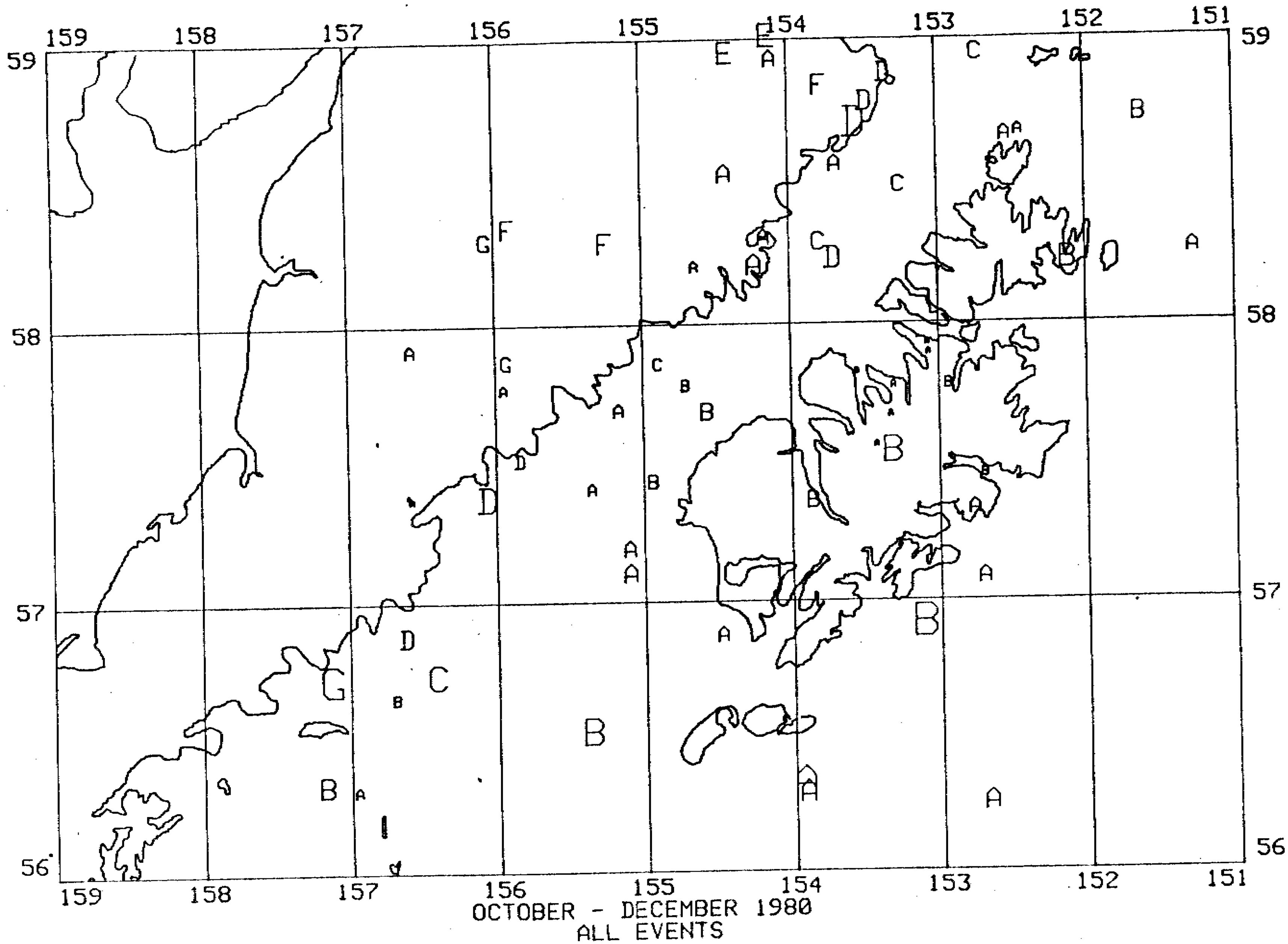

Figure 20. Alaska Peninsula/Kodiak epicenters.

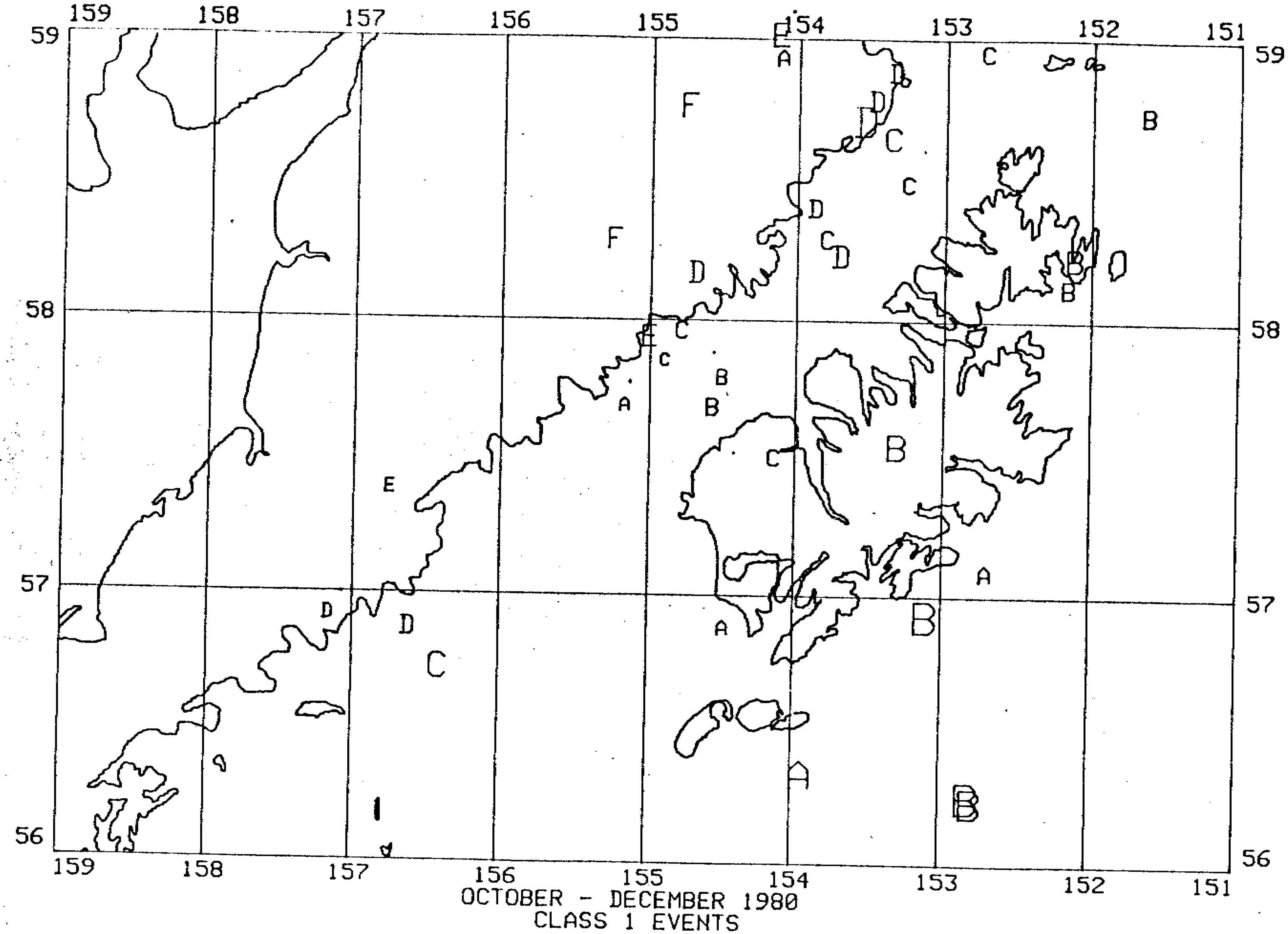

Figure 21. Alaska Peninsula/Kodiak epicenters.

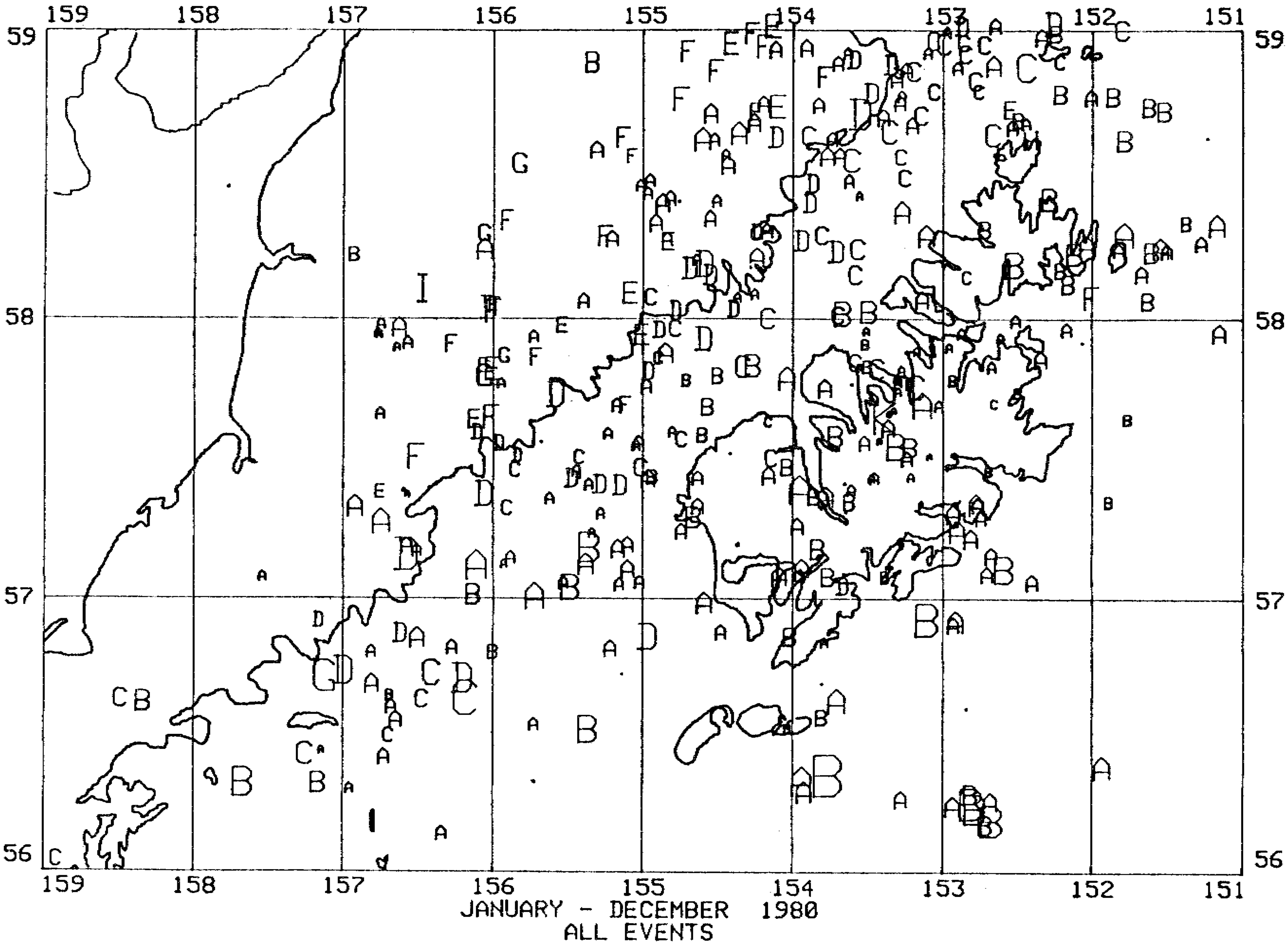

Figure 22. Alaska Peninsula/Kodiak epicenters.

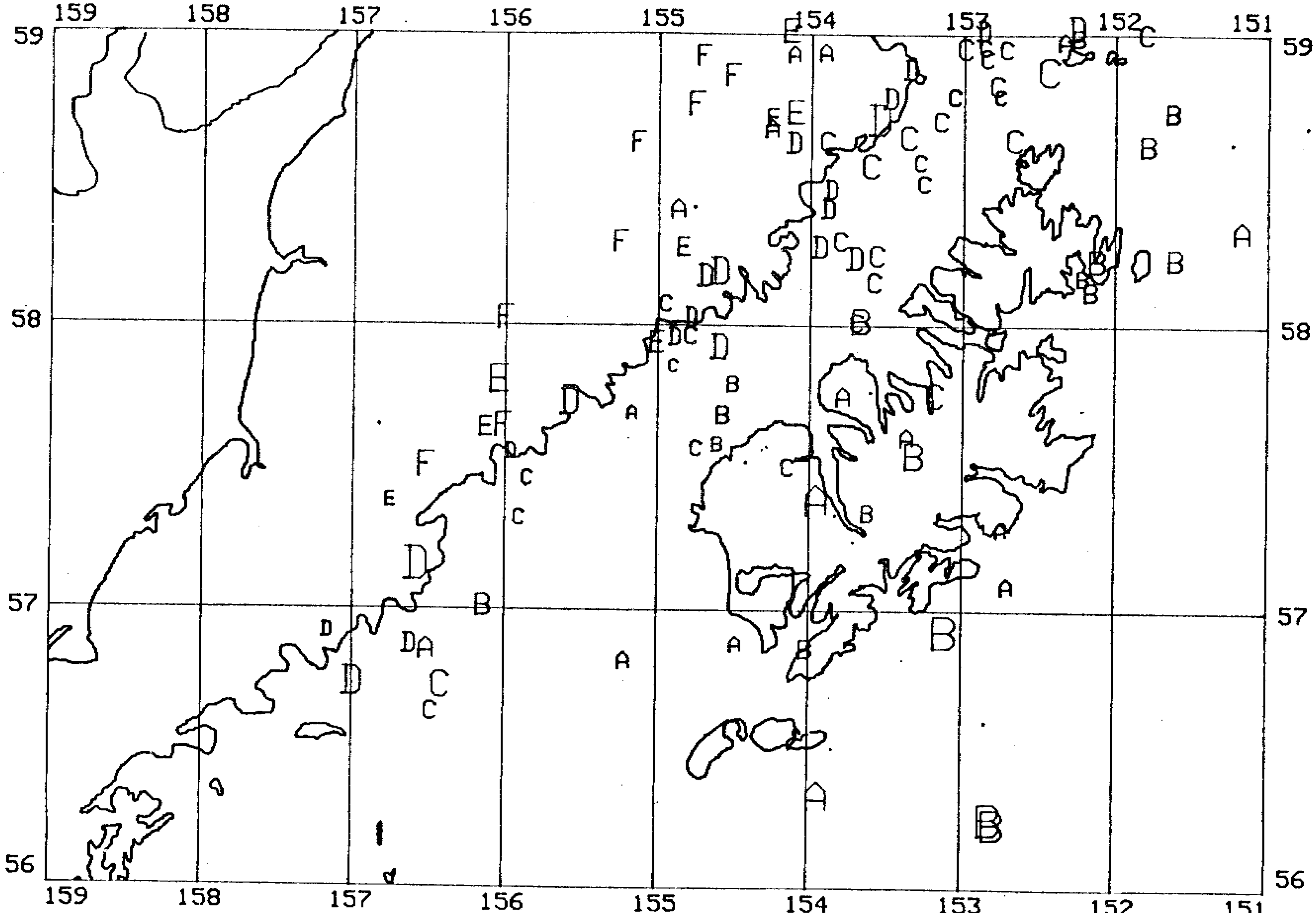

JANUARY - DECEMBER 1980
CLASS 1 EVENTS

Figure 23. Alaska Peninsula/Kodiak epicenters.

Davies et al. (1981) propose a model where the seismic activity in the shallow thrust zones displays a cyclic behavior:

(1) rupture in the form of a great earthquake across the shallow thrust zone with aftershock activity occurring over many years across most of that zone;

(2) locking of the shallow thrust zone and substantial decrease of seismic activity along it while strain is being accumulated along the thrust zone;

(3) stress concentrations building up at the lower edge of the thrust zone accompanied by an increased seismic activity. Eventually the accumulated strain along the thrust zone is released during the next great earthquake and the cycle resumes. Thus, if the concentration of locally determined events at the lower edge of the 1938 thrust zone is real, the 1938 rupture zone might just be entering stage (3) of the above cycle.

Shallow seismicity outside the two shallow thrust zones (1964, 1938) continues to be diffuse and no correlation appears to exist between it and known faults. Shallow earthquake swarms continue to be recorded beneath certain volcanoes that show hydrothermal activity. Activity in the Benioff zone at intermediate depths (focal depth >50 km) continues to show a tendency toward clustering beneath certain volcanoes, e.g., Iliamna, Augustine, Douglas, Peulik; the Iliamna cluster is by far the most prominent of these.

B. <u>Relocation of hypocenters off Kodiak Island using Ocean Bottom Seismometer data</u>

An array of Ocean Bottom Seismometers (OBS) was installed on the Kodiak Island shelf by the University of Texas under an OCSEAP sponsored program (RU 579). The eleven station array was first deployed from June 23 to August 14, 1979 and redeployed in 1980 on the continental shelf off southern Kodiak in the zone of unusually intense shallow seismicity. The purpose of the deployment was:

(1) to compare hypocenter locations based solely on the land-based network (the events lie outside this network) with locations obtained by combining land- and OBS-station data, and

(2) to study whether the hypocenters determined by the joint network do correlate with some of the active faults that have been mapped on this part of the Kodiak continental shelf.

Only 7 of the 11 deployed OBS instruments produced useful data. Unfortunately, too few earthquakes were recorded in the shelf area of interest to allow us to address the second problem. However, enough data were recorded by the OBS system to address problem (1). A total of 16 events were used for the study. These events were routinely located using first P-wave arrival times only. Only 7 of the 16 events (events 1, 2, 4, 5, 7, 15 and 16 in Table 1) were located with at least five P-readings and with an RMS travel time residual of less than .5 seconds (class 1 events; for definition see Appendix 1). After arrival times from the OBS-stations become available, the develocorder films were reread in order to obtain additional P- and also S-arrivals. The events were then located based upon 3 methods:

(1) P-readings from the land based network;

(2) P- and S-readings from the land-based network and;

(3) P- and S-readings from both the OBS and land based networks.

Hypocenter parameters for the 16 events based upon methods (2) and (3) are

Table 1. Comparison of earthquake hypocenter locations, based on P and S-readings for land stations only and based on combined land and OBS network data.

Event	Land Network Location	Land & OBS Network Location
1	57.556N 154.994W 86km	57.631 155.009 88km
2	57.263N 154.581W 55km	57.261N 154.586W 57km
3	57.247N 155.543W 94km	57.233N 155.440W 99km
4	57.472N 154.600W 69km	57.466N 154.587 69km
5	56.499N 155.871W 38km	46.497 155.873 36
6	56.516N 156.056W 75km	56.575N 156.072W 82km
7	55.977N 153.108W 29km	56.039N 153.333W 38km
8	56.021N 153.191W 29km	56.027N 153.267W 45km
9	55.491N 153.708W 55km	55.897N 153.614W 73km
10	56.053N 153.200W 36km	56.110N 153.309W 47km
11	56.297N 152.482W 20km	56.177N 152.445W 44km
12	56.152N 152.561W 18km	56.186 152.667 28km

13	56.408N 151.775W 23km	56.313 152.613 23km
14	56.302N 152.040W 21km	56.437N 152.183W 24km
15	56.913N 151.188W 33km	56.968 151.213 38km
16	57.241N 151.292W 40km	57.258N 151.349W 41km

given in Table 1. The locations based on method (3) are considered the best ones.

In deriving the locations, a dual velocity structure was used such that travel times from the hypocenter towards land based stations were calculated based upon the regional structure we use for this area routinely, while a special shelf velocity model derived by Shor et al. (1972) was used for calculating travel times to the OBS stations. A travel time correction for depth of deployment was also made for the OBS stations. Table 2 shows quality control parameters from the output of our routine hypocenter location program HYPOELLIPSE. N_p and N_s refer to the number of P and S readings, used for the locations. Gap refers to the largest azimuthal separation in degrees between neighboring stations and DMIN is the distance in kilometers from the epicenter to the closest station. Subscripts 2 to 3 correspond to the location methods 2 and 3 described above. D_a, D_b and D_c refer to the epicentral shift between the final epicenter based on all data from the combined network and the epicenter based on (a) the original routine P readings (D_a), (b) the epicenter based on additional P readings (D_b), and (c) the epicenter based on both P and S readings from the land network (D_c).

The events fall into two groups, one northeast of Kodiak Island (events 1-6) and the other in the shelf area to the south of Kodiak Island (events 7-16). Though the OBS network provides additional readings for the first group of events, the additional OBS data do not necessarily result in more accurate locations since neither the azimuthal coverage nor the distances from the epicenter to the closest stations are improved. This is reflected in the lower average epicentral shift between the final land network solutions and the combined network solutions of 4 km for

Table 2. Quality control parameters for the 6 events listed in Table 1 (see text for explanation of symbols used).

Event	Land Net N_p	Land Net N_s	OBS Net N_p	OBS Net N_s	Gap_2 [°]	Gap_3 [°]	$DMIN_2$ [km]	$DMIN_3$ [km]	D_a [km]	D_b [km]	D_c [km]
1	7	1	5	3	236	236	79	79	8	7	8
2	5	2	2	2	239	239	42	42	5	5	0
3	6	4	1	1	285	283	91	91	32	1	6
4	6	3	1	1	227	227	14	14	1	2	1
5	7	1	2	0	224	224	83	83	7	7	0
6	5	5	3	3	335	282	115	115	99	5	7
7	7	0	5	0	246	103	78	18	22	15	15
8	6	2	4	4	242	103	77	15	24	7	5
9	4	1	1	1	308	308	89	23	50	34	10
10	7	0	1	1	240	173	73	73	15	9	9
11	5	1	2	2	286	163	106	44	75	7	3
12	5	1	1	1	291	204	102	57	33	3	8
13	6	2	2	1	290	165	99	55	50	11	14
14	5	0	2	0	314	163	97	38	86	9	9
15	6	2	2	0	301	230	80	80	46	18	6
16	5	1	1	0	287	287	58	58	8	5	5
Averge mislocation with respect to final epicenters, based on all data									35	9	6

events of the first group if compared to 8 km for events of the second group for which the addition of OBS readings does generally improve the azimuthal coverage and closest station distance. Unfortunately, because of malfunctioning of some of the OBS stations, the azimuthal coverage for some of these events is still rather poor. The largest improvement in epicentral location (if we consider the solutions based upon P and S-readings from the combined network as the most accurate ones) comes not from the rather limited additional OBS data but from a more careful scrutiny of the P-arrivals (rereading) and the use of additional P-readings from the land network. The average epicentral mislocation of the original locations obtained from routine data analysis based upon the land network is 35 km, while the mislocation is only 9 km after the records had been reread and additional P-readings were incorporated (Table 2). Addition of S-readings further lowers the average mislocation to 6 km. The corresponding average values for well recorded events (events 1, 2, 4, 5, 7, 15 and 16) are 14 km (routine location), 8 km (after rereading; P arrivals only) and 5 km (after rereading P and S arrivals). Events 7 and 8 probably provide the best estimate of the location accuracy of the land network. For these events both azimuthal station coverage and distance to to the closest station from the epicenter where substantially improved by the OBS system and the two events were recorded well by both systems. The average distance betweeen the final land network epicenter and that from the combined network is 10 km. In addition to the hypocentral depths based on the land network are shallower by about 10 km than the depths calculated from the combined land and OBS system.

Although only a few events were recorded well by the combined land-OBS network, some conclusions can be drawn as to the accuracy of hypocenter locations in the shelf areas based on land network readings of poorly recorded events.

1. Hypocenters of poorly recorded (i.e., small magnitude) events determined from routinely processed data are mislocated on the order of several tens of kilometers, while hypocenters of better recorded events are on the average mislocated by about 15 km.
2. Careful scrutiny of the recorded data and greater care in their use in the location process greatly reduces the mislocation error.
3. Addition of S-phase readings in the location process generally improves the error but not to the extent as the careful rereading of the P-phase for each event does.
4. The average error of epicenters of shelf events that have been carefully located with land network data is about 10 km. This error estimate must be considered tentative since few events were recorded such that the hypocentral solution from the combined network could be considered well constrained. However, the indication that the land network can locate well recorded shelf events fairly accurately conforms with the results of a similar experiment in the central Aleutian area (Fröhlich, et al., personal communication).

C. Source Mechanism Studies

Focal mechanisms (or fault plane solutions) of earthquakes can be used to determine the type of faulting that is associated with the rupture process at the earthquake source. From the type of faulting, the stress regime that produced failure can be deduced. The mechanical behavior of a tectonic system (e.g., plate subduction) can thus be derived if a statistically significant set of solutions in both time and space can be accumulated.

e are currently compiling focal mechanisms of intermediate depth earthquakes in central Cook Inlet. The depth of these events range from about 60 to 200 km and the events originate within the deeper portion of the subducting Pacific Plate. Many of these events belong to the cluster of intermediate depth seismicity which we have persistently observed over the past years beneath Iliamna Volcano (Pulpan and Kienle, 1979).

The study uses the first motions of P-waves recorded at local Alaskan short-period stations of networks operated by (1) the U.S. Geological Survey (R.U. 210), (2) the NOAA tsunami warning system and (3) the University of Alaska. Stations of the first 2 networks are shown in Figure 24. The station locations of the Cook Inlet, Alaska Peninsula/Kodiak network operated by us under this contract are shown in Figure 3.

In principle, first motion polarities plotted onto the upper or lower hemisphere of a sphere surrounding the focus of an earthquake (the focal sphere) permit the definition of two perpendicularly intersecting planes through the center of the sphere (the focus) one of which is the fault plane. The orientation of the two planes is found by trying to separate the first-arriving P-wave ground motions into dilatational and compressional quadrants. Figure 25 shows the solutions for 20 events (the projection used for the lower focal sphere is Lambert equal area). The two possible rupture planes shown in each solution separate dilatational and compressional arrivals into 4 quadrants. The ambiguity as to which of the two planes is the actual fault plane is inherent in the method used. Additional data beyond P-wave first motion information is needed to make the choice between the two possible fault planes. However, irrespective of which plane actually ruptured the principal stress axes can be uniquely

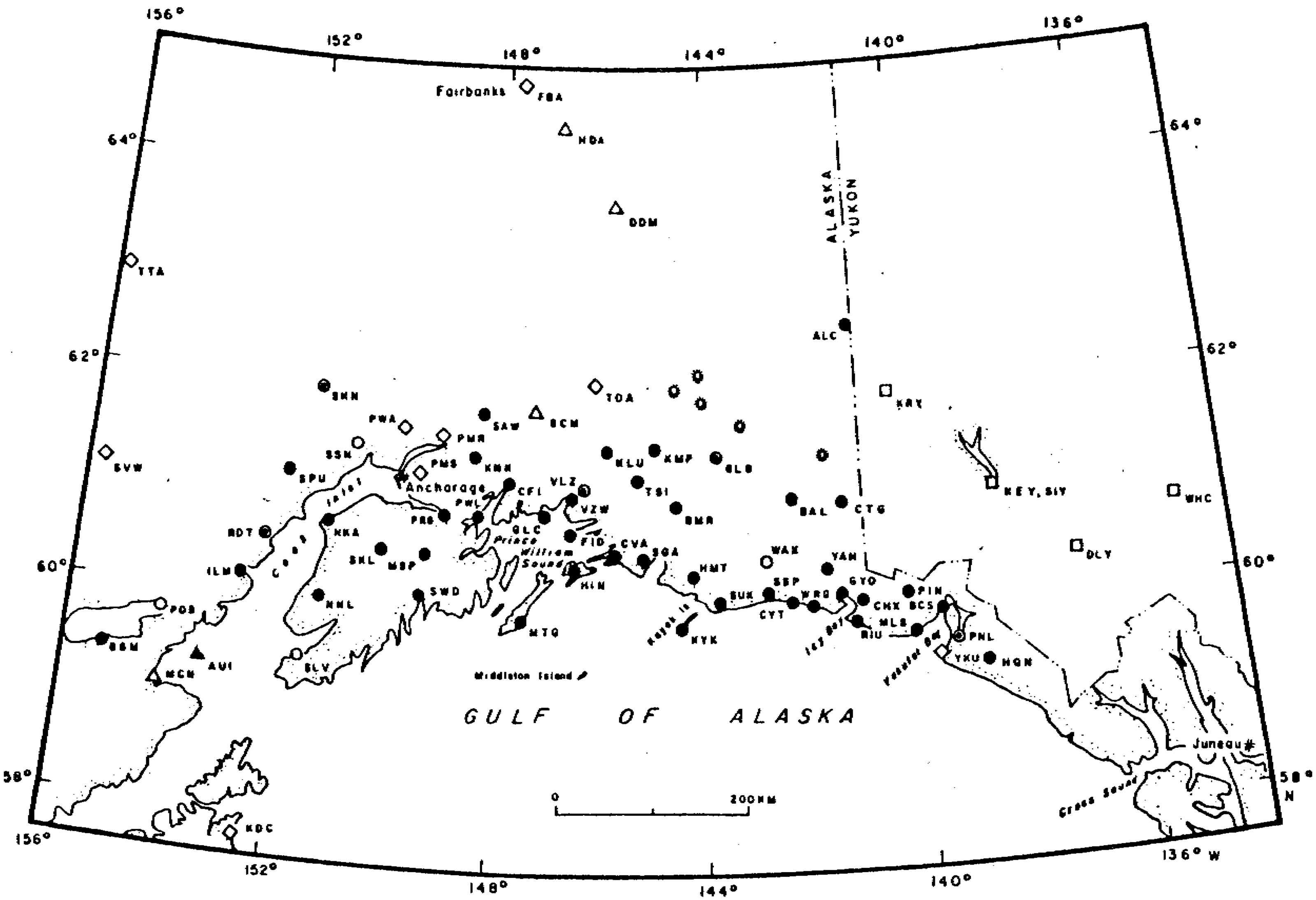

Figure 24. Map showing the locations of USGS, NOAA tsunami warning and other seismograph stations in southern Alaska. Several of these were used in preparing the fault plane solutions for Cook Inlet. The symbols are as follows: solid circles, vertical component USGS seismograph; circles with dots, three-component USGS seismographs; open circles, USGS stations not reporting during this quarter; diamonds, NOAA stations; triangles, Univ. of Alaska stations; squares, Dept. of Energy, Mines and Resources, Canada.

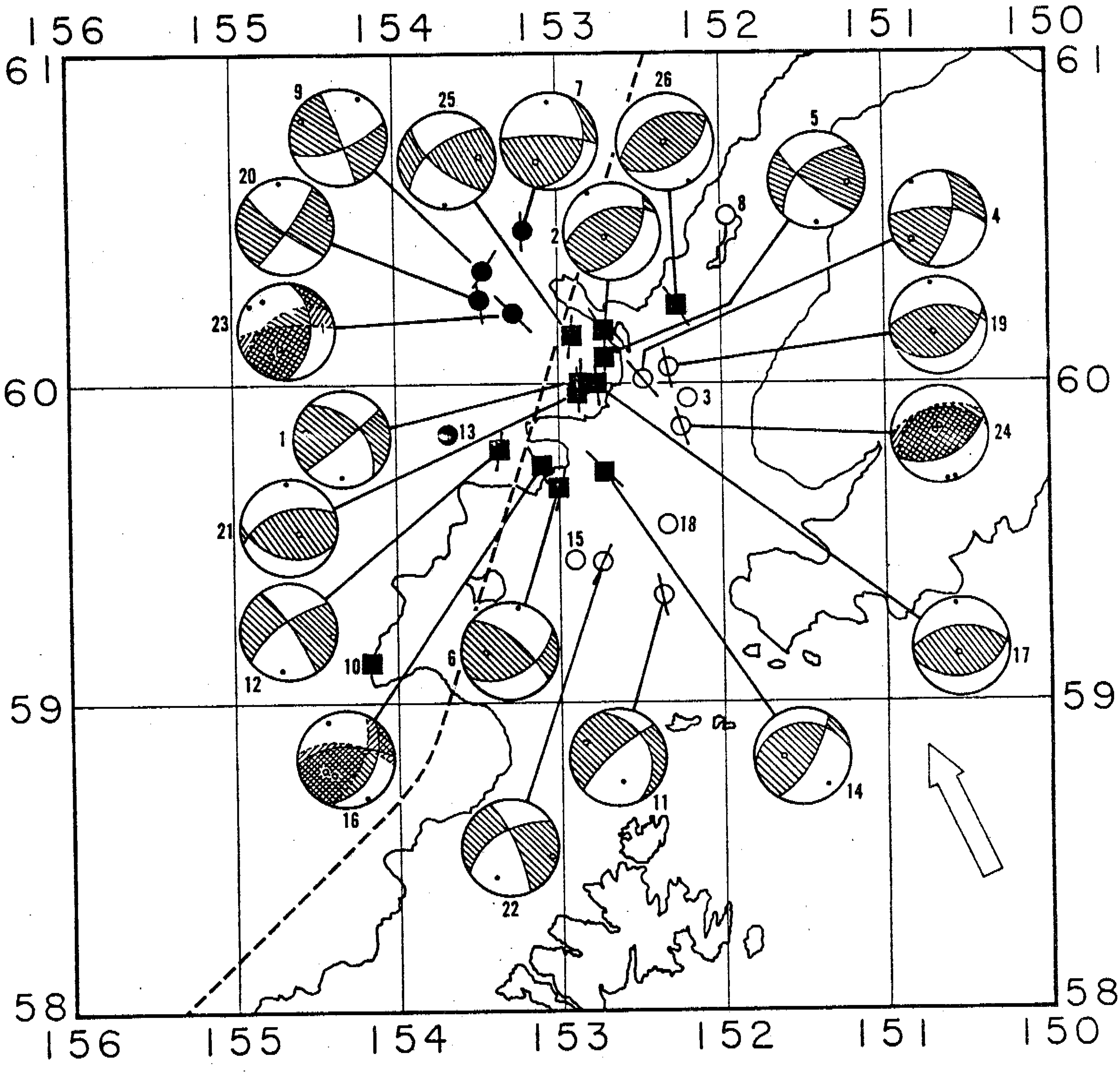

Figure 25. Twenty fault plane solutions for intermediate depth (77 to 206 km) Cook Inlet earthquakes plotted on a projection of the lower focal hemisphere. Quadrants with compressional arrivals are lined. Two possible solutions are given for some events. Open circles indicate tension (T) axes, solid dots indicate compression (P) axes. The epicenters of the 20 events are shown as open circles (shallower than 100 km), solid squares (100 to 150 km deep) and solid circles (deeper than 150 km). Horizontal bars through the epicenter symbols indicate the orientation of the nearly horizontal P-axes as derived from the fault plane solutions. Open arrow shows the plate convergence direction and the dashed line shows the strike of the Benioff zone.

determined for each event, the compressional stress axis bisecting the dilatational quadrants and the tensional axis bisecting the compressional quadrants. The intermediate stress axis is defined by the intersection of the two planes. In Figure 25 we show the compression and tension axis for each individual solution. Table 3 is a compilation of the hypocentral parameters and the orientation of the 3 principal stress axes for each event.

The data we show in Figure 25 does not conform with stress directions commonly found in other parts of the Aleutians or other island arcs. Stresses in the deeper portion of subducting plates that sink gravitationally are often characterized by stress alignments along the plunge of the plate; e.g., the down-dip stress is commonly tensional in slabs that penetrate less than 300 km, such as the Aleutian slab (e.g., Isacks and Molnar, 1971). Plates that reverse curvature, i. e., unbend, show again down-dip stress alignment but both down-dip compressional events as well as down-dip tensional events occur in two zones, in an upper compressional and in a lower tensional region, symmetric about the plane of zero bending stress (Hasegawa et al., 1978; Engdahl and Scholz, 1979).

In last years annual report we discussed 4 fault plane solutions of intermediate depth events orginating within the subducting plate in Cook Inlet. These seemed to indicate that the deeper portion of the Pacific plate beneath Iliamna Volcanoe may be in down-dip tensional stess, i.e., gravitationally sinking. However, the much larger 20 event data set for the same region we have now compiled in Figure 25 does not show any systematic trends pointing to stress regimes associated with either gravitational sinking, bending or unbending of the plate. In all three cases either the tension or compression axes should be

TABLE 3

FOCAL MECHANISMS OF INTRA SUBDUCTING PLATE EVENTS
IN COOK INLET, ALASKA

		Epicenter			Axis of Compression (P)		Axis of Tension (T)		Null Axis (B)	
Event #	Date	Latitude degrees	Longitude degrees	Depth km	Trend °E of N	Plunge Degrees	Trend	Plunge	Trend	Plunge
1	01/25/79	60°00.08'N	152°51.47'W	112.60	178	24	283	27	52	52
2	02/01/79	60°08.39'N	152°43.54'W	119.90	230	3	59	71	327	19
3	02/01/79	59°58.87'N	152°13.41'W	76.80						
4	02/09/79	60°00.87'N	152°29.38'W	83.80	324	1	234	30	57	60
5	02/21/79	60°05.65'N	152°43.83'W	118.10	184	16	95	35	296	52
6	03/09/79	59°40.58'N	152°59.34'W	107.60	08	12	266	45	110	43
7	04/04/79	60°26.63'N	153°13.09'W	185.10	342	30	212	48	88	28
8	04/04/79	60°30.79'N	151°57.57'W	91.90	161	18	266	38	51	48
9	04/04/79	60°19.58'N	153°27.22'W	205.90	26	12	292	16	151	70
10	04/16/79	59°07.17'N	154°09.45'W	129.90	180	4	275	40	85	50
11	04/20/79	59°19.97'N	152°21.42'W	79.95	170	48	294	26	40	32
12	06/26/79	59°47.42'N	153°22.10'W	136.80	191	16	99	5	354	72
13	07/04/79-a	59°50.13'N	153°40.10'W	150.10	13	8	276	54	108	37
	-b				26	18	282	40	132	46

Event #	Date	Latitude	Longitude	Depth	P AXIS Trend	P AXIS Plunge	T AXIS Trend	T AXIS Plunge	B AXIS Trend	B AXIS Plunge
14	08/15/79	59°43.62'N	152°43.60'W	101.60	138	22	271	59	40	22
15	10/27/79	59°26.12'N	152°53.31'W	82.51	35	17	126	6	240	73
16	02/01/80-a	59°43.79'N	153°05.64'W	106.10	335	12	227	56	73	30
	-b				151	4	246	39	54	51
17	06/03/80	60°00.35'N	152°48.34'W	108.10	350	7	224	80	81	7
18	06/11/80	59°33.38'N	152°19.56'W	59.25	09	16	268	33	121	53
19	06/15/80	60°02.29'N	153°20.38'W	148.00	349	10	218	77	81	10
20	06/17/80	60°16.07'N	153°28.92'W	193.80	353	14	83	2	177	78
21	08/12/80	59°59.14'N	152°52.61'W	104.20	355	11	121	72	262	14
22	08/30/80	59°26.82'N	152°44.06'W	77.45	201	29	105	10	357	60
23	09/05/80-a	60°12.25'N	153°17.43'W	167.40	323	20	215	40	72	43
	-b				305	6	204	61	38	29
24	09/13/80	59°51.69'N	152°14.81'W	95.16	153	4	331	85	72	11
25	09/21/80	60°08.30'N	152°54.17'W	122.50	181	6	86	37	281	53
26	01/01/80	60°13.45'N	152°15.96'W	93.08	154	1	259	86	63	5

aligned with the plunge direction of the plate (plunge of order 45° in our area with an azimuth of about 300°), yet most of the solutions given in Table 3 do not show this. What the solutions do show is a persuasive and consistent pattern of horizontal pressure axes that follow a northerly trend fairly close to the orientation of the strike of the Benioff zone (compare Figure 25, which shows the strike of the Benioff zone as a dashed line and the pressure axes orientation as horizontal bars across the epicentral symbols). This observation also holds for the 4 solutions reported in last years annual report.

We speculate that this peculiar orientation of the compressive stress may have to do with the misalignment of the convergence and plunge directions of the subducting plate in Cook Inlet. While the convergence direction and plunge of the subducting plate are nearly parallel for the Alaska Peninsula and McKinley segments of the plate, the convergence direction in Cook Inlet is oblique to the plunge of the plate (compare Figure 25, open arrow indicates the direction of plate convergence). Hence the Cook Inlet segment of the subducting plate may be obliquely driven north against the McKinley segment of the plate resulting in horizontal compression more or less along the strike of its deeper portions (60 to 200 km). Additional hydrostatic compressional stress perpendicular to the Cook Inlet segment of the plate could rotate the pressure axes of individual events counterclockwise slightly off the strike of the Benioff zone which would fit the observed pressure axes orientation better. If kinks (or bends in the deep plate with vertical axes) exit within the subducting plate near the lower and upper ends of Cook Inlet as perhaps reflected in the dramatic change of volcanic alignment from Katmai to Lower Cook Inlet and and absence of volcanoes in the McKinley arc segment north of Cook Inlet, such kinks or bends may actually strengthen the descending plate (like a T-bar) preventing the Cook Inlet segment to bend or unbend (hence the absence of solutions that fit bending or unbending).

Obviously, the current picture we have of the stress regime of the deeper portion of the Pacific plate in Cook Inlet is still very unclear and our current interpretation is highly speculative; we also do not yet really understand the significance of the persistent concentration of intermediate depth events beneath Iliamna Volcano. We clearly need more fault plane solutions of well constrained events to resolve the intriguing stress regime of the subducting plate in Cook Inlet.

D. Volcanology

During the past year we have principally concentrated on the identification of volcanic centers and associated hazards in the Katmai area. We have determined that Fourpeaked Mtn., Devils Desk, Mt. Stellar-Mt. Denison, Snowy Mt. and Kejulik Mtn. are also volcanic centers (Table 4), in addition to those already identified by Griggs (1922), Fenner (1926, 1950) and Muller et al. (1954) (Table 4 and Figure 2). Previously unreported fumarole activity was discovered at Kaguyak Crater and on Snowy Mtn. In 1980, we concentrated our field work on volcanic centers where little or no geologic and petrologic data were yet available.

Mt. Douglas is an ice-covered volcanic center with a well-developed cone that has been moderately dissected by glacial erosion. A summit crater approximately 200 m in diameter contains a blue-green, ice-free, crater lake. Dark-gray scum floating on the lake may represent sulfide minerals being deposited in the lake; a distinct sulfurous odor was noticed while flying around the lake. An active fumarole field on the west side of the crater has kept the crater walls and rim free of snow. Outcrops on the north flank of the mountain include a sequence of massive lava flows

TABLE 4

VOLCANIC CENTERS IN KATMAI

Name Latitude (N) Longitude (W) Of Feature Highest Point (ft)	Type of Volcanic Feature	Date of Last Eruption/ Type of Activity	Current Activity	Comments	Petrography
Douglas 58°51.3' 153°32.4' crater lake 7,020	stratocone	no historic activity	hot crater lake, steaming ground, shallow seismicity	heavily glaciated	two-pyroxene andesite, some olivine
Fourpeaked 58°46.1' 153°40.8' center of summits 6,903	stratocone	no historic activity	not active	hydrothermally altered summit but no apparent solfataric activity heavily glaciated and dissected	two-pyroxene andesite, minor hornblende
Kaguyak 58°36.8' 154°03.5' island in crater lake 2,956	caldera, 2.4 km diameter, contains lake up to 189 m deep (no elevated temperature)	no historic activity	weak solfataric activity and bubbling at shore of central island, shallow seismicity	not glaciated, pyroclastic flow apron, several internal and external lava domes	two-pyroxene dacite, minor rhyolite and andesite, some hornblende and quartz
Devils Desk 58°28.5' 154°17.9' highest peak 6,410	deeply dissected volcanic center	no historic activity	not active	central vent and dike complex, glaciated	two-pyroxene andesite, minor olivine and hornblende

Kukak 58°27.6' 154°20.9' fumarole field on northernmost peak 6,710	stratocone	no historic activity	summit solfatara field, occasional steam plumes, shallow seismicity	heavily glaciated	two-pyroxene andesite, minor dacite
Denison 58°25.1' 154°26.9' highest peak 7,520	stratocone includes Mt. Stellar, an erosional remnant	no historic activity	not active	heavily glaciated and dissected	two-pyroxene andesite
Snowy 58°20.1' 154°41.0' highest peak 7,090	dissected row of 3 peaks, aligned over 3.5 km in a NE-SW direction	no historic activity	fumarole field on peak 6,875, frequent intense shallow earthquake swarms	heavily glaciated	olivine, two-pyroxene andesite
Katmai 58°15.8' 154°58.5' center of crater lake 6,715	caldera, 2 x 2.5 km diameter, contains lake 200 m deep and rising at a rate of 3 m/yr (Motyka, 1978)	1912, paroxysmal caldera forming eruption, ash flow	lake has elevated temperature, there is a zone of up-welling (lake bottom fumarolic activity)	glaciated	andesite dominant, minor basalt, dacite and rhyolite (Fenner, 1926, 1950)
Griggs 58°21.2' 155°06.2' summit crater 7,650	stratocone, deeply covered with 1912 tephra	no historic activity	summit crater with hot ground and steam vents, high pressure fumarole on SW-flank	few small glaciers	andesite (Fenner, 1926)
Novarupta 58°16.0' 155°09.4' dome 2,760	dome	1912, believed by some to be source of Valley of 10,000 Smokes ash flow	weak steaming		rhyolite, minor andesite (Curtis, 1968)

Trident 58°13.8' 155°07.2' summit of new flank cone 3,800	cinder cone, lava flows and block avalanches, formed in 1953/54, 57, 58, 59/60, 63	1968, normal explosion (30,000 ft)	sulfurous fumaroles within and outside summit crater walls; vent plugs grown in 1961, 66, 74 (subsided again by 1975); normal explosions (plumes to 20-46,000 ft) in 1953, 60, 61, 62 (plug destroyed), 63, 64, 67 (plug destroyed), 68; no vent plug in 1980; shallow seismicity	located on SW-flank of Trident Group	two-pyroxene andesite (Ray, 1967)
Mageik 58°11.8' 155°14.6' summit crater lake 7,140	stratocone	1964, questionable event 1927, normal explosion	small crater lake at 70°C (Hildreth, personal communication) $P_H \approx 1$, frequently weak steam plume, shallow seismicity	heavily glaciated	dacite (Fenner, 1926)
Martin 58°10.2' 155°21.0' summit crater solfatara field 6,110	stratocone	no historic activity	almost continuous steam plume, fed from solfatara field in crater floor, small acid lake, shallow seismicity	glaciated	olivine, two-pyroxene andesite
Kejulik 58°01.7' 155°40.0' center of complex 5,510	deeply dissected volcanic center	no historic activity	not active	central vent and dike complex, few small glaciers	two-pyroxene andesite

3 to 10 m thick. Samples from two sites on the north flank of the volcano were two-pyroxene andesite; olivine is present in some samples.

Fourpeaked Mtn. is an extensively dissected ice-covered volcanic center. A deep. glacier-filled breach cuts the volcanic cone on the southwest side and exposes massive lava flows up to approximately 25 m in thickness that dip away from a central zone of hydrothermal alteration. The central altered zone may therefore represent a former vent for the volcanic center. No active hydrothermal activity was noted on Fourpeaked Mtn. Rock samples taken from a site on the southern flank of the volcano were two-pyroxene andesite.

Kaguyak Crater is a lake-filled circular caldera with an average diameter of 2.4 km. The maximum depth obtained from seven soundings in the lake was 189 m. The nearly circular form of the caldera has been altered by two small secondary craters along the western rim of the caldera (Fig. 26). At least two domes have been emplaced within the caldera and domes have also been emplaced outside of the caldera to the east and southeast (Fig. 26). Numerous dikes, sills and plugs intrude the cone-building lava and fragmental volcanic debris flows are exposed along the inner wall of the caldera. An extensive blanket of pyroclastic flows up to 100 m thick (Fig. 26) surrounds the caldera. These pyroclastic flows extend for several kilometers away from the caldera and are probably related to the caldera-forming eruption. A sample from soil immediatly overlying the pyroclastic flow deposit gave a single uncorrected C^{14} age of 1,060 ± 120 yrs. Low temperature (21°C), sulfurous fumaroles were found on the dome that forms a small island near the center of the crater lake (Fig. 26). We collected rock samples from over 20 localities during 10 days of geologic mapping of the Kaguyak Crater area. Dacite is the dominate rock type, but rhyolite and andesite are also found. Plagioclase, augite and hypersthene are common as phenocrysts together with smaller amounts of quartz and hornblende.

Devils Desks is a deeply dissected volcano, completely surrounded by the Hook Glacier system. The central vent has been breached on the east side exposing an extensive region of hydrothermal alteration. Thick lava flows and lahars, exposed in narrow ridges that extend above the ice, dip steeply away from the central vent on the north, west and south flanks of the volcano. Rock collections made on these ridges are dominated by two-pyroxene andesites. Hornblende or olivine is found in some of the samples. No active hydrothermal activity was observed at Devils Desk.

Kukak Volcano is a rugged cone virtually covered by the heavily crevassed Hook Glacier. Small exposures in a cliff-face on the east side of the summit reveal lava flows 10 to 30 m thick with crudely developed columnar jointing. An active fumarole field near the summit keeps some areas free from ice but other fumaroles form holes in the ice. The rock around the fumarole field is extensively altered and ranges in color from light pink to purple. We could only find one site to land on Kukak Volcano located 3 km west of the summit; all samples consisted of glacial debris. Striations on basement rock together with the present configuration of the glaciers suggest the debris we sampled was probably derived from Kukak Volcano. Two-pyroxene andesite is the most common lithology. Flow-banded rocks are common with the flow banding defined by alternating layers of clear and brown glass.

Mt. Stellar and Mt. Denison are rugged volcanic peaks that are also extensively covered by the Hook Glacier system. Lava flows exposed in cliffs near the summits of these peaks are approximately 20-50 m thick and some have poorly developed columnar jointing. The dip of these flows suggests a source for these lavas somewhere near the summit of Mt. Denison. Close to the summit of Mt. Denison, exposed coss-cutting tephra layers appear to represent a dissected volcanic vent. We suggest that the Mt. Stellar-Mt. Denison volcanic complex is one dissected volcanic center with a vent near the present summit of Mt. Denison and we name this center Denison Volcano. No active hydrothermal activity was found near this volcanic center. We were only able to sample one lava flow in this complex at a site approximately 5 km northwest from Mt. Denison. The lava flow is a two-pyroxene andesite about 50 m thick.

Snowy Mtn. is another heavily dissected volcanic center, largely covered by the Serpent Tongue Glacier system. The vent for the complex is probably located near the summit of Snowy Mtn. Lava flows 5 to 15 m thick are exposed south and west of the summit dipping away from the summit region suggesting a near summit vent. A previously unreported fumarole field was discovered on the 6,875 feet high peak 0.7 km east-northeast of Snowy Mtn. The fumaroles keep the area free of ice and rocks in the immediate area are altered to a light tan-pink color. Rock collections were made near the summit and from the lava flows on the southwest flank of the volcanic center. The most common rock type is an olivine-bearing two pyroxene andestie. Hornblende is found in some samples.

The Kejulik volcanic center is located southwest of Mt. Martin. Lava flows approximately 15 to 50 m thick dip away from an unnamed peak (elevation of 4,980 ft.); we propose to name this center Kejulik Volcano. Orientation of the lava flows and thick tephra layers suggest that the vent was near the present summit. The center is extensivley dissected and only remnants of lava flows are found preserved on basement rock ridge tops. These ridges form a radial pattern around the proposed vent. No hydrothermal activity was observed. The dominant rock type in our sample collections from two localities is two-pyroxene andesite.

Based on our preliminary examination of the geomorphology of volcanic centers in Katmai and the geochemistry of their eruptive products, we identify Kaguyak Crater and the group of volcanoes surrounding Mt. Katmai, including Mt. Katmai itself, Novarupta, Mt. Griggs, the Trident group, and Mt. Mageik as the volcanoes with the greatest potential for highly explosive future eruptions. The 2 major valleys draining from these volcanoes to Shelikof Strait, Big River and Katmai River, could become avenues for voluminous pyroclastic flows, lahars and mudflows and lava flows, should these erupt. Based on our limited sampling, the remaining volcanic centers we have now identified in Katmai erupted principally two-pyrexene andesite, which suggests that future eruptions maybe less violent than those of the first group. However, substantial additional hazards exist on those volcanoes that have an extensive ice cover (Douglas, Fourpeaked, Kukak, Snowy, Katmai, Mageik, Martin): During potential future volcanic activity subglacial heating and subsequent melting of the ice and snow cover could produce extensive flash floods. There are numerous examples in the literature to demonstrate just how voluminous and far reaching such outburst floods can be (e.g., chapter 8, fragmental flows, in Macdonald, 1972). For example, in 1963 a lava flow from the crater of Villarica Volcano, Chile, melted the ice and snow near the summit causing a mudflow to rush down the mountain side and out onto the plains tens of kilometers from the source vent, destroying crops and completely obliterating a village. In 1877, a mudflow originating from the glaciated summit of Cotopaxi Volcano, Ecuador, flooded a village 240 km (!)

distant. In Iceland, Katla Volcano and Grimsvötn frequently produce outburst floods caused by subglacial volcanic heating, so called "Jökulhlaups" that in one outburst have produced as much as 6 km^3 (1 1/2 cubic miles) of water at discharge rates of more than 120,000 m^3 per second (more than the discharge rate of the Amazon River). Such flash floods carry large amounts of sand and coarse debris that form extensive flood plains. The Katmai River delta is such a flood plain created during the 1912 eruption of Mt. Katmai. Another Alaskan example of this kind of volcano-glacier interaction is Mt. Redoubt, Cook Inlet, where lahars reached the shore of the Inlet 3,500 years ago burying most of the Crescent River valley with volcanic debris (Riehle et al., 1981) and again in 1966, when flash floods originating at the heavily glaciated summit crater reached the mouth of Drift River at the current tanker terminal site.

In Katmai, all valleys draining from active glaciated volcanic peaks of the Aleutian Range are potentially subject to this kind of flash flood activity. A detailed discussion of volcanic hazards in Katmai is forthcoming in a future report.

VIII. CONCLUSIONS

Seismic risk is greatest in the shallow inter-plate thrust zone between the subducting Pacific plate and the overriding American plate. The thrust zone extends from the Aleutian Trench to where the two plates decouple at depth. This decoupling occurs at a depth of about 50 km roughly beneath the surface trace of the Border Ranges fault on the Kenai Peninsula and along the northern shore of Kodiak Island (compare Figure 1). On the Kodiak shelf proposed lease blocks lie above the shallow thrust zone. There is a lower probability for a great earthquake ($M > 7.8$) to occur within the rupture zone of the great Alaska earthquake i.e., off-shore Kodiak, as compared to the adjacent shelf areas off the Semidi-Shumagin Islands further west, where the shallow thrust zone has not ruptured since the last great earthquake in 1938.

Another important seismic source region is the downgoing slab itself. This intraplate seismicity has not produced great ($M > 7.8$) earthquakes in historic times and probably will not do so in the future, based on comparison with other island arcs. Events associated with the deeper portion of the subducting plate (>60 km depth) seldom exceed $M = 7$. This deeper seismicity that is caused by stresses within the downgoing slab appears not to be uniformly distributed along the strike of the slab, but tends to occur in clusters. Earthquakes tend to cluster beneath certain volcanoes at depths of 100-130 km. The Iliamna cluster is the most intense one in our region and actually in the Aleutian arc.

Fault plane solutions for intermediate depth (60-200 km) earthquakes in the Cook Inlet area do not show the predominantly down-dip extensional or compressional stress that is commonly seen for intermediate depth intra-plate earthquakes elsewhere. The pattern we do see in Cook Inlet is one of generally horizontal pressure axes with orientation close to the strike of the subducting plate. The tension axes assume various non-systematic orientation. The divergence of plate convergence and plate plunge, and additional plate contortion in Cook Inlet may produce this unusual stress field within the downgoing plate.

Seismic activity in the overriding plate continues to be diffuse and does not correlate with known faults in our region. However, we see linear seismic trends in areas where no faults have been mapped, e.g., Deadman Bay, (Kodiak) and offshore Marmot Island (off Afognak). We also continue to locate shallow (< 5 km depth) earthquake swarms that are associated with hydrothermal systems beneath certain volcanoes of the eastern Aleutian arc.

A study of earthquake locations of outer continental shelf events off Kodiak based on combined Ocean Bottom Seismometer (OBS) and land based network data showed that well recorded (i.e., larger magnitude) events can be located quite well by the land network only. The average epicenter mislocation of 16 shelf events was about 10 km.

The volcanic reconnaissance work in Katmai has established that Mt. Douglas, Fourpeaked Mtn., Kaguyak Crater, Devils Desk, Kukak Volcano, Mt. Denison-Stellar, Snowy Mtn., Mt. Katmai, Novarupta, Mt. Griggs, the Trident group of volcanoes, Mt. Mageik, Mt. Martin, and the Kejulik Mtns., all are very young volcanic centers. Shallow (< 10 km deep) earthquake swarms have been located over the past years beneath the volcanoes Douglas, Kuguyak, Kukak, Snowy, Trident, Mageik and Martin. Pulpan and Kienle (1979) speculated that this seismicity may be the result of hydrofracturing in active shallow geothermal reservoirs beneath these volcanoes. During the past field season we did discover hitherto unknown hydrothermal activity at Kaguyak

Crater and Snowy Mtn. and we can now confirm that all volcanoes beneath which we have recorded shallow earthquake swarm activity in recent years do indeed have surface manifestations of hydrothermal activity.

The most silicic and hence explosive magmas have been erupted from the Katmai group of volcanoes (Katmai, Novarupta, Griggs, Tridents, Mageik) and from Kaguyak Crater which may have formed a little more than 1000 years ago (based on one C^{14} minimum age determination). The most common rock type found on the other volcanoes in Katmai is two-pyroxene andesite.

The principal volcanic hazards to offshore development in the Shelikof Strait region would probably be flash floods, mudflows and lahars in the main valleys radiating from the volcanic chain, caused by the interaction of volcanic heat with ice and snow. Pyroclastic flows (glowing clouds) could descend the Katmai River and Big River valleys if renewed explosive activity commences in the Katmai group of volcanoes or at Kaguyak crater. Further offshore, in Shelikof Strait and Bristol Bay volcanic hazards would probably be restricted to heavy tephra falls if one of the Katmai volcanoes becomes active again.

IX. NEED FOR FUTURE STUDY

We decided not to discuss this subject matter in this report in view of the current lease schedule and the winding down NOAA effort in our offshore areas.

X. SUMMARY OF 1981 STUDIES

Routine data analysis of earthquake data was completed for the time period January 1 to June 30, 1981. Hypocenter parameters and epicenter maps for this time window are being submitted to the Juneau Project Office.

Appendix 2 gives monthly epicenter plots of all events and class 1 events for both the Cook Inlet and Alaska Peninsula/Kodiak regions.

Chemical analyses are being obtained for all volcanic rock samples collected during the past field season.

XI. REFERENCES

Curtis, G. H., The Stratigraphy of the Ejecta of the 1912 Eruption of Mount Katmai and Novarupta, Alaska, Geological Society of America, Memoir 116, p. 153-210, 1968.

Davies, J., L. Sykes, L. House and K. Jacob, Shumagin Seismic Gap, Alaska Peninsula: History of Great Earthquakes, Tectonic Setting, and Evidence for High Seismic Potential, J. Geophys. Res., 86(B5), 3821-3855, 1981.

Engdahl, E. R., and C. H. Scholz, A Double Benioff Zone Beneath the Central Aleutians: an Unbending of the Lithosphere, Geophys. Res. Letters, 4(10), 473-476, 1977.

Evans, C. D., F. H. Buck, R. T. Buffler, S. G. Fisk, R. B. Forbes, and W. B. Parker, The Cook Inlet--An Environmental Background Study of Available Knowledge, prepared by the University of Alaska, Resource and Science Service Center, Alaska Sea Grant Program, Anchorage, Alaska, for the Alaska District Corps of Engineers, Anchorage, Alaska, 446 pp. 1972.

Fenner, C. N., The Chemical Kinetics of the Katmai Eruption: American Journal of Science, 248, 593-627, 1950

Fenner, C. N., The Katmai Magmatic Province, J. of Geology, 34, 673-772, 1926.

Griggs, R. F., The Valley of Ten Thousand Smokes: National Geographic Society, Washington, 341 pp, 1922.

Hampton, M. A., A. M. Bouma, R. Von Huene, and H. Pulpan, Geo-Environmental Assessment of the Kodiak Shelf, Proc. Offshore Tech. Conf., April 30-May 3, 1979, Houston, Texas, 1, 365-376, 1979.

Hasegawa, A., N. Umino, and A. Takagi, Double-Planned Structure of the Deep Seismic Zone in the Northeastern Japan Arc, Tectonophysics, 47, 43-58, 1978.

Hildreth, W., Novarupta 1912: Petrology of the Ejectas: Trans. Amer. Geophys. Union, 61, .66, 1980 (abstract)

Hildreth, W., The 1912 Eruption in the Valley of Ten Thousand Smokes, Katmai National Monument, Alaska, 1981 IAVCEI Symp. - Arc Volcanism, Tokyo and Hakone, Japan, Aug. 28 - Sept. 9, 1981, Abstracts, 126-127, 1981 (abstract).

Isacks, B., and P. Molnar, Distribution of Stresses in the Descending Lithosphere from a Global Survey of Focal-Mechanism Solutions of Mantle Earthquakes, Rev. Geophys. Space Phys., 9, 103-174, 1971.

Juhle, W., Iliamna Volcano and its Basement, U. S. Geol. Survey, Preliminary Rep., 74 pp. and map, 1955.

Keller, A. S. and H. N. Reisesr, Geology of the Mount Katmai Area, Alaska: U. S. Geol. Survey Bull., 1058-G, 298 pp. and map, 1959.

Kienle, J., and S. E. Swanson, Volcanic Hazards from Future Eruptions of Augustine Volcano, Alaska, Geophys. Inst. of the Univ. of Alaska, Rep. UAG R-275, 126 pp. and map, 1980.

Lahr, J. C., and G. Plafker, Holocene Pacific-North American Plate Interaction in Southern Alaska: Implications for the Yakataga Seismic Gap, Geology, 8, 483-486, 1980.

Macdonald, G. A., Volcanoes, Prentic-Hall, Englewood Cliffs, N.J., 170-181, 1972.

Magoon, L. B., A. H. Bouma, M. A. Fisher, M. A Hampton, E. W. Scott, and C. L. Wilson, Resource Report for Proposed OCS Sale No. 60 Lower Cook Inlet-Shelikof Strait, Alaska, U.S. Geol. Survey, Open-File Report 79-600, 38 pp., 1979.

Muller E. H., W. Juhle, and M. W. Coulter, Current Volcanic Activity in Katmai National Monument, Science, 119, 319-321, 1954.

Pulpan, H., and J. Kienle, Seismic and Volcanic Risk Studies, Western Gulf of Alaska, OCSEAP Annual Report of Princ. Investigators for Year ending March 1980, Vol. IV: Hazards, 427-496, 1980.

Pulpan, H., and J. Kienle, Western Gulf of Alaska Seismic Risk, Proc. Offshore Tech. Conf., April 30-May 3, 1979, Houston, Texas, 1, 2209-2219, 1979.

Ray, D. K., Geochemistry and Petrology of the Mt. Trident Andesites, Katmai National Monument, Alaska, Unpublished Ph.D. Thesis, University of Alaska, Fairbanks, 198 pp., 1967.

Riehle, J. R., J. Kienle, and K. S. Emmel, Lahars in Crescent River Valley, Lower Cook Inlet, Alaska, Alaska Geol. and Geophys. Survey, Rep. 53, 10 pp., 1981.

Shor, G. G., Jr., and R. Von Huene, Marine Seismic Refraction Studies near Kodiak, Alaska, Geophysics, 37(4), 697-700, 1972.

Snyder, G. L., Eruption of Trident Volcano, Katmai National Monument, Alaska, February-June, 1953, U.S. Geol. Survey Circ. 318, 7 pp., 1954.

Swanson, S. E., and J. Kienle, Volcanic Centers in Katmai, Alaska, in prep., 1982.

Ward, P. L. and T Matumoto, A Summary of Volcanic and Seismic Activity in Katmai National Monument, Alaska, Bull. Volcanol., 31, 107-129, 1967.

APPENDIX 1

<u>Definition of symbols used in earthquake epicenter plots; definition of class 1 events.</u>

In the epicenter maps shown in Figures 4 to 23 and A1-20 the one-letter code represents hypocentral depths as follows:

A	$0 \leq 25$
B	$26 \leq 50$
C	$51 \leq 100$
D	$101 \leq 125$
E	$126 \leq 150$
F	$151 \leq 200$
etc.	

The actual location of the event is the lower left hand corner of the letter. The size of the letter is proportional to the magnitude, the size used for the geographic coordinates corresponding to a magnitude 2.

Class 1 events have an RMS travel time residual of less than 0.5 second and the locations are based on a minimum of 5 stations.

APPENDIX 2

January-June, 1981, monthly epicenter plots for Cook Inlet and Alaska Peninsula/Kodiak.

Figures A1-20 are the latest monthly epicenter plots (all events and class 1 events) for the Cook Inlet and Alaska Peninsula/Kodiak regions for the period January to June, 1981. These plots are part of the data set which we have just submitted to the Juneau Project Office.

We have no data for the month of May, 1981, due to the failure of the power supply to the discriminator bank at the Homer recording site.

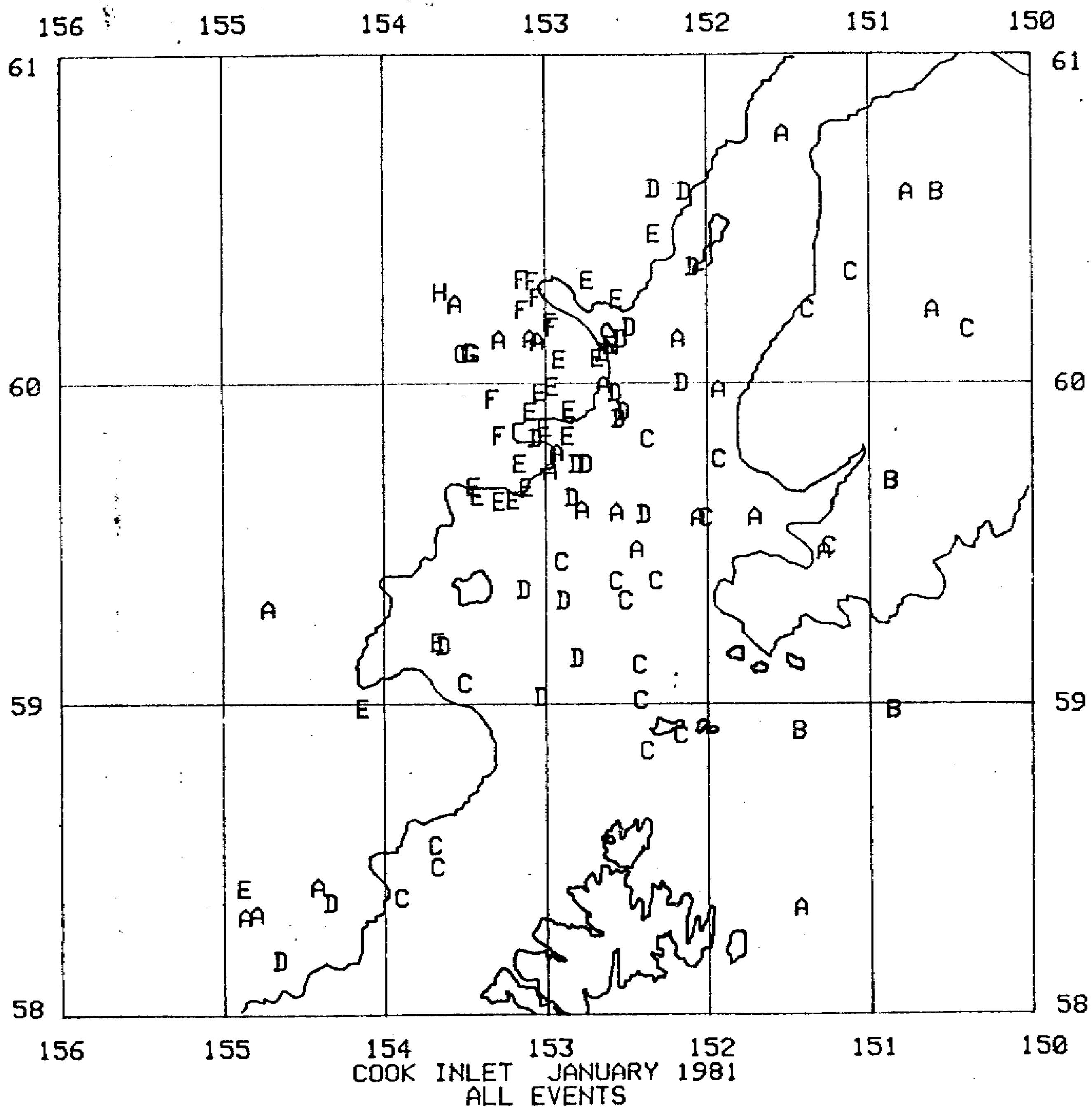

Figure A-1. Cook Inlet epicenters.

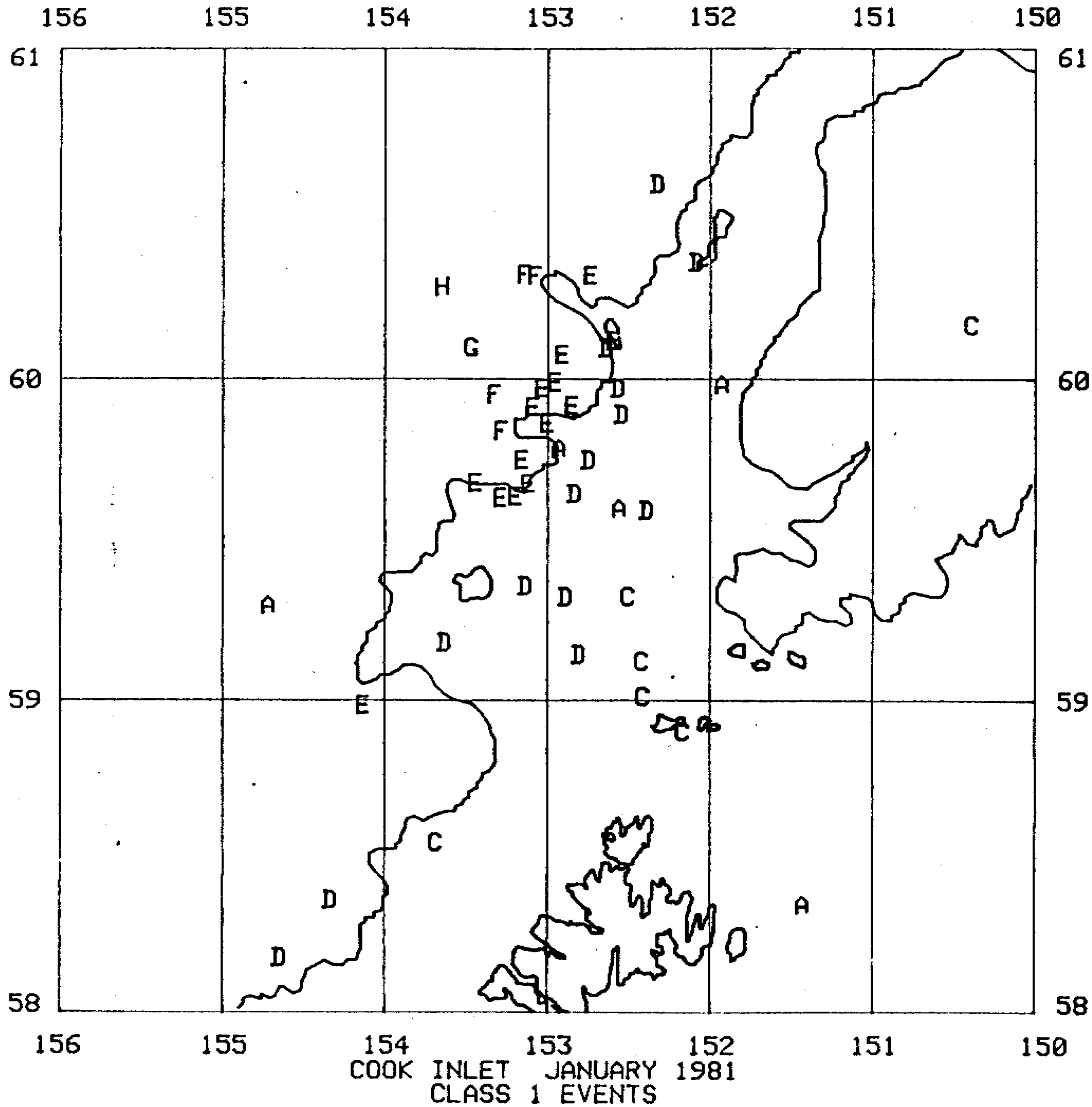

Figure A-2. Cook Inlet epicenters.

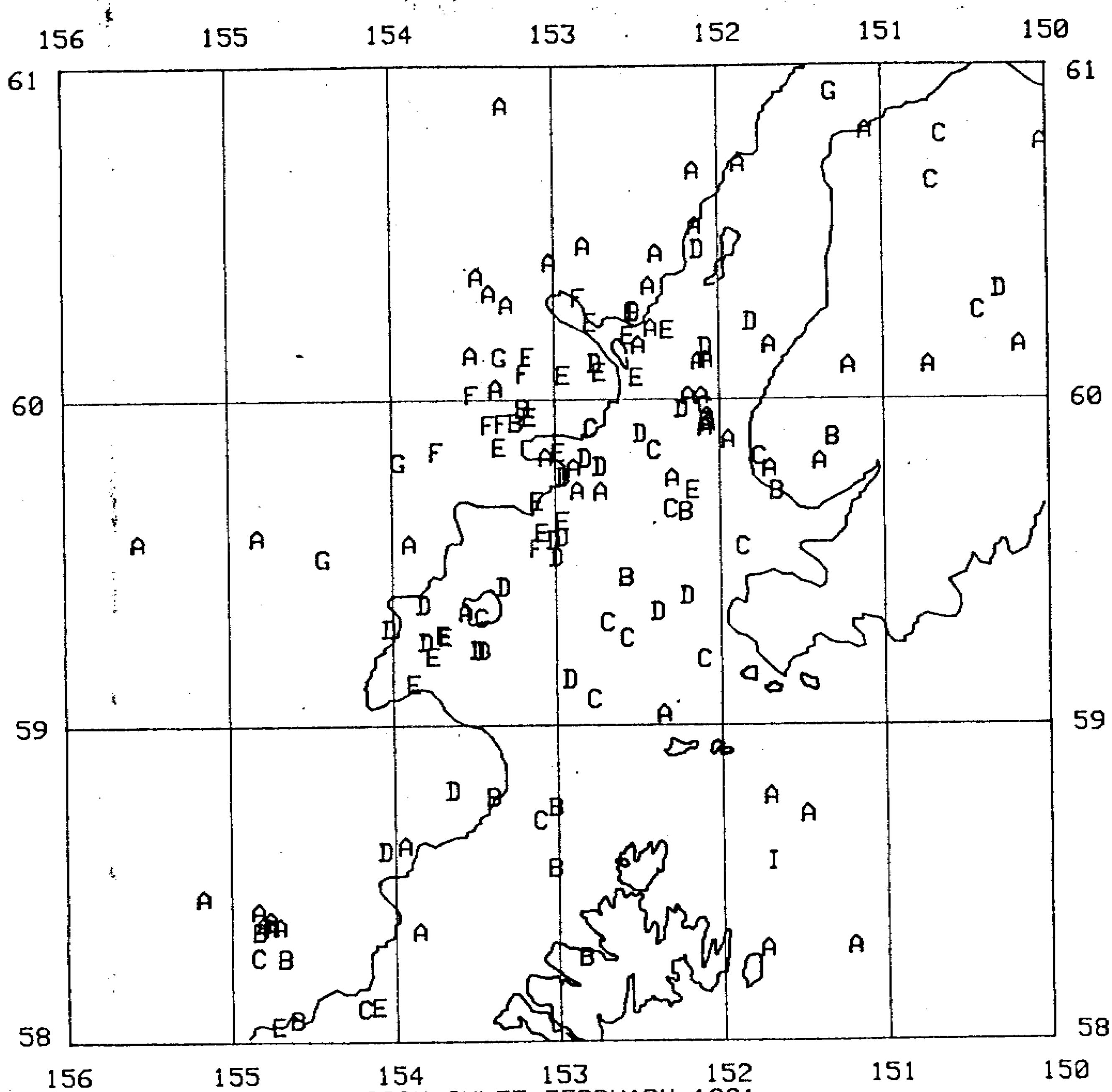

COOK INLET FEBRUARY 1981
ALL EVENTS

Figure A-3. Cook Inlet epicenters.

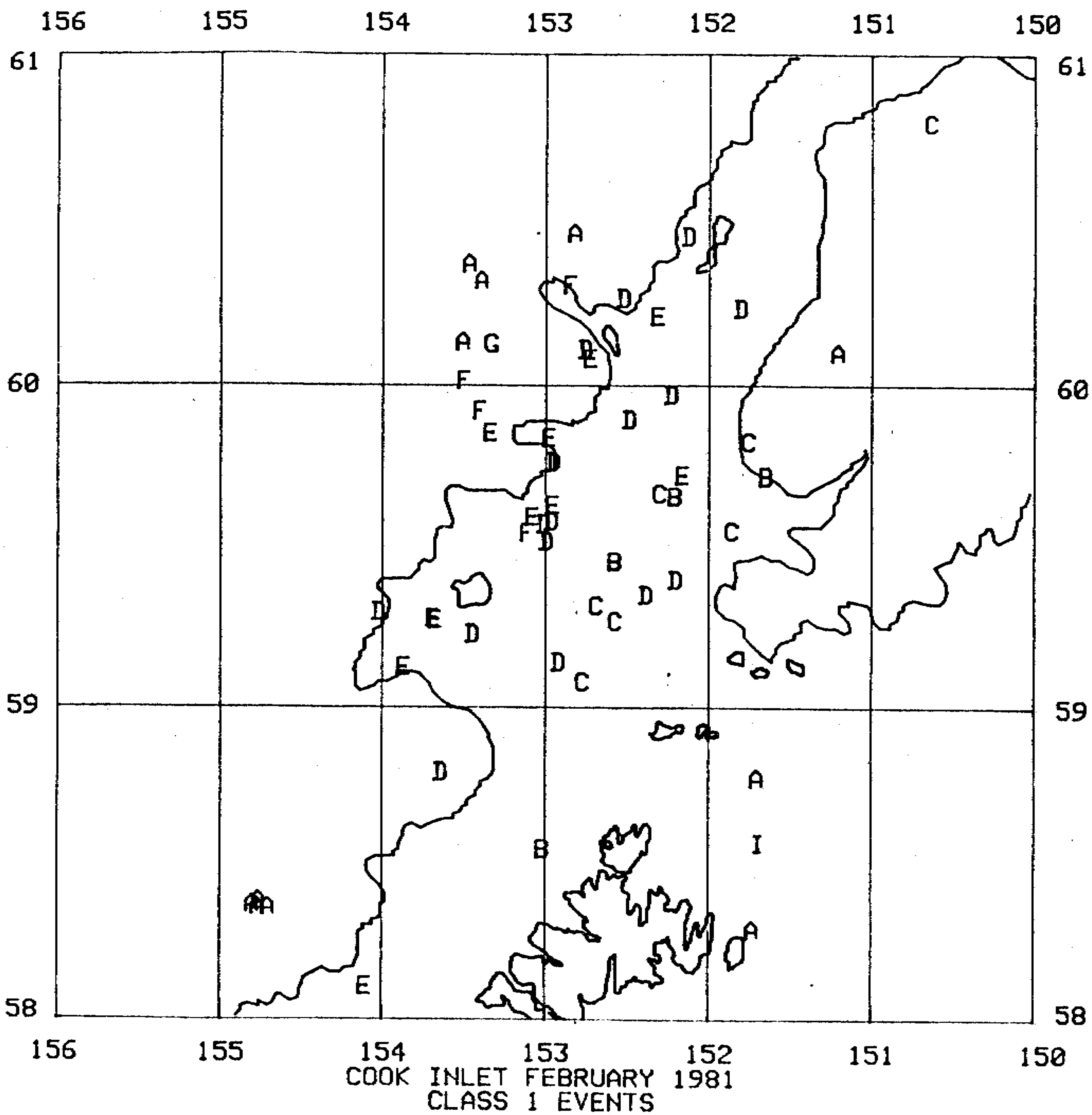

Figure A-4. Cook Inlet epicenters.

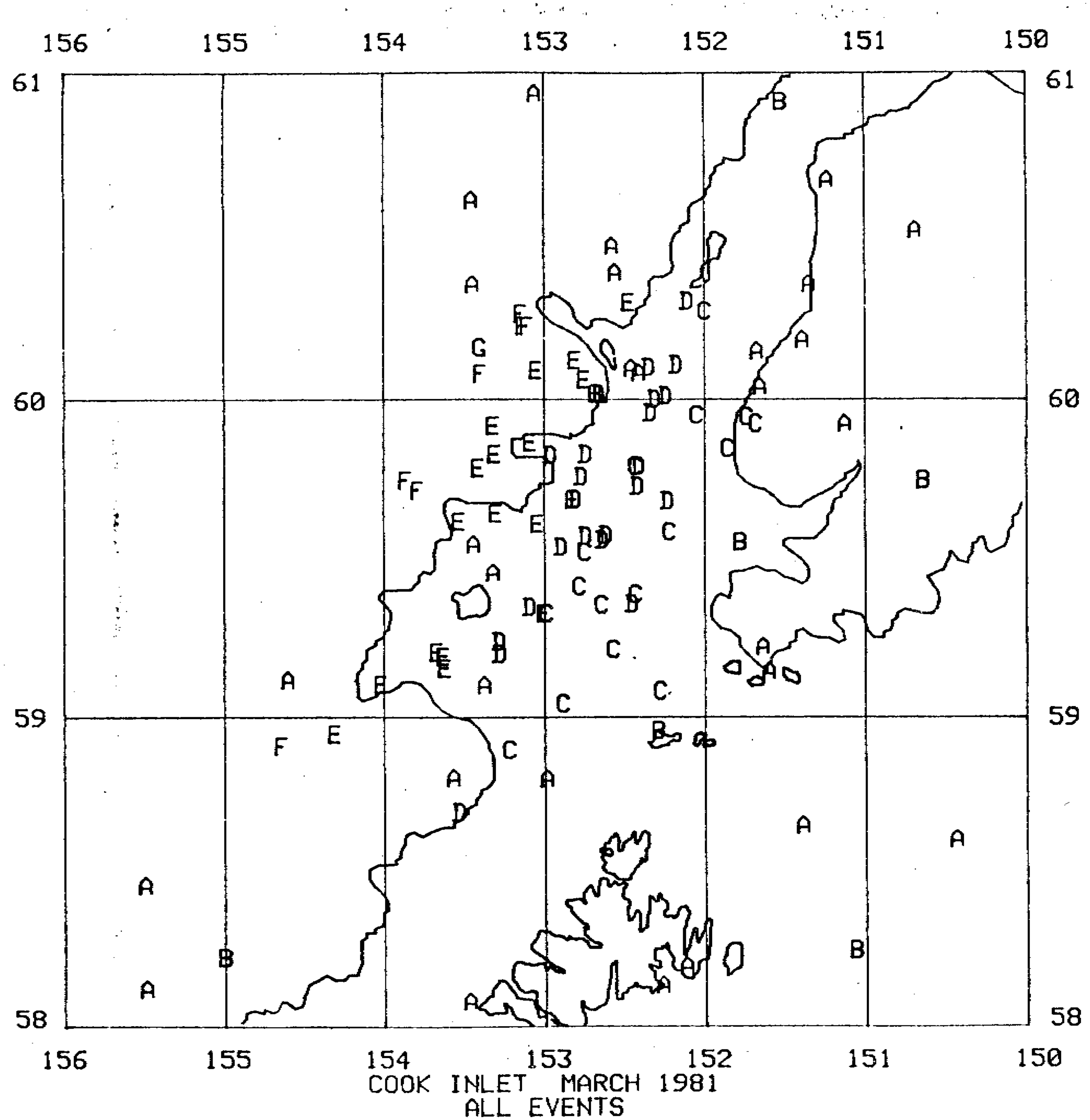

Figure A-5. Cook Inlet epicenters.

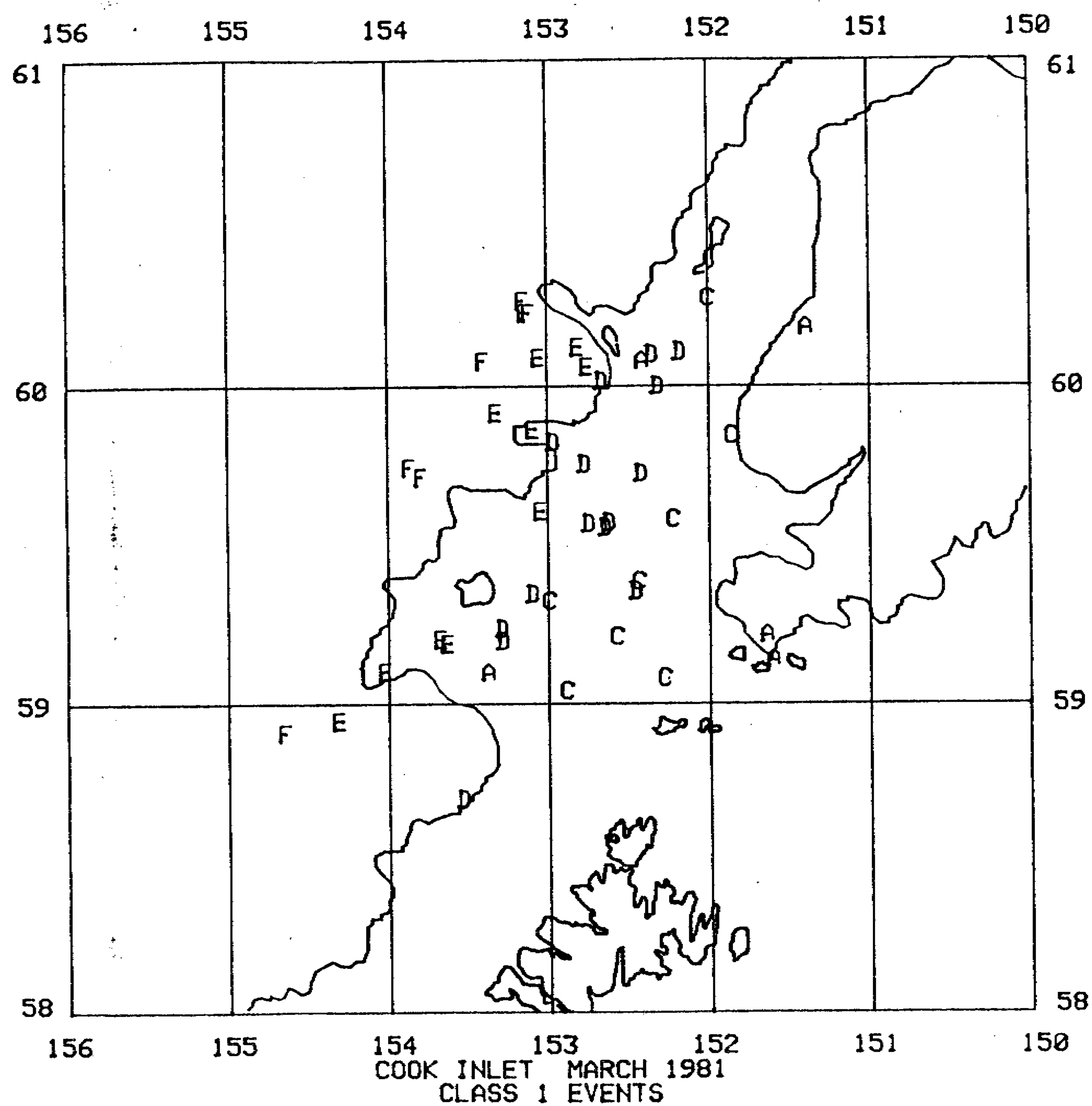

Figure A-6. Cook Inlet epicenters.

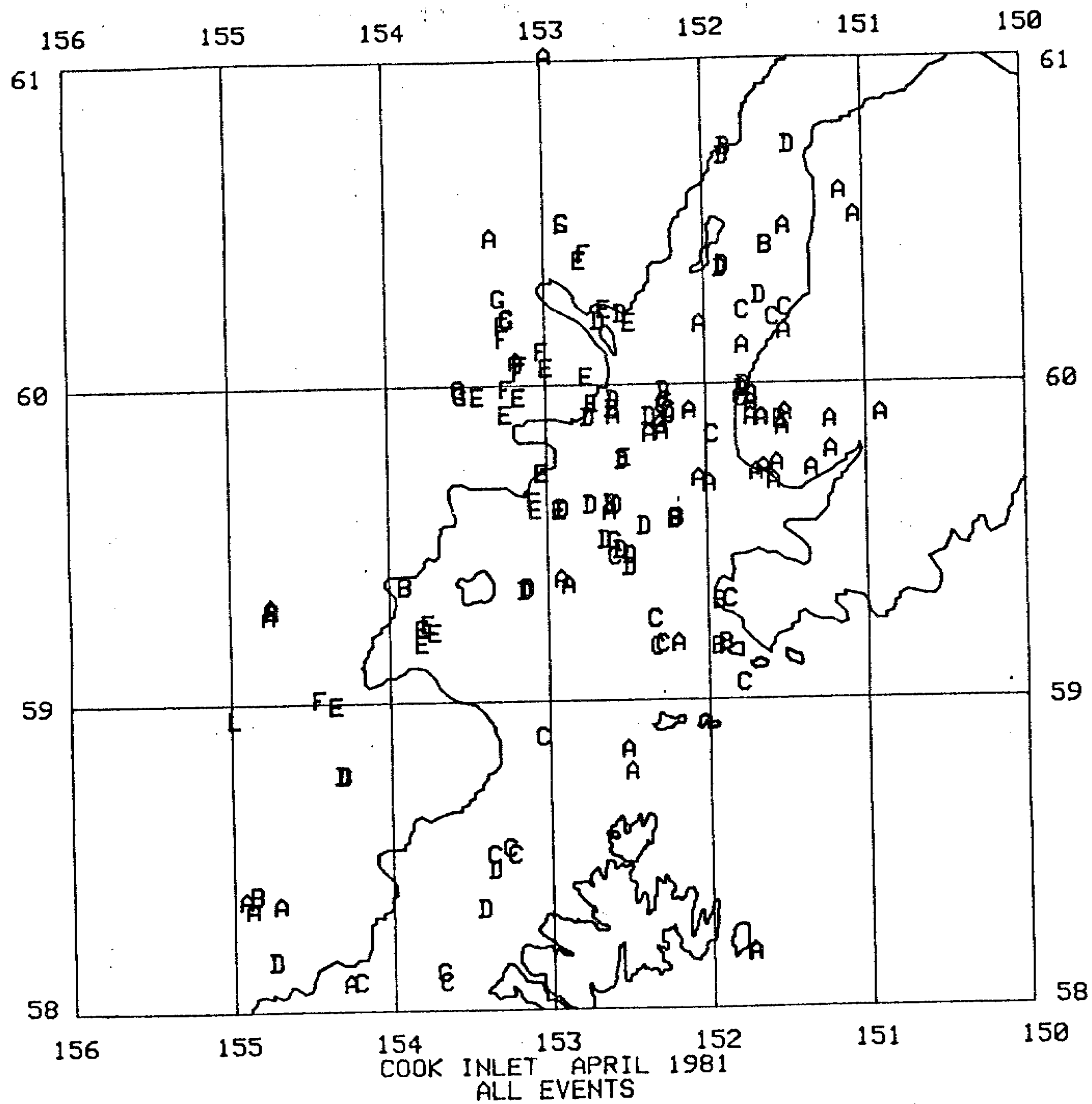

Figure A-7. Cook Inlet epicenters.

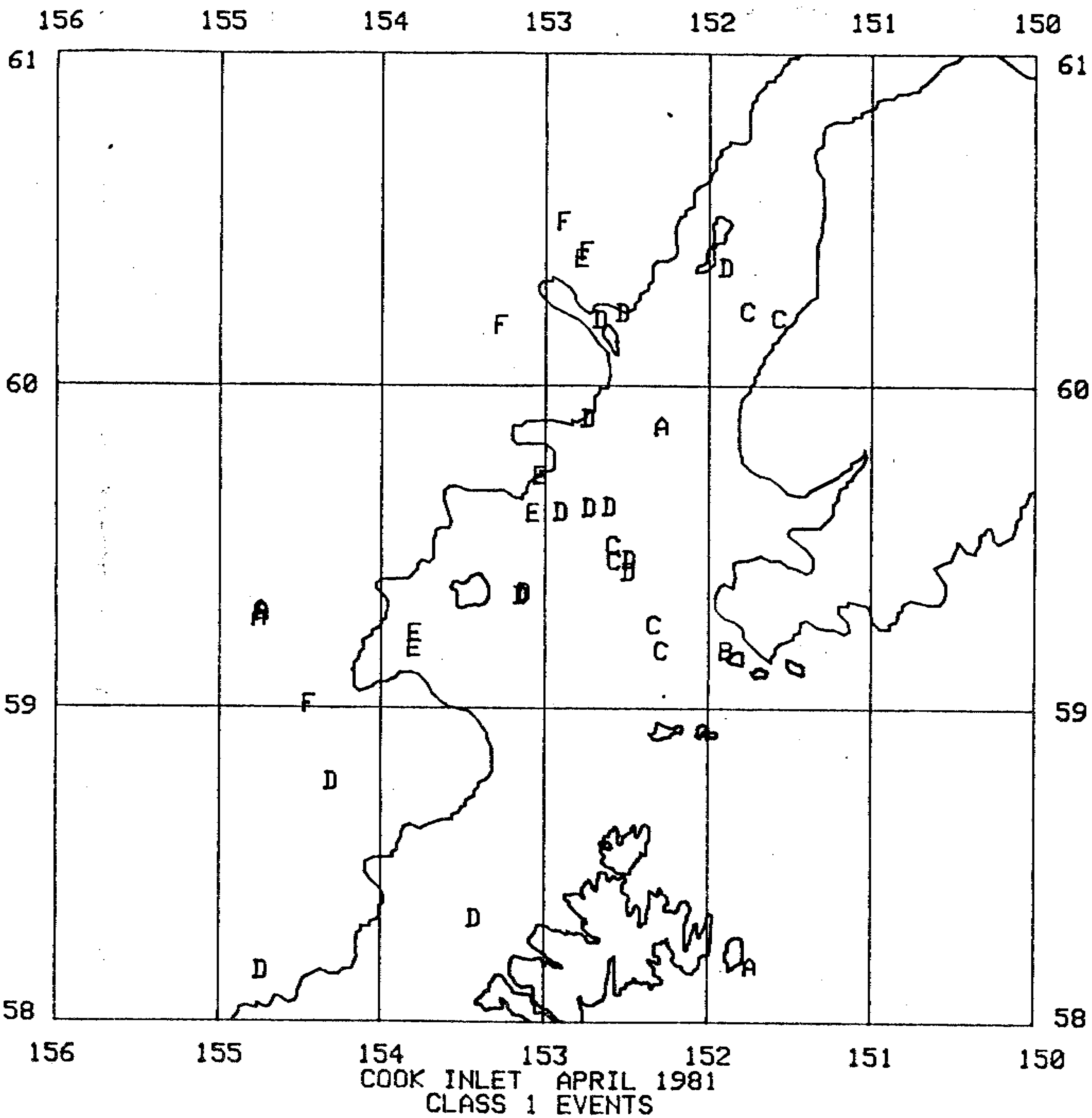

Figure A-8. Cook Inlet epicenters.

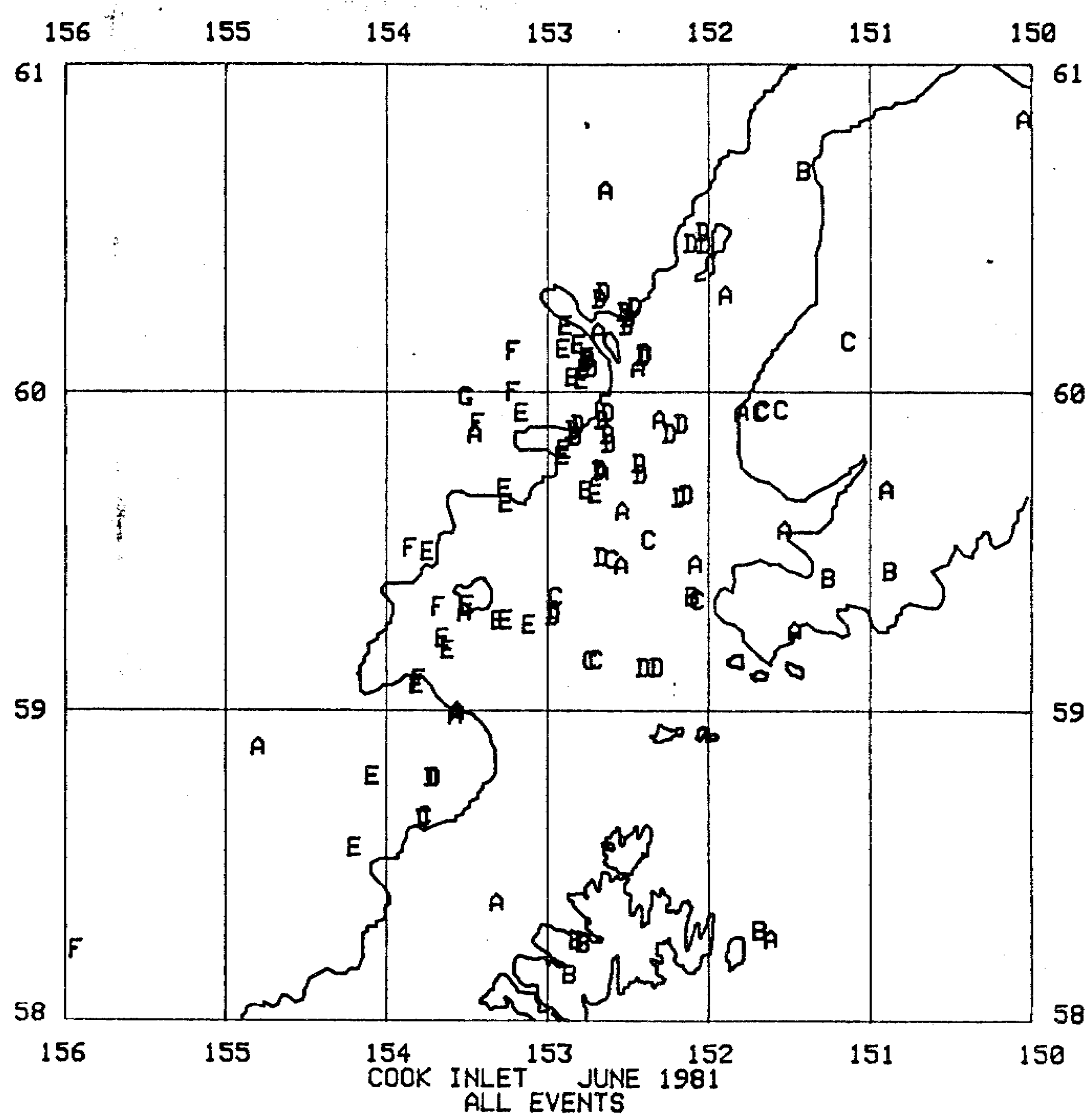

Figure A-9. Cook Inlet epicenters.

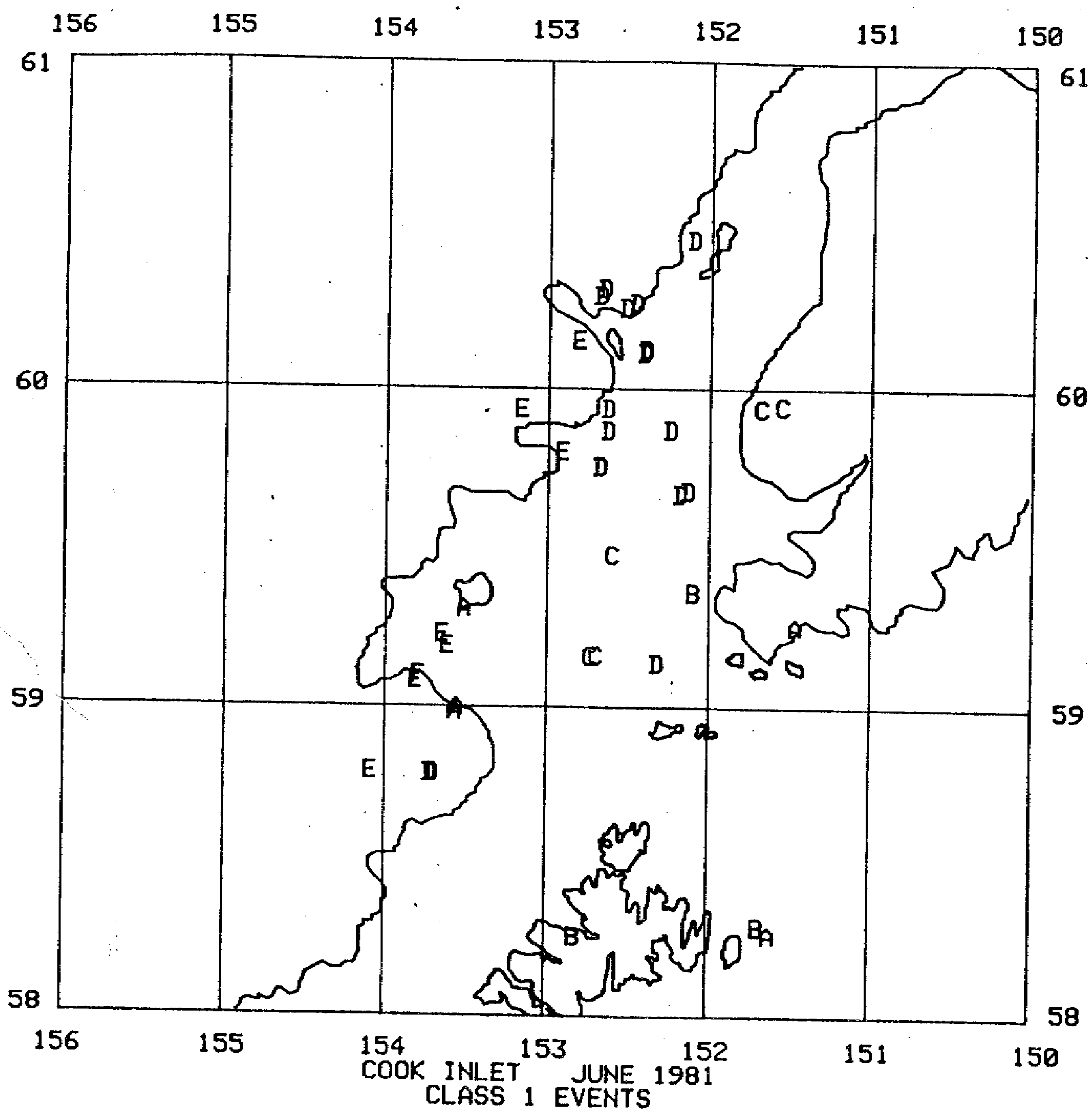

Figure A-10. Cook Inlet epicenters

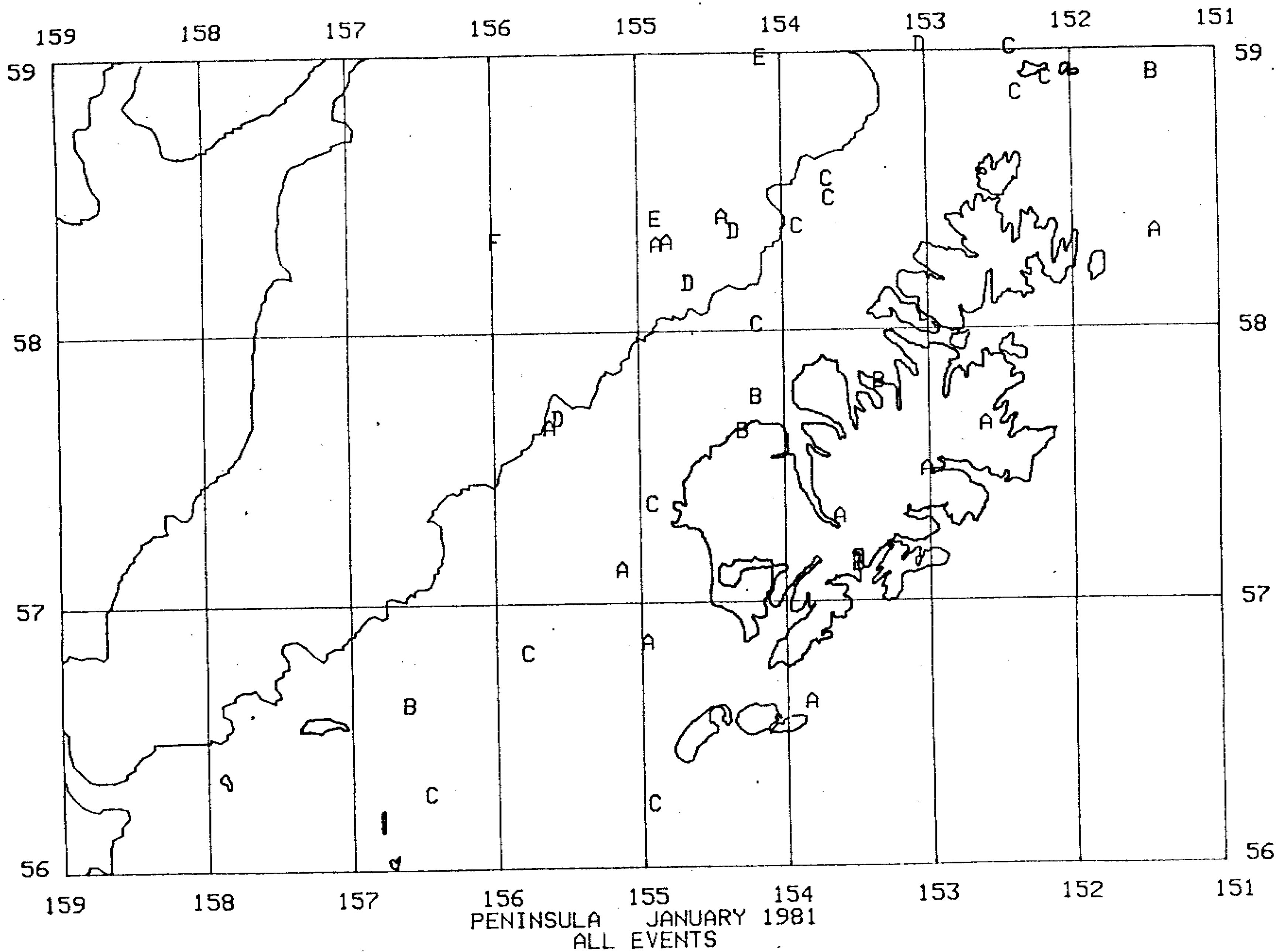

Figure A-11. Alaska Peninsula/Kodiak epicenters.

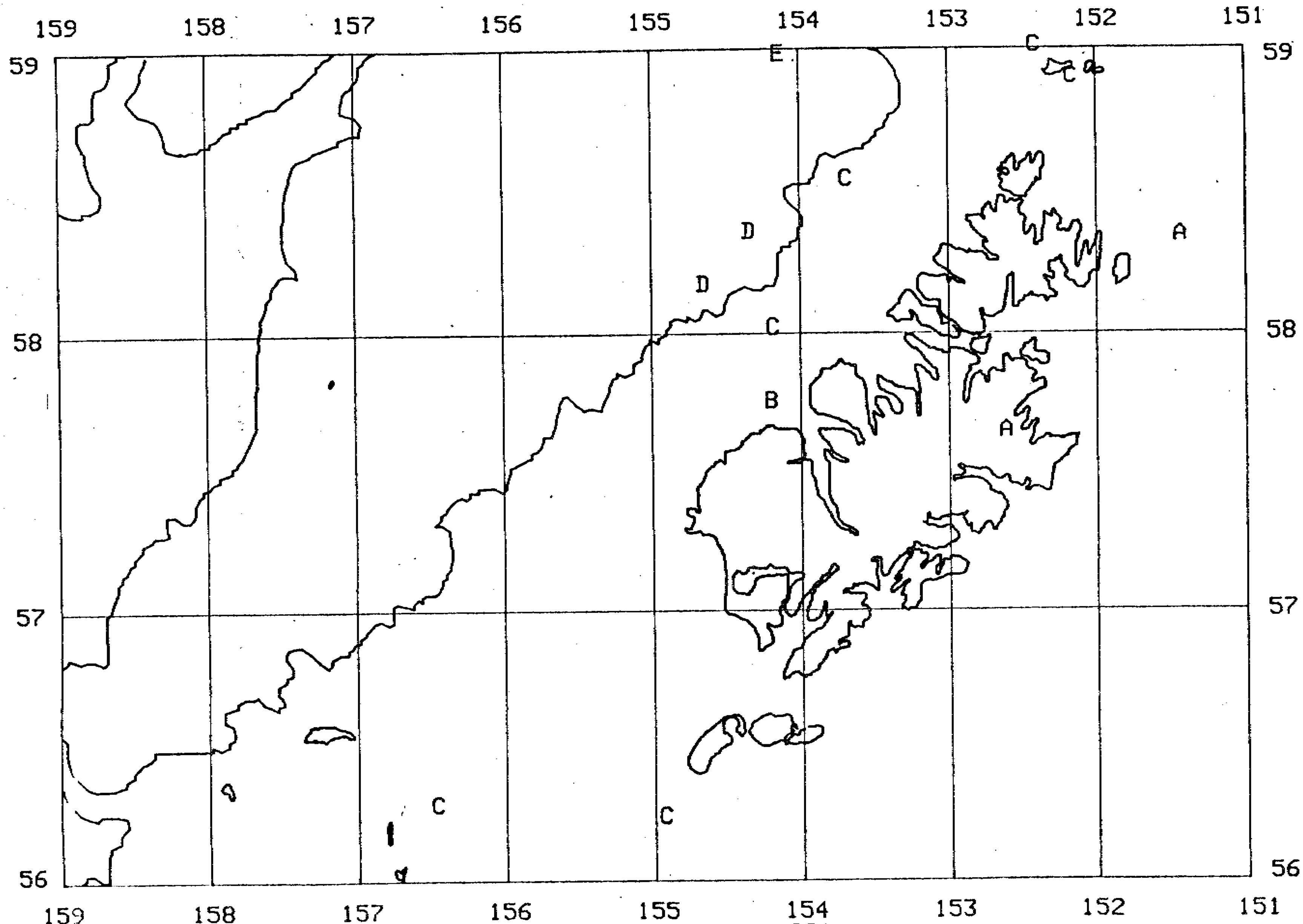

PENINSULA JANUARY 1981
CLASS 1 EVENTS

Figure A-12. Alaska Peninsula/Kodiak epicenters.

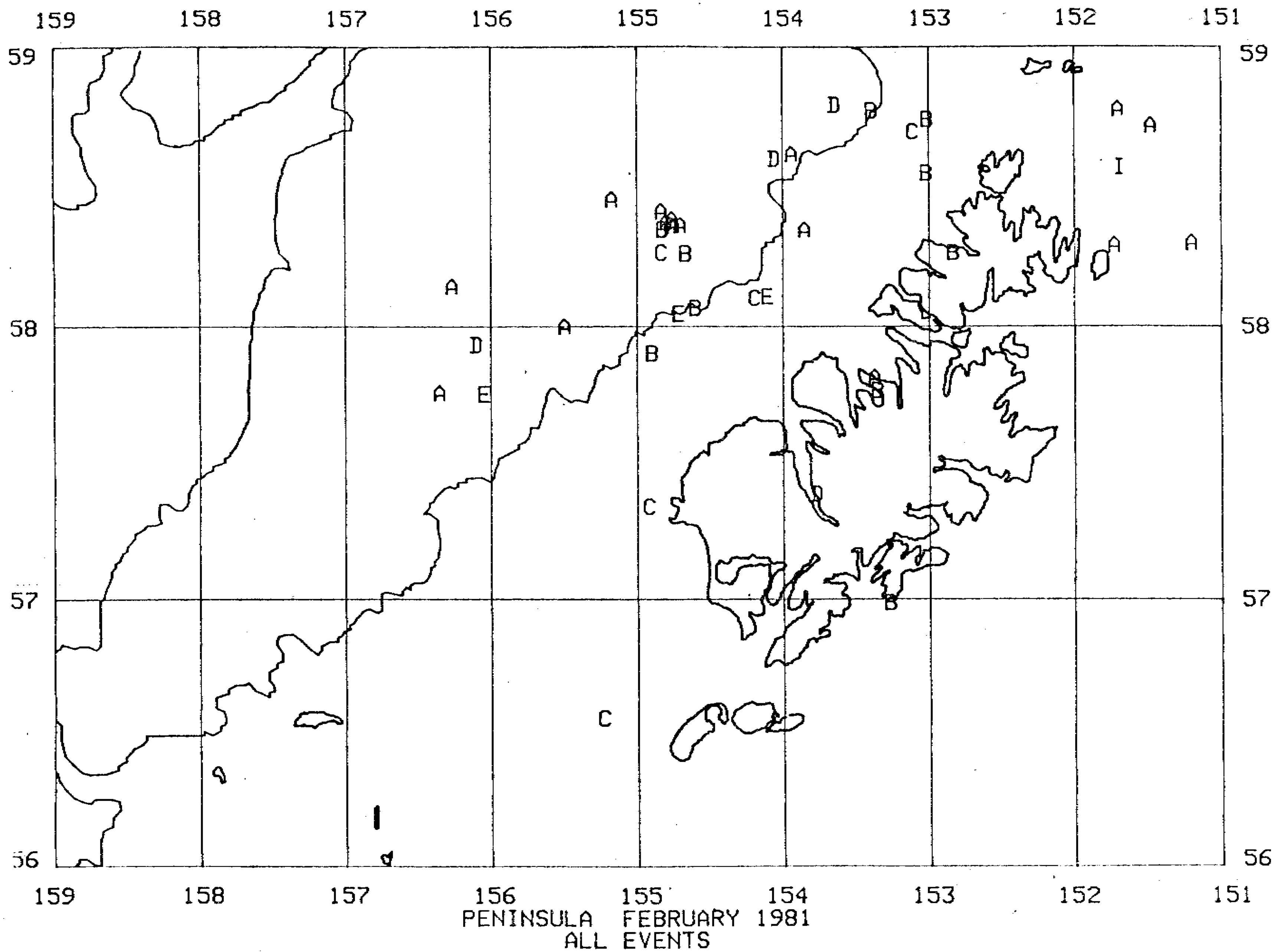

Figure A-13. Alaska Peninsula/Kodiak epicenters.

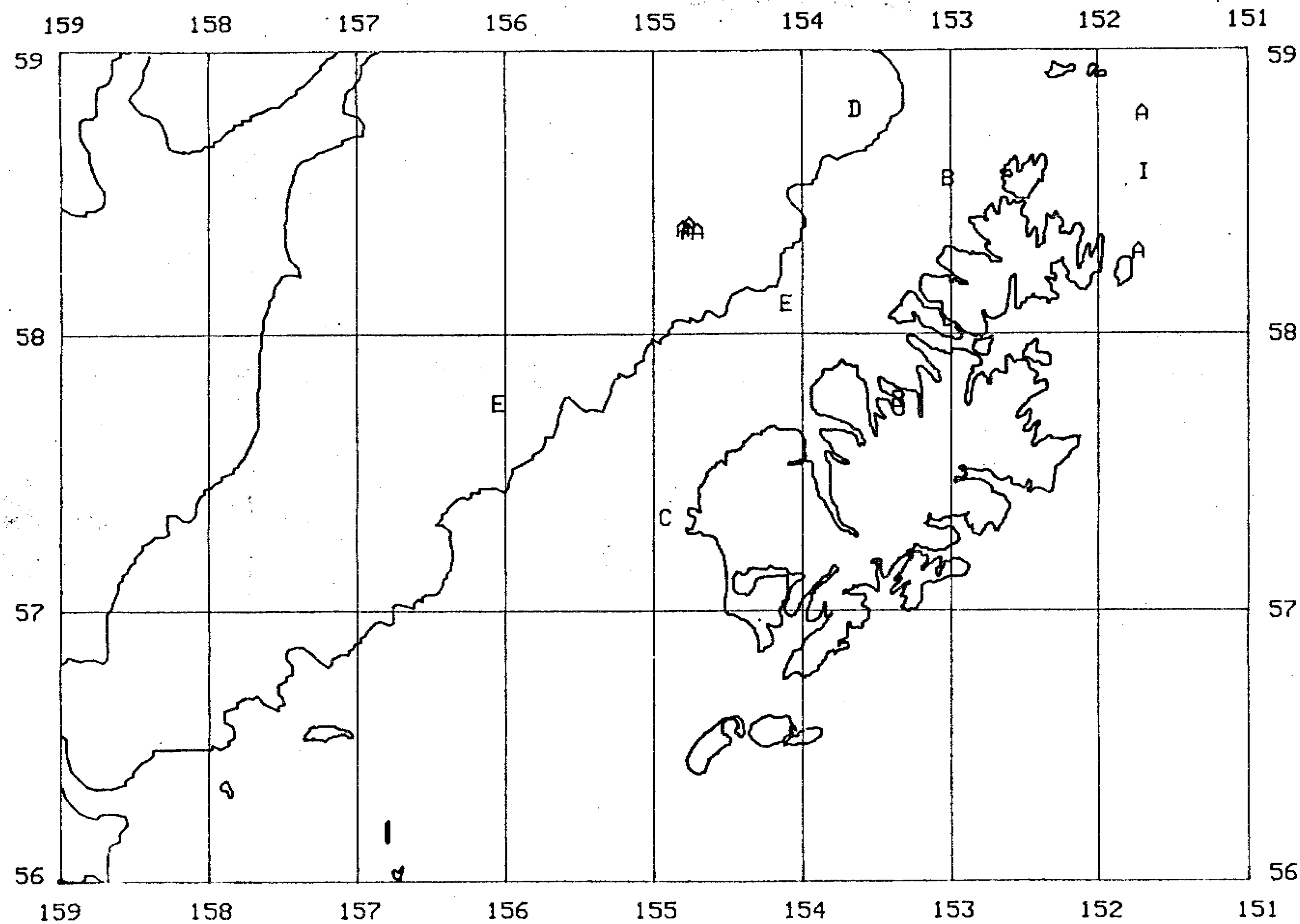

PENINSULA FEBRUARY 1981
CLASS 1 EVENTS

Figure A-14. Alaska Peninsula/Kodiak epicenters.

277

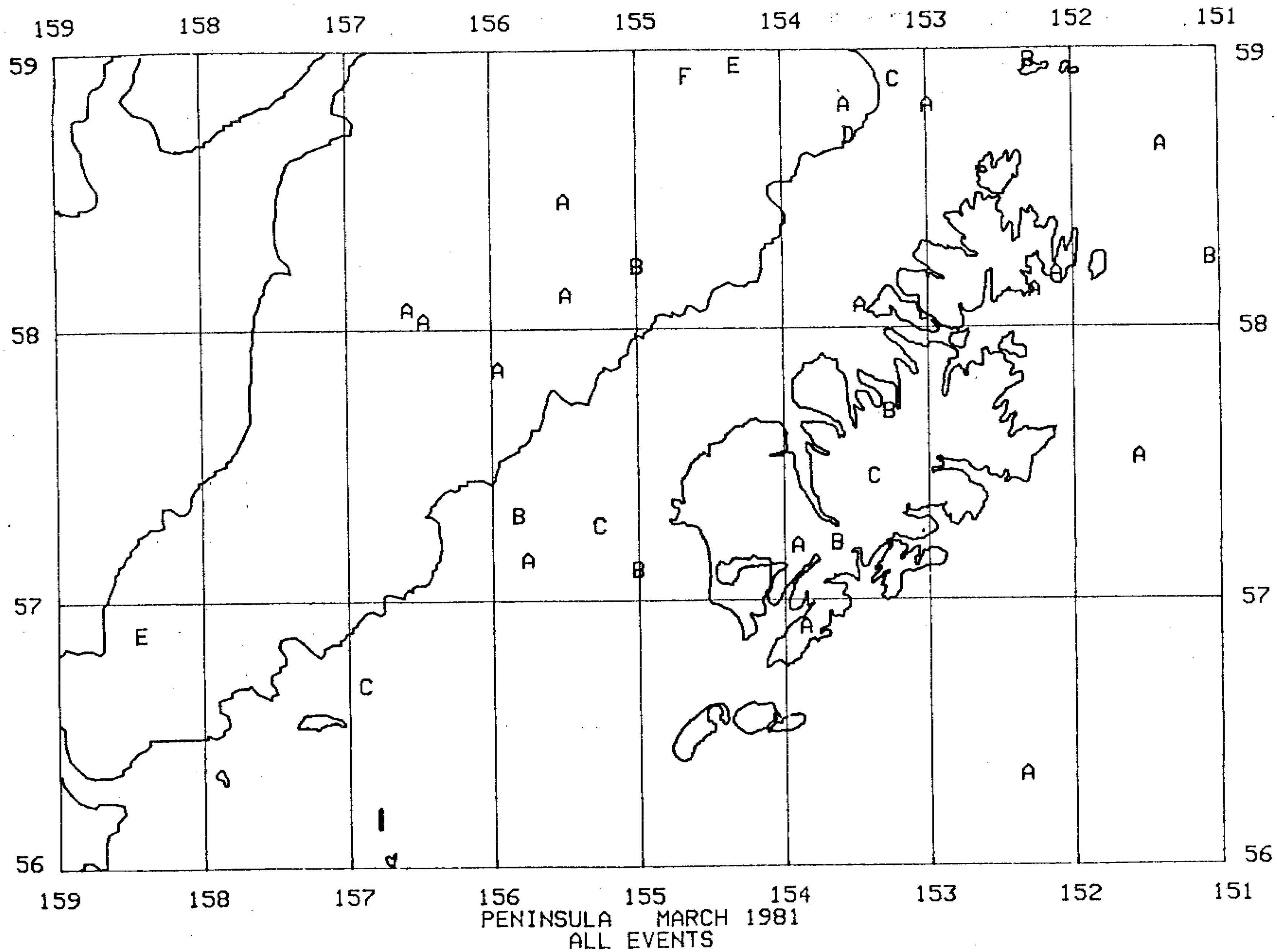

Figure A-15. Alaska Peninsula/Kodiak epicenters.

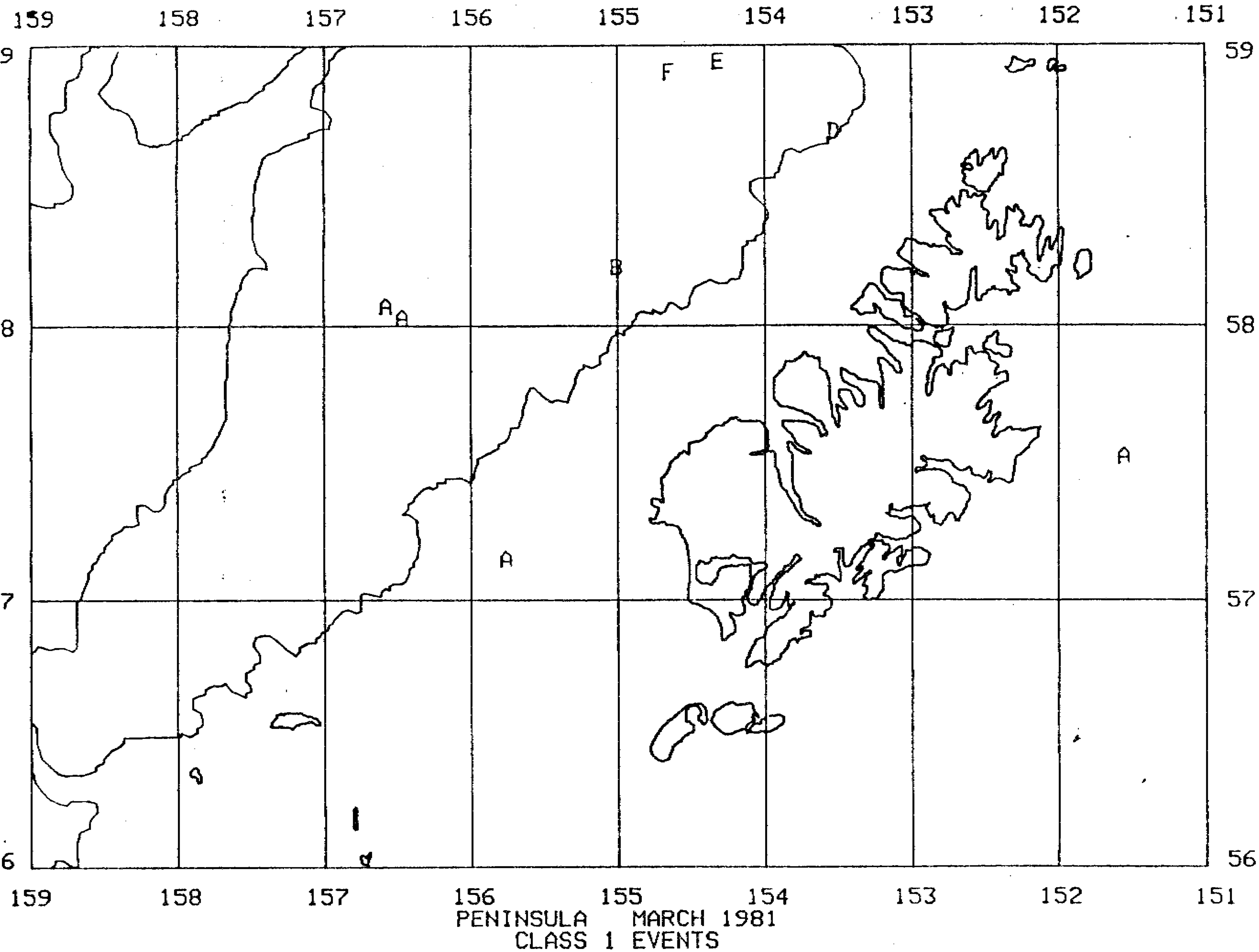

Figure A-16. Alaska Peninsula/Kodiak epicenters.

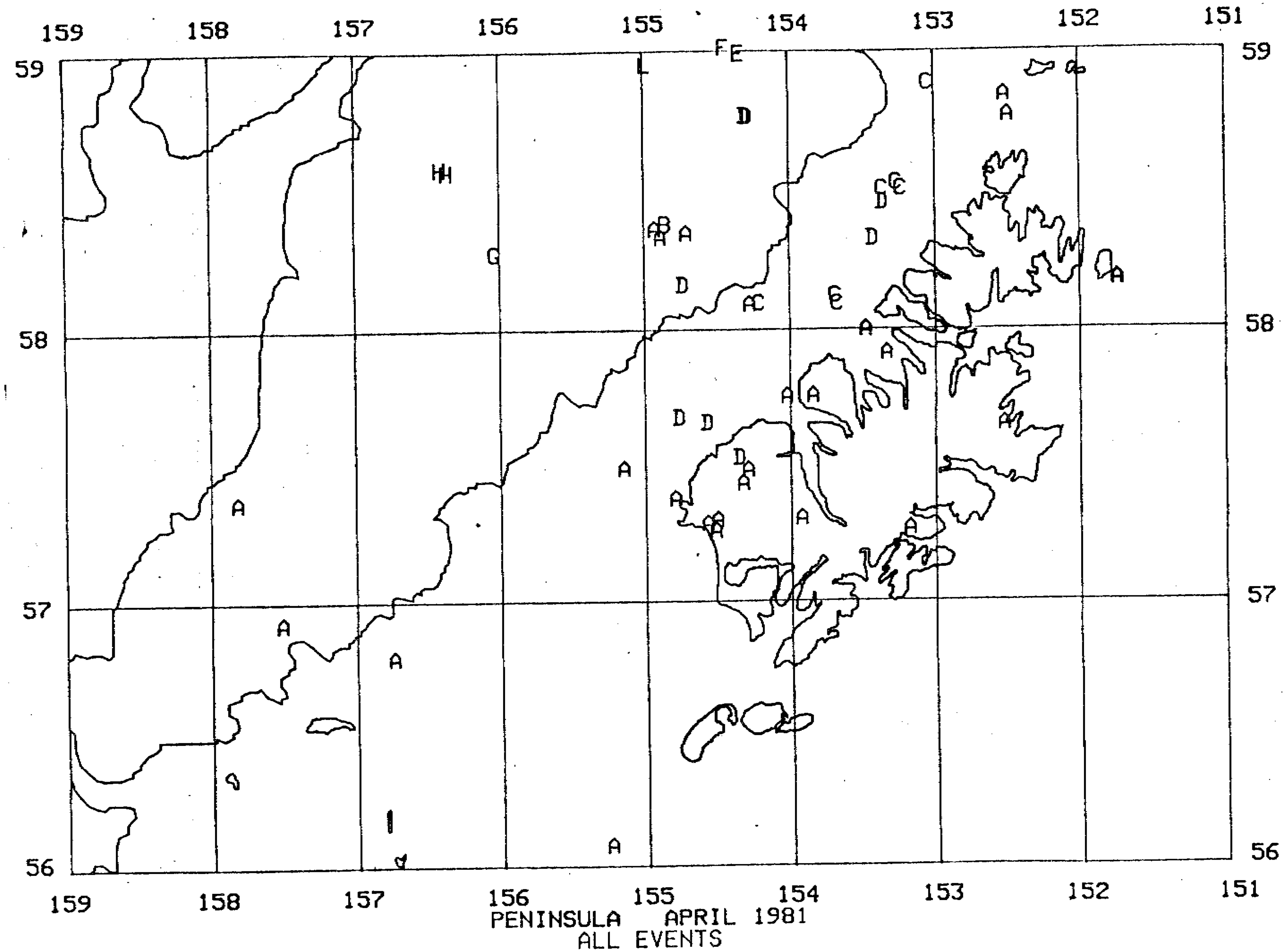

Figure A-17. Alaska Peninsula/Kodiak epicenters.

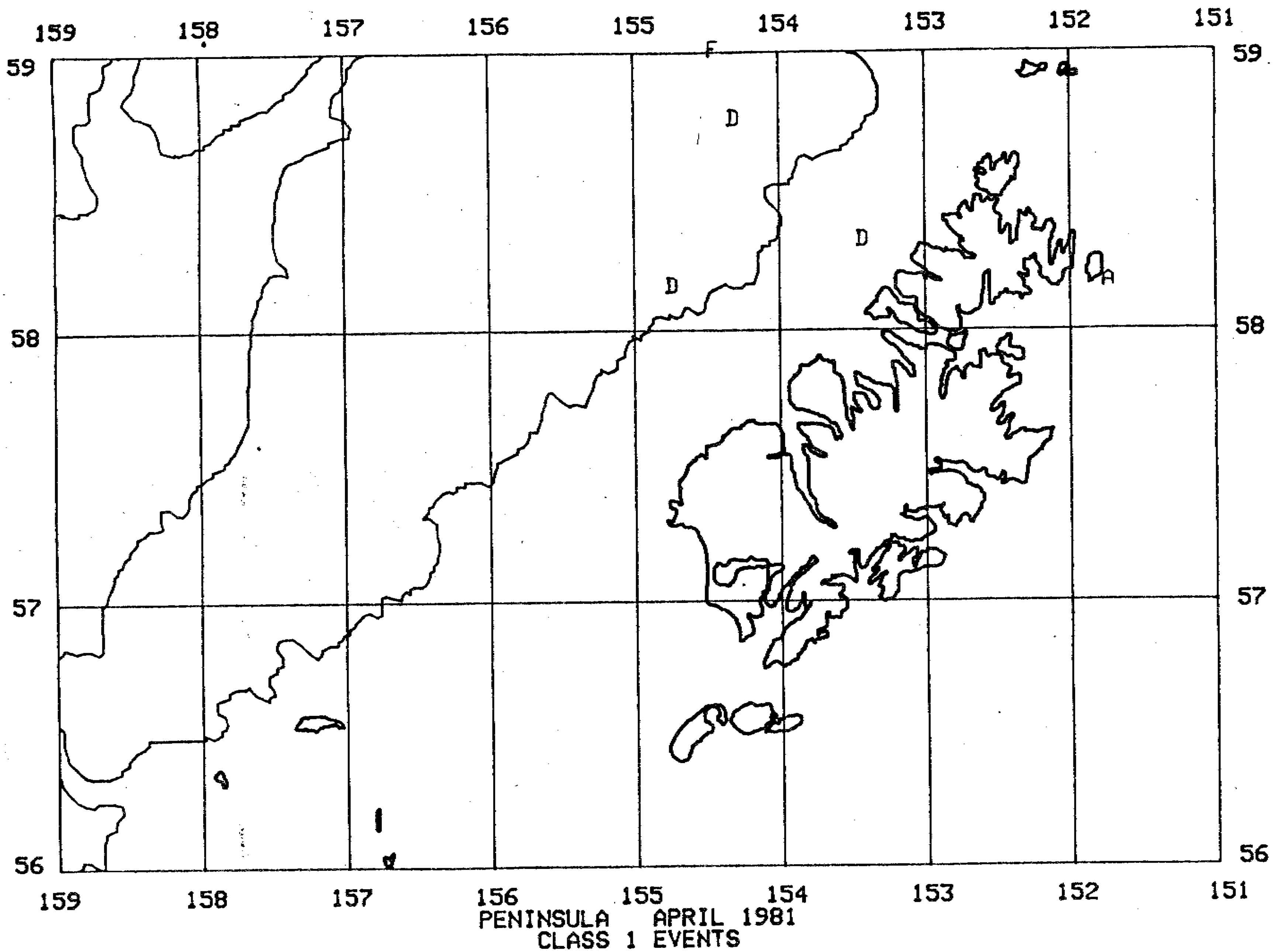

Figure A-18. Alaska Peninsula/Kodiak epicenters.

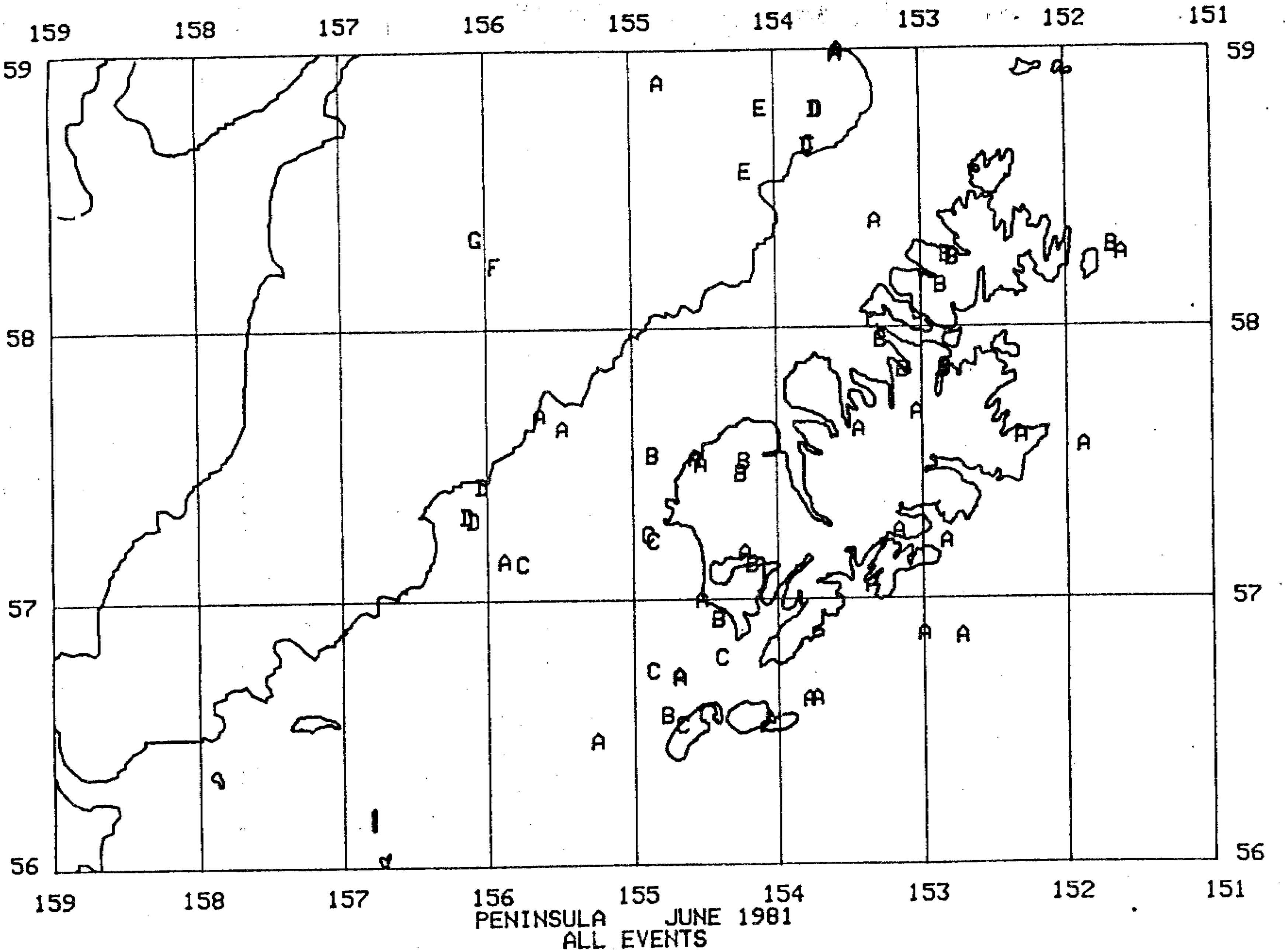

Figure A-19. Alaska Peninsula/Kodiak epicenters.

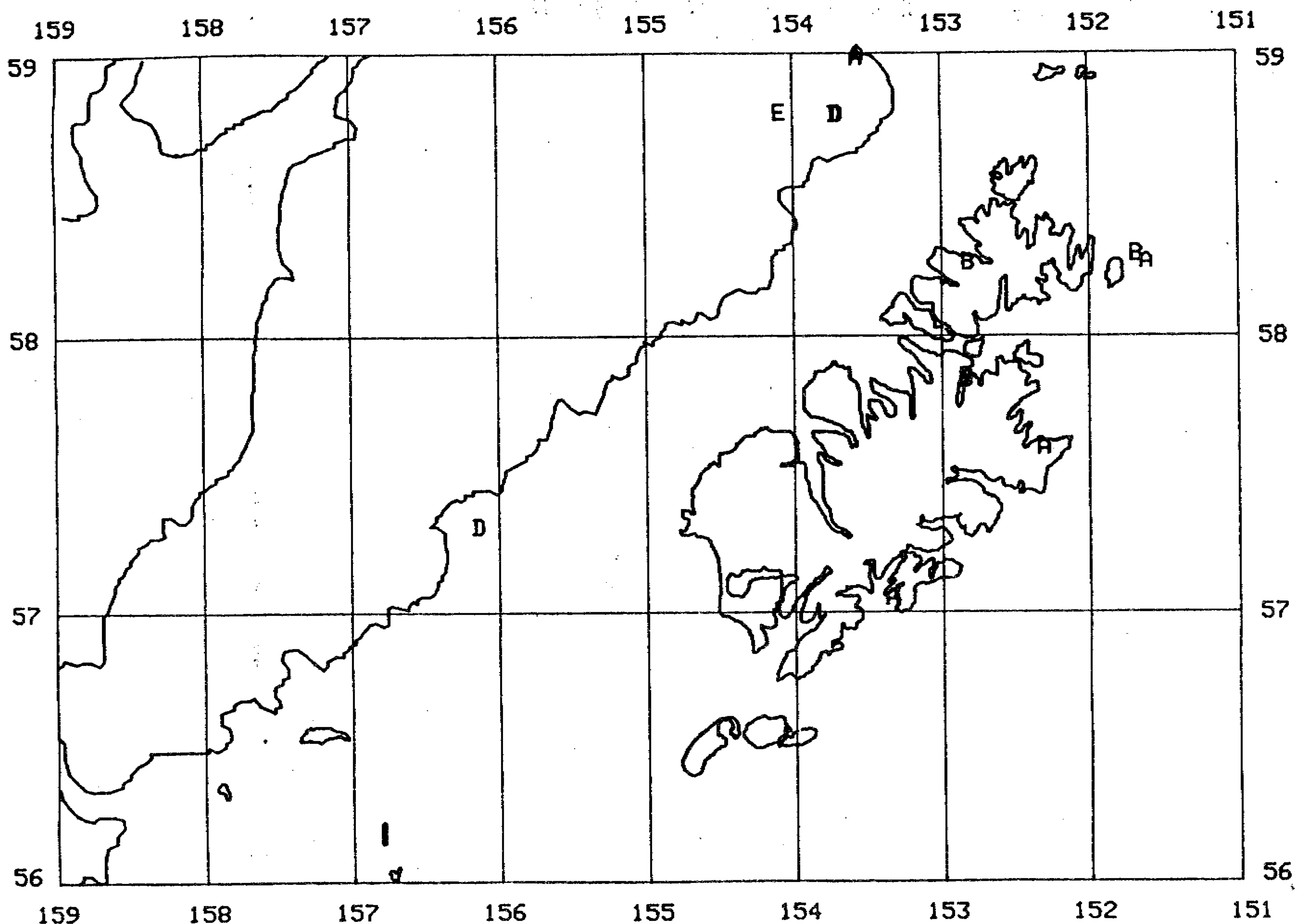

COOK INLET JUNE 1981
CLASS 1 EVENTS

Figure A-20. Alaska Peninsula/Kodiak epicenters.

APPENDIX 3

Abstracts of papers given at recent national and international meetings.

(1) Swanson, S. E. and J. Kienle, Volcanic hazards of Augustine Volcano, Lower Cook Inlet, Alaska, 31st Alaska Science Conference, AAAS, Anchorage, September 17-19, 1980, Proceedings, p. 71, 1980.

(2) Swanson, S. E. and J. Kienle, Volcanic hazards associated with Augustine Volcano, Lower Cook Inlet, Alaska, Geol. Soc. of Am., 93rd Ann. Meeting, Atlanta, Georgia, Nov., 1980, Abstracts with Programs, 12(7), 532, Aug. 1980 (abstract).

(3) Kienle, J., and S. E. Swanson, volcanic centers in the Katmai area, Alaska, EOS, Trans. Am. Geophys. Union, 62(17), 430, 1981 (abstract).

(4) Kienle, J. S. E. Swanson, and H. Pulpan, Subduction and magmatism in the eastern Aleutian arc, 1981 IAVCEI Symposium on Arc Volcanism, Tokyo and Hakone, Japan, Aug. 8-Sept. 9, 1981, Abstracts, pp. 177-178, 1981.

(5) Swanson, S. E., and J. Kienle, Geology and petrology of Kaguyak Crater, Alaska, EOS, Trans. Am. Geophys. Union, 1981 (abstract).

(1)

VOLCANIC HAZARDS OF AUGUSTINE VOLCANO, LOWER COOK INLET, ALASKA

Samuel E. Swanson and Juergen Kienle
Geophysical Institute
University of Alaska
Fairbanks, Alaska 99701

Augustine Volcano is the most active volcano in the eastern Aleutian arc and represents a significant hazard to the southcentral Alaska region. The volcano is situated on an unpopulated island in Lower Cook Inlet, about 285 km southwest of Anchorage. Offshore oil and gas lease blocks are located within 15 km of its shoreline.

Studies of Augustine's eruptive deposits reveal a constancy of eruptive style, magma chemistry and frequency of eruptions. Over the past 1,500 years magma chemistry has not changed; the bulk compositions of the eruptive products are in the andesite to dacite range (SiO_2 = 56 to 64 wt.%, for 22 analysis). This chemistry of the magma results in a rather high explosivity. Pyroclastic flow activity is common, initially of the eruptive column collapse type and later of the dome collapse type, as a new dome grows during the final stages of an eruptive cycle. Temperatures within the pyroclastic flows are over 600°C (Kienle and Forbes, 1976) and velocities of 180 km/hr have been measured at Augustine (Stith et al., 1977). Eruptions of the relatively young (15,000 years old) volcano average one to three per century (last in 1976) and this active pattern is expected to continue.

Based upon risk to human life and property, four volcanic hazard zones have been distinguished for future eruptions of Augustine Volcano. A key assumption in the hazard analysis is the continued constancy in the eruptive style. A zone of very high risk associated with pyroclastic flows, volcanic bomb fall, mudflows, tephra accumulation and poisonous gases characterizes all of Augustine Island and an offshore area to the northeast. Hazards from pyroclastic flows, volcanic gases and tephra accumulation result in a high risk zone in the area immediately offshore and extending up to 10 km from the island. A moderate hazard zone related to tsunamis (generated when pyroclastic flows enter the sea, run-ups nearshore up to 10 m) and tephra accumulation includes all of Lower Cook Inlet. Small amounts of tephra result in a low risk zone that covers much of southcentral Alaska, including Anchorage.

Two recommendations regarding development in the area around Augustine Volcano result from this study. All of Augustine Island is within a zone of very high risk and, therefore, no permanent structures of any kind should be built on the island. Secondly, the western limit of the oil and gas lease blocks is near the boundary between the very high and high risk hazard zones. Any drilling within the westernmost lease blocks near Augustine Island should be done as far away as possible from the volcano.

THE GEOLOGICAL SOCIETY OF AMERICA
Telephone (303) 447-8850
Publications Department

PLEASE SUBMIT THIS ORIGINAL AND FOUR COPIES

1980
ABSTRACT FORM

See instruction sheet for deadlines and details

Exact format shown on instruction sheet must be followed. Blue margins below are absolute limits.

(2)

Check the box below which best classifies your abstract for review (ONLY ONE PLEASE)

1 ☐ archaeological geology
2 ☐ coal geology
3 ☐ economic geology
4 engineering geology
5 ☒ environmental geology
6 ☐ extraterrestrial geology
7 ☐ general geology
8 ☐ geochemistry
9 ☐ geology education
10 ☐ geomorphology
11 ☐ geophysics
12 ☐ geoscience information
13 ☐ history of geology
14 ☐ hydrogeology
15 ☐ marine geology
16 ☐ mathematical geology
17 ☐ micropaleontology
18 ☐ mineralogy/crystallography
19 ☐ paleontology/paleobotany
20 ☐ petrology
21 ☐ experimental
22 ☐ igneous
23 ☐ metamorphic
☐ Precambrian geology
☐ Quaternary geology
☐ sedimentology
☐ sedimentary petrology
☐ stratigraphy
☐ structural geology
☐ tectonics
☐ volcanology
☐ Other

VOLCANIC HAZARDS ASSOCIATED WITH AUGUSTINE VOLCANO, LOWER COOK INLET, ALASKA

SWANSON, Samuel E. and KIENLE, J., Geophysical Institute, University of Alaska, Fairbanks, Alaska 99701

Augustine Volcano is the most active volcano in the eastern Aleutian arc and represents a significant hazard to the southcentral Alaska region. The volcano is situated on an unpopulated island in Lower Cook Inlet, within 15 km of oil and gas lease blocks, about 285 km southwest of Anchorage, Alaska. Studies of Augustine eruptive deposits reveal a constancy in magma chemistry, eruptive style and frequency. Eruptions of the relatively young (15,000 years old) volcano average one to three per century (last in 1976) and this active pattern is expected to continue. Andesites and dacites produce rather violent eruptions at Augustine characterized by pyroclastic flows. Temperatures within the pyroclastic flows were over 600°C and velocities of 180 km/hr have been measured at Augustine (Stith et al., 1977).

Based upon risk to human life and property, four volcanic hazard zones have been distinguished for future eruptions of Augustine Volcano. A key assumption in the hazard analysis is the continued constancy in the eruptive style of Augustine Volcano. A zone of very high risk associated with pyroclastic flows, volcanic bomb fall, mudflows, volcanic gas and tephra accumulation characterizes all of Augustine Island and an offshore area to the northeast. Hazards from pyroclastic flows, volcanic gases and tephra accumulation result in a high risk zone in the area immediately offshore and extending up to 10 km from the island. A moderate hazard zone related to tsunamis (generated when pyroclastic flows enter the sea, run- ups nearshore up to 10 m), volcanic gas and tephra accumulation covers all of Lower Cook Inlet. Small amounts of volcanic gas and tephra result in a low risk zone that covers much of southcentral Alaska, including Anchorage.

☒ Oral ☐ Poster ☐ Either

☐ Symposium ______
(title of symposium for which abstract was invited)

PLEASE NOTE: All invited symposium abstracts (original plus two copies) must be sent to the organizers of the respective symposia according to deadlines established by symposium organizers.

I will be available to serve as a cochairman for a technical session on or concerning ______

Speaker Samuel E. Swanson

For correspondence purposes, list address of speaker if different from above ______

Phone numbers and dates where speaker can be contacted ~~(907) 479-7660 until meeting~~

Note: All 1980 abstracts will be reviewed by the Joint Technical Program Committee (JTPC), which includes representatives from each of the associated societies. However, in order to compile statistics for possible future change in the review system, please check below the society you would have chosen to review this abstract if such a choice were available.

☒ GSA ☐ Cushman Foundation ☐ GS ☐ GIS ☐ MSA ☐ NAGT ☐ PS ☐ SEG

285

Mail to: Abstracts Coordinator, Geological Society of America, P.O. Box 9140, Boulder, CO 80301.

3/1/80

(3)

V 151

VOLCANIC CENTERS IN THE KATMAI AREA, ALASKA

Juergen Kienle
Samuel E. Swanson
Hans Pulpan (all at: Geophysical Institute,
University of Alaska, Fairbanks, AK. 99701)

In the Katmai area of the northern Alaska Peninsula identification of volcanic centers is difficult because of the extensive cover of glacial ice. Results of our reconnaissance study combined with the work of others in the region now give a clear picture of the distribution of volcanic centers in the Katmai area. Volcanic centers are associated with Mt. Douglas, Fourpeaked Mtn., Kaguyak Crater, Devils Desk, Kukak Volcano, Mt. Stellar/Mt. Denison, Snowy Mtn., Mt. Katmai, Novarupta, Mt. Griggs, Mt. Trident, Mt. Mageik, Mt. Martin and Kejulik Mtns. Active fumarole activity is currently associated with Douglas, Kaguyak, Kukak, Snowy, Katmai, Novarupta, Griggs, Trident, Mageik and Martin. Clusters of shallow (less than 10 km deep) earthquake swarms have been located over the past 5 years beneath the volcanoes Mt. Douglas, Kaguyak Crater, Kukak Volcano, Snowy Mtn., Trident, Mt. Mageik and Mt. Martin. This seismicity is apparently related to active magmatic-geothermal reservoirs beneath these volcanoes. Both Mt. Griggs and Katmai have active fumaroles, but no unusual seismic activity has yet been detected beneath these volcanoes. Two pyroxene andesite is the most common lithology in these volcanic centers except at Kaguyak Crater where dacite is the dominant bulk composition and at Novarupta where rhyolite is the most abundant rock type.

SUBDUCTION AND MAGMATISM IN THE EASTERN ALEUTIAN ARC

J. Kienle, S. E. Swanson and H. Pulpan, Geophysical Institute, University of Alaska, Fairbanks, Alaska, 99701, U.S.A.

Volcanism and tectonism in the eastern Aleutian arc are controlled by the subduction of the Pacific plate beneath the North American plate. Worldwide earthquake data and analysis of local network data in Cook Inlet and on the Alaska Peninsula have defined the arcuate plate boundary and depth to the Benioff zone. A calc-alkaline volcanic arc of approximately 20 volcanic centers is well developed above the subduction zone (Fig. 1).

Calc-alkaline volcanism and lithospheric plate subduction are intimately linked. However, the details of magma generation are still controversial. Figure 1 shows the position of the volcanic centers in the eastern Aleutian arc and the Benioff zone based on earthquake data from our local seismograph networks. The volcanoes in the Cook Inlet region (north of 59°N) have a regular spacing of 60 ± 19 km and follow a northerly trend which is parallel to the strike of the Benioff zone. In contrast, the Katmai volcanic centers (S of 59°N) are much closer together with a spacing of 13 ± 7 km and follow a cross-cutting trend with respect to the strike of the Benioff zone. A misorientation of 32° (from N17°E to N49°E) marks the change in trend of the volcanoes of Cook Inlet and Katmai. Augustine Volcano is the pivot point. Other more subtle links in the volcanic arc are found at Kaguyak and Katmai craters. This segmented nature of the volcanic arc is in contrast to the smooth trend of the Benioff zone.

Geochemical reconnaissance of the volcanic centers shown in Fig. 1 reveals 2 distinct types of patterns of magmatism based on major element chemistry. Volcanoes near arc segment boundaries (e.g., Augustine, Kaguyak and Katmai) are characterized by relatively high abundances of dacite and rhyolite while volcanoes within the segments are dominantly andesite.

Silicic volcanism associated with segmentation of the volcanic arc may be a reflection of (1) chemical heterogeneities in the subducting plate, (2) magma storage and fractionation in magma chambers in the overriding plate, (3) higher-heat flux in the zones of weakness along arc segment boundaries resulting in partial melting of the continental crust, or all three.

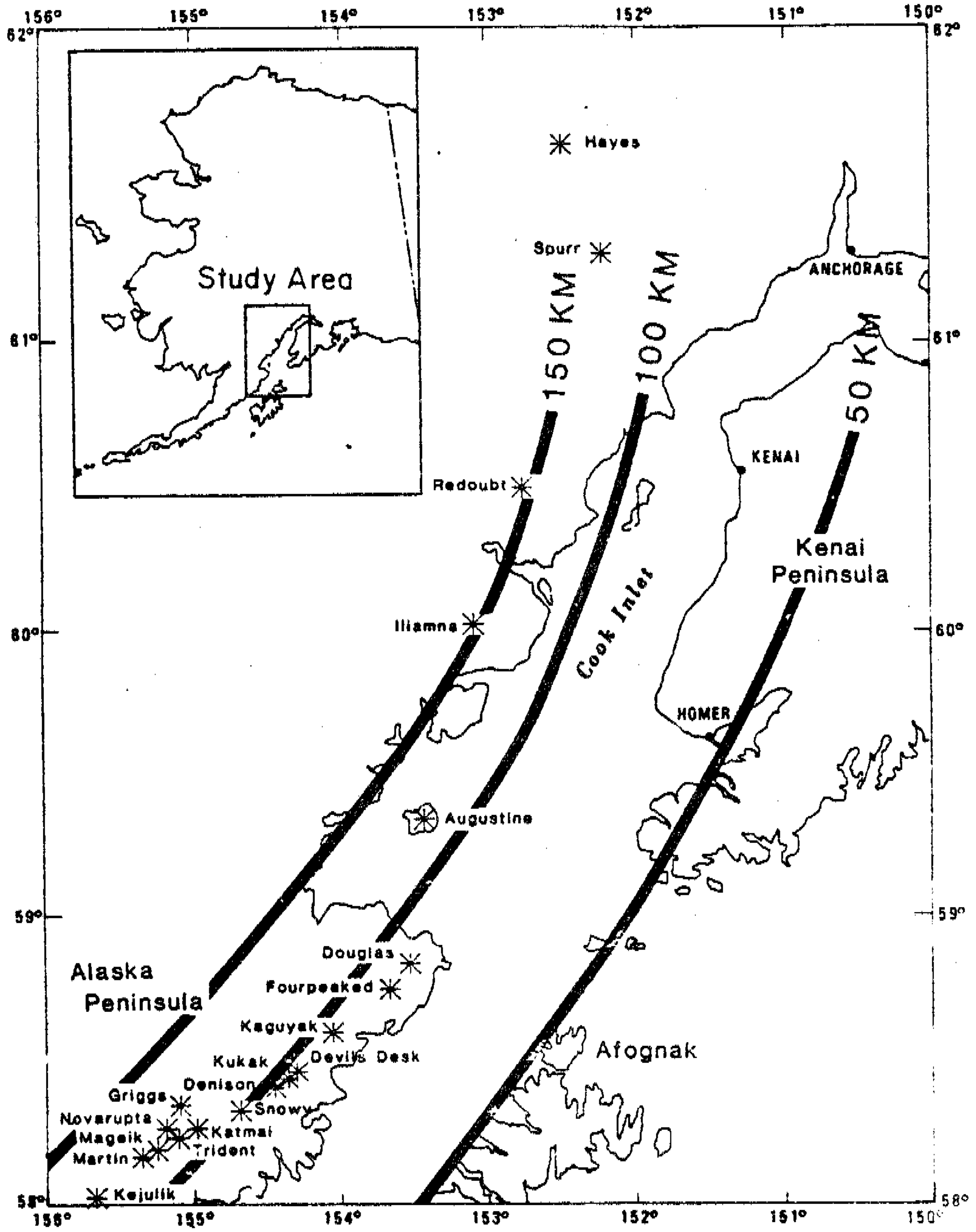
156°
155°
154°
153°
152°
151°
150°
62°
61°
60°
59°
58°
Study Area
Hayes
Spurr
ANCHORAGE
150 KM
100 KM
50 KM
KENAI
Redoubt
Kenai
Peninsula
Iliamna
Cook Inlet
HOMER
Augustine
Alaska
Peninsula
Douglas
Fourpeaked
Kaguyak
Kukak
Devils Desk
Denison
Griggs
Snowy
Novarupta
Katmai
Mageik
Trident
Martin
Kejulik
Afognak

GEOLOGY AND PETROLOGY OF KAGUYAK CRATER, ALASKA

Samuel E. Swanson
Juergen Kienle (both at: Geophysical Institute, University of Alaska, Fairbanks, AK 99701)
Philip M. Fenn (Geology Department, University of California, Davis, CA 95616)

Kaguyak Crater is a small (diameter=2.4 km), water-filled (average depth=190m) caldera on the Alaska Peninsula within Katmai National Park. An extensive apron of pyroclastic debris surrounds the crater lake and several post-caldera domes have been emplaced within and outside the caldera. A C^{14} age on a soil stratigraphically above the pyroclastic deposit gives a minimum age of caldera formation of 1000 years b.p. Weak fumarolic activity is associated with one of the post-caldera domes.

Pre-caldera lithologies are dominated by dacite (SiO_2 = 60-65), but small amounts of silica-rich andesite (SiO_2 = 59) are also found. Mineralogically, the two rock types are similar (dacite= pl + cpx + opx + qtz ± hb ± ol; andesite = pl + cpx + opx + altered hb ± qtz) with opx compositions of about $Wo_2En_{61}Fs_{37}$ and cpx compositions of $Wo_{45}En_{40}Fs_{15}$. Plagioclase phenocrysts within the lavas are complexly zoned with core compositions of An_{41-57} and rims of An_{40-73}; groundmass plagioclase shows a similar range of bulk composition.

Dacite (SiO_2 = 62-64) is the only rock type found in the post-caldera lavas. These younger dacites do not contain quartz (pl + opx + cpx ± hb), in contrast to the pre-caldera dacites.

The eruptive sequence at Kaguyak Crater (quartz-bearing lavas→caldera formation→quartz-absent lavas) may be related to the draining of a zoned magma chamber.

1. Fall Meeting
2. SWAN 403478
3. Corresponding address
   S.E. Swanson
   Geophysical Inst.
   Univ. of AK
   Fairbanks, AK 99701
4. VGP
5. none
6. 0
7. none
8. same as item 3
9. C

ANNUAL REPORT

Contract Number: 03-5-022-55
Research Unit Numbers: 253, 244, 256
OCSEAP Task Numbers: D8 and D9
Reporting Period: April 1, 1980 to March 31, 1981

SUBSEA PERMAFROST: PROBING, THERMAL REGIME AND DATA ANALYSIS

W. D. Harrison
T. E. Osterkamp

Geophysical Institute
University of Alaska
Fairbanks, Alaska 99701

TABLE OF CONTENTS

The last six pages of this appendix were omitted as copy provided was not of sufficient quality for reproduction.

I. SUMMARY OF OBJECTIVES, CONCLUSIONS AND IMPLICATIONS WITH RESPECT TO OCS DEVELOPMENT

The objectives of this study are to determine the distribution and properties of subsea permafrost in Alaskan waters, in cooperation with other OCSEAP investigators. Besides direct measurements, our program includes an effort to understand the basic physical processes responsible for the subsea permafrost regime, as a basis for predictive models.

The detailed conclusions of our 1980 field work are in Section VIII. Perhaps most notable are the apparent absence of subsea permafrost in Norton Sound (except possibly near shore in some areas undergoing rapid shoreline erosion), and the presence of ice-bearing permafrost near the sea bed out to at least 7.8 km off the Lonely DEW station in the Beaufort Sea. The latter observation emphasizes that shallow ice-bearing permafrost is probably widespread in the Beaufort Sea, especially where the sediments are fine-grained.

It is likely that problems posed by subsea permafrost for offshore hot oil production will be greater than for permafrost problems onshore at Prudhoe Bay, because subsea permafrost is warmer, saltier and more easily disturbed, and because it is often associated with fine-grained soils.

II. INTRODUCTION

This work is part of the OCSEAP study of the distribution and properties of permafrost beneath the seas adjacent to Alaska and of processes that control its development. The study involves coordination of the efforts of a number of investigators (RU 204, 271, 253, 255, 256, 473, 103, 407) and synthesis of the results of both field and laboratory work. Related work that is more focused on the scientific problems of heat and mass transfer in subsea permafrost is primarily funded by the National Science Foundation and supported by OCSEAP logistics.

More information on specific objectives, and relevance to problems of petroleum development, are given in our report of last year (Osterkamp and Harrision, 1980).

III. CURRENT STATE OF KNOWLEDGE

A summary of the current state of knowledge was given in Section III and Appendix B of our report of last year (Osterkamp and Harrison, 1980), and by the other OCSEAP investigators in their reports.

IV. STUDY AREA

Field investigations were carried out in the following areas in 1980: Norton Sound, the Chukchi Sea between Wainwright and the Naval Arctic Research Laboratory (NARL) at Barrow, the DEW site at Lonely, Prudhoe Bay, and on Thetis, Reindeer, Cross and Flaxman Islands.

V. METHODS AND RATIONALE OF DATA COLLECTION

Although there have been some refinements, our methods have not changed greatly from those described in our report of last year (Osterkamp and Harrison, 1980). We have recently published two reports (Harrison and Osterkamp, 1981; Osterkamp and Harrison, 1981) that give a fairly complete description of most of the methods; the abstracts are in Appendix A.

VI. AND VII. RESULTS AND DISCUSSION

A. NORTON SOUND

A discussion of the possible existence of permafrost beneath the northern Bering Sea has been given by Hopkins (1980). Although regional history suggests a long period of emergence and exposure to cold surface temperatures prior to 5000 years ago, the indirect evidence available suggests that permafrost is probably now absent except possibly in a narrow band off coastal areas that are undergoing rapid shoreline erosion, notably between the Koyuk River and Cape Denbigh, between St. Michael and the Apoon Pass (Yukon River), between Kivikloak Pass and Cape Romanzof, and in Norton Bay.

The data reported here are the results of a limited driving and jet drilling program to obtain temperature and lithologic data beneath Norton Sound in the eastern Bering Sea.

1. Nome Hole

A hole was driven near Nome, at a site about 326 m from shore and bearing about N208°E from Anvil Mountain as determined by tape and Brunton compass (Table 1 and Figure 1). The site was chosen because the equipment could be hauled by sled from the Nome airport, and because the lithology was very well known (Hopkins and others, 1960). The Atlas-Copco driver was used to place plastic tubing. Hard driving was encountered in what is probably glacial drift.

The temperature profile shown in Figure 2 was obtained 3 days after hole completion. It is probably within a few hundredths K of equilibrium. The water column temperature was ≈ -1.6°C near the sea bed but warmed to ≈ -0.2°C under the ice. It is believed that this warming was produced by a lens of fresh water under the ice, possibly from the Snake River. The hole was not deep enough (< 7 m) to allow an accurate estimate of the mean annual sea bed temperature (MASBT), but it appears to be between +1 and +3°C. A bottom hole temperature of +3.29°C at 6.8 m is very warm but appears to be reasonable judging from other holes in Norton Sound.

2. Charley Green Creek Holes

Two holes were driven near the mouth of Charley Green Creek at distances (paced from shore) of 610 and 630 m (Table 1 and Figure 3). The hole setting is shown in Figure 4. The site was chosen because it is one inferred to be undergoing rapid shoreline retreat (see Hopkins, 1980), and therefore a likely one for relict subsea permafrost. Hole 610 was completed with tubing and hole 630 with pipe. The lithology consisted of 5-7 m of silt overlying bed rock. The hard material encountered between 5 and 6 m in hole 610, which felt like ice-bonded fine-grained material, is of special interest. However, temperature data discussed below indicate that it is too warm to contain ice. It is probably soft rock.

Insufficient data were obtained to determine equilibrium temperatures. The pipe in hole 630 was partially jacked up out of the hole by tide, and both holes were finally destroyed by vandals before logging was completed. Hole 630 showed a bottom temperature of +3.38°C, 5.5 m below the sea bed on March 30. Hole 610 showed +3.73°C at the 6.72 m depth. Temperatures seemed to be positive 1 m or less below the sea bed. The water column and sea bed temperatures were -0.55°C, which corresponds to a salinity of about 10^{o}/oo. Yukon River water is probably responsible for the low value.

The holes are not quite deep enough to permit a test of the estimated shoreline retreat rate of 15-20 m a^{-1} (see Hopkins, 1980) or an assessment of the possibility of permafrost at depth.

3. St. Michael River Hole

A hole was drilled and completed with tubing about 3.9 ± 0.5 km from shore not far from the mouth of the St. Michael River (Table 1 and Figure 3). The hole location was determined from several compass bearings to prominant headlands and peaks, and checked by aircraft dead reckoning. The shoreline in this area is also retreating rapidly (see Hopkins, 1980). To the depth reached, the jetting was rapid and there was little caving in the silt and sandy silt sediments.

Problems with vertical movement of the tubing in the hole prevented determination of an extrapolated temperature profile. Therefore the last logging, obtained 34 days after drilling, is shown in Figure 5. The temperatures below 14 m are probably within a few hundredths K of equilibrium. A sea bed temperature of about -1.0°C, corresponding to a salinity of ≈ $18^{0}/oo$, was measured at the time of the last logging. Again, this low salinity, about 1/2 normal sea water, suggests mixing with the Yukon River water. The MASBT was about +3.3°C. Preliminary calculations suggest that the curvature just below the annual temperature variation was caused by warming at the sea bed within the past year. The temperature gradient near the bottom of the hole was positive, suggesting that subsea permafrost is absent at this site.

4. Yukon Delta Hole

A hole was jetted as far from shore to the north of the Yukon Delta as sea ice conditions safely permitted; the nearest portion of the delta is about 27 km distant (Table 1 and Figure 3). Hole position was determined by the Global Navigation System of the NOAA Bell 204 helicopter, calibrated to the position of the Charley Green Creek holes as determined from a map. Jetting was rapid and was accomplished with a long piece of radiator hose weighted with several pipe sections at the bottom. Silty sediments were encountered from the sea bed to the depth reached.

Figure 6 shows the temperature profile from the last logging, 31 days after drilling. Temperatures below 9 m are probably within a few hundredths K of equilibrium. A water temperature of ≃ -1.6°C was found within a few meters of the sea bed. The MASBT is ≃ +2.6°C. Preliminary calculations suggest that the curvature in the temperature profile just below the annual variations was produced by sea bed warming sometime during the past year.

5. General Comments

Sub-seabed temperaures on the south side of Norton Sound and near Nome are on the order of +3°C or higher at depth. These high temperatures and the presence of positive temperature gradients in the bottom portions of the deeper holes suggest that subsea permafrost is absent in these areas and probably over most if not all of Norton Sound. The possibility still exists that subsea permafrost may be found very close to shore in areas of high shoreline erosion rates. However, because of the positive MASBT, permafrost degradation should be rapid and not limited by salt transport rates as it may be in some areas of the colder Beaufort Sea. These conclusions cannot be extrapolated to the rest of the Bering Sea without additional data. Temperature data tabulations are in Appendix B.

B. CHUKCHI SEA

Few data on subsea permafrost exist between NARL, Barrow and Cape Lisburne, although some water temperature data have been compiled (Osterkamp and Harrison, 1980). A limited driving and rotary jet drilling program to fill some of this data gap was conducted, working from NARL. The area studied, SW from NARL, was limited by helicopter range and bad flying weather. Subsea permafrost was initially expected to be of limited importance in nearshore areas along much of this coast because bedrock probably exists near the sea bed in many places, although there are unconsolidated pleistocene sediments onshore (AEIDC, 1975, for example). However, it should be noted that a major break in the Trans-Alaska Pipeline occurred when ice-rich bedrock melted and settled.

1. Peard Bay

A site was rotary jet drilled in Peard Bay, roughly 500 m from shore as estimated from map bathymetry and measured water depth (Table 1). The drill was stopped about 2 m into the sea bed by what seemed to be rock.

2. Wainwright Terminal Hole (Hole 265)

A hole was rotary jet drilled and finished with plastic tubing near the proposed tanker terminal northeast of Wainwright (Table 1 and Figure 7). The distance from shore (265 m) was determined by taping, and the position along the coast, by the helicopter Global Navigation System. At this site, the tundra is about 35 m from the water edge and 2 to 3 m higher. Drilling was slow, particularly in some layers which may have been soft rock.

Two temperature profiles were obtained (Appendix B) and the second is shown in Figure 8. It was obtained 30 days after drilling and is probably within a few hundredths K of equilibrium below the 8 m depth. The water temperature a few meters above the sea bed increased from -1.734°C to -1.825°C between May 6 and 24. The MASBT is near 0.0°C. Warm water from the Kuk River flowing northeast along the coast from Wainwright may be responsible for this relatively warm sea bed temperature. There does not appear to be any evidence in the temperature data for ice-bearing permafrost except that the gradient is negative, ≈ -0.025 K m^{-1}, which would imply that ice could be present at depth. However, the negative gradient may be due to secular warming of the sea bed as noted in Norton Sound, and at NARL as discussed below.

This temperature gradient does not seem to be a steady state one. The steady state gradient, estimated by the simple method described by Osterkamp and Harrison (1978), and using parameters thought to be characteristic of Barrow, is roughly 1/2 of geothermal, or roughly +0.018 K m^{-1}. There is a large uncertainty in this value because the thermal conductivity is unknown. Nevertheless, it is sufficiently different from the measured value that there seems to be either present day coastal retreat or sea bed temperature warming. The latter effect may be important, given the evidence from NARL discussed below.

3. Naval Arctic Research Laboratory (NARL) holes

Three holes were rotary jet drilled off NARL in an effort to obtain deeper data than obtained in 1977 (Osterkamp and Harrison, 1978) (Table 1 and Figure 9). The hole line bears N330°E from the three mast (wood poles) radar tower as measured by Brunton compass. The holes were at distances from shore of 29, 78, and about 690 m. The first two distances were taped. The third was estimated with a device paying out string over a counting sheave, and also paced because a strong cross wind and rough ice conditions made the former measurement unreliable. Uncertainty in the third hole position is on the order of 100 m. The first two holes were finished with pipe; the third with plastic tubing.

4. NARL Hole 27 (hole A)

The temperature profile shown in Figure 10 was obtained on April 22, 1980. The hole is too shallow to justify much of an analysis effort. The water temperature was near -1.8°C which corresponds to near normal salinity under the ice, ≈ 33°/oo. As a rough guess, the MASBT may be about -1.0 to -1.3°C.

5. NARL Hole 78 (hole B)

Four temperature profiles were used to construct the extrapolated temperature profile shown in Figure 11. Water temperatures near the sea bed varied by a few hundredths K but were about -1.82°C. The curvature in the profile just below the level of annual variations is probably due to sea bed warming during the past year. A MASBT of -0.5°C was found by extrapolation of the linear portion of the profile to the sea bed. The effects of water forced into the formation during drilling are evident at 24 m. The temperature gradient is negative and suggests ice-bearing and possibly ice-bonded permafrost at depth. This temperature gradient is dominated by the nearby presence of land.

6. NARL Hole 690 (hole C)

Three temperature logs were obtained in this hole but problems with vertical movement of the tubing, and water forced into the formation prevent estimation of the equilibrium temperature. The hole was destroyed by vandals before a fourth log could be obtained. The third temperature log, obtained 15 days after drilling, is shown in Figure 12. Water temperatures just above the sea bed, for the three logs, were ≈ -1.81°C. The MASBT is ≈ -0.5°C, which is the same as at hole B, although the thermal gradient in the lower portion of the hole is positive. Extrapolation of the profile in the lower portion of the hole suggests that the 0°C isotherm is 80-90 m below the sea bed. The question of whether or not ice-bearing permafrost exists at this site cannot be answered directly although our past experience at other sites suggests that it may be absent.

Comparison of this temperature profile with one obtained in 1977 at a nearby site, about 705 m from shore, suggests a secular warming of the sea bed (Figure 13). The magnitude of this change is not certain since the 1977 data were somewhat less accurate than the 1980 data. This effect is perhaps best seen by ignoring the upper 5 or 10 m, which are subject to large seasonal variations in temperature. Judging by the curvature of the lower part of the 1977 profile, which should be relatively unaffected by seasonal variations, the warming had begun before 1977. The amount of warming cannot be estimated without a detailed analysis, but it is probably on the order of 0.5 K or larger. This is not the first time that a secular change has been noted in this area. Osterkamp and Harrison (1978) noted that the 1977 temperature was colder than that in the 1950's.

The apparent secular changes make it difficult to make simple estimates of mean annual sea bed temperature, depth to the 0°C isotherm, deep temperature gradient, or shoreline stability. The temperature gradient is also affected by the presence of the cold land at this site, although this effect is relatively minor, about 20%. With the uncertainties in its interpetation, our data are consistent with the conclusion of Lachenbruch and Brewer (1959) that the shoreline at NARL is relatively stable. The temperature data are in Appendix B.

C. BEAUFORT SEA

1. Lonely

A line of 5 holes was rotary jet drilled along a line bearing N328°E, as determined by Brunton compass, near the DEW line site (Table 1 and Figure 14). The holes were finished with pipe. Distances from shore were paced and checked by helicopter dead reckoning, but they may contain significant errors. This area is of considerable interest because it lies in a large data gap; there were no previous offshore hole data between Elson Lagoon and Harrison Bay. Also, extremely high shoreline retreat rates, up to 10 or 15 m a^{-1}, have been measured immediately to the west and to the east (Lewellen, 1977). The onshore surficial deposits are mapped as interglacial nearshore and lagoon sand, silty fine sand,

and pebbly sand (Hopkins and Hartz, 1978). Drilling data suggests that the offshore sediments are fine-grained. The ice-bearing permafrost onshore at Cape Simpson, about 55 km to the east, is about 300 m (Osterkamp and Payne, 1981).

It was difficult to assess the presence of ice from drilling data alone at this site, as is often the case when fine-grained soils are present. Therefore all the bore holes were heated after they had approached equilibrium, and the temperature response used to determine the presence of ice; a small response means buffering by the presence of ice.

Lonely Hole 88 (hole A)

The temperature profile measured 21 days after drilling is shown in Figure 15. The data point at 14.5 m is a measurement error. This profile should be within a few hundredths K of equlibrium. The water temperature under the ice at the time of first logging (May 14) was -2.2°C; the water depth was 1.96 m. The MASBT is ≈ -1.2°C, but the presence of a phase boundary near the sea bed makes it difficult to determine reliably. The temperature profile is nearly linear below 16 m and curved above. Borehole heating suggests that the sediments below 6 m contain ice; harder drilling was noticed below 7 m. The temperature at the probable location of the phase boundary, 6 m, is about -2.1°C.

Temperature data are in Appendix B Profile A4 was obtained after borehole heating.

Lonely Hole 950 (hole B)

The temperature profile measured 20 days after drilling is shown in Figure 16. It is probably within 0.05°C of equilibrium, which would be colder. The water temperature about 0.9 m above the sea bed was -1.94°C on May 29; the water depth was 3.12 m. The MASBT is probably ≈ -1.9°C, but the presence of a phase boundary near the sea bed makes it difficult to determine reliably. Drilling indicates that an ice-bonded permafrost boundary exists about 14 m below the sea bed where the temperature is -1.95°C; the temperature profile in Figure 16 suggests it might be about 1 m deeper. However, borehole heating suggests that ice exists below 7 m where the temperature is ≈ -1.50°C. An ice-bearing but unbonded transition zone is therefore suggested between 7 and 14 m.

Temperature data are in Appendix B. Profiles B3 to B6 were obtained after heating.

Lonely Hole 2560 (hole C)

The temperature profile, shown in Figure 17 was obtained 19 days after drilling. It is probably within 0.03°C of equilibrium, which would be colder. The water temperature above the sea bed was ≈ -1.9°C on May 22; the water depth was 4.8 m. The MASBT is ≈ -1.2°C, but the presence of a phase boundary near the sea bed makes it difficult to determine reliably. There is some curvature in the profile with possible breaks in slope near 13 1/2 and 17 1/2 m. Drilling indicated hard sediments below 16 m. However, borehole heating suggests the sediments were ice-bearing below 8 m, where the temperature ≈ -1.60°C. The combined information seems to suggest ice-bonding below 13 1/2 m, where the temperature is ≈ -1.91°C. An ice-bearing transition zone therefore appears to exist in this hole as well.

Temperature data are in Appendix B. Profile C3 was obtained after heating.

Lonely Hole 4360 (hole D)

The temperature profile shown in Figure 18 was obtained 17 days after drilling. It is probably within 0.02 K of equilibrium, which would be colder. The water temperature about 1/2 m above the sea bed was about -1.91°C on May 22; the water depth was 6.5 m. The MASBT is ≈ -1.2°C, but the presence of a phase boundary near the sea bed makes it difficult to determine reliably. Drilling, temperature and borehole heating suggest the sediments are ice-bearing below 7 m where the temperature is ≈ -1.52°C, and ice-bonded below 12 m, where the temperature is ≈ -1.71°C.

Temperature data are in Appendix B. Profile D3 was obtained after heating.

Lonely Hole 7770 (hole E)

The temperature profile measured 15 days after drilling is shown in Figure 19. This profile was probably within ± 0.03 K of equilibrium, judging from the previous temperature change. The water temperature 0.7 m above the sea bed was ≈ -1.87°C on May 22. The MASBT is about -1.3°C, but the presence of a phase boundary near the sea bed makes it difficult to determine reliably. Drilling suggests an ice-bonded permafrost boundary exists at about 16 1/2 m, where the temperature is -1.66°C; however, the temperature data suggests it might be at 15 m. Borehole heating suggests that the sediments are ice-bearing below 6 or 7 m, where the temperature is ≈ -1.45°C.

Temperature data are in Appendix B. Profile E3 was obtained after heating.

General Comments (Lonely)

These Lonely holes provide data in an area where none previously existed. The soil is fine-grained down to the maximum depth reached (31.3 m). The temperature data show evidence of rapid shoreline retreat; a simple preliminary analysis of the data in Figure 20 indicates a retreat rate on the order of several meters per year characteristic of the past 1000 years or so. Ice-bearing permafrost seems to exist at about 6 or 8 m below the sea bed all the way out to the most seaward hole about 7.8 km from shore. Ice-bonding exists somewhat deeper, characteristically at about 15 m below the sea bed.

Because of the fine-grained soils and presence of ice near the sea bed, subsea permafrost problems for offshore development are likely to be very serious in this area.

2. Barrier Islands

Our study of permafrost beneath the barrier islands of the Beaufort Sea was continued with holes rotary jet drilled on Thetis, Cross and Flaxman Islands (Table 1 and Figures 21, 22 and 23). All holes were finished with pipe and will be logged in 1981. A hole drilled on Reindeer Island (Hole D, Osterkamp and Harrison, 1980) was logged in 1980 (Appendix B).

3. Prudhoe Bay West Dock

Several new holes were driven along the UA-CRREL-USGS study line bearing about N31°E from North Prudhoe Bay State Number One well near the Arco West Dock. The main objective was to obtain more information about salt transport mechanisms by interstitial water sampling and temperature measurement. An existing onshore hole, CRREL PB-9, was logged for temperature. Lithology is described in several reports (see Sellmann, 1980).

West Dock Hole 300

A hole was augered 300 m from shore, as determined by taping (Table 1). Ice-bonded permafrost was encountered below 2 m and penetrated with difficulty by the auger. The hole was finished with pipe.

An approximate temperature profile is shown in Figure 24, which is probably not far from equilibrium. It is approximate because a calibration change in a thermistor (79-1) prevented precise reduction of the data. Comparison of data obtained in another hole (438) with data obtained with another thermistor (79-3) suggest a correction of -0.63°C between -2 and -3°C. At other temperatures, a correction of -0.6°C is assumed, which is probably accurate to ≈ ± 0.1°C. The temperature at the sea bed was ≈ -6 1/2 °C and the MASBT is ≈ -4°C.

Temperature data are in Appendix B.

West Dock Hole 438

A hole was driven 438 m from shore, as determined by taping (Table 1). The ice-bonded boundary was encountered between 16.5 and 16.8 m. The hole was made with the Atlas Copco Cobra driver, and finished with tubing.

The temperature profile in Figure 25 was measured four days after driving. It is probably within 0.05°C of equilibrium, which would be colder. The mean annual sea bed temprature ≈ -1.7°C. By downward extrapolation, the temperature at the ice-bonded boundary is between -2.4 and

-2.5°C. The ice-bearing and ice-bonded boundaries probably coincide. Curvature in the lower part of the profile could be caused by upward pore water motion of 0.1 to 0.2 ma^{-1}, or by warmer than normal sea bed temperatures during the previous year.

Temperature data are in Appendix B.

West Dock Hole 438 S

A hole was driven within a meter of the previously described hole 438 (Table 1). The ice-bonded boundary was encountered at about 13 m. Blow count data are shown in Figures 26 and 27. The hole was made with the conventional drop hammer driver and sampled for interstitial water with our special sampling probe (Harrison and Osterkamp, 1981). The electrical conductivity of the interstitial water at 25°C was measured in the lab to a precision and accuracy of 1/2% or better. The results are given in Figures 26 and 27 and in Table 2. The sharp increase above 2 m is due to seasonal partial freezing of the sea bed.

West Dock Hole 700

A hole was driven 700 m from shore, as determined by taping (Table 1). The direction of the hole line was determined by Brunton compass. It was intended to locate this hole and one at 701 m exactly at the site of similar 1979 holes (Osterkamp and Harrison, 1979), but this was not possible due to the destruction of one of the reference markers. There could be a 10 m relative lateral displacement. The ice-bonded boundary was encountered at about 25.0 m. Blow count data are shown in Figure 28. The hole was made with the conventional cathead and drop hammer driver and finished with plastic tubing.

The temperature profile shown in Figure 29 was measured 8 days after driving. It is probably within a few hundredths K of equilibrium, which would be colder. A damaged thermistor, and the calibration change in the one used to replace it, prevented the usual data reduction as it did with hole 300. However, by a somewhat similar procedure the profile was constructed and is probably accurate to ± 0.05 K or better. The MASBT is ≈ -0.7°C. Temperature at the ice-bearing boundary is about -2.44°C.

Temperature data are in Appendix B.

West Dock Hole 701

A hole was driven 1 m farther from shore than the previously described hole 700 (Table 1). The ice-bonded boundary was encountered at about 24.9 m. Blow count data near the boundary are shown in Figure 30. The hole was made for interstitial water sampling with the same procedure used in hole 438 S. The results are given in Figures 30 and 31, and in Table 2. The sharp increase above 2 m is due to seasonal partial freezing of the sea bed. We consider that the sharp decrease at about 15 m needs to be checked by further field measurements, but we have not been able to identify any obvious sources of error.

West Dock General Comments

A detailed study of the permafrost regime near the West Dock, Prudhoe Bay, which has as its objective the understanding of the heat and mass transport regimes operating there, was continued in 1980. This work is being done largely with NSF suport. Summaries of the status of this work, and of some of the features of our temperature measurement program were presented at the Fourth Canadian Permafrost Conference in Calgary, March 1980, and have been submitted for publication in the proceedings. The abstracts are in Appendix A.

VIII. SUMMARY AND CONCLUSIONS

Portable drilling and probing methods were used in studies of subsea permafrost beneath Norton Sound, and the Chukchi and Beaufort Seas in 1980. As in previous years, data on the thermal and chemical regimes of the permafrost were obtained. In one area, ice was detected by a borehole heating technique. On a regional basis some of the results are as follows:

A. NORTON SOUND

Sediment temperatures on the south side of Norton Sound and near Nome are on the order of +3°C or higher at depth. These high temperatures and the presence of positive temperature gradients observed in the bottom portions of the deeper holes indicate that subsea permafrost is absent in these areas and probably over most of Norton Sound, except possibly very close to shore in areas of high shoreline erosion rates.

B. CHUKCHI SEA

Holes were drilled in Peard Bay, offshore of the proposed Wainwright tanker terminal, and at NARL in an attempt to fill some of the data gaps on subsea permafrost between Cape Lisburne and NARL, Barrow. Rock or well-consolidated sediment was found at the Peard Bay site, which stopped the drilling at about 2 m below the sea bed. Possibly similar, but somewhat softer, material was penetrated at the Wainwright site, where the temperature profile shows evidence of shoreline retreat and/or secular sea bed warming. Secular sea bed warming appears to exist off NARL. The presence of ice-bearing material is still uncertain at these sites, although it may exist nearshore.

C. BEAUFORT SEA

1. Lonely

The soil is fine-grained off the Lonely DEW station and seems to contain ice within about 8 m of the sea bed at least out to 7.8 km from shore; ice-bonding begins at typically 15 m below the sea bed, or less, close to shore. Both temperature profiles and studies of recent shoreline erosion data indicate rapid shoreline erosion. The fine-grained soils and presence of ice near the sea bed suggest that subsea permafrost problems for offshore development are likely to be very serious in this area.

2. Barrier Islands

Additional barrier island holes, to be logged for temperature in 1981, have been drilled on Thetis, Cross and Flaxman Islands.

3. Prudhoe Bay West Dock

More data on the position of the ice-bonded permafrost boundary, its temperature, and the salinity distribution in the interstitial water above it have been obtained near the West Dock at Prudhoe Bay. This work is part of the heat and salt transport process studies in this area.

IX. REFERENCES

Harrison, W. D. and T. E. Osterkamp, 1981. Details of a probe method for interstitial soil water sampling and hydraulic conductivity and temperature measurement, Geophysical Institute Report UAG R-280, University of Alaska, Fairbanks, Alaska, 99701.

Hopkins, D. M. and R. W. Hartz, 1978. Shoreline history of Chukchi and Beaufort Seas as an aid to predicting offshore permafrost conditions. In: Environmental Assessment of the Alaskan Continental Shelf, Annual Reports, Vol. 12, p. 503-575.

Hopkins, D. M., 1980. Likelihood of encountering permafrost in submerged areas of northern Bering Sea. In: Smith, P., R. Hartz and D. Hopkins, Offshore permafrost and shoreline history as an aid to predicting offshore permafrost conditions, Environmental Assessment of the Alaskan Continental Shelf, Annual Reports, Vol. IV, p. 187-193.

Hopkins, D. M., F. S. MacNeil and E. B. Leopold, 1960. The coastal plain at Nome, Alaska--a late Cenozoic type section for the Bering Strait region: Dept. 21st. International Geological Congress, Copenhagen, Norden, pt. 4, p. 46-67.

Osterkamp, T. E. and W. D. Harrison, 1980. Subsea permafrost: probing, thermal regime, and data analysis. In: Environmental Assessment of the Alaskan Continental Shelf, Annual Reports, Vol. IV, p. 497-677.

Osterkamp, T. E. and W. D. Harrison, 1981. Methods and equipment for temperature measurements in subsea permafrost, Geophysical Institute Report UAG R-285, University of Alaska, Fairbanks, Alaska, 99701.

Osterkamp, T. E. and M. W. Payne, 1981. Estimates of permafrost thickness from well logs in Northern Alaska, Cold Regions Science and Technology (in press).

LIST OF FIGURES

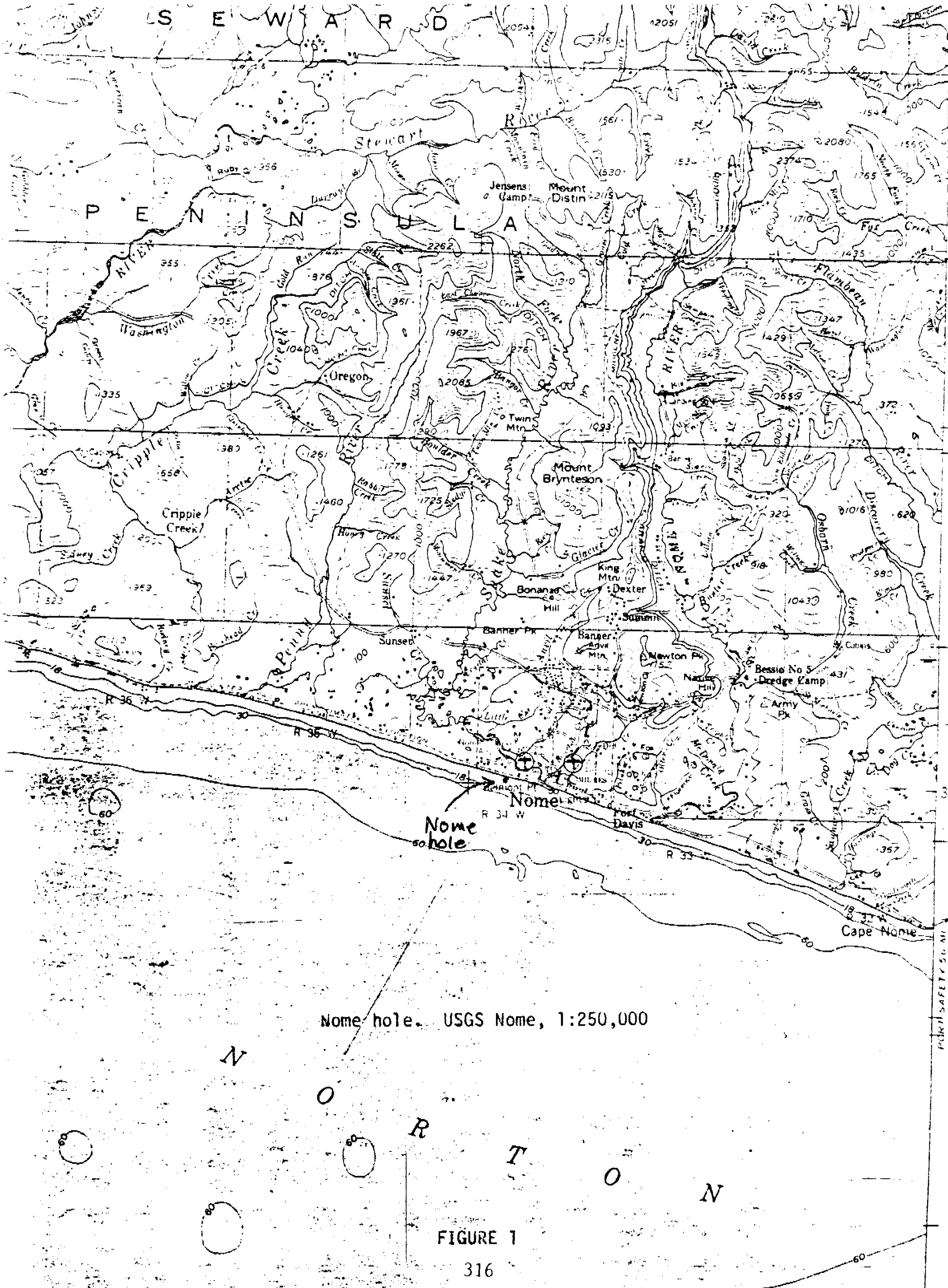

Nome hole. USGS Nome, 1:250,000

FIGURE 1

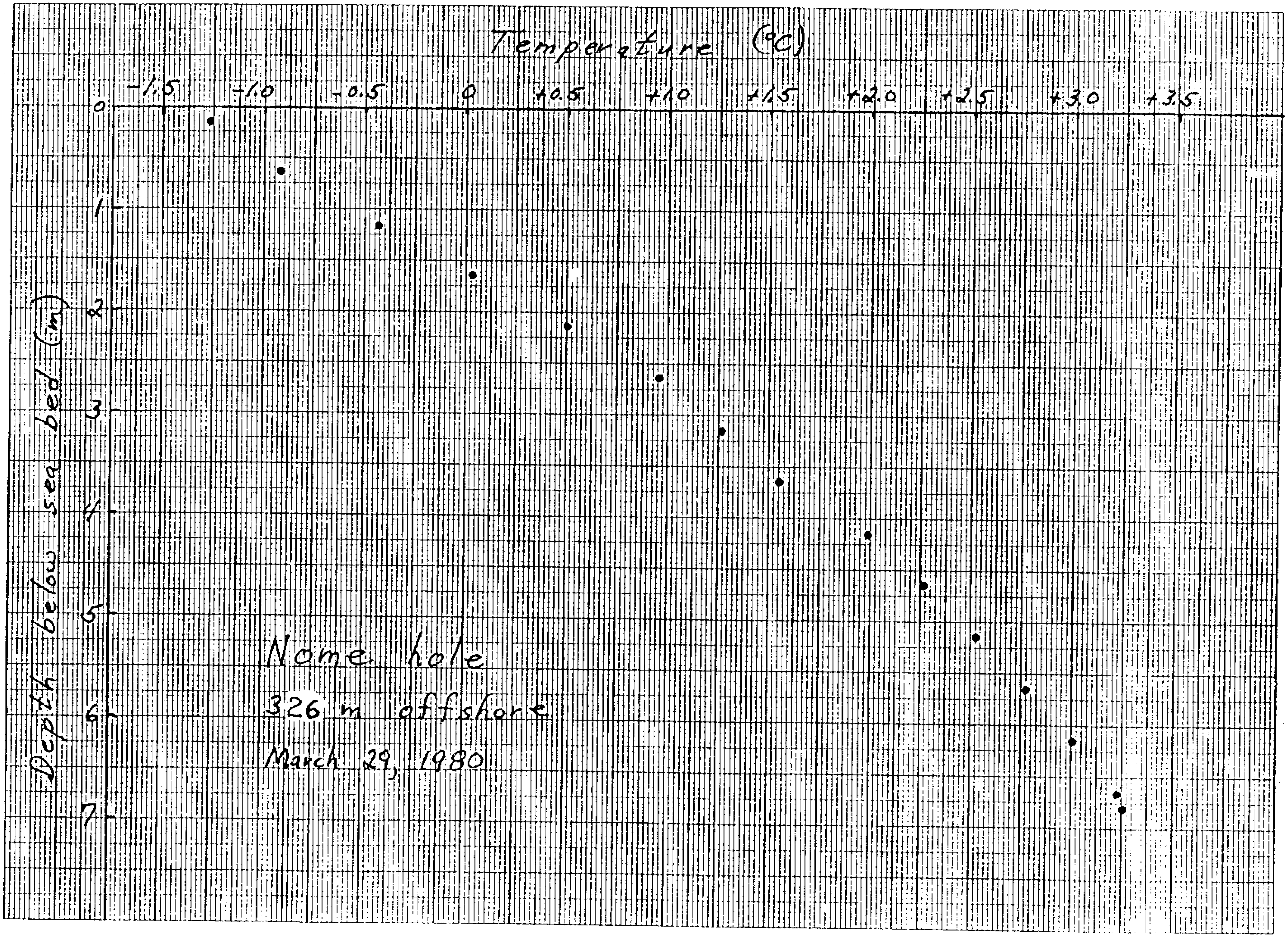
Temperature (°C)
-1.5
-1.0
-0.5
0
+0.5
+1.0
+1.5
+2.0
+2.5
+3.0
+3.5
Depth below sea bed (m)
0
1
2
3
4
5
6
7
Nome hole
326 m offshore
March 29, 1980

FIGURE 2

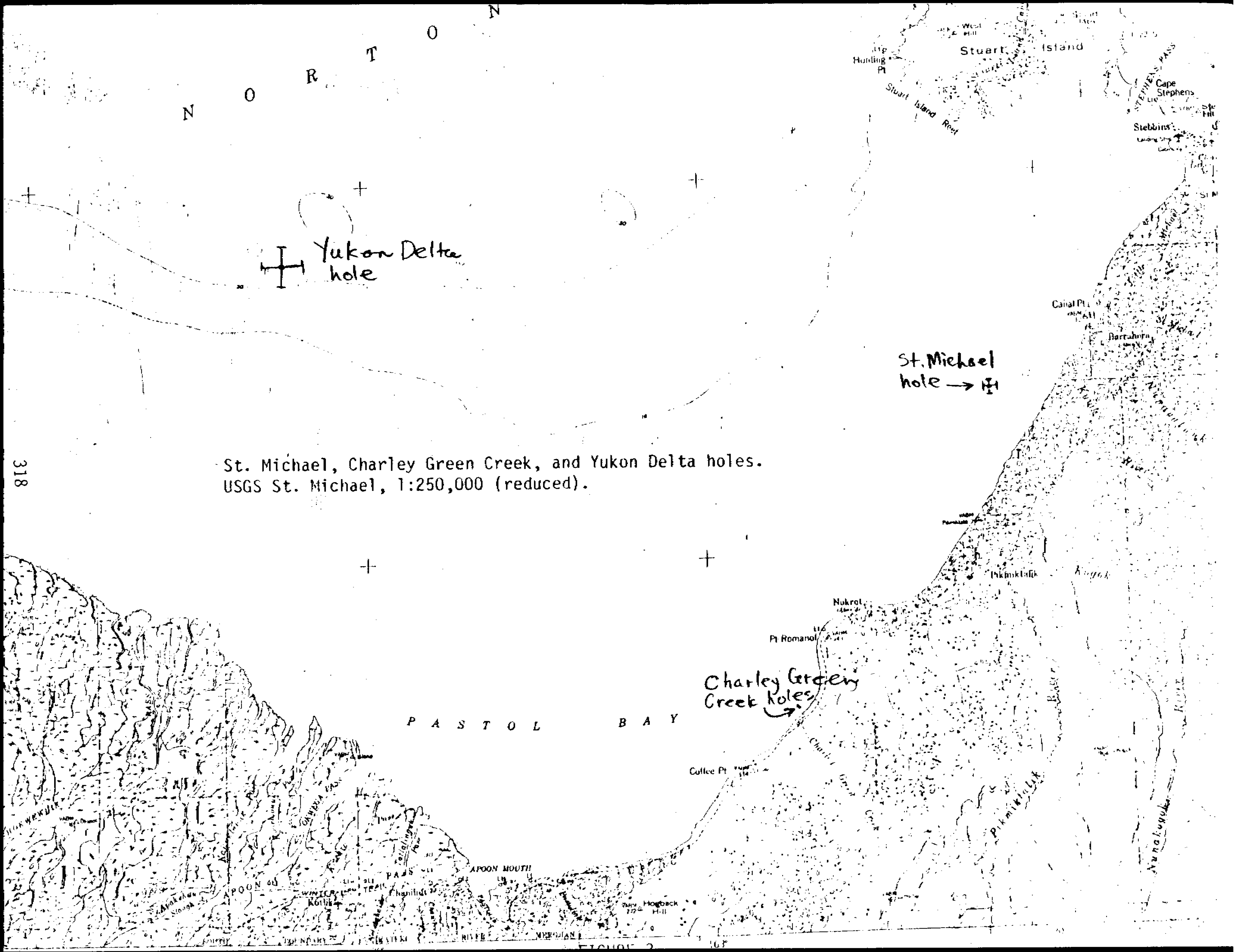

St. Michael, Charley Green Creek, and Yukon Delta holes.
USGS St. Michael, 1:250,000 (reduced).

FIGURE 3

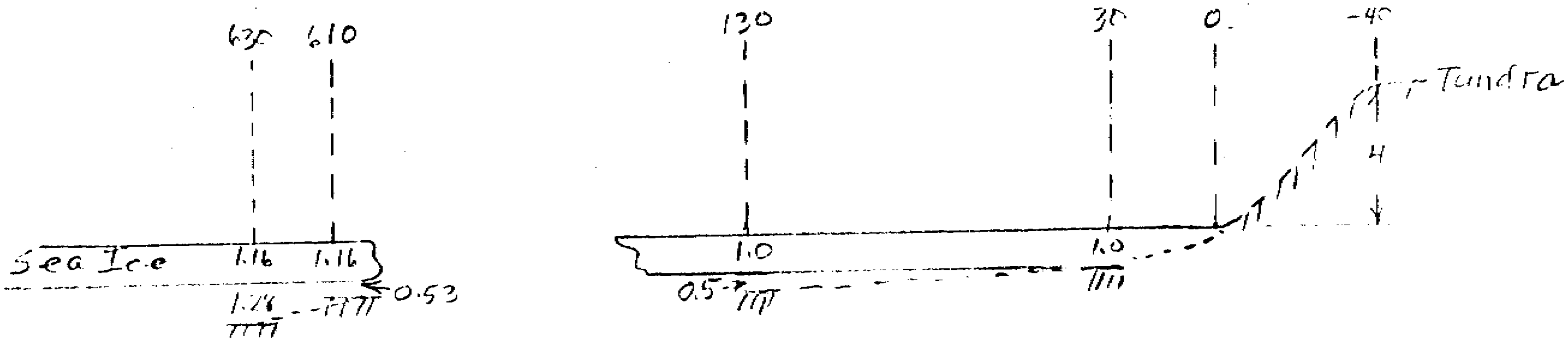

FIGURE 4

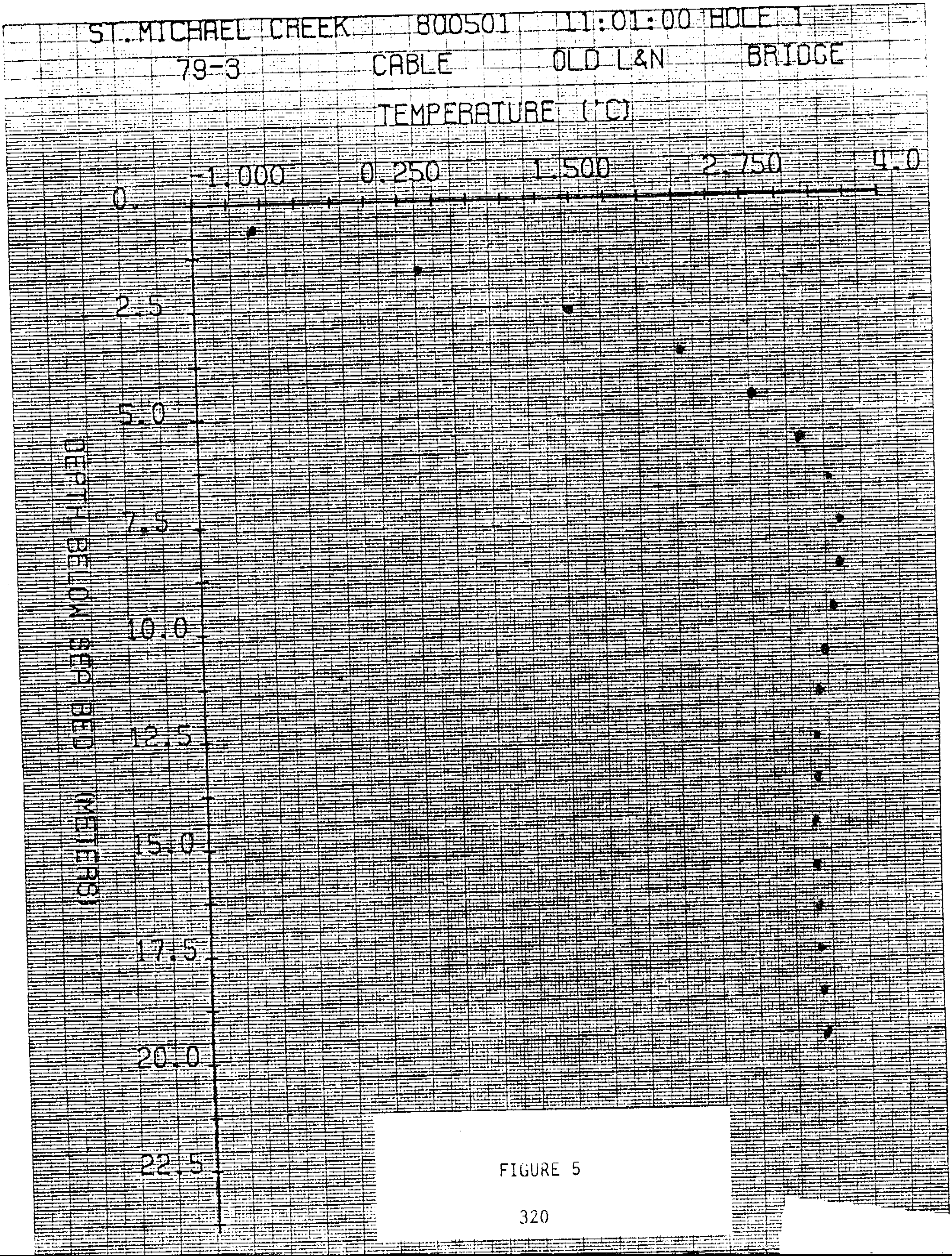

ST. MICHAEL CREEK 800501 11:01:00 HOLE 1
79-3 CABLE OLD L&N BRIDGE
TEMPERATURE (°C)
-1.000
0.250
1.500
2.750
4.0
0.
2.5
5.0
7.5
10.0
12.5
15.0
17.5
20.0
22.5
DEPTH BELOW SEA BED (METERS)

FIGURE 5

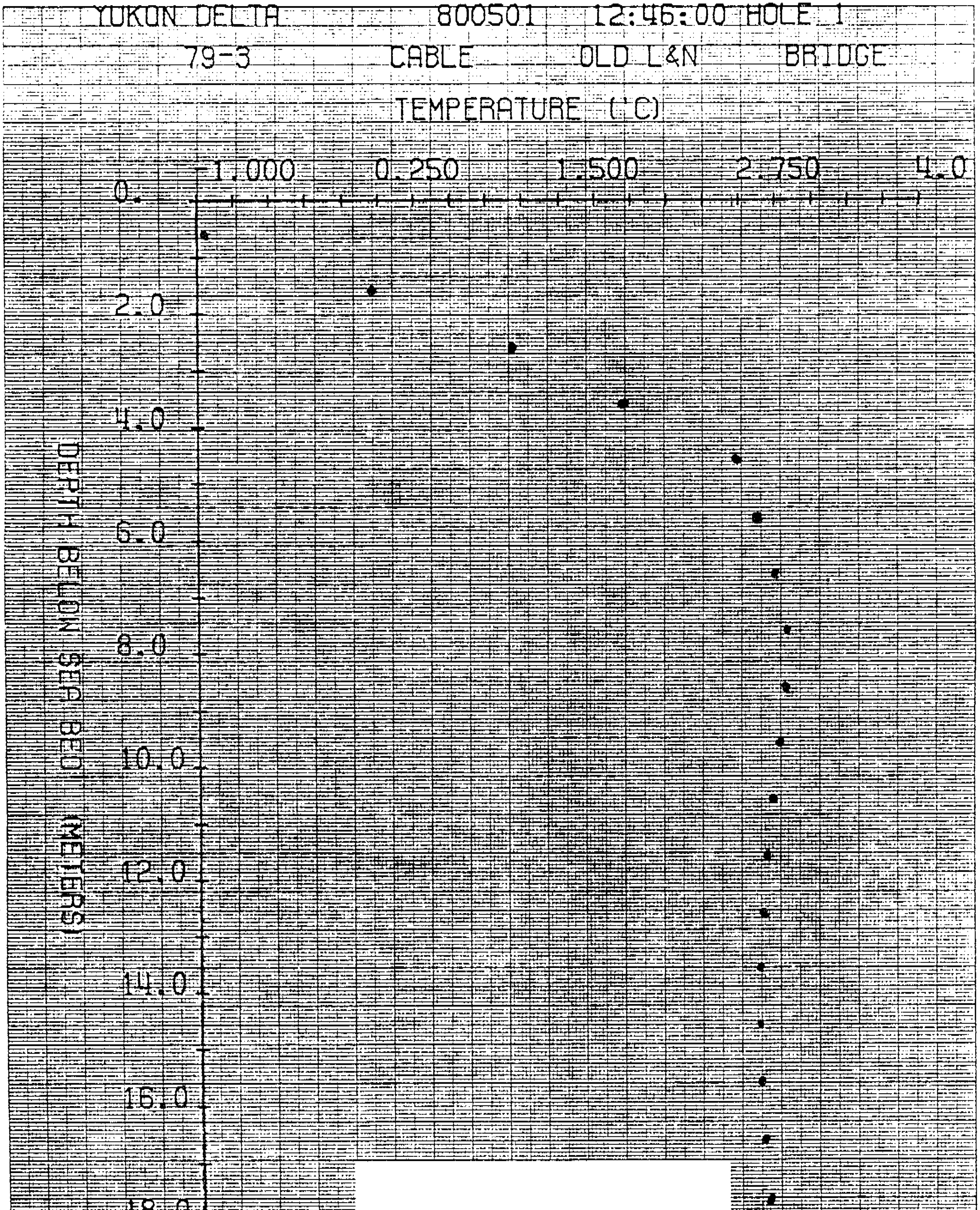
YUKON DELTA 800501 12:46:00 HOLE 1
79-3 CABLE OLD L&N BRIDGE
TEMPERATURE (°C)
-1.000
0.250
1.500
2.750
4.0
0.
2.0
4.0
6.0
8.0
10.0
12.0
14.0
16.0
18.0
DEPTH BELOW SEA BED (METERS)

FIGURE 6

FIGURE 7

Wainwright hole. USGS Wainwright (D-1), 1:63,360.

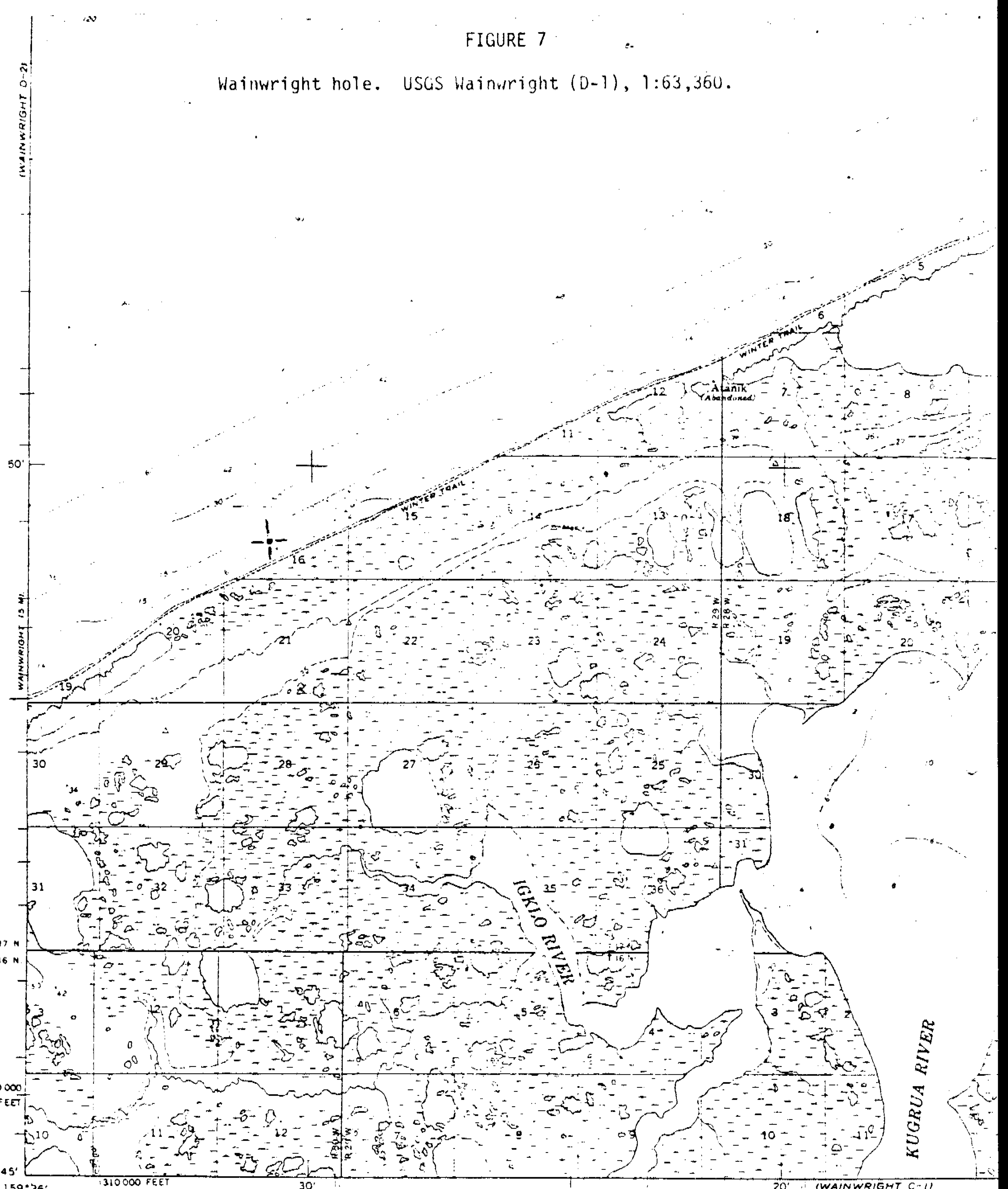

Mapped by the U.S. Army Topographic Command
Published for civil use by the Geological Survey

Control by USC&GS and USCE

Topography by photogrammetric methods from aerial photographs taken 1955, field annotated 1955. Map not field checked

Selected hydrographic data compiled from USC&GS

SCALE 1:63 360

CONTOUR INTERVAL 50 FEET
DASHED LINES REPRESENT 25-FOOT CONTOURS

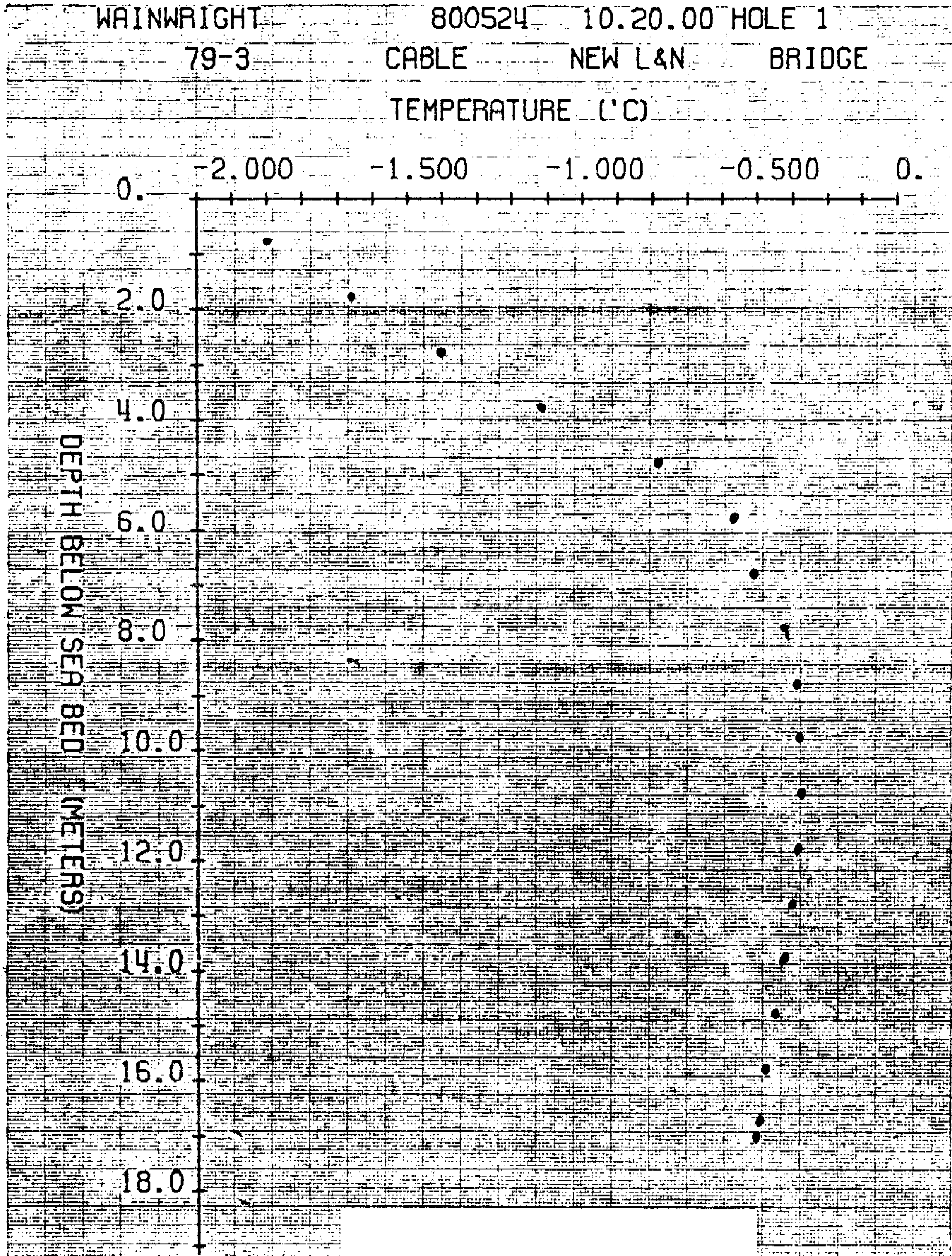
WAINWRIGHT 800524 10.20.00 HOLE 1
79-3 CABLE NEW L&N BRIDGE
TEMPERATURE ('C)
-2.000 -1.500 -1.000 -0.500 0.
0. 2.0 4.0 6.0 8.0 10.0 12.0 14.0 16.0 18.0
DEPTH BELOW SEA BED (METERS)

FIGURE 8

FIGURE 9

NARL holes. USGS Barrow (B-4), 1:63,360.

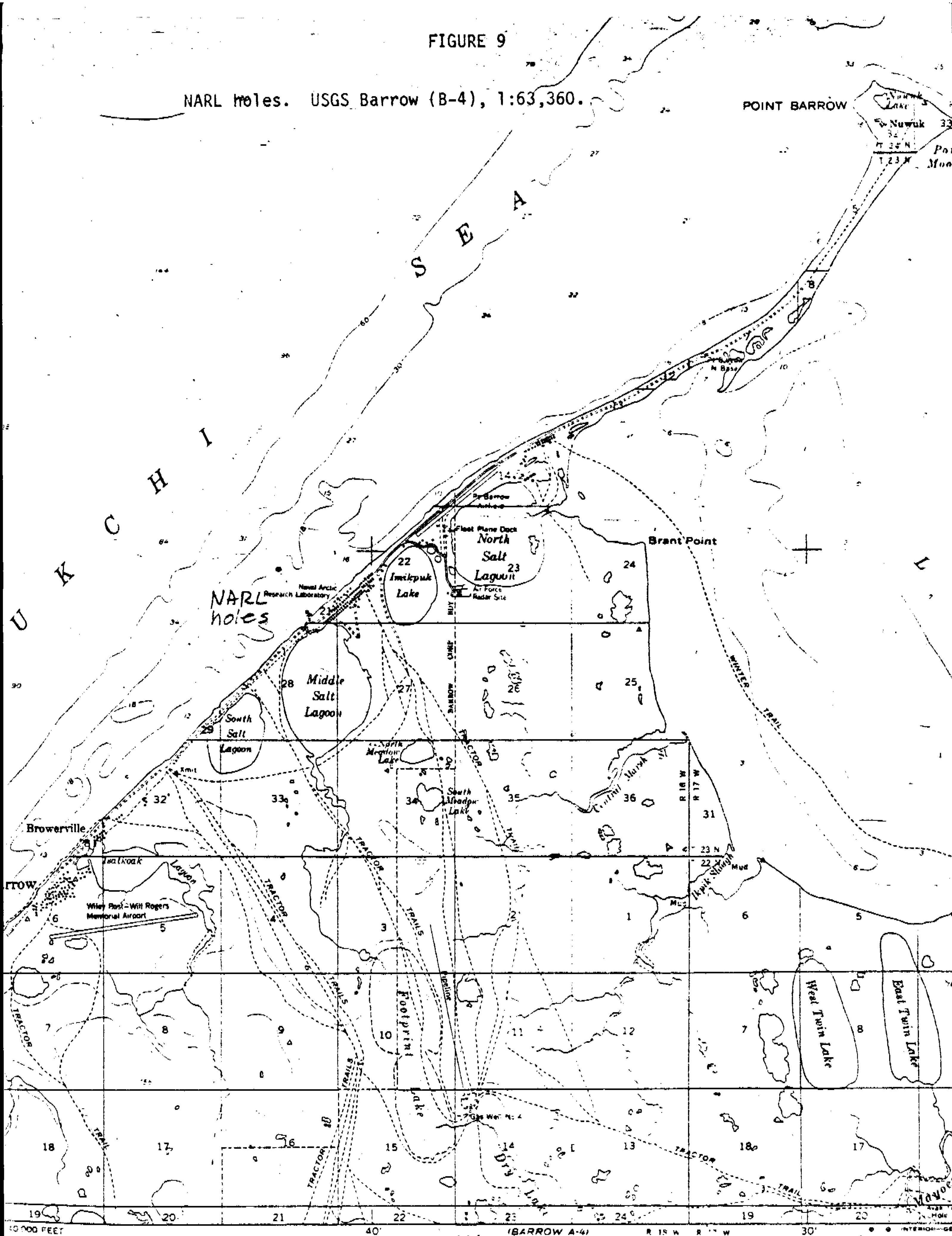

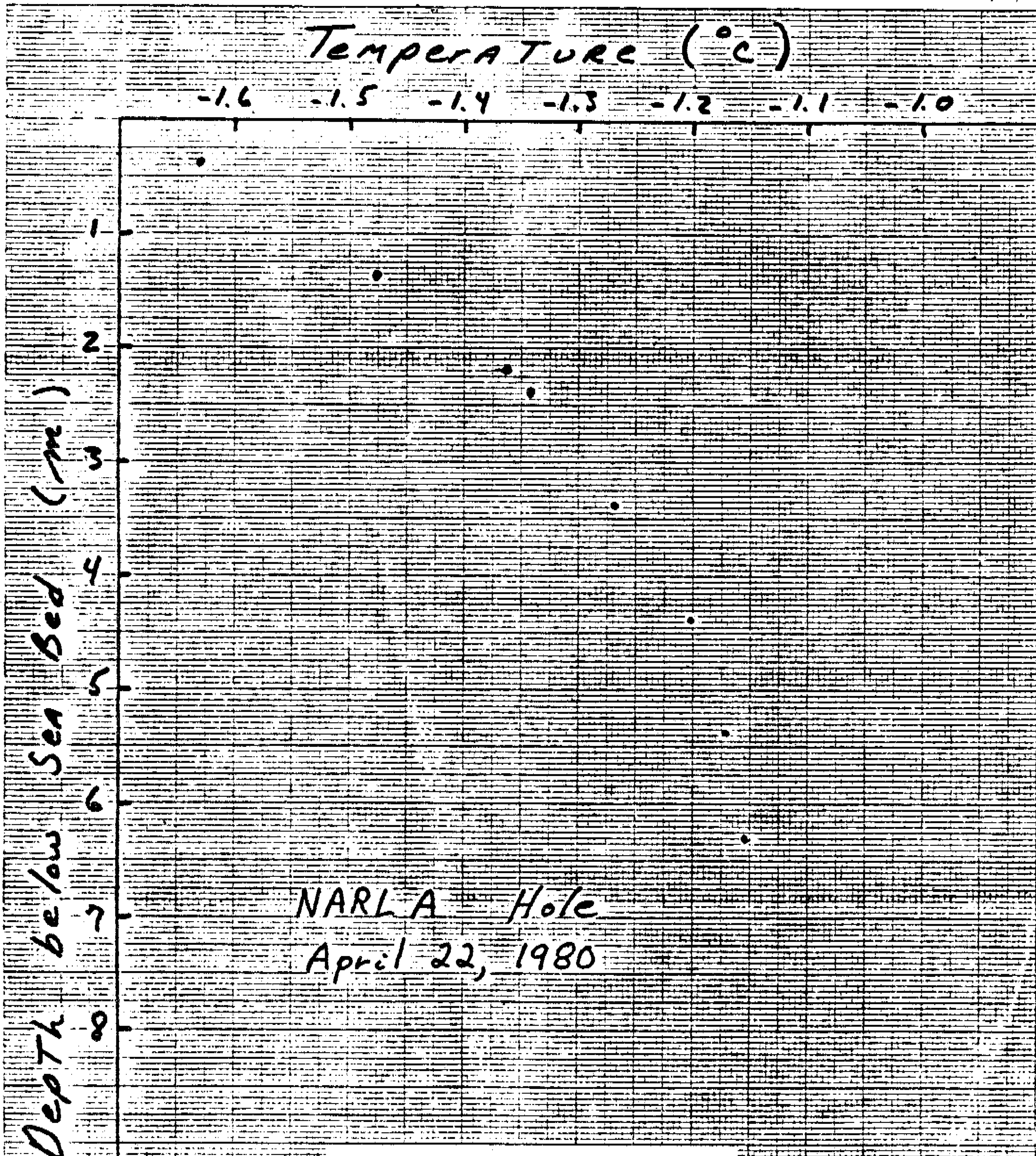
Temperature (°C)
-1.6
-1.5
-1.4
-1.3
-1.2
-1.1
-1.0
Depth below Sea Bed (m)
1
2
3
4
5
6
7
8
NARL A Hole
April 22, 1980

FIGURE 10

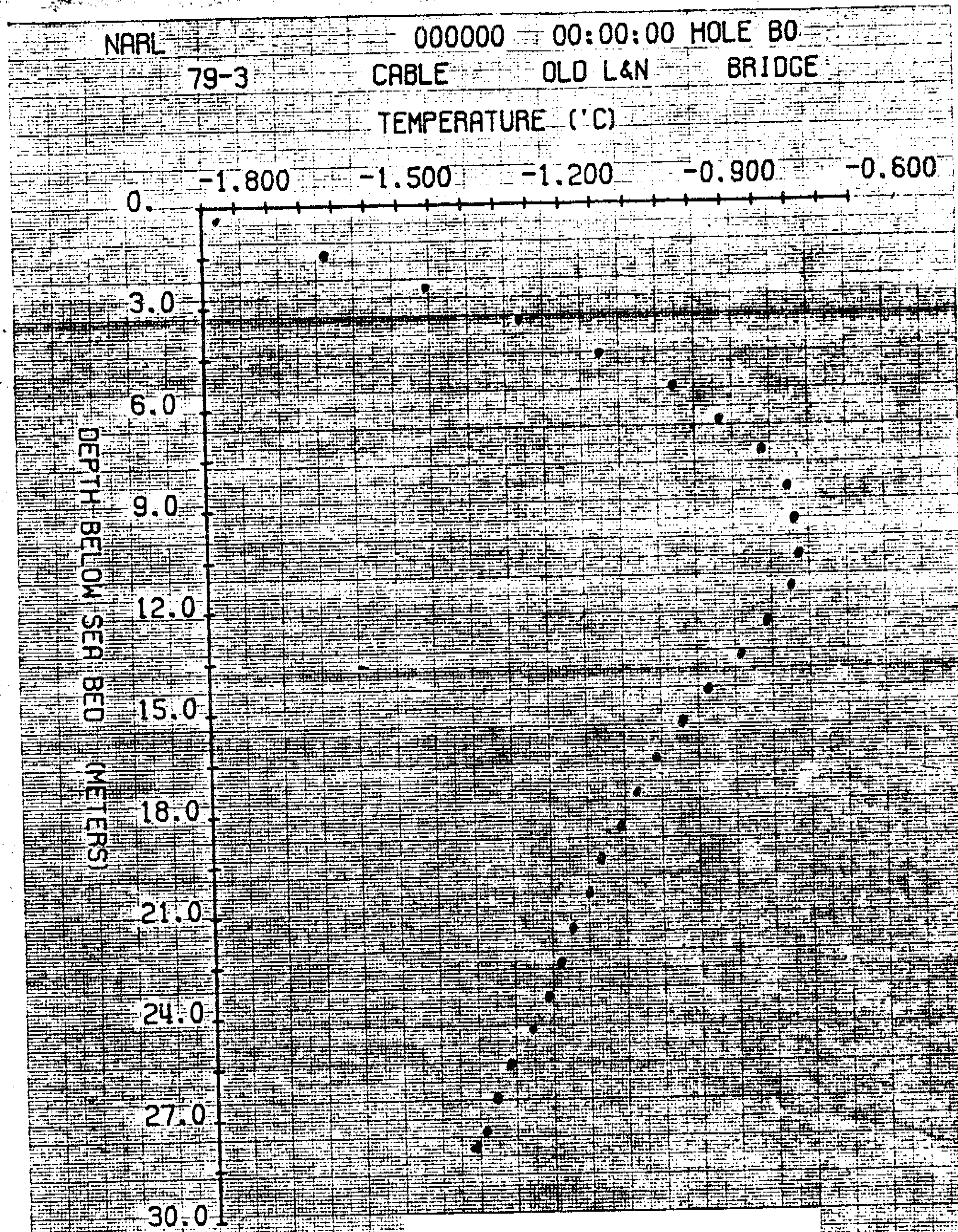
NARL
000000 00:00:00 HOLE B0
79-3
CABLE
OLD L&N
BRIDGE
TEMPERATURE ('C)
-1.800
-1.500
-1.200
-0.900
-0.600
0.
3.0
6.0
9.0
12.0
15.0
18.0
21.0
24.0
27.0
30.0
DEPTH BELOW SEA BED (METERS)

FIGURE 11

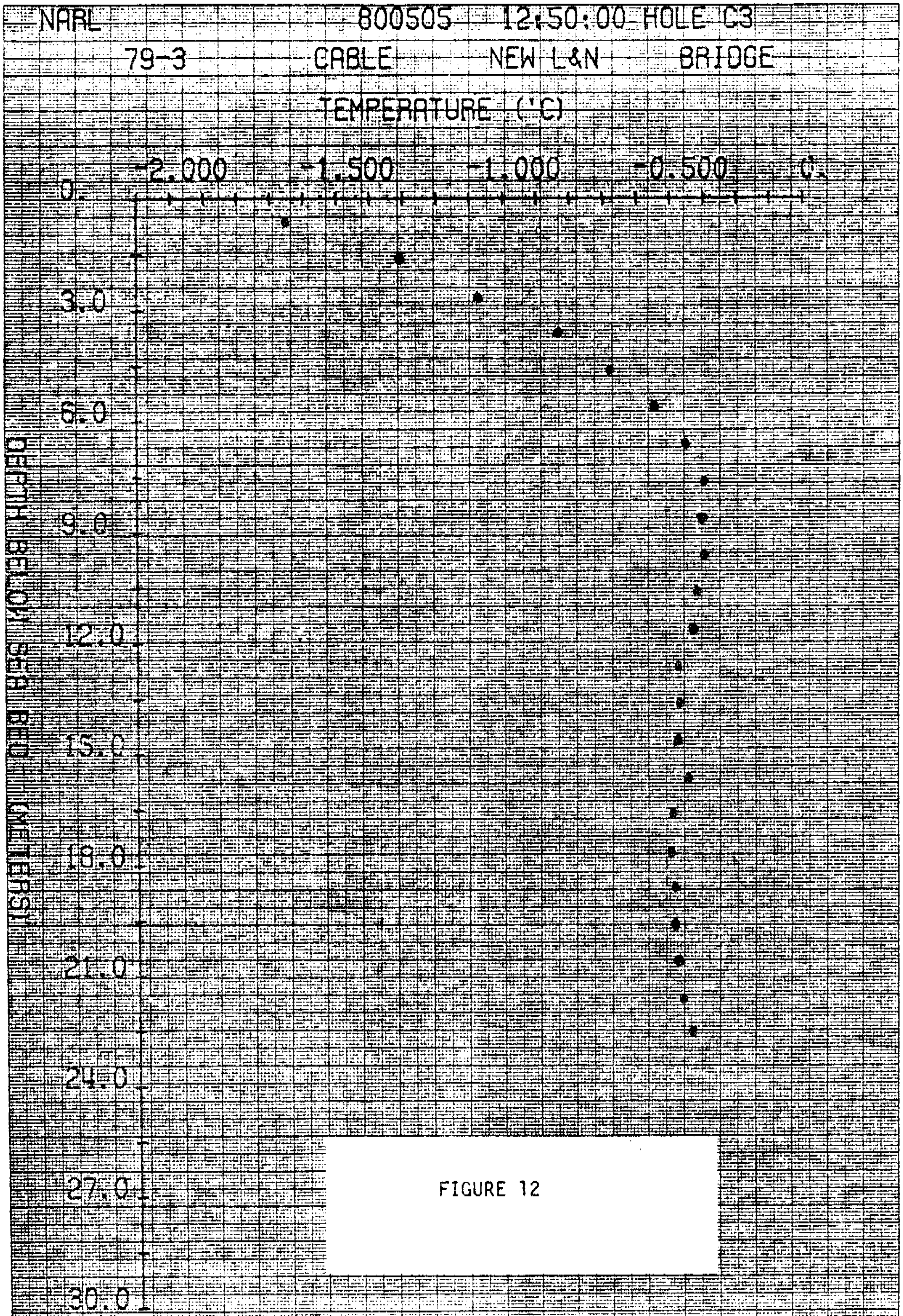
NARL
800505
12:50:00 HOLE C3
79-3
CABLE
NEW L&N
BRIDGE
TEMPERATURE ('C)
-2.000
-1.500
-1.000
-0.500
0.
0.
3.0
6.0
9.0
12.0
15.0
18.0
21.0
24.0
27.0
30.0
DEPTH BELOW SEA BED (METERS)

FIGURE 12

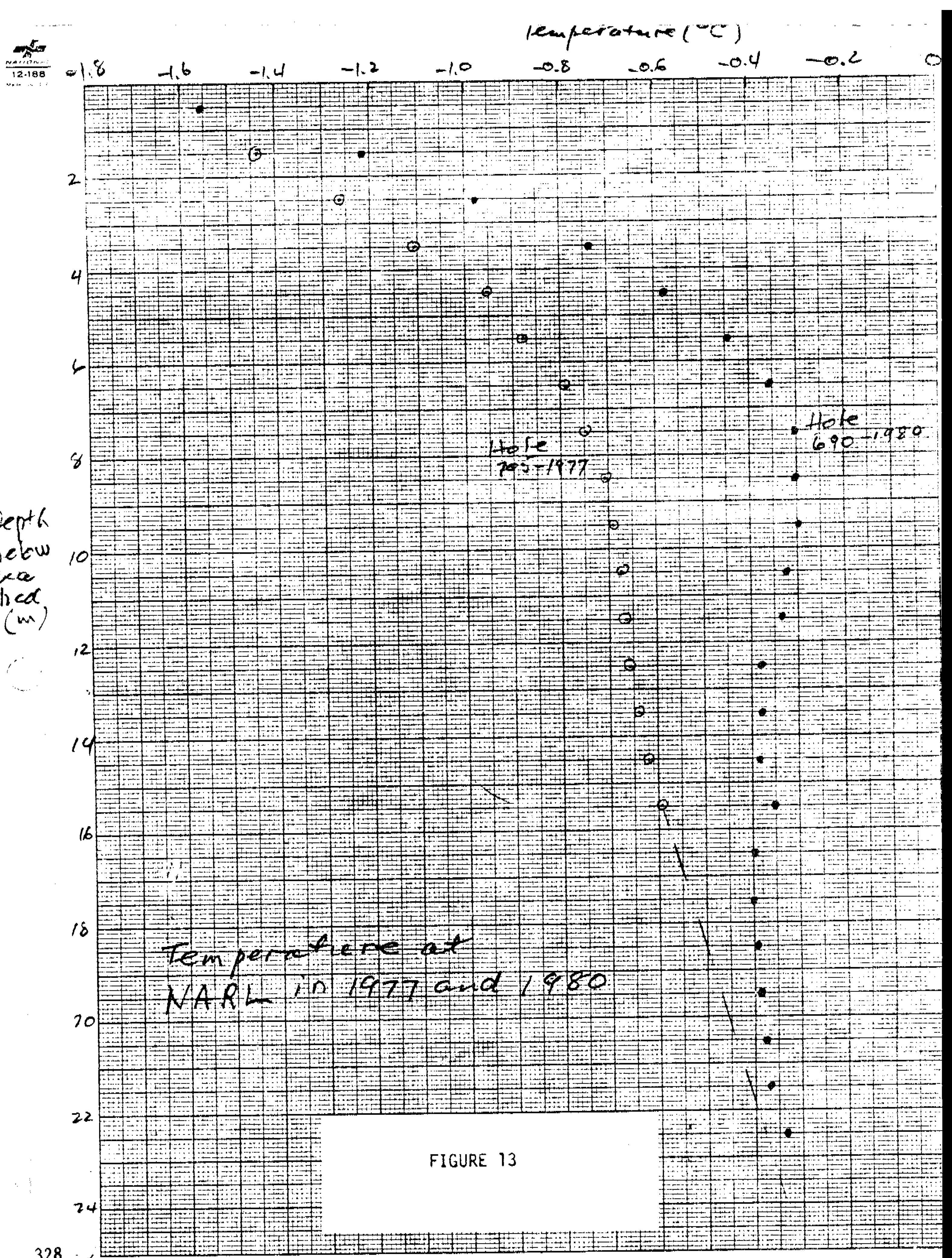
Temperature (°C)
-1.8
-1.6
-1.4
-1.2
-1.0
-0.8
-0.6
-0.4
-0.2
0
2
4
6
8
10
12
14
16
18
20
22
24
Depth below sea bed (m)
Hole 690-1980
Hole 705-1977
Temperature at NARL in 1977 and 1980

FIGURE 13

FIGURE 14

Lonely holes. USGS Teshekpuk (D-1), 1:63,360.

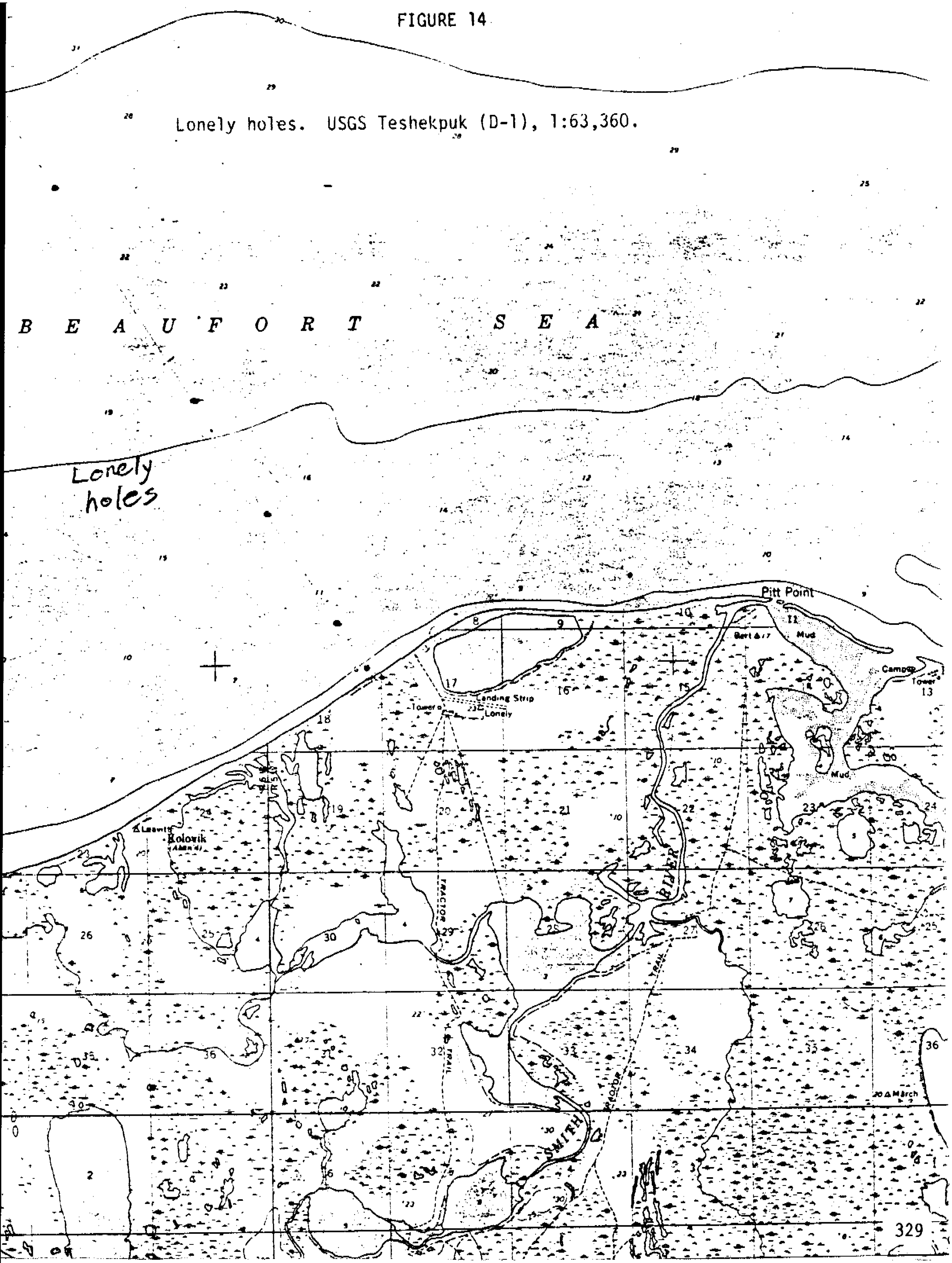

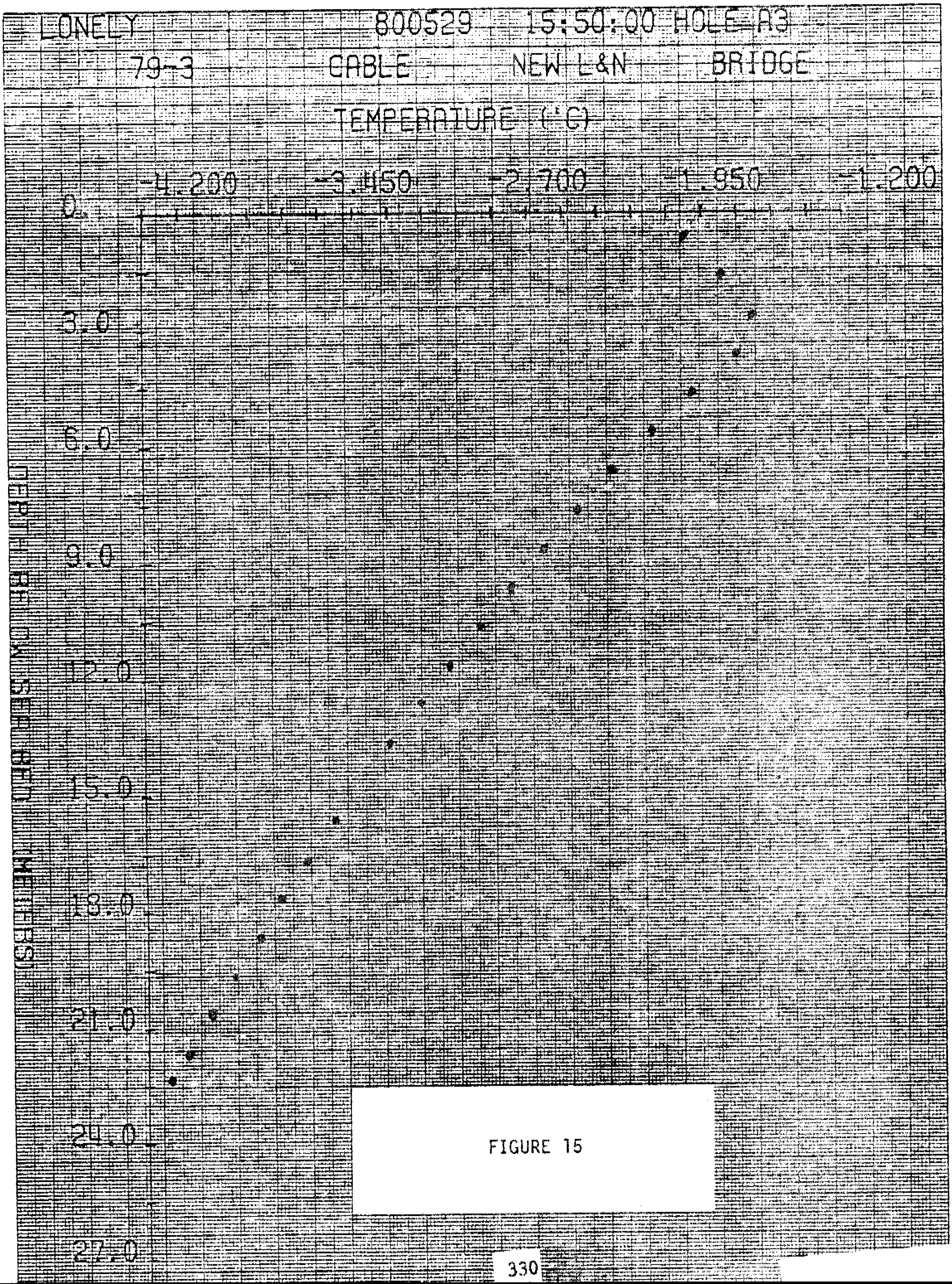

LONELY 800529 15:50:00 HOLE A3
79-3 CABLE NEW L&N BRIDGE
TEMPERATURE (°C)
-4.200 -3.450 -2.700 -1.950 -1.200
0.
3.0
6.0
9.0
12.0
15.0
18.0
21.0
24.0
27.0
DEPTH BELOW SEA BED (METERS)

FIGURE 15

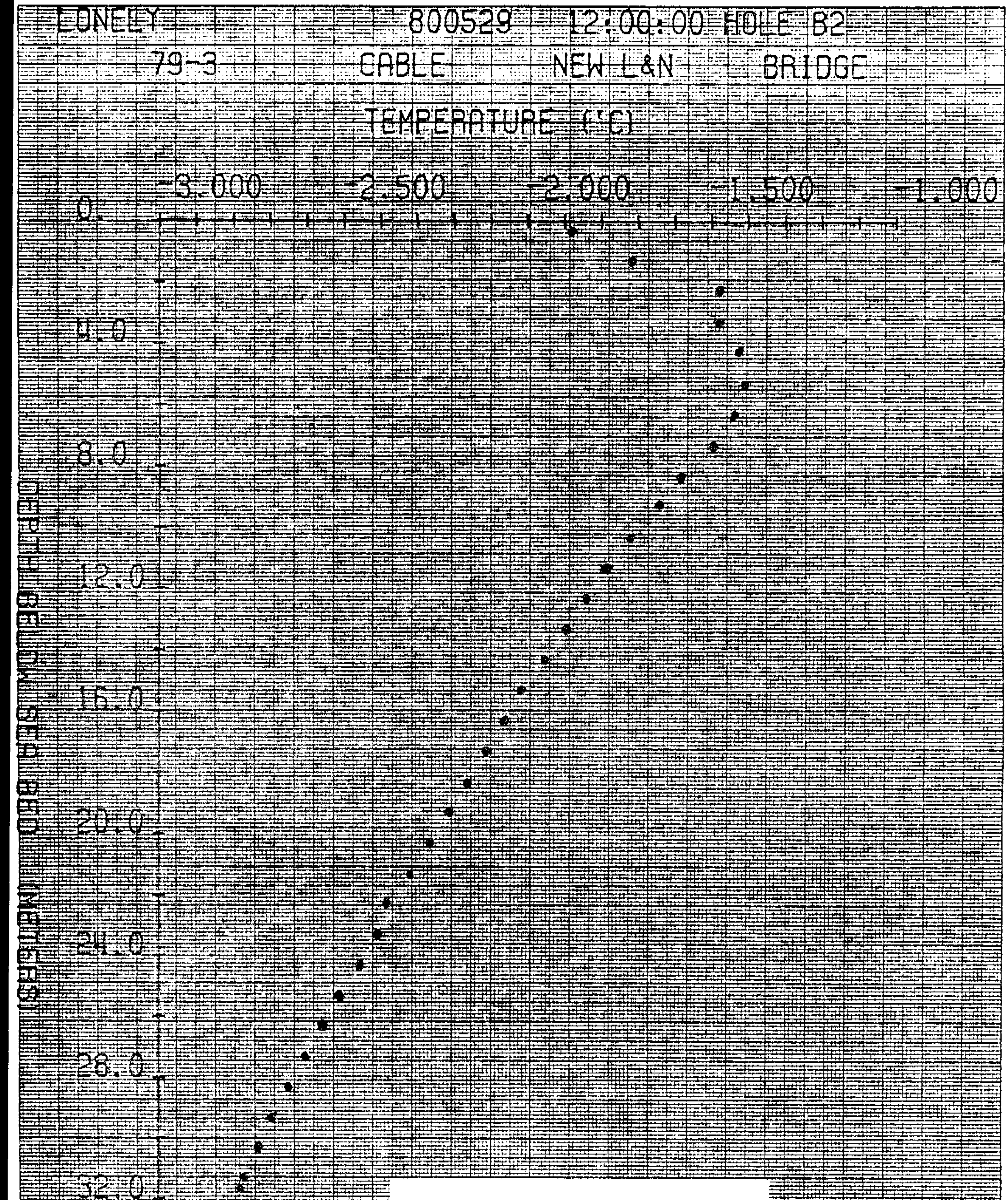
LONELY 800529 12:00:00 HOLE B2
79-3 CABLE NEW L&N BRIDGE
TEMPERATURE (°C)
-3.000 -2.500 -2.000 -1.500 -1.000
0.
4.0
8.0
12.0
16.0
20.0
24.0
28.0
32.0
36.0
DEPTH BELOW SEA BED (METERS)

FIGURE 16

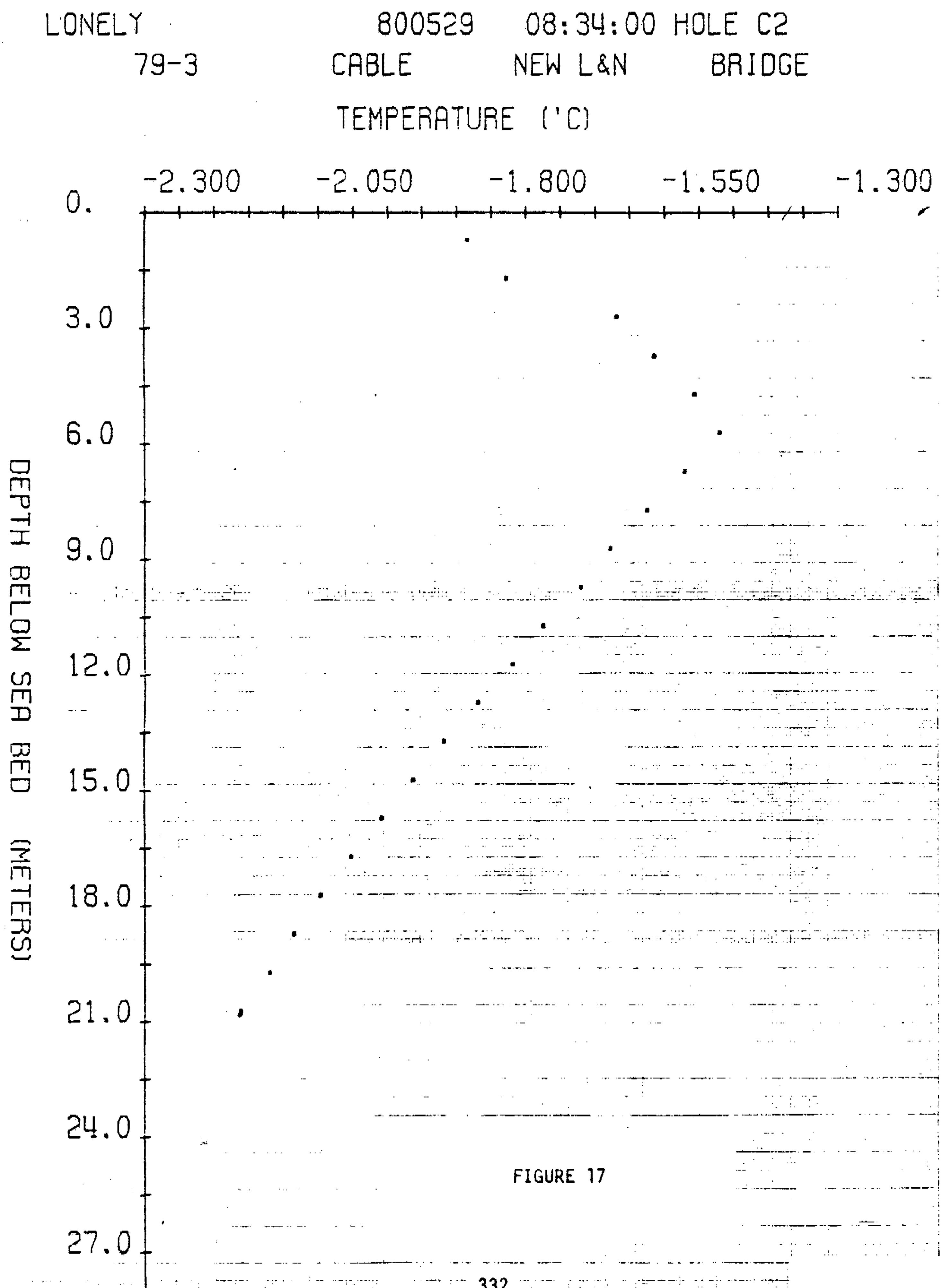
LONELY
800529 08:34:00 HOLE C2
79-3
CABLE
NEW L&N
BRIDGE
TEMPERATURE ('C)
-2.300
-2.050
-1.800
-1.550
-1.300
0.
3.0
6.0
9.0
12.0
15.0
18.0
21.0
24.0
27.0
DEPTH BELOW SEA BED (METERS)

FIGURE 17

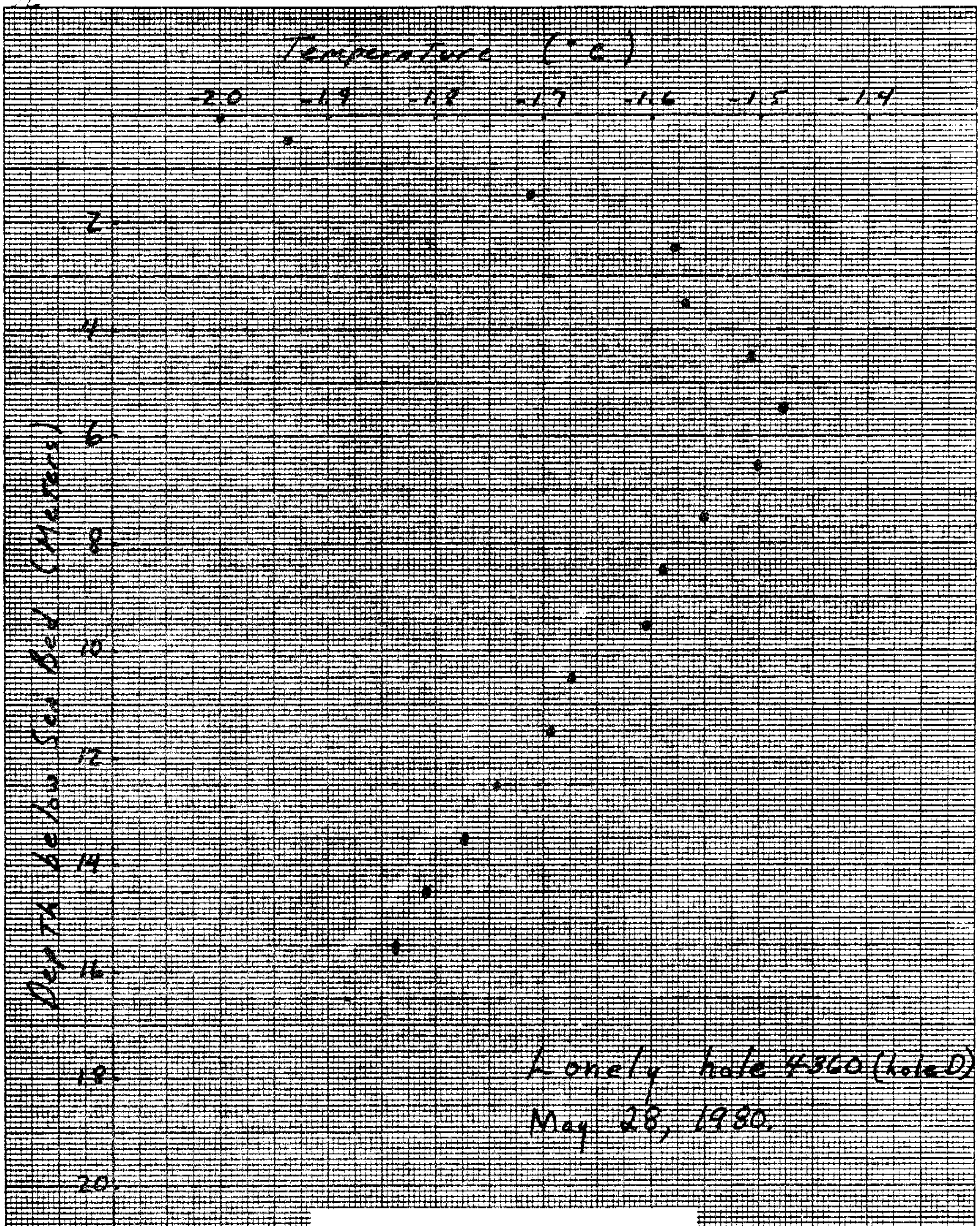
Temperature (°C)
-2.0
-1.9
-1.8
-1.7
-1.6
-1.5
-1.4
Depth below Sea Bed (Meters)
2
4
6
8
10
12
14
16
18
20
Lonely hole 4360 (hole D)
May 28, 1980.

FIGURE 18

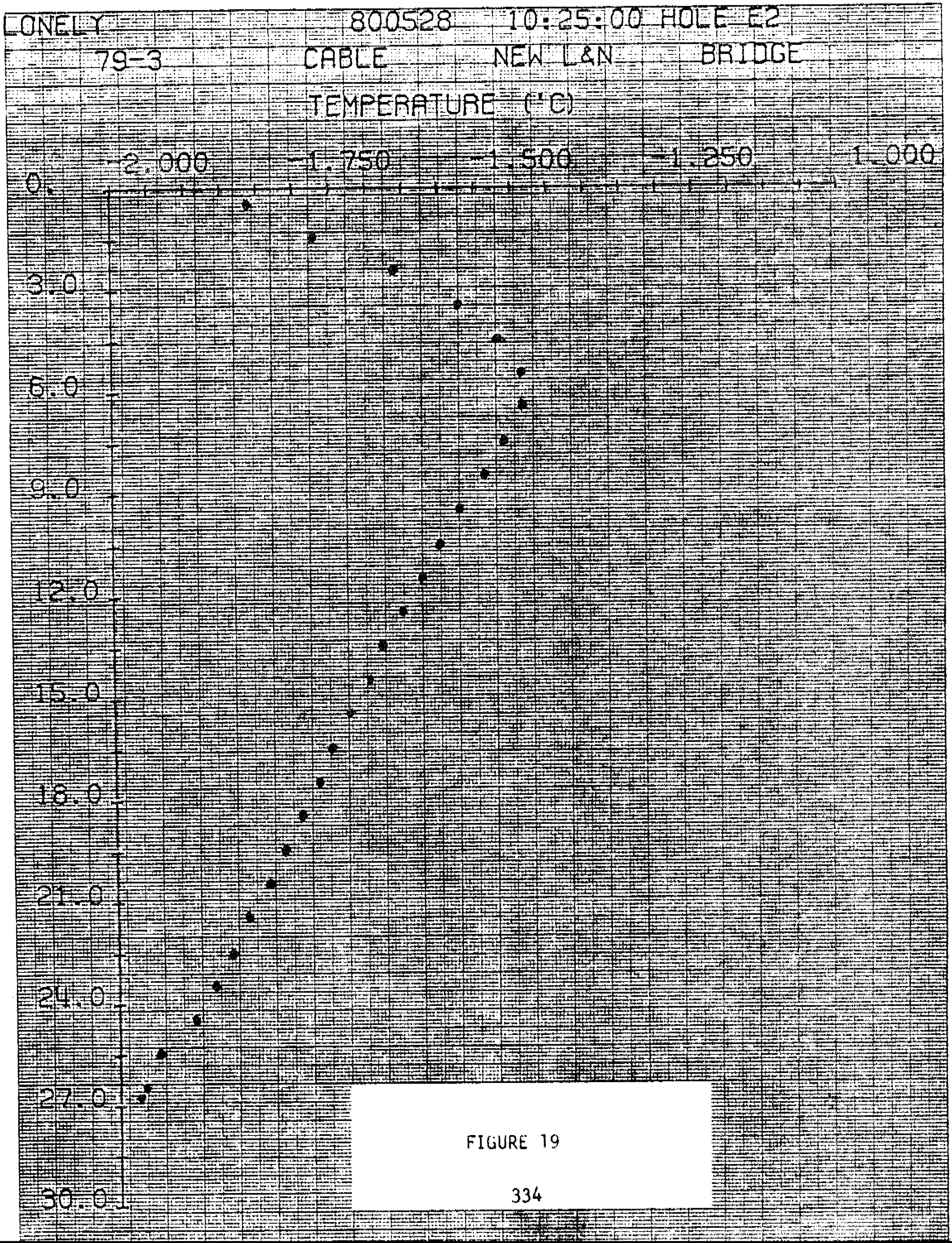

LONELY 800528 10:25:00 HOLE E2
79-3 CABLE NEW L&N BRIDGE
TEMPERATURE (°C)
-2.000
-1.750
-1.500
-1.250
-1.000
0.
3.0
6.0
9.0
12.0
15.0
18.0
21.0
24.0
27.0
30.0

FIGURE 19

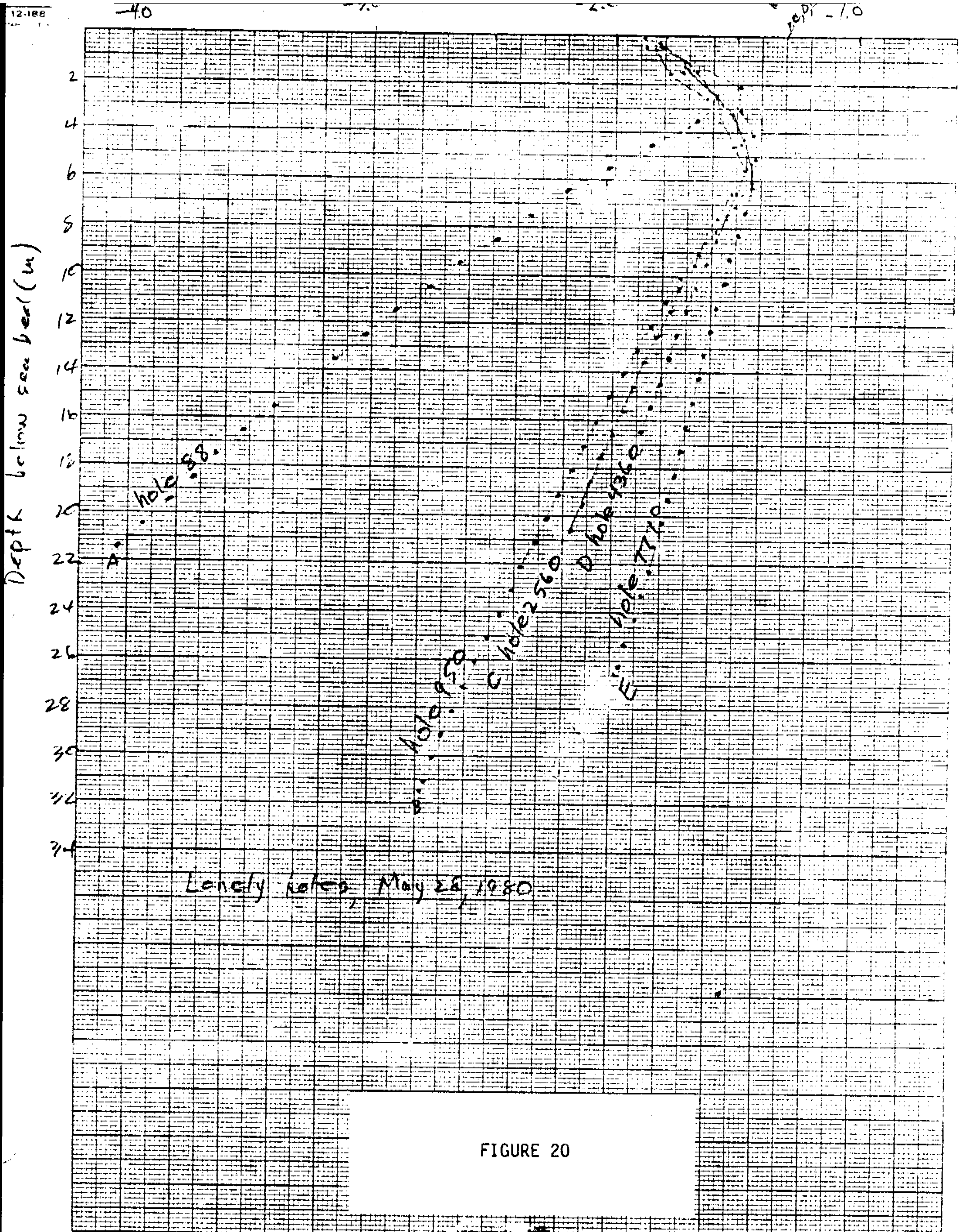

-4.0
-1.0
Depth below sea bed (m)
2
4
6
8
10
12
14
16
18
20
22
24
26
28
30
32
34
A
hole 88
B
hole 950
C hole 2560
D hole 4360
E hole 7720
Lonely Holes, May 28, 1980

FIGURE 20

FIGURE 21

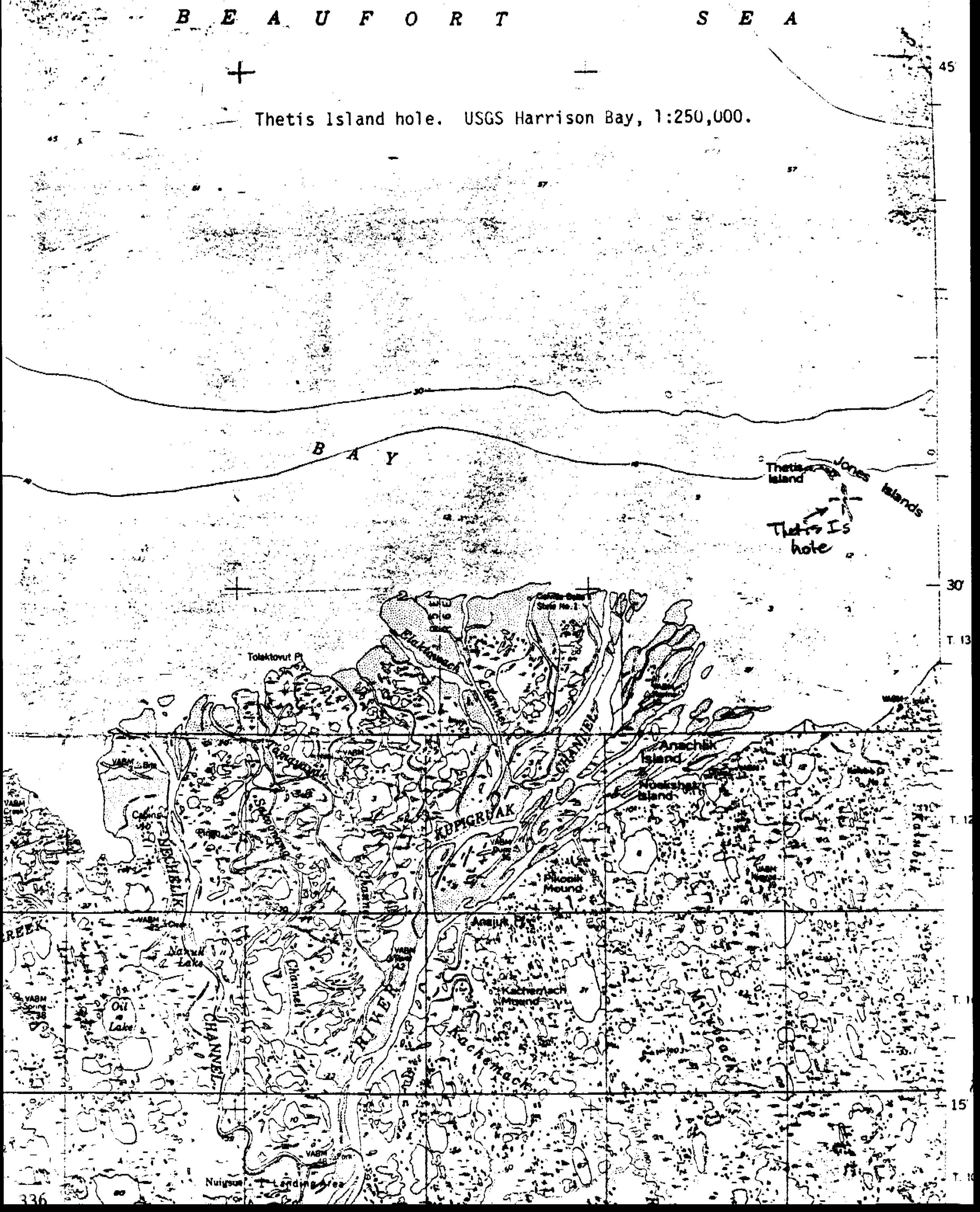

Thetis Island hole. USGS Harrison Bay, 1:250,000.

Cross Island holes. USGS Beechey Point, 1:250,000.

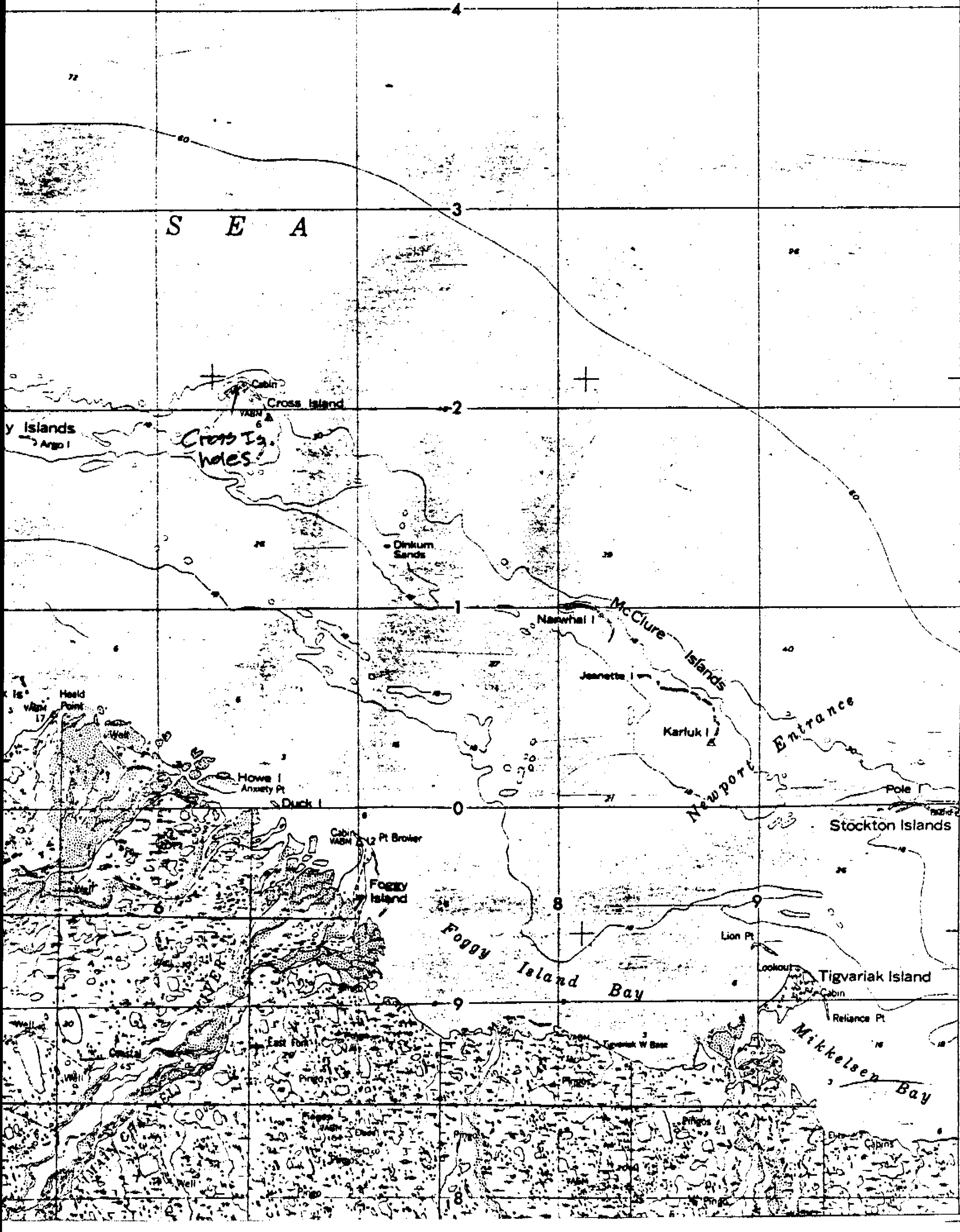

FIGURE 27

Flaxman Island hole. USGS Flaxman Island, 1:250,000.

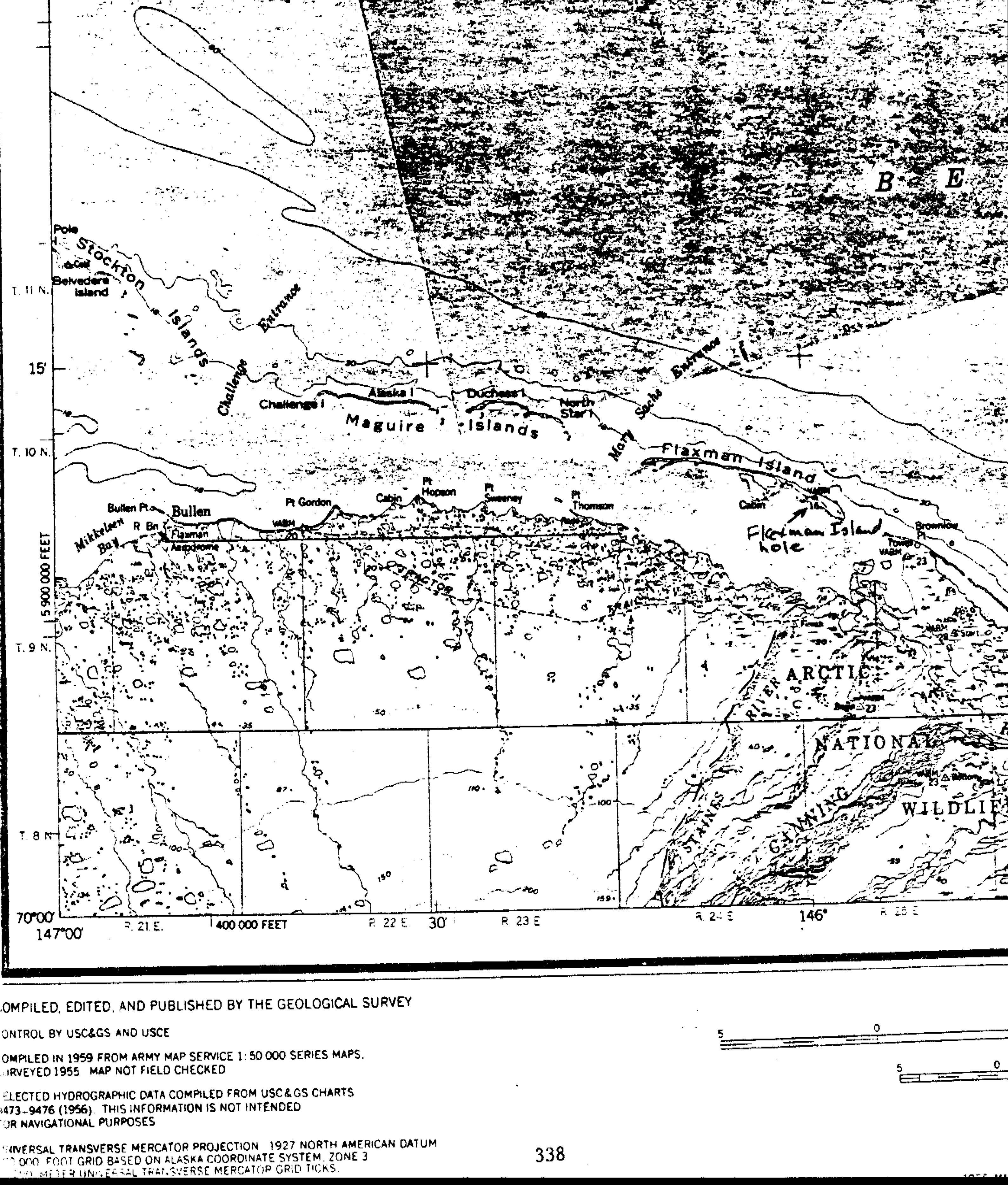

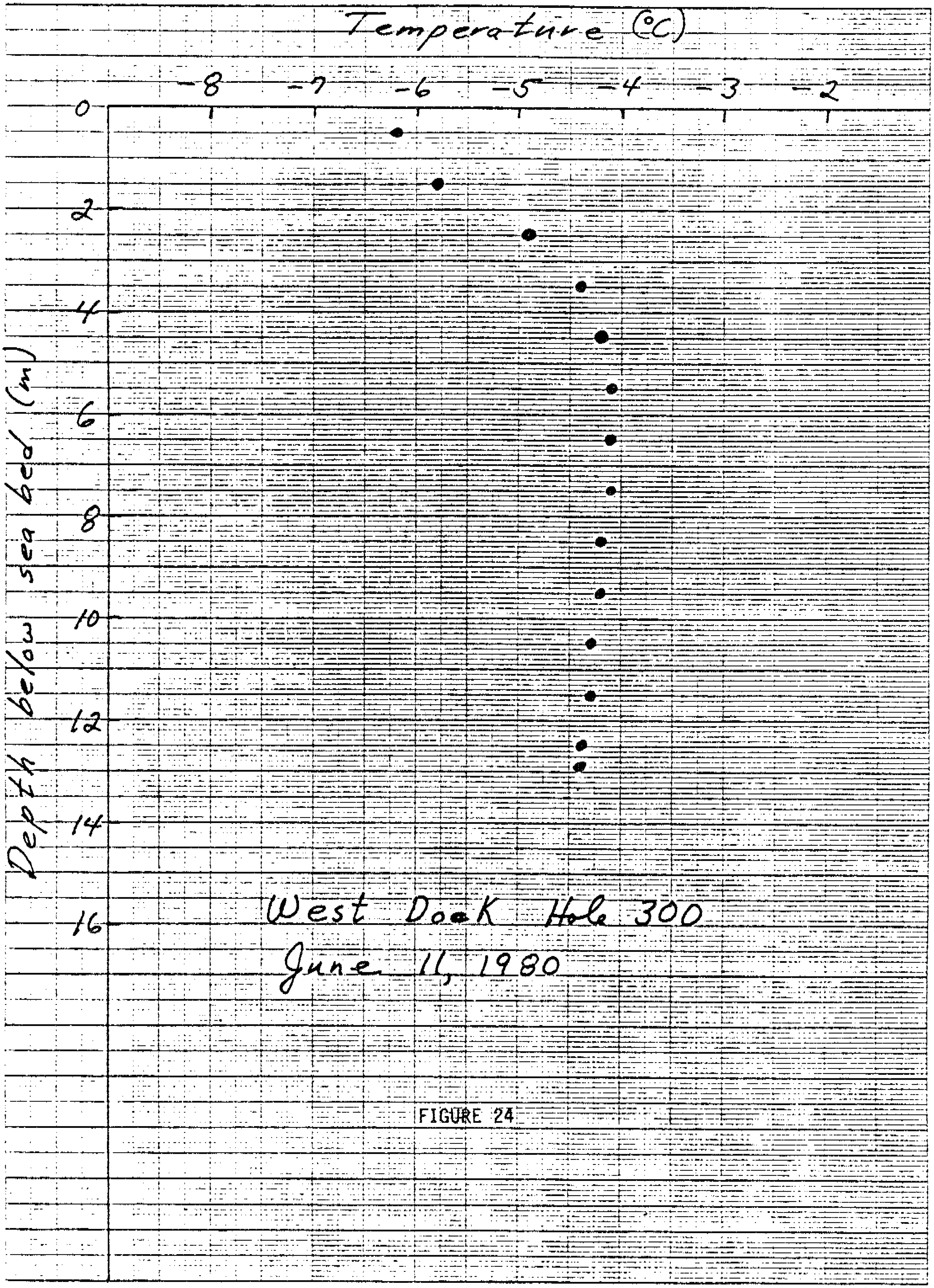

FIGURE 24

TO 80 04 29

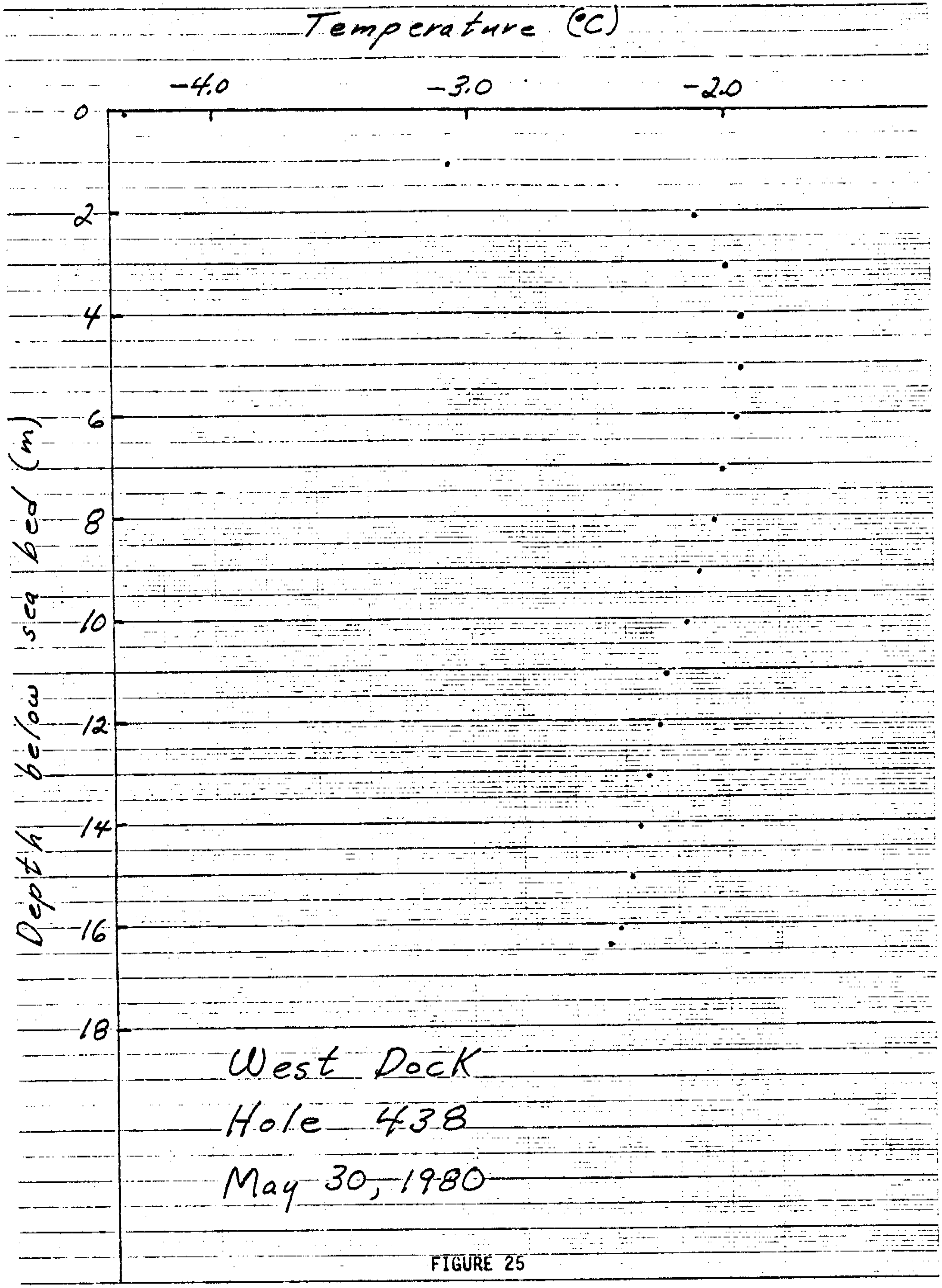

Temperature (°C)
-4.0
-3.0
-2.0
0
2
4
6
8
10
12
14
16
18
Depth below sea bed (m)
West Dock
Hole 438
May 30, 1980

FIGURE 25

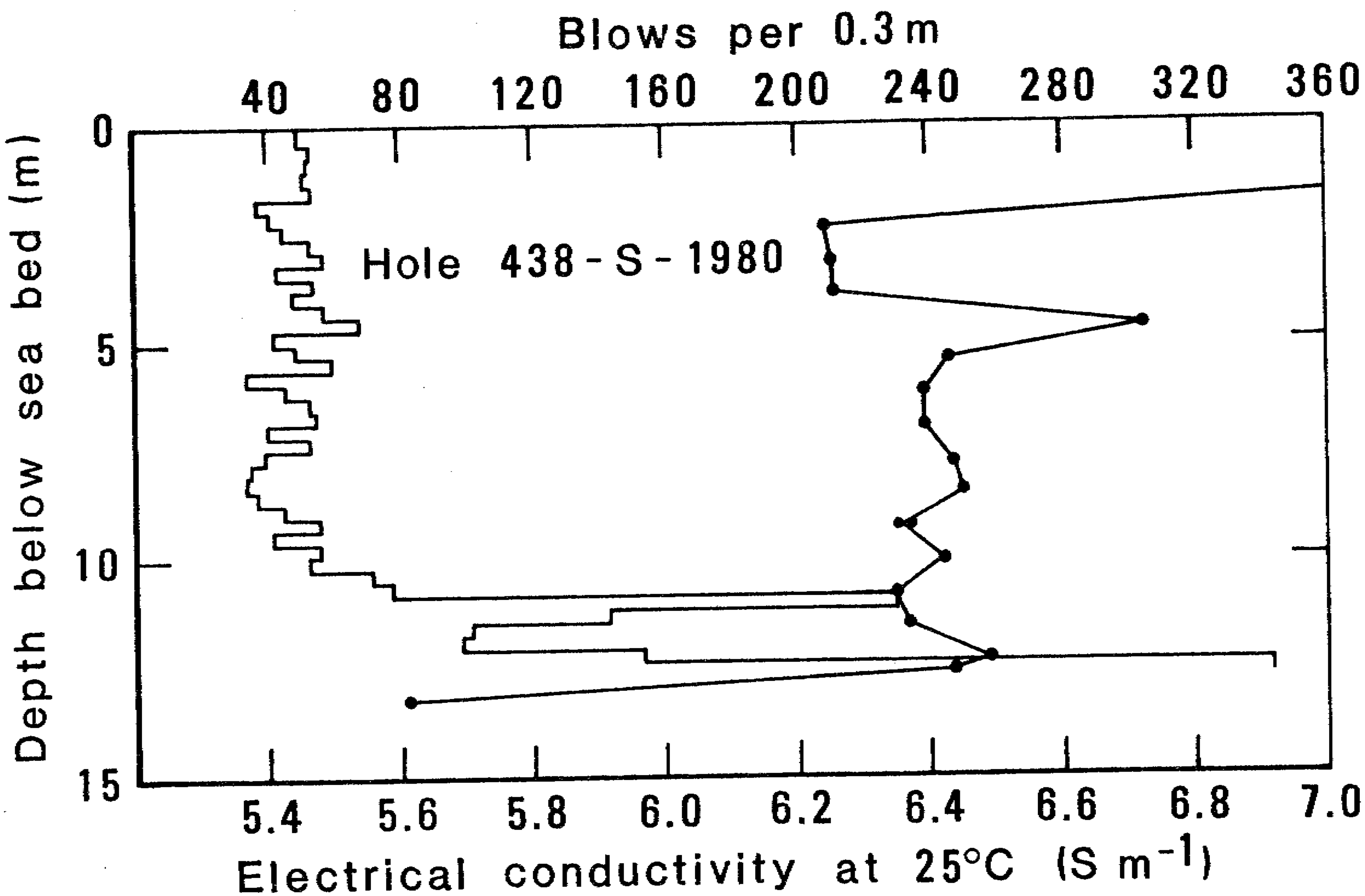
Blows per 0.3 m
40
80
120
160
200
240
280
320
360
Hole 438 - S - 1980
Depth below sea bed (m)
0
5
10
15
5.4
5.6
5.8
6.0
6.2
6.4
6.6
6.8
7.0
Electrical conductivity at 25°C (S m-1)

FIGURE 26

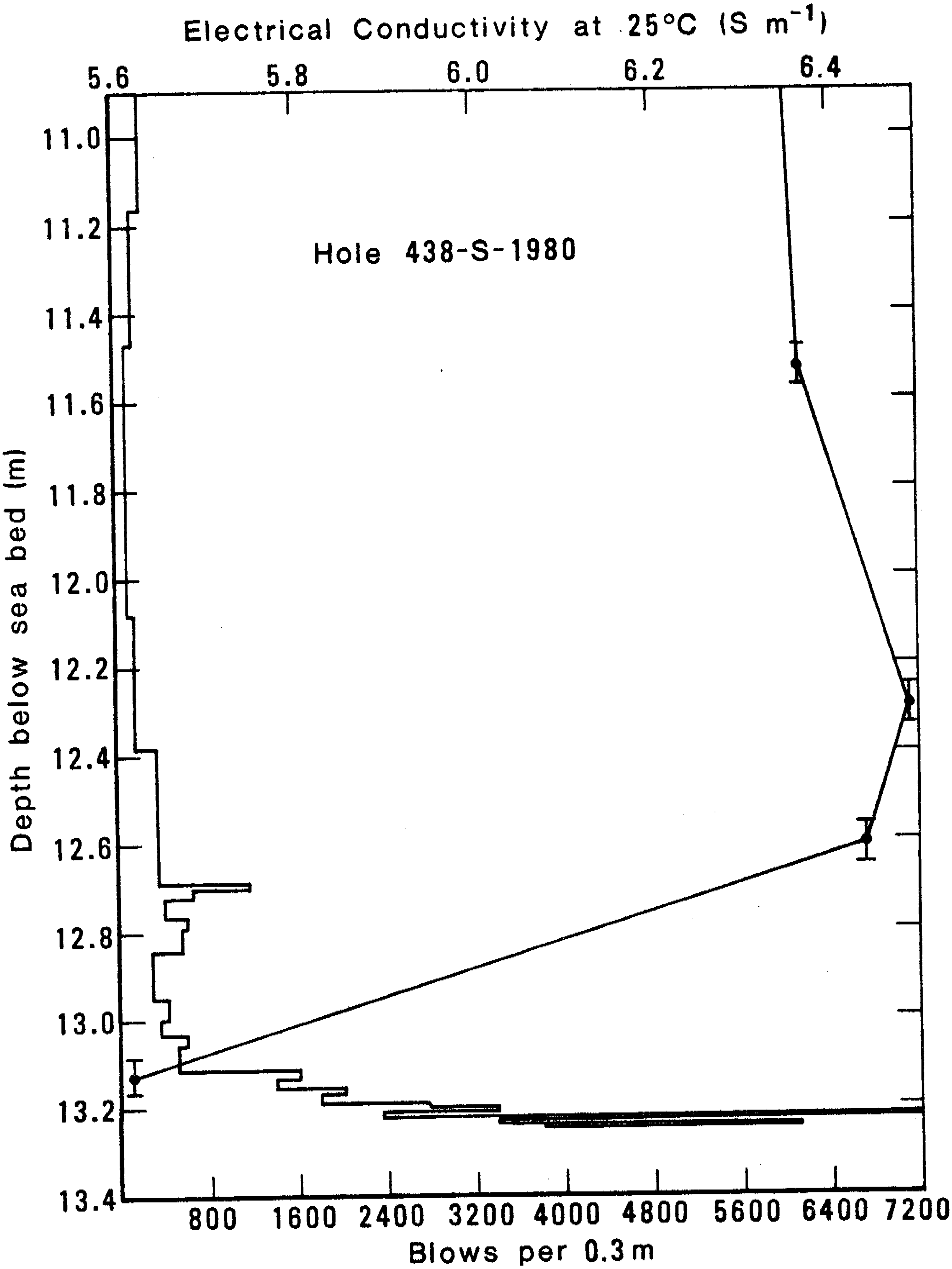
Electrical Conductivity at 25°C (S m⁻¹)
5.6
5.8
6.0
6.2
6.4
Hole 438-S-1980
Depth below sea bed (m)
11.0
11.2
11.4
11.6
11.8
12.0
12.2
12.4
12.6
12.8
13.0
13.2
13.4
800
1600
2400
3200
4000
4800
5600
6400
7200
Blows per 0.3 m

FIGURE 27

73

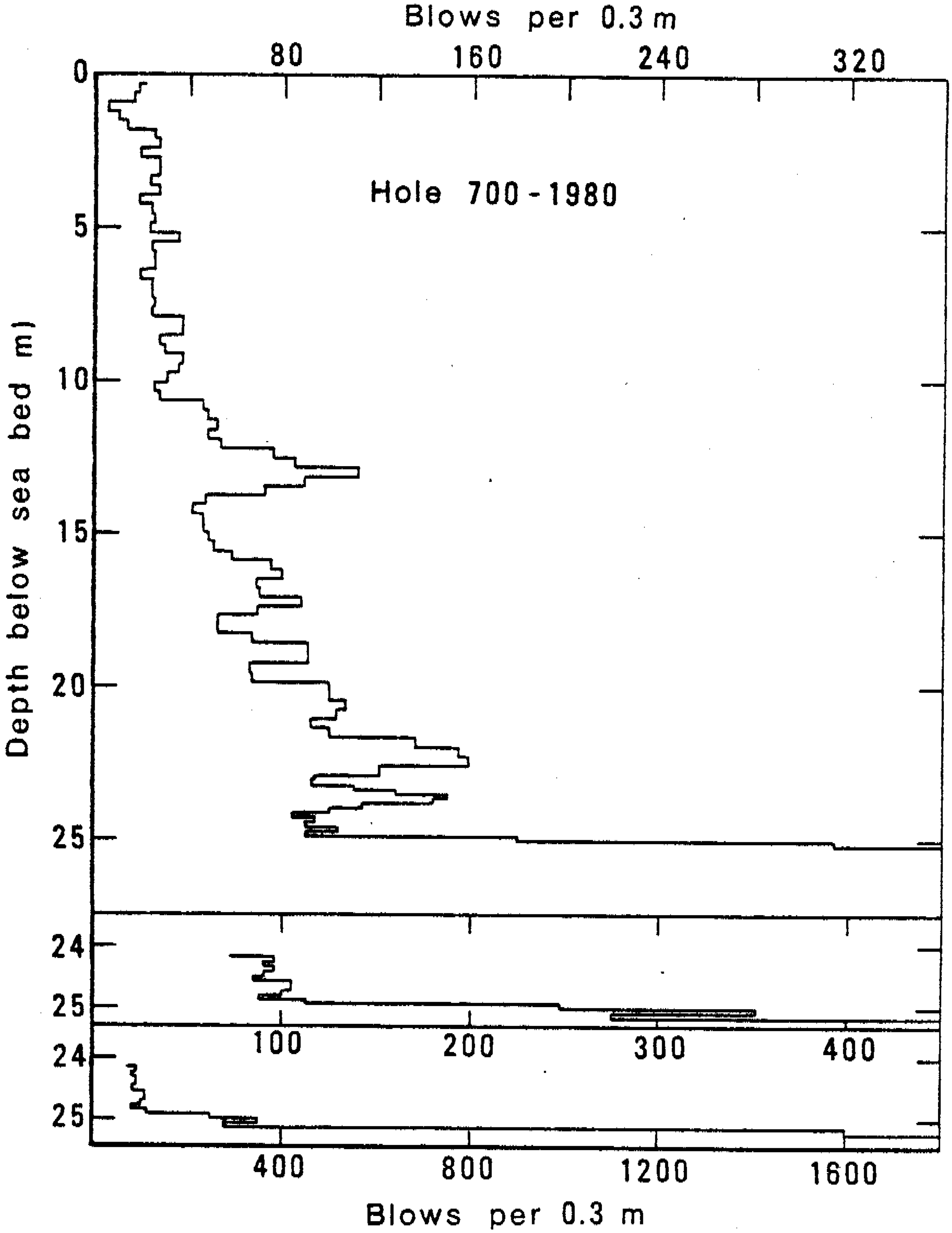

Blows per 0.3 m
80
160
240
320
Hole 700-1980
Depth below sea bed m)
0
5
10
15
20
25
24
25
100
200
300
400
24
25
400
800
1200
1600
Blows per 0.3 m

(73)

FIGURE 28

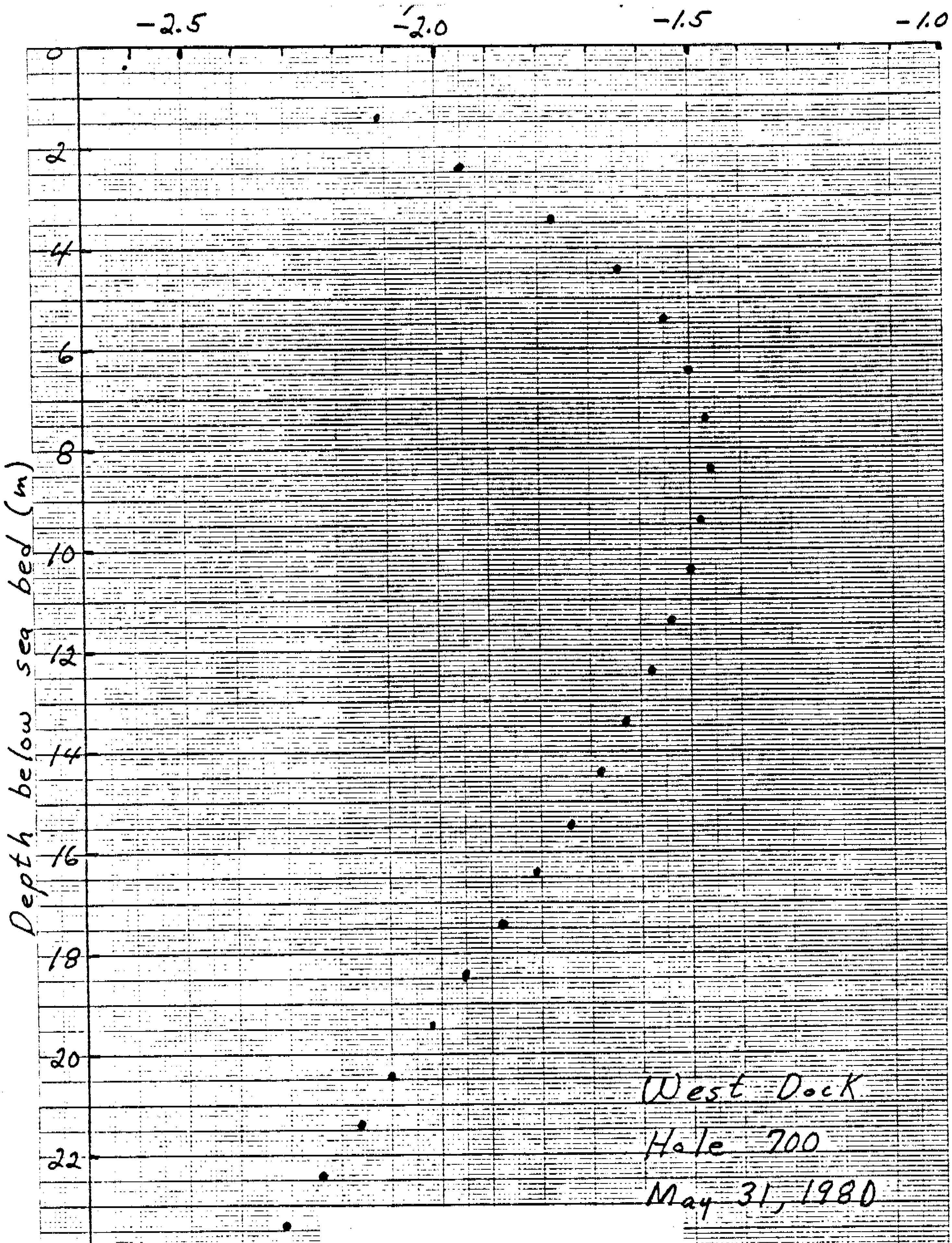

-2.5
-2.0
-1.5
-1.0
0
2
4
6
8
10
12
14
16
18
20
22
24
Depth below sea bed (m)
West Dock
Hole 700
May 31, 1980

FIGURE 29

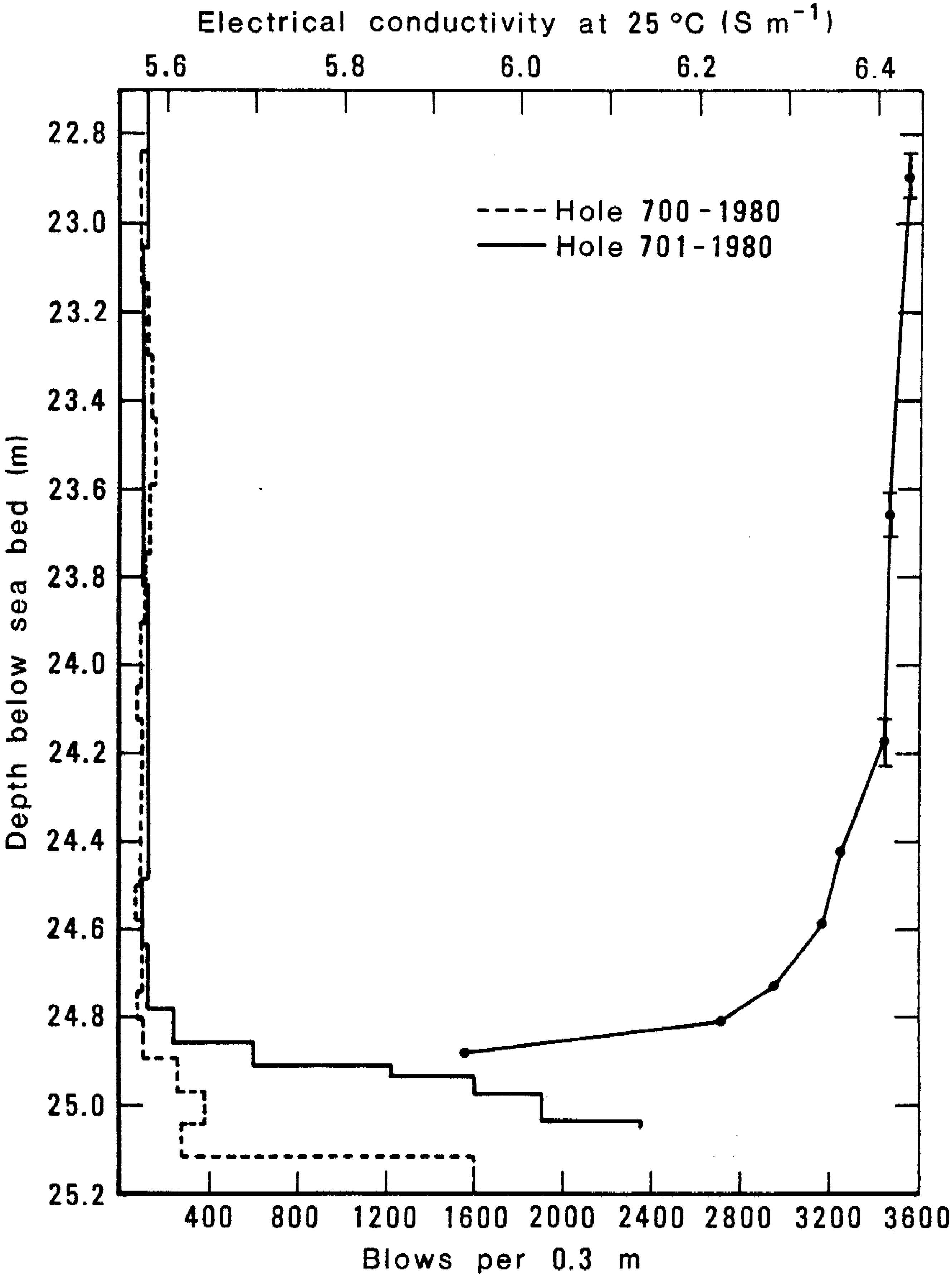

Electrical conductivity at 25 °C (S m^{-1})
5.6
5.8
6.0
6.2
6.4
Hole 700-1980
Hole 701-1980
22.8
23.0
23.2
23.4
23.6
23.8
24.0
24.2
24.4
24.6
24.8
25.0
25.2
Depth below sea bed (m)
400
800
1200
1600
2000
2400
2800
3200
3600
Blows per 0.3 m

FIGURE 30

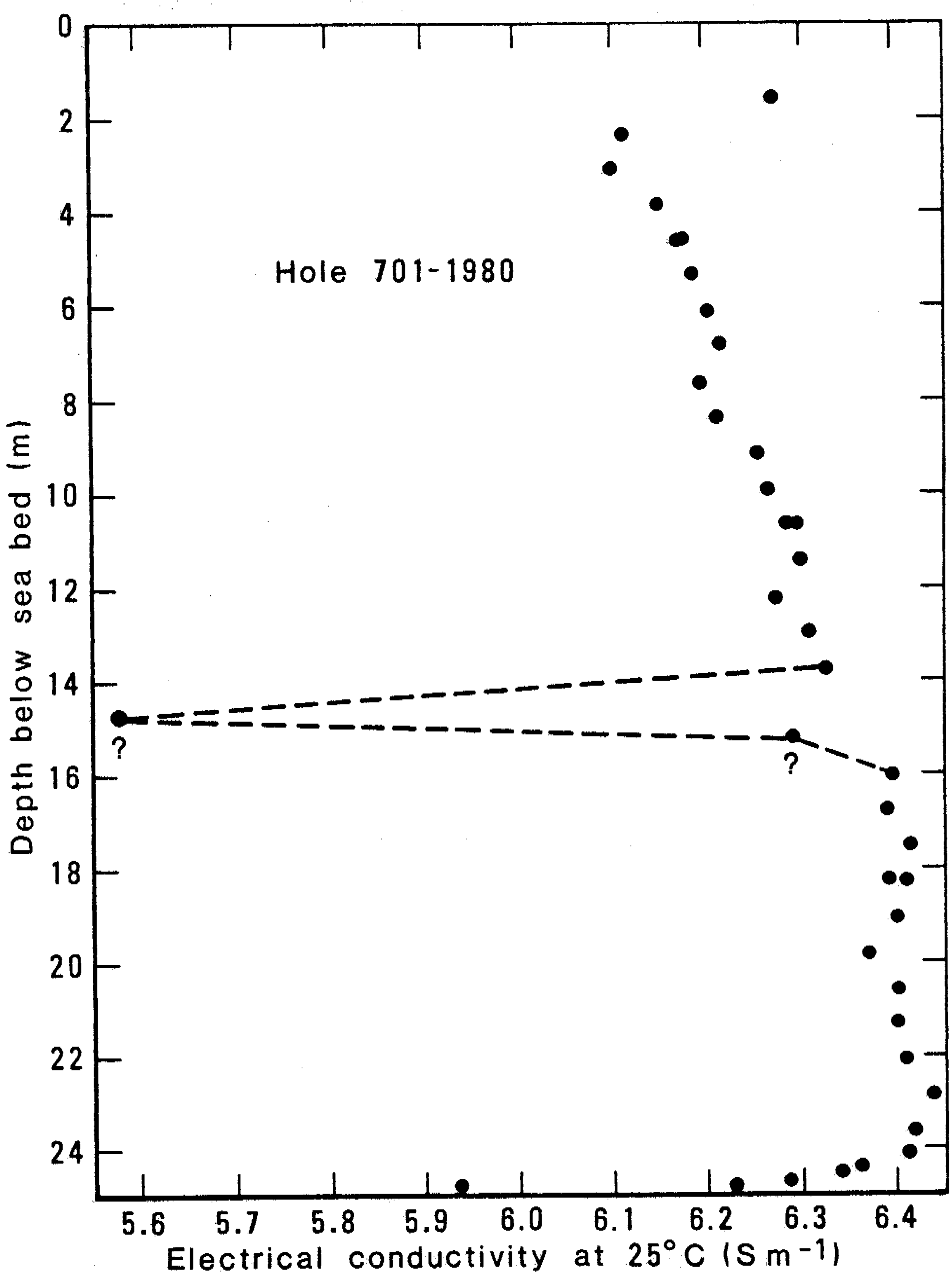
Hole 701-1980
Depth below sea bed (m)
0
2
4
6
8
10
12
14
16
18
20
22
24
?
?
5.6
5.7
5.8
5.9
6.0
6.1
6.2
6.3
6.4
Electrical conductivity at 25°C (S m⁻¹)

FIGURE 31

TABLE 1

DRILLING DATA FOR HOLES DRILLED DURING THE 1980 FIELD SEASON

Hole Designation	Location	Water Depth	Sea Ice Thickness	Drilling Method	Date of Drilling	Total Depth Below Sea Bed	Dates of Temperature Logging
Nome	N208°E from benchmark on Anvil Mt., 299 m from shore.	3.70 m	0.82 m	drive	3/25/80	6.50 m	March 26, 29, 1980
St. Michael River	About 8.7 km SW of mouth of St. Michael River	2.00	1.10	jet	3/28/80	25.3	March 30; April 3, 2; May 1
Charley Green Creek							
hole 630 (hole 1)	Near the mouth of Charley Green Creek, about 630 m from shore	2.44	1.16	jet	3/28/80	6.85(?)	March 30, 31
hole 630 (hole 2)	Same, but about 610 m from shore	1.69	1.16	jet	3/30/80	7.32(?)	March 31
Yukon Delta	63°27.2'N; 163°36.7'W 28 km from shore	10.30	1.05	jet	3/31/80	18.29	April 3, 12; May 1
NARL							
hole 27 (hole A)	On a line bearing N330°E from sea ice radar mass at NARL. 27 m from shore	4.12	1.80	rotary-jet	4/18/80	6.85	April 18, 22; May 5
hole 78 (hole B)	Same, but about 78 m from shore	5.0	1.75	rotary-jet	4/19/80	29.97	April 20, 22, 25; May 5
hole 690 (hole C)	Same, but 690 ± 100 m from shore	6.5	1.70	rotary-jet	4/21/80	18.3	April 20, 22, 25; May 5
Peard Bay	In line with runway near Tachinisok Inlet. About 500 m from shore.	6.5	rafted?	rotary-jet	4/23/80	2.0	--------
Wainwright (hole 265)	70°49.7'N; 159°31.2'W	4.75	rafted?	rotary-jet	4/24/80	17.26	May 6, 14
Lonely							
hole 88 (hole A)	Shore line reference point N294°E from DEW line radar dome. From this point hole line bears N328°E. About 88 m from shore.	1.98	1.45	rotary-jet	5/8/80	23.02	May 14, 22, 28, 29
hole 950 (hole B)	Same, but about 950 m from shore.	3.12	1.58	rotary-jet	5/9/80	31.24	May 23, 28, 29
hole 2560 (hole C)	Same, but about 2560 m from shore.	4.80	1.47	rotary-jet	5/10/80	20.65	May 22, 28
hole 4360 (hole D)	Same, but about 4360 m from shore.	6.50	2.1 (rafted?)	rotary-jet	5/11/80	16.53	May 22, 28
hole 7770 (hole E)	Same, but about 7770 m from shore.	7.70	1.39(?)	rotary-jet	5/13/80	26.50	May 22, 25

Table 1 (Continued)

Hole Designation	Location	Water Depth	Sea Ice Thickness	Drilling Method	Date of Drilling	Total Depth Below Sea Bed	Dates of Temperature Logging
Prudhoe Bay West Dock							
hole 300	On a line bearing N31°E from NPBS #1 Well. 300 m from shore.	1.37	1.37	auger	5/24/80	12.80	May 30, 31; June 11
hole 400	Same, but 400 m from shore	1.58	1.58	drive?	5/23/80	3.13	May 30, 31; June 11
hole 438	Same, but 438 m from shore	1.53	1.53	drive?	5/26/80	17.28(?)	May 30; June 11
hole 438 S	Same, but slightly displaced	1.53	1.53	drive?	5/28/80	?	(salinity)
hole 700	Same, but 700 m from shore	1.62	1.62	drive?	5/23/80	24.8	May 31; June 11
hole 701	Same, but 701 m from shore	1.62	1.62	drive?	5/22/80	24.8	(salinity)
Thetis Island	N301°E from Oliktok radar dome. Midway between cabin and SE end of island, 31 m from W shore	-	-	rotary-jet	7/29/80	28.8	July 29
Cross Island							
hole 1	N320°E and 276 m from USCG navigation tower	-	-	rotary-jet	7/23/80	4.5	---------
hole 2	N294°E from USCG tower, and 103 m from south shoreline	-	-	rotary-jet	7/23/80	13.6	July 23
Flaxman Island	N118°E from Flaxman Island exploratory well. N90°E from Leffingwell's cabin. 213 m due N of shoreline.	-	-	rotary-jet	7/28/80	9.9	July 28

XI. ACKNOWLEDGMENTS

We wish to acknowledge the cheerful and effective assistance of Robert Fisk, Sharon Frost, Foster Aviation of Nome, the NOAA helicopter crews and Geophysical Institute machine shop personnel. Logistical support was provided by OCSEAP. Part of the research was supported by NSF grant DPP 77-28451.

APPENDIX A

ABSTRACTS OF PAPERS AND REPORTS

MEASUREMENTS OF THE ELECTRICAL CONDUCTIVITY OF INTERSTITIAL WATER IN SUBSEA PERMAFROST

W. D. Harrison and T. E. Osterkamp

Geophysical Institute
University of Alaska
Fairbanks, Alaska 99701

April 1981

ABSTRACT

Interstitial water samples have been obtained from the thawed layer beneath the sea bed at Prudhoe Bay, Alaska, using a probe method. The electrical conductivities of the water samples, and therefore the salinities, are about 25^{o}/oo higher than those of normal sea water, which may be due to a density filtering process caused by convection of the interstitial water. The high salinity causes the phase boundary temperature at the bottom of the thawed layer, where ice bearing permafrost exists, to be lower than the freezing point of normal sea water. A rather uniform value of -2.4°C, corresponding to a salinity of about 43^{o}/oo, is found out to 3.5 km from shore. A downward salt flux exists at the bottom of the thawed layer, and the interstitial water electrical conductivity at one site shows evidence for a thin boundary layer there, in which the salt transport regime seems to change from convective to diffusive. Above this layer the salinity gradients are low, as would be expected in a well-developed convective regime. A characteristic interstitial water speed at a site 700 m from shore appears to be on the order of a few tenths of a meter per year.

TABLE 2

ELECTRICAL CONDUCTIVITIES OF 1980 INTERSTITIAL WATER SAMPLES FROM WEST DOCK HOLES 701 AND 438 S MEASURED IN THE LABORATORY AT 25°C

Sample Number	Depth Below Sea Bed (m)	Electrical Conductivity ($S\ m^{-1}$)
	HOLE 701	
701-1-80	1.558	6.271
701-2-80	2.320	6.112
701-3-80	3.082	6.100
701-4-80	3.844	6.155
701-5A-80	4.606	6.169
701-5B-80	4.606	6.176
701-6-80	5.368	6.186
701-7-80	6.130	6.202
701-8-80	6.892	6.213
701-9-80	7.654	6.195
701-10-80	8.416	6.211
701-11-80	9.178	6.253
701-12-80	9.940	6.267
701-13A-80	10.702	6.285
701-13B-80	10.702	6.295
701-14-80	11.464	6.249
701-15-80	12.226	6.275
701-16-80	12.988	6.309
701-17-80	13.750	6.327
701-18-80	14.741	5.586?
701-19-80	15.274	6.291
701-20-80	16.036	6.396
701-21-80	16.798	6.391
701-22-80	17.560	6.413
701-23A-80	18.322	6.389
701-23B-80	18.322	6.410
701-24-80	19.084	6.401
701-25-80	19.846	6.369
701-26-80	20.608	6.401
701-27-80	21.370	6.399
701-28-80	22.132	6.408
701-29-80	22.894	6.437
701-30-80	23.656	6.416
701-31A-80	24.164	6.412
701-31B-80	24.164	6.412
701-32A-80	24.432	6.359
701-32B-80	24.432	6.361
701-33-80	24.584	6.340
701-34-80	24.730	6.284
701-35-80	24.806	6.228
701-36-80	24.882	5.938
	HOLE 438 S	
440S-1-80	1.624	7.739
440S-2-80	2.386	6.241
440S-3-80	3.148	6.256
440S-4-80	3.910	6.257
440S-5A-80	4.672	6.723
440S-5B-80	4.672	6.725
440S-6-80	5.434	6.430
440S-7-80	6.196	6.394
440S-8-80	6.958	6.399
440S-9-80	7.720	6.437
440S-10-80	8.482	6.450
440S-11-80	9.244	6.355,6.373
440S-12-80	10.006	6.417,6.425
440S-13-80	10.768	6.350
440S-14-80	11.530	6.370,6.366
440S-15-80*	12.292	6.489
440S-16-80	12.609	6.440
440S-17-80	13.131	5.611

*Trouble clearing sample?

Samples 701-32 to 36 taken with 0.01 sampler length association; all others 2.1 m.

TEMPERATURE MEASUREMENTS IN SUBSEA PERMAFROST OFF THE COAST OF ALASKA

T. E. Osterkamp

and

W. D. Harrison

Geophysical Institute
University of Alaska
Fairbanks, Alaska 99701

April 1981

ABSTRACT

Temperature measurements have been made in shallow, small-diameter boreholes in the Beaufort, Chukchi and Bering Seas off the Alaskan coasts since 1975. Methods for making access holes with lightweight equipment are described. These included augering, water jet drilling, rotary water jet drilling and driving. Pipe or tubing was placed in the access holes and logged at discrete, closely-spaced depth intervals, usually 1 m, to obtain the temperature profiles.

Temperature profiles in the Norton Sound area of the Bering Sea show that permafrost is absent except possibly very nearshore in areas of rapid shoreline retreat. Sub-zero temperatures were found in all holes drilled in Kotzebue Sound, and in the Chukchi and Beaufort Seas. Holes drilled in the Chukchi Sea near Barrow suggest that the shoreline is stable or nearly so and that ice-bearing permafrost is probably thin or absent a kilometer or more offshore. In the Beaufort Sea (Elson Lagoon) near Barrow, the shoreline is retreating rapidly (i.e., a few meters per year) whereas temperature profiles near Prudhoe Bay suggest a retreat rate of a meter per year or less. The depth to ice-bonded permafrost, as determined by temperature measurements, increases with distance offshore when the soil conditions are constant. However, ice-bonded permafrost may be found near the sea bed in areas of very fine-grained compact soils even when these occur far offshore. The thermal data has been used to investigate the nature of heat and salt transport processes in subsea permafrost and to construct thermal models which infer its distribution and thickness in a general way.

DETAILS OF A PROBE METHOD FOR INTERSTITIAL SOIL WATER SAMPLING AND HYDRAULIC CONDUCTIVITY AND TEMPERATURE MEASUREMENT

by

W. D. Harrison

T. E. Osterkamp

M. Inoue

Geophysical Institute
University of Alaska
Fairbanks, Alaska 99701

January 1981

Geophysical Institute Report Number: UAG R-280

ABSTRACT

A technique for interstitial soil water sampling and hydraulic conductivity and temperature measurement that employs portable driving and sampling equipment is described. Some details of the equipment are given. A criterion is given for estimating when contamination by drilling fluid is likely to be a problem in a more standard soil and water sampling procedure, and therefore when a technique such as this may be particularly useful. A method for estimating shape factors for piezometers of odd geometry is given.

METHODS AND EQUIPMENT FOR TEMPERATURE MEASUREMENTS IN SUBSEA PERMAFROST

T. E. Osterkamp

and

W. D. Harrison

Geophysical Institute
University of Alaska
Fairbanks, Alaska 99701

April 1981

ABSTRACT

Temperature measurements have been made since 1975 in shallow, small-diameter boreholes in the subsea sediments of the Bering, Chukchi and Beaufort Seas off the coast of Alaska. Methods for making access holes with lightweight equipment are described. These include augering, water jet drilling, rotary water jet drilling, and driving. The holes were completed with iron or plastic water pipe or with plastic tubing and logged for temperature at discrete, closely spaced intervals. Methods for the calibration and use of the temperature-measuring equipment and for the reduction of temperature data are also described.

APPENDIX B

TABULATIONS OF TEMPERATURE DATA FOR THE 1980 FIELD SEASON

* BYE

NOME 1
HALF 1
800326
15:19:00

79-3 CABLE
OLD LAN BRIDGE

TIME	DEPTH (M)	R (OHMS)	T (C)
15.62	0.64	11611.0	-0.684
15.72	1.64	11222.0	0.093
15.82	2.64	10800.0	0.971
15.92	3.64	10468.0	1.690
16.02	4.64	10169.0	2.360
16.10	5.64	9955.5	2.852
16.18	6.64	9791.0	3.240
16.23	6.80	9770.2	3.289

LIST NOME2

NOME 2
HOLE 1
800329
11:09:00

79-3 CABLE
OLD L&N BRIDGE

TIME	DEPTH (M)	R (OHMS)	T (C)
11.82	0.14	11920.0	-1.280
11.88	0.64	11691.0	-0.840
11.95	1.14	11460.0	-0.386
12.02	1.64	11240.0	0.056
12.05	2.14	11020.0	0.508
12.12	2.64	10829.0	0.909
12.12	2.64	10829.0	0.909
12.15	3.14	10656.0	1.280
12.20	3.64	10504.0	1.611
12.25	4.14	10338.0	1.978
12.28	4.64	10205.0	2.278
12.33	5.14	10087.0	2.547
12.62	5.64	9979.9	2.795
12.47	6.14	9887.9	3.010
12.52	6.64	9805.0	3.206
12.55	6.80	9781.1	3.263

BYE

RIVER

ST.MICHAEL ~~CREEK~~

HOLE 1

800330

16:37

79-3 CABLE

OLD L&N BRIDGE

TIME	DEPTH (M)	R (OHMS)	T (C)
16.62	0.50	10992.0	0.567
16.78	1.50	10710.0	1.163
16.87	2.50	10275.0	2.120
16.92	3.50	10215.0	2.255
17.03	4.50	9831.0	3.145
17.08	5.50	9660.0	3.554
17.13	6.50	9611.0	3.672
17.20	7.50	9625.4	3.637
17.23	8.50	9653.2	3.570
17.28	9.50	9681.8	3.501
17.35	10.50	9704.5	3.446
17.42	11.50	9721.8	3.405
17.47	12.50	9761.2	3.311
17.52	13.50	9832.2	3.142
17.58	14.50	9761.0	3.311
17.62	15.50	9733.6	3.377
17.67	16.50	9724.2	3.399
17.72	17.50	9712.0	3.428
17.77	18.50	9703.5	3.449
17.82	19.50	9696.6	3.465
17.88	20.50	9689.8	3.482

ST.MICHAEL CREEK
HOLE 1
800403
17:14:00

79-3 CABLE
OLD L&N BRIDGE

TIME	DEPTH (M)	R (OHMS)	T (C)
18.35	0.50	11220.0	0.097
18.32	1.50	10670.0	1.249
18.27	2.50	10230.0	2.221
18.22	3.50	9510.0	2.958
18.13	4.50	9710.0	3.433
18.08	5.50	9600.0	3.699
18.03	6.50	9560.0	3.797
17.97	7.50	9570.0	3.772
17.90	8.50	9600.0	3.699
17.85	9.50	9630.0	3.626
17.80	10.50	9660.0	3.554
17.72	11.50	9680.0	3.505
17.70	12.50	9700.0	3.457
17.65	13.50	9710.0	3.433
17.60	14.50	9690.0	3.481
17.53	15.50	9690.0	3.481
17.48	16.50	9680.0	3.505
17.43	17.50	9670.0	3.529
17.37	18.50	9670.0	3.529
17.30	19.50	9580.0	3.748
17.25	20.50	9350.0	4.317

ST.MICHAEL CREEK
HOLE 1
800403
17:14:00

79-3 CABLE
OLD L&N BRIDGE

TIME	DEPTH (M)	R (OHMS)	T (C)
18.35	0.50	11220.0	0.097
18.32	1.50	10670.0	1.249
18.27	2.50	10230.0	2.221
18.22	3.50	9910.0	2.958
18.13	4.50	9710.0	3.433
18.08	5.50	9600.0	3.699
18.03	6.50	9560.0	3.797
17.97	7.50	9570.0	3.772
17.90	8.50	9600.0	3.699
17.85	9.50	9630.0	3.626
17.80	10.50	9660.0	3.554
17.72	11.50	9680.0	3.505
17.70	12.50	9700.0	3.457
17.65	13.50	9710.0	3.433
17.60	14.50	9690.0	3.481
17.53	15.50	9690.0	3.481
17.48	16.50	9680.0	3.505
17.43	17.50	9670.0	3.529
17.37	18.50	9670.0	3.529
17.30	19.50	9580.0	3.748
17.25	20.50	9350.0	4.317

* BYE
*cost: $ 2.62 to date: $ 2211.03= 80%
**on at 13.674 - off at 17.180 on 07/07/80

ST.MICHAEL CREEK
HOLE 1
800412
09:35:00

79-3 CABLE
NEW LAN BRIDGE

TIME	DEPTH (M)	R (OHMS)	T (C)
11.13	1.00	10694.0	1.203
11.05	2.00	10249.0	2.183
10.97	3.00	9930.7	2.915
10.88	4.00	9746.9	3.349
10.82	5.00	9635.9	3.616
10.73	6.00	9592.1	3.723
10.67	7.00	9594.7	3.716
10.60	8.00	9623.7	3.646
10.53	9.00	9643.6	3.598
10.47	10.00	9669.6	3.535
10.40	11.00	9690.8	3.484
10.32	12.00	9701.6	3.458
10.27	13.00	9706.1	3.447
10.20	14.00	9704.0	3.452
10.13	15.00	9700.5	3.461
10.07	16.00	9696.3	3.471
10.00	17.00	9690.4	3.485
9.92	18.00	9687.8	3.491
9.85	19.00	9683.8	3.501
9.75	20.00	9682.0	3.505

ST.MICHAEL CREEK
HOLE 1
800501
11:01:00

79-3 OLD LAN — CABLE BRIDGE

TIME	DEPTH (M)	R (OHMS)	T (C)
11.12	0.50	11551.0	-0.566
11.17	1.50	10963.0	0.627
11.22	2.50	10458.0	1.712
11.27	3.50	10098.0	2.522
11.33	4.50	9875.6	3.039
11.40	5.50	9724.4	3.399
11.45	6.50	9639.5	3.603
11.50	7.50	9611.8	3.670
11.57	8.50	9617.3	3.657
11.62	9.50	9639.1	3.604
11.67	10.50	9664.6	3.543
11.73	11.50	9684.6	3.494
11.78	12.50	9694.7	3.470
11.83	13.50	9700.6	3.456
11.88	14.50	9704.7	3.446
11.95	15.50	9703.5	3.449
12.00	16.50	9700.0	3.457
12.05	17.50	9697.4	3.463
12.10	18.50	9692.6	3.475
12.17	19.50	9686.5	3.490

BYE

CHARLEY
~~JAF~~ GREEN CREEK
HOLE 1 (hole 670)
800330
14:05:00

79-3 CABLE
OLD LAN BRIDGE

TIME	DEPTH (M)	R (OHMS)	T (C)
14.32	0.	11535.0	-0.534
14.80	0.50	10835.0	0.897
14.77	1.00	10500.0	1.619
14.75	1.50	10300.0	2.063
14.67	2.00	10107.0	2.501
14.58	2.50	9984.0	2.786
14.50	3.00	9918.8	2.938
14.42	3.50	9892.1	3.000
14.33	4.00	9809.9	3.195
14.25	4.50	9782.1	3.261
14.17	5.00	9749.0	3.340
14.10	5.50	9731.0	3.383

1

YUKON DELTA
HOLE 1
800501
12:46:00

79-3 CABLE
OLD L&N BRIDGE

TIME	DEPTH (M)	R (OHMS)	T (C)
13.12	0.50	11758.0	-0.969
13.50	1.50	11169.0	0.201
13.55	2.50	10705.0	1.174
13.62	3.50	10361.0	1.927
13.67	4.50	10010.0	2.725
13.72	5.50	9954.6	2.854
13.78	6.50	9898.3	2.986
13.83	7.50	9866.1	3.062
13.88	8.50	9868.9	3.055
13.93	9.50	9886.6	3.013
13.98	10.50	9907.2	2.965
14.03	11.50	9926.5	2.920
14.08	12.50	9939.2	2.890
14.13	13.50	9947.5	2.871
14.20	14.50	9948.2	2.869
14.25	15.50	9943.9	2.879
14.30	16.50	9935.6	2.898
14.42	17.60	9922.9	2.928

1

YUKON DELTA
HOLE 1
800412
12:23:00

79-3 NEW L&N   CABLE BRIDGE

TIME	DEPTH (M)	R (OHMS)	T (C)
13.82	0.50	11628.0	-0.711
13.77	1.50	11127.0	0.293
13.68	2.50	10775.0	1.030
13.62	3.50	10285.0	2.102
13.55	4.50	10203.0	2.287
13.50	5.50	9907.4	2.969
13.43	6.50	9879.7	3.034
13.37	7.50	9842.6	3.122
13.30	8.50	9867.1	3.064
13.22	9.50	9880.7	3.032
13.17	10.50	9908.6	2.967
13.07	11.50	9925.8	2.926
12.98	12.50	9933.3	2.909
12.93	13.50	9946.5	2.878
12.87	14.50	9942.3	2.888
12.82	15.50	9937.8	2.898
12.73	16.50	9931.7	2.912
12.67	17.60	9919.5	2.941

1

YUKON DELTA
HOLE 1
800403
14:10:00

79-3 SIMPSON — CABLE BRIDGE

TIME	DEPTH (M)	R (OHMS)	T (C)
16.03	0.50	11590.0	-0.642
15.97	1.50	11040.0	0.467
15.88	2.50	10720.0	1.142
15.83	3.50	10510.0	1.597
15.78	4.50	10210.0	2.267
15.72	5.50	9870.0	3.053
15.65	6.50	9660.0	3.554
15.63	7.50	9470.0	4.018
15.58	8.50	9680.0	3.505
15.52	9.50	9710.0	3.433
15.47	10.50	9820.0	3.171
15.42	11.50	9750.0	3.337
15.35	12.50	9750.0	3.337
15.32	13.50	9850.0	3.100
15.27	14.50	9860.0	3.076
15.22	15.50	9970.0	2.818
15.15	16.50	9970.0	2.818
15.08	17.60	9980.0	2.795

TO 800422 T-data NARL 7½ m out from Roller 2nd log
Book 17
p47

79-3 (Bronx) cable old L&N Bridge 800422 15:16

	Time	Depth	R	T	Std
3	15:18		12290	-1.971	
4	21		12179	-1.766	
bal → 5	24	0.38	12106	-1.630	
6	29	1.38	12025	-1.478	
7	32	2.38	11954	-1.344	
8	(?)	3.38	11915	-1.270	
9		4.38	11879	-1.202	
10		5.38	11864	-1.173	
~ 10.92		6.30	11855	-1.156	

NARL
HOLE 80
000000
00:00:00

79-3 OLD L&A

CABLE BRIDGE

TIME	DEPTH (M)	R (OHMS)	T (C)
0.	0.30	0.	-1.776
0.	1.30	0.	-1.579
0.	2.30	0.	-1.389
0.	3.30	0.	-1.217
0.	4.30	0.	-1.069
0.	5.30	0.	-0.936
0.	6.30	0.	-0.848
0.	7.30	0.	-0.770
0.	8.30	0.	-0.724
0.	9.30	0.	-0.710
0.	10.30	0.	-0.703
0.	11.30	0.	-0.732
0.	12.30	0.	-0.775
0.	13.30	0.	-0.826
0.	14.30	0.	-0.888
0.	15.30	0.	-0.938
0.	16.30	0.	-0.985
0.	17.30	0.	-1.022
0.	18.30	0.	-1.056
0.	19.3 0	0.	-1.090
0.	20.30	0.	-1.114
0.	21.30	0.	-1.146
0.	22.30	0.	-1.171
0.	23.30	0.	-1.194
0.	24.30	0.	-1.226
0.	25.30	0.	-1.266
0.	26.30	0.	-1.292
0.	27.30	0.	-1.317
0.	27.80	0.	-1.332

$$\nabla T = \frac{(1.317 - 1.02}{17.30 - 27.3} = -0.0295$$

NARL
HOLE 21
800420
11:20:00

79-3 CABLE
OLD LAN BRIDGE

TIME	DEPTH (M)	R (OHMS)	T (C)
11.47	0.30	12124.0	-1.664
11.55	1.30	11964.0	-1.363
11.62	2.30	11915.0	-1.270
11.68	3.30	11855.0	-1.156
11.73	4.30	11795.0	-1.041
11.80	5.30	11751.0	-0.956
11.85	6.30	11736.0	-0.927
11.90	7.30	11681.0	-0.820
11.95	8.30	11642.0	-0.744
12.00	9.30	11655.0	-0.770
12.05	10.30	11668.0	-0.795
12.10	11.30	11654.0	-0.768
12.13	12.30	11688.0	-0.834
12.18	13.30	11705.0	-0.867
12.23	14.30	11733.0	-0.921
12.28	15.30	11759.0	-0.971
12.33	16.30	11770.0	-0.993
12.38	17.30	11791.0	-1.033
12.42	18.30	11813.0	-1.075
12.45	19.30	11826.0	-1.100
12.48	20.30	11837.0	-1.121
12.52	21.30	11853.0	-1.152
12.55	22.30	11863.0	-1.171
12.58	23.30	11874.0	-1.192
12.62	24.30	11886.0	-1.215
12.67	25.30	11911.0	-1.263
12.70	26.30	11927.0	-1.293
12.73	27.30	11929.0	-1.297
12.77	27.76	11928.0	-1.295

NARL
HOLE 62
860422
09:23:00

79-3 CABLE
OLD L&N BRIDGE

TIME	DEPTH (M)	R (OHMS)	T (C)
9.43	0.30	12136.0	-1.686
9.53	1.30	12001.0	-1.433
9.60	2.30	11913.0	-1.266
9.65	3.30	11834.0	-1.116
9.70	4.30	11764.0	-0.981
9.77	5.30	11720.0	-0.896
9.82	6.30	11687.0	-0.832
9.87	7.30	11656.0	-0.772
9.92	8.30	11626.0	-0.713
9.97	9.30	11620.0	-0.701
10.02	10.30	11631.0	-0.723
10.07	11.30	11645.0	-0.750
10.12	12.30	11675.0	-0.809
10.17	13.30	11691.0	-0.840
10.22	14.30	11736.0	-0.927
10.27	15.30	11751.0	-0.956
10.32	16.30	11777.0	-1.006
10.38	17.30	11794.0	-1.039
10.43	18.30	11811.0	-1.071
10.48	19.30	11830.0	-1.108
10.55	20.30	11844.0	-1.135
10.60	21.30	11861.0	-1.167
10.65	22.30	11877.0	-1.198
10.70	23.30	11880.0	-1.203
10.75	24.30	11898.0	-1.238
10.80	25.30	11915.0	-1.270
10.87	26.30	11935.0	-1.308
10.93	27.30	11942.0	-1.321
10.98	27.76	11948.0	-1.333

[illegible]
HOLE 83
800425
[illegible]

79-3 CABLE
OLD LAN BRIDGE

TIME	DEPTH (M)	R (OHMS)	T (C)
17.05	0.30	12186.0	-1.779
17.10	1.30	12030.0	-1.488
17.17	2.30	11934.0	-1.306
17.20	3.30	11854.0	-1.154
17.23	4.30	11787.0	-1.025
17.27	5.30	11728.0	-0.911
17.32	6.30	11686.0	-0.830
17.37	7.30	11654.0	-0.768
17.40	8.30	11637.0	-0.734
17.45	9.30	11622.0	-0.705
17.50	10.30	11623.0	-0.707
17.57	11.30	11638.0	-0.736
17.62	12.30	11661.0	-0.781
17.65	13.30	11686.0	-0.830
17.70	14.30	11718.0	-0.892
17.80	15.30	11744.0	-0.942
19.28	16.30	11765.0	-0.983
19.33	17.30	11785.0	-1.021
19.38	18.30	11804.0	-1.058
19.45	19.30	11823.0	-1.094
19.53	20.30	11840.0	-1.127
19.60	21.30	11850.0	-1.146
19.65	22.30	11865.0	-1.175
19.70	23.30	11878.0	-1.200
19.75	24.30	11894.0	-1.230
19.80	25.30	11914.0	-1.268
19.83	26.30	11930.0	-1.299
19.88	27.30	11941.0	-1.319
19.93	27.76	11950.0	-1.337

1

NARL
HOLE B4
800505
15:32:00

79-3 CABLE
NEW LAN BRIDGE

TIME	DEPTH (M)	R (OHMS)	T (C)
15.65	0.30	12187.0	-1.775
15.68	1.30	12062.0	-1.542
15.73	2.30	11962.0	-1.354
15.78	3.30	11877.0	-1.192
15.83	4.30	11804.0	-1.052
15.87	5.30	11742.0	-0.933
15.92	6.30	11699.0	-0.849
15.95	7.30	11659.0	-0.772
15.98	8.30	11634.0	-0.723
16.03	9.30	11625.0	-0.705
16.07	10.30	11623.0	-0.701
16.12	11.30	11637.0	-0.729
16.15	12.30	11652.0	-0.758
16.18	13.30	11667.0	-0.787
16.23	14.30	11755.0	-0.958
16.28	15.30	11733.0	-0.915
16.33	16.30	11757.0	-0.962
16.37	17.30	11782.0	-1.010
16.42	18.30	11798.0	-1.041
16.45	19.30	11815.0	-1.073
16.48	20.30	11833.0	-1.108
16.53	21.30	11849.0	-1.139
16.57	22.30	11864.0	-1.167
16.60	23.30	11874.0	-1.186
16.65	24.30	11893.0	-1.223
16.70	25.30	11916.0	-1.266
16.73	26.30	11927.0	-1.287
16.75	27.30	11942.0	-1.316
16.78	27.76	11951.0	-1.333

NARL
HOLE C1
800422
12:58:00

79-3 CABLE
OLD L&N BRIDGE

TIME	DEPTH (M)	R (OHMS)	T (C)
13.17	0.50	12110.0	-1.637
13.23	1.50	11943.0	-1.323
13.30	2.50	11800.0	-1.050
13.35	3.50	11753.0	-0.960
13.42	4.50	11695.0	-0.847
13.50	5.50	11550.0	-0.564
13.57	6.50	11547.0	-0.558
13.65	7.50	11527.0	-0.518
13.73	8.50	11532.0	-0.528
13.82	9.50	11491.0	-0.447
13.90	10.50	11623.0	-0.707
13.98	11.50	11636.0	-0.732
14.08	12.50	11600.0	-0.662
14.17	13.50	11554.0	-0.572
14.23	14.50	11528.0	-0.520
14.32	15.50	11535.0	-0.534
14.42	16.50	11550.0	-0.564
14.50	17.50	11585.0	-0.633
14.58	18.50	11526.0	-0.516
14.67	19.50	11522.0	-0.509
14.75	20.50	11540.0	-0.544
14.83	21.50	11471.0	-0.408
14.92	22.40	11461.0	-0.388

NARL
HOLE C2
800425
14:10:00

79-3 OLD L&N

CABLE BRIDGE

TIME	DEPTH (M)	R (OHMS)	T (C)
14.52	0.50	12059.0	-1.542
14.58	1.50	11881.0	-1.205
14.63	2.50	11760.0	-0.973
14.70	3.50	11658.0	-0.775
14.75	4.50	11570.0	-0.603
14.80	5.50	11495.0	-0.455
14.85	6.50	11445.0	-0.356
14.90	7.50	11428.0	-0.322
14.95	8.50	11426.0	-0.318
15.02	9.50	11436.0	-0.338
15.17	10.50	11460.0	-0.386
15.22	11.50	11472.0	-0.410
15.25	12.50	11479.0	-0.423
15.33	13.50	11467.0	-0.400
15.40	14.50	11470.0	-0.406
15.47	15.50	11507.0	-0.479
15.58	16.50	11524.0	-0.513
15.63	17.50	11490.0	-0.445
15.67	18.50	11473.0	-0.412
15.77	19.50	11465.0	-0.396
15.80	20.50	11458.0	-0.382
15.83	21.50	11449.0	-0.364
15.93	22.40	11435.0	-0.336

NARL
HOLE C3
800505
12:50:00

79-3 CABLE
NEW L&N BRIDGE

TIME	DEPTH (M)	R (OHMS)	T (C)
13.00	0.50	12069.0	-1.555
13.05	1.50	11889.0	-1.215
13.08	2.50	11766.0	-0.979
13.13	3.50	11642.0	-0.739
13.17	4.50	11562.0	-0.582
13.20	5.50	11495.0	-0.450
13.25	6.50	11448.0	-0.356
13.30	7.50	11421.0	-0.302
13.33	8.50	11423.0	-0.306
13.38	9.50	11419.0	-0.298
13.43	10.50	11432.0	-0.324
13.47	11.50	11438.0	-0.336
13.52	12.50	11461.0	-0.382
13.68	13.50	11461.0	-0.382
13.73	14.50	11462.0	-0.384
13.80	15.50	11446.0	-0.352
13.88	16.50	11469.0	-0.398
14.13	17.50	11471.0	-0.402
14.18	18.50	11467.0	-0.394
14.22	19.50	11464.0	-0.388
14.25	20.50	11459.0	-0.378
14.30	21.50	11453.0	-0.366
14.47	22.40	11438.0	-0.336

WAINWRIGHT
HOLE A1
800506
11:15:00

79-3 CABLE
NEW LAN BRIDGE

TIME	DEPTH (M)	R (OHMS)	T (C)
12.28	0.70	12029.0	-1.480
12.23	1.70	11893.0	-1.223
12.17	2.70	11754.0	-0.956
12.12	3.70	11598.0	-0.652
12.07	4.70	11499.0	-0.457
11.93	6.70	11463.0	-0.386
11.88	7.70	11441.0	-0.342
11.83	8.70	11420.0	-0.300
11.78	9.70	11415.0	-0.290
11.72	10.70	11420.0	-0.300
11.67	11.70	11439.0	-0.338
11.62	12.70	11440.0	-0.340
11.55	13.70	11447.0	-0.354
11.50	14.70	11471.0	-0.402
11.45	15.70	11484.0	-0.428
11.40	16.70	11488.0	-0.436
11.33	16.95	11494.0	-0.448

WAINWRIGHT
HOLE A2
800524
10:20:00

79-3 NEW L&N

CABLE BRIDGE

TIME	DEPTH (M)	R (OHMS)	T (C)
10.73	0.70	12202.0	-1.803
10.93	1.70	12074.0	-1.564
11.08	2.70	11938.0	-1.308
11.17	3.70	11786.0	-1.018
11.33	4.70	11615.0	-0.686
11.42	5.70	11506.0	-0.471
11.58	6.70	11479.0	-0.418
11.72	7.70	11434.0	-0.328
11.77	8.70	11417.0	-0.294
12.03	9.70	11412.0	-0.284
12.13	10.70	11409.0	-0.278
12.22	11.70	11415.0	-0.290
12.35	12.70	11424.0	-0.308
12.45	13.70	11435.0	-0.330
12.50	14.70	11447.0	-0.354
12.58	15.70	11462.0	-0.384
12.67	16.70	11471.0	-0.402
12.75	16.95	11474.0	-0.408

LONELY
HOLE A1
800514
10:01:00

79-3 NEW L&N   CABLE BRIDGE

TIME	DEPTH (M)	R (OHMS)	T (C)
10.12	0.50	12262.0	-1.917
10.17	1.50	12140.0	-1.688
[illegible]	2.50	12105.0	-1.622
10.23	3.50	12128.0	-1.665
10.28	4.50	12216.0	-1.829
[illegible]	5.50	12306.0	-1.994
10.38	6.50	12388.0	-2.144
10.43	7.50	12459.0	-2.273
10.48	8.50	12542.0	-2.422
10.52	9.50	12615.0	-2.552
10.58	10.50	12688.0	-2.682
10.62	11.50	12741.0	-2.776
[illegible]	12.50	12824.0	-2.921
10.70	[illegible]	12957.0	-3.152
10.77	14.50	12974.0	-3.182
10.80	15.50	13046.0	-3.306
10.85	16.50	13120.0	-3.432
10.87	[illegible]	13191.0	-3.553
10.92	[illegible]	[illegible]	-3.649
10.93	[illegible]	[illegible]	-3.770
10.95	20.50	[illegible]	-3.895
10.98	21.50	[illegible]	-4.003
11.03	22.20	[illegible]	-4.095

COMMAND UNKNOWN

1

[illegible]
HOLE [illegible]
800[illegible]
09:40:00

79-3 CABLE
NEW L&N BRIDGE

TIME	DEPTH (M)	R (OHMS)	T ([illegible])
9.80	0.50	12232.0	-1.65[illegible]
9.85	1.50	12151.0	-1.708
9.93	2.50	12084.0	-1.583
10.00	3.50	12114.0	-1.63[illegible]
10.08	4.50	12223.0	-1.841
10.13	5.50	12319.0	-2.018
10.18	6.50	12408.0	-2.18[illegible]
10.23	7.50	12484.0	-2.318
10.32	8.50	12578.0	-2.486
10.38	9.50	12655.0	-2.623
10.50	10.50	12735.0	-2.765
10.58	11.50	12800.0	-2.879
10.67	12.50	12876.0	-3.012
10.73	13.50	12953.0	-3.145
10.83	14.50	13024.0	-3.268
10.92	15.50	13096.0	-3.391
10.98	16.50	13163.0	-3.505
11.07	17.50	13233.0	-3.624
11.15	18.50	13286.0	-3.713
11.23	19.50	13356.0	-3.830
11.32	20.50	13418.0	-3.933
11.38	21.50	13480.0	-4.036
11.47	22.20	13521.0	-4.103

1

LONELY
HOLE A3
800529
15:50:00

79-3 CABLE
NEW L&N BRIDGE

TIME	DEPTH (M)	R (OHMS)	T (C)
116.02	0.50	12244.0	-1.880
16.08	1.50	12162.0	-1.728
16.17	2.50	12089.0	-1.592
16.22	3.50	12127.0	-1.663
16.27	4.50	12228.0	-1.851
16.30	5.50	12324.0	-2.027
16.33	6.50	12419.0	-2.200
16.42	7.50	12500.0	-2.346
16.45	8.50	12580.0	-2.490
16.50	9.50	12662.0	-2.636
16.55	10.50	12739.0	-2.772
16.60	11.50	12809.0	-2.895
16.65	12.50	12884.0	-3.026
16.70	13.50	12959.0	-3.156
16.75	14.50	12033.0	-1.487
16.80	15.50	13102.0	-3.401
16.85	16.50	13172.0	-3.520
16.90	17.50	13238.0	-3.632
16.95	18.50	13295.0	-3.728
16.98	19.50	13359.0	-3.835
17.03	20.50	13419.0	-3.935
17.07	21.50	13480.0	-4.036
17.10	22.20	13522.0	-4.105

1

LONELY
HOLE A4
800529
18:50:00

79-3 CABLE
NEW L&N BRIDGE

TIME	DEPTH (M)	R (OHMS)	T (C)
18.90	0.50	11120.0	0.307
18.93	1.50	10958.0	0.643
18.97	2.50	11249.0	0.044
19.00	3.50	10629.0	1.343
19.03	4.50	11194.0	0.156
19.07	5.50	11533.0	-0.525
19.10	6.50	12037.0	-1.495
19.13	7.50	12081.0	-1.577
19.17	8.50	11798.0	-1.041
19.20	9.50	12212.0	-1.821
19.23	10.50	12204.0	-1.806
19.27	11.50	12304.0	-1.990
19.30	12.50	12434.0	-2.227
19.33	13.50	12481.0	-2.312
19.37	14.50	12514.0	-2.372
19.40	15.50	12555.0	-2.445
19.43	16.50	12585.0	-2.499
19.47	17.50	12586.0	-2.501
19.50	18.50	12724.0	-2.746
19.53	19.50	12693.0	-2.691
19.57	20.50	12818.0	-2.911
19.60	21.50	12945.0	-3.132
19.67	22.20	13189.0	-3.549

<50>FILE LONB1 -- NON-EXISTENT

1

LONELY
HOLE B
800523
07:45:00

79-3 CABLE
NEW L&N BRIDGE

TIME	DEPTH (M)	R (OHMS)	T (C)
7.78	0.10	12243.0	-1.878
7.83	1.10	12144.0	-1.695
7.88	2.10	12069.0	-1.555
7.93	3.10	12015.0	-1.454
7.98	4.10	11985.0	-1.397
8.03	5.10	11979.0	-1.386
8.08	6.10	11991.0	-1.408
8.13	7.10	12025.0	-1.472
8.18	8.10	12069.0	-1.555
8.25	9.10	12106.0	-1.624
8.30	10.10	12144.0	-1.695
8.35	11.10	12177.0	-1.756
8.42	12.10	12211.0	-1.819
8.47	13.10	12242.0	-1.876
8.52	14.10	12277.0	-1.941
8.57	15.10	12310.0	-2.001
8.62	16.10	12337.0	-2.051
8.67	17.10	12363.0	-2.098
8.72	18.10	12387.0	-2.142
8.78	19.10	12413.0	-2.189
8.83	20.10	12443.0	-2.244
8.88	21.10	12475.0	-2.301
8.97	22.10	12509.0	-2.363
9.03	23.10	12525.0	-2.391
9.08	24.10	12556.0	-2.447
9.13	25.10	12583.0	-2.495
9.18	26.10	12610.0	-2.543
9.25	27.10	12636.0	-2.590
9.30	28.10	12662.0	-2.636
9.35	29.10	12689.0	-2.684
9.40	30.10	12712.0	-2.724
9.45	31.10	12733.0	-2.761
9.5 0	31.50	12738.0	-2.770

1 LONELY HOLE B2

800529
12:00:00

79-3 NEW L&N

CABLE BRIDGE

TIME	DEPTH (M)	R (OHMS)	T (C)
12.17	0.10	12245.0	-1.882
12.22	1.10	12160.0	-1.725
12.27	2.10	12032.0	-1.486
12.30	3.10	12032.0	-1.486
12.33	4.10	12004.0	-1.433
12.37	5.10	11995.0	-1.416
12.40	6.10	12007.0	-1.439
12.43	7.10	12039.0	-1.499
12.47	8.10	12083.0	-1.581
12.50	9.10	12121.0	-1.652
12.53	10.10	12160.0	-1.725
12.57	11.10	12194.0	-1.788
12.60	12.10	12223.0	-1.841
12.65	13.10	12255.0	-1.900
12.68	14.10	12287.0	-1.959
12.73	15.10	12322.0	-2.023
12.77	16.10	12347.0	-2.069
12.80	17.10	12375.0	-2.120
12.83	18.10	12400.0	-2.166
12.88	19.10	12428.0	-2.216
12.92	20.10	12455.0	-2.265
12.98	21.10	12486.0	-2.321
13.03	22.10	12520.0	-2.382
13.08	23.10	12536.0	-2.411
13.13	24.10	12561.0	-2.456
13.18	25.10	12592.0	-2.511
13.23	26.10	12618.0	-2.558
13.28	27.10	12645.0	-2.606
13.33	28.10	12670.0	-2.650
13.38	29.10	12696.0	-2.696
13.43	30.10	12717.0	-2.733
13.48	31.10	12740.0	-2.774
13.52	31.50	12744.0	-2.781

1

LONELY
HOLE B3
800529
14:14:00

79-3 CABLE
NEW L&N BRIDGE

TIME	DEPTH (M)	R (OHMS)	T (C)
14.33	0.10	11203.0	0.137
14.37	1.10	10853.0	0.864
14.40	2.10	10901.0	0.763
14.43	3.10	10841.0	0.889
14.47	4.10	10959.0	0.641
14.50	5.10	11149.0	0.248
14.53	6.10	11191.0	0.162
14.57	7.10	11381.0	-0.222
14.60	8.10	11545.0	-0.548
14.63	9.10	11595.0	-0.647
14.67	10.10	11707.0	-0.865
14.70	11.10	11835.0	-1.112
14.73	12.10	11950.0	-1.331
14.77	13.10	12052.0	-1.523
14.80	14.10	12110.0	-1.632
14.83	15.10	12144.0	-1.695
14.87	16.10	12196.0	-1.792
14.90	17.10	12193.0	-1.786
14.93	18.10	12193.0	-1.786
14.97	19.10	12259.0	-1.908
15.00	20.10	12292.0	-1.968
15.03	21.10	12324.0	-2.027
15.07	22.10	12274.0	-1.935
15.10	23.10	12316.0	-2.012
15.13	24.10	12300.0	-1.983
15.17	25.10	12326.0	-2.031
15.20	26.10	12389.0	-2.146
15.23	27.10	12389.0	-2.146
15.27	28.10	12423.0	-2.207
15.30	29.10	12436.0	-2.231
15.33	30.10	12541.0	-2.420
15.37	31.10	12522.0	-2.386
15.40	31.50	12632.0	-2.583

LONELY
HOLE B4
800529
17:39:00

79-3 CABLE
NEW L&N. BRIDGE

TIME	DEPTH (M)	R (OHMS)	T (C)
17.52	1.10	12049.0	-1.518
17.55	2.10	11967.0	-1.363
17.58	3.10	11907.0	-1.249
17.62	4.10	11877.0	-1.192
17.65	5.10	11888.0	-1.213
17.68	6.10	11905.0	-1.245
17.72	7.10	12006.0	-1.437
17.75	8.10	12046.0	-1.512
17.78	9.10	12086.0	-1.587
17.82	10.10	12117.0	-1.645
17.85	11.10	12154.0	-1.714
17.88	12.10	12184.0	-1.769
17.92	13.10	12204.0	-1.806
17.95	14.10	12235.0	-1.864
17.98	15.10	12272.0	-1.932
18.02	16.10	12287.0	-1.959
18.05	17.10	12297.0	-1.978
18.08	18.10	12316.0	-2.012
18.12	19.10	12359.0	-2.091
18.15	20.10	12377.0	-2.124
18.18	21.10	12420.0	-2.202
18.22	22.10	12437.0	-2.233
18.25	23.10	12453.0	-2.262
18.28	24.10	12469.0	-2.291
18.32	25.10	12496.0	-2.339
18.35	26.10	12538.0	-2.415
18.38	27.10	12554.0	-2.443
18.42	28.10	12592.0	-2.511
18.45	29.10	12610.0	-2.543
18.48	30.10	12654.0	-2.622
18.52	31.10	12665.0	-2.641
18.55	31.50	12707.0	-2.716

1

LONELY
HOLE B5
800529
21:05:00

79-3 NEW L&N

CABLE BRIDGE

TIME	DEPTH (M)	R_t (OHMS)	T (C)
21.15	1.10	12097.0	-1.607
21.20	2.10	12011.0	-1.446
21.25	3.10	11966.0	-1.361
21.32	4.10	11938.0	-1.308
21.37	5.10	11943.0	-1.318
21.43	6.10	11958.0	-1.346
21.50	7.10	12021.0	-1.465
21.57	8.10	12060.0	-1.538
21.62	9.10	12095.0	-1.604
21.68	10.10	12133.0	-1.675
21.75	11.10	12171.0	-1.745
21.83	12.10	12223.0	-1.841
21.88	13.10	12234.0	-1.862
21.97	14.10	12254.0	-1.899
22.02	15.10	12294.0	-1.972
22.07	16.10	12309.0	-2.000
22.12	17.10	12332.0	-2.042
22.17	18.10	12354.0	-2.082
22.22	19.10	12393.0	-2.153
22.28	20.10	12411.0	-2.186
22.33	21.10	12454.0	-2.263
22.38	22.10	12479.0	-2.309
22.43	23.10	12498.0	-2.343
22.48	24.10	12523.0	-2.388
22.55	25.10	12551.0	-2.438
22.62	26.10	12583.0	-2.495
22.68	27.10	12605.0	-2.535
22.73	28.10	12636.0	-2.590
22.78	29.10	12654.0	-2.622
22.85	30.10	12683.0	-2.673
22.90	31.10	12704.0	-2.710
22.95	31.50	12730.0	-2.756

1

LONELY
HOLE B6
800530
07:07:00

79-3 CABLE
NEW L&N BRIDGE

TIME	DEPTH (M)	R (OHMS)	T (C)
7.15	1.10	12133.0	-1.675
7.20	2.10	12055.0	-1.529
7.25	3.10	12001.0	-1.427
7.30	4.10	11976.0	-1.380
7.35	5.10	11966.0	-1.361
7.40	6.10	11986.0	-1.399
7.45	7.10	12029.0	-1.480
7.50	8.10	12068.0	-1.553
7.55	9.10	12104.0	-1.620
7.60	10.10	12145.0	-1.697
7.65	11.10	12180.0	-1.762
7.70	12.10	12208.0	-1.814
7.75	13.10	12239.0	-1.871
7.80	14.10	12272.0	-1.932
7.85	15.10	12309.0	-2.000
7.90	16.10	12330.0	-2.038
7.95	17.10	12356.0	-2.086
8.00	18.10	12376.0	-2.122
8.15	19.10	12411.0	-2.186
8.10	20.10	12432.0	-2.224
8.20	21.10	12467.0	-2.287
8.25	22.10	12498.0	-2.343
8.30	23.10	12518.0	-2.379
8.37	24.10	12544.0	-2.425
8.43	25.10	12571.0	-2.474
8.48	26.10	12597.0	-2.520
8.58	27.10	12627.0	-2.574
8.63	28.10	12654.0	-2.622
8.72	29.10	12675.0	-2.659
8.78	30.10	12702.0	-2.707
8.87	31.10	12720.0	-2.739
8.93	31.50	12734.0	-2.763

1

LONELY
HOLE C
800522
16:47:00

79-3 CABLE
NEW L&N BRIDGE

TIME	DEPTH (M)	R (OHMS)	T (C)
16.88	0.60	12192.0	-1.784
16.97	1.60	12131.0	-1.671
17.02	2.60	12086.0	-1.587
17.07	3.60	12006.0	-1.437
17.12	4.60	11987.0	-1.401
17.17	5.60	12011.0	-1.446
17.22	6.60	12042.0	-1.504
17.28	7.60	12072.0	-1.561
17.33	8.60	12096.0	-1.606
17.38	9.60	12126.0	-1.662
17.43	10.60	12152.0	-1.710
17.48	11.60	12175.0	-1.753
17.53	12.60	12204.0	-1.806
17.58	13.60	12231.0	-1.856
17.63	14.60	12251.0	-1.893
17.70	15.60	12281.0	-1.948
17.75	16.60	12305.0	-1.992
17.80	17.60	12331.0	-2.040
17.87	18.60	12349.0	-2.073
17.92	19.60	12370.0	-2.111
17.97	20.60	12391.0	-2.149
18.02	20.70	12394.0	-2.155

1

LONELY
HOLE C2
800529
08:34:00

79-3 NEW L&N

CABLE BRIDGE

TIME	DEPTH (M)	R (OHMS)	T (C)
8.67	0.60	12220.0	-1.836
8.72	1.60	12190.0	-1.780
8.77	2.60	12104.0	-1.620
8.82	3.60	12075.0	-1.566
8.87	4.60	12044.0	-1.508
8.93	5.60	12025.0	-1.472
8.97	6.60	12052.0	-1.523
9.02	7.60	12081.0	-1.577
9.08	8.60	12109.0	-1.630
9.13	9.60	12132.0	-1.673
9.18	10.60	12161.0	-1.727
9.23	11.60	12185.0	-1.771
9.28	12.60	12212.0	-1.821
9.33	13.60	12239.0	-1.871
9.38	14.60	12263.0	-1.915
9.43	15.60	12288.0	-1.961
9.48	16.60	12312.0	-2.005
9.52	17.60	12336.0	-2.049
9.57	18.60	12357.0	-2.087
9.60	19.60	12376.0	-2.122
9.63	20.60	12399.0	-2.164
9.65	20.70	12400.0	-2.166

1

LONELY
HOLE C3
800529
10:36:00

79-3 CABLE
NEW L&N BRIDGE

TIME	DEPTH (M)	R_t (OHMS)	$\bar{T}$ (C)
10.67	0.60	10973.0	0.612
10.70	1.60	10680.0	1.233
10.73	2.60	10648.0	1.302
10.77	3.60	10723.0	1.141
10.80	4.60	11043.0	0.466
10.83	5.60	10938.0	0.685
10.87	6.60	10762.0	1.057
10.90	7.60	10985.0	0.587
10.93	8.60	11342.0	-0.144
10.97	9.60	11528.0	-0.515
11.00	10.60	11653.0	-0.760
11.03	11.60	11865.0	-1.169
11.07	12.60	11919.0	-1.272
11.10	13.60	12020.0	-1.463
11.13	14.60	12043.0	-1.506
11.17	15.60	12093.0	-1.600
11.20	16.60	12108.0	-1.628
11.23	17.60	12141.0	-1.689
11.27	18.60	12114.0	-1.639
11.30	19.60	12189.0	-1.779
11.33	20.60	12162.0	-1.728
11.37	20.70	12252.0	-1.895

1

LONELY
HOLE D1
800522
15:15:00

79-3 CABLE
NEW L&N BRIDGE

TIME	DEPTH (M)	R (OHMS)	T (C)
15.40	0.50	12181.0	-1.764
15.45	1.50	12122.0	-1.654
15.50	2.50	12090.0	-1.594
15.55	3.50	12035.0	-1.491
15.62	4.50	12018.0	-1.459
15.67	5.50	12014.0	-1.452
15.72	6.50	12037.0	-1.495
15.78	7.50	12059.0	-1.536
15.83	8.50	12084.0	-1.583
15.88	9.50	12108.0	-1.628
15.97	10.50	12125.0	-1.660
16.02	11.50	12144.0	-1.695
16.07	12.50	12166.0	-1.736
16.12	13.50	12186.0	-1.773
16.17	14.50	12206.0	-1.810
16.22	15.50	12222.0	-1.840
16.27	16.50	12245.0	-1.882

LONELY
HOLE D2
800528
15:57:00

79-3 NEW L&N

CABLE BRIDGE

TIME	DEPTH (M)	R (OHMS)	T (C)
16.12	0.50	12214.0	-1.825
16.18	1.50	12133.0	-1.675
16.23	2.50	12087.0	-1.589
16.28	3.50	12050.0	-1.519
16.33	4.50	12028.0	-1.478
16.38	5.50	12019.0	-1.461
16.42	6.50	12039.0	-1.499
16.47	7.50	12062.0	-1.542
16.52	8.50	12085.0	-1.585
16.55	9.50	12104.0	-1.620
16.60	10.50	12128.0	-1.665
16.63	11.50	12144.0	-1.695
16.68	12.50	12167.0	-1.738
16.73	13.50	12186.0	-1.773
16.77	14.50	12206.0	-1.810
16.82	15.50	12222.0	-1.840
16.85	16.50	12245.0	-1.882

LONELY
HOLE D3
800528
18:01:00

79-3 NEW L&N   CABLE BRIDGE

TIME	DEPTH (M)	R (OHMS)	T (C)
18.07	0.50	11029.0	0.495
18.10	1.50	10642.0	1.315
18.13	2.50	10757.0	1.068
18.17	3.50	10896.0	0.773
18.20	4.50	10811.0	0.953
18.23	5.50	10852.0	0.866
18.27	6.50	11013.0	0.528
18.30	7.50	11295.0	-0.049
18.33	8.50	11412.0	-0.284
18.37	9.50	11459.0	-0.378
18.40	10.50	11589.0	-0.635
18.43	11.50	11695.0	-0.842
18.47	12.50	11904.0	-1.243
18.50	13.50	11948.0	-1.327
18.53	14.50	11976.0	-1.380
18.57	15.50	12015.0	-1.454
18.60	16.50	12125.0	-1.660

LONELY
HOLE E1
800522
.13:30:00

79-3 NEW L&N CABLE BRIDGE

TIME	DEPTH (M)	R (OHMS)	T (C)
13.58	0.30	12204.0	-1.806
13.63	1.30	12154.0	-1.714
13.72	2.30	12048.0	-1.516
13.77	3.30	12037.0	-1.495
13.83	4.30	12024.0	-1.471
13.88	5.30	12013.0	-1.450
13.93	6.30	12016.0	-1.455
13.98	7.30	12032.0	-1.486
14.03	8.30	12053.0	-1.525
14.10	9.30	12071.0	-1.559
14.15	10.30	12085.0	-1.585
14.20	11.30	12098.0	-1.609
14.27	12.30	12109.0	-1.630
14.32	13.30	12123.0	-1.656
14.35	14.30	12133.0	-1.675
14.40	15.30	12142.0	-1.691
14.45	16.30	12152.0	-1.710
14.50	17.30	12163.0	-1.730
14.57	18.30	12178.0	-1.758
14.62	19.30	12193.0	-1.786
14.67	20.30	12209.0	-1.816
14.72	21.30	12219.0	-1.834
14.78	22.30	12231.0	-1.856
14.85	23.30	12243.0	-1.878
14.90	24.30	12262.0	-1.913
14.95	25.30	12289.0	-1.963
15.00	26.30	12297.0	--1.978
15.05	26.60	12299.0	-1.981

1

LONELY
HOLE E2
800528
10:25:00

79-3 CABLE
NEW L&N BRIDGE

TIME	DEPTH (M)	R (OHMS)	T (C)
10.75	0.30	12207.0	-1.812
10.78	1.30	12159.0	-1.723
10.85	2.30	12099.0	-1.611
10.92	3.30	12052.0	-1.523
10.97	4.30	12024.0	-1.471
11.02	5.30	12008.0	-1.440
11.05	6.30	12006.0	-1.437
11.07	7.30	12020.0	-1.463
11.10	8.30	12034.0	-1.489
11.17	9.30	12054.0	-1.527
11.23	10.30	12067.0	-1.551
11.28	11.30	12082.0	-1.579
11.32	12.30	12095.0	-1.604
11.35	13.30	12111.0	-1.634
11.40	14.30	12120.0	-1.650
11.45	15.30	12134.0	-1.676
11.48	16.30	12149.0	-1.704
11.52	17.30	12158.0	-1.721
11.55	18.30	12171.0	-1.745
11.62	19.30	12184.0	-1.769
11.65	20.30	12196.0	-1.792
11.68	21.30	12211.0	-1.819
11.73	22.30	12224.0	-1.843
11.77	23.30	12238.0	-1.869
11.80	24.30	12253.0	-1.897
11.85	25.30	12281.0	-1.948
11.88	26.30	12291.0	-1.967
11.95	26.60	12294.0	-1.972

1

LONELY
HOLE E3
800528
14:08:00

79-3 CABLE
NEW L&N BRIDGE

TIME	DEPTH (M)	R (OHMS)	T (C)
14.23	0.30	11308.0	-0.076
14.27	1.30	10820.0	0.934
14.30	2.30	10610.0	1.384
14.33	3.30	10630.0	1.341
14.37	4.30	10697.0	1.197
14.40	5.30	10868.0	0.832
14.43	6.30	11067.0	0.417
14.47	7.30	11269.0	0.003
14.50	8.30	11253.0	0.036
14.53	9.30	11433.0	-0.326
14.57	10.30	11462.0	-0.384
14.60	11.30	11635.0	-0.725
14.63	12.30	11613.0	-0.682
14.67	13.30	11806.0	-1.056
14.70	14.30	11789.0	-1.023
14.73	15.30	11954.0	-1.338
14.77	16.30	11980.0	-1.388
14.80	17.30	11982.0	-1.391
14.83	18.30	12002.0	-1.429
14.87	19.30	12009.0	-1.442
14.90	20.30	12012.0	-1.448
14.93	21.30	11989.0	-1.405
14.97	22.30	12013.0	-1.450
15.00	23.30	12056.0	-1.531
15.03	24.30	12081.0	-1.577
15.07	25.30	11997.0	-1.420
15.10	26.30	12061.0	-1.540
15.13	26.60	12177.0	-1.756

ANNUAL REPORT

Contract No.

Research Unit: RU429

Reporting Period: 1/1/81-7/30/81

Number of Pages: 35

Marine Geologic Hazards in the Northern Bering Sea

Final Report on data collected in FY 1980

Gordon R. Hess, Bradley R. Larsen, Darrell Klingman, and Deborah Moore

Pacific-Arctic Branch of Marine Geology

U.S. Geological Survey

Menlo Park, CA 94025

September 1981

I. Summary

Work completed in FY 1981 concentrated on analysis of sediment samples collected during 1980 field operations, analysis of sediment samples from previous USGS and non-USGS cruises, and examination of medium- and high-resolution seismic reflection records. Analysis of these data sets and all data collected throughout the northern Bering Sea will continue in 1982.

Sediment grain-size and carbon content analyses were incorporated to the extensive sediment data base. Revised sediment characteristic maps were produced. No major changes were observed other than the tightening of contours or additional contours in areas where new data filled in previous data gaps.

Post-glacial sediment accumulation is mapped on the basis of high-resolution reflection records. Two areas of significant accumulation are delineated. The largest volume of sediment occurs in the western portion of Chirikov Basin and probably accumulated during periods of lowered sea level during the Late Pleistocene. A second body of Late Pleistocene sediment is deposited between the modern Yukon delta and the Seward Peninsula. This accumulation of sediment probably reflects deposition during periods when sea level stood at or near its present level.

A number of buried channels are recognized within the sediment of Chirikov Basin. Combined with previously mapped subsurface and surface channel locations, an extensive ancient drainage system extends across the northern Bering Sea. Constraints imposed by the presence of gas-charged sediment, thick sediment accumulation, and trackline spacing prevent mapping

the drainage system. It is not possible to determine if the paleodrainage ties to the Yukon river or is related to rivers draining St. Lawrence Island or Seward Peninsula.

II. Introduction

The petroleum potential of the northern Bering Sea outer continental shelf (OCS) has produced a study of potential geologic hazards to resource development. In the past decade over 9000 km of high-resolution seismic reflection profiles have been run, hundreds of cores, grab samples, and photographs taken, and information has been gathered from current meters and hydrographic stations. Data collected in 1980 concentrated on the less well surveyed northwestern Bering Sea, especially in Chirikov Basin.

The aim of the entire geologic hazard assessment program has been to derive an understanding of the geologic history of the area, determine the active sediment erosion and deposition processes, and define potential hazards and areas where they are present or operate that would affect development of offshore resources. Mobile bedform movement, storm-sand deposition, current scouring, ice gouging, sediment liquefaction, sediment cratering produced by gas escape, biogenic gas saturation, thermogenic gas seepage, and active faulting comprise the natural processes and features judged to be potentially hazardous.

The FY 1980 study was conducted to collect data in Chirikov Basin. Work carried out in FY 1981 consisted of analysis of this data to identify and locate the occurrence of any hazards listed above. Additional work concentrated on the study of the shallow stratigraphy and identifying and locating subsurface channels.

The hazards listed above are deemed significant to resource development. Pockets of gas concentrated in the near-surface sediment may be unstable. Pipelines built across these areas may be unequally supported due to differences in sediment bearing strength or due to liquefaction of the gas-charged sediment. Sediment collapse may be associated with escape of near-surface gas leaving pipelines or structures unsupported or exposed. Migration of large-scale bedforms could leave pipelines unsupported. Scour potential is also high in the areas of bedforms. Artificial structures enhance the likelihood of scour and possibly hazardous undercutting may occur. Recent faulting implies direct hazard potential due to offset of the sea floor or severe shaking from earthquakes associated with fault movement. Ice-gouging presents a hazard to exposed pipelines and other structures. Subsurface channels pose a possible hazard due to different bearing strengths of channel-fill sediments contrasted to surrounding sediment. The stratigraphy of near-surface sediments is important for the placement of artificial structures, recognition of potentially hazardous features (slumps, faults), determining thickness of various sediments, and recognizing the presence of surface or near-surface bedrock outcrops.

III. Current State of Knowledge

Initial studies of seismic stratigraphy in this area were undertaken by Moore, 1964; Grim and McManus, 1970; and Nelson and Hopkins, 1972. Detailed surface sediment composition and texture studies were reported by McManus and others (1970, 1974, 1977). A general summary of the Cenozoic stratigraphic framework and sedimentary history was done by Nelson and others (1974). Nelson and Creager (1977) describe the Holocene sediment history and transport dynamics of the Norton Sound region.

In 1976 OCSEAP funded studies were initiated to begin collecting more data on nearsurface stratigraphy, sediments, geochemical and geotechnical characteristics, and high-resolution geophysical records. The high-resolution seismic data has been open-filed within several months of completion of field work (Thor and Nelson, 1978; Nelson and others, 1978; Larsen and others, 1979; Hess and others, 1981). The seismic stratigraphy has been used for numerous topical studies as has much of the sediment, lithologic, geochemical, and geotechnical information. Much of the geotechnical information including major, minor, and trace element content of surface sediment in Norton Basin is available in open-file (Larsen and others, 1980).

An open-file report on the physical characteristics of sediment in Norton Basin is in preparation (Larsen and others). It condenses information from a very broad sediment characteristics data base that includes analysis of sediment samples collected over the past 20 years. The report will include 2-dimensional contour and 3-dimensional perspective maps that display value surfaces depicting sediment composition, organic carbon, and statistical parameters commonly used to describe sediment character.

A broad data based of northern Bering Sea sediment analyses described above has provided information for the topical studies work completed over the past several years. These studies include several on the general hazards of gas-charged sediments (Nelson and others, 1978; Kvenvolden and others, 1979a, 1979b; Nelson and others, 1979). Research has also been completed on major thermogenic gas seeps (Cline and Holmes, 1977; Holmes, 1978) and biogenic gas generated cratering. Larsen and others (1979) describe these craters and also scour depressions. All of these topical studies have been summarized in short publications (Thor and Nelson, 1979a, 1979b).

A recent open-file report (Larsen and others, 1980) is comprised of a number of topical studies that are now in press including an updated summary of all hazards and sediment characteristics (Larsen and others, 1980). Clukey (1980) summarizes work on geotechnical problems and liquefaction. Regional geotechnical characteristics are described by Olsen and others (1980). Shallow gas accumulation and associated potential hazards are discussed by Holmes and Thor (1980). The hazard potential of ice gouging is the subject of a report by Thor and others (1980). Basic information on the stratigraphy from vibracores and high-resolution reflection profiling is summarized in a paper on transgressive history (Nelson, 1980). The necessary biostratigraphic information used to help construct the late Pleistocene and Holocene stratigraphy is presented in a paper by McDougall (1980). The seasonal nature of sedimentary processes in the modern Yukon delta, delta front platform, and prodelta region is described by Dupre (1980). The effects of these seasonal processes on the sedimentary history as recorded in sedimentary structures and biogenic processes are outlined by Howard and Nelson (1980). Cacchione (1980) and Nelson and others (1980) cover the dynamics of sediment transport, mobile bedforms, and storm surge sedimentation. The combination of instability due to cyclic wave loading and strong ebb flow currents of the major storm surges is described by Nelson (1980).

IV. Study Area

The northernmost part of the Bering Sea shelf between St. Lawrence Island and the Bering Straits encompasses two major divisions, Chirikov Basin and Norton Sound. Surveys have generally concentrated on that part of the area scheduled for lease sale 57 in Norton Sound. Other areas of topical interest have also been surveyed in some detail and broad reconnaisance surveying completed over most of the rest of the area. This report deals primarily with analysis of data collected in FY 1980 in Chirikov Basin and also examination of pertinent data from previous cruises. Chirikov Basin has been shown to be a product of tectonic, fluvial, glacial, and shallow marine processes (Hopkins and others, 1976; Grimm and McManus, 1970; Hopkins, 1973; McManus and others, 1974; Nelson and others, 1974).

V. Sources, Methods, and Rationale of Data Collection

Since 1967 the USGS has been collecting marine geologic/geophysical data in the northern Bering Sea. The seismic reflection data gathered during OCSEAP funded field operations in 1976, 1977, 1978, and 1980 are the principal sources of information contributing to our present knowledge of the shelf area. Cruises have been a combination of large-scale reconnaisance studies and more detailed, site-specific, topical work. Reports on these topical studies have been published in the past and summary articles are found in the open-file report of Larsen and others (1980).

The subject of the bulk of analyses conducted in FY 1981 were data from the survey of Chirikov Basin (Fig. 1). Several vibracores and bottom camera stations were occupied to aid stratigraphic analysis and to add to the sediment data base. Work was also done on samples and records from areas of topical interest.

All seismic records, side-scan sonar records, and navigation information and plots area available as open file reports (Hess and others, 1981, in prep.).

VI. Results

Moderate- and high-resolution reflection profiling records show nearsurface acoustic anomalies throughout Chirikov and Norton Basins. Distribution of these anomalies has been discussed in past reports and will not be extensively gone over in this paper.

The occurrence of reflector-termination acoustic anomalies in conjunction with high gas-content sediment in eastern Norton Sound (Nelson and others, 1979) can be related to similar anomalies in Chirikov Basin (Hess and others, 1980). Figures 2 and 3 depict the distribution of acoustic anomalies throughout the study area.

Not all acoustic anomalies shown are related to high gas concentrations in the nearsurface sediment. In western Chirikov Basin the anomalous acoustic response is related to the nature of the sediments at the sea floor. In this zone, layered sediments that are buried nearly 100 m in central Chirikov Basin, approach the seafloor and are mantled by a thin gravel-boulder veneer. The result is a highly reflective seafloor producing strong bottom multiples with no subbottom reflectors on the seismic-reflection profiles. Sidescan sonar records show a very rough, highly reflective surface with isolated boulders or some other large, isolated, targets. A few sand waves are observed around the margins of these rough areas.

To better understand the depositional history of the northern Bering Sea, a study of the near surface seismic stratigraphy has begun. As a starting point, the sediment accumulation on top of glacial moraines and associated tills was examined. Grim and McManus (1970), Hopkins and others (1972), Greene and Tagg (1970), all identify and describe the appearance of glacial moraines in high-resolution seismic records. Beginning at the locale of these various moraines, the thickness of overlying sediment was measured (in values of milliseconds of 2 way travel time). The surface of the moraines and associated tills is very irregular and hummocky, probably due to dissection by meltwater streams from the retreating glaciers. The overlying sediments are generally planar, well-bedded, and laterally continuous. Beyond the physical limits of the glacial moraines, a strong reflecting horizon is present that can be traced back to surface of the moraines. The sediment accumulation above this surface was measured throughout Chirikov and Norton Basins where the reflector could be recognized.

Thicknesses measured in milliseconds were converted to thickness in meters assuming a velocity of sound in the upper 50 m of sediment to be 1500 m/sec. (Holmes and Thor, 1980). An isopach map of this sediment accumulation is shown in figure 4. The sediment is divided into two major bodies separated by a broad area of less than 5 meters accumulation.

Previous studies noted the presence of some buried channel systems, notably along the margins of the basin near the Seward Peninsula. A more extensive distribution of buried channels was found during the 1980 field work. Generally the channels show no surface expression and are sediment filled. A range of channel shapes is seen on the seismic profiles. Some crossings record relatively narrow, steep-sided, isolated channels while other crossings show wide, irregular sided, multiple channel arrays. This variation is probably attributable to the variability in approach angle of the channel crossings. When crossed at nearly a right angle, the narrowest channel profile would be observed. When crossed obliquely, a much wider channel section would be recorded. Figure 5a and 5b are portions of seismic records showing typical channel crossings. Figure 6 shows all channels recognized on profiles from the 1980 field season and from previous studies.

Although desirable, it is not possible to tie the recorded channel crossings into a distinct drainage network. Trackline spacing is too great to relate crossings on adjacent tracks. The drainage network cannot be traced east to the Yukon as high resolution seismic systems are not able to penetrate through the sediments of the modern Yukon delta or the subbottom information is obscured by the abundance of gas-charged sediment and resulting acoustic anomalies. It is difficult to recognize channel features on the deeper-penetration airgun or sparker systems unless the channel crossing is at an oblique angle producing a broad channel cross-section. For the reasons discussed above it is not possible at this time to relate the drainage system to the modern Yukon or to rivers on St. Lawrence Island or Seward Peninsula. The drainage may be related to meltwater streams from the retreating glaciers. Greene and Tagg (1970) noted many buried valleys in their study of the sediments and stratigraphy along the coast off Nome.

Areas of mobile bedforms and ice-gouging were described by Hess and others (1980) and Thor and others (1980). Figures showing the distribution of these features are included without further discussion (Fig. 7, 8).

VII. Discussion

The acoustically anomalous sediments of the northern Bering Sea must be considered as indicators of potentially hazardous conditions to some types of structures. Gas-charged sediment could present foundation problems for any structure dependent on the sea bottom for support. Those areas of acoustic anomalies attributable to the near-surface presence of older, layered sediments and/or boulder-gravel lags do not constitute hazardous conditions.

Sediment accumulation above readily identifiable glacial features as shown in figure 4 probably reflects multiple processes. The two major portions of the deposit represent two separate phases of deposition.

The deposit in central Norton Basin in part reflects deposition by the modern Yukon River. This deposit includes all sediments from its base horizon to the present sea floor including Holocene sediments. The pattern of Holocene deposition shown by Nelson (1980) is similar to that shown for this deposit.

The sediment accumulated in western Chirikov Basin, where Holocene sediment is very thin or absent (Nelson, 1980) represents some earlier period of deposition when sea level stood much lower than at present. Nelson and Creager (1977) show that virtually no sediment is presently accumulating in this area. This absence of sediment accumulation is a product of present strong circulation northward through the Bering Strait. Conditions would likely be similar anytime sea level stood at or near its present level. The sediment deposit in western Chirikov Basin likely accumulated during pre-Holocene periods of lowered sea-level.

Glacial moraines used as a base level for this sediment body are attributed to the maximum glacial advance of stage 6 (Hopkins, 1973). The isopach map therefore records sediment accumulation over the past 130,000 years. Moore (1964) identified a delta deposit in central Norton Sound which Hopkins (1973) attributed to a middle Wisconsin transgression. This deposit is included in the sediment body shown by the isopach map. The delta sequence lies very close to or at the base of the deposit. The sediment accumulated in central Norton Sound probably represents deposition since the last 30-35,000 years.

Knebel and Creager (1973) show that the Yukon has followed its course for only a few thousand years and that throughout the previous 15-20,000 years reached the sea sounth of St. Lawrence Island. The presence of the delta sequence (Moore, 1964) and the extensive channel system mapped in this study suggest that the Yukon flowed to the northwest across the northern Bering Sea.

The masking effect of modern Yukon delta sediments prevents the tracing of subsurface channels directly back to the Yukon. The limit on the west end of Chirikov Basin is posed by lack of trackline coverage and thicker accumulation of sediment masking subbottom information. Closer study of deeper penetration airgun and sparker system profiles may reveal additional details of this drainage system.

References Cited

Cacchione, D. A., Drake, D. E., and Wiberg, P., 1980, Velocity and bottom-stress measurements in the boundary layer, outer Norton Sound, Alaska, in Larsen, M. C., Nelson, C. H., and Thor, D. R., Geological, geochemical, and geotechnical observations on the Bering Shelf, Alaska, U.S.G.S. Open-File Report 80-979.

Cline, J. D. and Holmes, M. L., 1977, Submarine seepage of natural gas in Norton Sound, Alaska: Science, v. 198, p. 1149-1153.

Clukey, E. C., Cacchione, D. A., and Olsen, H. W., 1980, Liquefaction potential of the Yukon prodelta: Proceedings of the Offshore Technology Conference, Houston, Texas, 1980, Paper no. 3773, in press.

Dupre, W. R., 1980, Seasonal variations in deltaic sedimentation on a high-altitude epicontinental shelf in S. C. Nio, R. T. Schattenhelm, and T. C. E. Van Weering, eds., IAS Special Publication, London, Blackwell Science Publications (in press).

Grim, M. S. and McManus, D. A., 1970, A shallow seismic-profiling survey of the northern Bering Sea: Marine Geology, v. 8, p. 293-320.

Hess, G. R., Larsen, B. R., Nelson, C. H., Klingman, D., and Mango, P., 1981, Summary of 1980 cruise results, geohazard program. Norton Basin-Chirikov Basin; and Summary of surface sediment characteristics, Norton Basin, End-of-year report to NOAA-OCSEAP, 25 pp.

Hess, G. R., Larsen, B. R., and Klingman, D., 1981 (in preparation), Seismic reflection profiles of U.S.G.S. cruise Lee-7-80-BS, U.S.G.S. Open File Report 81-   , 5 pp.

Holmes, M. L., 1979b, Distribution of gas-charged sediment in Norton Sound and Chirikov Basin, in C. H. Nelson, D. R. Thor, and M. C. Larsen, Faulting, sediment instability, erosion, and depositional hazards of the Norton Basin seafloor, Annual Report of Principal Investigators for the year ending March 1979, Environmental Research Laboratory, Boulder, Colorado, NOAA, U.S. Dept. of Commerce, p. B1-B16.

Holmes, M. L., Cline, J. D., and Johnson, J. L., 1978, Geologic setting of the Norton Basin gas seep, Proceedings of Offshore Technology Conference, Houston, Texas, OTC Paper no. 3051, p. 73-80.

Holmes, M. L. and Thor, D. R., 1980, Distribution of gas-charged sediment in Norton Basin, northern Bering Sea, in Larsen, M. C., Nelson, C. H., and Thor, D. R., Geological, geochemical, and geotechnical observations on the Bering shelf, Alaska, U.S.G.S. Open-File Report 80-979.

Hopkins, D. M., 1973, Sea-level history in Beringia during the past 250,000 years, Quat, Res. v. 3, p. 520-540.

Hopkins, D. M., Rowland, R. W., and Patton, W. W. Jr., 1972, Middle Pleistocene mollusks from St. Lawrence Island and their significance for the paleo-oceanography of the Bering Sea, Quaternary Research, v. 2, p. 119-134.

Hopkins, D. M., Nelson, C. H., Perry, R. B., and Alpha, T. R., 1976, Physiographic subdivisions of the Chirikov Basin, northern Bering Sea: U.S. Geological Survey Professional Paper 759-B, 7 p.

Howard, J. D. and Nelson, C. H., 1980, Sedimentary structures on a delta-influenced shallow shelf, Norton Sound, Alaska, in Larsen, M. C., Nelson, C. H., and Thor, D. R., Geological geochemical, and geotechnical observations on the Bering Shelf, Alaska, U.S.G.S. Open-File Report, 80-979.

Knebel, H. J. and Creager, J. S., 1973, Yukon River; evidence for extensive migration during the Holocene transgression, Science, v. 179, p. 1230-1232.

Kvenvolden, K. A., Nelson, Hans, Thor, D. R., Larsen, M. C., Redden, G. D., Rapp, J. B., and Des Marais, D. J., 1979a, Biogenic and thermogenic gas in gas-charged sediment of Norton Sound, Alaska: Proceedings Offshore Technical Conference, Paper No. 3412.

Kvenvolden, K. A., Weliky, K., Nelson, C. H., and Des Marais, D. J., 1979b, Submarine seep of carbon dioxide in Norton Sound, Alaska: Science, v. 205, p. 1264-1266.

Larsen, M. C., Nelson, C. H., and Thor, D. R., 1979, Geologic implications and potential hazards of scour depressions on Bering shelf, Alaska: Environmental Geology, v. 3, p. 39-47.

Larsen, M. C., Nelson, C. H., and Thor, D. R., 1980, Sedimentary processes and potential hazards on the sea floor of northern Bering Sea, in Larsen, M. C., Nelson, C. H., and Thor, D. R., Geological, geochemical, and geotechnical observations on the Bering Shelf, Alaska, U.S.G.S. Open-File Report 80-979.

Larsen, B. R., Nelson, C. H., Heropoulos, C., and Patry, J., 1980, Distribution of trace elements in bottom sediment of northern Bering Sea, U.S. Geological Survey Open-File Report 80-399A, 122 p.

Larsen, B. R., Nelson, C. H., Heropoulos, C., and Patry, J., 1980, Map-plots and value/location lists of trace element concentrations in northern Bering Sea bottom sediment, U.S. Geological Survey Open-File Report 80-399B, microfiche.

McDougall, K., 1980, Microfaunal analysis of late Quaternary deposits of the northern Bering Sea, in Larsen, M. C., Nelson, C. H., and Thor, D. R., Geological, geochemical, and geotechnical observations on the Bering Shelf, Alaska, U.S.G.S. Open-File Report, 80-979.

McManus, D. A., Venkatarathnam, K., Echols, R. J., and Holmes, M. L., 1970, Bottom samples and seismic profiles of the northern Bering Sea and associated studies, U.S. Geological Survey, Office of Marine Geology Final Report, Contract No. 14-08-0001-11995, 115 p.

McManus, D. A., Venkatarathnam, K., Nelson, C. H., and Hopkins, D. M., 1974, Yukon sediment on the northernmost Bering Sea shelf, Journal of Sedimentary Petrology, v. 44, p. 1052-1060.

McManus, D. A., Kolla, V., Hopkins, D. M., and Nelson, C. H., 1977, Distribution of bottom sediments on the continental shelf, northern Bering Sea: U.S. Geological Survey Professional Paper 759-C, 31 p.

Moore, D. G., 1964, Acoustic-reflection reconnaisance of continental shelves: eastern Bering and Chukchi seas, in Miller, R. L., ed., Papers in Marine Geology - Shepard Commemorative Volume. McMillan, New York, N.Y., pp. 319-362.

Nelson, C. H. and Hopkins, D. M., 1972, Sedimentary processes and distribution of gold in the northern Bering Sea, U.S.G.S. Professional Paper 689, 27 p.

Nelson, C. H., Hopkins, D. M., and Scholl, D. W., 1974, Tectonic setting and Cenozoic sedimentary history of the Bering Sea, in Y. Herman, ed., Marine

Geology and Oceanography of the Arctic Seas, New York, Springer-Verlag, p. 119-140.

Nelson, C. H. and Creager, J. S., 1977, Displacement of Yukon-derived sediment from Bering Sea to Chukchi Sea during the Holocene: Geology, v. 5, p. 141-146.

Nelson, C. H., Thor, D. R., Sandstrom, M. W., and Kvenvolden, K. A., 1978, Modern biogenic gas-generated craters (sea-floor pockmarks) on the Bering shelf, Alaska: Geological Society of America Bulletin, v. 90, p. 1144-1152.

Nelson, C. H., 1980a, Graded storm sand layers from the Yukon prodelta, Bering Sea, in Larsen, M. C., Nelson, C. H., and Thor, D. R., Geological, geochemical, and geotechnical observations on the Bering Shelf, Alaska, U.S.G.S. Open-File Report 80-979.

Nelson, C. H., 1980b, Late Pleistocene-Holocene transgressive sedimentation in deltaic and non-deltaic areas of the Bering epicontinental shelf, in Larsen, M. C., Nelson, C. H., and Thor, D. R., Geological, geochemical, and geotechnical observations on the Bering Shelf, Alaska, U.S.G.S. Open-File Report 80-979.

Nelson, C. H., Dupre, W. R., Field, M. E., and Howard, J. D., 1980, Linear sand bodies in the Bering Sea epicontinental shelf, in Larsen, M. C., Nelson, C. H., and Thor, D. R., Geological, geochemical, and geotechnical observations on the Bering Shelf, Alaska, U.S.G.S. Open-File Report 80-979.

Olsen, H. W., Clukey, E. C., and Nelson, C. H., 1979, Geotechnical characteristics of bottom sediments in the northern Bering Sea, in Larsen, M. C., Nelson, C. H., and Thor, D. R., Geological, geochemical, and geotechnical observations on the Bering Shelf, Alaska, U.S.G.S. Open-File Report 80-979.

Tagg, A. R. and Greene, H. G., 1973, High-resolution seismic survey of an offshore area near Nome, Alaska, U.S.G.S. Prof. Paper 759-A, p. A1-A23.

Thor, D. R. and Nelson, C. H., 1979a, A summary of interacting surficial geologic processes and potential geologic hazards in the Norton Basin, northern Bering Sea: Proceedings Offshore Technical Conference, Paper No. 3400, p. 377-381.

Thor, D. R. and Nelson, C. H., 1979b, A summary of interacting surficial geologic processes and potential geologic hazards in the Norton Basin, northern Bering Sea: Journal of Petroleum Technologists, March 1980, p. 355-362.

Thor, D. R. and Nelson, C. H., 1980, Ice gouging on the subarctic Bering Shelf, in Larsen, M. C., Nelson, C. H., and Thor, D. R., Geological, geochemical, and geotechnical observations on the Bering Shelf, Alaska, U.S.G.S. Open-File Report, 80-979.

Figure Captions

Figure 1. Station locations and tracklines for 1980 field operations.

Figure 2. Acoustic anomalies observed on high-resolution uniboom records prior to 1980 field studies from Nelson and others, 1979.

Figure 3. Acoustic anomalies observed on uniboom records from 1980 survey.

Figure 4. Isopach map of post-glacial sediment accumulation.

Figure 5. Subsurface channels observed on uniboom high-resolution profiles. a) Narrow channel judged to represent a near orthogonal crossing of the channel axis. b) Wide, complex channel judged to represent an oblique channel crossing. For locations of profiles see figure 6.

Figure 6. Distribution of surface and subsurface channels. Modified from Nelson and others, 1979. Data from 1980 studied added as shown. Dark lines denote location of profiles in figure 5.

Figure 7. Occurrence of ice-gouging throughout the northern Bering Sea.

Figure 8. Areas of intense current activity and presence of mobile bedforms as recognized on sidescan from 1980 survey.

Figure 9. Location map of all samples from Norton Sound and Chirikov Basin.

Figure 10-16. Updated sediment character maps for northern Bering Sea.

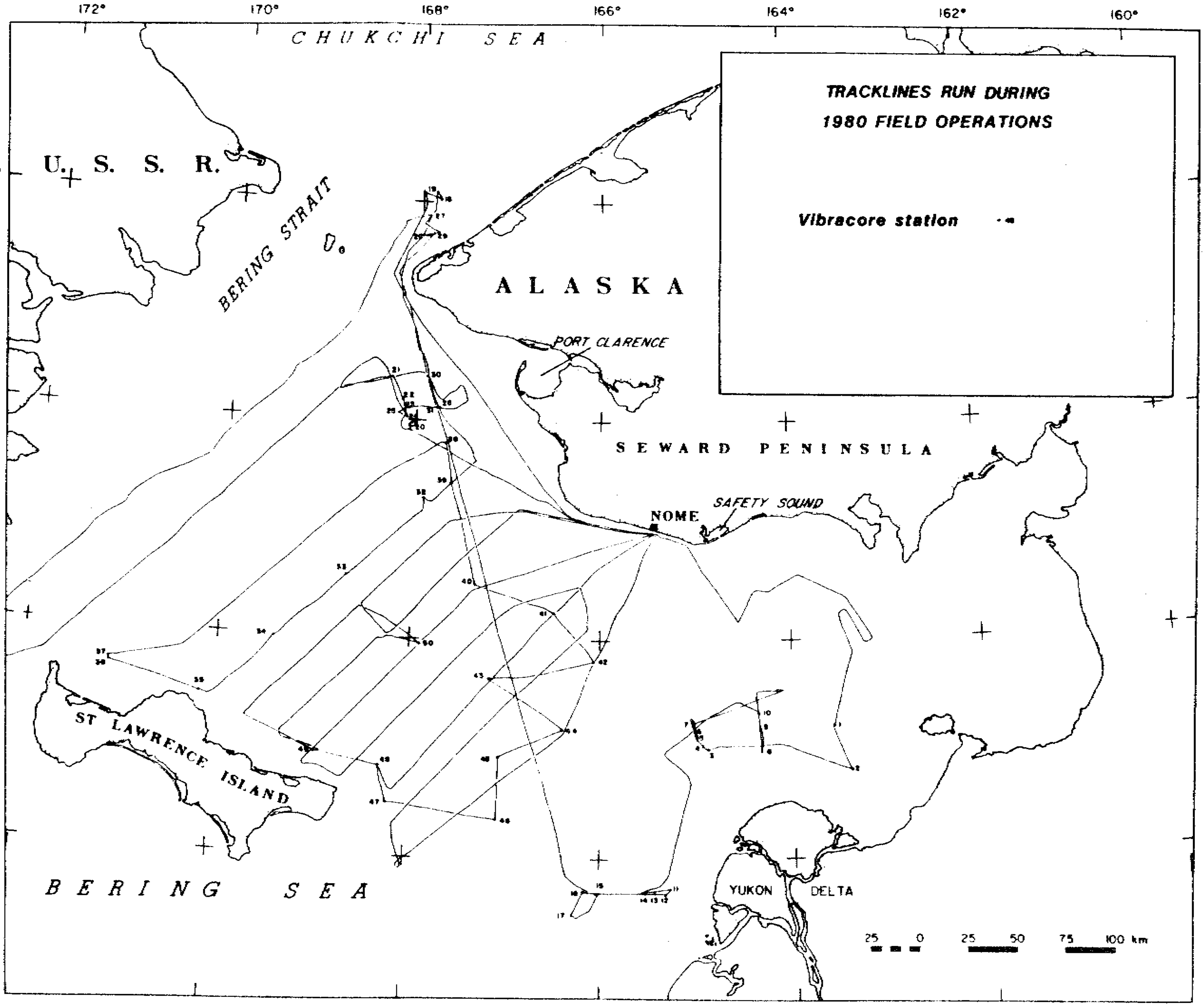
172°
170°
168°
166°
164°
162°
160°
66°
65°
64°
63°
CHUKCHI SEA
TRACKLINES RUN DURING
1980 FIELD OPERATIONS
Vibracore station
U. S. S. R.
BERING STRAIT
ALASKA
PORT CLARENCE
SEWARD PENINSULA
NOME
SAFETY SOUND
ST LAWRENCE ISLAND
BERING SEA
YUKON
DELTA
25 0 25 50 75 100 km

Figure 1.

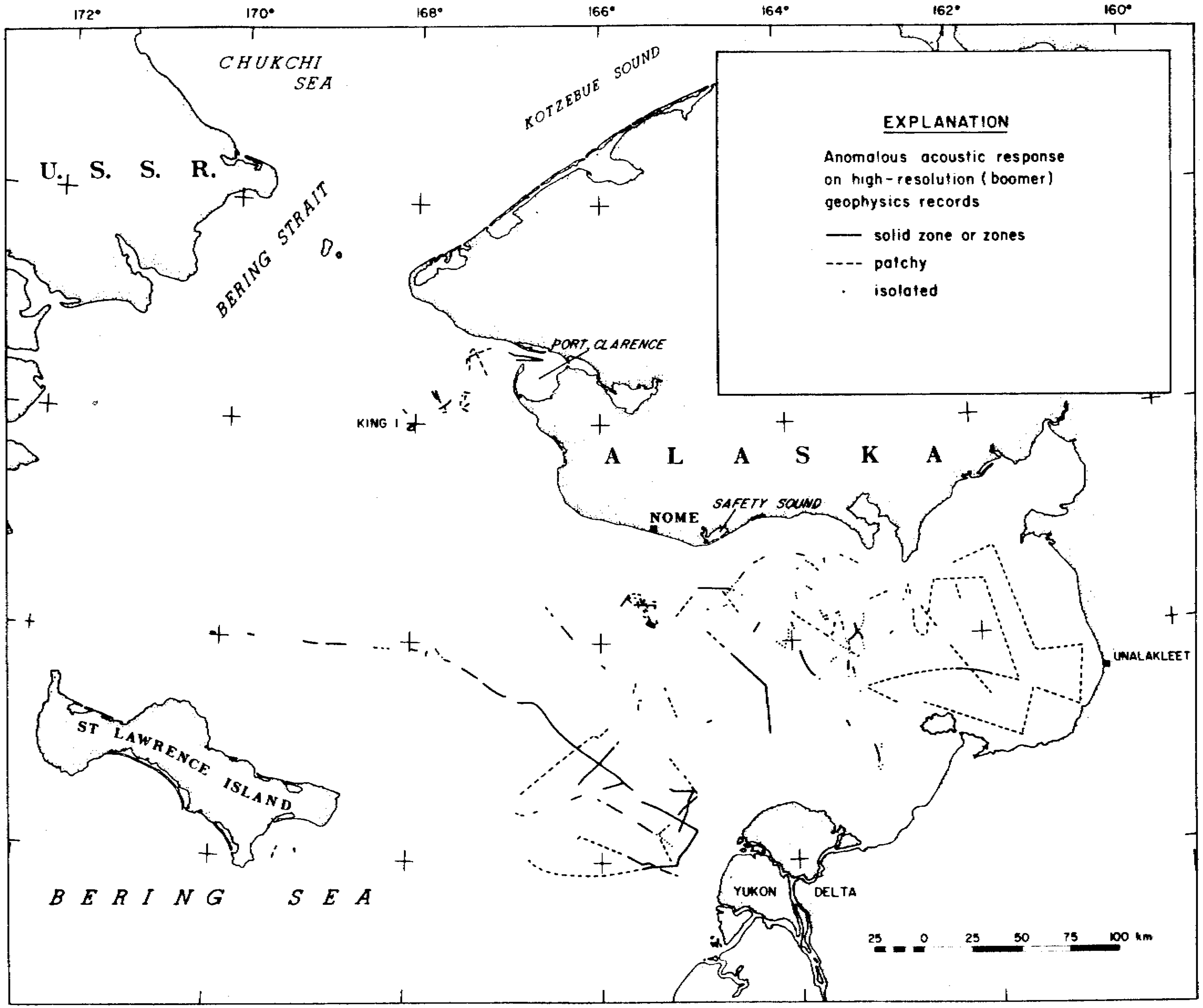
172°
170°
168°
166°
164°
162°
160°
66°
65°
64°
63°
CHUKCHI SEA
KOTZEBUE SOUND
U. S. S. R.
BERING STRAIT
PORT CLARENCE
KING I
A L A S K A
NOME
SAFETY SOUND
UNALAKLEET
ST LAWRENCE ISLAND
YUKON DELTA
BERING SEA
EXPLANATION
Anomalous acoustic response on high-resolution (boomer) geophysics records
solid zone or zones
patchy
isolated
25 0 25 50 75 100 km

Figure 2.

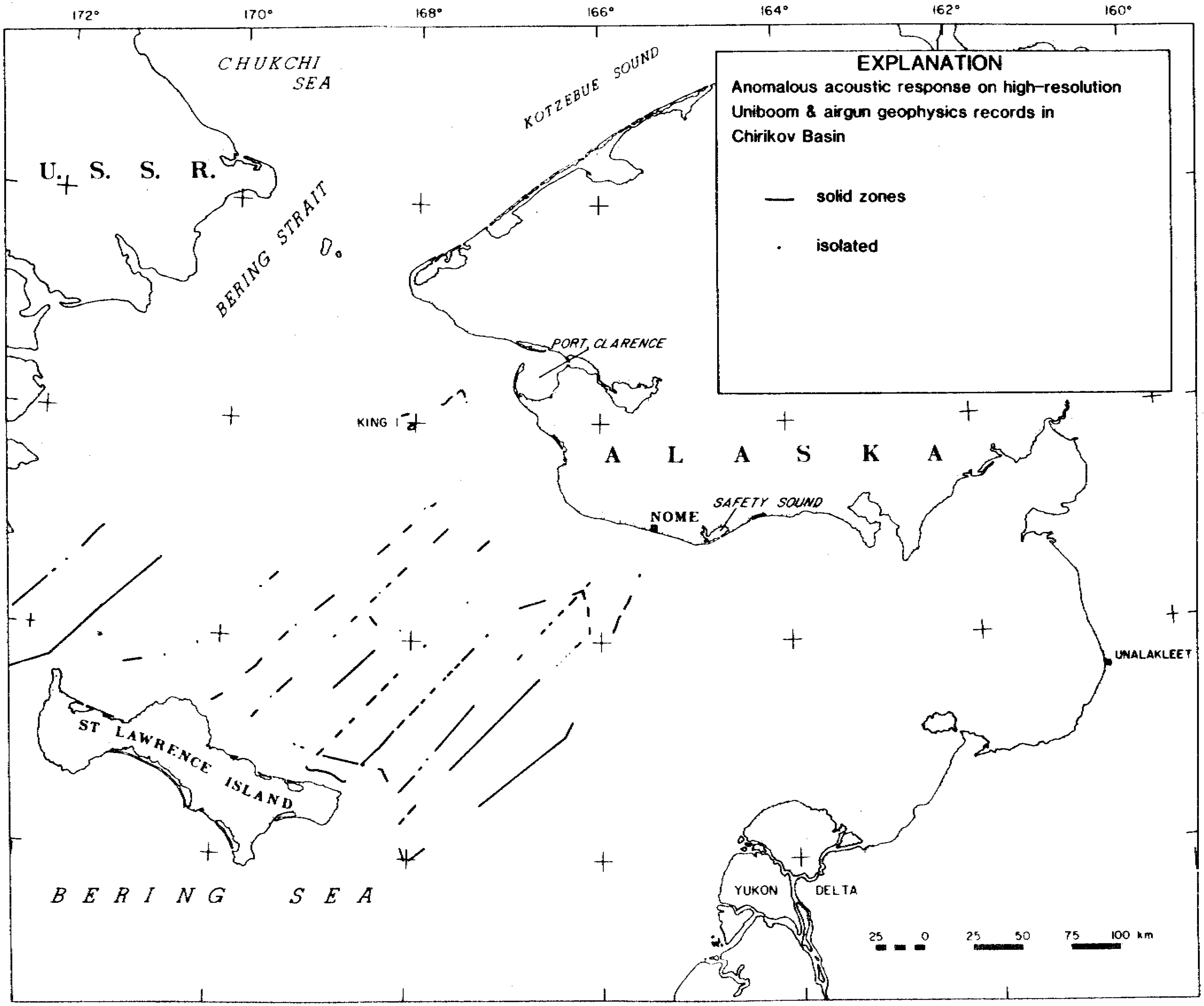
172°
170°
168°
166°
164°
162°
160°
66°
65°
64°
63°
CHUKCHI SEA
KOTZEBUE SOUND
U. S. S. R.
BERING STRAIT
PORT CLARENCE
KING I
A L A S K A
NOME
SAFETY SOUND
UNALAKLEET
ST LAWRENCE ISLAND
YUKON DELTA
BERING SEA
25 0 25 50 75 100 km
EXPLANATION
Anomalous acoustic response on high-resolution Uniboom & airgun geophysics records in Chirikov Basin
solid zones
isolated

Figure 3.

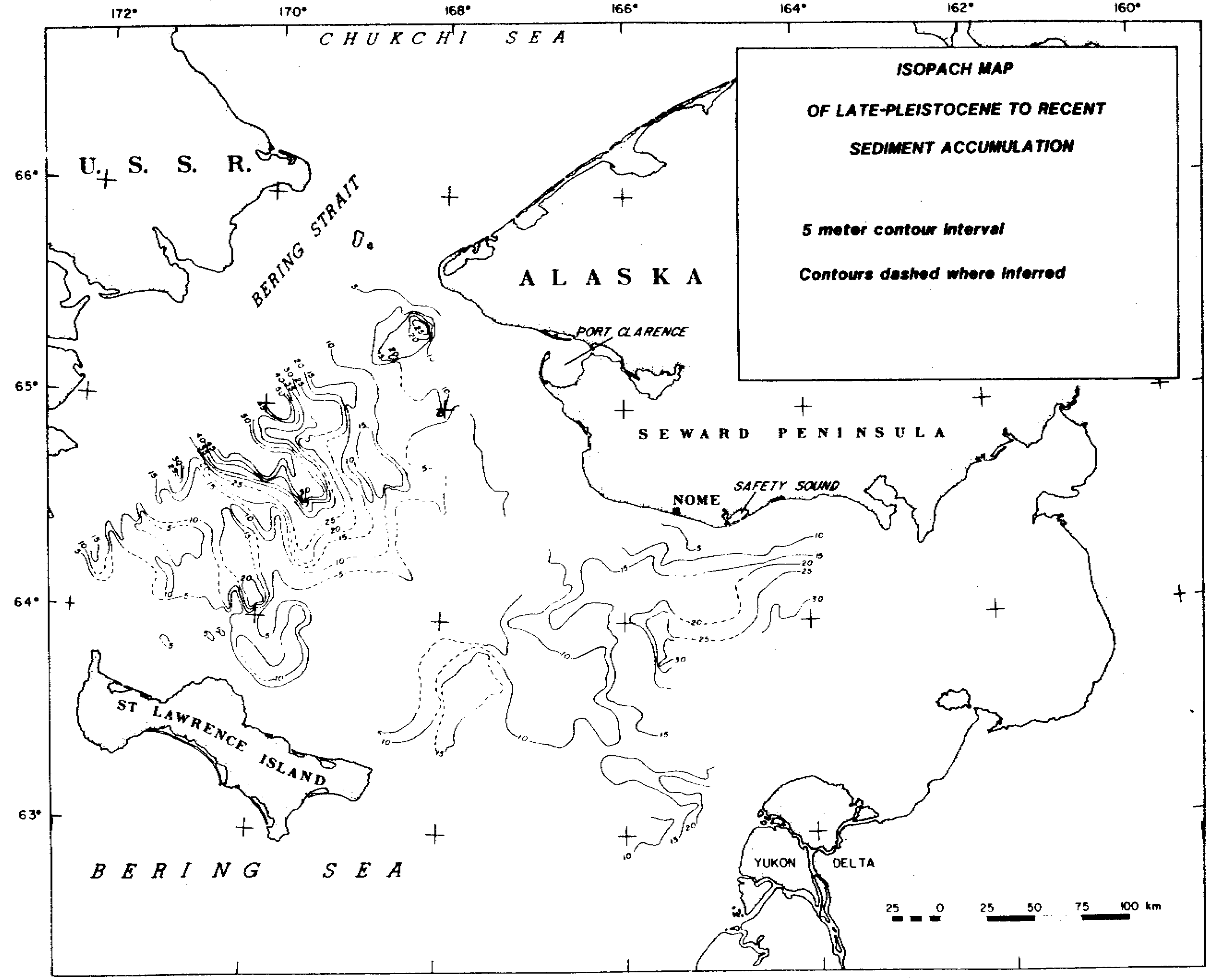

172°
170°
168°
166°
164°
162°
160°
66°
65°
64°
63°
CHUKCHI SEA
U. S. S. R.
BERING STRAIT
ALASKA
ISOPACH MAP
OF LATE-PLEISTOCENE TO RECENT
SEDIMENT ACCUMULATION
5 meter contour interval
Contours dashed where inferred
PORT CLARENCE
SEWARD PENINSULA
NOME
SAFETY SOUND
ST LAWRENCE ISLAND
BERING SEA
YUKON DELTA
25 0 25 50 75 100 km

Figure 4.

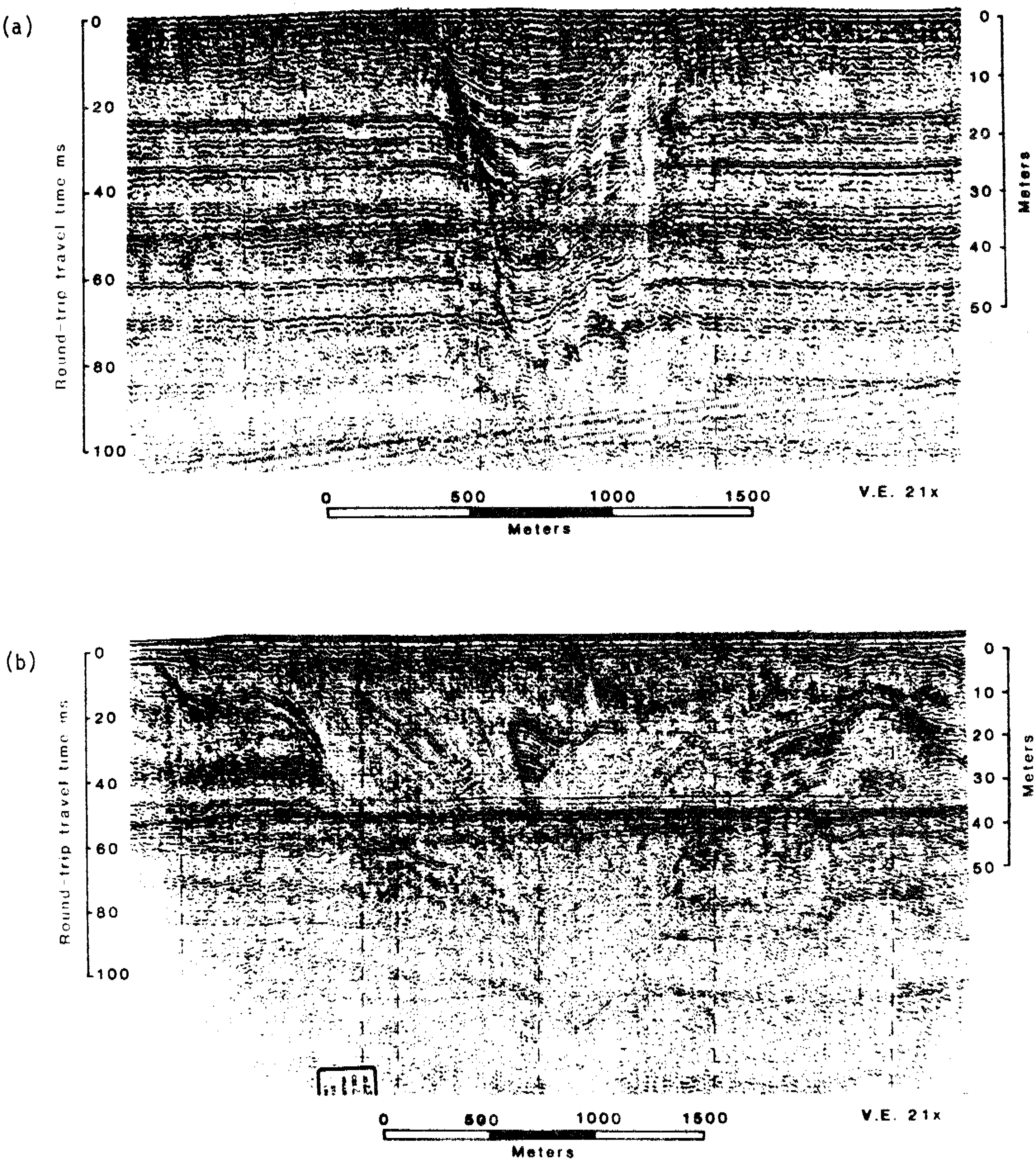

(a)
Round-trip travel time ms
0
20
40
60
80
100
Meters
0
10
20
30
40
50
0
500
1000
1500
Meters
V.E. 21x
(b)
Round-trip travel time ms
0
20
40
60
80
100
Meters
0
10
20
30
40
50
0
500
1000
1500
Meters
V.E. 21x

Figure 5.

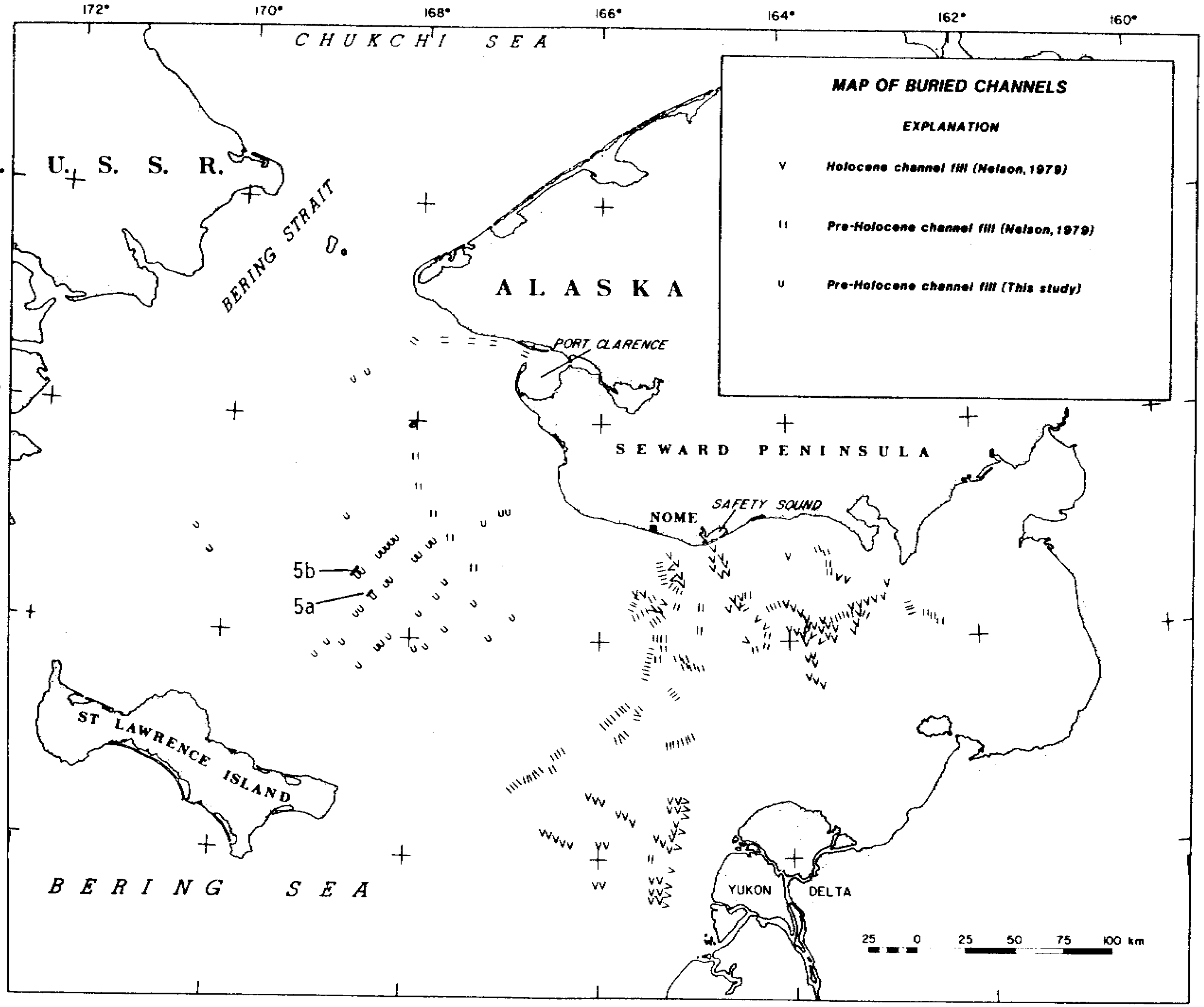

MAP OF BURIED CHANNELS
EXPLANATION
v Holocene channel fill (Nelson, 1979)
ıı Pre-Holocene channel fill (Nelson, 1979)
u Pre-Holocene channel fill (This study)
CHUKCHI SEA
U. S. S. R.
BERING STRAIT
ALASKA
PORT CLARENCE
SEWARD PENINSULA
NOME
SAFETY SOUND
5b
5a
ST LAWRENCE ISLAND
BERING SEA
YUKON DELTA
172°
170°
168°
166°
164°
162°
160°
66°
65°
64°
63°
25 0 25 50 75 100 km

Figure 6.

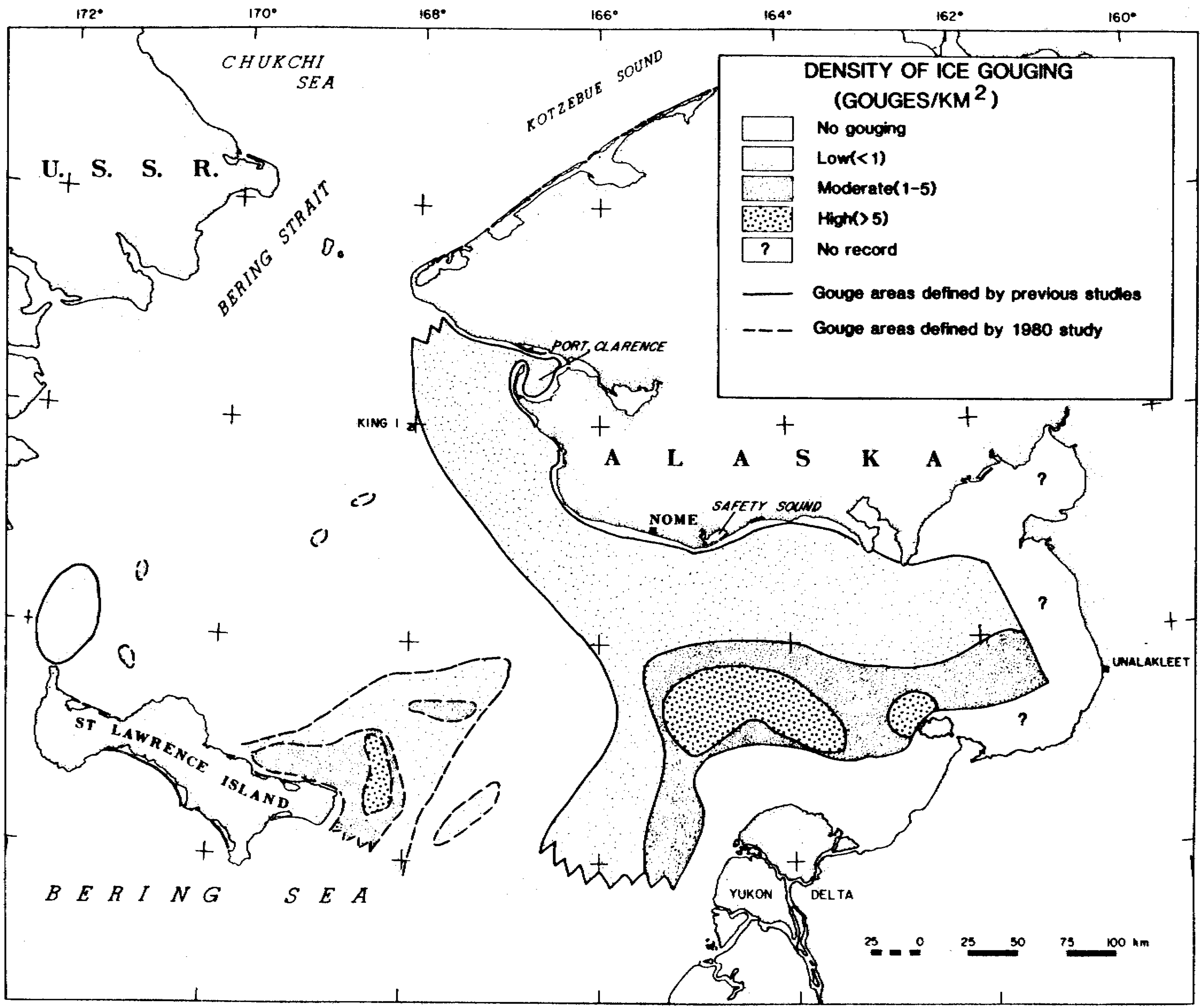

172°
170°
168°
166°
164°
162°
160°
66°
65°
64°
63°
CHUKCHI SEA
KOTZEBUE SOUND
U. S. S. R.
BERING STRAIT
PORT CLARENCE
KING I
A L A S K A
NOME
SAFETY SOUND
UNALAKLEET
ST LAWRENCE ISLAND
B E R I N G S E A
YUKON DELTA
DENSITY OF ICE GOUGING
(GOUGES/KM 2)
No gouging
Low(< 1)
Moderate(1-5)
High(> 5)
?
No record
Gouge areas defined by previous studies
Gouge areas defined by 1980 study
25 0 25 50 75 100 km

Figure 7.

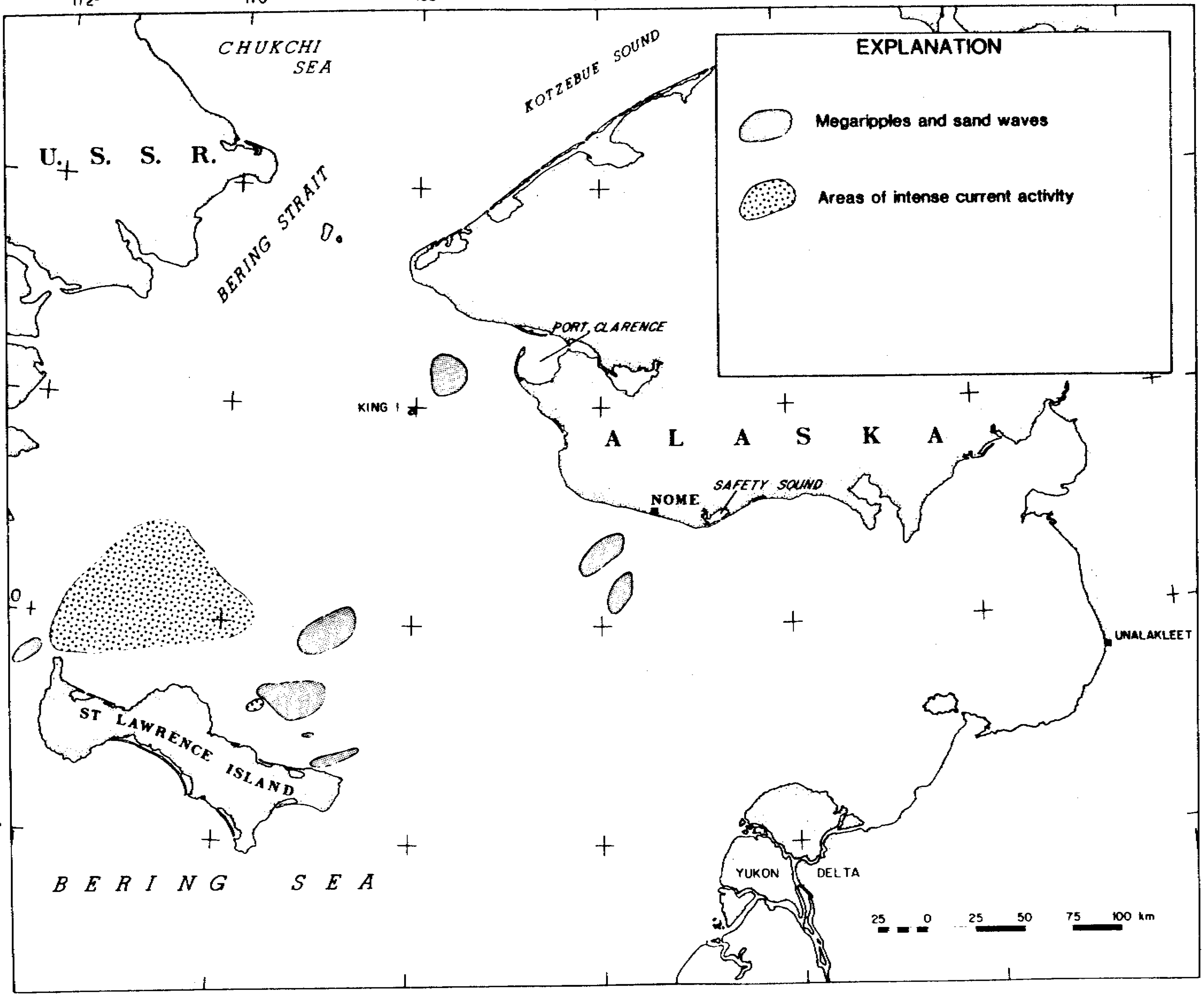
172°
170°
168°
166°
164°
162°
160°
66°
65°
64°
63°
CHUKCHI SEA
KOTZEBUE SOUND
EXPLANATION
Megaripples and sand waves
Areas of intense current activity
U. S. S. R.
BERING STRAIT
PORT CLARENCE
KING I
A L A S K A
NOME
SAFETY SOUND
UNALAKLEET
ST LAWRENCE ISLAND
YUKON DELTA
25 0 25 50 75 100 km
B E R I N G S E A

Figure 8.

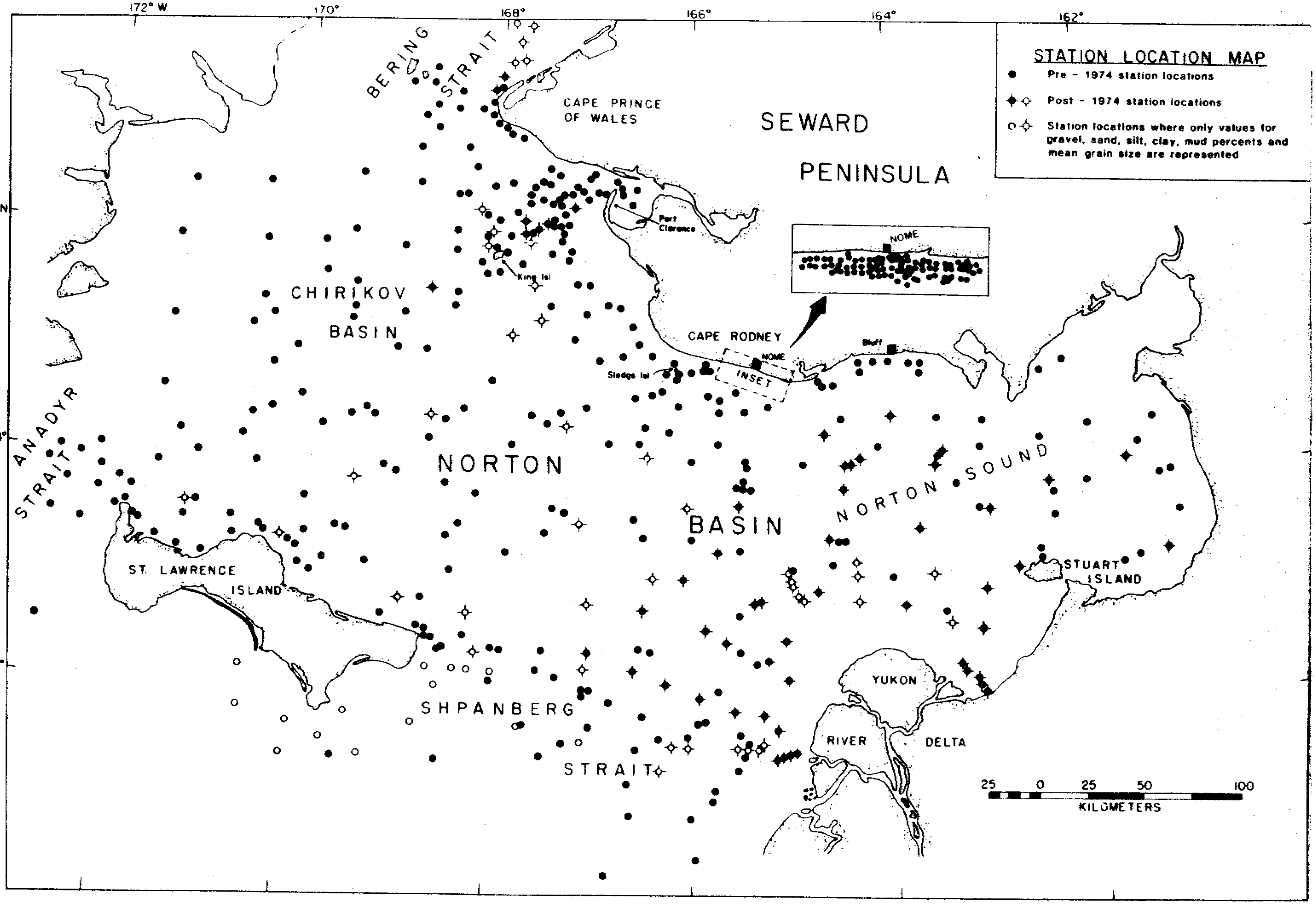

172° W
170°
168°
166°
164°
162°
65°N
64°
63°
STATION LOCATION MAP
Pre - 1974 station locations
Post - 1974 station locations
Station locations where only values for gravel, sand, silt, clay, mud percents and mean grain size are represented
BERING STRAIT
CAPE PRINCE OF WALES
SEWARD PENINSULA
Port Clarence
King Isl
NOME
CHIRIKOV BASIN
CAPE RODNEY
Bluff
Sledge Isl
INSET
ANADYR STRAIT
NORTON BASIN
NORTON SOUND
ST. LAWRENCE ISLAND
STUART ISLAND
YUKON RIVER DELTA
SHPANBERG STRAIT
25 0 25 50 100
KILOMETERS

Figure 9.

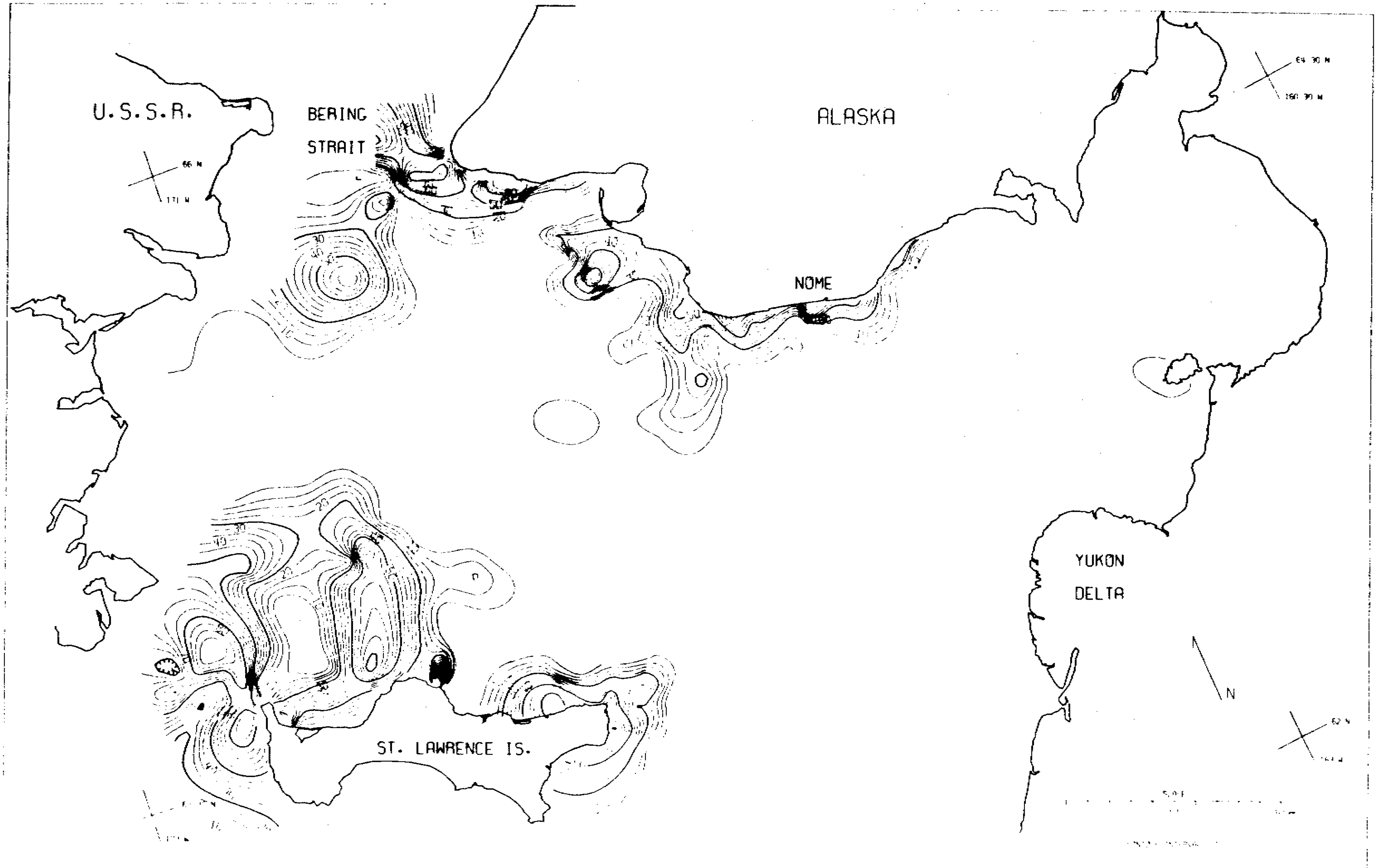

10 %

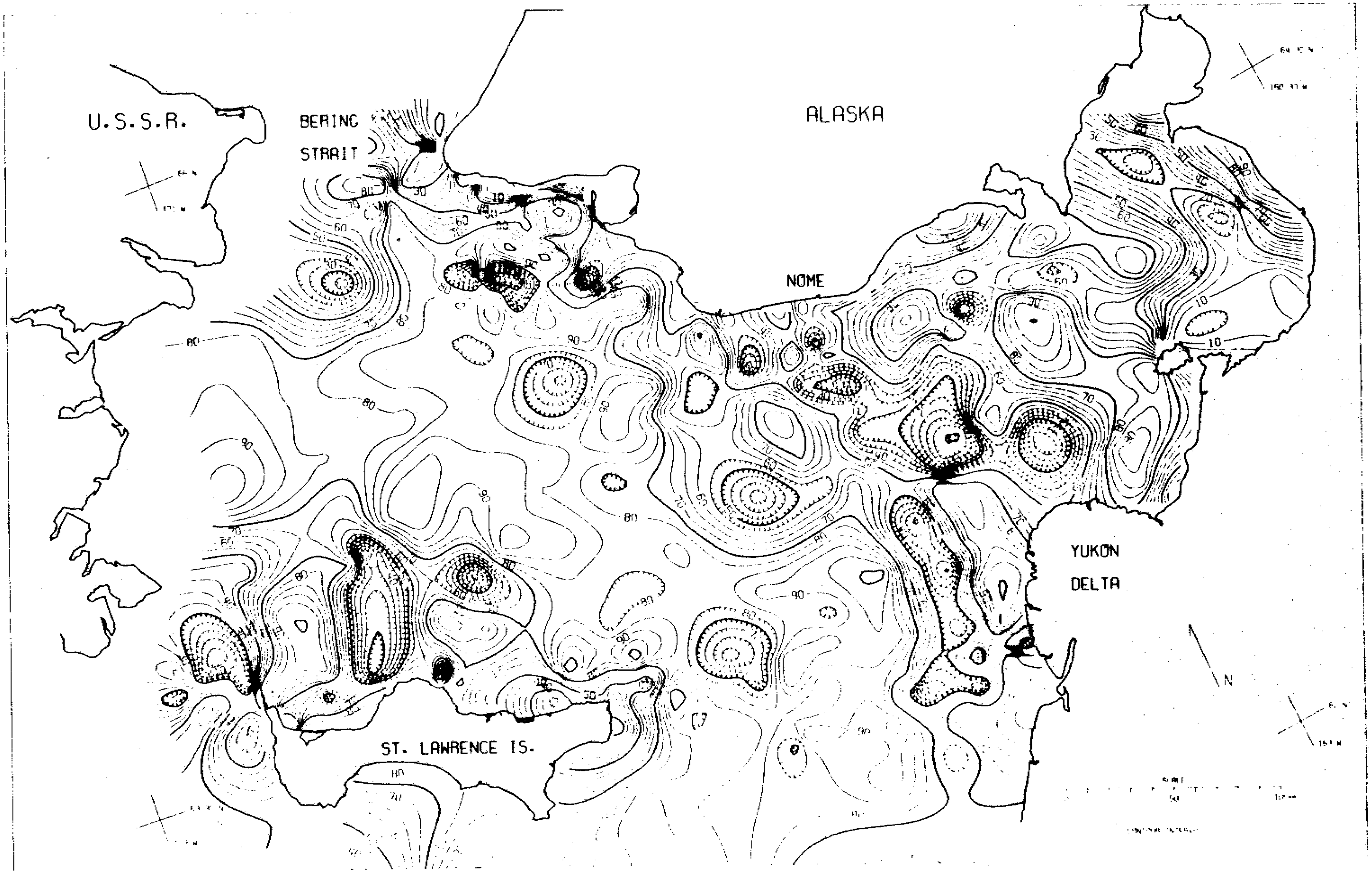

11 %

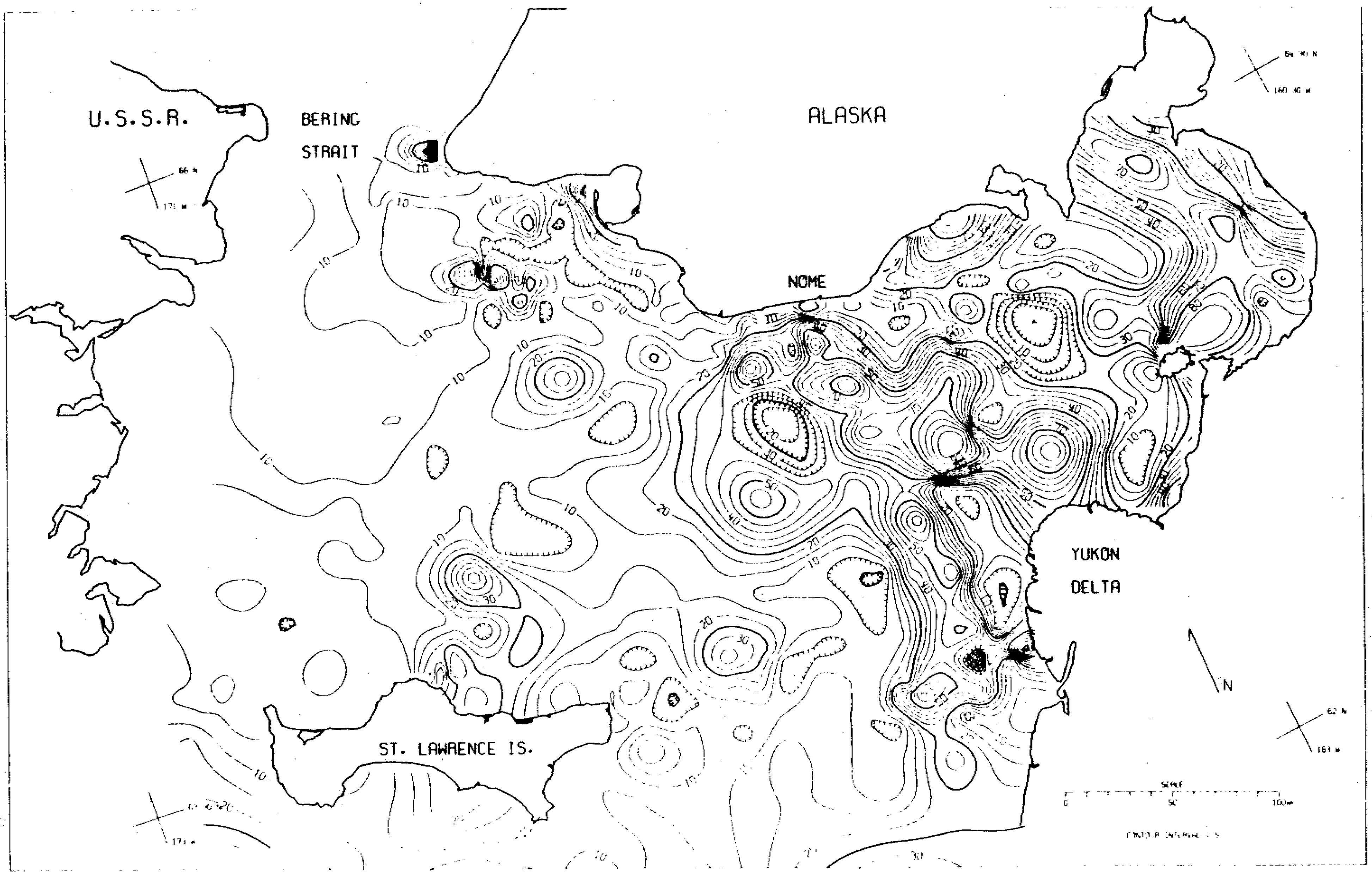

FIG. 12 % SILT IN SURFACE SEDIMENT OF NORTON BASIN, NORTHERN BERING SEA

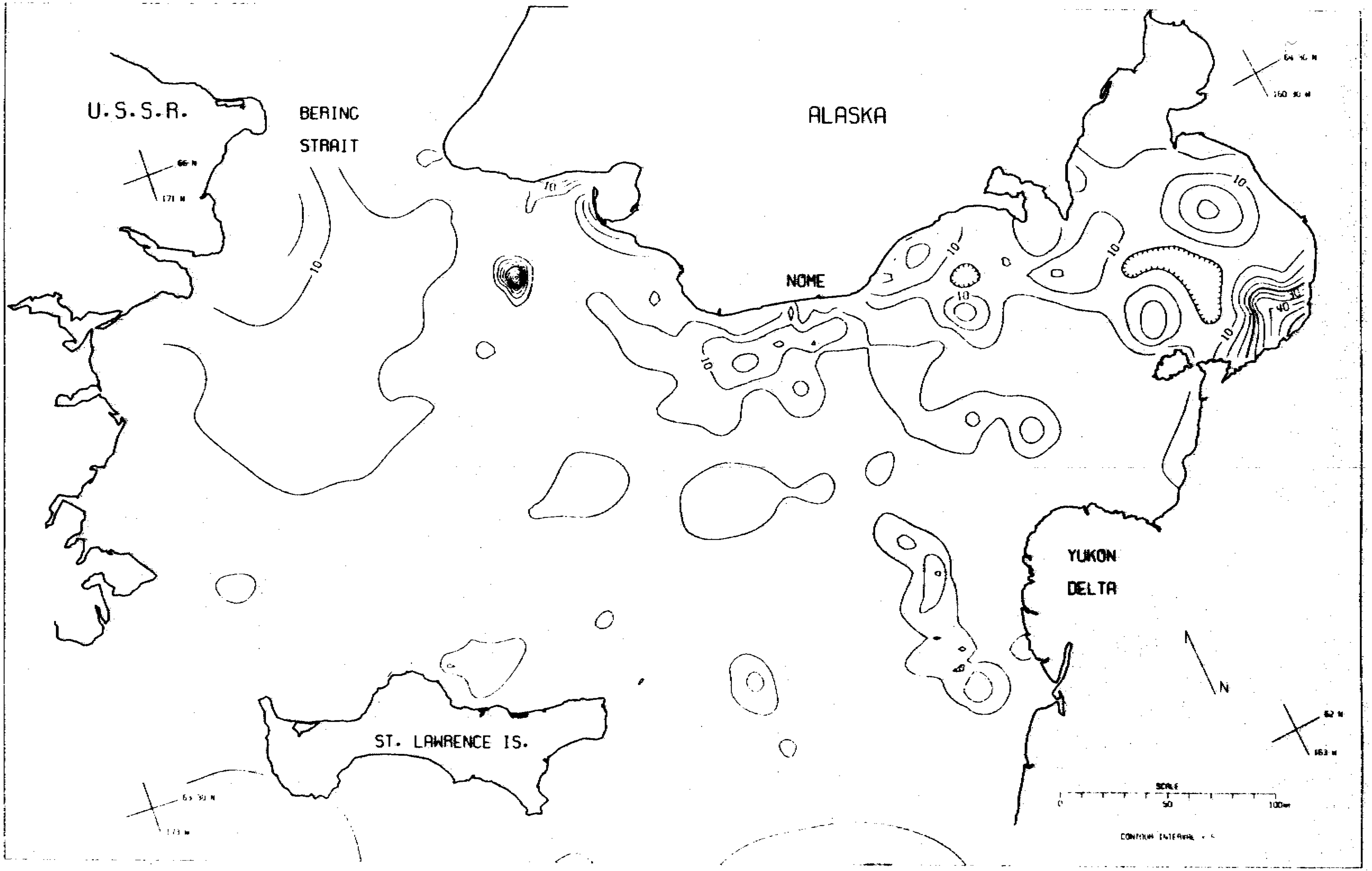

FIG. 13 % CLAY IN SURFACE SEDIMENT OF NORTON BASIN, NORTHERN BERING SEA

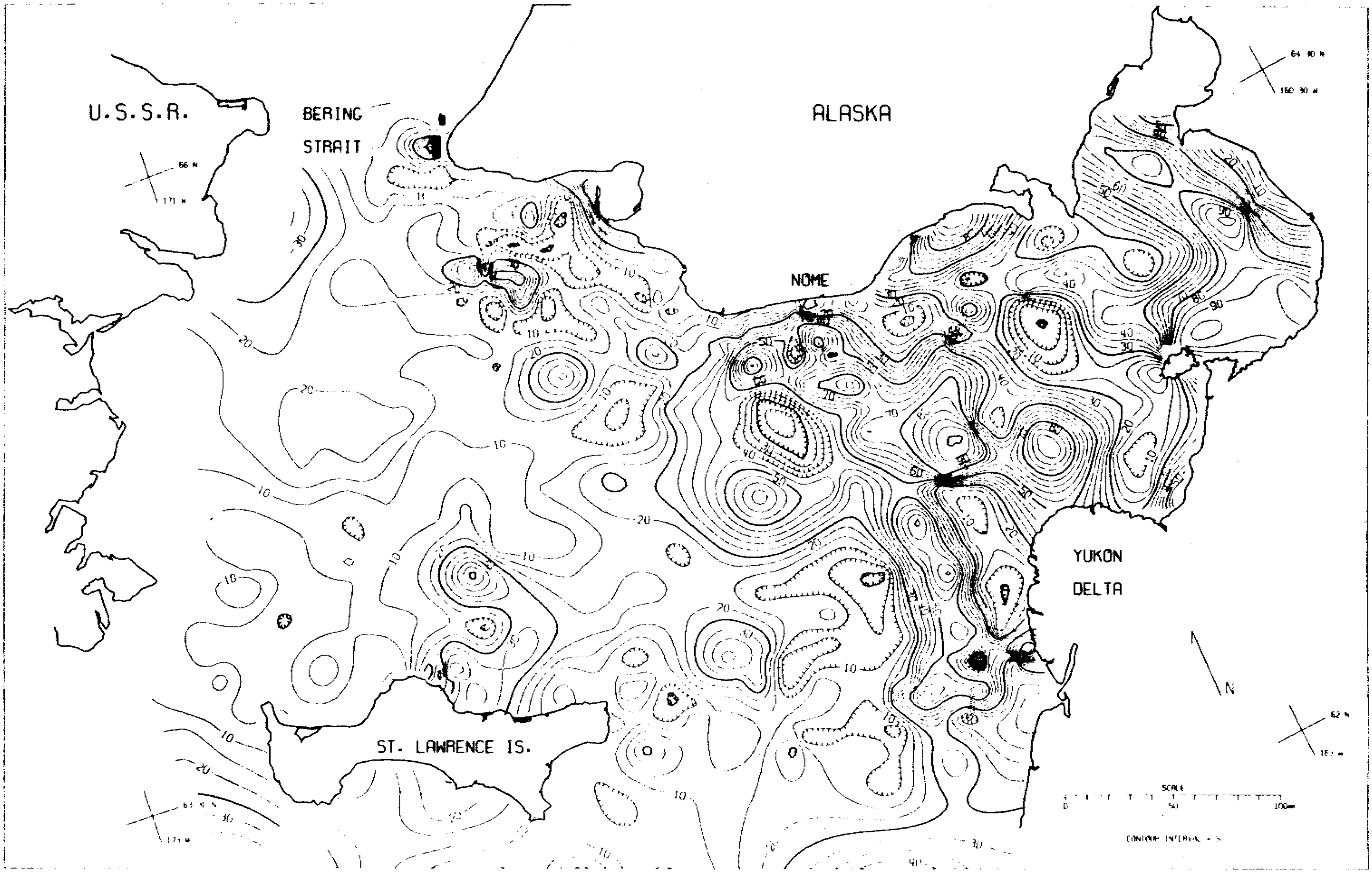

FIG. 14 % MUD IN SURFACE SEDIMENT OF NORTON BASIN, NORTHERN BERING SEA

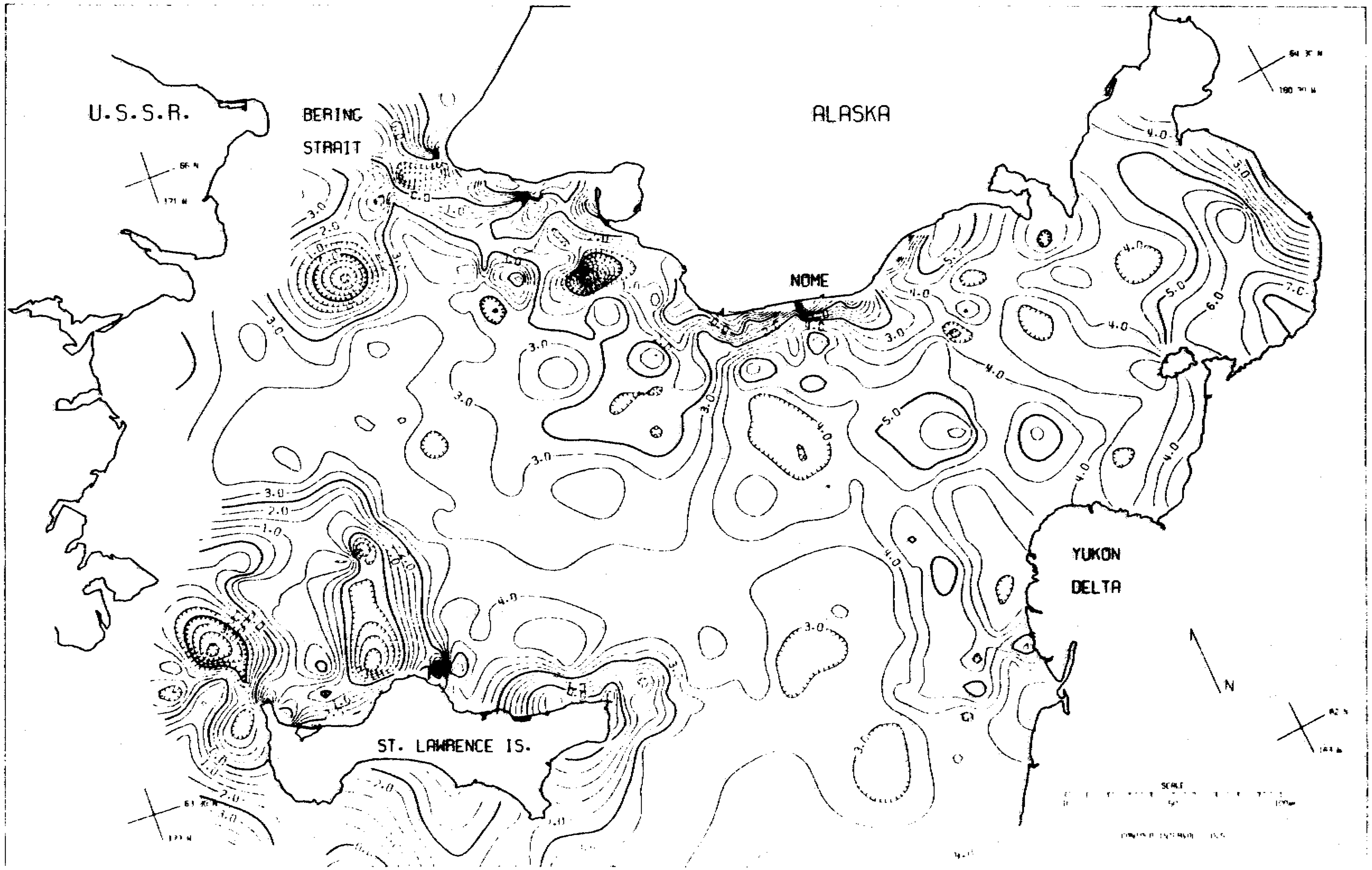

FIG. 15

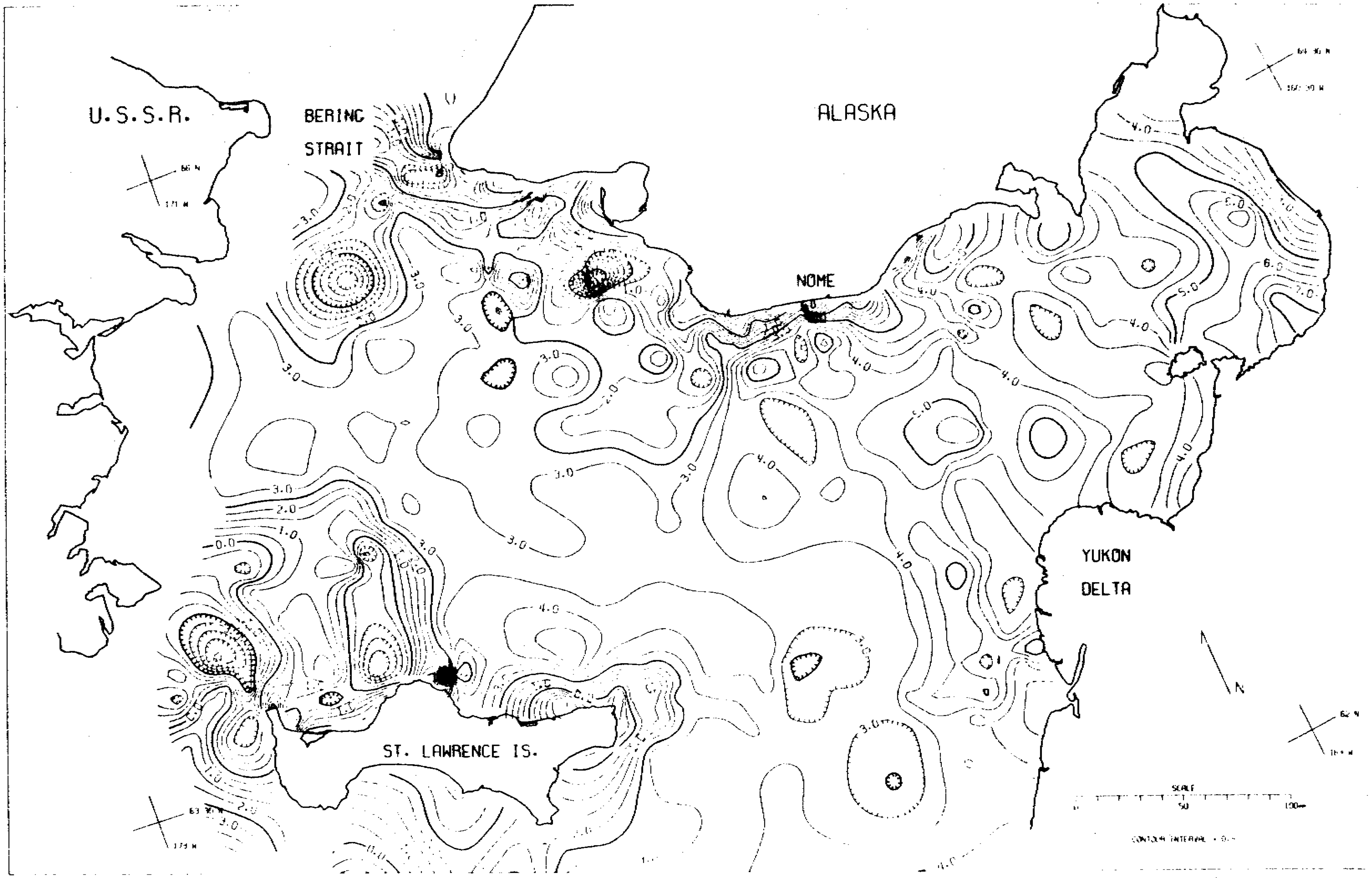

FIG. 16 MEAN GRAIN SIZE [illegible] SEDIMENT IN NORTON BASIN, NORTHERN BERING SEA

SUMMARY OF 1980 CRUISE RESULTS,

GEOHAZARD PROGRAM

Norton Basin-Chirikov Basin

and

SUMMARY OF SURFACE SEDIMENT CHARACTERISTICS

Norton Basin

by

Gordon R. Hess
Brad R. Larsen
C. Hans Nelson
Patrice Mango
Darrell Klingman

Published as the Appendix to the Annual Report for RU 429.

This report is preliminary and has not been edited or reviewed for conformity with Geological Survey standards and nomenclature.

PRELIMINARY
SUBJECT TO REVISION

NOAA ANNUAL REPORT to provide information for the draft environmental impact statement.

I. SUMMARY

More than 2300 km of high-resolution and deep-penetration seismic reflection profiling records were collected in Norton and Chirikov Basins. In addition, over 2400 km of side-scan sonar records were collected along these same tracklines. These data, collected in 1980, combined with data collected in previous years, provide the data base for evaluation of potential hazards in the northern Bering Sea. Previous papers and reports have discussed many of the hazards and areas of potential problems in offshore development.

This report in part presents a preliminary summary of the data collected in Chirikov Basin and in part augments reports previously prepared on Norton Basin. Potential geologic hazards discussed include gas-charged sediment, ice-gouging, areas of mobile bedforms, and zones of intense current scour.

<u>Sediment Instability</u> - Gas-charged sediment creates a potentially unstable surficial-sediment condition in Chirikov Basin (Clukey and others, 1978; Olsen and others, 1980; Clukey and others, 1980). Acoustic anomalies as identified on high-resolution and deep penetration seismic reflection records, occur throughout Chirikov Basin but are most prevalent in the eastern portion and decrease in abundance, continuity, and extent to the west. The presence of gas in the nearsurface sediment presents a possible hazard for any resource development activity in these areas. Any man-made structure penetrating the gas accumulation may provide direct avenues for gas migration to the sea floor. Gas-charged sediment also has a lower shear strength than gas-free sediment (Clukey and others, 1978). Rapid sediment collapse associated with gas venting may also pose a potential hazard to offshore structures and pipelines.

<u>Erosion and Deposition Hazards</u> - Ice gouging occurs throughout the northern Bering Sea beyond the shorefast zone, generally in 20 m or less of water but occasionally

in water depths of 30 m or more. Gouges are generally cut to 1 m depth or less and occur as single gouges and as numerous parallel furrows (raking). A heretofore unidentified zone of concentrated ice-gouging is located off the northeast end of St. Lawrence Island. Several other areas of isolated gouges are found throughout Chirikov Basin. Design of offshore facilities must take into account the scouring capability of ice.

Strong currents caused by storm waves, sea-level set-up, and constricted passages create migrating fields of mobile bedforms. The bedform field north of St. Lawrence Island, although already defined (Nelson and others, 1980), is shown to be more extensive than previously mapped.

Strong bottom currents are also associated with areas of bottom scour and scour depressions (Larsen, 1979) and irregular lag-covered sea floor. The straits west of St. Lawrence Island are the site of an extensive area of scoured sea floor and scour depressions. Sand movement associated with scouring and with the bedform fields present potential hazards to any underwater structures.

This NOAA Report not only summarizes the new cruise information of 1980 but is also accompanied by one U.S.G.S. Open-File Report and extracts from another in the process of being compiled. The complete U.S.G.S. Open-File Report provides numerous scientific reports on topical studies in the Norton Basin region. The extracts from the U.S.G.S. Open-File Report in preparation provide baseline information on textural and geochemical properties of the nearsurface sediment in Norton Basin and includes numerous computer-generated contour maps outlining much of this information.

Sediment texture in Norton Sound is shown to grade from silts in the inshore regions off the Yukon Delta to very fine sands in the more northerly and westerly parts of Norton Sound. The finest sediment is found in the eastern regions of Norton Sound. The complex mosaic of surface texture in Chirikov Basin is shown to result from coarser nearshore surface sediment interleaved with a widespread blanket of fine sand that covers the central areas of Chirikov Basin. Profiles from 15 selected Kiel vibracores taken on the 1980 cruise are presented to show the extent and thickness of the medium to fine sand layer in the Chirikov Basin (see Appendix A).

The map for organic carbon content in surface sediment, though limited in coverage, shows organic carbon concentrations highest near the Yukon Delta and grading off to less than 1 percent in northern Norton Sound and to the low average value of 0.2 percent in the western Chirikov Basin region of fine sand. At depth, the pre-Holocene sediment of the Late Pleistocene silts contain a high quantity of organic carbon.

Topical reports in the U.S.G.S. Open-File 80-979 provide information on several potential geological hazards as well as general information on the sedimentary history of the Norton Basin. The report by Thor and Nelson shows intense ice gouging along the shorefast ice edge and seaward in southern Norton Sound. This gouging penetrates up to 1 m beneath the sea-floor surface and can occur anywhere up to a depth of 30 m and is common in water 20 m deep or less. The study by Holmes and Thor (1980) on acoustic anomalies in potentially gas-charged sediments shows that anomalies are very common in the region of Norton Sound, whereas fewer and fewer anomalies are encountered towards the west as the Yukon mud blanket thins and transgressive sands cover the surface of the Chirikov Basin.

A study by Olsen and others (1980) indicates that geotechnical properties of semi-cohesive sediments in Norton Sound are affected by the gas content so that loose or less consolidated zones of sediment occur in the thicker Yukon mud near the delta and that more consistently consolidated sediment is found towards the north in Norton Sound and in the Chirikov Basin. The subsurface pre-Holocene sediment is even more highly overconsolidated because of its diagenetic history, except in regions where gas-charged sediment occurs such as in the numerous areas of shallow gas pockets and the local faulted regions over the large thermogenic gas cap 30 km south of Nome.

The study by Nelson (1980) on the history of transgressive sedimentation in Norton Sound provides the basic stratigraphic framework for nearsurface deposits in the Norton Basin region. This study shows that the oldest underlying sediment may be basement rock that occurs at the sea-floor surface in nearshore areas off the Seward Peninsula and off the northwestern region near St. Lawrence Island. Throughout most of Chirikov Basin, basal transgressive gravels and sands, generally a few centimeters thick, are overlain by fine inshore sand facies, varying from a few centimeters thick in much of the area to about 1 m thick.

In the Yukon delta region of Norton Sound a wedge of Holocene sediment is deposited which may be up to 12 m or more thick. In most of central and northern Norton Sound this Holocene sediment is only 1 to 2 m thick. In much of northern and central Norton Sound this is a homogeneous, bioturbated refined sand grading to coarse silt. In southern Norton Sound, towards the delta, there is an increasing quantity of interbedded sand deposited by storm surge events as described by Nelson. Major prograding sheets of sand are deposited up to 100 km from the modern Yukon lobate delta. The process suggested is one of a combination of liquefaction of the very fine sand-size Yukon deposits (see Clukey and others, 1980) in combination with strong bottom return flow currents from storm-surge ebb flow currents (see Cacchione and others, 1980, in this same topical Open-File).

This synergistic storm surge process has been described previously and may play an extremely important role in the sedimentary processes of the continental shelves and may provide a potential mechanism for scouring and rapid deposition which should be considered when planning for pipeline installations in such places as nearshore Norton Sound. Similarly, studies of gas-charged sediment, ice gouging, and geotechnical characteristics of Norton Basin sediments provide important baseline information in potential geologic hazards of the Norton Basin region.

II. INTRODUCTION

Surveys for potential geologic hazards on the northern Bering Sea floor have been conducted by the U.S.G.S. in preparation for leasing of the outer continental shelf (OCS) areas. Over 9000 km of high-resolution geophysical track lines have been run, hundreds of cores, grab samples, and photographs have been taken, and information has been gathered from current meters and hydrographic stations. In FY 1980, data collection was concentrated in the northwest Bering Sea, principally in the Chirikov Basin.

Processes related to sediment stability, erosion, and deposition all pose potential hazards to the development of offshore resources in northern Bering Sea. Thermogenic gas seepage, biogenic gas saturation, cratering of sediment, sediment liquefaction, ice gouging, current scouring, storm-sand deposition, and mobile bedform movement comprise the processes judged to be potentially hazardous.

The FY-1980 study was carried out to identify areas of shallow gas concentration, areas of mobile bedforms, to locate zones of active faulting, and to define areas of active ice gouging in Chirikov Basin. Shallow gas pockets are potentially unstable. Pipelines built across these areas may be unequally supported due to differences in sediment strength or due to actual liquefaction of the gas-charged sediment. Sediment collapse may be associated with escape of nearsurface gas, leaving pipelines or structures unsupported or exposed. Large-scale bedforms could subject pipelines to stress by leaving portions of the pipe unsupported during bedform migration. Potential for scour is highest in areas where bedforms exist. Scour is enhanced where artificial structures are emplaced and potentially hazardous undercutting may occur. Recent faulting implies direct hazard potential due to offset of the sea floor or severe shaking due to earthquakes may be associated with the fault movement. Ice gouging presents a hazard to exposed pipelines and other structures.

III. CURRENT STATE OF KNOWLEDGE

Explanation of past work:

Initial studies of seismic stratigraphy in this area were provided by Grim and McManus (1970) and similarly Nelson and Hopkins (1972) provided an initial study of the stratigraphy, sedimentary history, and nearsurface sediment. More detailed surface sediment composition and texture were provided by McManus and others (1970, 1974, 1977). A general summary of the Cenozoic stratigraphic framework and sedimentary history is provided by Nelson and others, (1974). Nelson and Creager (1977) describe the Holocene sedimentary history and dynamics of the Norton Sound region.

In 1976 the OCSEAP began collecting more nearsurface data on stratigraphy, sediments, high-resolution geophysics, geochemical, and geotechnical characteristics in Norton Basin. The high-resolution seismic data has been open-filed within several months after field work each season (Thor and Nelson, 1978; Nelson and others, 1978; Larsen and others, 1979).

The seismic stratigraphy has been used for numerous topical studies as has much of the sediment lithological, geochemical, and geotechnical information. Up to this point all of the seismic records have been put on microfilm and open-filed and are available to the public. Much of the geochemical information including major, minor, and trace element content in surface sediments of Norton Basin is available in Open-File (Larsen and others, 1980).

A U.S.G.S. Open-File on the physical characteristics of sediments in Norton Basin is in preparation. It condenses and selects information from a very broad sediment characteristics data base that includes thousands of statistical, geotechnical, geochemical, radiometric, and biological analyses of sediment samples collected over the past 20 years. The report will include computer-generated generated 2-dimensional contour and 3-dimensional perspective maps that display value surfaces depicting sediment composition, statistics, and organic carbon content. It will also include vibracore profiles that display geotechnical, stratigraphic and textural information (Larsen, and others, in press).

The broad data base of Norton Basin sediment analyses just described has provided information for the topical work completed over the past several years on the OCSEAP Program. These studies include several on the general hazards of gas-charged sediments (Nelson and others, 1978; Kvenvolden and others, 1979a, 1979b; Nelson and others, 1979). Research has also been completed on a major thermogenic gas seep (Cline and Holmes, 1977; Holmes, 1978) and biogenic gas cratering. Additional research has reported on scour depressions (Larsen and others, 1979). All of these topical studies have been summarized in short publications for potential users in the oil and gas industry (Thor and Nelson, 1979a, 1979b). A recent Open-File (Larsen and others, 1980) includes a number of topical studies that are now in press. The first of these is an updated summary of all hazard and sedimentary process work (Larsen and others, 1980). Work on geotechnical problems of potential instability was summarized in an article on geotechnical calculations suggesting liquefaction problems in the prodelta area (Clukey, 1980) and the regional geotechnical characteristics of sediments described by Olsen and others (1980). The hazards of shallow gas pockets, as shown by acoustic anomalies in high-resolution profiles is outlined by Holmes and Thor (1980). A summary of the potential hazards of ice gouging is given by Thor and others (1980) in this same report.

Basic information on the sedimentary stratigraphy provided by the new vibracore stratigraphy and in part by high-resolution profiling is summarized in a paper on transgressive history (Nelson, 1980). The necessary biostratigraphic information used to help construct the Late Pleistocene and Holocene stratigraphy is outlined in a paper by McDougall (1980). The importance of seasonality in sedimentary processes in the delta front platform and prodelta region off the modern Yukon lobate delta is described by Dupré (1980). The effects of these seasonal processes on the sedimentary history are recorded in the sedimentary structures and biogenic processes outlined by Howard and Nelson (1980). The nearsurface dynamics influencing sediment transport and especially sedimentary processes critical to the dynamics of mobile bedforms and storm-surge sedimentation are described by Cacchione (1980). Dynamics of the large mobile bedform region off Pt. Clarence are described in a paper by Nelson and others (1980). The unusual synergistic combination of instability provided by cyclic wave loading plus strong ebb flow currents of the major storm surges that occur periodically in the Norton Basin region are described in the storm sand sedimentation paper by Nelson (1980).

IV. STUDY AREA

Surveys conducted in FY 1980 concentrated on Chirikov Basin, that part of the northern Bering Sea north of St. Lawrence Island and south of the Bering Strait. Survey lines were confined to east of the 1867 U.S.-Russian convention border.

Previous studies (Hopkins and others, 1976; Grimm and McManus, 1970; Hopkins, 1973; McManus and others, 1974; Nelson and others, 1974) show the Chirikov Basin floor to be a complex result of tectonic, fluvial, glacial, and shallow marine processes. Shallow marine processes are actively modifying old features and forming new relief features and sedimentary environments.

Figure 1 shows the trackline coverage and sampling stations completed in FY 1980.

V. DATA COLLECTION AND COMPILATION

A. Geophysical data

Field operations in FY 1976, 1977, and 1978 concentrated on both reconnaissance studies in Norton Basin and on more detailed surveys which evolved from the reconnaissance studies. These topical studies focused on the sand wave fields west of Port Clarence, thermogenic gas seeps south of Nome, biogenic gas craters in central and eastern Norton Sound, and scour depressions west and northwest of the Yukon Delta.

The 1980 cruise concentrated on a broad reconnaissance survey of Chirikov Basin to collect high-resolution geophysics and side-scanning sonar records. A few vibracores and TV and bottom camera stations were also occupied to aid stratigraphic analysis and to add sediment data to the baseline study of northern Bering Sea sedimentation. Additional sampling and geophysics were done at some of the topical study areas.

The R/V S.P. Lee was utilized to conduct gheophysical and geological studies in Norton Sound and Chirikov Basin in August 1980. Acoustic profiling systems used included single channel airgun, uniboom, 3.5 kHz, and 12 kHz subbottom profilers. Side-scan sonar records were collected along most ot the tracklines using an E.G. & G. SMS-960 digital side-scan system. This system provides records corrected for slant-range distortion and ship speed variation. The side-scan data were also recorded on magnetic tape for possible replay.

All seismic records, side-scan records, and navigation tracklines are copied on microfilm and will be available as open-file reports. Core profiles of 15 Kiel vibracore samples are presented in this report to display down-core stratigraphy and sedimentation. The final DEIS report to NOAA will contain core profiles for all cores collected on the 1980 cruise. These profiles will display all sediment analyses work done up to that time; to include textural, geochemical and geotechnical information.

Navigation:

Navigation information was provided by a Motorola satellite navigation system with integrated Loran-C and inputs from ship's speed log and gyro. Dead-reckoned positions were calculated and displayed on a teleprinter. Satellite determined positions were also printed out and provide the best position determination. All navigation data are stored on magnetic tape. Positions were plotted every 15 minutes or more frequently during maneuvers. The performance of the system was handicapped by a faulty satellite which caused the computer to malfunction and by the close proximity of the Loran-C master station at Port Clarence. Notation of major course and speed changes was kept in a handwritten navigation log. Radar and line-of-sight fixes were used to augment the integrated navigation system. Navigation accuracy is probably $\pm$150 m.

Updated navigation plots were produced following completion of the cruise. The Honeywell-Multics computer system was used to generate plots of satellite and dead-reckoned positions. Post-cruise processing included editing of bad positions, smoothing between plotted positions, and use of written navigation logs to fill in gaps in the computer plotted navigation.

Geophysical methods:

Figure 2 shows which acoustic systems were in operation along the tracklines for the 1980 field operations. Seismic profiling and side-scan operations were conducted at speeds of 4-7 knots depending on weather conditions, sea state, and the nature of data being collected.

Singe channel airgun. A Teledyne single channel streamer was used in conjunction with an array of two 40 cubic inch air guns to collect single channel seismic reflection data. The signals were processed through a Teledyne amplifier and printed on a Raytheon recorder. Filters were set at 25-98 Hz., firing rate was 4 seconds with a 1- or 2-second sweep rate. Records were annotated at 15 minute intervals with date, time, water depth, and line number. Changes in course, speed, or instrument setting were noted when they occurred.

Uniboom. A hull-mounted E.G.& G. uniboom system of four transducer plates and a towed E.G.& G. hydrophone streamer as a receiver were used to collect high-resolution records. Records were printed on a Raytheon recorder after filtering through a Krohn-Hite amplifier. Time marks were made at 5-minute intervals with detailed annotation every 15 minutes. Sweep rate was 1/4 second and firing rate was 1/2 second.

3.5 and 12 kHz. These records were collected continuously during underway and station operations. Hull-mounted transducer and receiver arrays are used in both systems. Sweep and fire rates of 1/4 second were normally used. Annotation was similar to that of the uniboom records.

Side-scan sonar. An E.G.&.G. SMS-960 digital side-scan sonar provided generally good quality data along the reconnaissance tracklines. Scales were normally set at 100 m to either side of the fish path but 200 m was occassionally used. An instrument altitude of 5 to 7 m was maintained as closely as possible. In addition to the analog record, data were also recorded on magnetic tape. The side-scan was operated simultaneously with the other seismic systems with no adverse effects.

B. Geologic Data

The sediment characteristics maps in this report are compiled from analyses on over 467 sediment cores and grab samples collected from Norton Basin over the past twenty years (see Fig.3). The samples were collected on 15 different cruises in the years 1960, 1961, 1967, 1968, 1969, 1970, 1976, 1977, and 1978. Detailed size analyses on cores collected in 1980 are not yet available. Grain size analyses on 250 surface grab samples were provided by the University of Washington, analyses on 77 surface grab samples came from Woods Hole Oceanographic Institute, and 11 Kiel Vibracores were analyzed for their grain size distributions at Rice University. The remainder of the samples which include Van Veen grabs, box cores and vibracores were analyzed with equipment located at the Branch of Marine Geology, U.S.G.S., Menlo Park, California. A variety of techniques were used including sieves and settling tubes for the coarse fraction, and hydrometer, pipette and hydrophotometer for the fine size fraction. These various techniques were used in different combinations at different times. As a consequence the data are mixed and non-synoptic and therefore, can't be expected to yield more than a general approximation to exact present-day sediment distribution.

The common denominator, however, is that all the data, whether it was in the form of size-fraction weight percents, size-fraction cummulative weight percents, or size-fractions weights, were run through the same computer program (SDSZ) to generate or re-generate grain-size distribution breakdowns and statistics. The data generated by SDSZ were then added to a large sediment characteristics data base from which computer plots were made using the Surface Display Library computer graphics system. The resulting maps, employing greater sample station coverage, are meant to be an extension and refinement of maps generated earlier by McManus and others at the University of Washington. McManus et al. treat sediment source, provenance, distribution, destination, heavy minerals, and statistical characteristics in great detail in U.S.G.S. Professional Paper 759-C, and in a final report to the U.S.G.S. in 1970.

Caution should be used in interpreting contoured data. Contours may imply a gradation in value from one area to the next that does not exist. In general, areas of relatively close-spaced contours are suspect and may represent simply a sharp boundary between widely different sediment types.

VI. RESULTS

A. Geophysical Surveys

Moderate- and high-resolution reflection profiling records show nearsurface acoustic anomalies throughout the Chirikov Basin. One type of anomaly consists of a sharp reduction in subbottom reflectors and a very weak multiple indicating complete absorption of the acoustic energy. Another type of acoustic anomaly is characterized by loss of subbottom reflectors but very strong surface multiple, seen lower in the record. This type of anomaly is generated by a highly reflective sea floor (Nelson and others, 1978). Side-scan records over the tracklines along which this second type of anomaly occurs show a patchy, rough or "bouldery" pattern. Isolated sand waves are also seen on the margins of these rough stretches.

The first type of acoustic anomaly is judged to be produced by peat and/or gas-charged sediment that acts as an acoustic sponge absorbing all reflective energy. The occurrence of reflector-termination acoustic anomalies in conjunction with high gas content sediment in eastern Norton Sound (Nelson and others, 1979) makes it reasonable to relate similar anomalies to gas-charged sediment in Chirikov Basin. Reflector terminations and acoustic anomalies occur as kilometers-long features and as short, discrete features. Both are seen in Chirikov Basin (Fig. 4). Long, continuous stretches of anomaly diminish in abundance west and north in the basin. The most extensive and continuous anomaly zone is located just north and east of St. Lawrence Island. The central and northern areas of the basin are nearly void of any acoustic anomalies.

The second anomaly type and associated sea-floor features are seen in western Chirikov Basin along lines 47 and 48 (Figs. 1 and 4). The airgun profiling system shows a somewhat less extensive area of this anomaly type than that indicated by the uniboom or 3.5 kHz records. The greater power of the airgun system is probably capable of seeing through part of the high reflectivity bottom.

Bedforms are observed in scattered locales in Chirikov Basin. The aforementioned sandwaves associated with rough, highly reflective sea floor are the only extensive area of bedforms. Other scattered occurrences are identified on Figure 5. The large sand wave field west and south of Nome was seen on several tracks across the area as was the previously identified sand wave field west of Port Clarence.

An extensive area of concentrated ice-gouging was seen on several tracks in southeast Chirikov Basin just east of St. Lawrence island (Fig. 6). The general trend of these gouges is north-south but northwest-southeast sets are also seen.

B. Sediment analysis

The silt map of this report (Fig. 7, also 8) is generally the same as McManus' silt map but with some differences in coverage and configuration due to more complete sample coverage in this report but possibly due in part to actual differences in the extent of each distinct sediment type.

This report shows silt concentrations in lobes just off the north central coast of St. Lawrence Island, 60 km due east of the NE Cape of St. Lawrence Island, in the area surrounding King Island, in areas off Nome and Bluff, and in a wide arc surrounding the Yukon Delta that fingers off in the direction of the Bering Strait, similar to the silt distribution pattern shown by McManus. But additionally, Fig. 8 shows a greater silt concentration east of Stuart Island and just west of Cape Prince of Wales than McManus shows. Also, in contrast to the dearth of silt in a large elongate lobe trending EW in northern Norton Sound, as shown in McManus' map, the same area in this report appears broken up into smaller silt-free areas and exhibits a more northerly incursion of the Yukon River silt into the area. Perhaps the most striking difference between the two maps is what appears to be a disruption of the NW trending extensions of the Yukon River silt as shown in McManus' map by large NNE trending sand lobes (see Fig. 9, also 10). These sand-dominated areas are defined by post-1974 samples (i.e., mostly 1976 samples). The great storm surge of 1974 (Fathauer, 1975) was in a NNE to NE direction and it is suggested that these two lobes, centered 20 and 80 km west of the Yukon Delta, may be residual effects of this storm event and could thus give some indication of just how changeable the surface sediment coverage in shallow water shelf environments can be over a relatively short period of time and under the influence of major storms. The actual change in sediment coverage of this area may be much greater than indicated by the few recent samples because they simply supplement or overlay the older sample assemblage which would tend to mask recent changes in sediment type. Also, these sand lobes, in so far as they are storm-surge related, probably represent either an encroachment of sand onto an area formerly dominated by Yukon silt - or they might simply be storm lag deposits.

The mud map (Fig.11, also 12) is simply an amplification of the silt map, because it represents all of the fine-sized material.

The clay map (Fig. 13, also 14) generally shows clay content below 5% but with scattered lobes as high as 10 to 20%. Significant clay concentrations are found in the SE corner of Norton Sound and in an area centered on King Island. King Island is an exposed granitic-like stock and thus may be a source of minerals readily weathered to clay. The source of the very high clay content in SE Norton Sound is due to one sample collected in 1961 from the vessel Northwind. It is flanked by two more recent samples within 20 km distance that have only 11 to 12% clay content. The EW trending lobes of high and low clay content in northern Norton Sound as shown in McManus' map are disrupted on our plot which includes data from a more recent, closely-spaced sampling. This change either reflects greater variability in the actual extent of the clay coverage outlined by McManus or perhaps indicates changes through time in the coverage.

The sand map shows a distribution pattern complementary to the silt-clay or gravel distribution maps. Noticeable sandy areas or shoals are observable in central and western Shpanberg Strait, eastern Bering Strait, north-central and northeast Norton Sound, west of Stuart Island, south of St. Lawrence Island, in a shoal west of the mouth of the Yukon River, and uniformly distributed over much of Chirikov Basin. Rather striking differences between the map in this report and McManus' map are to be found in the enlarged central Shpanberg Strait shoal which gives the appearance of encroaching on the formerly Yukon River silt domain in a NNE direction, the Yukon River mouth shoal which extends in the same NNE direction over Yukon River silt, and in the high percentage of sand appearing in almost a NS axis in central Norton Sound. As suggested above, these differences may in part reflect changes in sediment distribution wrought by the great storm surge of 1974.

The gravel map of this report (Fig. 15, also 16) shows a gravel distribution pattern very close to that depicted by McManus, and, as he points out, the pattern largely represents residual glacial outwash and morainal debris as well as material derived from bedrock and alluvium deposits (McManus, and others, 1977).

The mean sediment grain size distribution in Norton Basin was determined using the method of Folk and Ward and by calculating the first moment parameter for each sediment sample. The maps displaying these values are virtually identical (Figs. 17 and 18) and the values depicted represent an entire sample not just the sand fraction. Inspection reveals that these maps are composites of the areas of maximum content of each sediment type. This means that the contour configurations of areas corresponding to those areas of concentrated gravel, sand, silt, and clay will be almost identical. Once again, caution should be used in the interpretation of these maps. Apparent transition or grading from one average grain-size to another may not be real, but strictly a function of the contour interval and the contouring technique. This is especially probable in areas of close contours where more abrupt changes from one sediment type to another may be the actuality.

The maps show the areas of concentrated Yukon River silt to be largely coarse silt. This pattern is interrupted however, by very fine sand coverage just west of the Yukon Delta and along a north-south axis dividing Norton Sound. Eastern Norton Sound shows a gradation of coarse to fine silt in an eastward direction. Shpanberg Strait is dominated by fine to very fine sand, whereas central Chirikov Basin is covered by sediment with an average size in the coarse end of the very fine sand-size range. Two large areas of medium to fine sand are centered 50 km west of Cape Rodney and 45 km NW of the northern tip of St. Lawrence Island. The coarsest sediment corresponds approximately to those areas on the gravel map previously discussed.

The map showing a plot of the sediment modal classes (Fig.19) is very similar to the mean grain-size map but in general shows values on the average of 1/2 Ø interval coarser than the values displayed on the mean-grain-size maps.

The sorting maps (Figs. 20 and 21) show that most of Norton Basin sediments are poorly to very poorly sorted. Extremely poorly sorted sediment is found on the south coast of the eastern end of Seward Peninsula and very poorly sorted sediment is found generally in the areas of high gravel content. Much of Chirikov Basin sand as well as Norton Sound silt are poorly sorted. Extremely well-sorted sediment generally coincides with those areas with 90% or greater amounts of sand, notably the very fine sand off the western edge of the Yukon Delta, the sandy areas in Shpanberg Strait, an extensive area 50 km north of NE Cape on St. Lawrence Island, the patchy areas of central Norton Sound, and in the ridge and swale area west of Port Clarence. McManus says many of the very well-sorted patchy areas correspond to 20 and 34 meter depths on various shoals in the area and could possibly be relict beach sands.

These same areas of well-sorted, concentrated sand are actually shown by the modal class map to be coarser than the mean-grain-size map indicates, i.e., they are generally in the fine-size range. This fits with the observation based theoretically on the Hjulstrom Diagram that it is the fine-sand range that is most susceptible to sorting (Blatt et al., 1972). The same considerations would explain why fluvially derived silt is generally poorly sorted.

The skewness map (Fig.22) shows the sediments of Norton Basin to be moderately skewed in the positive direction which means that the distributions tail off somewhat in the fine-size direction. The average skewness value range of 0.4 to 0.8, coupled with generally poor to very poor sorting indices may indicate that sediments in this particular type of shelf environment are characteristically rather poorly sorted and somewhat positively skewed. It is possible that these particular statistical characteristics are more directly related to the fairly recent fluvial origin of most Norton Basin sediments. According to Blatt, et al., (1972) river sands are usually positively skewed and moderately to poorly sorted.

There is a modest visual correlation between low or negative skewness values (approximately 0.2) and areas of very well-sorted sediment. This is another indication that these areas may be relict beach deposits because beach sands are generally negatively skewed and well sorted (Blatt et al., 1972). An exception to this possibility would be the area with the most negative skewness value located 50 km NW of the north tip of the Yukon Delta. Sediment here is also very well sorted but it is predominantly coarse silt which rules out a beach origin. The most positive skewness value was in sediment in the Bering Strait. Sorting is not too good here and the existence of almost continually high current speeds in a northward direction may simulate a quasi-fluvial environment.

The kurtosis map (Fig. 23, also 24) is included as an item of possible interest but without comment.

The percent organic carbon map (Fig. 25) is limited in its definition of the carbon distribution in surface sediment of Norton Basin due to a lack of analyses throughout most of the region. It can be seen that organic carbon concentrations as high as 2.5% are found in sediment close in to the western edge of the Yukon Delta and that relatively high concentrations are found in a halo around the Delta and throughout the area of Yukon River sediment distribution. These values tail off to a background of 0.2% in a direction away from the delta. The background value of 0.2% is confirmed by similar values from the central Chirikov Basin. It is also apparent that organic carbon is concentrated in nearshore sediments, undoubtedly reflecting the large amount of organic detritus usually found in fluvial runoff.

VIII. Discussion

Since the first discussion of bubble-phase gas in nearsurface sediment (Cline and Holmes, 1977) several detailed studies of deep-penetration and high-resolution seismic reflection records (Holmes and Cline, 1978; Nelson and others, 1978; Holmes, 1979) have shown the widespread distribution of acoustic anomalies. An additional 2300 km of single-channel airgun records and uniboom records were collected in Chirikov Basin in 1980.

The distribution of acoustic anomalies (Fig. 4) suggests that they are most common in eastern Chirikov Basin and decrease in abundance to the west. This westerly decrease was suggested by Holmes (1979) to be caused by the differing nature of Quaternary deposits in western Chirikov Basin. The glacial and glacio-marine sediment of western Chirikov Basin does not have a high potential for biogenic gas generation because growth of tundra derived peats was not possible (Holmes, 1979). Holmes also suggests that the thinner

Tertiary section beneath Chirikov Basin has not attained sufficient thickness to subject the basal sediment to the thermogenic levels necessary to generate hydrocarbon gases. We would further add that the generally sandier sediments of western Chirikov Basin do not trap gas as readily as the finer sediment in eastern Chirikov Basin. The acoustic anomalies in eastern Chirikov Basin pose a potential hazard to pipeline crossings and to penetration by structures.

More than 2300 km of side-scan sonar survey lines were run in Norton Basin and Chirikov Basin to identify bedform and ice-gouge features. Major areas of mobile bedforms throughout Norton Basin and Chirikov Basin have been identified and described (Nelson and others, 1980; Hunter and others, 1980). Survey lines run in 1980 identify no large areas of bedforms that have not been identified before. The large area of bedforms north of St. Lawrence Island was mapped and defined in greater detail and found to be more extensive in area than previously determined. Scattered, isolated, bedform fields were seen on rare occasions throughout Chirikov Basin. An area of intensive scouring was reconfirmed off the west end of St. Lawrence Island. The large bedform field west of Port Clarence, the area of previously concentrated study (Nelson and others, 1980), was also briefly surveyed. This extensive bedform field is judged to pose a potential hazard but the scattered small fields throughout the basin do not.

The most significant area of sea-floor activity is the area of intense ice gouging northeast of St. Lawrence Island. Ice gouging occurs in this area due to concentration of ice as it is diverted around St. Lawrence Island. Isolated ice gouges are seen at various locations in Chirikov Basin and do not appear to be as rare as previously thought.

The sediment characteristics maps by and large are similar to those in U.S.G.S. Professional Paper 759-C. The differences between these two sets of maps reflect either the more extensive sample coverage used by this report or actual changes in surface sediment coverage in Norton Basin over the time between the sampling used for each report. One possible cause of change in sediment coverage may be major storm events such as the one in 1974. Such an event may move sand into an area or winnow silt out to leave sand lag deposits. Sand concentrations greater than that shown by McManus appear in three general areas: in a north-south axis in central Norton Sound, just west and northwest of the Yukon Delta, and in a lobe extending from central Shpanberg Strait into western Norton Sound. Gravel distribution remains essentially the same as described by McManus. The silt coverage is almost the inverse of the sand distribution and reflects the same changes.

Insofar as these differences reflect actual changes in sediment coverage, they portray the dynamic and potentially hazardous nature of a shallow-shelf environment, especially during major storms.

References Cited

Blatt, H., Middleton, G., and Murray, R., 1972, Origin of Sedimentary Rocks, Englewood Cliffs, N.J., Prentice-Hall, 634 p.

Cacchione, D.A., and Drake, D.E., and Wiberg, P., 1980, Velocity and bottom-stress measurements in the boundary layer, outer Norton Sound, Alaska, in Larsen, M.C., Nelson, C.H., and Thor, D.R., Geological, geochemical, and geotechnical observations on the Bering Shelf, Alaska, U.S.G.S. Open-File Report 80-979.

Cline, J.D., Holmes, M.L., 1977, Submarine seepage of natural gas in Norton Sound, Alaska: Science, v. 198, p. 1149-1153.

Clukey, E.C., Nelson, C.H., and Newby, J.E., 1978, Geotechnical properties of northern Bering Sea sediment, U.S.G.S. Open-File Report 78-408.

Clukey, E.C., Cacchione, D.A., and Olsen, H.W., 1980, Liquefaction potential of the Yukon prodelta: Proceedings of the Offshore Technology Conference, Houston, Texas, 1980, Paper no. 3773, in press.

Duprè, W.R., 1980, Seasonal variations in deltaic sedimentation on a high-latitude epicontinental shelf in S.C. Nio, R.T. Schattenhelm, and T.C.E. Van Weering, eds., IAS Special Publication, London, Blackwell Science Publications (in press)

Fathauer, T.F., 1975, The great Bering Sea storms of 9-19 November, 1974: Weatherwise Magazine, American Meteorological Society, v. 28, p. 76-83.

Grim, M.S., and McManus, D.A., 1970, A shallow seismic-profiling survey of the northern Baring Sea: Marine Geology, v. 8, p. 293-320.

Holmes, M.L., 1979b, Distribution of gas-charged sediment in Norton Sound and Chirikov Basin, in C.H. Nelson, D.R. Thor, and M.C. Larsen, Faulting, sediment instability, erosion, and depositional hazards of the Norton Basin seafloor, Annual Report of Principal Investigators for the year ending March 1979, Environmental Research Laboratory, Boulder, Colorado, NOAA, U.S. Dept. of Commerce, p. B1-B16.

Holmes, M.L., Cline, J.D., and Johnson, J.L., 1978, Geologic setting of the Norton Basin gas seep, Proceedings of Offshore Technology Conference, Houston, Texas, OTC Paper no. 3051, p. 73-80.

Holmes, M.L., and Thor, D.R., 1980, Distribution of gas-charged sediment in Norton Basin, northern Bering Sea, in Larsen, M.C., Nelson, C.H., and Thor, D.R., Geological, geochemical, and geotechnical observations on the Bering shelf, Alaska, U.S.G.S. Open-File Report 80-979.

Hopkins, D.M., 1973, Sea-level history in Beringia during the past 250,000 years, Quat. Res., v. 3, p. 520-540.

Hopkins, D.M., Nelson, C.H., Perry, R.B., and Alpha, T.R., 1976, Physiographic subdivisions of the Chirikov Basin, northern Bering Sea: U.S. Geological Survey Professional Paper 759-B, 7 p.

Howard, J.D., and Nelson, C.H., 1980, Sedimentary structures on a delta-influenced shallow shelf, Norton Sound, Alaska, in Larsen, M.C., Nelson, C.H., and Thor, D.R., Geological, geochemical, and geotechnical observations on the Bering Shelf, Alaska, U.S.G.S. Open-File Report, 80-979.

Hunter, R., and Thor, D.R., and Swisher, M.L., 1980, Depositional and erosional features of the northeastern Bering Sea inner shelf, in: Larsen, M.C., Nelson, C.H., and Thor, D.R., Geological, geochemical, and geotechnical observations on the Bering Shelf, Alaska, U.S.G.S. Open-File Report, 80-979.

Kvenvolden, K.A., Nelson, Hans, Thor, D.R., Larsen, M.C., Redden, G.D., Rapp, J.B., and Des Marais, D.J., 1979a, Biogenic and thermogenic gas in gas-charged sediment of Norton Sound, Alaska: Proceedings Offshore Technical Conference, Paper No. 3412.

Kvenvolden, K.A., Weliky, K., Nelson, C.H., and DesMarais, D.J., 1979b, Submarine seep of carbon dioxide in Norton Sound, Alaska: Science, v. 205, p. 1264-1266.

Larsen, M.C., Nelson, C. H., and Thor, D.R., 1979, Continuous seismic reflection data, S9-78-BS cruise, northern Bering Sea: U.S. Geological Survey Open File Report 79-1673, 7 p.

Larsen, M.C., Nelson, C.H., and Thor, D.R., 1979, Geologic implications and potential hazards of scour depressions on Bering shelf, Alaska: Environmental Geology, v. 3, p. 39-47.

Larsen, M.C., Nelson, C.H., and Thor, D.R., 1980, Geological, geochemical, and geotechnical observations on the Bering Shelf, Alaska, U.S.G.S. Open-File Report, 80-979.

Larsen, M.C., Nelson, C.H., and Thor, D.R., 1980, Sedimentary processes and potential hazards on the sea floor of northern Bering Sea, in Larsen, M.C., Nelson, C.H., and Thor, D.R., Geological, geochemical, and geotechnical observations on the Bering Shelf, Alaska, U.S.G.S. Open-File Report 80-979.

Larsen, B.R., Nelson, C.H., Heropoulos, C., and Patry, J., 1980, Distribution of trace elements in bottom sediment of northern Bering Sea, U.S. Geological Survey Open-File Report 80-399A, 122 p.

Larsen, B.R., Nelson, C.H., Heropoulos, C., and Patry, J., 1980, Map-plots and value/location lists of trace element concentrations in northern Bering Sea bottom sediment, U.S. Geological Survey Open-File Report 80-399B, microfiche.

McDougall, K., 1980, Microfaunal analysis of late Quaternary deposits of the northern Bering Sea, in Larsen, M.C., Nelson, C.H., and Thor, D.R., Geological, geochemical, and geotechnical observations on the Bering Shelf, Alaska, U.S.G.S. Open-File Report, 80-979.

McManus, D.A., Venkatarathnam, K., Echols, R.J., and Holmes, M.L., 1970, Bottom samples and seismic profiles of the northern Berng Sea and associated studies, U.S. Geological Survey, Office of Marine Geology Final Report, Contract No. 14-08-0001-11995, 115 p.

McManus, D.A., Venkatarathnam, K., Nelson, C.H., and Hopkins, D.M., 1974, Yukon sediment on the northernmeost Bering Sea shelf, Journal of Sedimentary Petrology, v. 44, p. 1052-1060.

McManus, D.A., Kolla, V., Hopkins, D.M., and Nelson, C.H., 1977, Distribution of bottom sediments on the continental shelf, northern Bering Sea: U.S. Geological Survey Professional Paper 759-C, 31 p.

Nelson, C.H., and Hopkins, D.M., 1972, Sedimentary processes and distribution of gold in the northern Bering Sea, U.S.G.S. Professional Paper 689, 27 p.

Nelson, C.H., Hopkins, D.M., and Scholl, D.W., 1974, Tectonic setting and Cenozoic sedimentary history of the Bering Sea, in Y. Herman, ed., Marine Geology and Oceanography of the Arctic Seas, New York, Springer-Verlag, p. 119-140.

Nelson, C.H., and Creager, J.S., 1977, Displacement of Yukon-derived sediment from Bering Sea to Chukchi Sea during the Holocene: Geology, v. 5, p. 141-146.

Nelson, C.H., Holmes, M.L., Thor, D.R., and Johnson, J.L., 1978, Continuous Seismic reflection data, S5-76-BBS cruise, northern Bering Sea: U.S. Geological Survey Open File Report 78-609, 6 p.

Nelson, C.H., Thor, D.R., Sandstrom, M.W., and Kvenvolden, K.A., 1978, Modern biogenic gas-generated craters (sea-floor pockmarks) on the Bering shelf, Alaska: Geological Society of America Bulletin, v. 90, p. 1144-1152.

Nelson, C.H., 1980, Graded storm sand layers from the Yukon prodelta, Bering sea, in Larsen, M.C., Nelson, C.H., and Thor, D.R., Geological, geochemical, and geotechnical observations on the Bering Shelf, Alaska, U.S.G.S. Open-File Report, 80-979.

Nelson, C.H., 1980, Late Pleistocene-Holocene transgressive sedimentation in deltaic and non-deltaic areas of the Bering epicontinental shelf, in Larsen, M.C., Nelson, C.H., and Thor, D.R., Geological, geochemical, and geotechnical observations on the Bering Shelf, Alaska, U.S.G.S. Open-File Report, 80-979.

Nelson, C.H., Duprè, W.R., Field, M.E., and Howard, J.D., 1980, Linear sand bodies in the Bering Sea epicontinental shelf, in Larsen, M.C., Nelson, C.H., and Thor, D.R., Geological, geochemical, and geotechnical observations on the Bering Shelf, Alaska, U.S.G.S. Open-File Report, 80-979.

Olsen, H.W., Clukey, E.C., and Nelson, C.H., 1979, Geotechnical characteristics of bottom sediments in the northern Bering Sea, in Larsen, M.C., Nelson, C.H., and Thor, D.R., Geological, geochemical, and geotechnical observations on the Bering Shelf, Alaska, U.S.G.S. Open-File Report, 80-979.

Thor, D.R., and Nelson, Hans, 1978, Continuous seismic reflection data. S5-77-BS cruise, northern Bering Sea: U.S. Geological Survey Open File Report 78-608, 8 p.

Thor, D.R., and Nelson, C.H., 1979a, A summary of interacting surficial geologic processes and potential geologic hazards in the Norton Basin, northern Bering Sea: Proceedings Offshore Technical Conference, Paper No. 3400, p. 377-381.

Thor, D.R., and Nelson, C.H., 1979b, A summary of interacting surficial geologic processes and potential geologic hazards in the Norton Basin, northern Bering Sea: Journal of Petroleum Technologists, March 1980, p. 355-362.

Thor, D.R., and Nelson, C.H., 1980, Ice gouging on the subarctic Bering Shelf, in: Larsen, M.C., Nelson, C.H., and Thor, D.R., Geological, geochemical, and geotechnical observations on the Bering Shelf, Alaska, U.S.G.S. Open-File Report, 80-979.

FIGURE CAPTIONS

Figure 1. Tracklines run and stations occupied in 1980 field operations.

Figure 2. Type of geophysical data collected along tracklines run in 1980.

Figure 3. Station location map for sediment size analyses stations occupied by cruises in 1960, 1961, 1967, 1968, 1969, 1970, 1976, 1977, and 1980.

Figure 4. Distribution of acoustic anomalies observed on geophysical records collected in 1980.

Figure 5. Areas of strong current activity and associated large-scale bedforms.

Figure 6. Areas of ice gouging. This is a composite of previous work (enclosed by solid lines) and preliminary interpretation of 1980 data.

Figure 7. % silt in surface sediment of Norton Basin.

Figure 8. % silt in surface sediment of Norton Basin.

Figure 9. % sand in surface sediment of Norton Basin.

Figure 10 % sand in surface sediment of Norton Basin.

Figure 11. % mud in surface sediment of Norton Basin.

Figure 12. % mud in surface sediment of Norton Basin.

Figure 13. % clay in surface sediment of Norton Basin.

Figure 14. % clay in surface sediment of Norton Basin.

Figure 15. % gravel in surface sediment of Norton Basin.

Figure 16. % gravel in surface sediment of Norton Basin.

Figure 17. Mean grain size (Folk and Ward) for surface sediments.

Figure 18. Mean grain size (first moment) for surface sediments.

Figure 19. Modal phi sizes for surface sediment.

Figure 20. Sorting values (Folk and Ward) for surface sediments.

Figure 21. Sorting values (Folk and Ward) for surface sediments.

Figure 22. Skewness values (Folk and Ward) for surface sediments.

Figure 23. Kurtosis values (Folk and Ward) for surface sediments.

Figure 24. Kurtosis values (Folk and Ward) for surface sediments.

Figure 25. % organic carbon in surface sediments in Norton Basin.

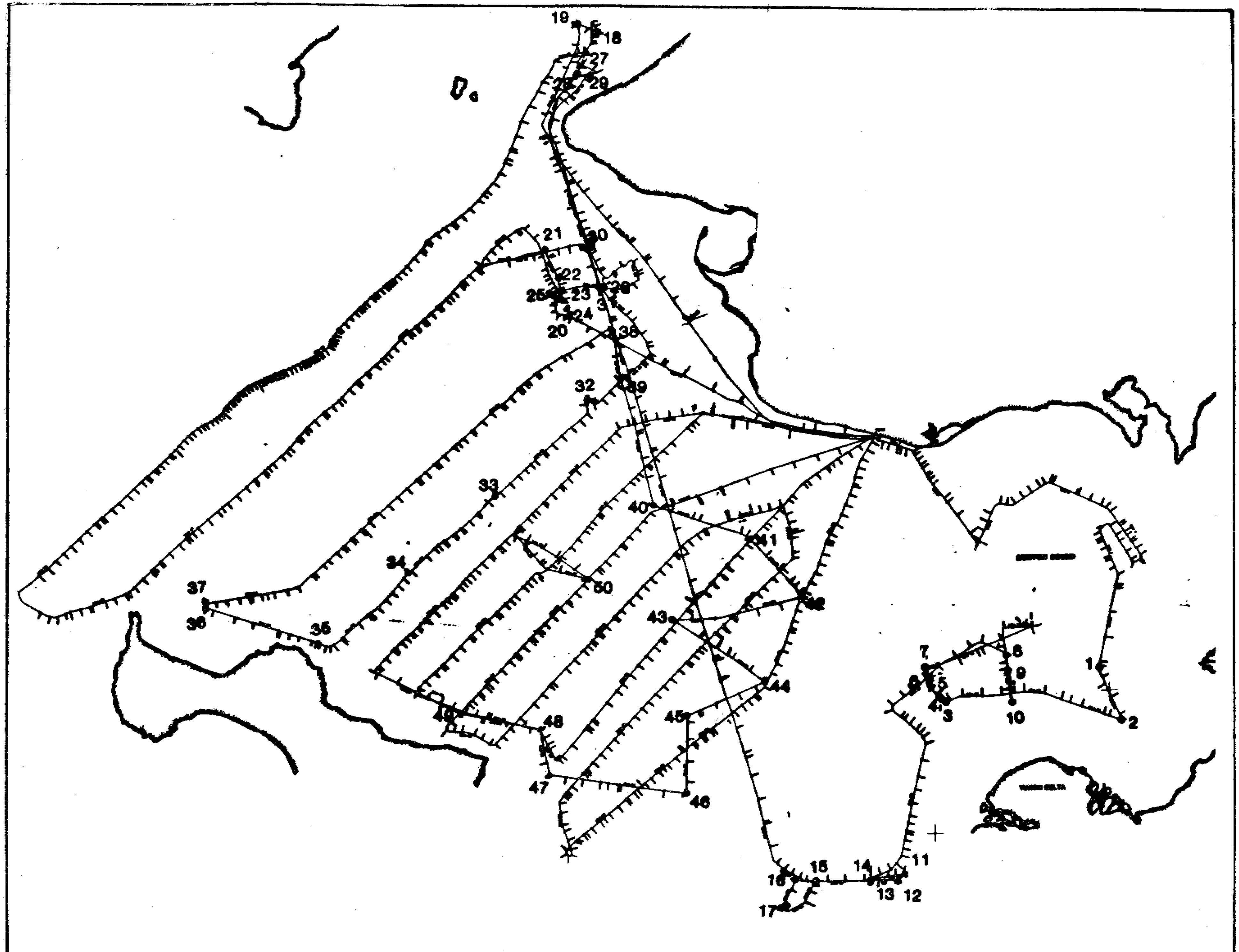

FIG. 1 Tracklines run and stations occupied in 1980 field operations.

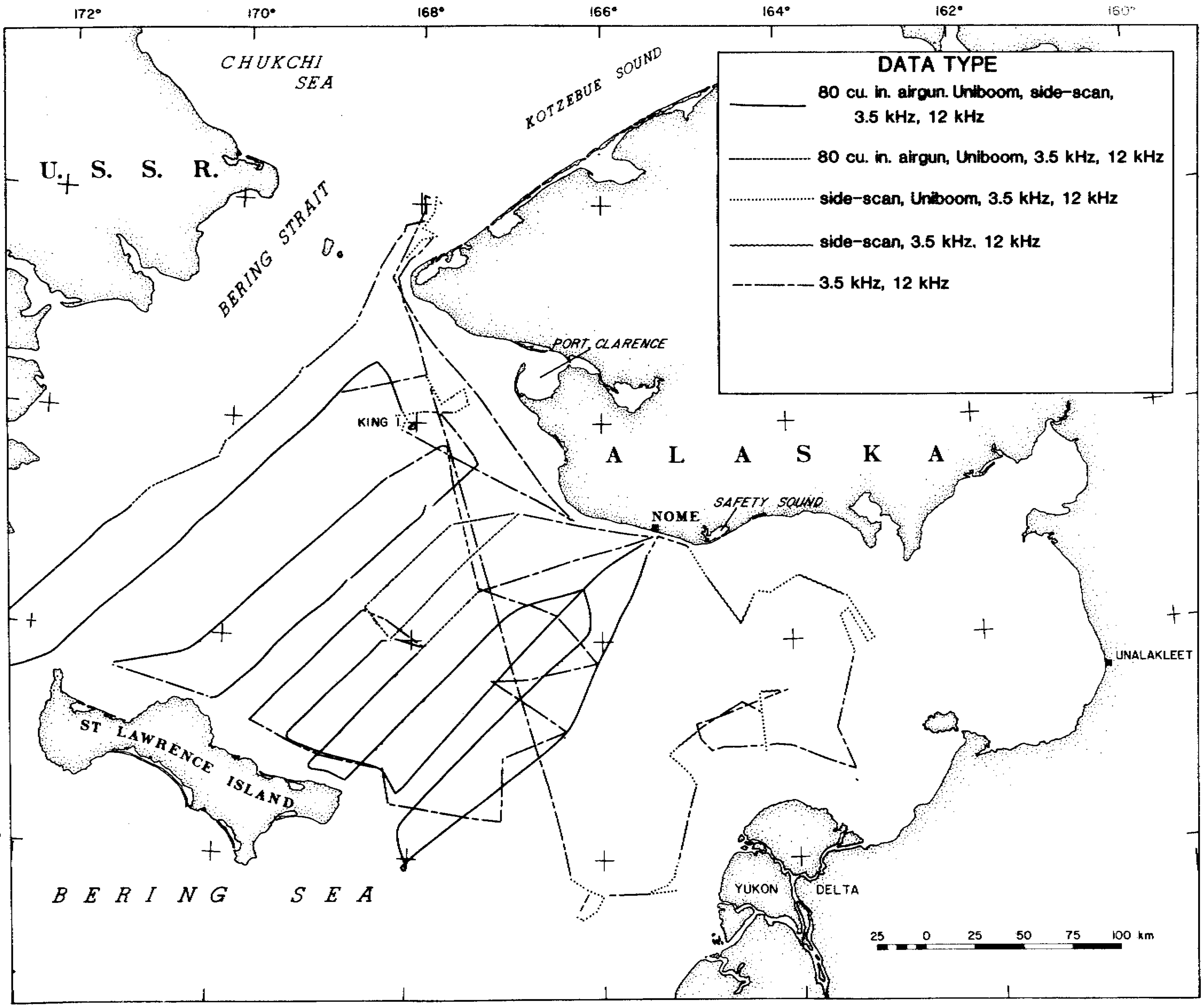

FIG. 2 Type of geophysical data collected along tracklines run in 1980.

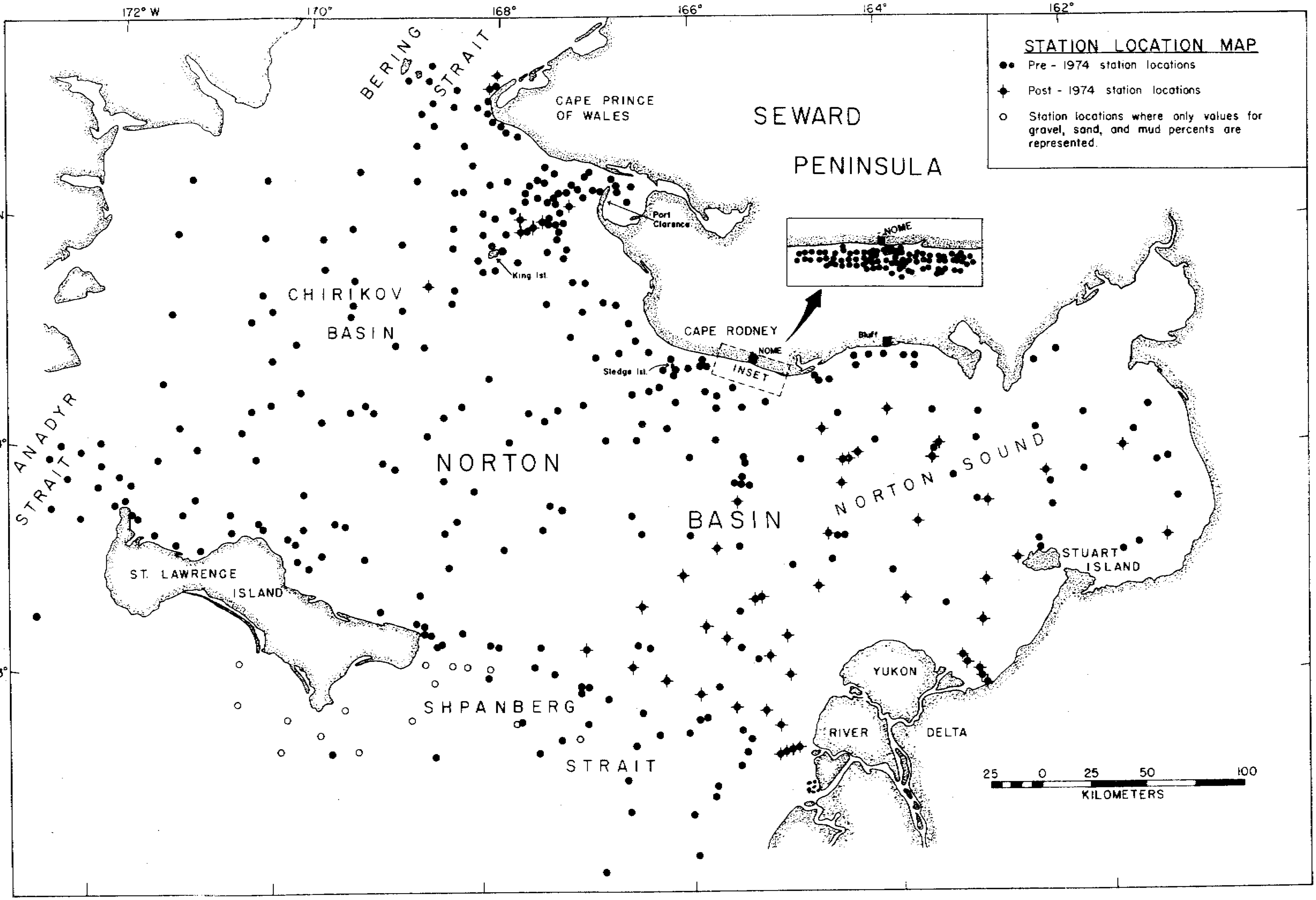

FIG 3 Station location map for sediment size analyses stations occupied by cruises in 1960, 1961, 1967, 1968, 1969, 1970, 1976, 1977 and 1980.

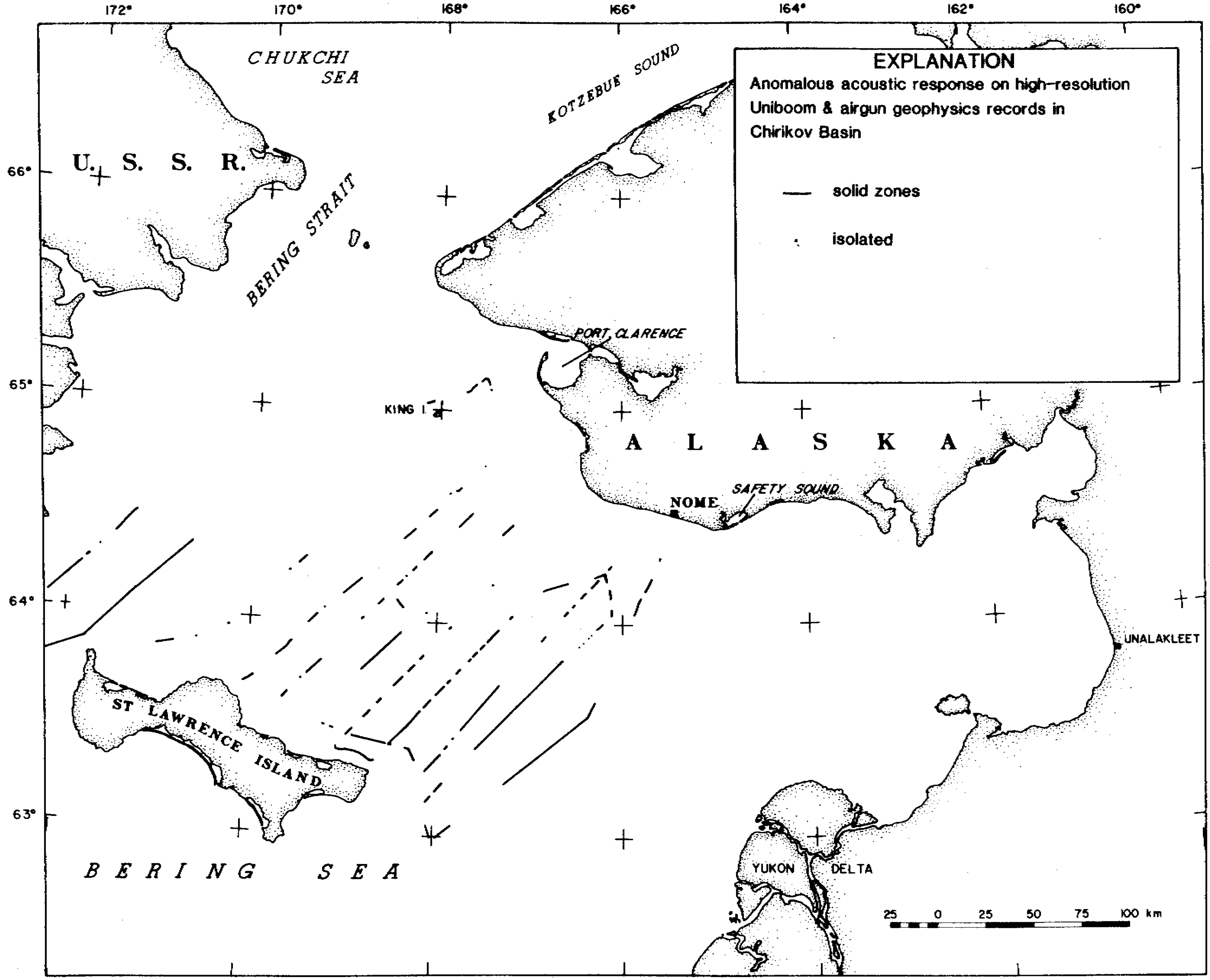

FIG. 4 Distribution of acoustic anomalies observed on geophysical records collected in 1980.

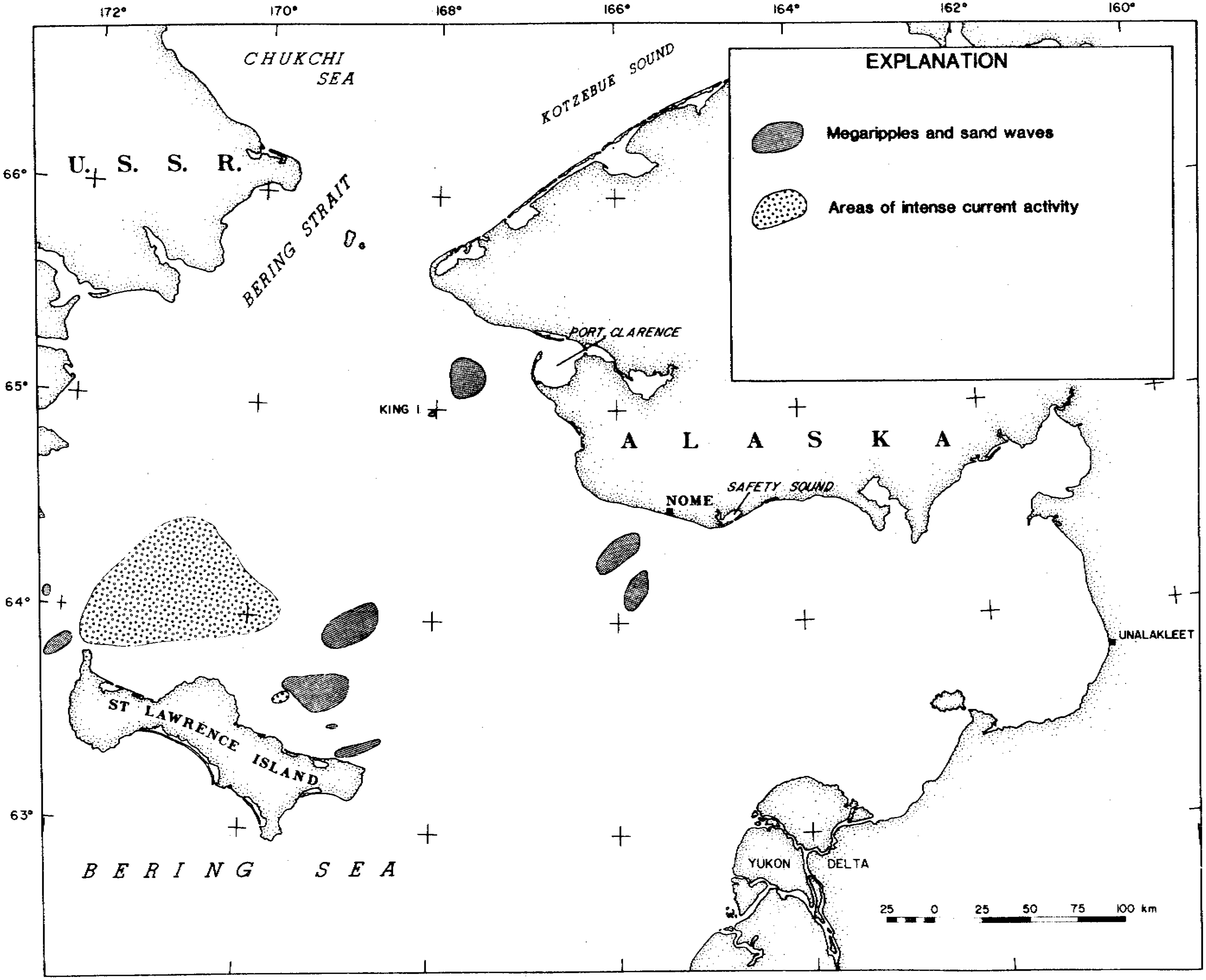

FIG. 5 Areas of strong current activity and associated large-scale bedforms.

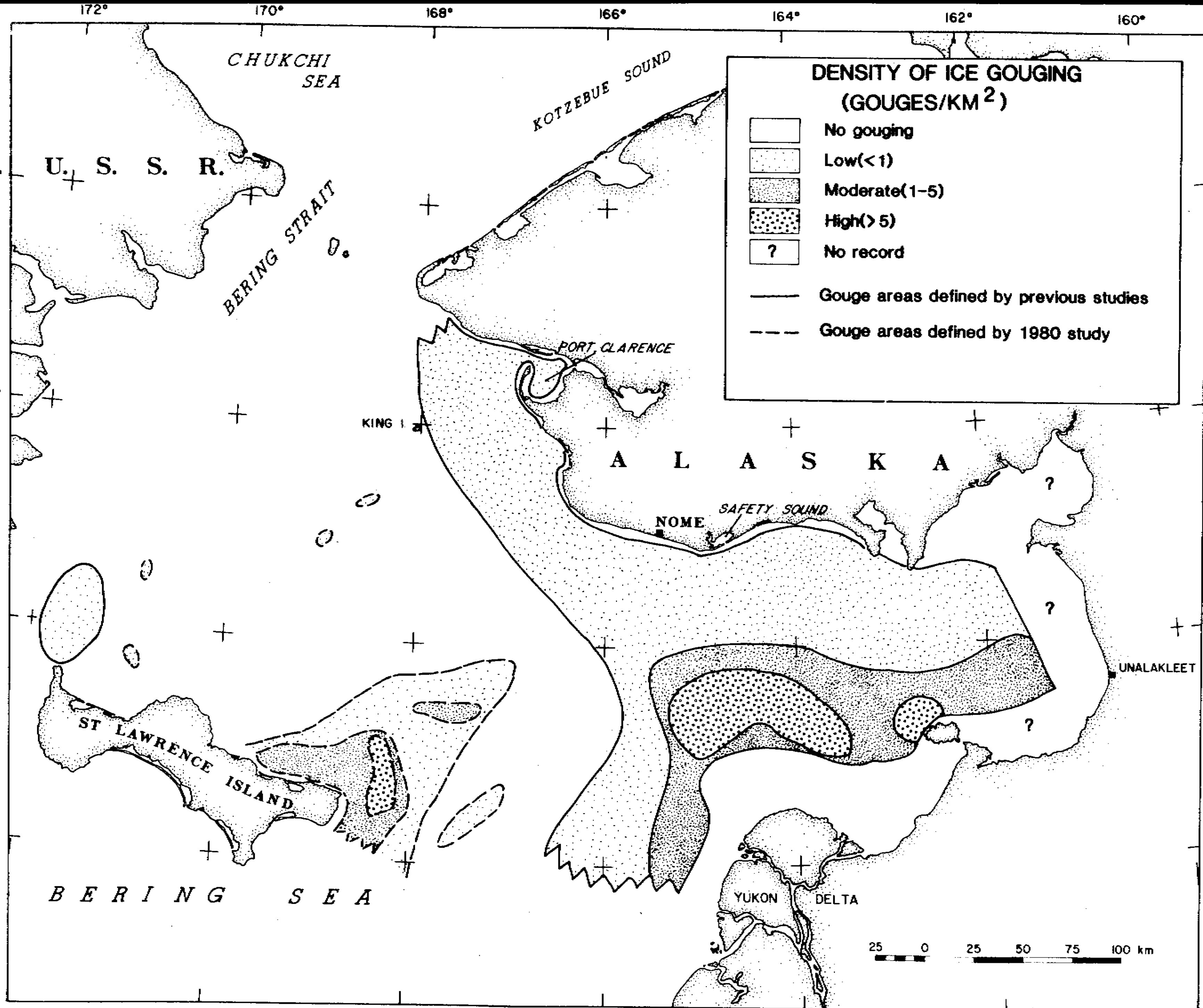

FIG. 6 Areas of ice gouging. This is a composite of previous work (enclosed by solid lines) and preliminary interpretation of 1980 data.

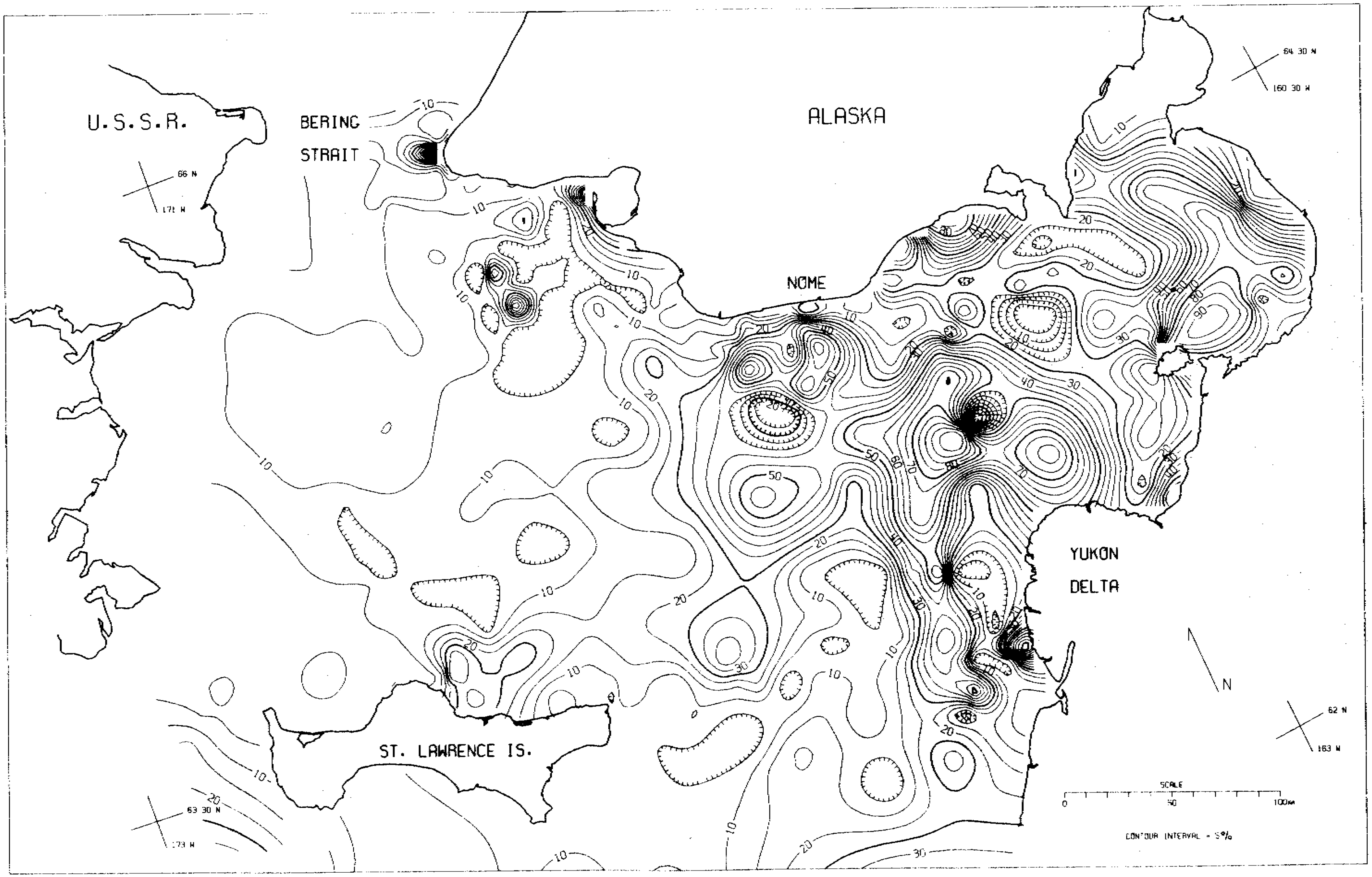

FIG 7 % SILT IN SURFACE SEDIMENT OF NORTON BASIN, NORTHERN BERING SEA

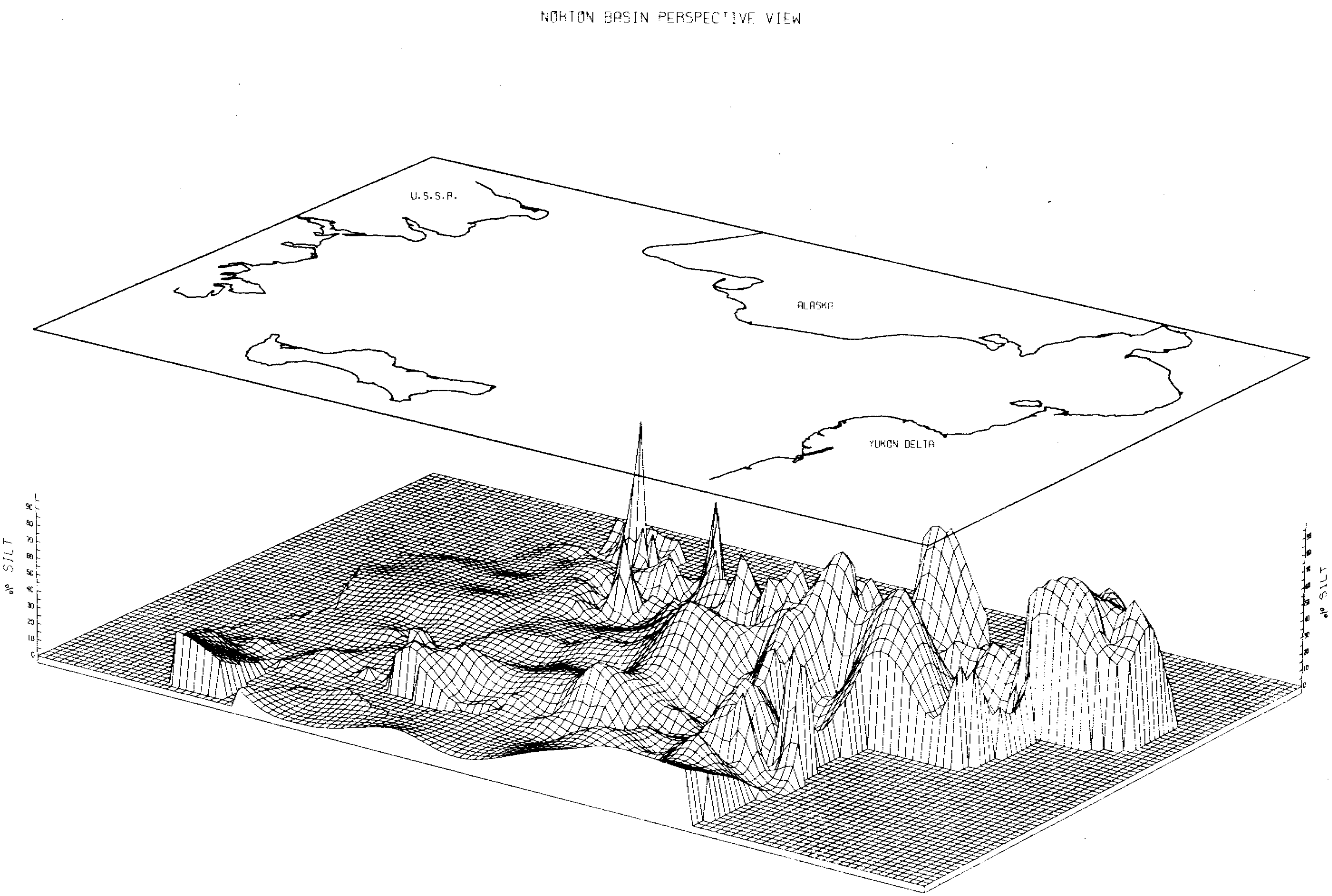

FIG 8 % SILT IN SURFACE SEDIMENT OF NORTON BASIN, NORTHERN BERING SEA

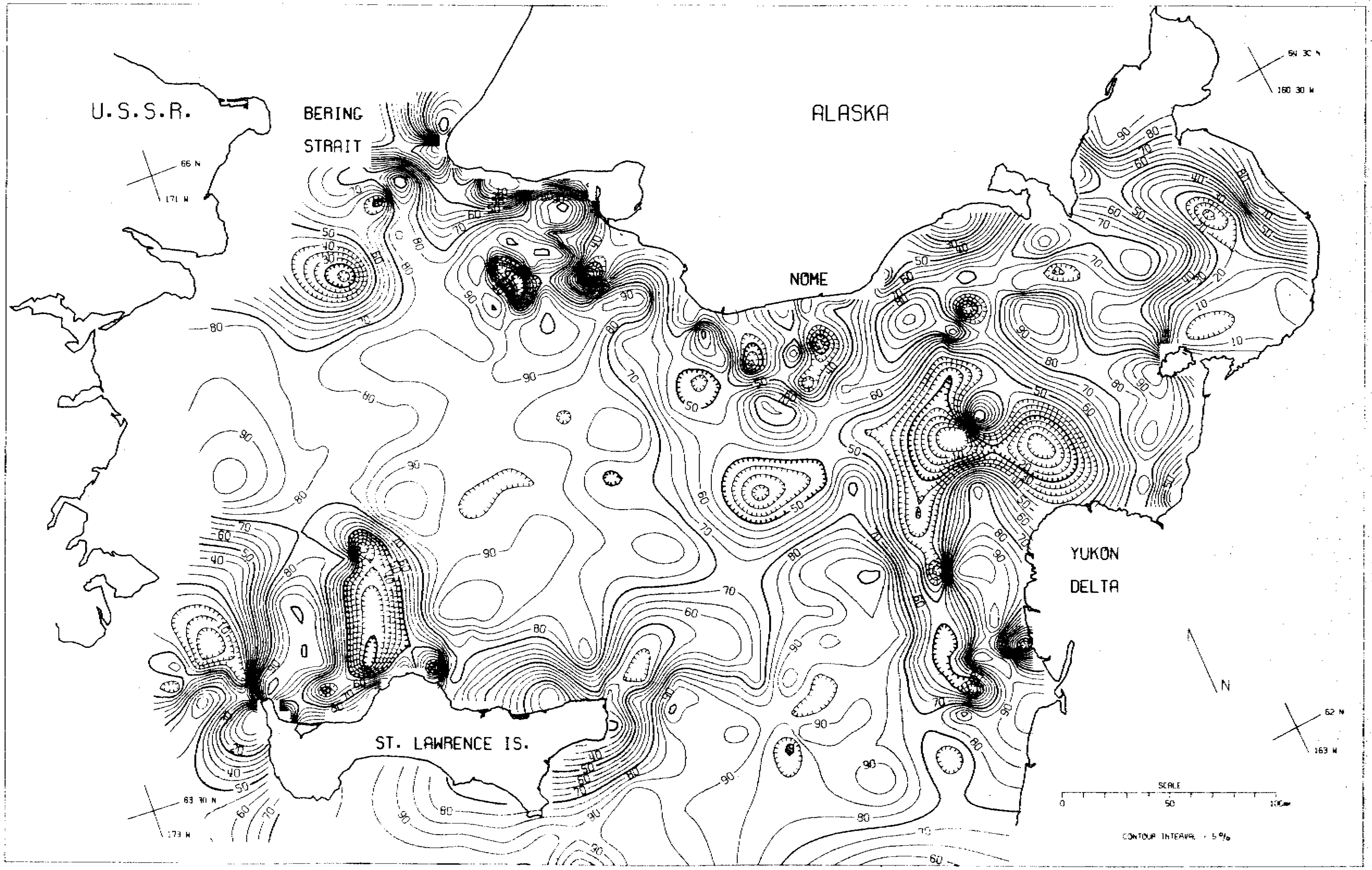

FIG 9 % SAND IN SURFACE SEDIMENT OF NORTON BASIN, NORTHERN BERING SEA

NORTON BASIN PERSPECTIVE VIEW

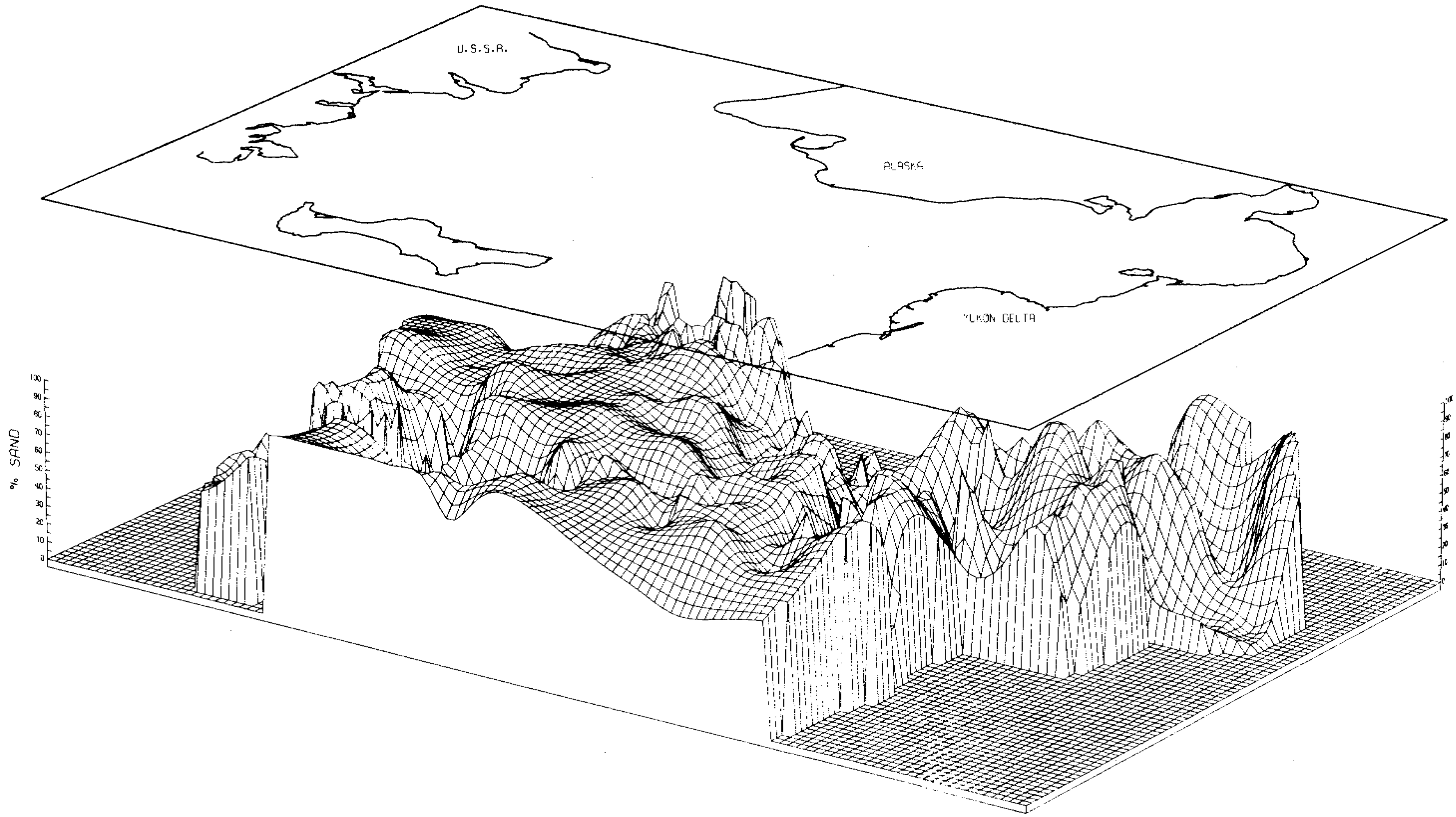

FIG 10 % SAND IN SURFACE SEDIMENT OF NORTON BASIN, NORTHERN BERING SEA

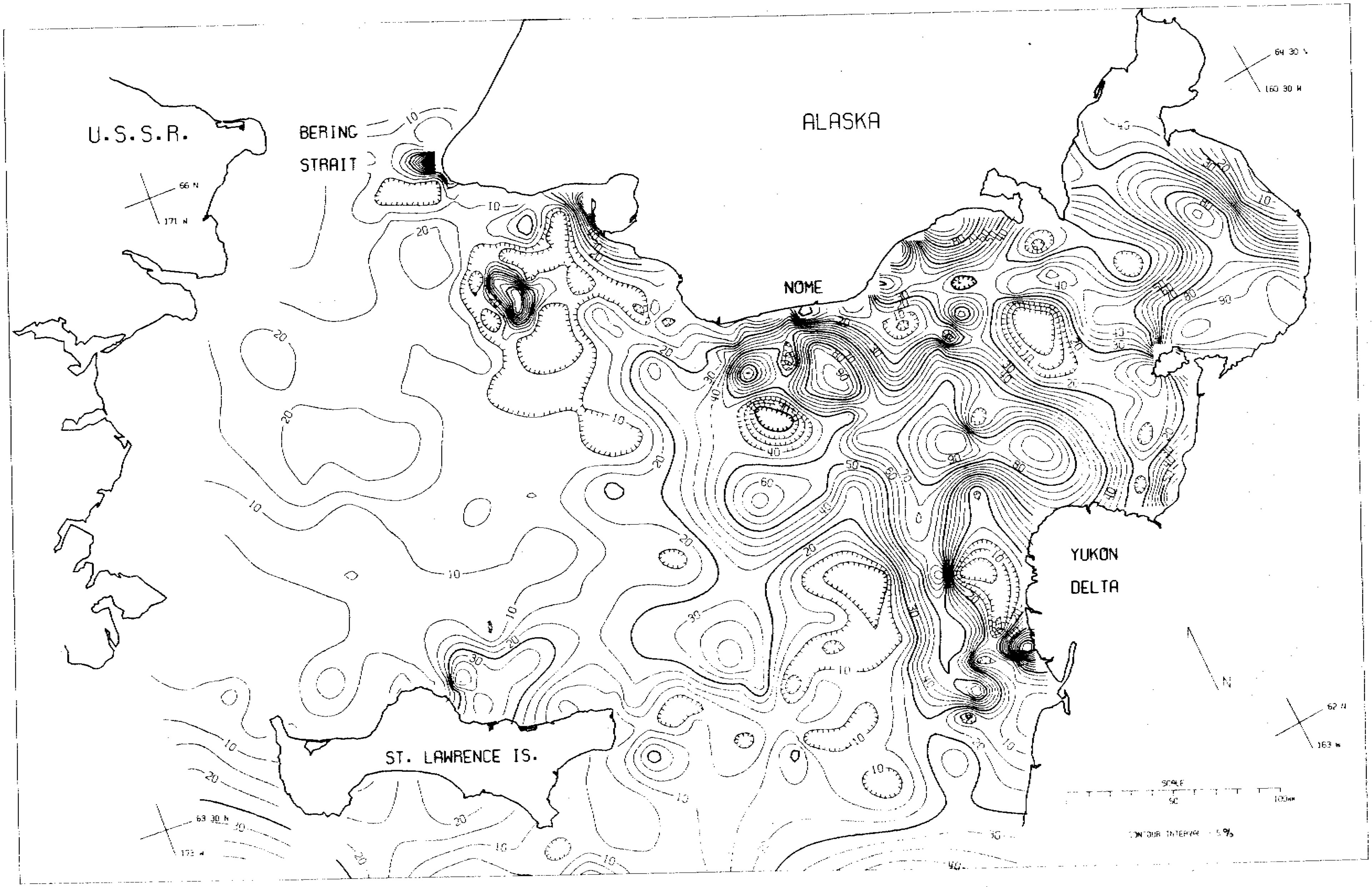

FIG 11 % MUD IN SURFACE SEDIMENT OF NORTON BASIN, NORTHERN BERING SEA

(MUD = SILT + CLAY)

NORTON BASIN PERSPECTIVE VIEW

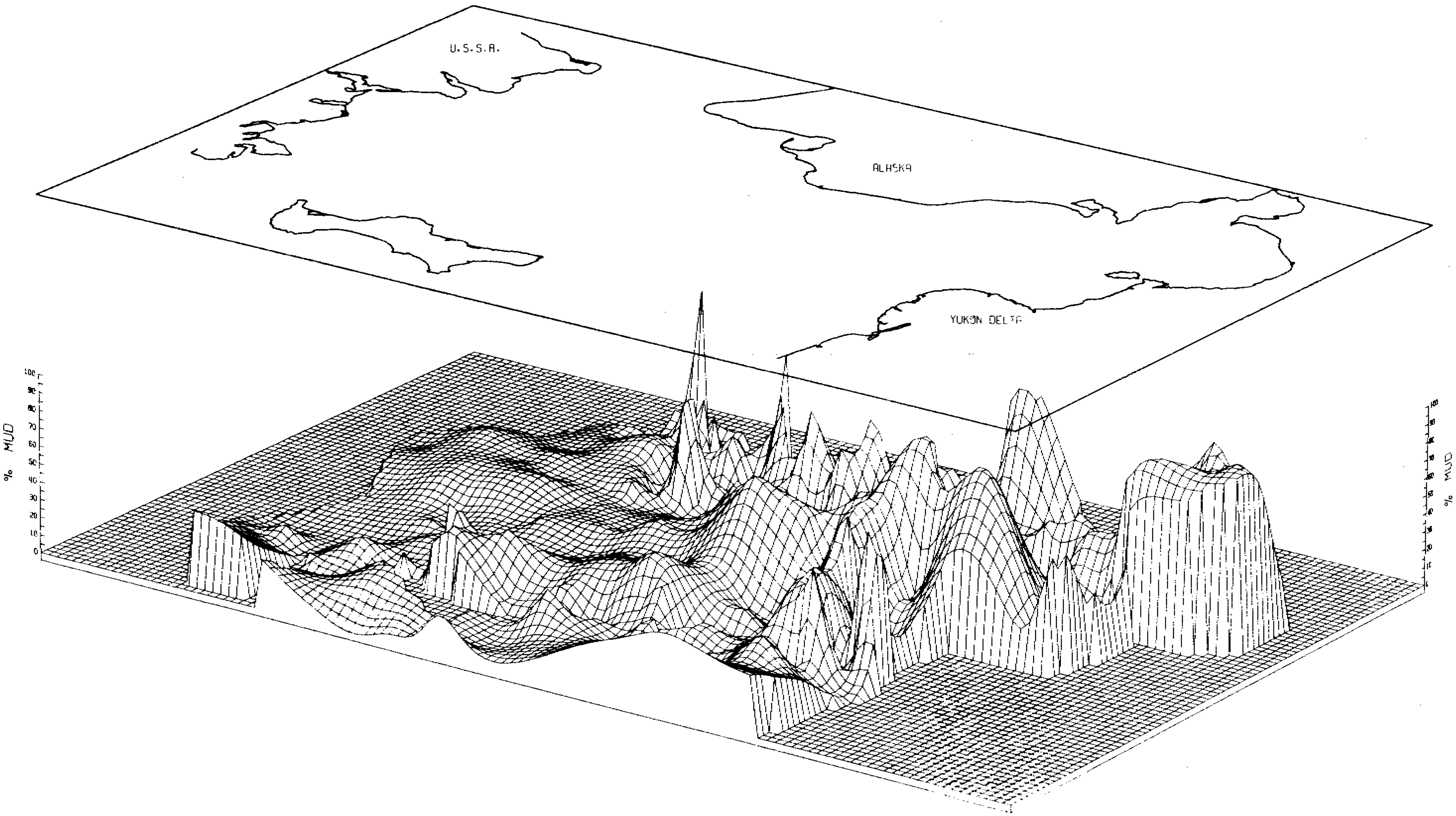

FIG 12 % MUD IN SURFACE SEDIMENT OF NORTON BASIN, NORTHERN BERING SEA
(MUD = SILT + CLAY)

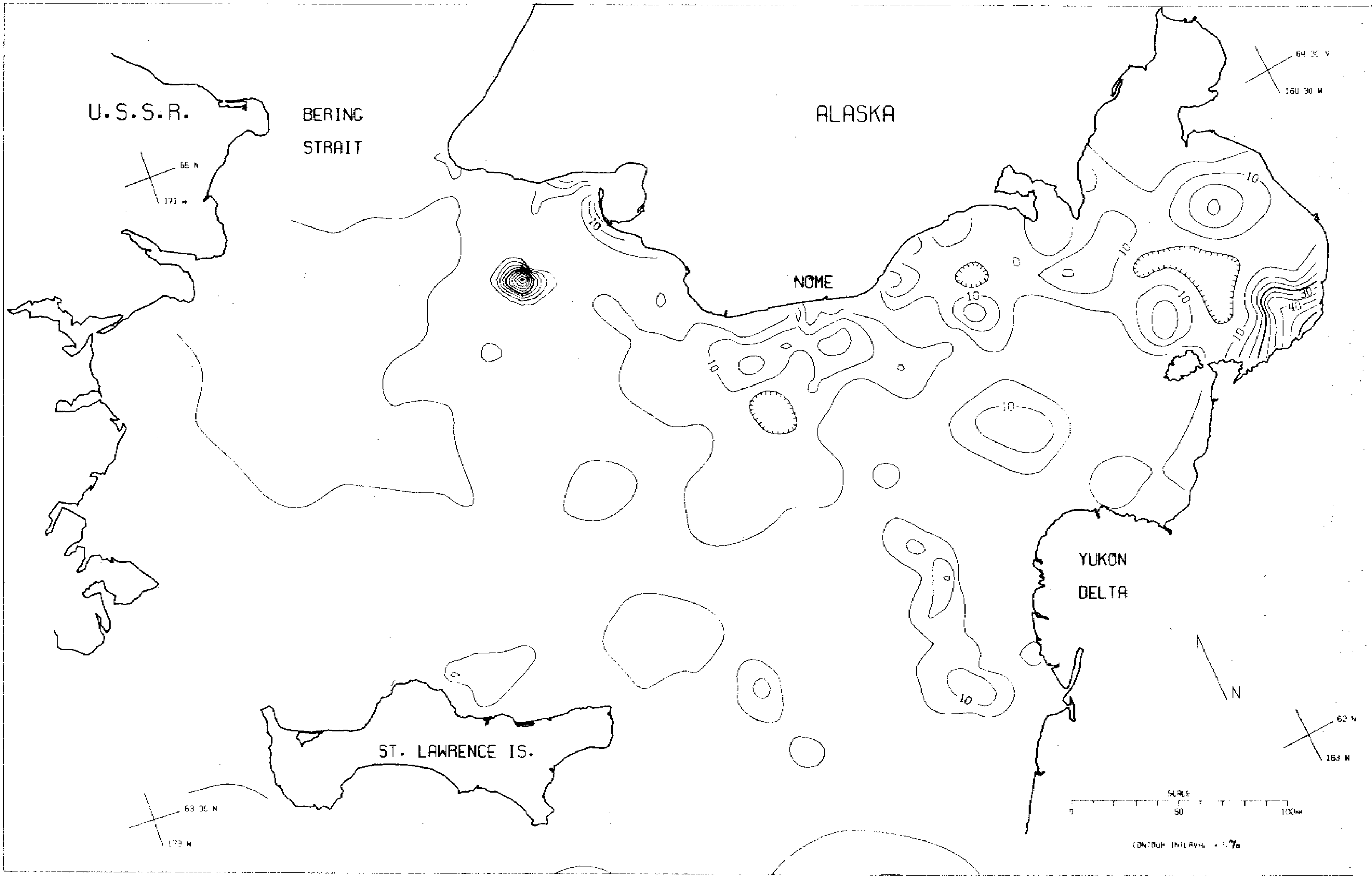

FIG. 13 % CLAY IN SURFACE SEDIMENT OF NORTON BASIN, NORTHERN BERING SEA

NORTON BASIN PERSPECTIVE VIEW

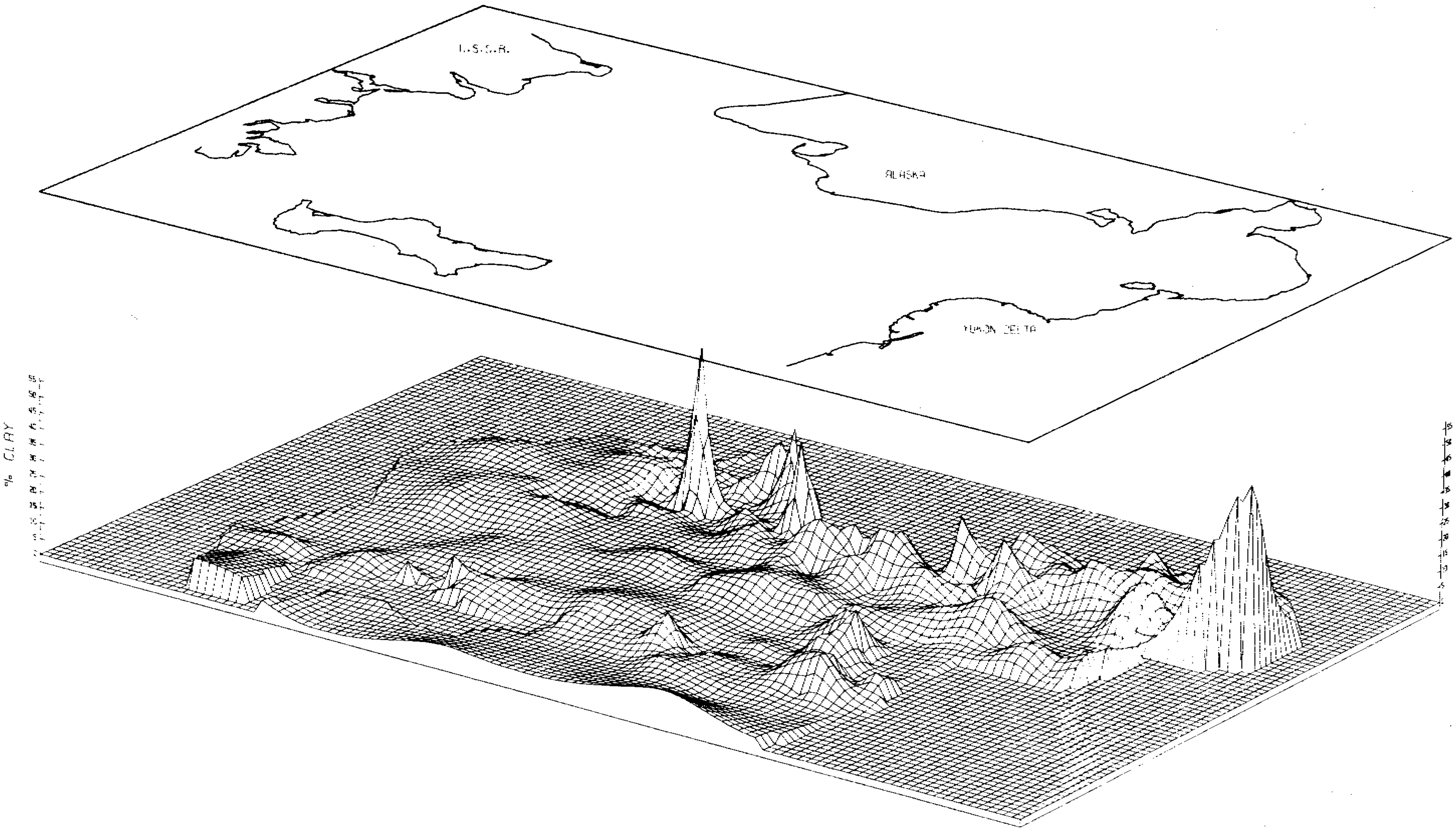

FIG 14 % CLAY IN SURFACE SEDIMENT OF NORTON BASIN, NORTHERN BE

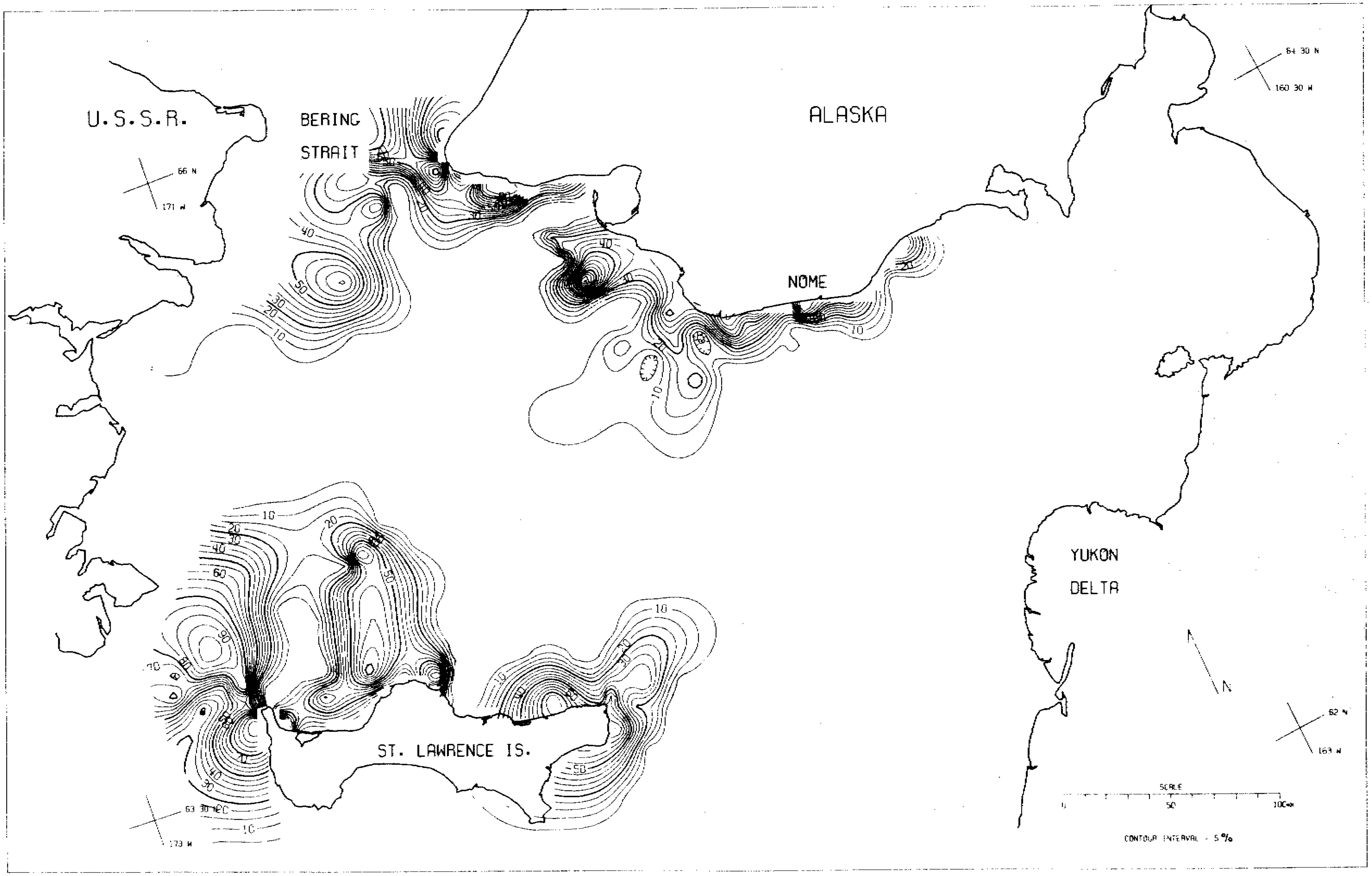

FIG 15 % GRAVEL IN SURFACE SEDIMENT OF NORTON BASIN, NORTHERN BERING SEA

NORTON BASIN PERSPECTIVE VIEW

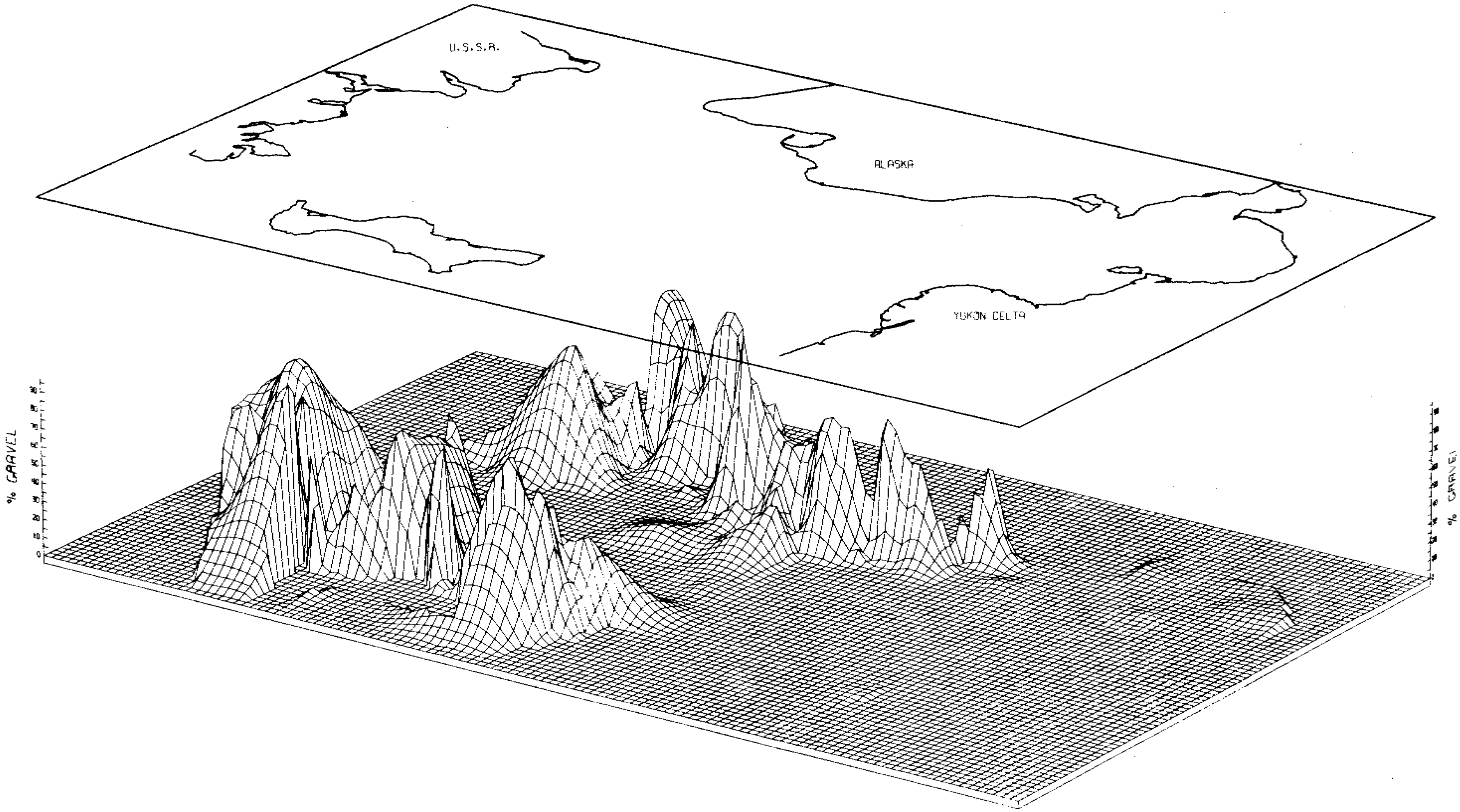

FIG 16 % GRAVEL IN SURFACE SEDIMENT OF NORTON BASIN, NORTHERN BERING SEA

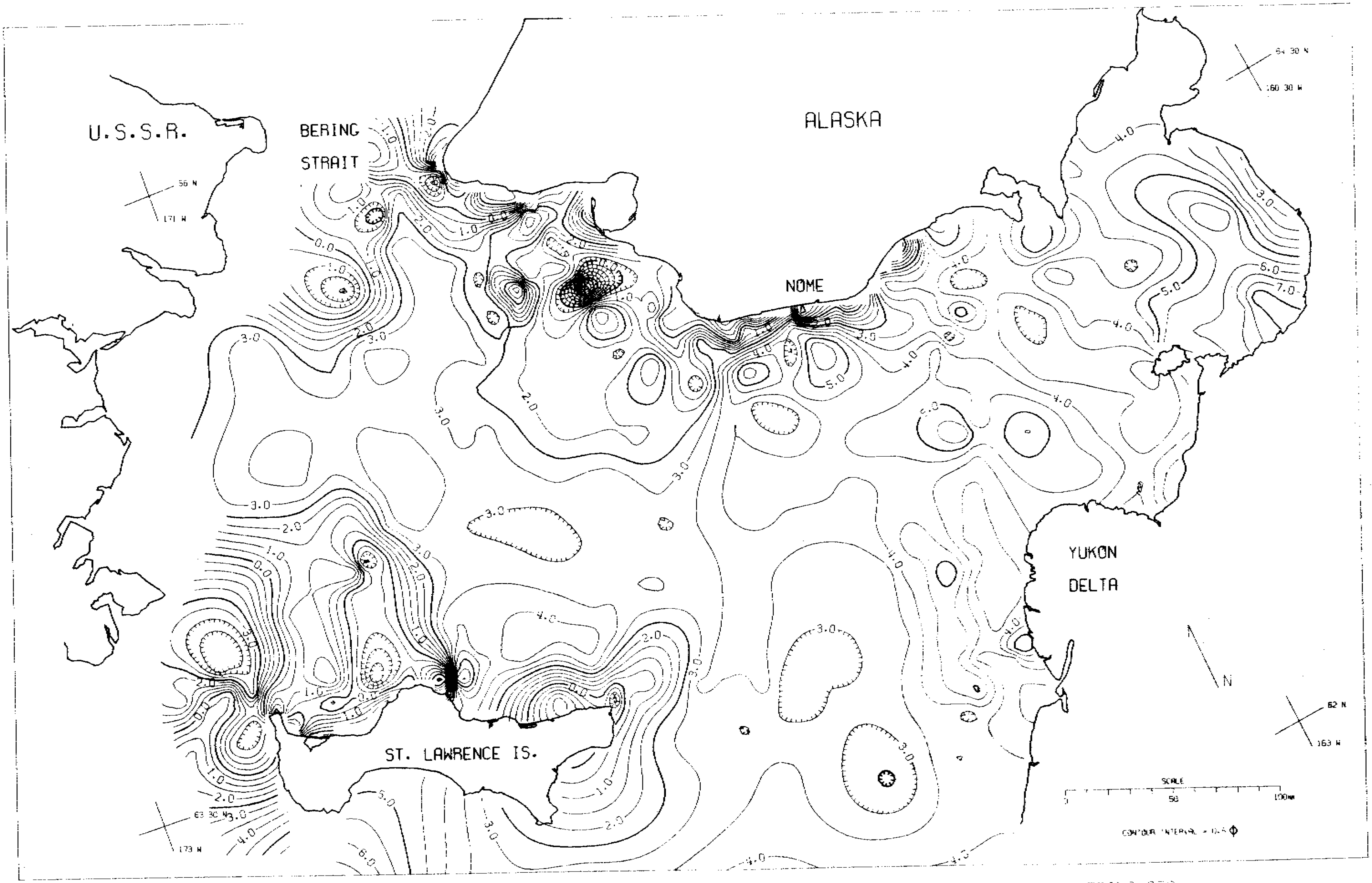

FIG 17 MEAN GRAIN SIZE (FOLK AND WARD) FOR SURFACE SEDIMENT IN NORTON BASIN, NORTHERN BERING SEA

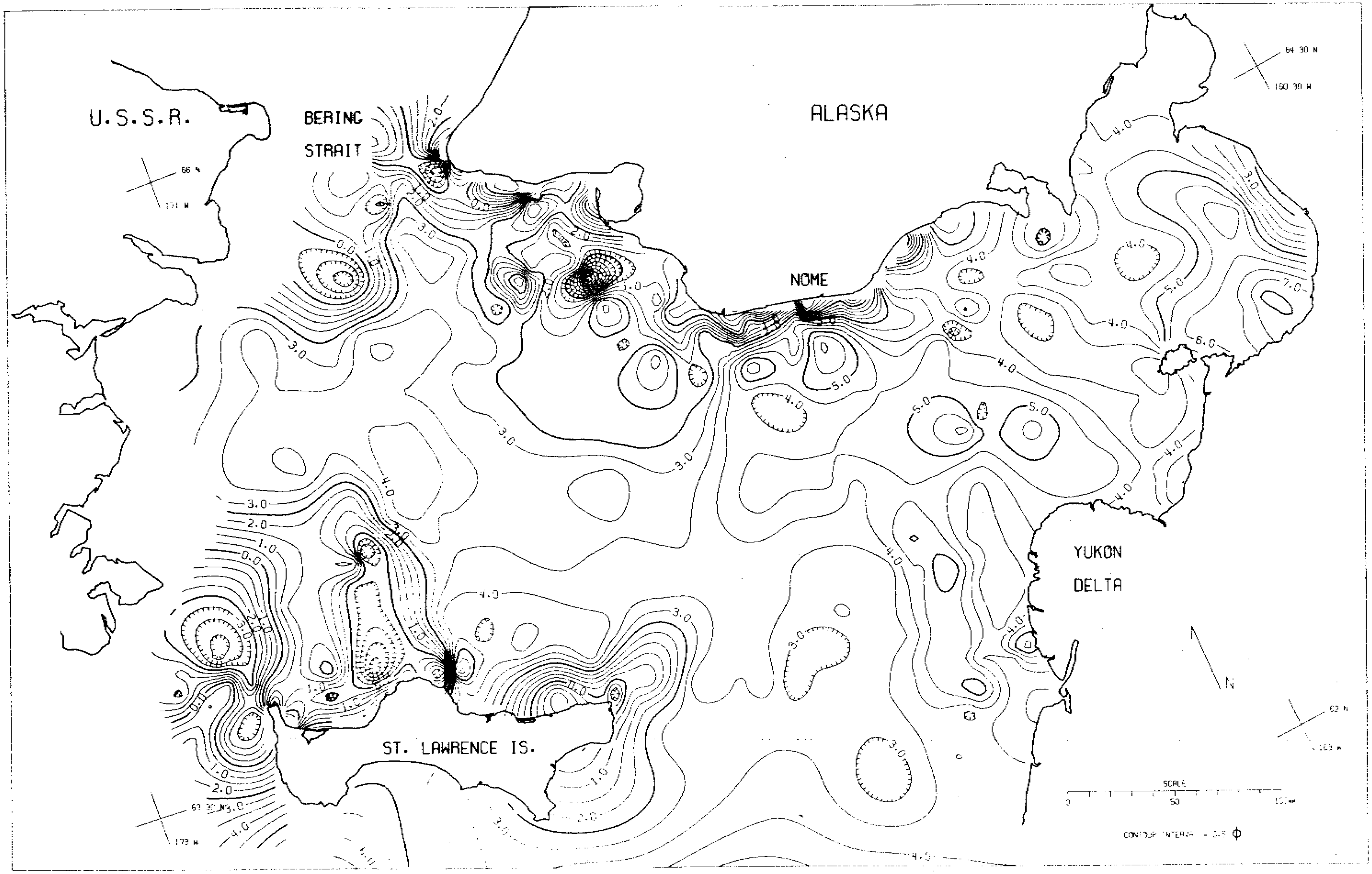

FIG 18 MEAN GRAIN SIZE (FIRST MOMENT) FOR SURFACE SEDIMENT IN NORTON BASIN, NORTHERN BERING SEA

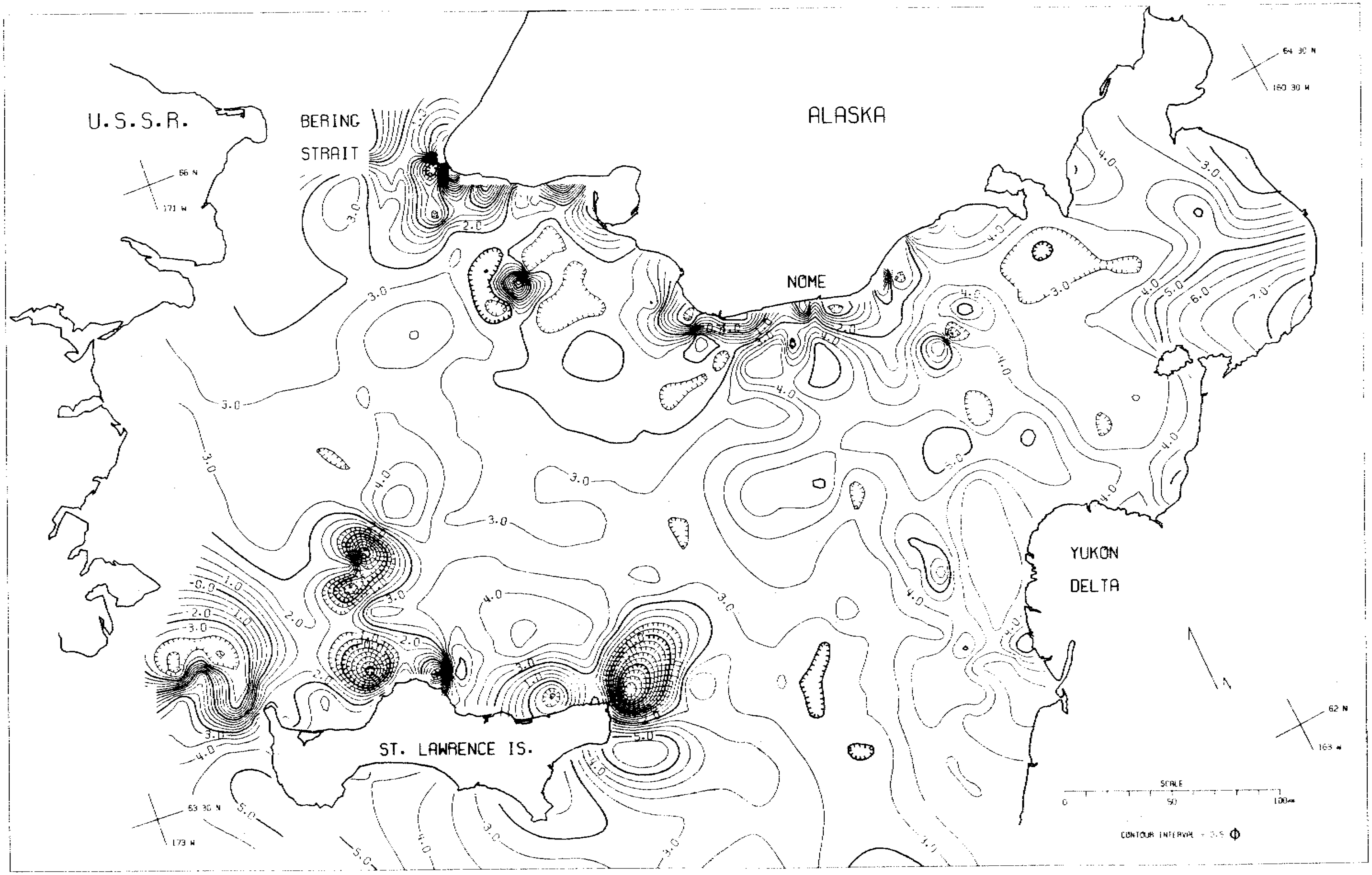

FIG 19 PLOT OF MODAL CLASSES (IN PHI) FOR SURFACE SEDIMENT IN NORTON BASIN, NORTHERN BERING SEA

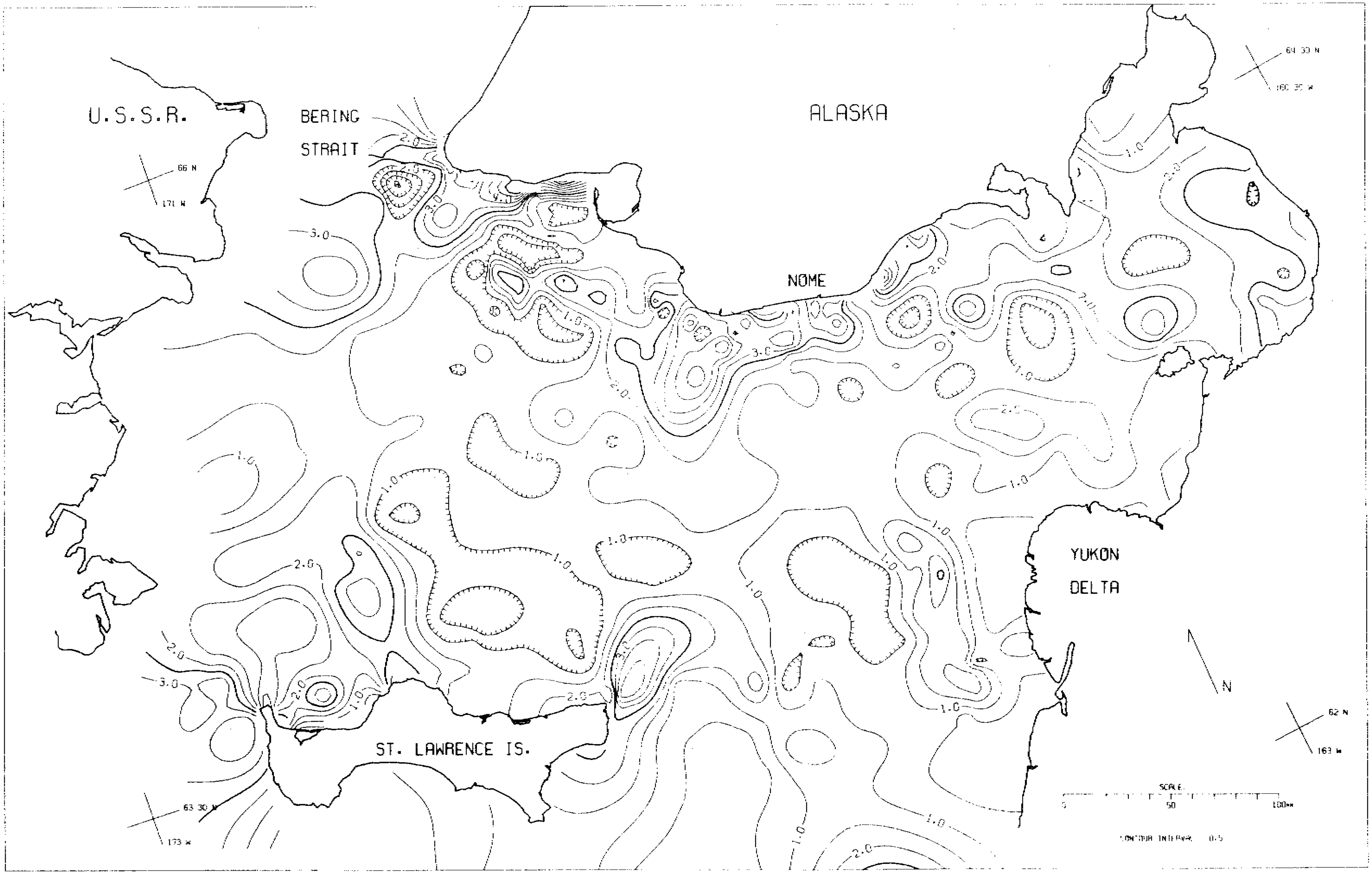

FIG 20 SORTING VALUES (FOLK AND WARD) FOR SURFACE SEDIMENT IN NORTON BASIN, NORTHERN BERING SEA

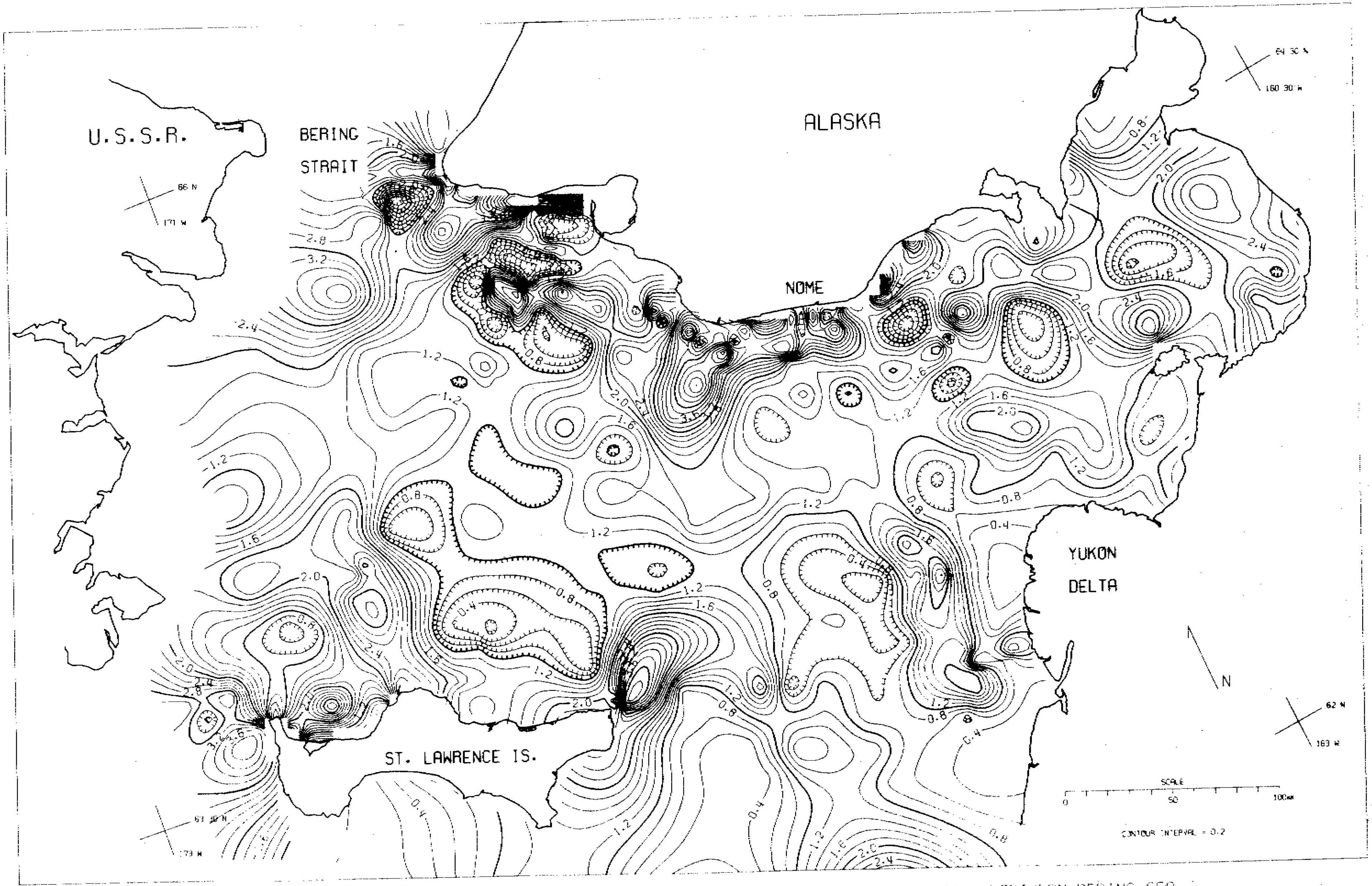

FIG. 21 SORTING VALUES (FOLK AND WARD) FOR SURFACE SEDIMENT IN NORTON BASIN, NORTHERN BERING SEA

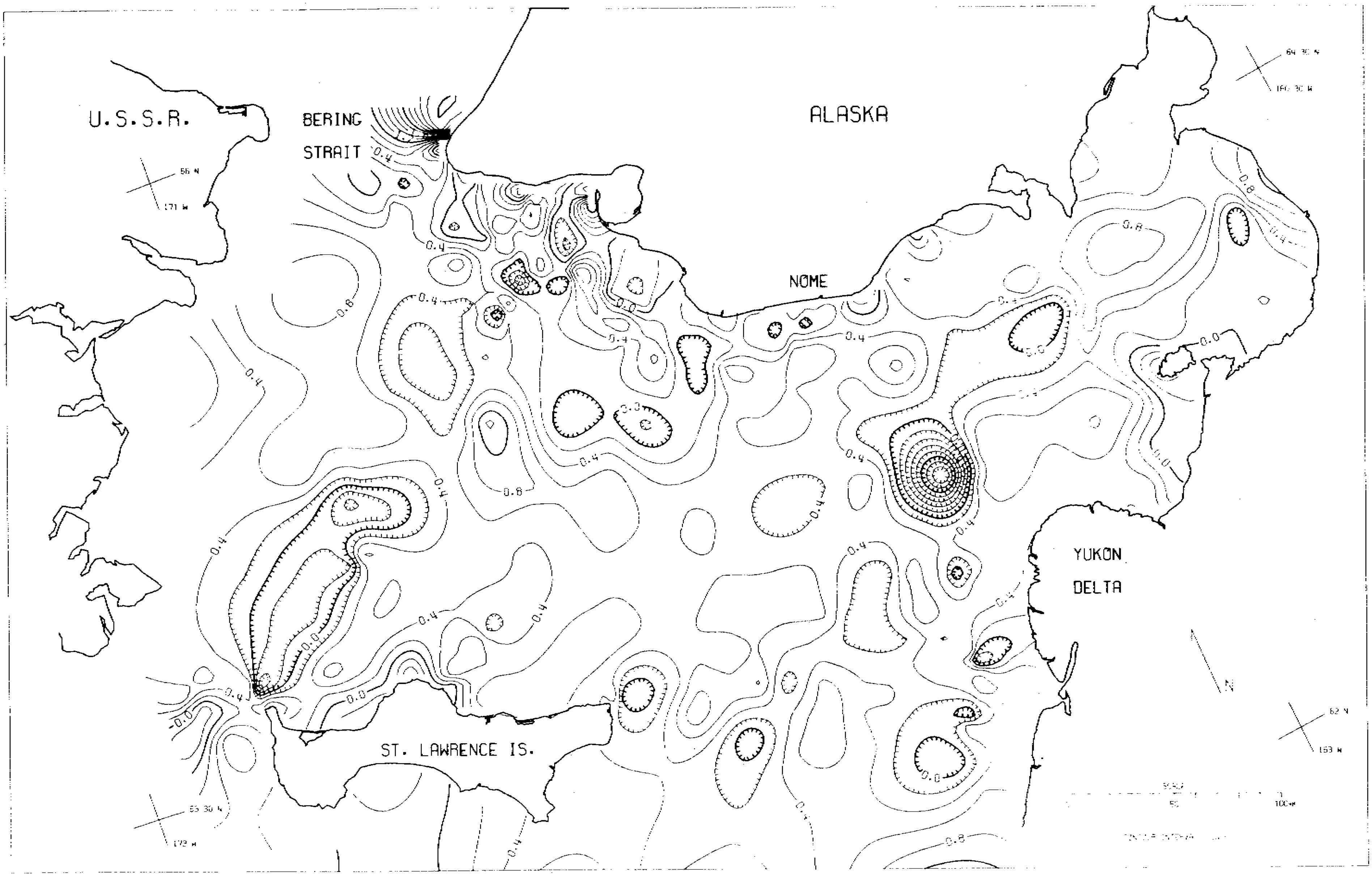

FIG 22 SKEWNESS VALUES (FOLK AND WARD) FOR SURFACE SEDIMENT IN NORTON BASIN, NORTHERN BERING SEA

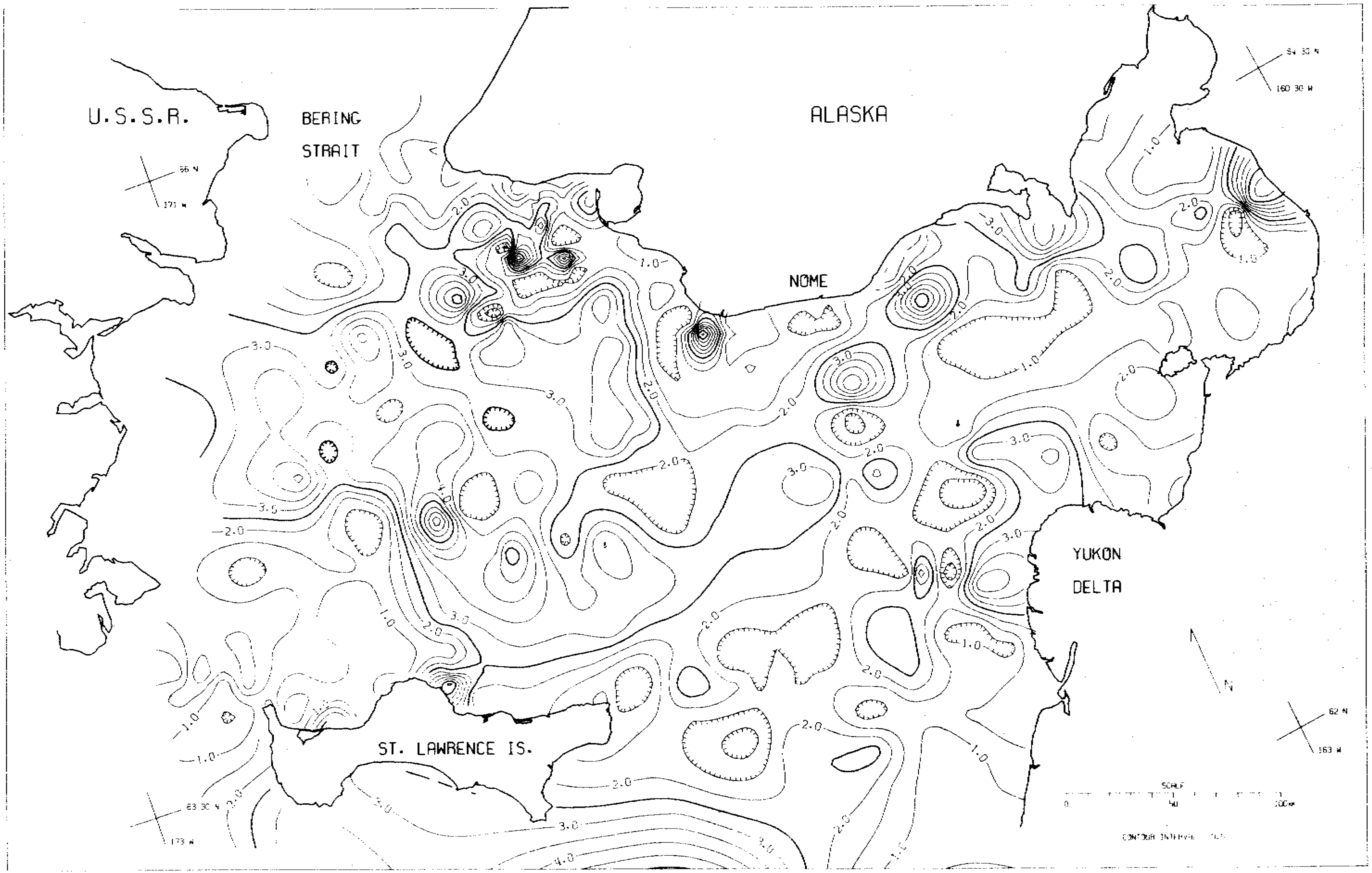

FIG 23 KURTOSIS VALUES (FOLK AND WARD) FOR SURFACE SEDIMENT IN NORTON BASIN, NORTHERN BERING SEA

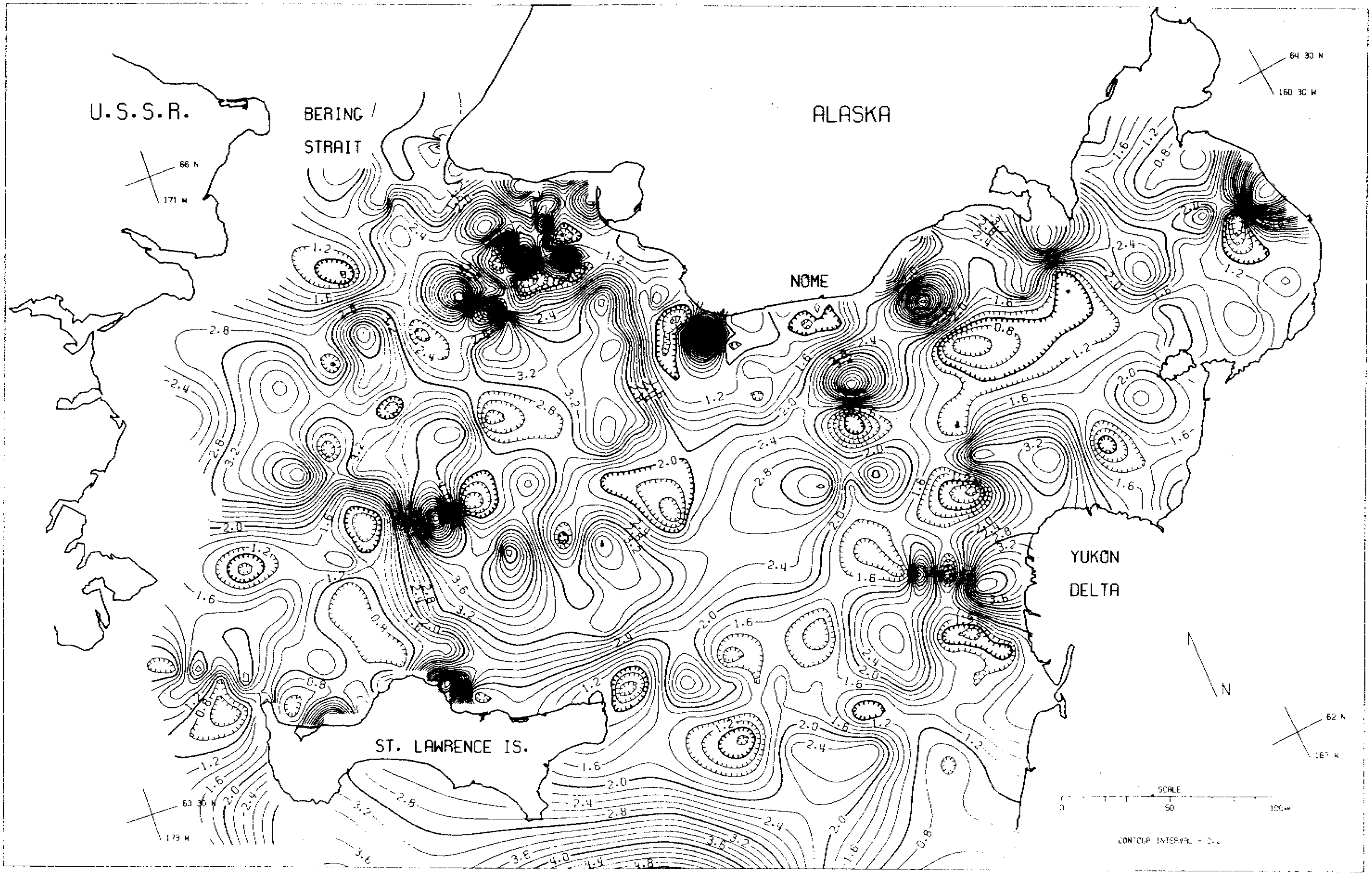

FIG 24 KURTOSIS VALUES (FOLK AND WARD) FOR SURFACE SEDIMENT IN NORTON BASIN, NORTHERN BERING SEA

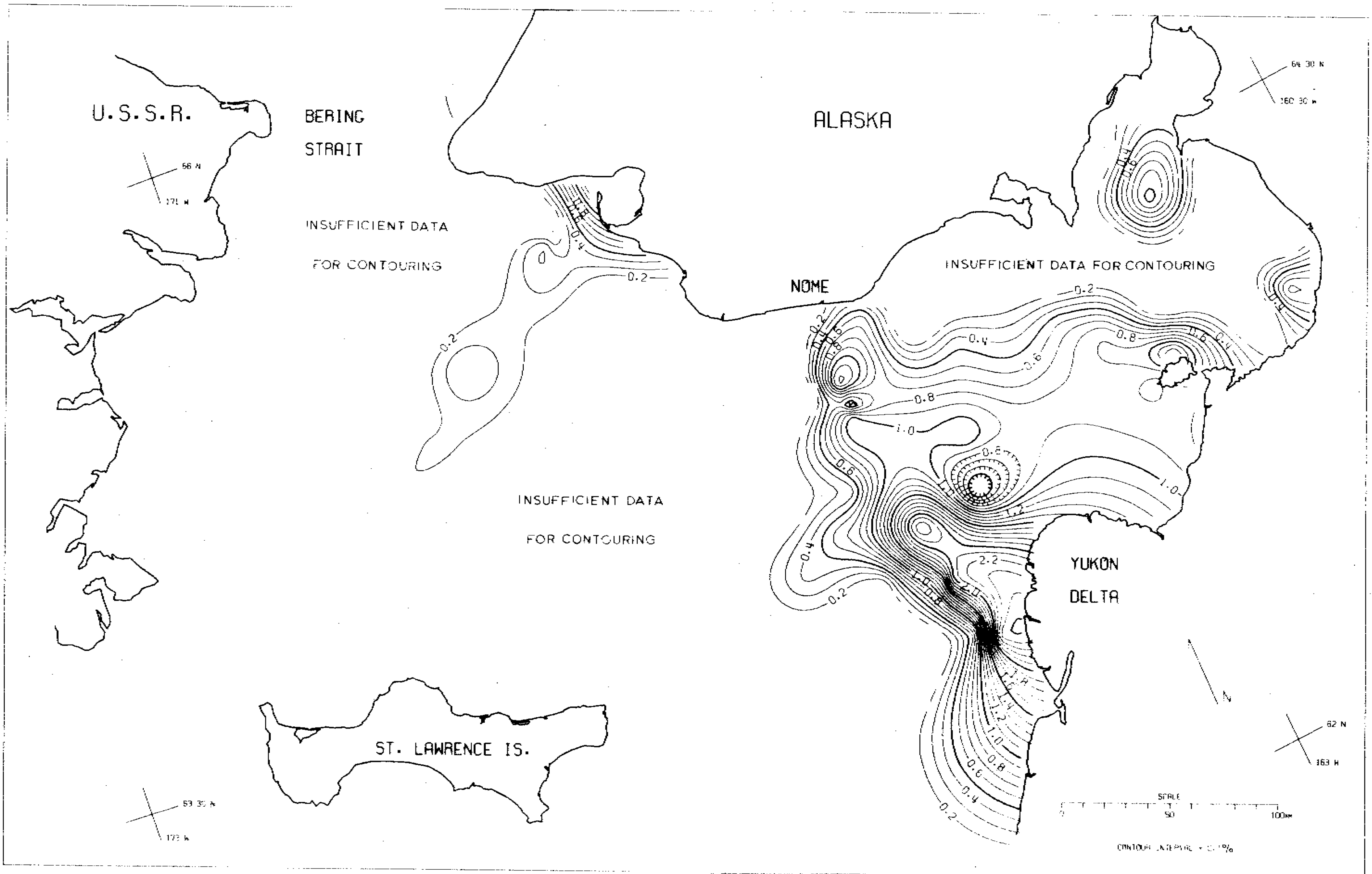

FIG 25 PERCENT ORGANIC CARBON IN SURFACE SEDIMENT OF NORTON BASIN, NORTHERN BERING SEA

APPENDIX A

LOGS OF SELECTED KIEL VIBRACORES

1980

SOIL CLASSIFICATION CHART
AND
KEY TO TEST DATA

UNIFIED SOIL CLASSIFICATION SYSTEM

MAJOR DIVISIONS				TYPICAL NAMES
COARSE GRAINED SOILS MORE THAN HALF IS LARGER THAN #200 SIEVE	GRAVELS MORE THAN HALF COARSE FRACTION IS LARGER THAN NO. 4 SIEVE SIZE	CLEAN GRAVELS WITH LITTLE OR NO FINES	GW	WELL GRADED GRAVELS, GRAVEL - SAND MIXTURES
			GP	POORLY GRADED GRAVELS, GRAVEL - SAND MIXTURES
		GRAVELS WITH OVER 12% FINES	GM	SILTY GRAVELS, POORLY GRADED GRAVEL - SAND - SILT MIXTURES
			GC	CLAYEY GRAVELS, POORLY GRADED GRAVEL - SAND - CLAY MIXTURES
	SANDS MORE THAN HALF COARSE FRACTION IS SMALLER THAN NO. 4 SIEVE SIZE	CLEAN SANDS WITH LITTLE OR NO FINES	SW	WELL GRADED SANDS, GRAVELLY SANDS
			SP	POORLY GRADED SANDS, GRAVELLY SANDS
		SANDS WITH OVER 12% FINES	SM	SILTY SANDS, POORLY GRADED SAND - SILT MIXTURES
			SC	CLAYEY SANDS, POORLY GRADED SAND - CLAY MIXTURES
FINE GRAINED SOILS MORE THAN HALF IS SMALLER THAN #200 SIEVE	SILTS AND CLAYS LIQUID LIMIT LESS THAN 50		ML	INORGANIC SILTS AND VERY FINE SANDS, ROCK FLOUR, SILTY OR CLAYEY FINE SANDS, OR CLAYEY SILTS WITH SLIGHT PLASTICITY
			CL	INORGANIC CLAYS OF LOW TO MEDIUM PLASTICITY, GRAVELLY CLAYS, SANDY CLAYS, SILTY CLAYS, LEAN CLAYS
			OL	ORGANIC CLAYS AND ORGANIC SILTY CLAYS OF LOW PLASTICITY
	SILTS AND CLAYS LIQUID LIMIT GREATER THAN 50		MH	INORGANIC SILTS, MICACEOUS OR DIATOMACIOUS FINE SANDY OR SILTY SOILS, ELASTIC SILTS
			CH	INORGANIC CLAYS OF HIGH PLASTICITY, FAT CLAYS
			OH	ORGANIC CLAYS OF MEDIUM TO HIGH PLASTICITY, ORGANIC SILTS
HIGHLY ORGANIC SOILS			Pt	PEAT AND OTHER HIGHLY ORGANIC SOILS

KEY TO TEST DATA

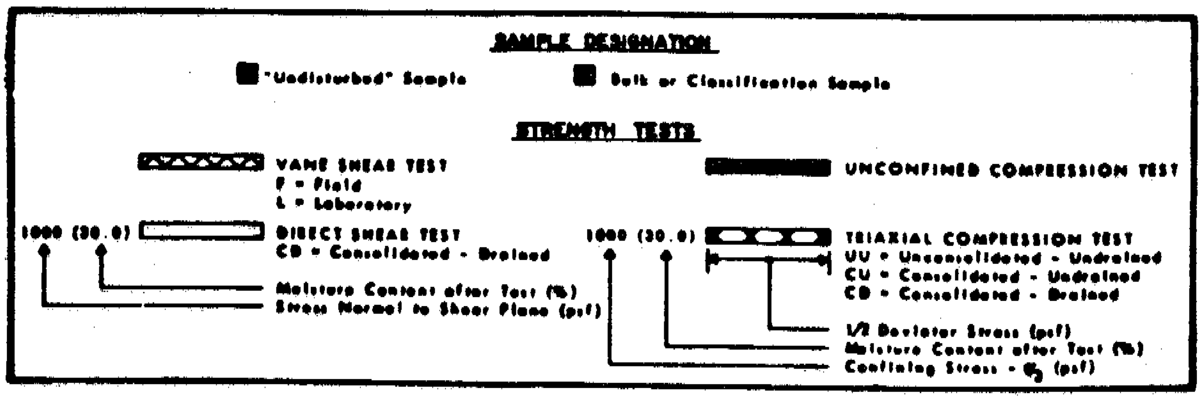

LOG OF KEIL CORE L780BS #31

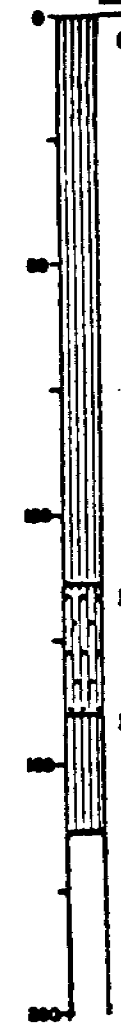

0-112 Olive brown to grayish olive silty sand with lenses of grayish olive clay and rare shell horizons.

112-143 Grayish olive fine to medium grained sand. Well developed ripple, flat, and tabular cross laminations.

143-164 Grayish olive to olive gray bioturbated fine grained sand.

LOG OF KEIL CORE L780BS #32

0-20 Light olive gray fine to coarse grained poorly sorted clayey sand with pebbles and shell fragments.

20-52 Dark gray bioturbated silt with sand stringers.

LOG OF KEIL CORE L780BS #33

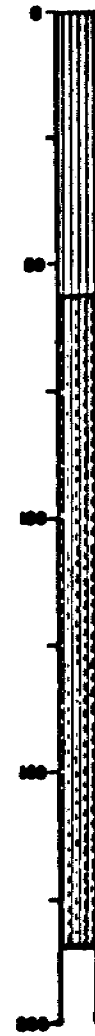

0-56 Grayish olive green to olive black bioturbated fine grained sand.

56-180 Olive gray to olive black silt and clayey silt. Occasional flat laminae and varves of yellowish brown peaty mud.

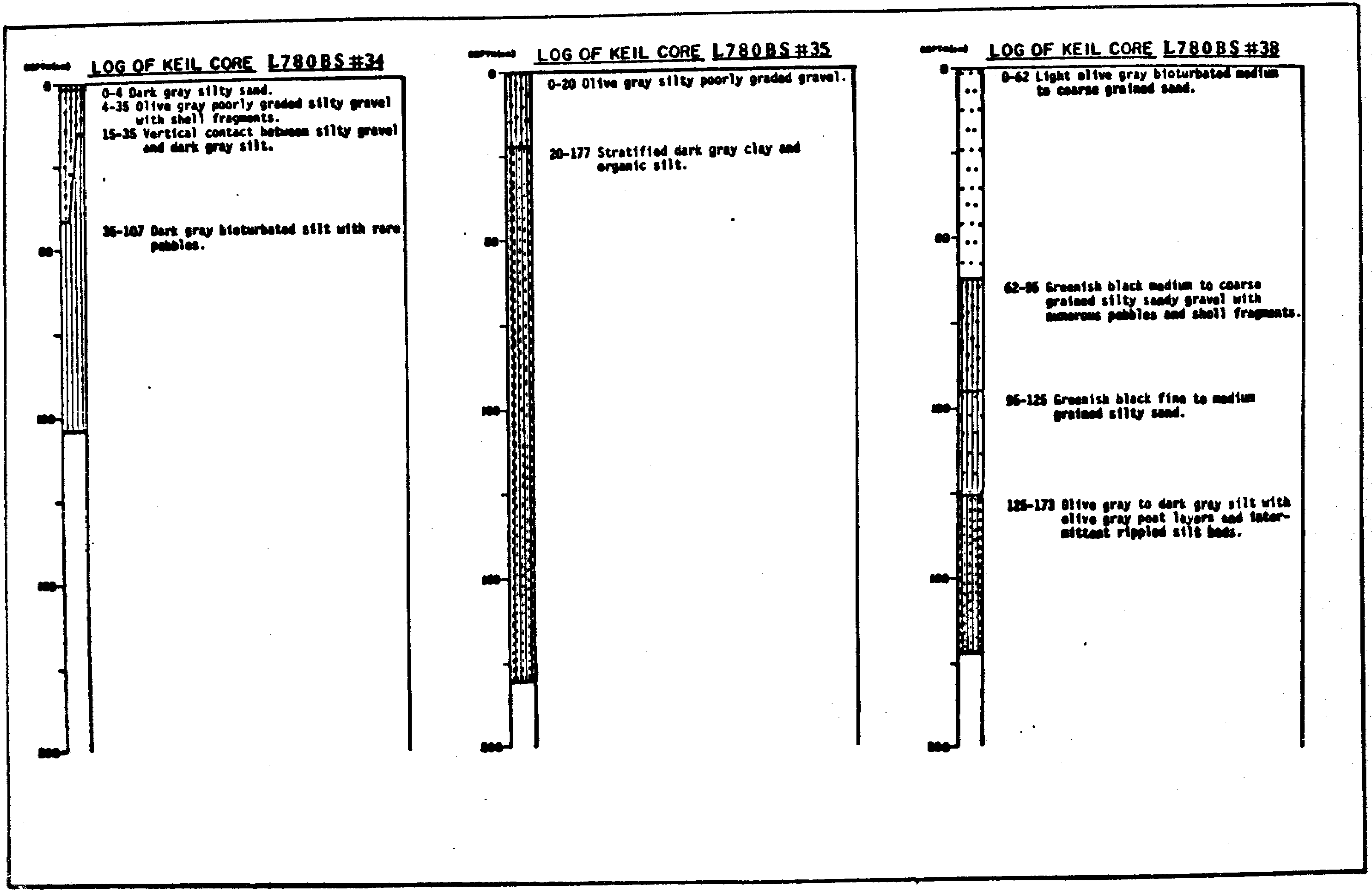
LOG OF KEIL CORE L780BS #34
0-4 Dark gray silty sand.
4-35 Olive gray poorly graded silty gravel with shell fragments.
15-35 Vertical contact between silty gravel and dark gray silt.
36-107 Dark gray bioturbated silt with rare pebbles.
LOG OF KEIL CORE L780BS #35
0-20 Olive gray silty poorly graded gravel.
20-177 Stratified dark gray clay and organic silt.
LOG OF KEIL CORE L780BS #38
0-62 Light olive gray bioturbated medium to coarse grained sand.
62-96 Greenish black medium to coarse grained silty sandy gravel with numerous pebbles and shell fragments.
96-125 Greenish black fine to medium grained silty sand.
125-173 Olive gray to dark gray silt with olive gray peat layers and intermittent rippled silt beds.

LOG OF KEIL CORE L780BS #39

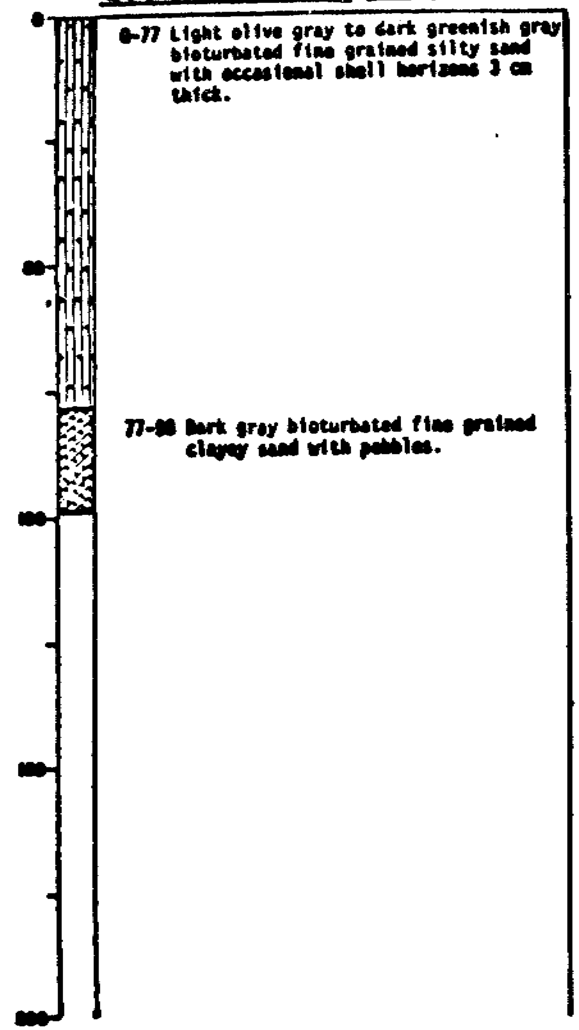

LOG OF KEIL CORE L780BS #40

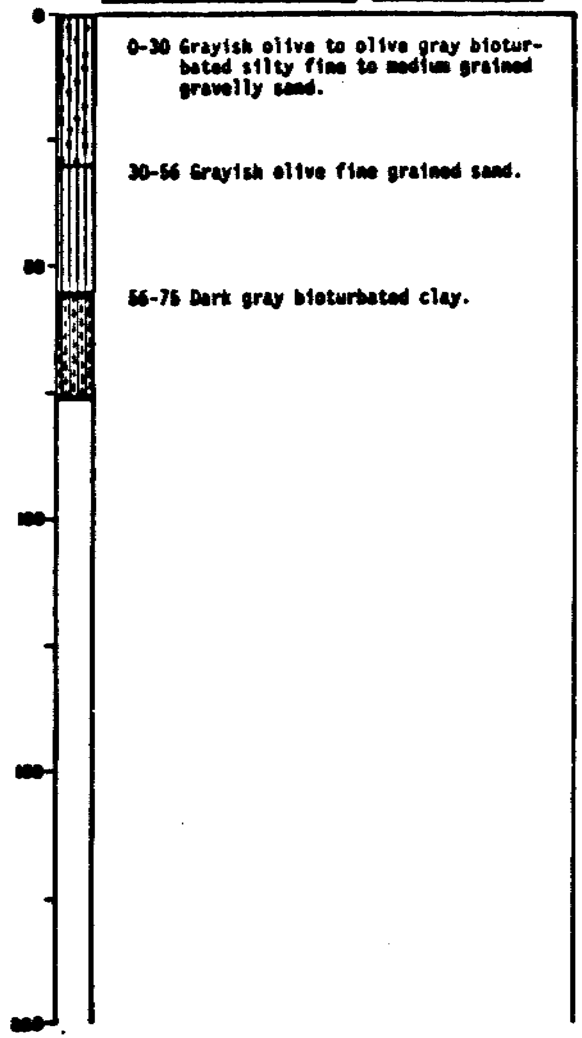

LOG OF KEIL CORE L780BS #41

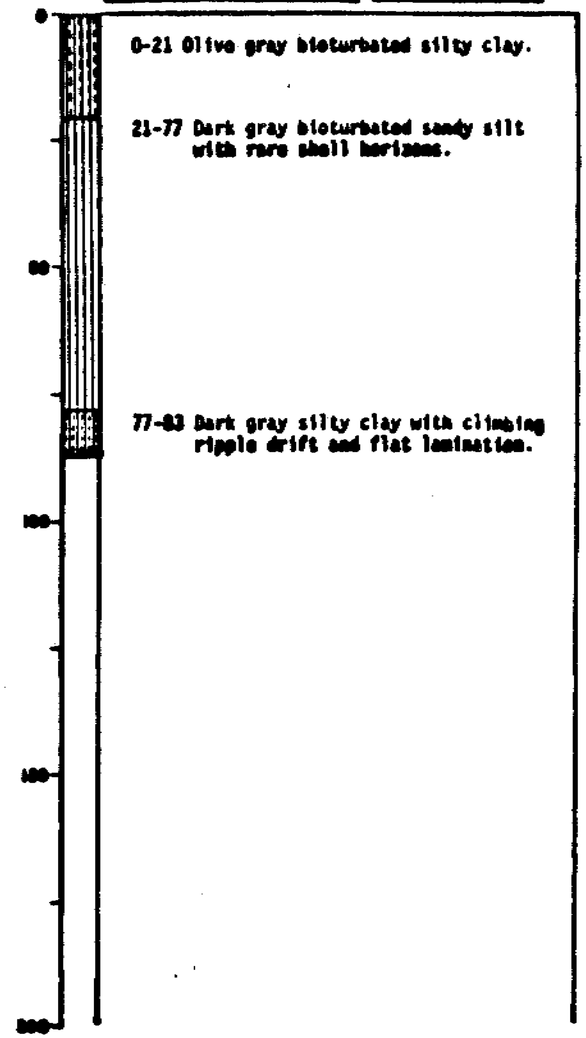

LOG OF KEIL CORE L780BS #42

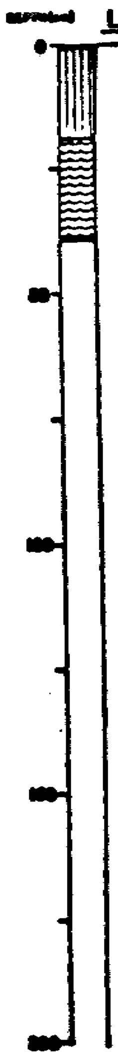

0-20 Olive gray silt and fine grained sand with rare shell horizons.

20-36 Olive gray to dusky yellowish brown pasty mud.

LOG OF KEIL CORE L780BS #45

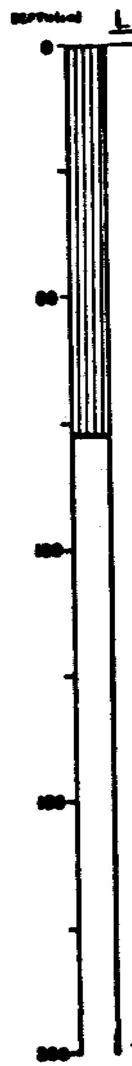

0-76 Olive gray to grayish black bioturbated silty very fine grained sand with rare shell horizons.

LOG OF KEIL CORE L780BS #46

0-90 Olive gray to greenish black bioturbated silty fine sand with rare shell horizons.

LOG OF KEIL CORE L780BS#47

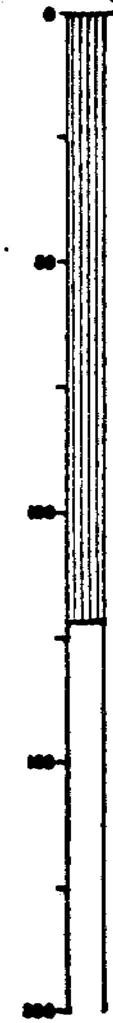

0-120 Light olive gray to greenish black silty fine grained bioturbated sand. Occasional shell hash layers 5-10 cm thick.

LOG OF KEIL CORE L780BS#48

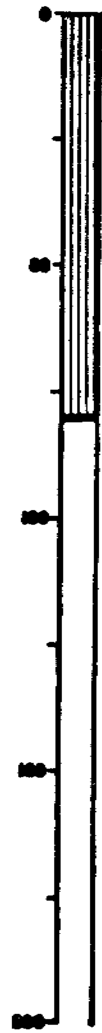

0-77 Grayish olive green to dark gray bioturbated silty fine sand with rare shell fragments.

LOG OF KEIL CORE L780BS#49

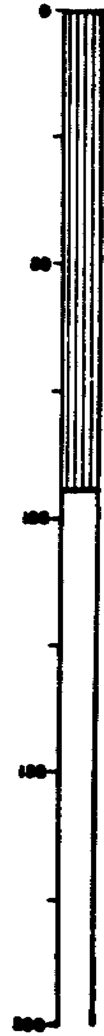

0-90 Grayish olive green to grayish black bioturbated fine grained silty sand with occasional shell hash layers 5 cm thick.

ANNUAL REPORT

CONTRACT #: 03-5-022-55
RESEARCH UNIT #: 483
REPORTING PERIOD: 1 April 1980 -
31 March 1981
NUMBER OF PAGES: 30

SEISMOTECTONIC STUDIES OF WESTERN ALASKA

Principal Investigators

N.N. Biswas
J. Pujol

Geophysical Institute
University of Alaska, Fairbanks
Fairbanks, Alaska 99701

Prepared for the

National Oceanic and Atmospheric Administration

Under Contract No. 03-5-022-55

TABLE OF CONTENTS

LIST OF FIGURES

LIST OF FIGURES (cont'd)

LIST OF TABLES

I. SUMMARY: OBJECTIVES, CONCLUSIONS AND IMPLICATIONS FOR OIL AND GAS DEVELOPMENTS

The objectives under the present study are to evaluate the extent of seismic hazards posed by earthquakes around Norton and Kotzebue Sounds. The ongoing locations of earthquakes employing the local seismographic network continue to show offshore and onshore seismic activity. The observed earthquake distribution patterns closely follow the mapped traces of geologic features, principally faults. Seismicity in the region is tentatively identified as of the intraplate type.

II. INTRODUCTION

A. General Nature and Scope of Study

In this report a preliminary attempt is made to synthesize the available earthquake data for the western Alaska area. The general trends of concentration of Alaskan earthquakes is shown in Figure 1. The locations of earthquake epicenters shown in this figure were compiled by Meyers (1976) from the Alaskan earthquake catalog of the United States Geological Survey. The data represent the time period from 1867 through 1974.

As Figure 1 illustrates, the predominant seismically active areas of Alaska are distributed along the southern coastal belts and in the central interior. West of 145^{O}W, earthquake activity is much more diffuse. The earthquakes in Meyers' (1976) catalog of magnitude 4.0 and above in the region of interest are labeled and shown at a larger scale in Figure 2. In this figure, a distinct concentration of epicenters with a northwest-southwest trend can be seen near 66^{O}N, 156^{O}W. This concentration reflects the magnitude

7.3 (m_b) Huslia earthquake of 1958 and its aftershock sequence. The surface effects on and around the epicenter of this earthquake have been reported by Davis (1960).

West of 156^{o}W, and around the Seward Peninsula, a number of earthquakes of magnitude greater than 5.0 occurred during the past 30 years. Because the area is sparsely populated, local effects passed largely undocumented. However, it could be demonstrated from this study that the areas offshore and onshore of Seward Peninsula are seismically quite active.

B. Scientific Objectives

The specific objectives of this study are the following:

(i) To determine the spatial and temporal characteristics of the seismicity, and its relationship to mapped tectonic features.

(ii) To determine the predominant failure mechanisms associated with the earthquakes located along or near the known geological features or trends.

(iii) To determine magnitudes, and if possible, recurrence rates of strong earthquakes in Norton Sound for use in projections as to possible activity in the future.

(iv) To determine the characteristics of velocity spectra and seismic energy attenuation as function of spicentral distance.

(v) To synthesize results of studies under (i)-(iv) in order to integrate the seismotectonic settings of the study areas with the overall tectonic framework of Alaska.

C. Relevance to Problems of Petroleum Development

Large scale exploration programs for hydrocarbon concentrations, and their eventual development in the offshore areas around Seward Peninsula are anticipated to take place in the near future. Consequently, the evaluation of the level of seismicity for these areas is a logical undertaking to assist in the planning and design of future construction projects.

III. CURRENT STATE OF KNOWLEDGE

As mentioned earlier, it appears from the past data that seismic activity around Seward Peninsula in western Alaska tends to occur in both offshore and onshore areas. The largest earthquake to have been instrumentally documented in western Alaska occurred about 30 km inland from the northern coast of Norton Sound in 1950, and was of magnitude 6.5. Since then, recording at stations remote from the area has failed to reveal any further significant seismic activity. However, the present study utilizing a localized seismographic network demonstrates clearly that a characteristic of the ongoing seismicity is an approximate north-south distribution of epicenters passing through the area of the 1950 earthquake. In addition, earthquakes located during a four-year period (1977-80) were widely distributed throughout the entire area, including Norton and Kotzebue Sounds. Most significantly, there are a number of instances where earthquake clusters tend to lie along, or parallel to, mapped faults or linear structural trends. A preliminary estimate of the magnitudes of earthquakes recorded during the reporting period ranged from about 2.0 to 5.6. The largest one of magnitude 5.6 was located just north of Kotzebue during July, 1981 and was felt there quite widely.

IV. STUDY AREA, SOURCES, METHODS AND RATIONAL OF DATA COLLECTION

The outline of the study area by heavy lines shown in Figure 1 and the locations of the seismograph stations of the operational network around Norton and Kotzebue Sounds are shown in Figure 3. It may be noted in these figures that the area of interest is relatively large. However, the densification of the network around Norton Sound carried out during the reporting period has improved the location capabilities of earthquakes in and around Seward Peninsula.

Each station of the operational network consists of a short period vertical component seismometer (Geotech S13), set to a nominal one-second natural period with 0.5 of critical damping. However, the station located at Kotzebue (KTA) has three components (vertical, north-south and east-west) and is equipped with different model seismometers (Geotech S500) than the other stations. This model of seismometer is small enough (0.057 m diameter and 0.165 m length) to facilitate installation, and has the added benefit of being insensitive to ground tilt. This is particularly important because a layer of permafrost is encountered at shallow depth (1-2 ft) at this station site.

The signals from the seismometers are preamplified by either Geotech Model 42-21 or Monitron Model 2000 amplifiers. The electronic systems of all stations, except for the one at Kotzebue (KTA), are powered by a set of Carbonaire Model ST-22 batteries delivering 1100 AMP-hr of service. The electronic package at KTA is powered by locally available 110V lines. The data from the stations are telemetered to the central recording site at the Northwest Community College at Nome by frequency-modulated audio subcarriers via a combination of VHF (transmitter: Monitron T15F; receiver: Monitron R15F) and microwave (leased Alascom circuits).

The central recording setup at the Northwest Community College, Nome, consists of an uninterruptable power supply system (TOPAZ), a discriminator bank (EMTEL), synchronized digital clock (True-Time) and a 16 mm film recorder (Geotech). The recording system is well stabilized. The film record is changed daily and shipped to Fairbanks on a weekly basis.

The short and long-period data from the local Nome seismographic station AVN are telemetered to the Geophysical Institute by Alascom microwave circuit. This long circuit has been leased by the Alaska Tsunami Warning Center, Palmer. Though the station is operated by us, the data are shared by both the organizations. Station location details are given in Table 1.

At the Geophysical Institute, the telemetered data from AVN are recorded on heat sensitive paper by Helicorder (Geotech RV-301B). This recording mode facilitates the identification of local earthquakes and approximate origin time for rapid scaling of the daily film records recorded at the central recording site (Nome). The following data are scaled from the records: first arrival times of the P-wave and the S-wave when possible, direction of P-wave first motion, and the maximum amplitude and period in the recorded trace.

For impulsive arrivals, the first onset times for P-waves could be scaled with a precision of $\pm$ 0.1 sec, while for emergent arrivals, the uncertainty in the arrival times might be as high as $\pm$ 0.5 sec. For S-wave arrivals, uncertainty of the measurements is even larger.

Scaled data for each earthquake are input in appropriate format to the VAX 11/780 computer and processed by the computer program of Lee and Lahr (1975) for location purposes. The magnitude (M_L) of the earthquakes are computed by using the formula of Richter (1958) for local earthquakes, incorporating a correction factor for the instrumentation used.

V. RESULTS

The crust and upper mantle structure of western Alaska is not yet known. However, an attempt will be made to resolve this problem, particularly for the Norton Sound area, from the data of the present densified network in the near future. At present, P-wave travel time used in the location of earthquakes are based on a plane layered P-wave velocity model for the crust obtained from central Alaskan data from earthquakes and quarry blasts. The upper mantle section is taken from Biswas and Bhattacharya (1974). The details of this model are shown in Table 2. A ratio of 1.78 between P- and S-wave velocities, corresponding to Poisson's solid, is used for the computation of S-wave travel times.

With the limitations mentioned above, a preliminary computer run on the scaled data is made and the output is examined for reading errors. If the time residuals for an earthquake (that is, the difference between the observed and computed travel times) for any station exceed 1 sec, the records are rescaled to reduce the uncertainties to a minimum. The corrected data are then used for a second computer run allowing all focal parameters to vary.

The details of the earthquakes located by following the above procedure during the reporting period are given in Table 3. All solutions are based on a weighted least squares minimization technique. The symbols NO, GAP, DMIN, RMS, ERH and ERZ of this table refer, respectively, to the number of station readings used to locate each earthquake, largest azimuthal difference between two neighboring stations with respect to the epicenter, distance of the epicenter from the nearest station, the root mean square of travel time residuals, the standard error in epicentral location and the standard error in focal depth.

It may be noted in Table 3 that for a number of earthquakes, the locations are associated with significant uncertainty. It is planned to rescale the data for these events in the very near future. In this effort we also plan to recompute the magnitudes for all events incorporating the latest setting of system response. Thus, at this stage, the magnitude values were not incorporated in the list of Table 3. The locations of the earthquakes listed in this table are shown in Figure 4.

VI. DISCUSSION

To relate the epicenter locations to known tectonic features, all earthquakes located so far in the study area are plotted on an overlay of the mapped structural traces. The result is shown in Figure 5. The mapped geologic features located north of Kotzebue Sound, on Seward Peninsula and offshore in Norton Sound were taken from Eittreim et al. (1979), Grantz et al. (1979), Hudson (1977), and Johnson and Holmes (1977), respectively. The traces were enlarged photographically by a factor of about 10, digitized at close intervals, and converted to the same projection and scale as that used to plot the epicenters.

Despite the considerable scatter in the distribution of earthquakes seen in Figure 5, a number of distinct trends can be discerned. The inland trace of the Kaltag fault, a major tectonic element of the area, appears to traverse through the clusters labeled A. Offshore in Norton Sound, the earthquakes align along a trend (B-B) which appears to be offset 20-30 km northwest from the trace of the Kaltag fault. Along the trend B-B, a number of faults have been mapped by Johnson and Holmes (1977) from using marine geophysical data.

The seismic trend C-C in Norton Sound appears to follow closely a series of mapped faults and a basement ridge identifeid by Johnson and Holmes (1977). They also mapped a number of offshore faults (Figure 5) trending east-west from Port Clarence where earthquakes tend to cluster.

In Kotzebue Sound, where published results from marine geophysical surveys are lacking, two trends in the east-west direction (E-E and G-G) and one in the north-south direction (F-F) appear in the earthquake data. The trends E-E and G-G parallel the young geologic structures of Hope Basin and the mountains east of the basin, but it would be necessary to extend the marine surveys to this area to see if there are structural implications to the observed trends in seismicity.

Inland on the Seward Peninsula, the clustering of earthquakes and mapped fault traces is quite significant. For instance, the cluster H-H closely follows a well-defined fault system along the Darby mountains, and traverses the epicentral area of the 1950 earthquake (m_b = 6.5). About 75-100 km to the west of this zone, a second trend in seismicity (I-I) cuts across the Bendeleben-Kigluaik mountain trend, and closely follows the en-echelon type of fault system mapped there. Similar clustering of earthquakes apparently associated with mapped faults appears immediately to the east and northeast of Port Clarence. Grantz (1979, personal communication) suggests that the seismicity on the lower third of the Seward Peninsula may represent the tectonic activity along the young fault systems of the Kigluaik, Bendeleben and Darby complexes. Inland further east, the cluster labeled J coincides with the aftershock zone of the Huslia earthquake of 1958 (A_1-A_2, Figure 2). There are also a number of earthquakes located inland which cannot be associated with any mapped structures.

East of the study area, in central Alaska, earthquakes are a direct consequence of lithospheric plate subduction as shown by Bhattacharya and Biswas (1979). This phenomenon results in normal and strike-slip faulting at earthquake foci in the depth interval of 0-60 km, and underthrusting at greater depth. However, it is difficult to invoke this phenomenon as being the immediate cause of earthquakes in western Alaska, an area approximately 500 km distant from the Alaskan subduction zone. Rather, the seismicity in the study area appears to be of intraplate type and to belong to a separate tectonic regime.

In the evolutionary sequency, the region around Bering Strait in northwest Alaska and northeast Siberia have been interpreted by Grantz (1966), Churkin (1970, 1972) and Patton and Tailleur (1977) as having passed through compression in an east-west direction in the geologic past. This interpretation is based on the observed change in the orientation of structural grains from east-west and northwest-southeast directions in the Brooks Range and the Chukchi Sea (Figure 5), respectively, to a predominantly north-south direction on and around Seward Peninsula. The structural trend in the latter area undergoes an oroclinal bend (Patton and Tailleur, 1977) on and near St. Lawrence Island in the northern Bering Sea and terminates on Chukotsk Peninsula.

A number of authors have used lithologic correlation to substantiate the above interpretation and to classify the area of interest as a representative of a tectonic province separate from the adjoining section (Yukon-Koyukuk) of Alaska. These features, as summarized by Patton and Tailleur (1977), are shown in Figure 6.

The current tectonic orientation of the stress distribution in the study area is not understood well. It needs to be ascertained from the data concurrently gathered by the local seismographic installation. However, in collaboration with Prof. K. Aki of Massachusetts Institute of Technology, we are studying the source mechanisms of strong earthquakes located in the area.

The study just mentioned involves the analyses of Rayleigh waves recorded by the long-period vertical component World Wide Standard Seismographic Network (WWSSN). In order to test the computer programs adopted on the VAX 11/780 computer of the Geophysical Institute, we acquired the WWSSN data from the National Data Center, Boulder, for the earthquake (magnitude of 5.8) located just northeast of Norton Sound. This earthquake occurred in 1965 and labeled in Figure 2.

The focal mechanism of the above earthquake has been compiled by Sykes and Sbar (1974), the solution shows normal faulting with the tension axis oriented approximately northeast-southwest. This solution was obtained from short-period data which were analyzed in time domain.

The present study consists of the analyses of complex spectra of Rayleigh waves in frequency domain to evaluate the components of moment tensor which in turn provide the values of the parameters of faulting mechanisms. The results are summarized in Table 4 and compared with those of Sykes and Sbar (1974) in Figure 7. As can be seen in this figure, the solutions show close agreement and we conclude that the computer programs are checked well and they can now be used for other events.

Concerning the inferred intraplate nature of seismicity of western Alaska, note that the trend of seismicity H-H (Figure 5), in addition to lying on a fault zone, tends to follow closely a plutonic belt with alkaline magnetism (Figure 6). Further, this belt is aligned transversely to the northern coast line of Norton Sound. These features are some of the typical characteristics of many other zones of intraplate seismicity as noted by Sykes (1978). However, the seismic data (Figure 5) do not show any correlation between the locations of earthquakes and similar zones or magnetism (Figure 6) occurring immediately east of Kotzebue Sound, on the southern coast of St. Lawrence Island, or at the northeastern corner of Chukotsk Peninsula.

VII. CONCLUSION

Within the last 20 years, the strongest instrumentally recorded earthquake in western Alaska was a magnitude 7.3 earthquake, located near Huslia in the Koyukuk River basin. Several earthquakes of magnitude greater than 5.0 have occurred on and around the Seward Peninsula with one event located about 400 km offshore in the Chukchi Sea. Because the areas around the epicenters of these earthquakes are thinly populated, their seismic impact passed largely undocumented.

Crustal earthquakes commonly migrate with time along a fault or fault system. This means that if a given section of an active fault yields (resulting in an earthquake), then at a later time a somewhat distant point of the same fault may yield to accumulated stresses. This points to the necessity of determining the trend of the faults both in offshore and onshore areas for an appropriate geohazard assessment for an area.

Since the installation of a local seismographic network, about 450 earthquakes, predominantly of crustal origin, and in the magnitude range of $2.0 < M_L < 5.4$ have been located. Despite location uncertainties due to unknown crust-upper mantle velocity structure, the epicenters of these earthquakes are found in some cases to follow closely the offshore and onshore traces of mapped faults. Some of these seismic trends traverse the epicentral areas of the past strong earthquakes.

We make no attempt at this stage of our study to interpret the detailed tectonic significance of the observed trends in seismicity and the associated seismic hazards posed by these features from the available data. However, in contrast to the contiguous areas of central Alaska, the Seward Peninsula area appears to represent a separate tectonic province with associated seismicity of the intraplate type.

ACKNOWLEDGEMENTS

We thank Mr. R. Cobelliek, Dr. L. Thorsteinson and J. Gravitz of the Arctic Project Office (OCSEAP) for their continuous support and encouragement during the study period. We express appreciation to Mr. R. Eppley and other members of the Alaskan Tsunami Warning Center of NOAA for their cooperation in operating the seismographic network. We are also grateful to Mr. G. Lapin and Ms. Jody Hilton of OCSEAP for logistic support in time.

This research was supported by the NOAA Contract No. 03-6-022-55, Task #12, and by the State of Alaska funds appropriated to the Geophysical Institute through the University of Alaska.

REFERENCES

Bhattacharya, B. and N.N. Biswas (1979). Implications of North Pacific plate tectonics in central Alaska: focal mechanisms of earthquakes, Tectonophysics, 53, 99-130.

Biswas, N.N. and B. Bhattacharya (1974). Travel-time relations for the upper mantle P-wave phases from central Alaskan data, Bull. Seism. So. Am., 64, 1953-1965.

Churkin, M., Jr. (1970). Fold belts of Alaska and Siberia and drift between North America and Asia, the Proceedings of the Geological Seminar on the North Slope of Alaska, Am. Assoc. Petroleum Geologists, Pacific Sec., W.L. Adkinson and M.M. Brosġe, Editors, Los Angeles.

Churkin, M., Jr. (1972). Western boundary of the North American continental plate in Asia, Bull. Geol. Soc. Am., 83, 1027-1036.

Davis, T.N. (1960). A field report on the Alaskan earthquakes of April 7, 1958, Bull. Seism. Soc. Am., 50, 489-490.

Eittreim, S., A. Grantz, and O.T. Whitney (1979). Cenozoic sedimentation and tectonics of Hope Basin, southern Chukchi Sea, in The Relationship of Plate Tectonics to Alaskan Geology and Resources, Proceedings of the Sixth Alaska Geological Society, B-1 to B-11.

Grantz, A. (1966). Strike-slip faults in Alaska, U.S. Geol. Surv., Open-File Rept. 267.

Grantz, A., S. Eittreim, and D.A. Dinter (1979). Geology and tectonic development of the continental margin north of Alaska, Tectonophysics, 59, 263-291.

Hudson, T. (1977). Geologic map of Seward Peninsula, Alaska, U.S. Geol. Surv., Open-File Rept. 77-796A.

Johnson, J.L. and M.L. Holmes (1977). Preliminary report on surface and subsurface faulting in Norton and northeastern Chirikov Basin, Alaska, in Environmental Assessment of the Alaskan Continental Shelf: Hazards and Data Management, NOAA, Report XVIII, 14-41.

Lee, W.H.K. and J.C. Lahr (1975). A computer program for determining hypocenter, magnitude, and first motion patterns of local earthquakes, U.S. Geol. Surv., Open-File Rept. 75-311.

Meyers, H. (1976). A historical summary of earthquake epicenters in and near Alaska, NOAA, Technical Memorandum EDS NDSDG-1.

Patton, W.W., Jr. and I.L. Tailleur (1977). Evidence in the Bering Strait region for differential movement between North America and Eurasia, Bull. Geol. Soc. Am, 88, 1298-1304.

Richter, C. (1958). Elementary Seismology, W.H. Freeman and Co., San Francisco.

Sykes, L.R. (1978). Intraplate seismicity, reactivation of pre-existing zones of weakness, alkaline magmatism, and other tectonic post-dating continental fragmentation, Rev. Geophys. Space Phys., 16, 621-688.

Sykes, L.R. and M.L. Sbar (1974). Focal mechanism solutions of intraplate earthquakes and stress in the lithosphere, in Geodynamics of Iceland and the North Atlantic Area, proc. NATO Advanced Study Inst. Reykjavik, Iceland, L. Kristjanssen, Editor, D. Reidel Publishing Co., U.S.A.

Table 1

Location Details of the Seismographic Network

Station Name	Code	Lat. (N) Deg.	Lat. (N) Min.	Long. (W) Deg.	Long. (W) Min.	Elevation (m)	Site Geologic Formation	Satellite Delay at Nome (sec)
Anvil Mt.	AVN	64	33.90	165	22.28	323	Metamorphic (fractured schist and gneiss)	0.00
Alder Creek	ACK	66	00.50	162	11.70	377	Parmafrost	0.54
Besboro Is.	BBO	64	07.27	161	18.30	244	Volcanic (large fractured blocks)	0.00
Cape Derby	CDY	64	20.75	162	47.60	335	Metamorphic (fractured schist and gneiss)	0.00
Christmas Creek	CKR	64	45.60	160	39.50	305	Sedimentary (fractured sandstone)	0.00
Devil Mt.	DMA	66	17.80	164	31.35	238	Volcanic (piles of small grains)	0.54
Ear Mt.	EAM	65	55.34	166	12.30	701	Metamorphic (fractured schist and geniss)	0.54
Kogog River	KGR	63	09.70	162	03.10	320	Sedimentary (weathered sand stone)	0.00
Kotzebue	KTA	66	50.48	162	35.22	24	Permafrost	0.54
Teller	TLR	65	19.10	166	12.70	122	Volcanic (weathered)	0.54
Tin City	TCY	65	33.98	167	57.35	72	Sedimentary (fractured shales and limestone)	0.54

Table 1 (cont'd)

Station Name	Code	Lat. (N) Deg.	Lat. (N) Min.	Long. (W) Deg.	Long. (W) Min.	Elevation (m)	Site Geologic Formation	Satellite Delay at Nome (sec)
Topkok Pt.	TPK	64	33.36	163	59.80	122	volcanic (large fractured blocks)	0.00
Savoonga	SOV	63	38.79	170	26.94	198	volcanic (large fractured blocks)	0.54
Stuart Is.	SUE	63	35.84	162	26.11	140	volcanic (piles of medium size pieces)	0.00
Stations Closed in September 1981								
Kanguksam Mt.	KGS	63	18.13	168	59.25	488	Intrusives	0.54
Kookooligit Mt.	KKL	63	35.33	170	22.53	655	volcanic (large fractured blocks)	0.54
Poovook Mt.	PVK	63	26.34	171	33.13	411	volcanic (large fractured blocks)	0.54

Table 2

P-Wave Velocity Structure of the Crust and Upper Mantle Used to Compute Travel Times for Hypocenter Locations

Layer Thickness (km)	P-Wave Velocity (km/sec)
24.4	5.9
15.8	7.4
35.8	7.9
225.0	8.29
244.0	10.39
∞	12.58

TABLE 3

Location Details of Earthquakes Located in 1981

Date (Yr.Mo.Day)	O.T. (Hr.Min.Sec)	Lat. (Deg.Min)	Long. (Deg.Min)	Depth (km)	NO	GAP	DMIN	RMS	ERH	ERZ
810104	1227 38.33	64N42.27	165W 0.79	2.23	5	220	262.9	2.48	8.2	16.3
810104	1227 44.42	64N58.88	155W34.10	39.31	4	203	248.0	2.33	8.6	99.0
810110	123 45.02	64N45.67	170W43.17	39.33	7	220	157.5	5.55	99.0	99.0
810110	123 39.81	65N21.74	171W31.56	2.51	4	255	214.4	0.76	42.5	99.0
810110	811 27.30	65N50.54	163W25.61	5.59	5	117	145.9	3.08	10.8	26.4
810110	811 26.99	65N54.21	163W59.35	5.00*	4	133	150.3	2.19	21.3	48.2
810120	15 6 43.21	64N 6.76	161W17.68	0.42	6	159	77.3	16.69	99.0	99.0
810120	1753 2.35	65N58.35	166W10.74	0.00*	3	183	93.1	1.15	8.6	99.0
810121	336 45.20	65N49.84	166W36.26	2.18*	5	174	107.6	0.08	73.5	93.2
810121	336 45.20	65N49.80	166W36.25	2.11*	4	173	107.6	0.09	82.0	99.0
810121	1443 51.28	66N 6.42	164W18.32	16.30	5	157	97.6	0.22	6.4	5.6
810121	1443 51.09	66N 5.39	164W15.43	14.94	4	159	95.1	0.00	7.5	9.2
810126	1150 12.92	64N26.73	164W11.27	5.00*	3	301	207.0	0.00	54.5	99.0
810126	236 32.64	65N43.96	166W 7.20	0.40	9	93	96.0	0.52	3.8	10.3
810126	236 32.94	65N44.99	166W 7.81	0.22*	6	91	95.1	0.41	5.7	13.7
810126	20 9 52.99	64N48.63	165W 7.32	0.00*	13	99	134.5	10.65	62.6	81.9
810126	20 9 48.70	64N24.54	165W11.94	0.56*	7	183	175.7	0.56	15.5	12.4
810128	1346 10.69	65N37.80	164W 7.74	92.92	8	138	102.1	1.97	28.5	75.4
810128	1345 38.44	66N27.09	165W19.73	428.63	5	215	129.1	0.63	49.3	99.0
810130	831 54.31	65N31.56	164W 7.49	0.31*	5	210	106.8	0.49	6.3	6.5
810201	1339 14.29	64N11.89	169W38.61	2.50*	5	180	172.2	2.19	7.4	19.5
810201	1339 14.46	64N 9.87	170W 9.89	5.00*	3	174	188.1	0.00	99.0	99.0
810112	854 53.66	65N31.90	166W58.29	1.69	8	130	131.6	0.15	1.1	2.8
810112	854 53.61	65N32.15	166W59.80	3.92	4	130	132.5	0.00	3.2	7.3
810214	222 14.50	65N46.98	166W11.21	5.00*	4	201	94.8	0.50	99.0	99.0
810214	222 14.72	65N47.85	166W 7.49	5.00*	3	200	91.6	0.00	99.0	99.0
810214	1512 5.16	67N 3.91	166W 5.75	0.00*	5	294	186.8	0.84	9.0	7.8
810214	1512 7.25	66N54.81	166W12.48	5.00*	3	285	169.6	0.00	99.0	99.0
810214	1855 26.07	65N30.76	168W18.53	0.00*	4	353	193.5	0.36	51.2	11.6
810214	1855 28.72	65N35.04	167W58.11	0.00*	3	260	176.0	0.16	99.0	99.0
810216	625 15.74	64N13.59	165W19.53	0.16	4	273	242.6	2.32	99.0	8.1
810216	710 53.25	65N55.62	165W51.02	19.94	4	147	153.5	5.06	23.6	19.2
810217	1514 2.52	65N57.17	172W19.89	5.00*	10	283	279.5	2.53	69.7	74.4
810217	1514 17.54	65N11.72	169W46.61	23.19*	5	234	182.0	1.43	19.9	93.1
810229	1049 52.20	62N16.99	168W46.21	57.77	4	300	424.0	0.67	99.0	99.0
810219	1849 10.12	62N18.04	167W30.23	5.27	5	290	408.4	1.78	99.0	99.0
810219	1426 7.54	65N55.41	166W14.22	0.00*	3	185	192.6	4.35	99.0	99.0
810221	1429 20.44	63N32.51	167W 7.84	6.47	4	263	100.0	0.39	99.0	99.0
810222	854 5.33	69N 7.70	167W 6.29	77.32	4	329	359.5	0.34	99.0	99.0
810223	713 13.04	64N51.00	166W12.12	47.31*	6	205	249.0	3.78	10.6	99.0
810223	713 12.68	64N39.73	166W22.17	5.00*	3	220	251.6	0.00	99.0	99.0
810223	537 13.94	64N59.06	160W17.69	5.00*	5	312	182.3	5.50	33.3	22.6
810223	536 42.87	67N41.69	162W 6.32	5.00*	3	341	400.2	5.25	99.0	99.0
810223	4 2 8.40	65N43.47	166W 9.99	10.77	9	93	203.2	6.83	99.0	99.0
810223	4 2 6.79	65N41.46	165W50.14	10.77	6	87	194.2	8.17	99.0	99.0
810224	22 4 31.10	65N11.94	151W11.87	29.27	4	317	548.6	0.77	99.0	99.0
810224	22 5 7.60	65N45.16	158W11.56	45.38	8	271	234.1	4.30	99.0	99.0
810224	22 4 26.81	65N 7.82	150W52.07	5.20	4	318	565.3	0.37	99.0	99.0
810224	525 25.20	64N33.71	164W51.21	25.64	6	233	165.1	10.81	17.2	99.0
810224	524 45.96	61N 1.99	165W37.00	5.00	4	335	545.9	3.15	99.0	99.0
810215	747 36.68	64N46.24	162W43.52	6.19	4	313	100.0	0.20	99.0	99.0
810226	1953 34.04	64N15.95	162W24.11	0.31*	7	111	100.5	0.77	12.0	24.2

TABLE 3 (cont'd)

Location Details of Earthquakes Located in 1981

Date (Yr.Mo.Day)	O.T. (Hr.Min.Sec)	Lat. (Deg.Min)	Long. (Deg.Min)	Depth (km)	NO	GAP	DMIN	RMS	ERH	ERZ
810225	2138 25.64	65N38.72	162W58.58	5.00*	3	270	134.5	0.00	99.0	99.0
810227	2019 59.95	65N 1.74	167W52.82	1.25*	10	140	130.0	1.00	4.4	8.3
810227	2019 59.95	65N 2.15	167W56.71	1.25*	5	143	133.1	0.79	4.2	7.6
810227	6 2 20.97	63N52.97	160W 2.46	5.88	8	247	128.5	3.43	52.8	61.4
810227	6 2 12.16	63N19.75	159W20.36	0.00*	4	284	160.1	1.01	25.3	13.0
810228	1033 6.88	64N21.20	162W39.77	3.55	11	90	108.3	0.46	4.6	5.1
810228	217 19.24	65N17.81	167W11.52	29.05*	4	177	165.4	0.65	12.2	60.0
810228	217 19.02	65N18.98	166W50.19	5.00*	3	158	152.2	0.00	99.0	99.0
810228	555 54.32	64N51.69	168W14.93	77.87	9	154	150.6	24.34	99.0	99.0
810228	556 3.48	65N13.99	167W 3.63	1.25*	7	85	115.3	0.98	5.3	9.5
810301	1120 33.41	65N58.87	165W 3.61	40.80	6	158	158.6	9.44	43.2	99.0
810301	1120 40.79	65N57.44	165W23.24	5.00*	3	164	162.3	0.00	99.0	99.0
810302	1430 35.00	63N37.73	152W16.58	2.50	17	119	241.1	3.67	39.7	99.0
810302	1416 58.76	65N 6.01	167W52.73	38.04	6	239	133.3	5.49	99.0	99.0
810302	1416 59.38	65N 7.01	167W51.40	5.00*	3	237	133.2	0.00	99.0	99.0
810303	639 38.98	64N55.79	162W29.75	2.50*	10	179	178.8	1.17	14.1	32.6
810303	639 39.67	64N53.59	162W25.27	2.50*	6	180	184.1	0.96	21.6	30.4
810303	139 45.57	65N33.59	166W57.84	0.35*	8	128	133.8	0.75	4.8	99.0
810303	139 46.31	65N37.68	167W 1.45	5.85	4	147	135.9	0.00	6.6	8.0
810304	12 3 37.44	64N25.31	162W43.06	5.74	7	158	108.6	0.32	6.7	6.5
810304	12 3 37.43	64N25.36	162W43.16	5.77	5	158	108.7	0.38	4.2	4.0
810305	1921 35.27	64N52.18	162W 9.73	15.27	8	107	93.1	0.84	19.5	26.2
810305	1921 35.19	64N54.63	162W13.85	9.16	5	108	98.6	0.84	8.0	14.5
810306	439 58.72	63N30.68	163W58.31	24.38	6	275	289.8	4.17	99.0	99.0
810306	439 48.83	63N 0.26	164W40.17	5.00	5	294	334.0	4.04	57.7	99.0
810306	439 58.72	63N30.68	163W58.31	24.38	6	275	289.8	4.17	99.0	99.0
810306	439 48.83	63N 0.26	164W40.17	5.00	5	294	334.0	4.04	57.7	99.0
810307	1025 11.60	65N20.94	165W37.11	2.50*	6	104	117.0	1.12	54.7	99.0
810307	20 3 42.94	66N14.91	165W51.73	5.00	5	213	122.0	3.68	99.0	99.0
810307	20 3 41.70	66N 5.71	165W25.49	5.00*	3	182	130.0	3.21	99.0	99.0
810307	919 37.85	64N19.77	163W26.53	5.74	4	294	146.2	6.41	31.6	32.9
810307	919 33.78	64N22.59	164W 7.46	0.00*	3	310	168.5	6.80	99.0	99.0
810307	458 53.09	64N54.08	165W 7.23	40.82	5	193	244.2	2.60	17.9	99.0
810307	458 53.37	64N59.09	164W43.96	5.00*	3	179	240.6	0.00	99.0	99.0
810307	1025 11.52	65N20.63	165W36.78	1.25*	6	105	117.4	1.11	54.1	99.0
810307	20 3 38.17	66N27.06	166W15.69	5.00*	5	245	125.1	2.34	99.0	99.0
810307	20 3 40.37	66N 3.97	165W32.01	5.00*	3	183	124.1	0.85	99.0	99.0
810307	919 38.51	64N21.45	163W21.67	6.47	4	298	147.0	6.40	99.0	99.0
810307	919 33.51	64N18.28	164W12.02	0.00*	3	306	164.8	6.77	99.0	99.0
810307	458 53.09	64N54.08	165W 7.23	40.82	5	193	244.2	2.60	17.9	99.0
810307	458 53.37	64N59.09	164W43.96	5.00*	3	179	240.6	0.00	99.0	99.0
810307	1025 11.02	65N17.29	165W38.97	2.50*	9	60	111.6	1.30	9.6	18.0
810307	20 3 36.97	65N34.67	165W 7.04	2.25	6	167	113.6	2.03	52.5	99.0
810307	20 3 36.17	65N38.59	164W57.32	2.50*	4	174	121.8	1.76	4.2	7.8
810307	19 2 18.31	64N14.39	162W17.47	5.00*	3	178	152.9	0.00	99.0	99.0
810307	919 33.59	64N23.63	163W49.86	3.57	6	172	126.0	5.33	99.0	99.0
810307	919 34.33	64N19.34	164W 4.56	3.05	4	154	136.5	5.73	10.5	10.0
810307	458 53.95	65N19.83	163W56.77	47.58	7	195	184.5	3.31	99.0	99.0
810307	458 55.28	65N25.67	163W46.61	38.57	4	205	187.2	1.01	8.2	99.0
810311	2026 27.42	66N 9.35	163W48.90	45.76	4	256	343.3	3.91	39.8	99.0
810311	1017 45.47	64N47.97	163W15.05	0.31*	4	219	137.9	0.42	7.6	9.5
810311	2026 28.99	65N13.57	164W43.25	36.50*	5	169	204.3	0.79	55.4	99.0
810311	2026 27.30	65N16.56	164W18.02	5.00*	3	183	192.4	0.00	99.0	99.0

TABLE 3 (cont'd)

Location Details of Earthquakes Located in 1981

Date (Yr.Mo.Day)	O.T. (Hr.Min.Sec)	Lat. (Deg.Min)	Long. (Deg.Min)	Depth (km)	NO	GAP	DMIN	RMS	ERH	ERZ
810312	15 6 31.26	64N47.90	162W16.40	0.33*	7	180	181.9	0.49	10.8	9.9
810312	15 6 31.78	64N45.87	162W16.51	0.06*	4	178	178.1	0.31	5.2	8.5
810312	756 36.54	63N20.71	172W55.05	0.00*	3	360	100.0	1.21	99.0	99.0
810312	457 51.72	65N28.03	161W50.45	5.00*	3	183	208.5	0.00	8.0	99.0
810312	23 0 35.26	64N 5.50	160W18.25	13.52	6	297	135.0	0.39	14.1	7.9
810312	23 0 39.33	63N56.04	160W58.48	5.00*	3	250	101.0	0.00	99.0	99.0
810312	15 6 30.67	64N49.60	162W12.96	0.60*	11	102	90.0	0.62	6.0	7.8
810312	15 6 30.79	64N49.15	162W12.72	2.50*	7	101	89.2	0.79	10.3	20.1
810312	457 44.51	65N 4.47	162W31.68	181.25	7	152	196.2	9.22	99.0	99.0
810312	457 51.72	65N28.03	161W50.45	5.00*	3	183	208.5	0.00	8.0	99.0
810312	23 0 36.32	64N 3.15	160W24.39	13.89	8	225	120.5	0.48	7.1	6.4
810312	23 0 35.40	64N 0.33	160W20.18	10.36	4	230	125.3	0.00	7.3	6.7
810313	22 0 4.39	64N50.92	162W21.20	7.01	9	106	95.5	1.15	16.5	31.5
810313	22 0 4.65	64N48.19	162W19.16	9.08	5	103	90.3	0.22	7.8	13.6
810314	2 6 57.99	65N13.01	165W49.43	0.22	6	222	173.7	0.72	39.4	44.2
810314	2 6 58.42	65N14.04	165W52.70	1.25*	4	224	176.9	0.66	8.6	10.9
810314	1539 48.79	65N 2.66	168W59.21	1.16	6	197	175.6	0.28	99.0	42.3
810314	1539 48.18	65N 9.57	169W20.20	0.00*	3	219	182.1	0.05	99.0	99.0
810314	855 8.71	64N26.69	161W30.39	60.28	4	265	144.9	0.00	12.3	10.4
810314	854 19.40	67N 9.60	156W 2.17	5.00*	3	348	527.0	0.61	99.0	99.0
810315	2 6 57.99	65N13.01	165W49.43	0.22	6	222	173.7	0.72	39.4	44.2
810315	2 6 58.42	65N14.04	165W52.70	1.25*	4	224	176.9	0.66	8.6	10.9
810315	1539 50.00	64N23.15	166W57.29	35.33	4	231	100.0	0.05	99.0	99.0
810315	855 13.28	64N 5.92	161W59.84	5.00*	3	140	103.7	0.00	99.0	99.0
810315	1244 7.20	64N 9.67	161W32.61	5.00*	3	182	113.6	0.00	99.0	99.0
810316	1939 6.97	65N42.12	167W22.54	0.06*	5	182	145.5	5.97	99.0	11.6
810316	1939 7.50	65N37.63	167W36.42	0.00*	3	185	158.7	7.28	99.0	99.0
810316	859 8.36	65N56.13	166W15.51	2.89	5	181	98.2	0.78	99.0	99.0
810316	859 8.54	65N56.04	166W10.09	5.00*	3	182	91.5	0.51	99.0	99.0
810316	7 2 17.09	64N57.86	162W22.10	25.26	4	230	100.0	0.17	99.0	99.0
810316	219 21.80	65N46.87	167W12.09	5.00*	3	189	134.5	0.33	99.0	99.0
810316	215 39.85	65N44.29	167W17.61	2.50*	6	186	140.4	1.29	99.0	32.2
810316	215 39.43	65N43.11	167W11.09	5.00*	3	182	137.0	0.03	99.0	99.0
810317	459 1.43	65N13.99	165W52.80	2.50*	7	186	133.9	0.53	15.2	15.8
810317	459 1.43	65N13.98	165W52.72	2.50*	6	186	133.9	0.59	23.3	22.3
810317	1831 10.95	64N53.22	162W13.74	14.66	9	106	96.2	0.58	6.9	10.8
810317	1831 10.73	64N54.46	162W16.48	2.72	6	106	99.3	0.51	12.9	28.2
810318	1731 12.88	64N45.17	162W32.22	37.57*	4	168	195.2	0.19	99.0	99.0
810318	1731 11.58	64N52.27	162W18.83	5.00*	3	193	188.8	0.00	99.0	99.0
810318	1720 14.89	66N 6.66	162W44.76	17.96	9	251	82.7	1.08	62.6	78.8
810318	1720 8.37	65N45.89	162W 0.23	4.97*	5	278	128.8	0.97	74.3	47.9
810318	2111 13.52	65N 3.86	167W 1.91	5.00*	3	204	100.0	0.00	99.0	99.0
810320	1910 26.58	65N11.52	157W 2.69	0.63*	4	162	169.1	0.35	6.1	8.0
810323	1451 12.34	65N19.71	162W21.64	1.58	4	184	146.4	0.24	99.0	99.0
810328	9 7 12.06	63N15.95	163W57.63	0.13*	4	238	160.5	0.29	13.7	12.9
810328	9 7 12.44	63N17.60	163W55.39	5.00*	3	235	158.6	0.00	99.0	99.0
810329	351 30.31	66N 1.43	163W16.49	5.00*	3	235	188.5	0.00	99.0	99.0
810330	1324 16.95	66N 2.53	167W30.25	1.25*	5	237	137.3	0.48	99.0	99.0
810330	1324 18.01	65N58.38	167W18.15	5.00*	3	221	130.8	0.00	99.0	99.0
810402	116 9.52	62N43.25	166W 8.36	5.00*	4	218	246.2	1.82	23.0	29.9
810402	116 12.15	63N15.24	166W 3.05	5.00*	3	187	219.3	0.00	12.3	99.0

TABLE 3 (cont'd)

Location Details of Earthquakes Located in 1981

Date (Yr.Mo.Day)	O.T. (Hr.Min.Sec)	Lat. (Deg.Min)	Long. (Deg.Min)	Depth (km)	NO	GAP	DMIN	RMS	ERH	ERZ
810404	1118 2.86	66N 2.91	165W40.17	5.00*	3	180	100.0	5.25	99.0	99.0
810404	1038 15.87	65N57.26	167W21.89	5.00*	3	221	134.1	0.00	99.0	99.0
810405	1755 56.29	65N46.86	169W15.11	5.00	4	323	222.3	0.90	65.1	39.1
810405	1756 5.26	65N35.20	167W42.86	5.00*	3	197	165.6	0.15	99.0	99.0
810406	2345 43.62	63N10.03	162W 4.81	4.58	6	310	417.3	10.12	99.0	99.0
810406	2346 14.80	65N13.21	169W 6.63	0.00*	3	216	191.8	2.13	99.0	99.0
810406	2333 31.76	62N46.25	161W11.79	4.72	6	316	470.9	9.47	99.0	99.0
810406	2334 14.82	65N11.19	167W55.72	5.00*	3	170	213.7	0.00	99.0	99.0
810407	716 32.56	65N41.77	168W11.71	4.16	6	285	179.7	6.42	99.0	99.0
810407	716 34.95	65N35.64	168W 4.73	0.04*	5	291	180.1	5.76	95.8	34.9
810407	132 37.06	66N 3.58	165W31.84	0.10	4	184	123.9	2.71	99.0	99.0
810407	132 36.77	66N 2.64	165W37.15	5.00*	3	183	119.5	2.97	99.0	99.0
810410	4 7 43.97	66N 1.19	166W23.38	5.00*	3	195	89.6	0.00	99.0	99.0
810410	545 53.15	63N 2.77	164W32.85	5.00*	3	251	330.8	0.00	99.0	99.0
810410	1142 20.21	63N10.46	171W57.96	5.00*	3	336	411.7	9.04	99.0	99.0
810410	433 58.47	65N56.19	167W28.26	5.00*	3	225	139.3	0.00	99.0	99.0
810411	8 8 18.06	66N 9.47	168W53.74	0.63*	5	299	197.6	1.02	5.1	10.2
810411	8 8 25.40	65N49.40	167W53.46	5.00*	3	245	161.2	0.00	99.0	99.0
810412	415 8.97	65N55.63	166W38.30	8.30*	4	190	104.2	0.28	99.0	99.0
810412	415 8.91	65N54.89	166W39.95	5.00*	3	190	105.9	0.00	99.0	99.0
810412	1824 54.33	65N42.01	167W17.15	0.06	6	182	142.0	0.42	99.0	99.0
810412	1824 54.53	65N40.46	167W17.26	5.00*	3	188	143.5	0.43	99.0	99.0
810413	3 8 7.25	66N 0.83	166W26.59	0.63*	5	188	92.1	0.66	5.3	9.6
810413	3 8 7.47	65N49.38	166W 6.14	2.50*	4	197	89.8	0.31	5.8	9.0
810413	2041 22.66	66N 2.08	167W50.05	0.63*	5	253	152.0	1.08	6.0	10.0
810413	2041 25.04	65N40.46	167W23.64	5.00*	3	183	147.7	0.06	99.0	99.0
810416	1931 24.73	65N16.99	175W 4.85	4.96	5	303	496.2	0.48	99.0	99.0
810417	2229 52.35	62N50.37	164W41.32	0.62	4	237	298.1	3.22	24.1	99.0
810417	253 35.65	66N32.76	164W54.32	1.25*	4	201	107.5	0.67	5.9	9.6
810420	1654 4.89	64N54.39	165W23.23	2.50*	8	122	139.0	1.50	23.3	27.8
810420	1654 4.96	64N57.94	165W 6.51	0.63*	5	117	130.3	1.05	5.4	7.0
810402	116 9.52	62N43.25	166W 8.36	5.00*	4	218	246.2	1.82	23.0	29.9
810402	116 12.15	63N15.24	166W 3.05	5.00*	3	187	219.3	0.00	12.3	99.0
810404	1117 51.76	65N38.99	167W33.73	25.55	4	180	155.7	7.12	99.0	29.2
810404	1117 30.43	65N36.86	171W23.19	0.00*	3	344	320.8	5.55	99.0	99.0
810404	1038 16.10	65N55.19	167W20.68	6.74	6	216	134.4	0.10	7.5	4.2
810404	1038 15.87	65N57.26	167W21.89	5.00*	3	221	134.1	0.00	99.0	99.0
810405	1755 56.29	65N46.86	169W15.11	5.00	4	323	222.3	0.90	65.1	39.1
810405	1756 5.26	65N35.20	167W42.86	5.00*	3	197	165.6	0.15	99.0	99.0
810406	2345 43.62	63N10.03	162W 4.81	4.58	6	310	417.3	10.12	99.0	99.0
810406	2346 14.80	65N13.21	169W 6.63	0.00*	3	216	191.8	2.13	99.0	99.0
810406	2333 31.76	62N46.25	161W11.79	4.72	6	316	470.9	9.47	99.0	99.0
810406	2334 14.82	65N11.19	167W55.72	5.00*	3	170	213.7	0.00	99.0	99.0
810407	716 34.00	65N38.35	167W58.76	2.93	6	253	173.2	6.40	99.0	99.0
810407	716 34.95	65N35.13	168W 4.76	0.00*	5	291	180.5	5.75	66.7	27.5
810407	132 37.06	66N 3.58	165W31.84	0.10	4	184	123.9	2.71	99.0	99.0
810407	132 36.77	66N 2.64	165W37.15	5.00*	3	183	119.5	2.97	99.0	99.0
810410	4 7 43.97	66N 1.19	166W23.38	5.00*	3	195	89.6	0.00	99.0	99.0
810410	545 53.15	63N 2.77	164W32.85	5.00*	3	251	330.8	0.00	99.0	99.0
810410	1142 20.21	63N10.46	171W57.96	5.00*	3	336	411.7	9.04	99.0	99.0

TABLE 3 (cont'd)

Location Details of Earthquakes Located in 1981

Date (Yr.Mo.Day)	O.T. (Hr.Min.Sec)	Lat. (Deg.Min)	Long. (Deg.Min)	Depth (km)	NO	GAP	DMIN	RMS	ERH	ERZ
810410	433 58.47	65N56.19	157W28.25	5.00*	3	225	139.3	0.00	99.0	99.0
810425	1049 15.37	64N59.29	152W46.79	5.00*	3	173	205.7	0.00	99.0	99.0
810425	1357 15.04	65N44.55	167W 4.21	0.16	5	357	235.6	15.19	99.0	47.8
810425	1357 19.35	65N52.42	156W27.56	0.00*	3	356	203.9	17.52	99.0	99.0
810426	150 11.36	64N30.30	156W 9.46	18.07	8	228	153.2	1.04	25.3	35.5
810425	150 9.23	64N25.23	156W16.58	5.00	4	234	158.4	0.79	11.3	99.0
810426	1911 55.54	66N 3.23	156W16.43	5.00*	3	207	99.6	0.00	99.0	99.0
810429	9 9 18.65	65N11.29	170W36.61	0.00*	4	335	369.7	7.38	99.0	99.0
810430	21 3 20.71	67N13.67	154W13.03	10.77*	4	252	173.5	1.28	61.0	39.9
810501	425 13.43	65N42.46	170W25.55	0.00*	3	338	275.0	1.73	99.0	99.0
810501	724 5.98	65N15.57	165W38.61	0.16	5	254	126.5	1.34	4.0	99.0
810501	724 10.72	66N 8.68	156W54.49	5.00*	3	225	108.8	0.00	99.0	99.0
810501	2041 14.30	65N45.97	165W57.37	0.31	5	174	125.3	0.55	20.1	8.0
810502	528 53.27	66N19.31	165W42.18	38.26*	5	238	101.8	1.07	46.1	75.3
810502	528 52.07	66N20.49	166W55.47	5.00*	3	244	107.9	0.00	99.0	99.0
810502	1749 46.79	66N 9.62	157W32.71	8.64*	5	248	137.0	0.37	7.1	9.9
810502	1749 47.19	66N 6.75	157W29.58	5.00*	3	242	135.4	0.00	99.0	99.0
810503	552 30.34	65N46.98	157W22.58	5.00*	3	198	141.7	0.32	99.0	99.0
810503	1254 13.95	64N56.22	159W43.92	0.31*	5	218	195.9	2.07	99.0	38.8
810503	1616 48.32	63N 7.70	168W21.75	0.12*	5	172	197.2	1.30	5.4	18.6
810503	1616 49.19	65N12.77	168W13.48	5.00*	3	168	208.7	0.00	99.0	99.0
810503	2254 22.84	66N20.52	166W 7.35	5.00	5	220	120.1	4.16	99.0	99.0
810503	2254 22.37	66N 3.08	155W33.10	5.00*	3	184	122.6	3.55	99.0	99.0
810504	11 8 36.25	66N16.86	164W31.25	0.53	4	245	100.0	12.41	99.0	99.0
810511	920 10.64	64N24.93	154W 7.01	5.00*	3	189	64.3	0.00	99.0	99.0
810515	1441 54.43	66N53.24	168W24.78	69.23	7	279	148.7	20.51	99.0	99.0
810515	1441 38.17	63N18.20	168W20.90	5.00	6	307	280.9	21.02	99.0	99.0
810515	2043 36.73	64N15.80	165W25.90	3.46*	9	235	187.6	3.44	72.0	91.8
810515	2043 39.99	64N31.63	154W48.92	2.12*	5	206	169.3	3.52	15.4	32.5
810516	1424 47.96	66N40.42	160W27.22	5.00*	3	257	287.3	0.00	99.0	99.0
810518	225 26.72	64N18.37	163W24.08	0.08*	4	233	228.0	0.73	15.9	9.5
810518	225 25.32	64N10.14	163W25.81	0.00*	3	270	242.7	0.58	99.0	99.0
810518	12 9 14.88	65N51.46	166W26.45	0.00*	3	354	100.0	5.21	99.0	99.0
810522	2017 19.60	66N 7.93	156W42.40	5.00*	3	217	100.1	0.00	99.0	99.0
810522	2234 55.09	65N35.80	155W37.99	5.00*	3	175	139.2	0.00	99.0	99.0
810522	550 56.34	65N32.52	159W 5.65	28.73	6	232	224.7	1.33	99.0	96.5
810522	550 50.38	65N44.10	159W46.85	0.26	5	249	241.0	0.94	23.9	15.1
810522	550 56.34	65N32.52	159W 5.65	28.73	6	232	224.7	1.33	99.0	96.5
810522	550 50.38	65N44.10	159W46.85	0.26	5	249	241.0	0.94	23.9	15.1
810526	240 44.09	65N34.13	153W13.80	2.74	4	334	100.0	0.17	99.0	99.0
810526	057 22.48	65N19.76	162W47.23	5.00*	3	216	135.5	0.00	99.0	99.0
810530	6 9 33.90	64N20.25	163W32.24	0.00*	3	330	223.2	13.36	99.0	99.0
810531	2122 50.25	65N14.63	157W24.62	2.50*	6	280	178.9	0.40	12.6	8.3
810531	2122 51.00	65N14.09	157W12.45	0.00*	3	274	170.6	0.40	99.0	99.0
810605	2336 11.19	65N13.70	170W25.04	0.00*	6	322	313.2	2.40	99.0	99.0
810605	2336 26.40	65N 6.51	157W26.99	0.00*	3	291	138.8	1.07	99.0	99.0
810605	117 59.39	66N59.54	154W11.15	24.96*	4	291	346.5	3.49	69.7	99.0
810606	333 33.04	67N43.17	154W34.35	5.00*	3	299	213.5	0.00	53.6	99.0
810606	22 4 37.36	65N30.40	156W14.50	8.78	4	140	113.0	0.05	6.6	10.3
810613	1725 17.38	64N46.05	165W15.02	31.08	4	229	173.3	0.00	78.1	99.0
810621	1 4 37.16	66N41.64	163W28.70	18.18	4	201	100.3	0.00	21.8	13.4
810621	1 4 37.76	66N39.04	163W25.07	5.00*	3	189	95.3	0.00	99.0	99.0
810621	2342 0.58	64N20.36	168W18.89	5.00*	3	305	280.1	1.38	99.0	99.0
810623	1030 37.68	67N13.11	160W52.41	6.76	8	296	190.6	0.83	99.0	34.3
810625	20 0 14.05	64N53.38	152W31.08	15.91	5	129	97.9	0.44	7.5	11.3
810625	1354 1.96	64N27.45	163W35.05	10.11	6	190	148.1	0.45	25.9	20.3

Table 4

Values of Component of Moment Tensor M_{ij} (i, j = x, y z) and Azimuth and Dip of Pressure (P), Null (B) and Tenson (T) Axes

Hypocentral depth for best-fit model = 10 km

Moment Tensor:	Std. Error:
MXX = 0.372E+25	±0.651E+24
MXY = 0.341E+25	±0.557E+24
MYY = 0.581E+25	±0.651E+24
MXZ = -0.396E+25	±0.700E+24
MYZ = -0.489E+25	±0.795E+24
MZZ = -0.953E+25	±0.782E+24

Axes	Azimuth	Std. Error	Dip	Std. Error
P	-139.59	±10.63	72.40	±1.81
B	-232.66	± 3.37	0.97	±2.96
T	-322.97	± 3.28	17.58	±1.82

EARTHQUAKES IN AND NEAR ALASKA (MEYERS, 1976)

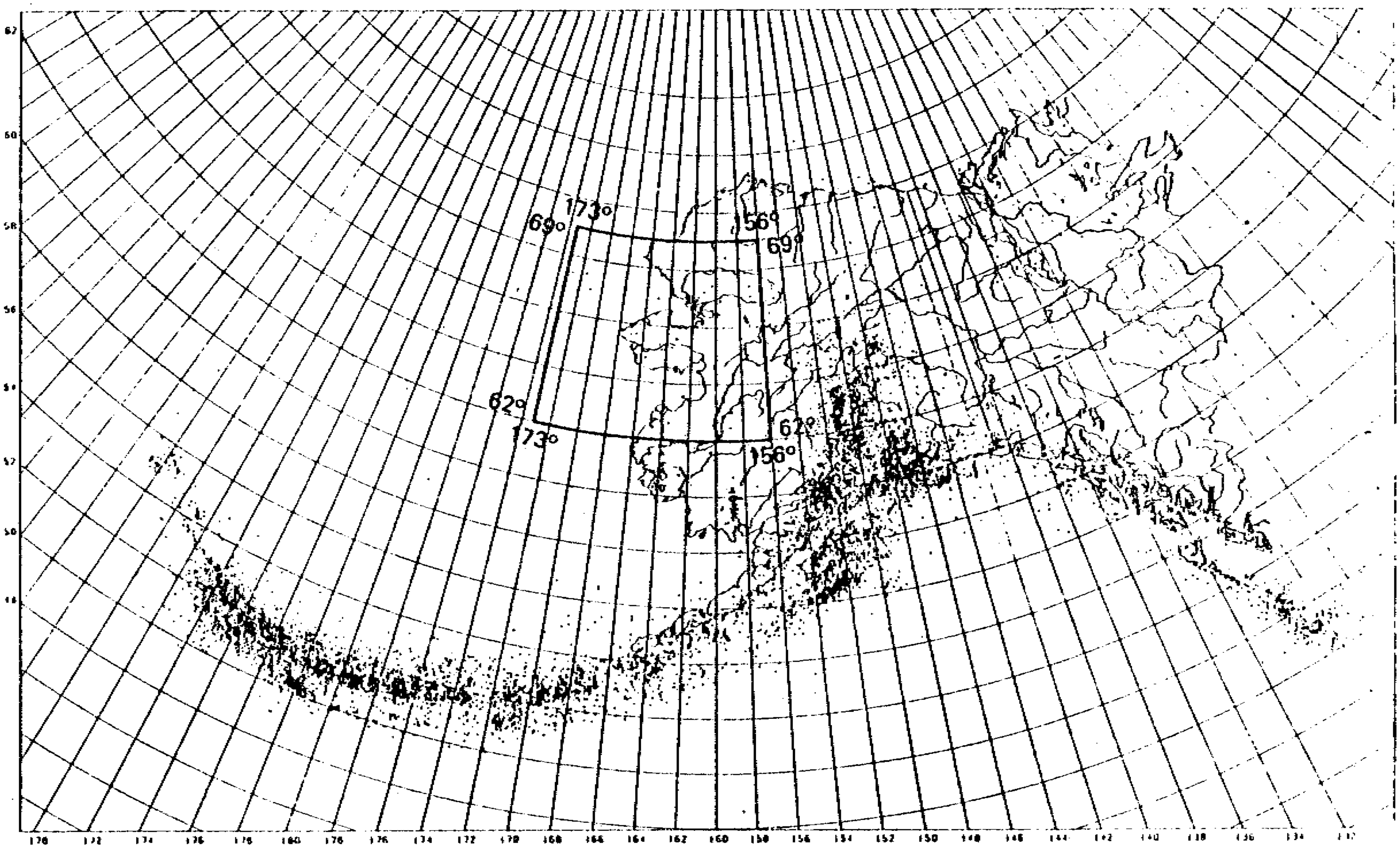

Fig. 1

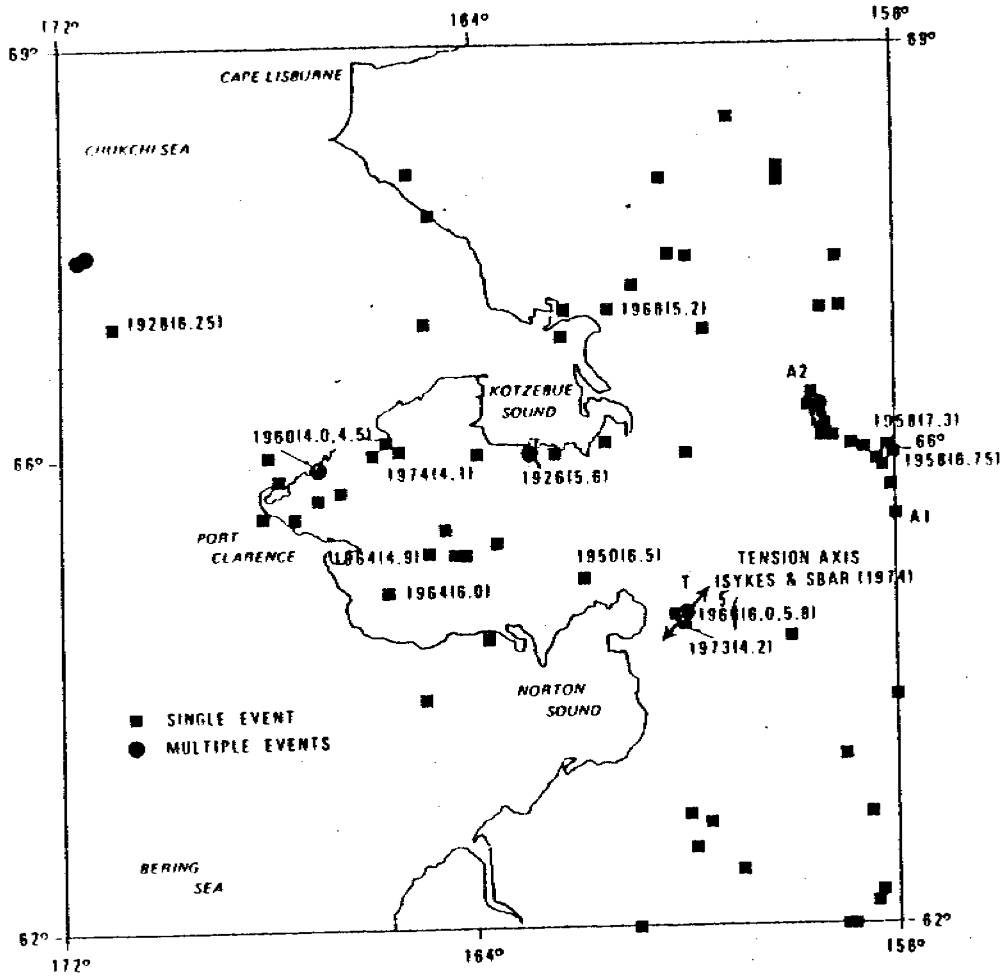
172°
164°
158°
69°
66°
62°
CAPE LISBURNE
CHUKCHI SEA
1928(6.25)
1968(5.2)
KOTZEBUE
SOUND
A2
1958(7.3)
1958(6.75)
A1
1960(4.0,4.5)
1974(4.1)
1926(5.6)
PORT
CLARENCE
1964(4.9)
1964(6.0)
1950(6.5)
TENSION AXIS
(SYKES & SBAR (1974)
T
1973(4.2)
NORTON
SOUND
SINGLE EVENT
MULTIPLE EVENTS
BERING
SEA

Fig. 2

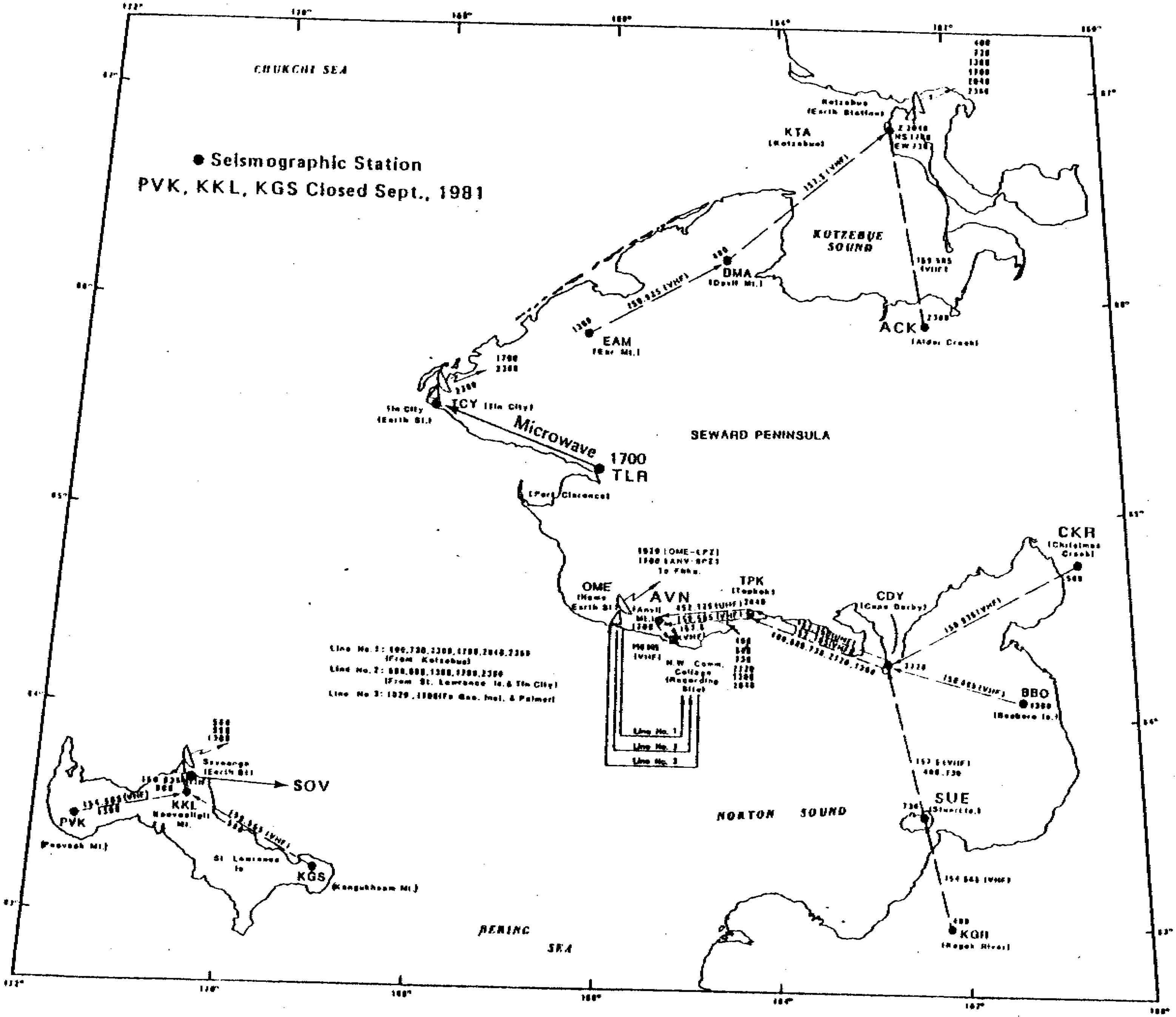

● Seismographic Station
PVK, KKL, KGS Closed Sept., 1981
CHUKCHI SEA
KTA
KOTZEBUE SOUND
DMA
EAM
ACK
TCY
Microwave
1700
TLR
SEWARD PENINSULA
OME
AVN
TPK
CDY
CKR
BBO
SUE
NORTON SOUND
KGH
SOV
KKL
PVK
KGS
BERING SEA
Line No. 1
Line No. 2
Line No. 3

Fig. 3

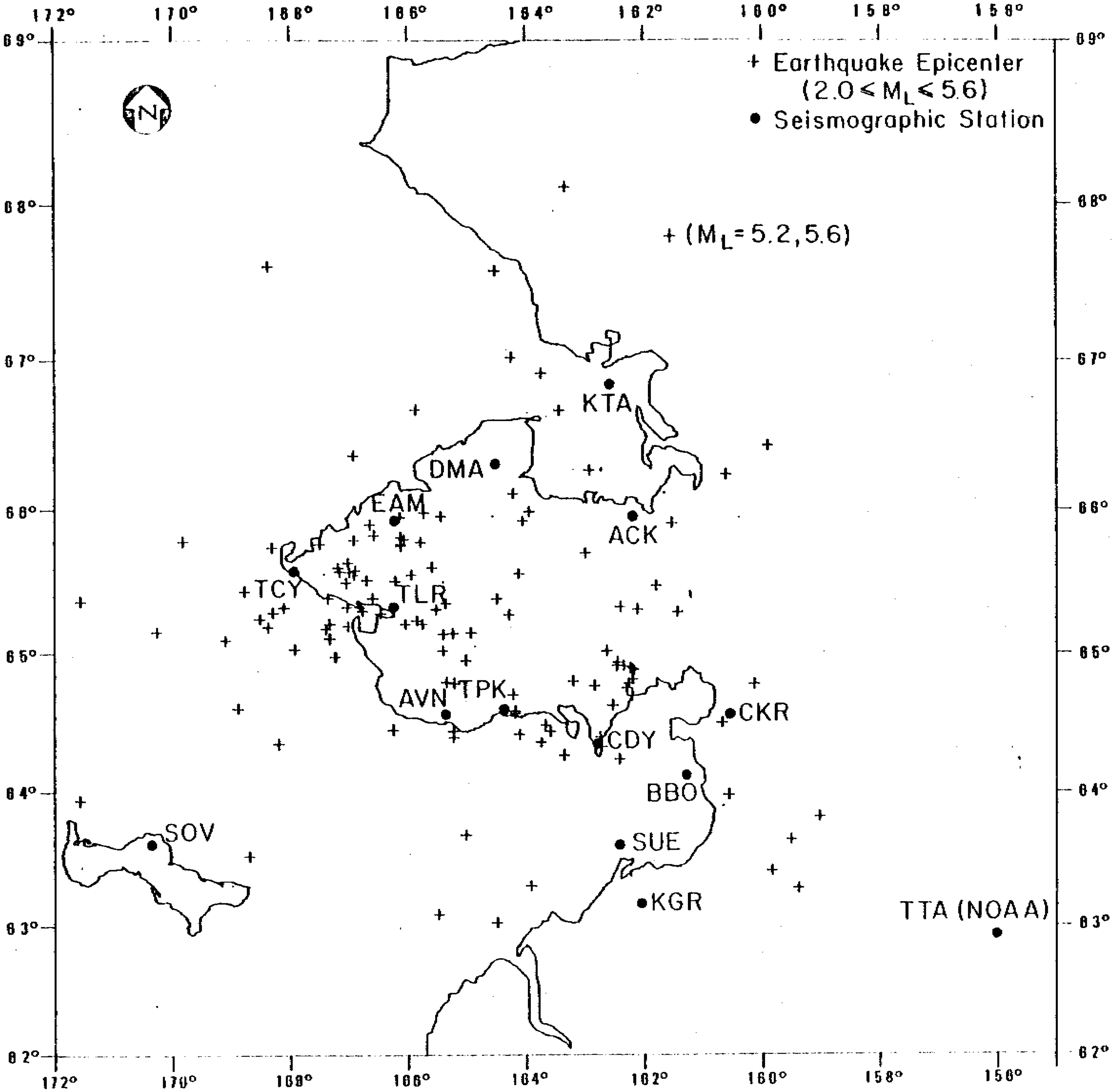
+ Earthquake Epicenter
($2.0 \leq M_L \leq 5.6$)
● Seismographic Station
+ (M_L=5.2,5.6)
N
KTA
DMA
EAM
ACK
TCY
TLR
AVN
TPK
CKR
CDY
BBO
SOV
SUE
KGR
TTA (NOAA)
172°
170°
168°
166°
164°
162°
160°
158°
156°
69°
68°
67°
66°
65°
64°
63°
62°

Fig. 4

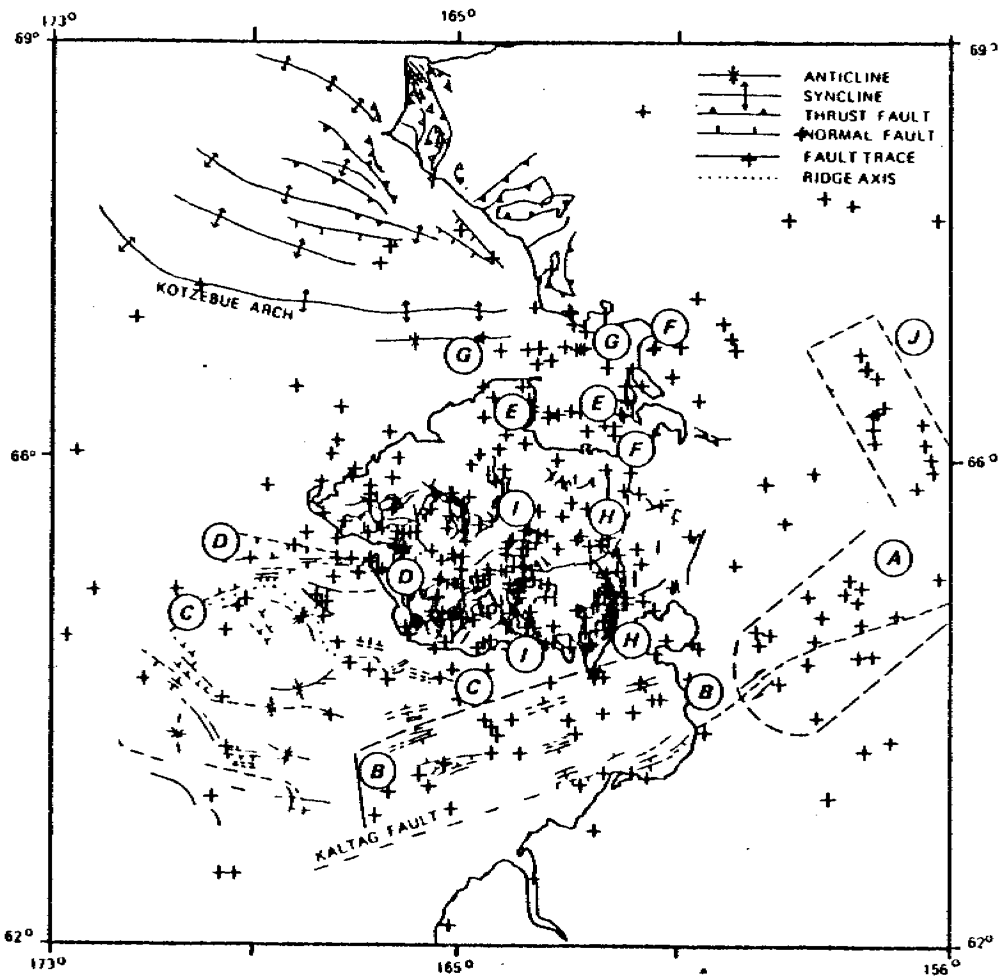
173°
165°
69°
66°
62°
156°
ANTICLINE
SYNCLINE
THRUST FAULT
NORMAL FAULT
FAULT TRACE
RIDGE AXIS
KOTZEBUE ARCH
KALTAG FAULT
A
B
C
D
E
F
G
H
I
J

Fig. 5

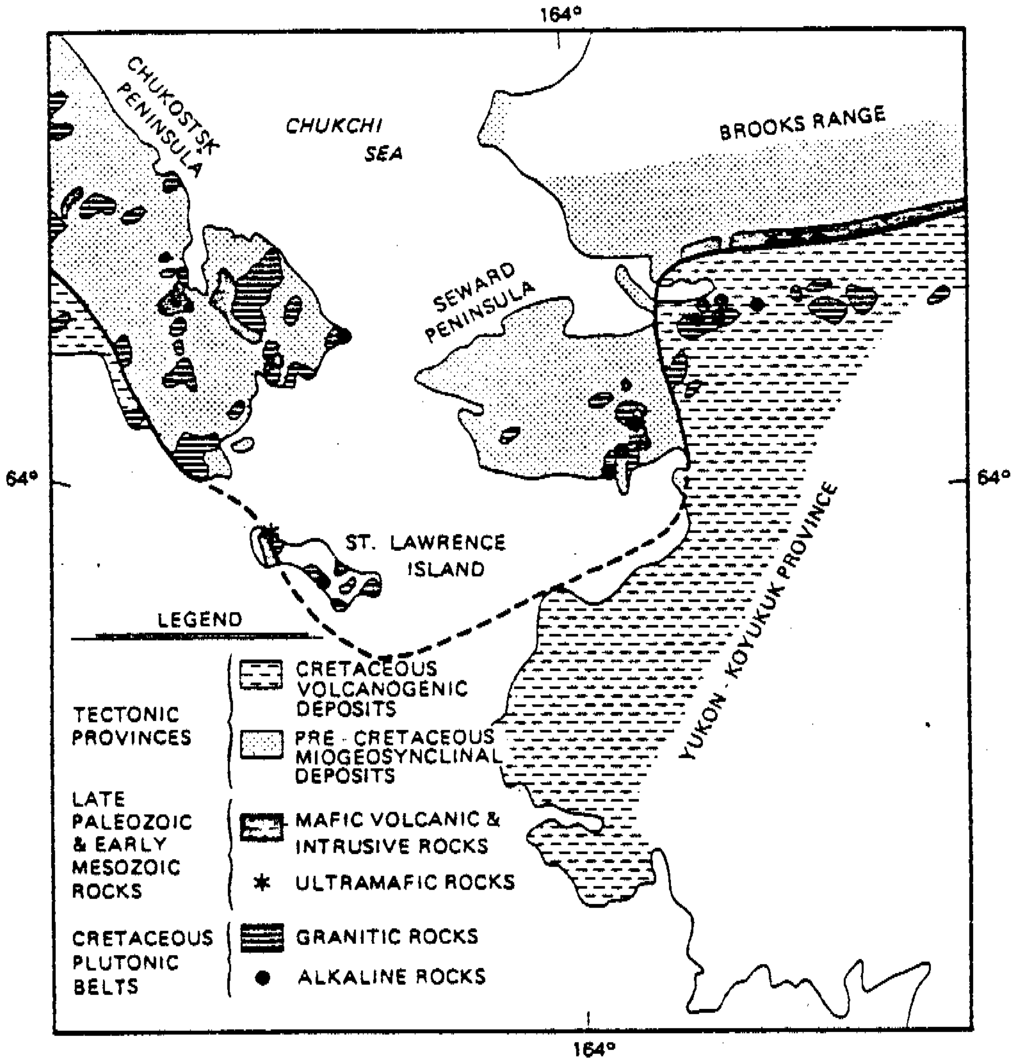

164°
CHUKOSTSK PENINSULA
CHUKCHI SEA
BROOKS RANGE
SEWARD PENINSULA
64°
64°
ST. LAWRENCE ISLAND
YUKON - KOYUKUK PROVINCE
LEGEND
TECTONIC PROVINCES
CRETACEOUS VOLCANOGENIC DEPOSITS
PRE - CRETACEOUS MIOGEOSYNCLINAL DEPOSITS
LATE PALEOZOIC & EARLY MESOZOIC ROCKS
MAFIC VOLCANIC & INTRUSIVE ROCKS
ULTRAMAFIC ROCKS
CRETACEOUS PLUTONIC BELTS
GRANITIC ROCKS
ALKALINE ROCKS
164°

Fig. 6

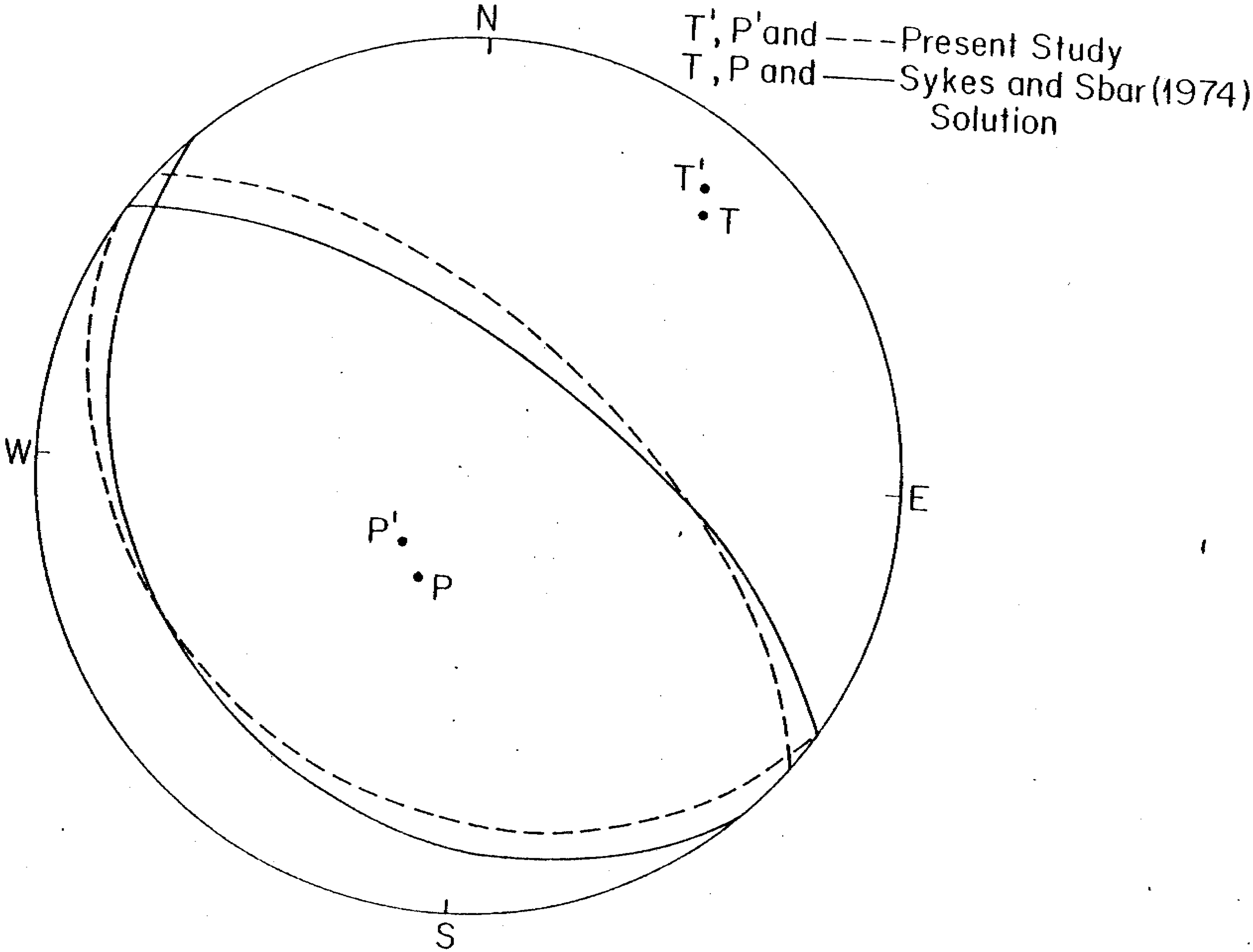
N
T', P'and ---Present Study
T , P and ——Sykes and Sbar (1974) Solution
T'
T
W
E
P'
P
S

Fig. 7

Annual Report
1980 - 1981
Research Unit 588

GEOLOGIC HAZARDS IN NAVARIN BASIN PROVINCE, NORTHWESTERN BERING SEA

Paul R. Carlson
Herman A. Karl
U.S. Geological Survey
Menlo Park, California

April 1, 1981

I. Summary of Objectives, Conclusions and Implications with Respect to OCS Oil and Gas Development.

The principal objective of this study is to provide interpretive maps and reports of seafloor hazards in the Navarin Basin province preparatory for OCS lease sale 83 presently scheduled for December, 1984. Several geologic processes that are active in Navarin Basin province are potentially hazardous to commercial development. Preliminary conclusions and implications pertaining to OCS development follow:

1. Navarin Basin province appears to be aseismic and no faults mapped to date rupture the seafloor. However, several faults indicate movement in the last 12,000 years and, thus, are potentially active.

2. Submarine landslides are common in the heads of submarine canyons and on the upper continental slope and must be considered in the design of any seafloor structures.

3. Fields of large sediment waves have been discovered near the heads of the three large canyons. These sediment waves if active could be hazardous to seafloor structures.

4. Gas-charged sediment, present throughout a large part of the province, has reduced strength and bearing capacity as compared to strength of gas-free sediment.

5. Intense storms produce exceptionally large waves which are not only capable of eroding bottom sediment, but are also dangerous to surface structures and vessels.

6. Sea-ice commonly covers much of the Navarin Basin province for several months of the year and could pose a significant problem to exploration, development, or production of oil and gas during years of heavy concentrations.

II. Introduction

A. General Nature and Scope of Study

Navarin Basin Province is an OCS (Outer Continental Shelf) lease sale area that is scheduled for leasing in 1984. This basin potentially contains vast accumulationsof oil and gas and with the escalating energy problems will be the subject of extensive exploration activity. Preliminary to the sale, an environmental impact statement must be released by BLM. Our study in Navarin Basin will provide information about the seafloor geologic hazards that need to be considered during the exploration for and development of petroleum on the outer continental shelf. No previous geohazards investigations had been conducted in the Navarin Basin province. Thus, we began in the summer of 1980, to collect reconnaissance geophysical and geological data. This report includes preliminary findings from the past field season. We will build on this data base, proceeding toward the investigation of specific geohazards problems in the study area in subsequent field seasons.

B. Specific Objectives

Our objectives in FY 1981 are to continue the collection of broadly spaced high resolution seismic reflection lines and seafloor samples in order to determine the regional characteristics of the marine geology of Navarin Basin province and to investigate in detail a few areas of potential seafloor hazards identified during the FY 80 field season. The seismic profiles and samples will allow us to continue the mapping of seafloor hazards in OCS lease area 83 that we began in FY 1980. Preliminary maps are being prepared to show the location of near-surface faults, submarine slides, zones of gas-charged sediment, fields of large bedforms and areas of erosion, deposition and sediment bypassing. Maps showing preliminary interpretations of the various hazards are included in the results and discussion sections of this report. These maps will be modified as additional data become available.

C. Relevance to Problems of Petroleum Development

The Navarin Basin province encompasses an area of 45,000 km^2 and contains three sedimentary basins filled with thick sequences of Cenozoic strata. Interpretation of the stratigraphy and structure of these basins suggests areas which could trap accumulations of economically exploitable hydrocarbon deposits. The province, which includes the outer continental shelf and upper slope, is deeply dissected by large submarine canyons. The steep gradients within the canyons and along the upper continental slope result in potential instability problems in a large part of the province. Zones of gas-charged sediment that also may cause problems of seafloor instability are present over much of the outer continental shelf in the Navarin province. All areas of unstable seafloor must be carefully considered during the design and the installation of exploration and development platforms. Preliminary data from this potential petroleum province have revealed the existence of large bedforms near the heads of the large submarine canyons. The potential impact of these bedforms as well as the occurrences of gas-charged sediment and sediment slides must be considered during development phases when planning pipelines and holding tanks.

III.Current State of Knowledge

Prior to the summer of 1980, no geohazards data had been collected in the Navarin Basin province. Several marine geology and geophysics cruises to the Bering Sea had, however, collected data adjacent to and even within part of the province. The thick sedimentary sequence that makes up Navarin Basin was first discovered on a 1970 cruise of the R/V Bartlett (Scholl and others, 1975, 76). Marlow and others (1976) named this 10-15 km thick sedimentary sequence of Mesozoic and Cenozoic age deposits. However, detailed mapping of the "acoustic basement" was not completed until seismic-reflection surveys of 1976, 1977, and 1980 provided multi-channel coverage necessary to allow delineation of the northwest-trending basins (Marlow and others, 1981).

The Russians published the first generalized maps of sediment distribution in the study area (Lisitsyn, 1966). Without access to the original data, we only have been able to extract a few data points along the northern border of the Navarin province which we are using to supplement our sediment distribution maps. Of much greater use are data from the University of Washington cores and grab samples, some of which were collected in the eastern part of Navarin Basin (Knebel, 1972). Other studies that will provide comparative sedimentologic data have been conducted in adjacent parts of the Bering Sea (Anadyr Basin, Kummer and Creager, 1971; Bristol Bay, Sharma and others, 1972; Norton Basin, Nelson and others, 1974; McManus and others, 1977; Kvenvolden and others, 1979; Drake and others, 1980 ; St. George Basin, Gardner and others, 1980; Vallier and others, 1980).

Although oceanographic data have been gathered from the Bering Sea for at least 100 years (Dall, N. H., 1881 to Cacchione and others, in press) and by scientists from numerous countries (e.g. USSR-Natarov, 1963; Japan Takenouti and Ohtani, 1974; U.S.A.-Hughes and others, 1974), very little is known about the details of circulation and other oceanographic parameters within the Navarin Basin province. These other studies have involved water mass characteristics (Sayles and others, 1979) or large scale circulation (Hughes and others, 1974) of the entire Bering Sea or the deep Aleutian Basin or have concentrated on movement and characteristics of the water in and through the major outlets, the Bering Strait (Coachman and others, 1975) or the passes in the Aleutian Chain (Favorite, 1974).

Sea-ice is often present throughout most of the Navarin Basin province for about five months of the year, January through May. Whereas the average monthly limit of sea-ice in the Bering Sea has been determined (Webster, 1979), little is known about the movement and deformation of the sea-ice field (Tabata, 1974). The increasing availability of satellite imagery (Muench, 1974; Ahlnas and Wendler, 1980) together with winter field work (Drake and others, 1979; Paquette and Bourke, 1980) will provide needed detailed information helping to delineate the sea-ice fields in the Navarin Basin province.

IV. Study Area

The Navarin Basin province is located on the outer continental shelf and upper slope in the northwestern Bering Sea (Fig. 1). This promising petroleum region, scheduled for lease sale in 1984, is bounded on the northwest by the U.S.-USSR Convention Line of 1867, on the southwest by the base of the continental slope and extends to within 100 km of St. Matthew Island to the northeast and St. Paul Island to the southeast, an area of about 45,000 km^2. This province consists of a very flat continental shelf (average gradient 0.02^o) and a rugged continental slope (gradient ranges from 3^o to 8^o) that has been deeply dissected by three massive submarine canyons. Bathymetric maps of the Bering Sea constructed by Pratt and Walton (1972) and Schumacher (1976), include very limited bathymetric data from the Navarin area. We have made a more detailed bathymetric map of the study area by combining the bathymetric data obtained on the DISCOVERER cruise of 1980 with data from several U.S. Geological Survey cruises during the past decade (Scholl and Marlow, 1980; Scholl, Buffington, and Marlow, 1976; Marlow and Cooper, 1979 and 1980). The map and a discussion of the morphology of the Navarin continental margin are included in the appended results section.

V. Sources, Methods and Rationale of Data Collection

The principal sources of data for this study have been the seismic reflection profiles and sediment samples collected on the 1980 R/V DISCOVERER cruise. Some additional data were collected in 1980 from the USCG POLAR STAR and the R/V S.P. LEE. We are also incorporating into our data base seismic reflection records that were collected over the past fifteen years by the U.S.G.S. for resource evaluation (Marlow and others, 1981). Other sources of data include studies by the University of Washington and Alaska, Russian, and Japanese scientists (e.g. Knebel, 1972; Sharma, 1979; Lisitsyn, 1966; Takenouti and Ohtani, 1974).

We acknowledge the assistance provided by the officers and crew of the NOAA Ship DISCOVERER (July 2 - August 22, 1980) in collecting seismic reflection profiles along 6700 km of track lines (Fig. 2), 300 suspended sediment samples, and 115 bottom samples (Fig. 3, 104 gravity cores, 10 grab samples, and 1 dredge haul). NOAA officers and survey technicians provided navigational control using LORAN C and satellite fixes.

Following is a list of the U.S.G.S. scientific party on DC 4/5 - 80 cruise.

Paul Carlson	Co-Chief scientists
Herman Karl	" "
Brian Edwards	Engineering Geologist
Jeff Fischer	Physical Science Tech.
George Ford	" " "
Sarah Griscom	" " "
Ken Johnson	" " "
Beth Lamb	Data coordinator
Grant Lichtman	Physical Science Tech.
Paula Quinterno	Micropaleontologist
Jeff Rupert	Mechanical Tech.
John Saladin	Electronics Tech.
Rick Viall	Electronics Tech.
Tim Vogel	Geochemist
Pat Wiberg	Physical Science Tech.
Bob Wilson	Mechanical Tech.
Mark Yeats	Physical Science Tech.

On the cruise of the U.S.C.G. cutter POLAR STAR (May 2 - 29, 1980), Rick Herrera (USGS representative), with assistance from Coast Guard personnel, collect 55 samples (22 gravity cores and 33 grab samples).

Sampling Methods:

State of the art high-resolution geophysical equipment (air gun, mini-sparker, 3.5 kHz), bottom samplers (gravity corer, grab, dredge) near-bottom suspended sediment samplers, and navigation (Satellite and Loran C) were used for our six weeks of shipboard operations during the summer of 1980. Spacing between track lines was approximately 30 km. During the second leg of the six week cruise, geologic samples were collected at the intersections of tracklines and at locations deemed to be geologically important by the chief scientists. These sets of data provide the regional information necessary to identify areas of special interest to be investigated during future cruises.

The geophysical systems used on the Navarin Basin cruise were as follows:

System	Resolution
1. Air gun (40 in^3)	5 - 10 m
2. Minisparker (800 J)	1 - 3 m
3. 3.5 kHz	1 m

The bottom samplers used were: gravity corer, dredge, and grab samplers.

Analytical Methods:

The geophysical records are analyzed by standard methods, whereby slumps and shallow faults are identified by discontinuity of reflectors and by characteristic geometry, and seismic stratigraphic units are correlated by their continuity and seismic-reflection signature. The sediment cores are being studied megascopically and microscopically in order to classify sedimentary units and to gather data for deciphering dispersal patterns. Cores have been X-radiographed for study of internal structures that provide inferences as to depositional mechanics and post-depositional disturbance. Grain size and mineralogy will be used to determine provenance and sediment pathways.

The types of analytical systems used in the Sedimentological Laboratory are described below:

A. General

(1) PDP-11/34 computer serving as controller for several analytical devices. Used to store analyzed data and interface with the main USGS computer.

(2) X-radiography unit for analyzing sedimentary structures in core samples.

(3) Suspended sediment concentrations are determined by gravimetric analysis of material collected on filters.

B. Particle Size Analysis

(1) Rapid sediment analyzer (height: 2.3 m; diameter: 20 cm) to measure grain-size distribution in the range of 2000 to 64 microns; fall velocities measured by a semi-conductor strain-gauge element.

B. Particle Size Analysis (cont'd)

(2) Coulter Counter for analysis of fine-grained sediments in the size range 2 to 64 microns.

(3) Hydrophotometer for analysis of fine-grained sediments in the size range 2 to 64 microns by measuring changes in light transmission.

C. Mineral and Chemical Analysis

(1) LECO Carbon Analyzer - automatic analysis of total and organic carbon concentrations in sediments.

(2) Carbonate Determiner for measuring the amount of calcium carbonate in marine sediments. (Attached to LECO Unit).

(3) Scanning Electron Microscope (a Mini-SEM) having a capability for magnifications up to 40,000 X for viewing, identifying and photographing particulate matter.

In addition to routine geologic analysis, core samples will be subjected to several routine laboratory tests to determine geotechnical index properties. Most routine tests will be conducted on subsamples from the core surface and at intervals downcore. Laboratory procedures will follow American Society for Testing and Materials (ASTM) standards where available.

Test	ASTM
Water content	D2216
Specific gravity of solids	D 854
Bulk unit weight	--
Atterberg limits	D423, 424
Vane shear strength	--

Specialized tests, such as one-dimensional consolidation (ASTM D 2435) and triaxial compression are being conducted on replicate cores taken at a few selected stations in an endeavor to characterize different sedimentary facies. Core sections taken for these and other laboratory tests were sealed in wax, refrigerated and stored in an upright position until analyzed.

VI - VIII. Results, Discussion, and Conclusions

We have chosen to incorporate these three parts as a series of chapters. to this annual progress report. Each chapter, written by several different authors, is an independent report on a specific topic complete within itself. We must stress the preliminary nature of these reports and caution the readers that as additional data are collected on our 1981 DISCOVERER cruise many additional data points will be added and results and maps modified. The reports are organized into the following sections:

A. Morphology of Navarin Basin Province
B. Distribution and Physical Characteristics of Navarin Sediments
C. Seafloor Geologic Hazards

VI - VIII. Results, Discussion, and Conclusions (cont'd)

D. Geotechnical Properties of Navarin Basin Sediment
E. Hydrocarbon gases in near-surface sediments of Navarin Basin
F. Distribution of Microfossils in Navarin Sediments
G. Amino Acid Diagenesis in Fossil Mollusks

IX. Needs for Further Study

The large size of the Navarin Basin province 45,000 km^2 necessitates several years of field work to permit collection of adequate seismic reflection lines and seafloor samples in order to accurately assess the geohazards in this promising petroleum province. In one field season of six weeks, we collected seismic-reflection profiles along about 7,000 km of track lines and a total of 115 bottom samples. This first cruise was a successful venture and we feel that we obtained very useful data, but we need many more closely-spaced seismic reflection lines to be able to delineate the major slumps and to map and understand the fields of large bedforms which were identified on the regional survey lines. Additional high-resolution seismic profiles in specific areas are also needed to determine the extent of the numerous areas of gas-charged sediment, to trace near-surface fault zones, and to attempt to decipher any cause and effect relations between the trends of faults and zones of gas-charged sediment. At present our 115 samples scattered throughout the huge 45,000 km^2 (11 million acres) province amounts to one sample per 39/km^2 (95,650 acres), hardly a dense sampling grid. Therefore, we conclude that a minimum of two years additional field work, after FY 81, will be necessary to complete evaluations of faulting, slumping, and sediment dynamics for OCS lease area 83.

REFERENCES CITED

Ahlnas, K. and Wendler, G., 1980, Meteorological parameters affecting the location of the ice edge in the Bering Sea: Transactions Am. Geophys. Union, EOS, v. 61, p. 1006.

Cacchione, D. A., Drake, D. E., and Wiberg, P., in press, Velocity and bottom-stress measurements in the bottom boundary layer, outer Norton Sound, Alaska: in Nio, S. D., ed., Holocene marine sedimentation.

Coachman, L. K., Aagaard, K., and Tripp, R. B., 1975, Bering Strait, The regional physical oceanography: Seattle, Univ. of Washington Press, 186 p.

Dall, N. H., 1881, Hydrologie des Bering-Meeres und der benachbarten Gewasser: Pet. Geog. Mitt., v. 27, p. 361-380.

Drake, D. E., Totman, C. E., and Wiberg, P. L., 1979, Sediment transport during the winter on the Yukon prodelta Norton Sound, Alaska: Journal of Sedimentary Petrology, v. 49, p. 1171-1180.

Drake, D. E., Cacchione, D. A., Muench, R. D., and Nelson, C. H., 1980, Sediment transport in Norton Sound, Alaska: Marine Geology, v. 36, p. 97-126.

Favorite, F., 1974, Flow into the Bering Sea through Aleutian island passes: in Hood, D. W. and Kelley, E. J., ed., Oceanography of the Bering Sea. Inst. Mar. Sci., Univ. Alaska Occas. Publ. 2, p. 3-37.

Gardner, J. V., Dean, W. E., and Vallier, T. L., 1980, Sedimentology and geochemistry of the surface sediments, outer continental shelf, southern Bering Sea: Marine Geology, v. 35, p. 299-329.

Hughes, F. W., Coachman, L. K., and Aagaard, K., 1974, Circulation, transport and water exchange in the western Bering Sea: in Hood, D. W. and Kelley, E. J., ed., Oceanography of the Bering Sea. Univ. Alaska Inst. Marine Science, Occas. Publ. 2, p. 59-98.

Knebel, H. J., 1972, Holocene sedimentary framework of the east-central Bering Sea continental shelf: Ph.D. thesis, Univ. Washington, Seattle, 186 p.

Kummer, J. T., and Creager, J. S., 1971, Marine geology and Cenozoic history of the Gulf of Anadyr: Marine Geology, v. 10, p. 257-280.

Kvenvolden, K. A., Nelson, C. H., Thor, D. R., Larsen, M. C., Redden, G. D., Rapp, J. V., and Des Marias, D. J., 1979, Biogenic and thermogenic gas in gas-charged sediment of Norton Sound, Alaska: Offshore Technology Conference, Houston, Texas, Proceedings, v. 1, p. 479-486.

Lisitsyn, A. P., 1966, Protessy Sovremennogo Osodko' obrazovaniya v Beringovom More: Akad. Nauk SSR Inst. Okeal., Moskva, 574 p. (Recent sedimentation in the Bering Sea: Israel Program for Sci. Translations, 1969, Jerusalem; U.S. Dept. of Commerce, Clearinghouse for Federal Sci. Tech. Info., Springfield, VA, 614 p.).

Marlow, M. S., Scholl, D. W., Cooper, A. K., and Buffington, E. C., 1976, Structure and Evolution of Bering Sea shelf south of St. Lawrence Island, Bulletin of the American Association of Petroleum Geologists, v. 60, no. 1, p. 161-183.

Marlow, M. S., and Cooper, A. K., 1979, Multichannel seismic reflection profiles collected in 1977 in the northern Bering Sea: U.S. Geological Survey open-file report 79-1147.

Marlow, M. S. and Cooper, A. K., 1980, Multichannel seismic reflection profiles collected in 1976 in the southern Bering Sea shelf: U.S. Geological Survey open-file report 80-389.

Marlow, M. S., Carlson, P. R., Cooper, A. K., Karl, H. A., McLean, H., McMullin, R., and Lynch, M. B., 1981, Resource report for proposed OCS sale number 83 Navarin Basin, Alaska: U.S. Geological Survey open-file report 81-252, 82 p.

McManus, D. A., Kolla, Venkatarathnam, Hopkins, D. M., and Nelson, C. H., 1977, Distribution of bottom sediments on the continental shelf, northern Bering Sea: U.S. Geological Survey Prof. Paper 759-C, 31 p.

Muench, R. D., 1974, Satellite observations of Bering Sea ice: in Hood, D. W. and Takenouti, Y., eds., Bering Sea oceanography: an update: Univ. Alaska, Inst. Marine Science, Report No. 75-2, p. 191-192.

Nelson, C. H., Hopkins, D. M., and Scholl, D. W., 1974, Tectonic setting and Cenozoic sedimentary history of the Bering Sea, in Herman, Yvonne, ed., Marine geology and oceanography of the Arctic seas: New York, Springer-Verlag, p. 119-140.

Paquette, R. G. and Bourke, R. H., 1980, Winter conditions in the Bering Sea: Transactions Am. Geophys. Union, EOS, v. 61, p. 1006.

Pratt, R. and Walton, F., 1974, Bathymetric map of the Bering Shelf: Geological Society of America, Boulder, Colorado.

Sayles, M. A., Aagaard, K., and Coachman, L. K., 1979, Oceanographic atlas of the Bering Sea Basin: Seattle, Univ. of Washington Press, 155 p.

Scholl, D. W., Buffington, E. C., and Marlow, M. S., 1975, Plate tectonics and the structural evolution of the Aleutian Bering Sea region, in Forbes, R. B., ed., Contributions to the geology of the Bering Sea Basin and adjacent regions: Geol. Soc. of America Spec. Paper 151, p. 1-32.

Scholl, D. W., Buffington, E. C., Marlow, M. S., 1976, Aleutian-Bering Sea region seismic reflection profiles: U.S. Geol. Survey Open-File Rept. 76-748.

Schumacher, G. M., 1976, Bathymetric map of the Aleutian Trench and Bering Sea U.S. Geological Survey open-file map 76-821, scale 1:2,500,000.

Sharma, G. D., Naidu, A. S., and Hood, D. W., 1972, Bristol Bay: model contemporary graded shelf: Am. Assoc. Petroleum Geologists, v. 56, p. 2000-2012.

Sharma, G. D., 1979, The Alaska shelf, hydrographic, sedimentary, and geochemical environment: Springer-Verlag, New York, 498 p.

Tabata, T., 1974, Movement and deformation of drift ice as observed with sea ice radar: in Hood, D. W. and Kelley, E. J., eds., Oceanography of the Bering Sea, Univ. Alaska, Inst. Marine Science, Occas. Publ. 2, p. 373-382.

Takenouti, A. Y. and Ohtani, K., 1974, Currents and water masses in the Bering Sea: a review of Japanese work: in Hood, D. W. and Kelley, E. J., eds., Oceanography of the Bering Sea, Univ. Alaska, Inst. Marine Science, Occas. Publ. 2, p. 39-57.

Vallier, T. L., Underwood, M. B., Gardner, J. V., and Barron, J. A., 1980, Neogene sedimentation on the outer continental margin, southern Bering Sea: Marine Geology, v. 36, p. 269-287.

Webster, B. D., 1979, Ice edge probabilities for the eastern Bering Sea: NOAA Technical Memorandum NWS AR-26, 20 p.

RESULTS, DISCUSSION, AND CONCLUSIONS
FOR ANNUAL REPORT R.U. 588

The results and discussions of the various geological and geophysical data sets collected for this Navarin Basin (Fig. 1) investigation are included in the following sections. The very preliminary nature of these studies precludes drawing many firm conclusions. Most of the data were obtained during the 1980 cruise of the NOAA ship DISCOVERER. Seismic reflection lines and sample locations are shown on figures 2 and 3 respectively.

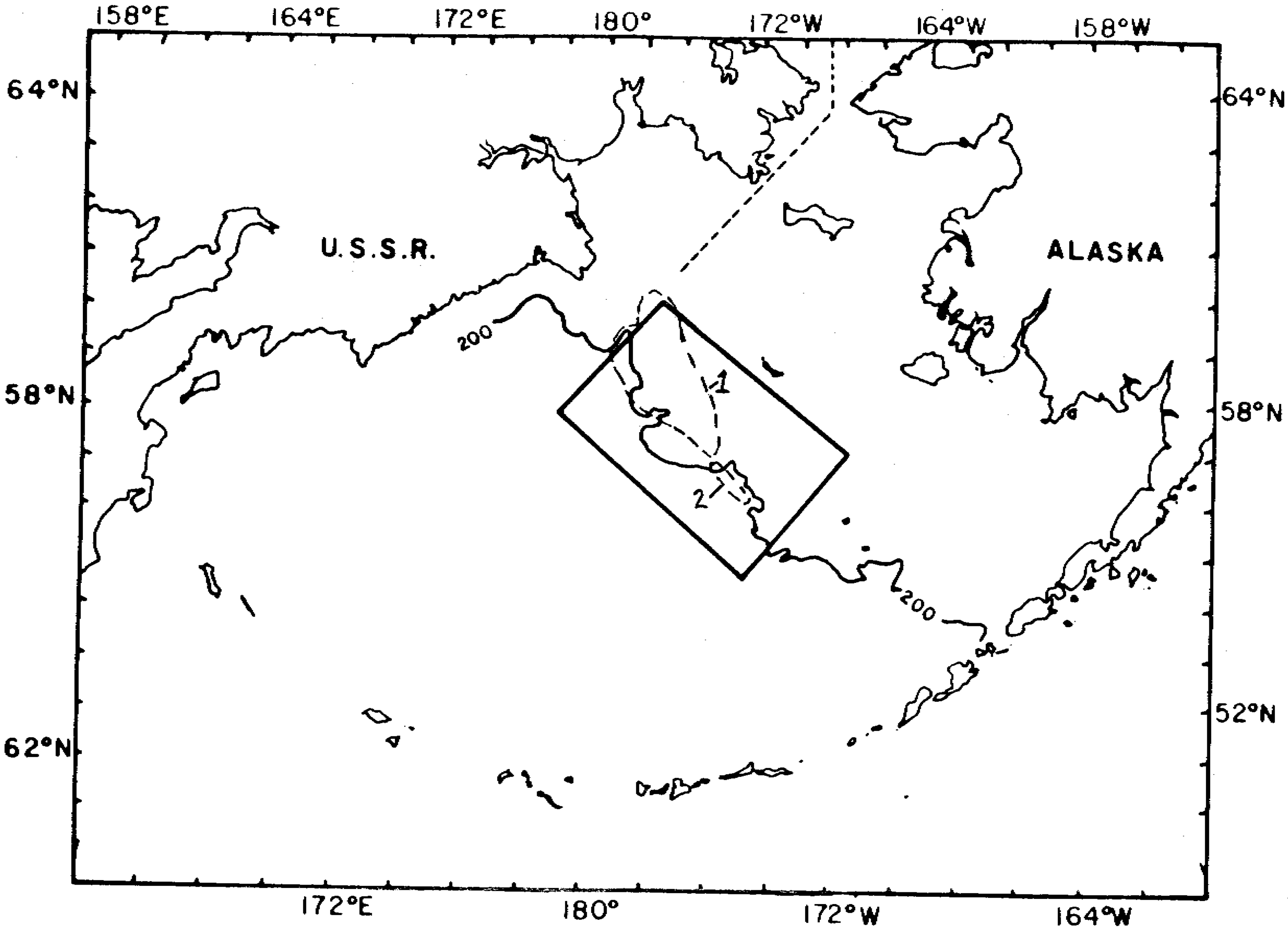

Figure 1. Location map of the study area that includes Navarin(1) and Zhemchug(2) basins as delineated by the 2 km thickness of strata contour (after Marlow and others, 1979).

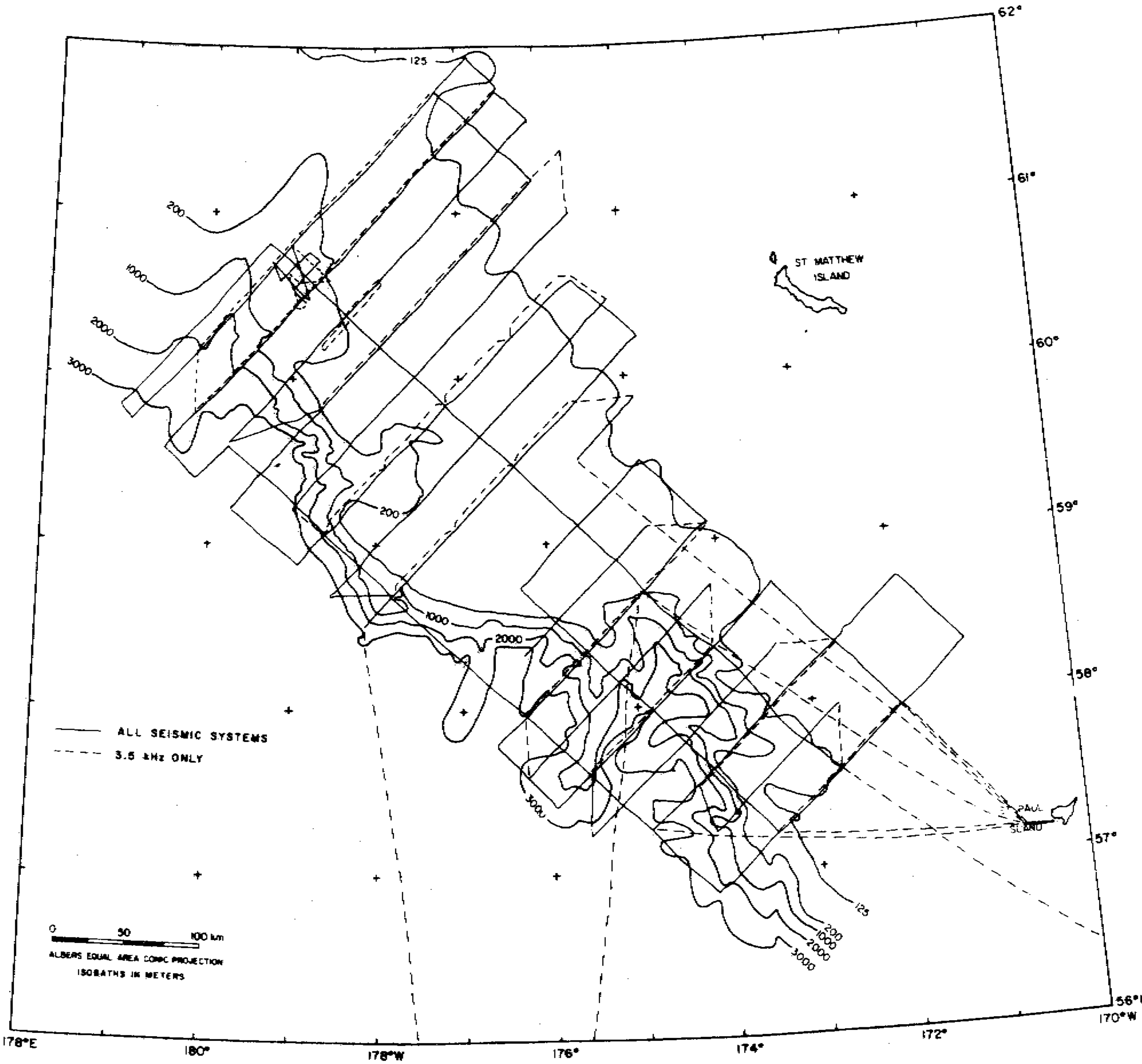

Figure 2. Trackline chart of seismic reflection profiles across the Navarin Basin province, collected on DISCOVERER cruise DC4/5-80-BS/NB.

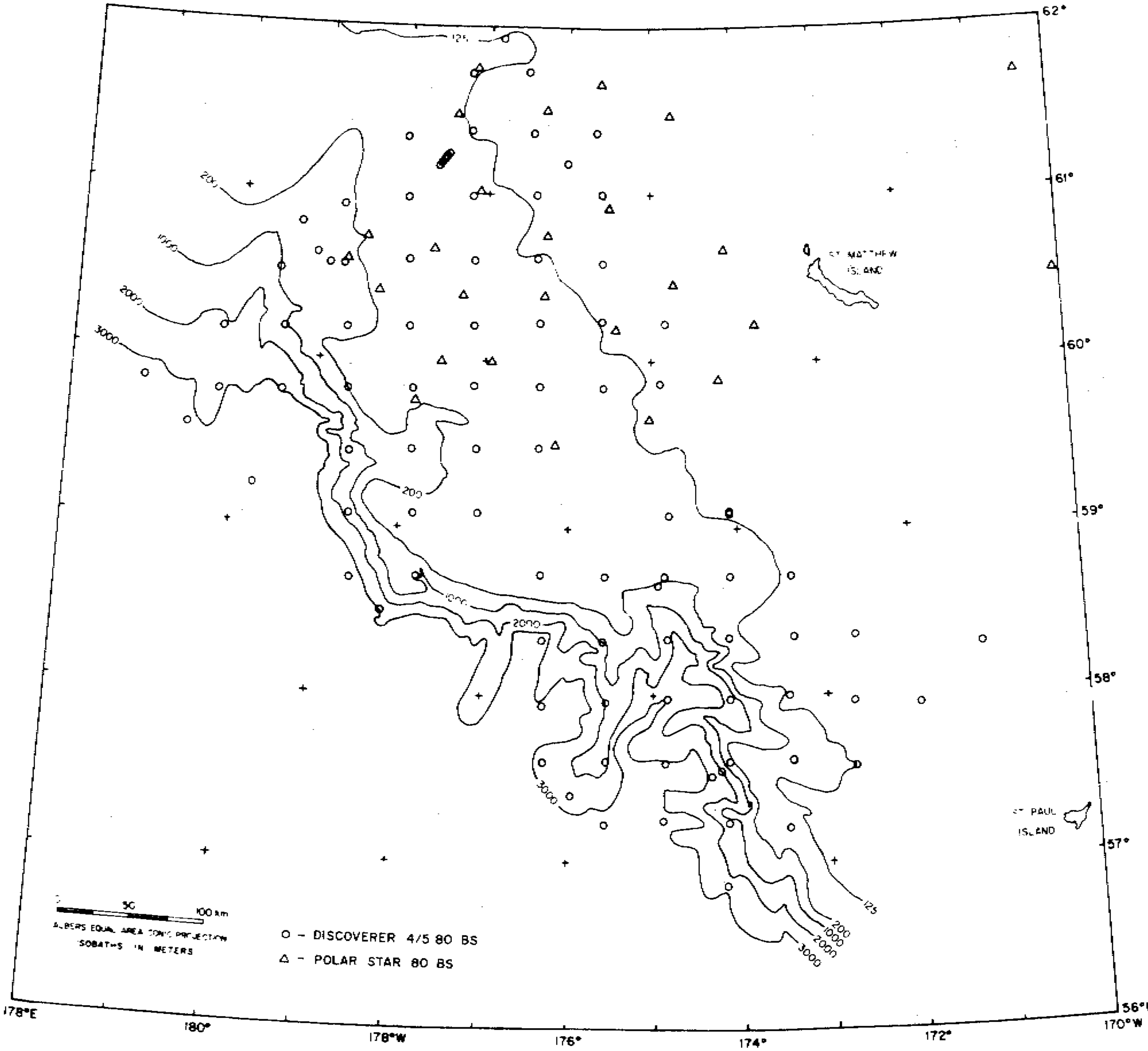

Figure 3. Location map of bottom samples collected in 1980 in Navarin Basin province.

CONTENTS

INTRODUCTION

The study area, referred to in this report as the Navarin basin province, is located on the outer continental shelf and upper slope in the northwestern Bering Sea (Fig. 1). The area is bounded on the northwest by the US-USSR Convention line of 1867, on the southwest by the base of the continental slope and extends to within 100 km of St. Matthew Island to the northeast and St. Paul Island to the southeast. This region potentially contains significant vast accumulations of oil and gas and is likely to be the subject of extensive exploration activity.

The principal purpose of this report is to provide preliminary interpretations of seafloor hazards and related sediment and microfaunal studies of the Navarin Basin province preparatory to OCS lease sale 83. Several geologic processes that are active in Navarin Basin province are potentially hazardous to commercial development and will be discussed in this report.

Previous Studies

Prior to the summer of 1980, systematic geohazard surveys data had not been conducted in the Navarin Basin province. However, several earlier marine geology and geophysics cruises had collected dredge samples and seismic data adjacent to and within part of the province. A thick sedimentary sequence that underlies much of the present study area was first discovered on a 1970 cruise of the R/V Bartlett (Scholl and others, 1975, 1976). Marlow and others (1976) named this 10-15 km thick sedimentary sequence of Mesozoic and Cenozoic age deposits Navarin Basin. However, detailed mapping of the "acoustic basement" was not completed until seismic-reflection surveys of 1976, 1977, and 1980 provided multi-channel seismic coverage necessary to allow delineation of the northwest-trending basins (Marlow and others, 1981).

Bathymetric maps of the Bering Sea constructed by Pratt and Walton (1972) and Schumacher (1976), include very limited bathymetric data from the Navarin area. We have made a more detailed bathymetric map of the study area by combining the bathymetric data obtained on the DISCOVERER cruise of 1980 with data from several U. S. Geological Survey cruises during the past decade (Scholl and Marlow, 1970; Scholl, Buffington, and Marlow, 1976; Marlow and Cooper, 1979 and 1980).

Lisitsyn (1966) Russians published the first generalized maps of sediment distribution in the study area; without access to the original data, we only have been able to extract a few data points along the northern border of the Navarin province that we are using to supplement our sediment distribution maps. Data from the University of Washington cores and grab samples, some of which were collected in the eastern part of Navarin Basin (Knebel, 1972), are of much greater use. Other studies that provide comparative sedimentologic data have been conducted on nearby parts of the Bering Sea (Anadyr Basin, Kummer and Creager, 1971; Bristol Bay, Sharma and others, 1972; Norton Basin, Nelson and others, 1974, McManus and others, 1977, Kvenvolden and others, 1979, Drake and others, 1980; St. George Basin, Gardner and others, 1980; Vallier and others, 1980).

Although oceanographic data have been gathered from the Bering Sea for at least 100 years (Dall, N.H., 1881 to Cacchione and others, in press) and by scientists from numerous countries (e.g. USSR-Natarov, 1963; Japan-Takenouti and Ohtani, 1974; U.S.A.-Hughes and others, 1974), very little is known about the details of circulation and other oceanographic parameters within the Navarin Basin province. These other studies have involved water mass characteristics (Sayles and others, 1979) or large scale circulation (Hughes and others, 1974) of the entire Bering Sea or the deep Aleutian Basin or have concentrated on movement and characteristics of the water in and through the major outlets, the Bering Strait (Coachman and others, 1975) or the passes in the Aleutian Chain (Favorite, 1974).

Sea-ice is often present throughout of the Navarin basin province for about five months of the year (January through May). Whereas the average monthly limit of sea-ice in the Bering Sea has been determined (Webster, 1979), little is known about the movement and deformation of the sea-ice field (Tabata, 1974). The increasing availability of satellite imagery (Muench, 1974; Ahlnas and Wendler, 1980) together with winter field work (Drake and others, 1979; Parquette and Bourke, 1980) will provide needed detailed information helping to delineate the sea-ice fields in the Navarin Basin province.

Data Collection

The principal sources of data for this study have been the seismic-reflection profiles and sediment samples collected on the 1980 R/V DISCOVERER cruise (Figs. 2 and 3).

The geophysical systems used on the 1980 Navarin Basin cruise were as follows:

System	Resolution
1. Air gun (40 in ^{3})	5 - 10 m
2. Minisparker (800 J)	1 - 3 m
3. 3.5 kHz	1 m

The bottom samplers used were: gravity corer, dredge, and grab samplers. Suspended particulate samples were collected at the sea surface and near the seafloor.

Spacing between geophysical tracklines was approximately 30 km and seafloor geological samples were taken at intersections of track lines and at selected sites deemed geologically significant. Navigational control was LORAN C updated with satellite positioning.

Some additional data were collected in 1980 from the USGC POLAR STAR and the R/V S. P. LEE. We are also incorporating into our data base seismic-reflection records that were collected over the past fifteen years by the U.S.G.S. for resource evaluation (Marlow and others, 1981). Other sources of data include studies by the University of Washington and Alaska, Russian, and Japanese scientists (e.g. Knebel, 1972; Sharma, 1979; Lisitsyn, 1966; Takenouti and Ohtani, 1974).

Acknowledgments

We acknowledge the assistance provided by the officers and crew of the NOAA Ship DISCOVERER (July 2 - August 22, 1980) in collecting seismic reflection profiles along 6700 km of track lines (Fig. 2), 300 suspended samples, and 115 bottom samples (Fig. 3; 104 gravity cores, 10 grab samples, and 1 dredge haul). NOAA officers and survey technicians provided navigational control.

On the cruise of the U.S.C.G. cutter POLAR STAR (May 2 - 29, 1980), Rick Herrera (USGS representative), with assistance from Coast Guard personnel, collect 55 samples (Fig. 3; 22 gravity cores and 33 grab samples).

This study was funded jointly by the U.S. Geological Survey and by the Bureau of Land Management through interagency agreement with the National Oceanic and Atmospheric Administration, as part of the Outer Continental Shelf Environmental Assessment Program.

REFERENCES CITED

Ahlnas, K. and Wendler, G., 1980, Meteorological parameters affecting the location of the ice edge in the Bering Sea: Transactions Am. Geophys. Union, EOS, v. 61, p. 1006.

Cacchione, D. A., Drake, D. E., and Wiberg, P., in press, Velocity and bottom-stress measurements in the bottom boundary layer, outer Norton Sound, Alaska: in Nio, S. D., ed., Holocene marine sedimentation.

Coachman, L. K., Aagaard, K., and Tripp, R. B., 1975, Bering Strait, The regional physical oceanography: Seattle, Univ. of Washington Press, 186 p.

Dall, N. H., 1881, Hydrologie des Bering-Meeres und der benachbarten Gewasser: Pet. Geog. Mitt., v. 27, p. 361-380.

Drake, D. E., Totman, C. E., and Wiberg, P. L., 1979, Sediment transport during the winter on the Yukon prodelta Norton Sound, Alaska: Journal of Sedimentary Petrology, v. 49, p. 1171-1180.

Drake, D. E., Cacchione, D. A., Muench, R. D., and Nelson, C. H., 1980, Sediment transport in Norton Sound, Alaska: Marine Geology, v. 36, p. 97-126.

Favorite, F., 1974, Flow into the Bering Sea through Aleutian island passes: in Hood, D. W. and Kelley, E. J., ed., Oceanography of the Bering Sea. Inst. Mar. Sci., Univ. Alaska Occas. Publ. 2, p. 3-37.

Gardner, J. V., Dean, W. E., and Vallier, T. L., 1980, Sedimentology and geochemistry of the surface sediments, outer continental shelf, southern Bering Sea: Marine Geology, v. 35, p. 299-329.

Hughes, F. W., Coachman, L. K., and Aagaard, K., 1974, Circulation, transport and water exchange in the western Bering Sea: in Hood, D. W. and Kelley, E. J., ed., Oceanography of the Bering Sea. Univ. Alaska Inst. Marine Science, Occas. Publ. 2, p. 59-98.

Knebel, H. J., 1972, Holocene sedimentary framework of the east-central Bering Sea continental shelf: Ph.D. thesis, Univ. Washington, Seattle, 186 p.

Kummer, J. T., and Creager, J. S., 1971, Marine geology and Cenozoic history of the Gulf of Anadyr: Marine Geology, v. 10, p. 257-280.

Kvenvolden, K. A., Nelson, C. H., Thor, D. R., Larsen, M. C., Redden, G. D., Rapp, J. V., and Des Marias, D. J., 1979, Biogenic and thermogenic gas in gas-charged sediment of Norton Sound, Alaska: Offshore Technology Conference, Houston, Texas, Proceedings, v. 1, p. 479-486.

Lisitsyn, A. P., 1966, Protessy Sovremennogo Osodko' obrazovaniyá v Beringovom More: Akad. Nauk SSR Inst. Okeal., Moskva, 574 p. (Recent sedimentation in the Bering Sea: Israel Program for Sci. Translations, 1969, Jerusalem; U.S. Dept. of Commerce, Clearinghouse for Federal Sci. Tech. Info., Springfield, VA, 614 p.).

Marlow, M. S., Scholl, D. W., Cooper, A. K., and Buffington, E. C., 1976, Structure and Evolution of Bering Sea shelf south of St. Lawrence Island, Bulletin of the American Association of Petroleum Geologists, v. 60, no. 1, p. 161-183.

Marlow, M. S., and Cooper, A. K., 1979, Multichannel seismic reflection profiles collected in 1977 in the northern Bering Sea: U.S. Geological Survey open-file report 79-1147.

Marlow, M. S. and Cooper, A. K., 1980, Multichannel seismic reflection profiles collected in 1976 in the southern Bering Sea shelf: U.S. Geological Survey open-file report 80-389.

Marlow, M. S., Cooper, A. K., Parker, A. W., and Childs, J. R., 1981, Isopach map of strata above acoustic basement in the Bering Sea: U.S. Geological Survey miscellaneous field studies map MF-1164

Marlow, M. S., Carlson, P. R., Cooper, A. K., Karl, H. A., McLean, H., McMullin, R., and Lynch, M. B., 1981, Resource report for proposed OCS sale number 83 Navarin Basin, Alaska: U.S. Geological Survey open-file report 81-252, 82 p.

McManus, D. A., Kolla, Venkatarathnam, Hopkins, D. M., and Nelson, C. H., 1977, Distribution of bottom sediments on the continental shelf, northern Bering Sea: U.S. Geological Survey Prof. Paper 759-C, 31 p.

Muench, R. D., 1974, Satellite observations of Bering Sea ice: in Hood, D. W. and Takenouti, Y., eds., Bering Sea oceanography: an update: Univ. Alaska, Inst. Marine Science, Report No. 75-2, p. 191-192.

Nelson, C. H., Hopkins, D. M., and Scholl, D. W., 1974, Tectonic setting and Cenozoic sedimentary history of the Bering Sea, in Herman, Yvonne, ed., Marine geology and oceanography of the Arctic seas: New York, Springer-Verlag, p. 119-140.

Paquette, R. G. and Bourke, R. H., 1980, Winter conditions in the Bering Sea: Transactions Am. Geophys. Union, EOS, v. 61, p. 1006.

Pratt, R. and Walton, F., 1974, Bathymetric map of the Bering Shelf: Geological Society of America, Boulder, Colorado.

Sayles, M. A., Aagaard, K., and Coachman, L. K., 1979, Oceanographic atlas of the Bering Sea Basin: Seattle, Univ. of Washington Press, 155 p.

Scholl, D. W., Buffington, E. C., and Marlow, M. S., 1975, Plate tectonics and the structural evolution of the Aleutian Bering Sea region, in Forbes, R. B., ed., Contributions to the geology of the Bering Sea Basin and adjacent regions: Geol. Soc. of America Spec. Paper 151, p. 1-32.

Scholl, D. W., Buffington, E. C., Marlow, M. S., 1976, Aleutian-Bering Sea region seismic reflection profiles: U.S. Geol. Survey Open-File Rept. 76-748.

Schumacher, G. M., 1976, Bathymetric map of the Aleutian Trench and Bering Sea U.S. Geological Survey open-file map 76-821, scale 1:2,500,000.

Sharma, G. D., Naidu, A. S., and Hood, D. W., 1972, Bristol Bay: model contemporary graded shelf: Am. Assoc. Petroleum Geologists, v. 56, p. 2000-2012.

Sharma, G. D., 1979, The Alaska shelf, hydrographic, sedimentary, and geochemical environment: Springer-Verlag, New York, 498 p.

Tabata, T., 1974, Movement and deformation of drift ice as observed with sea ice radar: in Hood, D. W. and Kelley, E. J., eds., Oceanography of the Bering Sea, Univ. Alaska, Inst. Marine Science, Occas. Publ. 2, p. 373-382.

Takenouti, A. Y. and Ohtani, K., 1974, Currents and water masses in the Bering Sea: a review of Japanese work: in Hood, D. W. and Kelley, E. J., eds., Oceanography of the Bering Sea, Univ. Alaska, Inst. Marine Science, Occas. Publ. 2, p. 39-57.

Vallier, T. L., Underwood, M. B., Gardner, J. V., and Barron, J. A., 1980, Neogene sedimentation on the outer continental margin, southern Bering Sea: Marine Geology, v. 36, p. 269-287.

Webster, B. D., 1979, Ice edge probabilities for the eastern Bering Sea: NOAA Technical Memorandum NWS AR-26, 20 p.

MORPHOLOGY OF NAVARIN BASIN PROVINCE

Paul R. Carlson, Jeffrey M. Fischer, and Herman A. Karl

INTRODUCTION

There are three physiographic provinces in the Navarin study area. These are (1) the flat, wide, 100,000 km^2 continental shelf that extends from the 100 to the 150 m isobath and has an average gradient of 0.02°; (2) the steep, rugged 47,000 km^2 continental slope that extends from the 150 to the 2800 m isobath and has a range of gradients from 3° to 8°; and (3) the 40,000 km^2 rise which extends from the base of the slope to the 3600 m isobath. Three large submarine canyons deeply dissect the outer shelf and slope. Coalescing fans at the mouths of these canyons have contributed in part to the wedge of sediment that forms the continental rise.

The purpose of this chapter is to show a preliminary detailed bathymetric map (Fig. 4) of the Navarin basin province and to discuss characteristics of the principal geomorphic features.

The remoteness of the Navarin basin province has undoubtedly contributed to the lack of detailed published bathymetric maps of the area. Although Soviet scientists have discussed morphologic features of the Bering Sea (Lisitsyn, 1966; Gershanovich, 1968), they have not published detailed maps of the Navarin basin margin. Scholl and others (1970) published a detailed geomorphic diagram of Zhemchug Submarine Canyon and a bathymetric map of the adjacent continental slope that included the southern part of the study area. Four years later Scholl and others (1974) published a map that included the entire continental slope of the Bering Sea. At the same time, Pratt and Walton (1974) released a bathymetric map that included coverage of the Navarin continental shelf. However, both of these maps were contoured using very sparse depth control especially in the northern part of the Navarin basin province.

DATA COLLECTION AND PROCESSING

Shipboard

Depth soundings collected on several cruises by the U.S. Geological Survey scientists were used in compilation of a preliminary bathymetric map of the Navarin Basin province (Fig. 4). The bulk of the soundings were made on the 1980 cruise of the NOAA ship DISCOVERER (DC 4/5-80-BS/NB); supplemental soundings were added to the data set from previous cruises by U.S. Geological Survey ships R/V S. P. LEE and R/V SEA SOUNDER (S3-77-BS,L5-76-BS, L8-77-BS, L5-78-BS, L6-80-BS). Navigation for all cruises included LORAN C and Satellite.

Laboratory

The bathymetric profiles (3.5 and 12 kHz records) were digitized on a Tektronix plotter. Depths were "picked" at 5 minute intervals and at major changes in slope. The digitized data were merged with corrected navigation, computer plotted, and hand contoured at a scale of 1:1,000,000.

THE NAVARIN MARGIN

Shelf

The Bering Sea continental shelf is one of the widest and flattest in the world, is about 700 km wide and has a gradient of 0.02° seaward of the Yukon River delta. By comparison, Shepard (1963) reported a world-wide average for continental shelves of 0.12°. The portion of the Bering shelf that includes the Navarin basin province lies between the 100 m and 150 m isobaths and ranges in width from about 120 km at the northern and southern parts of the study area to a maximum width of about 235 km in the central part (Fig. 4). These boundaries define an area of about 100,000 km^2. The gradient of the Navarin basin shelf averages approximately 0.02° (range 0.01 to 0.03°). Although, the outer continental shelf is cut by three massive submarine canyons, there are no apparent morphologic expressions of these canyons landward of the 125 m isobath.

Slope

The continental slope forming the southeastern boundary of the Navarin Basin province begins at the 150 m isobath and extends to a depth of 2800 m northwest of Zhemchug Canyon (Fig. 4). Southeast of this magnificent canyon the slope abruptly changes gradient at 2400 m. The slope includes an area of about 47,000 km^2. The gradients of the Navarin slope range from 3° to 8° with even steeper gradients over shorter segments of slope. This compares with world-wide average gradient for continental slopes of about 4.3° (Shepard, 1963). The width of the continental slope ranges from 47 km in the middle of the province to 19 km south of Zhemchug Canyon. Exceptions to these width and gradient values are within the three submarine canyons that are deeply incised in the shelf and on either side of Zhemchug Canyon where pronounced ridges extend as much as 105 km seaward of the base of the slope. The longest of these ridges also functions as the northwestern wall of Zhemchug Canyon. These prominent ridges have several hundred to more than a thousand meters of relief.

Submarine Canyons

The three major submarine canyons that cut deeply into the Bering continental margin (Fig. 4) are Navarinsky (named after Cape Navarin), Pervenets, and Zhemchug (both named after Russian research vessels) (Kotenev, 1965). All three canyons head in water depths less than 150 m. Extensive deep-sea fans have been built at the mouths of the canyons in water depths of about 3000 m. Navarinsky is the longest canyon (340 km), Pervenets the shortest (125 km) and Zhemchug intermediate in length (240 km). Both Navarinsky and Zhemchug Canyons are about 100 km wide at the shelf break, but the smaller Pervenets Canyon is only 30 km wide. Wall relief of the three canyons at the shelf break ranges from 700 m for Navarin and 800 m for Pervenets, to a spectacular 2600 m for Zhemchug. Each of the three canyons consist of two main branches or tributaries on the landward side of the shelf break. The two tributaries in Zhemchug Canyon trend 180° away from each other, forming a large trough-shaped basin. Each of these tributaries is about 150 km long. The average gradient along the thalweg of each branch is about 1.2°, but a maximum gradient of 2.2° occurs along the steepest parts of these tributary canyons. In contrast, the two main branches or tributaries in Navarinsky and Pervenets Canyon intersect at a 90° angle. The length of the northern tributary of Navarinsky Canyon is 270 km and the southern 180 km. The thalweg gradients of these broad, shallow branches average 0.33° and 0.50°, respectively. The smaller Pervenets Canyon has a 90 km long northern tributary and a 80 km long southern one. These shorter tributaries average 0.30° and 0.33° in gradient, respectively.

These canyons are incised into Neogene and older more-lithified Paleogene rocks, principally mudstones, that are thought to make up much of Navarin Basin (Marlow and others, 1976). The canyons, especially Zhemchug, are apparently structurally controlled, the structures dating back at least into the Paleogene (Scholl and others, 1975). The major cutting of the canyons probably occurred when glacio-eustatically lowered sea-levels exposed most of the Bering shelf.

Rise

The continental rise in this remote part of the world has been sparsely sounded, but is a prominent enough feature to be easily recognized on profiles that traverse the bounding features - the Bering continental slope and the Aleutian abyssal plain. The rise includes 40,000 km^2 of the Navarin Basin province and begins at the base of the slope, a depth of 2800 m northwest of Zhemchug Canyon and 2400 m south of the canyon, and extends to the 3600 m isobath that marks the beginning of the abyssal plain. The width of the rise averages about 75 km, ranging from a minimum of 25 km northwest of Zhemchug Canyon to a width of more than 100 km adjacent to the mouths of the three large canyons. The gradients across the rise range from a low of 0.5° adjacent to the canyon mouths to 1.8° off the two prominent ridges located northwest of Zhemchug Canyon. Deep-sea channels cross the rise in the area of the canyon mouths and are apparently connected to the submarine canyons. Gravity cores collected near the mouths of the canyons and on the adjacent rise contain sand lenses that indicate deposition by turbidity currents (see Karl and others, this report). Seismic reflection profiles of the rise also indicate the presence of turbidites which together with the cores suggest that the rise, at least adjacent to the canyons, consists of deep-sea fan deposits. The gradients measured across the rise near the canyons are also similar to gradients reported from other deep-sea fans (Nelson and others, 1970, p. 282-283).

REFERENCES CITED

Gershanovich, D. E., 1968, New data on geomorphology and recent sediments of the Bering Sea and the Gulf of Alaska: Marine Geology v.6, p. 281-296.

Kotenev, B. N., 1965, Submarine valleys in the zone of the continental slope in the Bering Sea: All-Union Research Inst. of Marine Fisheries and Oceanography. Transactions, v. 58, p. 35-44. (U.S. Navy Electronics Lab., San Diego, Ca., NEL Translation 112).

Lisitsyn, A. P., 1966, Recent sedimentation in the Bering Sea (in Russian): Inst. Okeanol. Akad. Nauk USSR, (translated by Israel Program for Scientific Translations, available from U. S. Dept. Commerce, Clearinghouse for Fed. Sci. and Tech. Info. 1969, 614 p.).

Nelson, C. H., Carlson, P. R., Byrne, J. V., and Alpha, T. R., 1970, Development of the Astoria Canyon-Fan physiography and comparison with similar systems: Marine Geology, v. 8, p. 259-291.

Marlow, M. S., Scholl, D. W., Cooper, A. K., and Buffington, E. C., 1976, Structure and evolution of Bering Sea shelf south of St. Lawrence Island: American Assoc. Petroleum Geol. Bull., v. 60, p. 161-183.

Pratt, R. and Walton, F., 1974, Bathymetric map of the Bering shelf: Geological Soc. of America, Boulder, Colo.

Shepard, F. P., 1963, Submarine geology: 2nd. ed. New York, Harper, 557 p.

Scholl, D. W., Alpha, T. R., Marlow, M. S. and Buffington, E. C., 1974, Base map of the Aleutian Bering Sea region: U. S. Geological Survey Map I-879, scale 1:2,500,000.

Scholl, D. W., Buffington, E. C., Hopkins, D. M., and Alpha, T. R., 1970, The structure and origin of large submarine canyons of the Bering Sea: Marine Geology v. 8, p. 187-210.

Scholl, D. W., Buffington, E. C., and Marlow, M. S., 1975, Plate tectonics and the structural evolution of the Aleutian-Bering Sea region: Forbes, R. B., ed., Contributions to the geology of the Bering Sea basin and adjacent regions: Geol. Soc. America Special Paper 151, p. 1-32.

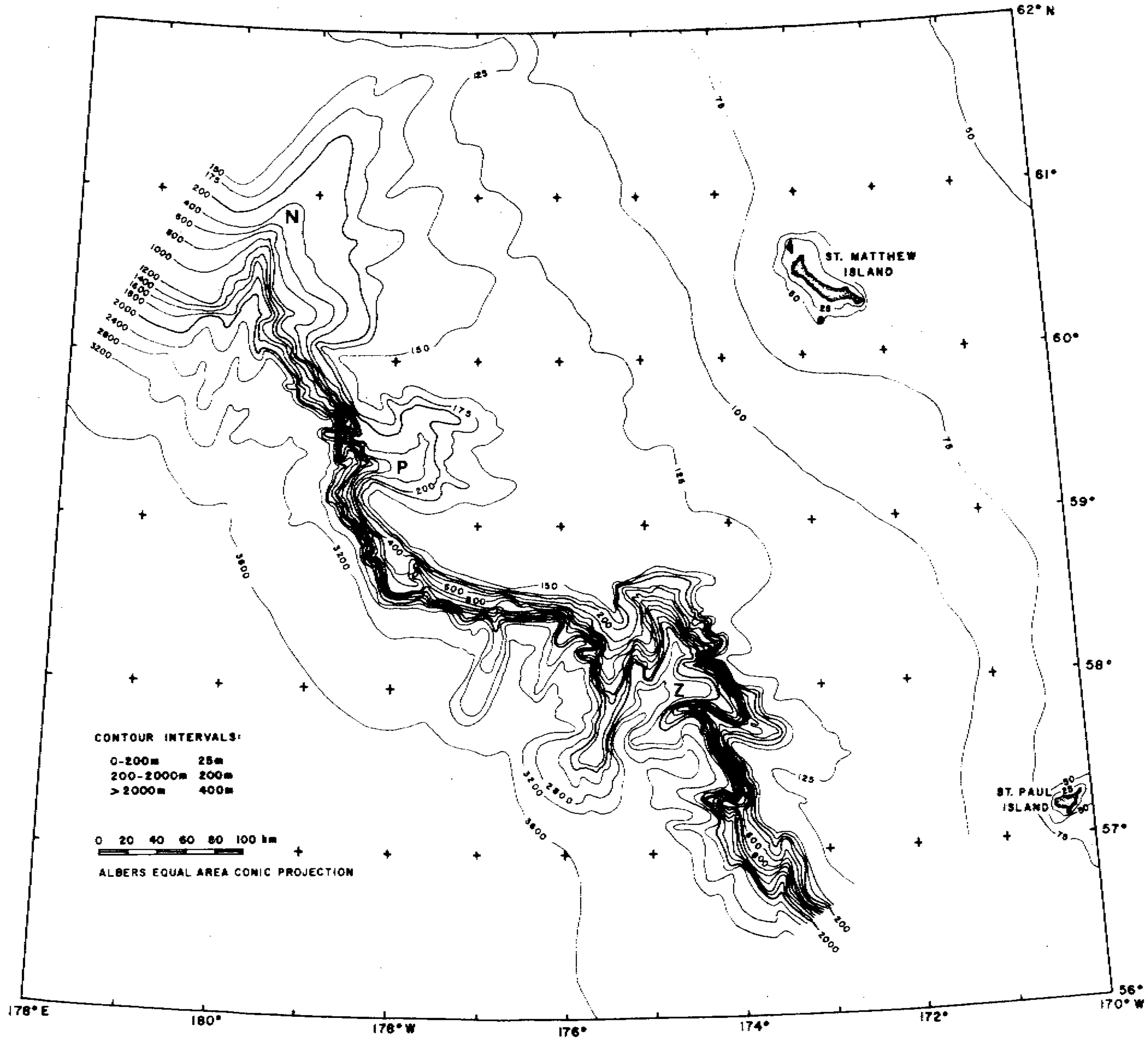

Figure 4. Preliminary bathymetry of Navarin Basin province. Letters N, P, and Z locate the three major submarine canyons, Navarinsky, Pervenets, and Zhemchug.

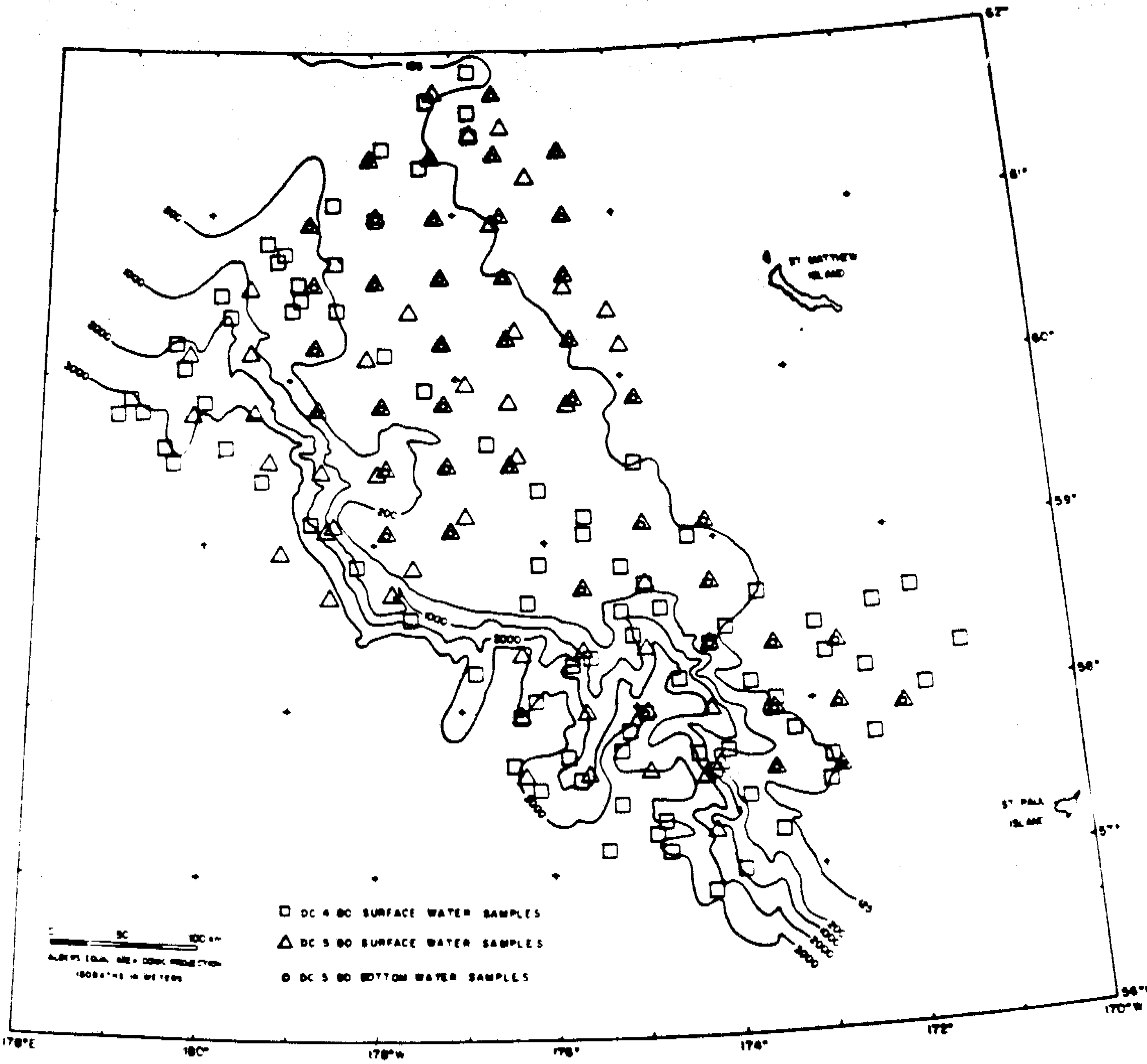

Figure 5. Suspended particulate matter station locations.

SUSPENDED PARTICULATE MATTER IN NAVARIN BASIN PROVINCE, SUMMER, 1980

H. A. Karl, B. Lamb, and P. R. Carlson

INTRODUCTION

Distribution, concentration, and composition of particulate matter suspended in the water column reflect oceanographic conditions prevailing in Navarin Basin province. Terrigenous sediment and plankton in large part constitute the total suspended matter (TSM) in the water column. In addition, waves and currents resuspend fine-grained material previously deposited on the bottom. Particulate matter occurs in suspension throughout the water column, but is concentrated at density discontinuities where particles accumulate as they settle. Major concentrations of suspensates occur at the water surface, along density gradients within the thermocline, and near the bottom. Spatial and temporal variations in the distribution, concentration, and composition of suspended sediment define pathways of sediment dispersal and zones of erosion and deposition.

Methods

Samples of TSM were collected at the surface and within 1-2 m of the sea floor. Samples of surface water were collected by casting a PVC bucket from the ship at 4-hour intervals while seismic profiling and 1-2 minutes before coming to a stop at each core station. Water near the bottom was sampled using a 5 liter Niskin bottle modified to close when a weighted line contacted the seabed. Vacuum pumps sucked a 1-4 liter aliquot of water taken from these samples through preweighed 47 mm diameter polycarbonate Nuclepore filters with a nominal pore size of 0.4 um. The filters were rinsed with distilled water and placed in covered plastic petri dishes. Onshore the filters were dried for 24 hours at 50°C and reweighed to an accuracy of 10 ug. In addition, one-half of each filter was combusted for 5-6 hours at 550°C in tared platinum foil crucibles in order to obtain an estimate of organic matter concentration. Concentrations of TSM, organic matter, and ash residue were calculated as milligrams of suspensate per liter of seawater.

RESULTS

During the 1980 DISCOVERER cruise, from July 6 to August 18, we collected 187 surface samples and 38 bottom samples (Fig 5). Table 1 shows the concentrations of TSM, organic matter, and ash residue of those samples processed to date. Concentrations of surface suspended sediment averaged 0.55 mg/l ranging from a low of 0.04 mg/l to a high of 2.32 mg/l. The average bottom TSM concentration, exclusive of 3 contaminated samples (BS-6, BS-12, BS-17) and a non-contaminated sample (BS-18), but one with an unusually high TSM concentration is 1.91 mg/l that is 3.5 times the average surface concentration. By including the highest concentration recorded, 18.32 mg/l, the mean is raised to 2.33 mg/l. The lowest concentration measured was 0.39 mg/l. We have calculated the percent of organic matter in 144 surface samples and 13 near bottom samples. The mean percentage of organic matter for surface samples is 65.7%; the range is from 12.2% to 95.2%. The organic content of the near bottom samples which have been analyzed is less than half the surface mean averaging 29.1% and ranging from 10.9% to 85.5%.

Maps of the spatial distribution of TSM and ash residue percent (the non-combustible portion of the sample which is taken to be the inverse of the organic matter percentage) reveal several trends. Regionally, concentrations of surface TSM tend to be greater in the southeastern part of the province than elsewhere (Fig. 6). There is no clear cut cross-shelf gradient in concentration. Instead isopleths form lobes, plumes and closures. Although sample coverage is meager, bottom TSM concentrations tend to decrease seaward (Fig. 7). Higher than average concentrations occur at the heads of Pervenets and Zhemchug canyons. Percentage of ash residue in surface samples also tends to be greater in the southeastern part of the area (Fig. 8). A narrow, elongate band of anamolously-low values extending across the upper slope and outer shelf perpendicular to isobaths is an exception to this trend (Fig. 8). Higher percentage occur in the northwest to the east of Pervenets Canyon, and to the southeast of Navarinsky canyon. Except for the transect northeast of Pervenets Canyon, percentages of ash residue in near bottom samples decrease seaward (Fig. 9).

DISCUSSION

Surface TSM

The relatively low concentrations of TSM in the surface water is not surprising in that Navarin Basin lies several hundred kilometers from major sources of terrigenous sediment. The higher concentrations of surface TSM in the southeast in the vicinity of Zhemchug Canyon, over the upper slope and outer shelf, and near Pervenets and Navarinsky Canyons may reflect populations of plankton. Similarly isolated areas of higher TSM values may be the result of concentrated pockets of plankton. This interpretation is conjecture, because no suspended matter compositions have as yet been determined. A major point which must be considered when interpreting our areal distribution of suspended particulates is the time required to sample such an enormous area. Distributions and concentrations may have changed from the first sample collected to the last. Temporal changes in concentrations may in part account for the patchy and convoluted distributions. Alternately, these patterns may reflect eddies in the shelf and slope current systems. The percentage of ash residue tends to be correlated positively with higher TSM concentrations. Ash residue is composed not only of terrigenous debris, but includes the non-combustible, often siliceous, parts of organisms. Diatoms (see Baldauf, this report) dominate and radiolarians (Blueford, this report) are important contributors to the micro-organism assemblages. The siliceous tests of these organisms could contribute to the ash residue.

Near-bottom TSM

Distribution patterns of TSM and ash residue near the bottom of the water column are more readily interpreted than surface distributions. Decreasing gradients seaward suggest less energy is available to resuspend sediment. This might be explained by shoaling surface waves that affect bottom sediments more in shallow water than in deep water. Other oceanic processes affect sedimentation, but not enough is known about Bering Sea shelf currents to discuss the role of various currents on the transport of near bottom sediment.

Three near-bottom samples (BS-6, BS-12, and BS-17) of anamolously high concentrations were discounted as being contaminated. Even discounting these samples, there is a plume of higher than average TSM extending from the shelf towards the head of Pervenets Canyon (Fig. 7). Another plume is located near the head of Zhemchug Canyon. These canyons possibly may modify currents around their heads in such a way as to intensify resuspension of bottom sediment on the adjacent shelf and to draw water from the shelf down canyon. Such canyon effects on shelf sediment dynamics have been postulated elsewhere (Karl, 1980). Alternately, these higher concentrations may reflect greater numbers of benthic and planktonic microorganisms near the canyon heads.

CONCLUSIONS

A substantial number of suspended sediment samples have been collected from a virtually unstudied area of the Bering Sea. The preliminary stage of data reduction does not warrant making detailed statements about the processes that influence sediment dynamics in Navarin basin. Generally, the concentration of total suspended matter near the bottom is more than 3 times that on the surface. This very likely reflects fine-grained material resuspended by currents generated by surface waves but may involve other processes. The patchy distribution of surface suspended sediment suggests not only that plankton may influence the TSM concentrations, but also may reflect complex shelf and slope currents. The submarine canyons may affect both surface and near-bottom distributions by supplying nutrient-rich upwelled water and by modifying current patterns on the adjacent shelf.

REFERENCES CITED

Karl, H. A., 1980, Influence of San Gabriel submarine canyon on narrow shelf sediment dynamics, southern California: Marine Geology, v. 34, p. 61-78.

Table 1.: Analyses of suspended particulate matter

SAMPLE NO.	DEPTH (m)	TSM[1] (mg/l)	NCM[2] (mg/l)	NCM %	CM[3] (mg/l)	CM %
SS-1	Surface	0.64	0.33	51.3	0.31	48.7
SS-2	"	0.73	0.21	28.0	0.52	72.0
SS-3	"	0.64	0.27	42.9	0.36	57.1
SS-4	"	0.53	0.27	51.7	0.25	48.3
SS-5	"	0.67	0.28	42.5	0.38	57.5
SS-6	"	1.20	0.23	19.0	0.97	81.0
SS-7	"	1.04	0.26	25.0	0.76	75.0
SS-8	"	0.66	0.12	19.3	0.53	80.7
SS-9	"	0.29	0.12	42.6	0.16	57.4
SS-10	"	0.72	0.30	42.0	0.41	58.0
SS-11	"	0.93	0.41	44.4	0.51	55.6
SS-12	"	0.65	0.22	34.7	0.42	65.3
SS-13	"	1.25	0.46	37.4	0.78	62.6
SS-14	"	0.23	0.10	42.7	0.13	47.3
SS-15	"	0.54	0.11	20.8	0.43	79.2
SS-16	"	0.34	0.14	40.3	0.20	59.7
SS-17	"	0.27	0.13	48.8	0.14	51.2
SS-18	"	0.75	0.17	23.7	0.57	76.3
SS-19	"	0.70	0.06	09.5	0.63	90.5
SS-20	"	0.26	0.07	28.7	0.18	71.2
SS-21	"	0.28	0.10	35.5	0.18	64.5
SS-22	"	0.82	0.28	34.1	0.54	65.9
SS-23	"	0.26	0.08	33.7	0.17	66.3
SS-24	"	0.28	0.10	35.8	0.18	64.2
SS-25	"	0.24	0.07	32.8	0.16	67.2
SS-26	"	0.34	0.13	38.9	0.21	61.1
SS-27	"	0.62	0.32	51.5	0.30	48.5
SS-28	"	0.63	0.30	48.5	0.32	51.5
SS-29	"	0.33	0.09	26.8	0.24	73.2
SS-30	"	0.45	0.08	19.4	0.37	80.6
SS-31	"	0.29	0.05	19.8	0.23	80.2
SS-32	"	0.27	0.10	39.5	0.16	60.5
SS-33	"	0.30	0.08	26.1	0.22	73.9
SS-34	"	0.42	0.13	32.5	0.28	67.5
SS-35	"	0.24	0.09	37.1	0.15	62.9
SS-36	"	0.38	0.11	28.8	0.27	71.2
SS-37	"	0.36	0.14	39.6	0.22	60.4
SS-38	"	0.31	0.07	25.4	0.23	74.6
SS-39	"	0.18	0.04	25.7	0.13	74.3
SS-40	"	0.23				
SS-41	"	0.66	0.31	48.1	0.34	51.9
SS-42	"	0.59	0.30	52.1	0.28	48.9
SS-43	"	0.40	0.13	31.8	0.27	58.2
SS-44	"	0.48	0.16	34.6	0.31	65.4
SS-45	"	0.81	0.17	21.4	0.63	78.6
SS-46	"	0.65	0.24	36.8	0.47	63.2
SS-47	"	0.44	0.12	28.5	0.31	71.5

[1] concentration of total suspended matter in the sample

[2] concentration of non-combustible matter in the sample; this matter is assumed to be terrigenous particles and/or the non-combustible parts of organisms.

[3] concentration of combustible matter in the sample; this matter is assumed to be the organic constituents of the total suspended sediment.

* C = contaminated sample.

Table 1.: Analyses of suspended particulate matter (cont'd)

SAMPLE NO.	DEPTH (m)	TSM[1] (mg/l)	NCM[2] (mg/l)	NCM %	CM[3] (mg/l)	CM %
SS-48	Surface	0.46	0.15	32.9	0.31	67.1
SS-49	"	0.38	0.13	34.8	0.25	65.2
SS-50	"	0.50	0.14	29.5	0.35	70.5
SS-51	"	0.34	0.11	34.7	0.22	65.3
SS-52	"	0.40	0.19	44.9	0.20	55.1
SS-53	"	0.40	0.10	26.2	0.29	73.8
SS-54	"	0.35	0.12	34.0	0.23	66.0
SS-55	"	0.41	0.14	35.6	0.26	64.4
SS-56	"	0.58	0.30	52.7	0.27	47.3
SS-57	"	1.76	1.14	65.0	0.62	35.0
SS-58	"	1.66	0.08	04.8	1.58	95.2
SS-59	"	0.49	0.22	45.1	0.27	54.9
SS-60	"	0.62	0.25	41.0	0.36	59.0
SS-61	"	0.66	0.23	34.8	0.43	65.2
SS-62	"	0.35	0.10	29.3	0.24	70.7
SS-63	"	0.35	0.08	25.1	0.26	74.9
SS-64	"	0.38	0.10	27.9	0.27	72.1
SS-65	"	0.44	0.11	25.6	0.32	74.4
SS-66	"	0.38	0.07	19.1	0.31	80.9
SS-67	"	0.80	0.34	42.6	0.46	57.4
SS-68	"	0.74	0.10	14.8	0.63	85.2
SS-69	"	0.44	0.27	62.1	0.16	37.9
SS-70	"	0.72	0.13	19.0	0.58	81.0
SS-71	"	0.60	0.09	14.7	0.51	85.3
SS-72	"	0.51	0.14	27.5	0.37	72.5
SS-73	"	0.50	0.16	32.1	0.34	67.9
SS-74	"	0.57	0.15	26.5	0.42	73.5
SS-75	"	0.60	0.14	24.3	0.46	75.7
SS-76	"	0.46	0.13	30.0	0.32	70.0
SS-77	"	0.57	0.18	52.2	0.39	47.8
SS-78	"	0.37	0.16	48.6	0.21	51.4
SS-79	"	0.94	0.35	37.2	0.59	62.8
SS-80	"	0.31	0.09	29.4	0.22	70.6
SS-81	"	0.59	0.18	31.2	0.40	68.8
SS-82	"	0.66	0.21	17.1	0.45	82.9
SS-83	"	0.61	0.23	38.0	0.38	62.0
SS-84	"	0.28	0.11	39.3	0.17	60.7
SS-85	"	0.32	0.07	22.0	0.25	78.0
SS-86	"	0.33	0.06	19.6	0.26	80.4
SS-87	"	0.78	0.33	42.3	0.45	57.7
SS-88	"	1.47	0.90	61.3	0.56	38.7
SS-89	"	0.53	0.14	26.8	0.39	73.2
SS-90	"	0.40	0.11	28.2	0.28	71.8
SS-91	"	0.92	0.44	47.8	0.48	52.2
SS-92	"	0.44	0.10	23.7	0.33	76.3
SS-93	"	0.41	0.11	26.9	0.30	73.1
SS-94	"	0.26	0.09	34.8	0.17	65.2

Table 1.: Analyses of suspended particulate matter (cont'd)

SAMPLE NO.	DEPTH (m)	TSM[1] (mg/l)	NCM[2] (mg/l)	NCM %	CM[3] (mg/l)	CM %
SS-95	Surface	0.37	0.13	35.8	0.23	64.2
SS-96	"	0.40	0.14	35.4	0.26	64.6
SS-97	"	0.32	0.09	30.6	0.22	69.4
SS-98	"	0.48	0.19	41.3	0.28	58.8
SS-99	"	0.17	0.65	38.0	1.06	62.0
SS-100	"	0.40	0.14	35.5	0.26	64.5
SS-101	"	0.25	0.06	24.6	0.19	75.4
SS-102	"	0.24	0.05	21.6	0.19	78.4
SS-103	"	0.34	0.04	14.1	0.29	85.9
SS-104	"	0.44	0.11	26.7	0.32	73.3
SS-105	"	0.24	0.07	31.6	0.16	83.4
SS-106	"	0.28	0.09	34.6	0.18	65.4
SS-107	"	0.31	0.05	19.1	0.25	80.9
SS-108	"	0.21	0.07	33.5	0.14	66.5
SS-109	"	0.24	0.12	50.0	0.12	50.0
SS-110	"	0.56	0.21	38.8	0.34	65.5
SS-111	"	0.41	0.11	39.5	0.29	60.5
SS-112	"	0.41	0.16	39.8	0.25	60.2
SS-113	"	0.23	0.06	28.8	0.16	71.2
SS-114	"	0.64	0.10	16.9	0.53	83.1
SS-115	"	0.17	0.02	16.8	0.14	83.2
SS-116	"	0.21	0.04	21.2	0.16	78.8
SS-117	"	0.18	0.03	17.6	0.14	82.4
SS-118	"	0.13	0.02	21.5	0.10	78.5
SS-119	"	0.38	0.10	25.9	0.28	74.1
SS-120	"	0.45	0.13	29.6	0.32	70.4
SS-121	"	0.60	0.32	54.3	0.27	45.7
SS-122	"	0.24	0.08	34.9	0.15	65.1
SS-123	"	0.89	0.69	51.7	0.20	48.3
SS-124	"	0.32				
SS-125	"	0.74	0.35	48.2	0.38	51.8
SS-126	"	0.76	0.37	48.7	0.39	51.3
SS-127	"	0.38	0.12	32.3	0.26	67.7
SS-128	"	0.34	0.10	28.0	0.24	72.0
SS-129	"	0.23	0.65	27.9	0.16	72.1
SS-130	"	0.27	0.56	20.2	0.22	79.8
SS-131	"	0.29	0.07	23.2	0.22	76.8
SS-132	"	1.34	0.25	18.2	1.09	81.8
SS-133	"	0.34	0.09	27.0	0.25	73.0
SS-134	"	0.41	0.12	28.0	0.29	72.0
SS-135	"	0.24	0.10	42.0	0.14	58.0
SS-136	"	0.78	0.27	34.0	0.51	66.0
SS-137	"	1.02	0.38	37.0	0.64	63.0
SS-138	"	0.46	0.11	23.0	0.35	77.0
SS-139	"	0.63	0.24	38.0	0.39	62.0
SS-140	"	0.37	0.13	36.0	0.24	64.0

Table 1.: Analyses of suspended particulate matter (cont'd)

SAMPLE NO.	DEPTH (m)	TSM[1] (mg/l)	NCM[2] (mg/l)	NCM %	CM[3] (mg/l)	CM %
SS-141	Surface	0.37	0.15	42.7	0.21	57.3
SS-142	"	0.37	0.13	36.4	0.23	76.2
SS-143	"	0.35	0.19	54.2	0.16	45.8
SS-144	"	0.40	0.35	87.8	0.04	12.2
SS-145	"	0.52	0.27	51.4	0.25	48.6
SS-146A	"	0.56	0.25	44.0	0.31	56.0
SS-146B	"	0.64	0.25	39.0	0.39	61.0
SS-147	"	0.35	0.09	27.0	0.26	73.0
SS-148	"	0.31	0.06	19.0	0.15	81.0
SS-149	"	0.28	0.09	31.0	0.19	69.0
SS-150	"	0.24	-	-	-	-
SS-151	"	0.40	0.02	05.0	0.38	95.0
SS-152	"	0.79	0.23	28.0	0.56	72.0
SS-153	"	0.43	0.16	37.0	0.27	63.0
SS-154	"	0.68	0.27	39.0	0.31	61.0
SS-155	"	0.92	0.34	37.3	0.58	62.7
SS-156	"	0.59	0.14	24.7	0.44	75.3
SS-157	"	0.77	0.34	44.6	0.43	55.4
SS-158	"	1.13	0.19	17.1	0.94	82.9
SS-159	"	0.51	0.14	26.0	0.37	74.0
SS-160A	"	1.22	0.93	76.6	0.28	23.4
SS-160B	"	1.09	0.43	39.0	0.56	61.0
SS-161	"	0.64	0.18	27.9	0.46	72.1
SS-162	"	0.58	0.24	41.6	0.34	58.4
SS-163	"	1.30	0.78	60.1	0.52	39.9
SS-164	"	1.21	0.65	53.5	0.56	46.5
SS-165	"	1.45	0.67	45.8	0.78	54.2
SS-166	"	1.13	0.46	40.4	0.67	59.6
SS-167	"	0.51	0.20	38.5	0.31	61.5
SS-168	"	0.40	0.16	39.0	0.24	84.0
SS-169	"	1.13	0.69	61.1	0.44	38.9
SS-170	"	2.32	0.12	55.8	1.03	44.6
SS-171	"	1.00	0.53	53.3	0.47	46.7
SS-172	"	1.36	0.83	60.9	0.53	39.1
SS-173	"	0.73	0.32	51.0	0.41	49.0
SS-174	"	0.46	0.20	43.7	0.26	56.3
SS-175	"	0.40	0.19	46.8	0.21	53.2
SS-176	"	0.45	0.21	47.1	0.24	52.9
SS-177	"	0.46	0.16	33.2	0.30	66.8
SS-178	"	0.74	0.38	51.2	0.36	48.8
SS-179	"	0.77	0.47	31.3	0.30	68.7
SS-180	"	0.70	0.35	50.5	0.35	49.5
SS-181	"	0.40	0.14	36.3	0.26	63.7
SS-182	"	0.45	0.18	40.2	0.27	59.8
SS-183	"	0.60	0.31	50.4	0.29	49.6
SS-184	"	0.75	0.31	40.9	0.34	59.1
SS-185	"	1.15	0.49	42.6	0.56	57.4

Table 1.: Analyses of suspended particulate matter (cont'd)

SAMPLE NO.	DEPTH (m)	TSM[1] (mg/l)	NCM[2] (mg/l)	NCM %	CM[3] (mg/l)	CM %
BS-1	150	0.41	0.06	14.5	0.35	85.5
BS-2	210	0.54	0.33	60.8	0.21	39.2
BS-3	230	0.39	0.21	55.0	0.17	45.0
BS-4	148	1.51	1.08	67.5	0.42	32.5
BS-5	124	1.97	1.54	78.0	0.43	21.9
BS-6 *	108	214.34C	187.45	87.0	27.85	13.0
BS-7	110	2.19	1.67	76.0	0.42	24.0
BS-8	123	2.35	1.67	70.9	0.68	29.1
BS-9	159	2.31	1.65	71.3	0.66	20.7
BS-10	300	0.50	0.33	65.0	0.17	35.0
BS-11	159	0.71	0.53	73.0	0.18	27.0
BS-12 *	145	376.79C	341.60	90.0	35.10	10.0
BS-13	118	2.35	1.66	70.6	0.69	29.4
BS-14	98	3.79	3.06	81.0	0.73	19.0
BS-15	106	3.73	2.94	78.9	0.78	21.1
BS-16	125	3.82	2.93	76.5	0.89	23.5
BS-17 *	140	59.64C	51.96	87.1	7.68	12.8
BS-18	147	18.32	16.33	89.1	1.99	10.9
BS-19	378	0.74	0.48	64.0	0.26	36.0
BS-20	140	1.75	1.37	78.0	0.38	22.0
BS-21	133	3.47	2.77	80.0	0.70	20.0
BS-22	111	2.70	1.65	61.0	1.05	39.0
BS-23	117	2.20	-	-	-	-
BS-24	151	0.77	0.49	63.0	0.28	37.0
BS-25	140	0.70	0.32	45.0	0.38	55.0
BS-26	147	0.62	0.43	69.6	0.19	30.4
BS-27	137	2.02	1.64	73.4	0.37	26.6
BS-28	128	3.38	2.66	78.7	0.72	21.3
BS-29	117	2.49	1.86	74.0	0.63	26.0
BS-30	105	0.76	6.48	84.0	1.19	15.9
BS-31	120	1.09	2.08	83.0	1.01	17.0
BS-32	112	9.01	7.76	86.0	1.25	14.0
BS-33	145	0.64	0.37	56.6	0.27	43.4
BS-34	119	2.38	1.86	78.0	0.52	22.0
BS-35	109	2.16	1.56	72.4	0.60	27.6
BS-36	117	3.31	2.89	78.0	0.41	22.0
BS-37	134	0.56	0.40	71.2	0.16	29.8
BS-38	142	0.97	0.68	69.8	0.29	30.2
BS-39	165	0.56	0.24	43.2	0.32	56.7
BS-40	122	1.97	1.21	61.2	0.76	38.8
BS-41	129	1.14	0.76	66.5	0.38	33.5
BS-42	136	0.74	0.44	59.4	0.30	40.6

[1] Concentration of total suspended matter in the sample.

[2] Concentration of non-combustible matter in the sample; this matter is assumed to be terrigenous particles and/or the non-combustible parts of organisms.

[3] Concentration of combustible matter in the sample; this matter is assumed to be the organic constituents of the total suspended sediment.

* C = contaminated sample.

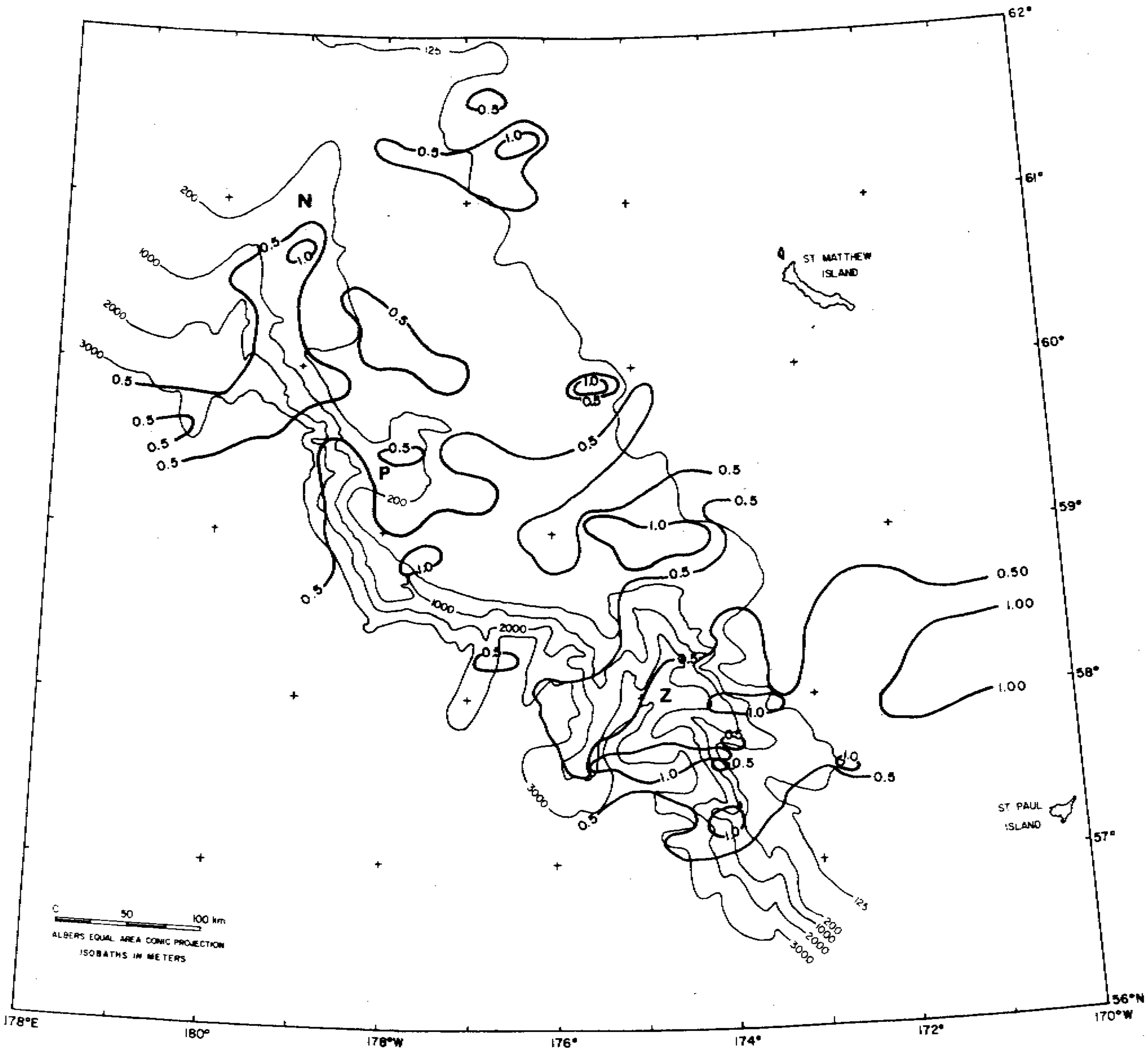

Figure 6. Areal distribution of absolute concentration (mg/l) of total suspended matter collected at the surface. Letters N, P, Z locate Navarinsky, Pervenets, and Zhemchug Canyons.

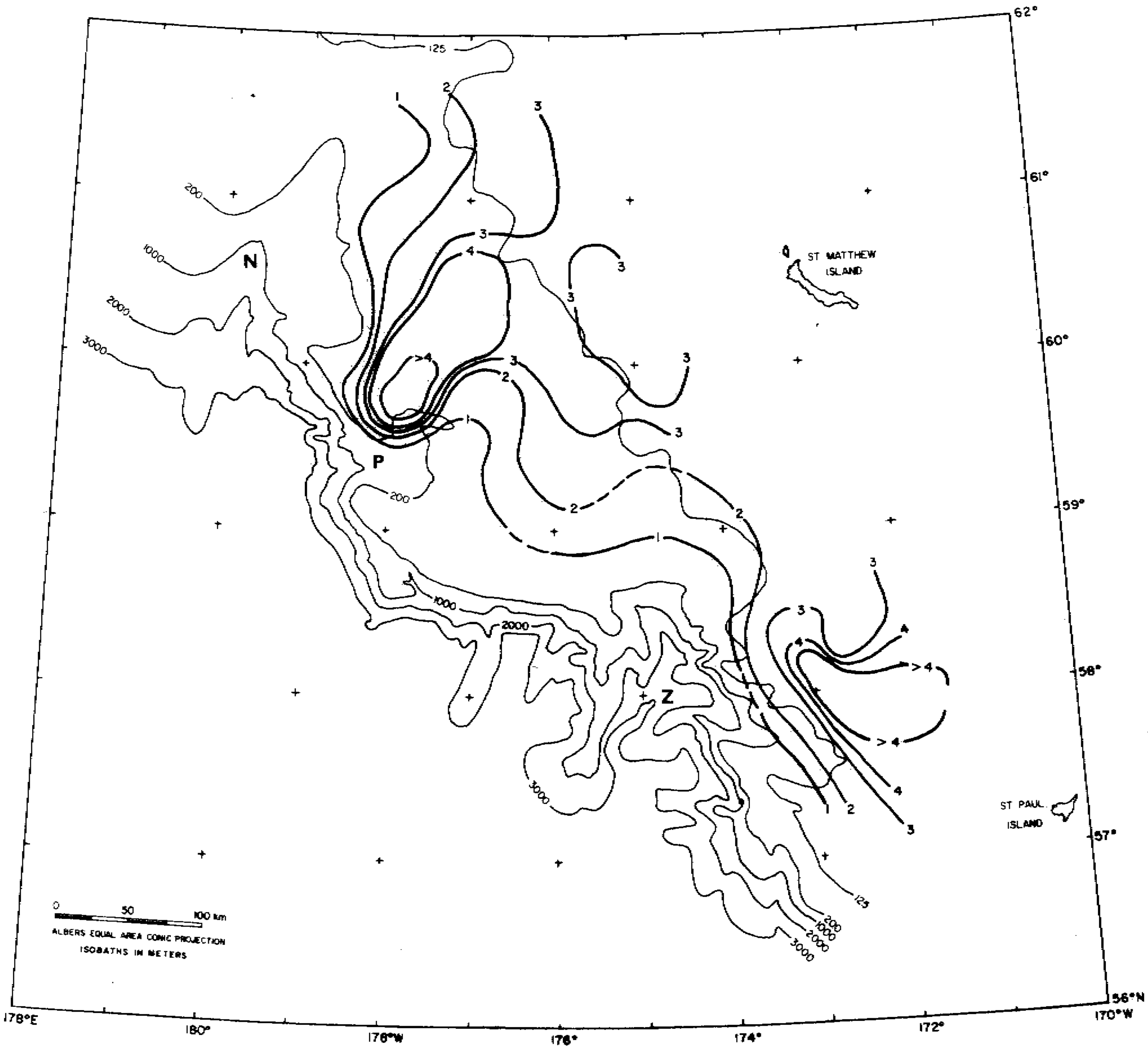

Figure 7. Areal distribution of absolute concentration (mg/l) of total suspended matter collected 1 m above the sea bed. Letters N, P, Z locate Navarinsky, Pervenets, and Zhemchug Canyons.

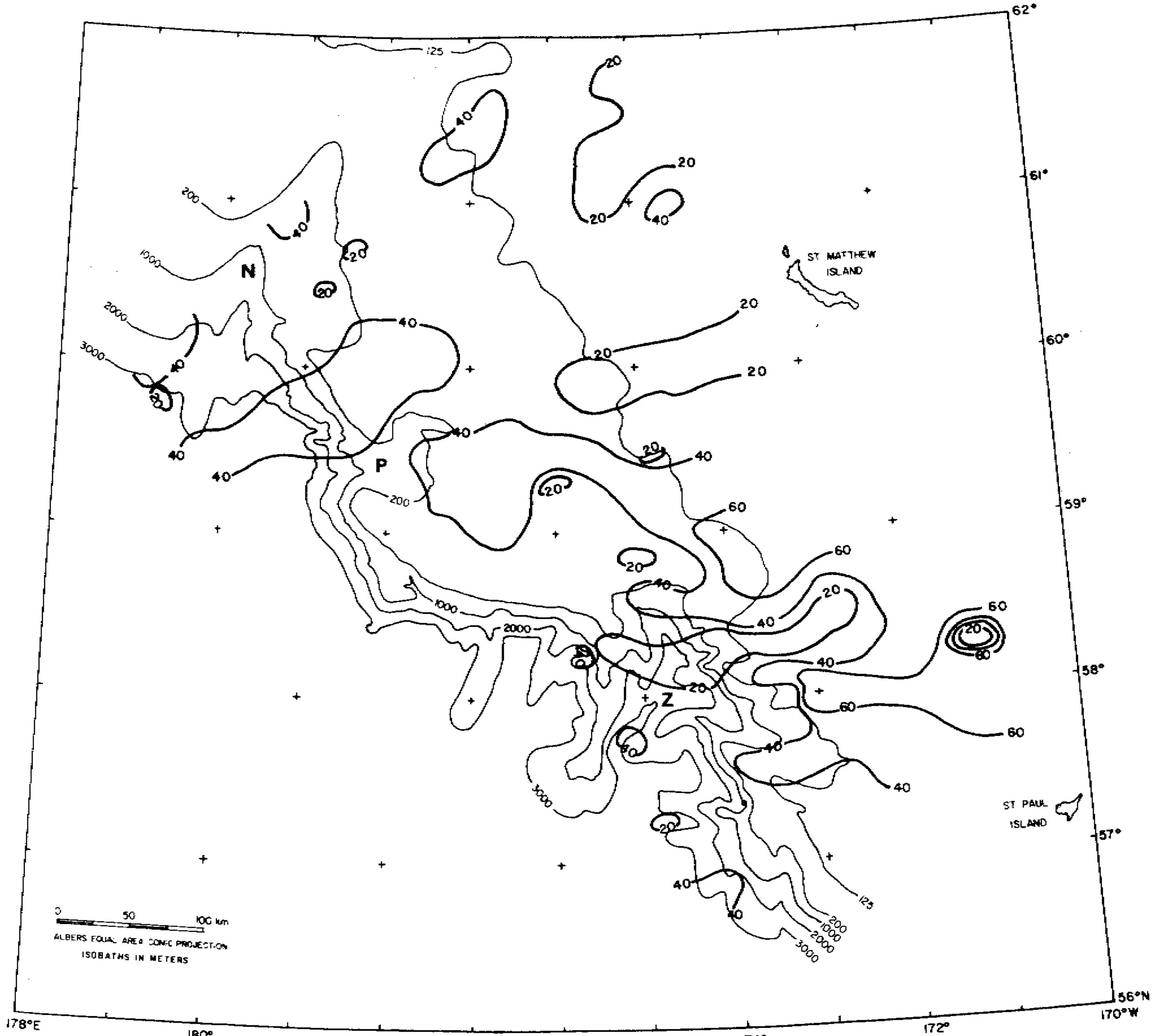

Figure 8. Areal distribution of the percentage of non-combustible material in surface suspended sediment samples. Letters N, P, Z locate Navarinsky, Pervenets, and Zhemchug Canyons.

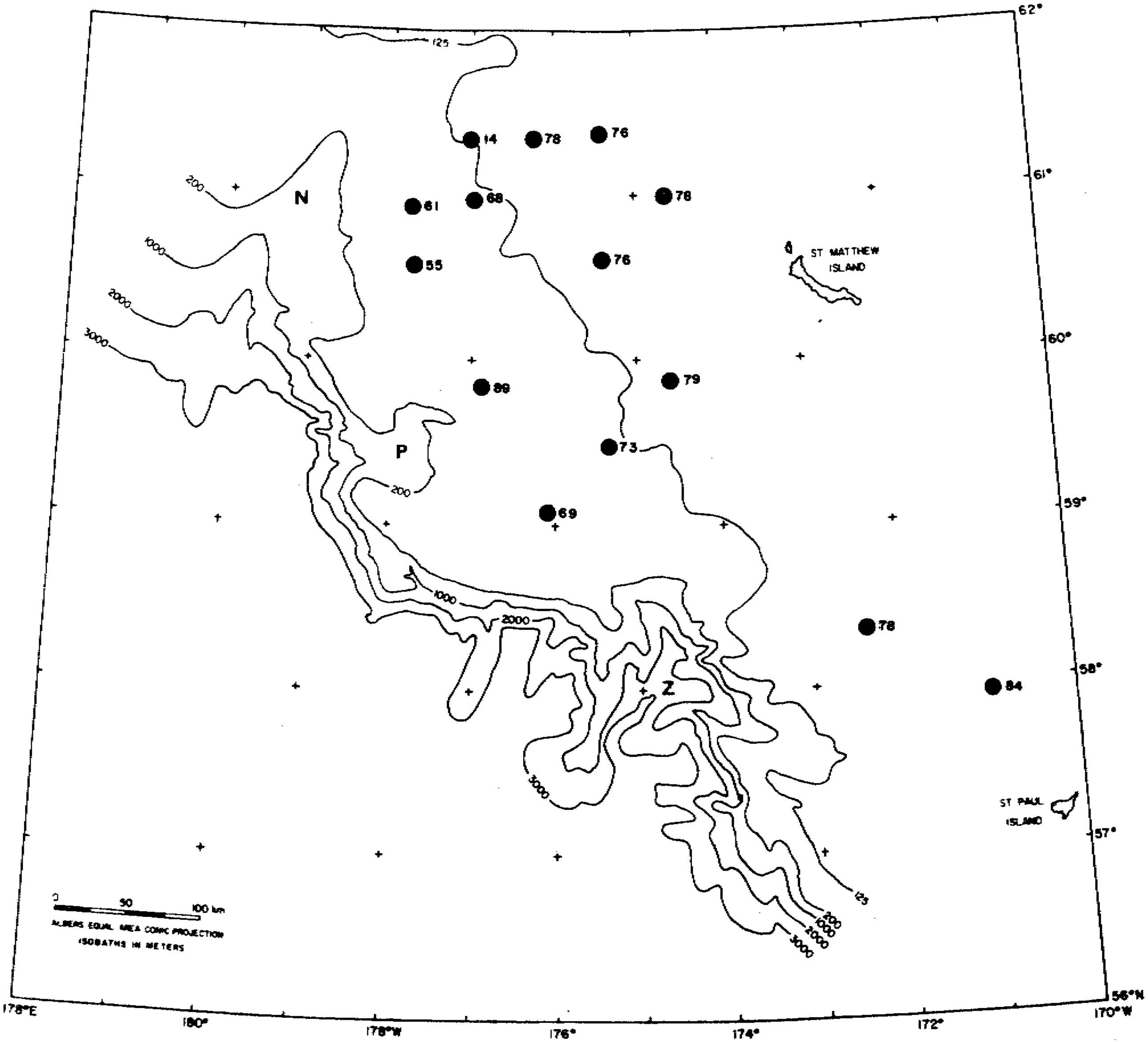

Figure 9. Areal distribution of the percentage of non-combustible material in suspended sediment samples collected 1 m above the sea bed. Letters N, P, Z locate Navarinsky, Pervenets, and Zhemchug Canyons.

TEXTURAL VARIATIONS AND COMPOSITION OF BOTTOM SEDIMENT

H. A. Karl, P. R. Carlson, J. Fischer, K. Johnson, and B. Lamb

In this section we present the available data from our analyses of sediment subsamples taken from gravity cores and grab samples. Subsamples were soaked in H_2O_2 solution to remove organic matter. The samples were then wet sieved at >63 µm to separate mud and sand fractions. If gravel (> 2 mm) was present, it was separated from sand by dry sieving. The percentage of biogenic material in the sand fraction was determined by counting 500 grains under low power magnification.

Sediment sampling stations are plotted in Figure 10. Sediment types are derived from qualitative visual descriptions of surface samples. We consider bulk subsamples from grab samples and discrete subsamples from the upper 35 cm of gravity cores as surface samples. Figure 11 is a contour map of the sand/mud ratios of surface samples. Figures 10 and 11 show two trends. Whereas silts generally characterize the shelf and slope, there is a zone of coarser sediment at the shelf break, on the upper slope, and in the heads of submarine canyons. Also, surficial sediment on the shelf is slightly coarser in the southeastern part of the area than elsehwere. The percentages of various components identified in the sand fraction are shown in Table 2. The small amounts of volcanic glass may be important stratigraphic markers are discussed by Carlson and others elsewhere in this volume.

Characteristics of gravity cores collected along a shelf-to-slope profile are shown in Figure 12. The cores collected on the shelf are representative of many shelf cores in that there is very little variation in texture and structure down core. Cores collected within submarine canyons (see e.g., Core 37, Fig. 12) and deep-sea fan channels often contain lenses and laminae of sand and coarse silt.

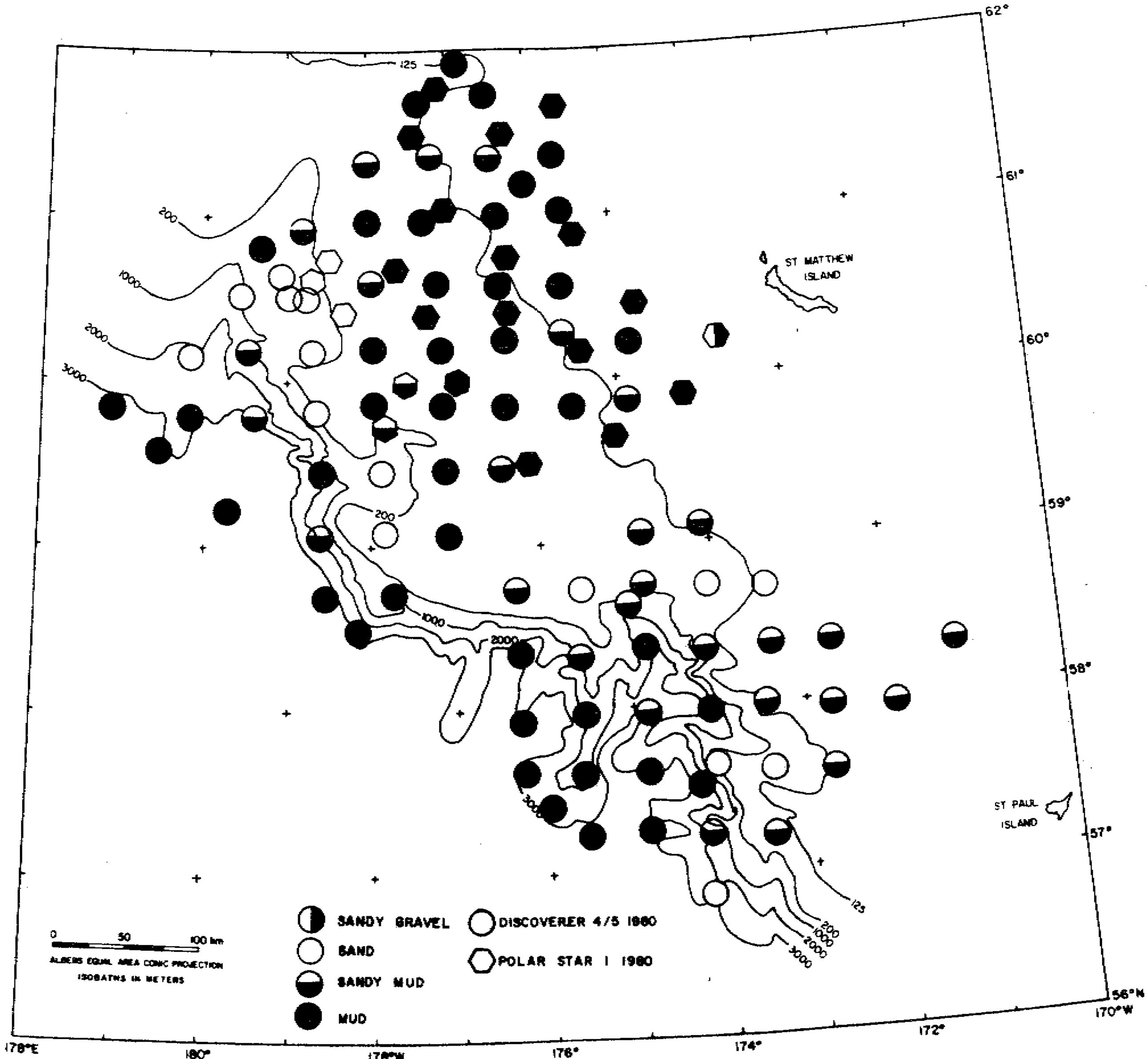

Figure 10. Preliminary map of sediment types in Navarin Basin province derived from visual inspection of core samples onboard ship.

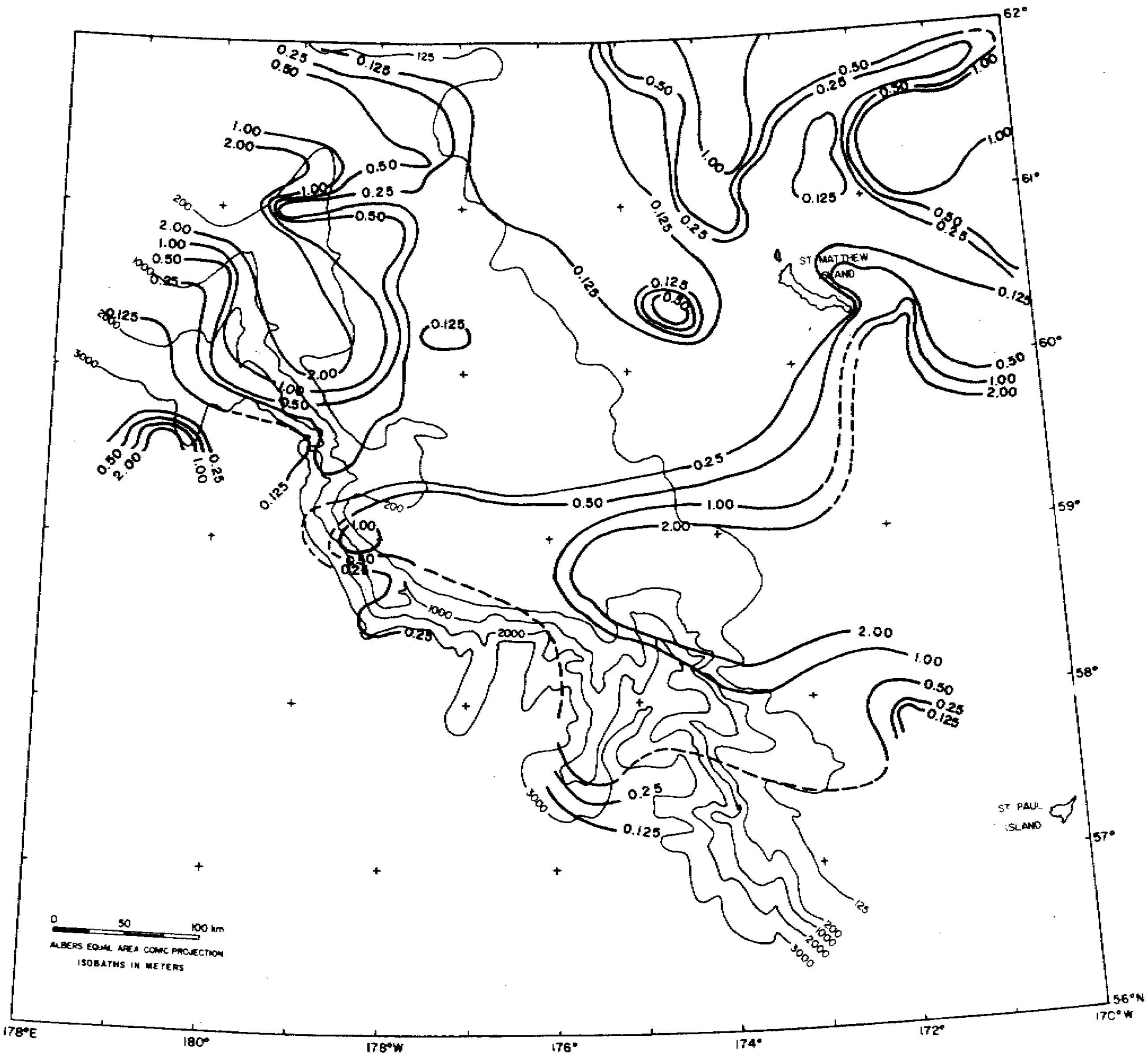

Figure 11. Areal distribution of sand-to-mud ratio for sediment.

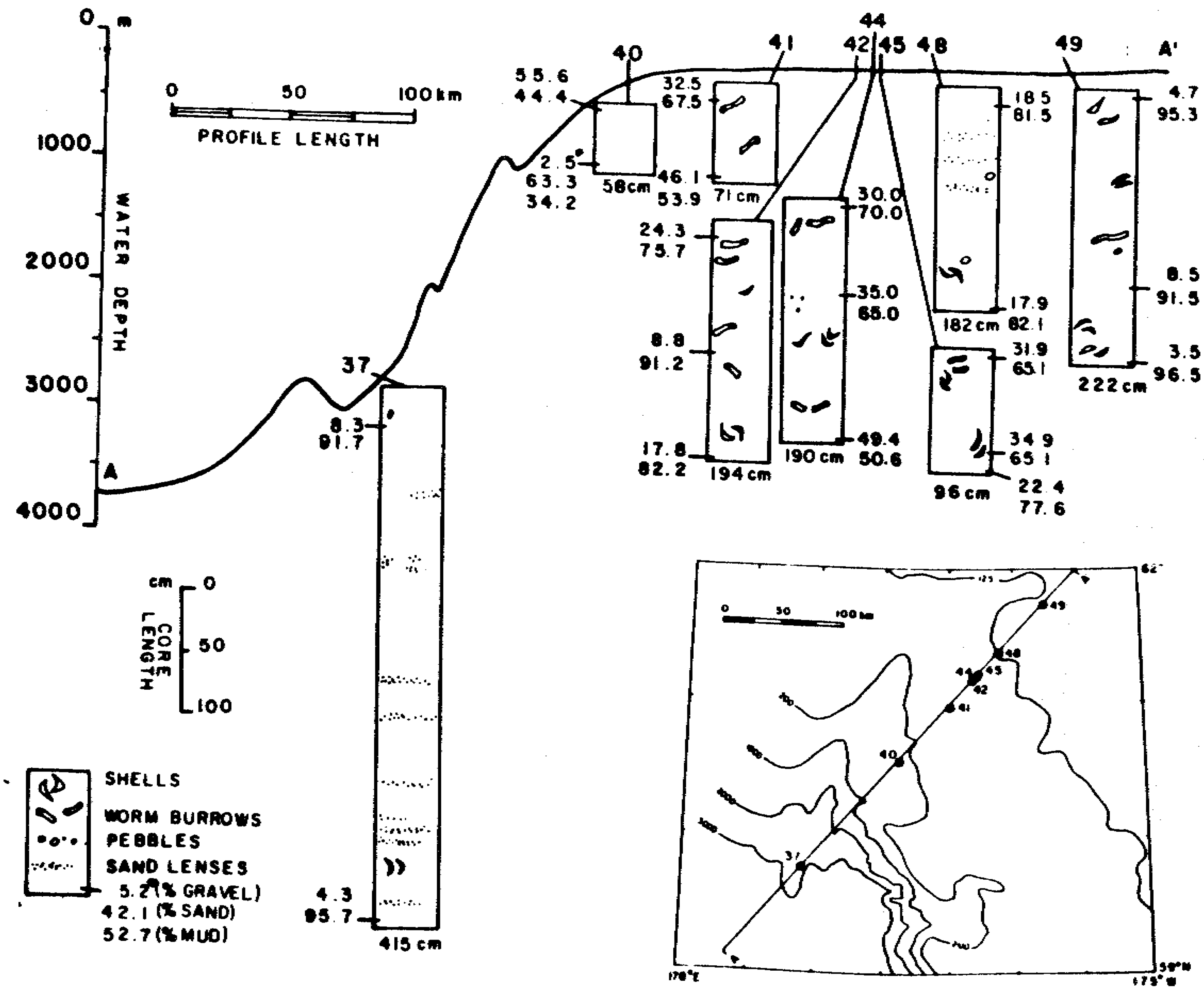

Figure 12. Sedimentary structures observed in gravity cores along bathymetric profile A-A'.

Table 2 Composition of sand fractions (values in percent).

Sample #	Core Interval (cm.)	Minerals and Rock Fragments	Vol. Glass	Diatoms	Rads	Misc.	Water Depth (M)
1		44.8	10.0	44.4	0.8	--	580
2*		96.6	2.8	0.2	0.4		533
4	5-7	96.6	3.0	TR	--	0.4	3,232
12	13-14	4.8	--	92.2	1.0	2.0	3,188
21		93.6	2.8	2.4	0.2	1.0	235
22	25-26	13.6	--	85.2	1.2		2,842
23	8-10	97.6	0.8	1.6	--	TR	110
35		95.2	1.4	3.2	0.2	--	868
38		94.0	1.8	2.2	1.0	TR	990
39		91.8	2.8	4.8	0.6	TR	229
40	5-7	96.4	1.2	1.0	1.2	0.2	230
41	12-13	90.0	--	10.0	TR	--	148
42	12-14	83.4	TR	16.8	--	TR	141
43	5-7	95.2	1.4	3.4	TR	TR	148
44	8-10	93.2	TR	6.8		TR	138
45	8-10	94.8	1.4	3.0	0.4	0.4	137
46	12-14	99.3	--	0.8	TR	--	134
47	5-7	94.8	1.6	3.6	--	--	134
48	11-12	90.2	5.2	4.2	0.4	--	124
60	27-29	62.2	5.0	32.0	--	0.2	106
62	5-7	91.0	2.6	6.4	--	--	125
63	8-10	86.2	0.2	12.6	1.0	--	150
64	9-10	74.8	2.2	22.4	0.6	--	147
65	5-7	19.8	2.0	76.2	1.2	0.8	1,609

Table 2. Composition of sand fractions (values in percent). cont'd

Sample #	Interval (cm.)	Minerals and Rock Fragments	Vol. Glass	Diatoms	Rads	Misc.	Water Depth (M)
75	5-7	23.6	2.0	74.0	0.4	TR	951
77	5-7	89.8	2.8	6.6	0.6	0.2	147
79	11-12	81.2	1.8	16.4	0.2	0.4	136
80	10-11	90.8	0.8	7.8	--	--	128
83	7-10	88.8	1.6	9.6	--	--	105
84	3-4	59.2	0.8	39.6	0.4	--	119
96	9-11	88.0	1.6	10.2	0.2	TR	116
98	5-7	95.2	0.8	2.8	--	1.2	1,610
101	40-42	6.8	0.2	91.8	1.2	--	2,155
102	62-64	83.0	2.4	13.4	TR	0.8	2,960
110		96.0	1.6	2.2	0.2	--	164

*Samples with no values for core interval are grab samples.

CLAY MINERAL DISTRIBUTION IN NAVARIN BASIN, BERING SEA

Kenneth A. Johnson

INTRODUCTION

Previous analyses of clay minerals of Bering Sea sediment are predominantly restricted to the southern reaches of the sea, Hein and others (1976), and Hein and Scholl (1978) reported on clay mineralogical analyses of D.S.D.P. cores in the southern Bering Sea and northern Pacific Ocean. Gardner and others (1980) mapped the distribution of clay minerals in surface sediments in the St. George Basin region just southeast of the Pribilof Islands. This study discusses the distribution of clay minerals in sediments of the Navarin Basin province.

Acknowledgements

Progress of this study was greatly enhanced by discussion with James R. Hein. I would also like to thank Carol Madison and J. Mark Yeats for their assistance during the course of the X-ray work.

METHODS

Subsamples from 58 cores were analyzed and relative percentages of illite, chlorite, smectite and kaolinite were determined (Table 3). Twenty-three of these samples were from near surface (defined as within 35 cm of top of core) sediments. The remainder of samples ranged from 37 to 513 cm in depth. Generally only two samples per core were analyzed, one from the top and bottom of each core. The exception is in core 26 where eight samples were collected from different colored units separated by distinct horizons.

Samples were first treated with equal parts of hydrogen peroxide and Morgan's solution (sodium acetate plus glacial acetic acid diluted with distilled water). Clays were dispersed with a 2% sodium carbonate solution before isolating the less than two micron fraction by centrifugation. This size fraction was saturated with a 1 M $MgCl_2$ solution and subsequently washed twice with distilled water to remove excess salts. Analyses were run on a Picker Integrated high angle diffractometer using nickel filtered copper K radiation at 34 kV and 16 mA. Slides were prepared using the smear technique (Gibbs, 1968) and X-rayed from 3-14° 2θ at 1° per minute. Slides were then glycolated at 65°C for 1 hour and run again at 1° per minute from 3-14° 2θ, and also from 24-26° 2θ at slow scan (1/4° per minute) to distinguish kaolinite and chlorite (Biscaye, 1964).

Peak areas were measured using an electronic planimeter. These values were then multiplied by Biscaye's (1965) weighting factors (4 x 10Å illite peak, 2 x 7Å chlorite peak and 1 x 17Å smectite peak). Relative percentages were calculated by dividing the weighted area of each peak by the total of all three weighted peaks and multiplying by 100. Only clay mineral groups were considered in this study. All minerals whose d-spacing expands to 17Å upon glycolation are called smectite. Kaolinite and chlorite were distinguished by their respective second -order (3.58Å) and fourth-order (3.54Å) basal diffraction peaks. Values of kaolinite + chlorite are also presented because this analytical method does not always provide clear peak distinction (Martin Vivaldi and Gallego, 1961). Random mixed layering of smectite and illite was seen in all samples. Percentages of expandable layers in these mixed-layer minerals were determined from the charts of Perry and Hower (1970) and Reynolds and Hower (1970).

RESULTS

The distribution of clay minerals in near-surface samples is shown in Figure 13. Areal distribution of smectite was plotted and contoured with a 5% contour interval (Fig. 14). Distribution of other clay minerals did not show any significant trends. The surface distribution of smectite exhibits a band of relatively high concentration (>30%) across the middle of the study area, roughly parallel to the shelf break (Fig. 14). Within this band smectite seems to be slightly more concentrated at the northwest and southeast ends of the study area, roughly coincident with the heads of Navarinsky and Zhemchug canyons. No distinct trend is exhibited by kaolinite + chlorite distribution; however, their concentration also shows a subtle increase in the vicinity of the canyon heads. Conversely, illite distribution, shows a slight decrease in concentration around the canyon heads. No downcore trends could be reliably discerned, due to the irregular sampling intervals throughout this study. However, a downcore increase in chlorite was noticed in approximately 70% of the cores.

DISCUSSION

The average percentages of clay minerals in the Navarin region are similar to those determined by Gardner and others (1980) and Hein and others (1976) in other parts of the Bering Sea (Table 4).

Illite and chlorite are generally believed to have a detrital origin at high latitudes (Biscaye, 1965). Smectite however, while commonly associated with alteration of volcanic rocks, can have both detrital and authigenic origins (Hein and Scholl, 1978; Biscaye, 1965). Detrital smectite is usually not pure smectite, but most often some combination of random and/or ordered illite-smectite interlayers (Reynolds and Hower, 1970). Smectite with 50-70% expandable layers is associated with a detrital origin (Hein and Griggs, 1972) whereas authigenic smectite usually has expandable layers in the 90-100% range (Hein and others, 1979). The smectites from this study were found to contain 50-75% expandable layers, thus implying a detrital origin.

Source Area

The location of the study area, near the center of the Bering Sea, suggests the Navarin area could conceivably be supplied with clay material from many sources. The Yukon and Kuskokwim Rivers, with respective runoff totals of 185 and 45 km^3 per year (Lisitsyn, 1966) are likely sources of much Bering shelf sediment. Problems arise with this source in that modern Yukon and Kuskokwim suspended clay minerals include virtually no smectite (Hein, person. commun., 1981). The Anadyr River, emptying into the Bering Sea just north of the study area has a runoff of 41 km^3 per year (Lisitsyn, 1966). Lisitsyn describes a Cenozoic effusive terrain at the mouth of the Anadyr, that could also supply sediment to the area. The Aleutian island chain also provides a source of volcanic detritus. The smectite distribution throughout the Bering Sea is described by Lisitsyn (1966, p. 57) as being " ... very nonuniform. Its content being very low in the north of the sea, whereas it is the most widespread mineral of the clay fraction in the south." Gardner and others (1980) also note that the highest percentages of smectite occur closest to the Aleutians, but a uniform decrease in smectite concentration away from the Aleutians is not proposed. Comparison of mean smectite percentage between Navarin and southern Bering shelf sediments also agrees with a general decrease in smectite with distance from the Aleutians; however, the distribution determined in this study also precludes a simple trend throughout the Bering Sea.

The Navarin region is one of the least studied and hence hydrographically unknown areas in the Bering Sea. Hughes and others (1974) give a summary of surface current studies that generally show northward flow across this part of the shelf, ultimately passing through the Bering Strait into the Chukchi Sea. However, one must be wary of only using surface currents in discussing clay distribution because bottom currents potentially play the most important role in determining ultimate sites of deposition. Kinder others (1975) and Kinder and Schumacher (1980) propose a hydrographic regime that suggests a source area to the south. Their Bering Slope Current supports the additional possibility of the clay mineral distribution being the product of a reworked sediment source.

REFERENCES CITED

Biscaye, P. E., 1965, Mineralogy and sedimentation of Recent deep sea clay in the Atlantic Ocean and adjacent seas and oceans: Geol. Soc. Amer. Bull., v. 76, p. 803-831.

Biscaye, P. E.,1964, Distinction between kaolinite and chlorite in recent sediments by X-ray diffraction: Amer. Mineralogist, v. 49, p. 1281-1289.

Caroll, D., 1970, Clay minerals: A guide to their X-ray identification: Geol. Soc. Amer. Spec. Paper 126; 80p.

Favorite, F., 1974, Flow into the Bering Sea through Aleutian island passes: in Oceanography of the Bering Sea, D. W. Hood and E. J. Kelley, eds., Institute of Marine Science, Univ. of Alaska, p. 3-37.

Gardner, J. V., Dean, W. E., and Vallier, T. L., 1980, Sedimentology and geochemistry of surface sediments, outer continental shelf, southern Bering Sea: Marine Geology, v. 35, p. 299-329.

Gibbs, R. J., 1968, Clay mineral mounting techniques for X-ray diffraction analysis: A Discussion, Journ. Sed. Pet. v. 38, p. 242-244.

Gibbs, R. J.,1965, Error due to segregation in quantitative clay mineral X-ray diffraction mounting techniques: Amer. Mineralogist, v. 50, p. 741-751.

Griffin, J. and Goldberg, E. D., 1963, Clay mineral distributions in the Pacific Ocean: in The Sea, M. N. Hill, ed., V. III, p. 728-741.

Hein, J. R., Ross, C. R., and Alexander, E. A., 1979a, Mineralogy and diagenesis of surface sediments from D.O.M.E.S. areas A, B, and C: in Marine Geology and Oceanography of the Pacific manganese nodule province, J. L. Bischoff and D. Z. Piper eds., Plenum Publishing Corp. p. 365-396.

Hein, J. R., Bouma, A. H., Hampton, M. A., and Ross, C. R., 1979b, Clay mineralogy, fine grained sediment dispersal, and inferred current patterns, Lower Cook Inlet and Kodiak shelf Alaska; Sedimentary Geol. v. 24, p. 291-306.

Hein, J. R., Yeh H-W, and Alexander, E. A., 1979c, Origin of iron-rich montmorillonite from the manganese nodule belt of the north equatorial Pacific: Clay and Clay Minerals, v. 27, p. 185-194.

Hein, J. R. and Scholl, D. W., 1978, Diagenesis and distribution of late Cenozoic volcanic sediment in the Southern Bering Sea: Geol. Soc. Amer. Bull., v. 89, p. 197-210.

Hein, J. R., Scholl, D. W. and Miller, J., 1978, Episodes of Aleutian Ridge explosive volcanism: Science, v. 199, p. 137-141.

Hein, J. R., Scholl, D. W., and Gutmacher, C. E., 1976, Neogene clay minerals of the far northwest Pacific and southern Bering Sea: Sedimentatin and diagenesis: in A.I.D.E.A. Proceedings, International Clay conference, Mexico City, S. W.Bailey, ed. p. 71-80.

Hughes, F. W., Coachman, L. K., and Aagaard, K., 1974, Circulation, transport, and water exchange in the western Bering Sea: in Oceanography of the Bering Sea, D. W. Hood and E. J. Kelley eds., Inst. of Marine Sciences, Univ. of Alaska, p. 59-98.

Johns, W. D., Grim, R. E., and Bradley, W. F., 1954, Quantitative estimations of clay minerals by diffraction methods: Journ. Sed. Pet. v. 24, p. 242-251.

Kinder, T. H. and Schumacher, J. D., 1980, Circulation over the continental shelf of the southeastern Bering Sea, in The Bering Sea shelf, oceanography and Resources, D. W. Hood, ed., Dept. of Commerce, N.O.A.A.

Kinder, T. H., Coachman, L. K. and Galt, J. A., 1975, The Bering slope current system: Journ. of Physical Oceanog., v. 5, p. 231-244.

Knebel, H. J., 1972, Holocene Sedimentary framework of the east-central Bering Sea continental shelf, Ph.D. Thesis, Univ. of Washington, Seattle, 186 p.

Lisitsyn, A. P., 1966, Recent Sedimentation in the Bering Sea (in Russian): Inst. Okeanol. Akad. Nauk U.S.S.R., (Translated by Israel Program for Scientific Translations, available from U. S. Dept. Commerce, Clearinghouse for Fed. Sci. and Tech. Info., 1969), 614 p.

Martin Vivaldi, J. L. and Gallego, M., 1961, Some problems in the identifications of clay minerals by X-ray diffraction. 1. Chlorite-aolinite mixtures: Clay Minerals Bull. v. 4, p. 288-292.

Naidu, A. S., Burrell, D. C. and Hood, D. W., 1971, Clay mineral composition and geologic significance of some Beaufort Sea sediments: Journ. Sed. Pet. v. 41, p. 691-694.

Perry, E. and Hower, J., 1970, Burial and diagenesis in Gulf Coast pelitic sediments: Clays and clay minerals, v. 18, p. 165-177.

Pierce, J. W. and Siegel, F. R., 1969, Quantification in clay mineral studies of sediments and sedimentary rocks: Journ. Sed. Pet., v. 39, p. 187-193.

Reynolds, R. C. and Hower, J., 1970, The nature of interlayering in mixed layer illite montmorillonite, Clays and clay minerals, v. 18, p. 25-36.

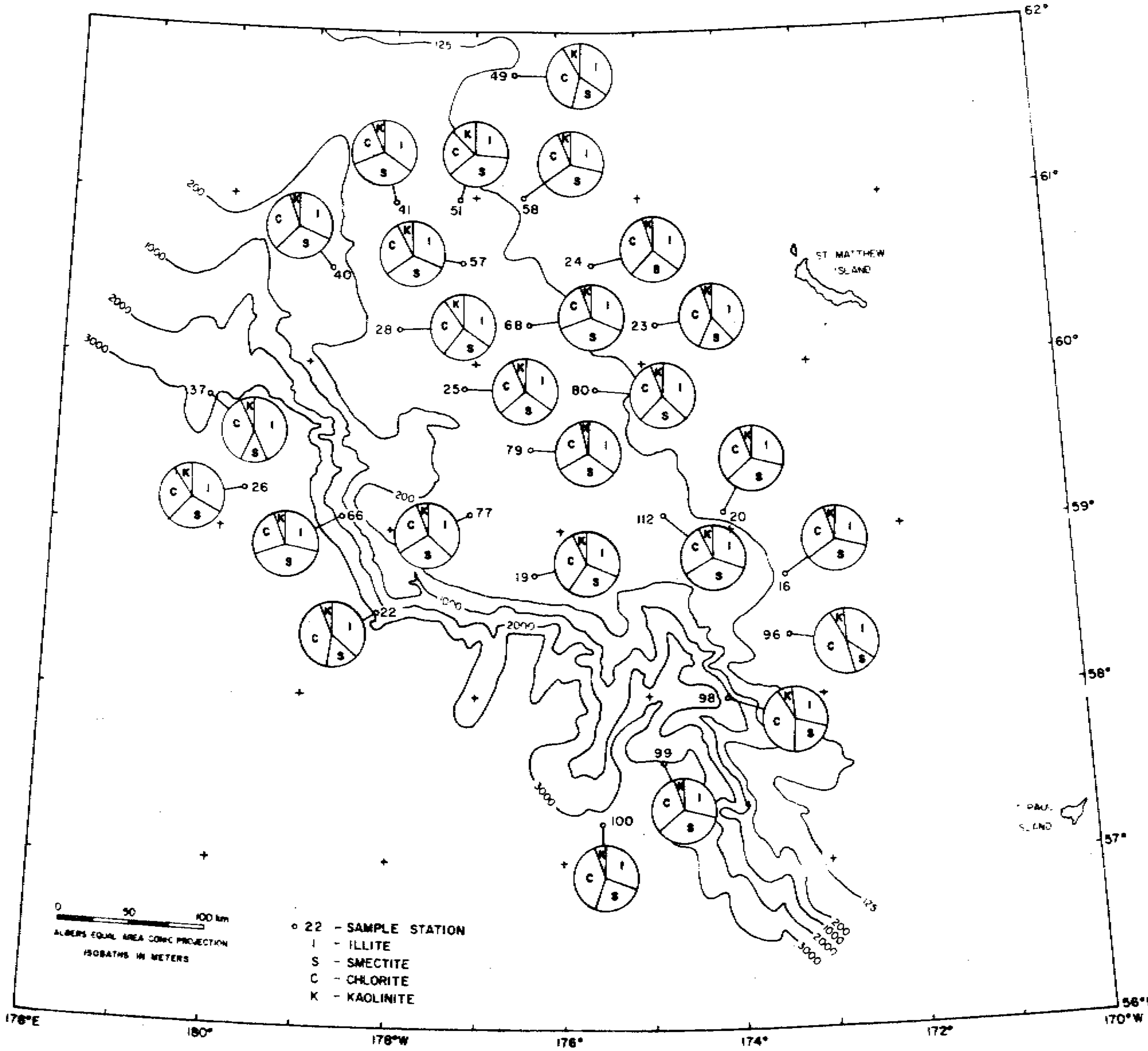

Figure 13. Distribution of relative percentages of clay minerals in surface sediments from Navarin Basin province.

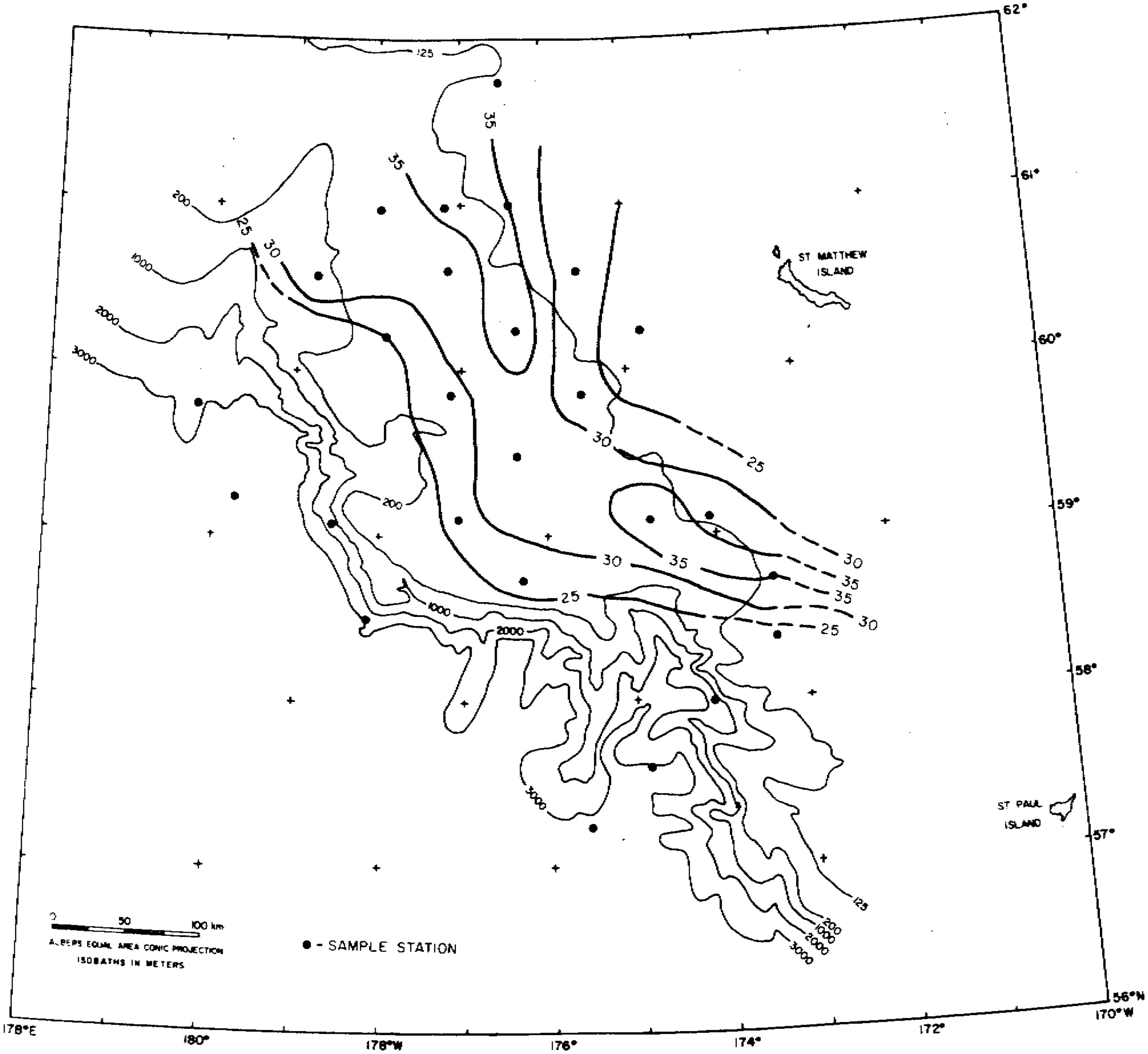

Figure 14. Contour map of relative percentages of smectite in surface sediment. Contour internal 5%.

Table 3. Relative percentages of clay minerals

Core No.	Depth Interval (cm)	Illite	Smectite	Chlorite	Kaolinite	Kaolinite & Chlorite
16G	10-12	29	35	31	5	36
	67-69	29	33	31	7	38
19G	9-11	31	28	34	7	41
	31-32	31	26	35	8	43
20G	10-12	28	34	32	6	38
	94-96	28	29	33	10	43
22G	30-32	36	16	42	6	48
	503-513	41	22	31	6	37
23G	8-10	38	19	38	6	43
	140-142	36	17	41	6	47
24G	10-12	35	27	33	5	38
	94-96	30	34	32	4	36
25G	12-13	34	28	31	7	38
	178-180	36	28	30	6	36
26G	22-24	33	29	29	9	38
	214-216	31	37	25	7	32
	225-230	32	38	24	6	30
	231-232	34	28	31	7	38
	255-260	36	26	31	7	38
	275-280	30	33	29	8	37
	295-300	31	28	34	7	41
	348-350	30	33	29	8	37
28G	12-14	35	25	30	10	40
	70-77	35	25	31	9	40
37G	35-37	42	14	38	6	44
	441	34	16	41	9	50
40G	10-12	32	31	32	5	37
	58	34	31	29	6	35
41G	11-12	34	34	26	6	32
	81	43	12	35	10	45
49G	12-14	33	20	39	8	47
	232	32	23	39	6	45
51G	15-17	27	37	29	7	36
	217	33	29	32	6	38

Table 3. Relative percentages of clay minerals (cont'd)

Core No.	Depth Interval (cm)	Illite	Smectite	Chlorite	Kaolinite	Kaolinite & Chlorite
57G	10-12	31	33	29	7	36
	83	35	30	26	9	35
58G	15-17	29	35	30	6	36
	231	31	32	30	9	39
66G	10-12	30	40	25	6	31
	531	34	28	32	6	38
68G	43-45	32	37	25	6	31
	159	29	35	30	6	36
77G	10-12	37	28	30	5	35
	54	42	28	25	5	30
79G	12-13	34	32	30	4	34
	111	30	34	30	6	36
80G	8-10	36	26	32	6	38
	211	34	26	34	6	40
96G	5-7	34	12	48	6	54
	58-61	33	15	45	7	52
98G	5-7	29	23	41	7	48
	171	36	22	37	5	42
99G	57-58	28	36	32	24	36
	408-431	24	31	40	5	45
100G	24-26	31	25	39	5	44
	382	31	24	41	4	45
112G	6-8	30	36	27	7	34
	74	30	34	28	8	36

Table 4. Comparison of relative percentages of clay minerals from several parts of the Bering Sea.

Mineral	Minimum	Maximum	Mean	Standard deviation
This study				
Smectite	12	40	28.0	6.9
Illite	24	43	32.8	3.8
Kaolinite	4	10	6.6	1.5
Chlorite	24	48	32.6	5.3
Kaolinite + Chlorite	30	54	39.2	5.4
Gardner and others, 1980				
Smectite	13.0	57.5	31.2	9.4
Illite	17.0	47.0	29.8	6.9
Kaolinite	0	11.8	6.0	3.5
Chlorite	24.3	44.3	33.2	5.6
Hein and others, 1976				
Site 184				
Smectite	-	-	31	4
Illite	-	-	30	4
Kaolinite	-	-	10	3
Chlorite	-	-	29	4
Kaolinite & Chlorite	-	-	38	5
Site 185				
Smectite	-	-	32	10
Illite	-	-	30	7
Kaolinite	-	-	7	2
Chlorite	-	-	34	2
Kaolinite + Chlorite	-	-	40	2
Site 188				
Smectite	-	-	32	5
Illite	-	-	26	2
Kaolinite	-	-	8	1
Chlorite	-	-	37	5
Kaolinite + Chlorite	-	-	42	4

CARBON CONTENTS OF NAVARIN BASIN SEDIMENTS

Jeffrey M. Fischer

INTRODUCTION

Carbon plays an important role in sedimentation, even though it is a relatively small component of the sediments. The relation between organic carbon content and depositional environment has long been established (Dow, 1975). Factors such as basin morphology, grain fabric, sedimentation rates, and source areas all affect carbon distribution. Organic matter also has a role in diagenetic processes that affect mineralogy and chemistry of sediments (Lisitsyn, 1972), as well as its bearing as a possible petroleum source. The purpose of this chapter is to discuss the distribution of organic and carbonate carbon in the Navarin Basin province.

Previous work

Various studies of carbon contents for the entire Bering Sea area have been conducted. Gershanovich (1962) and Lisitsyn (1966) discussed variations in carbonate and organic carbon based mainly on data from the western Bering Sea. Carbonate values were universally low, whereas organic carbon showed relatively high concentrations in coastal areas and at the base of the continental slope. Studies of the distribution of carbon in the sediments northeast and southeast of Navarin Basin were conducted by Knebel (1972) and Gardner and others (1980). Both studies showed sediments almost devoid of carbonates; the largest concentrations of organic carbon occurred in the fine-grained sediments.

Methods

Two centimeter subsamples were taken within the top 35 centimeters of 14 of the cores (considered a near surface sample for this study). Each succeeding 100 centimeters length of core was subsampled; subsamples also were taken from the core catchers. Samples were freeze dried, ground to a fine powder, and stored in a dessicator. Analyses for carbonate and organic carbon were done at a commercial laboratory by the direct organic carbon-wet oxidation method (Bush, 1970). Knebel (1972) data were determined on a LECO induction furnace and carbon determinator using the Walkley-Black analysis. Lisitsyn (1966) does not discuss analytical methods.

RESULTS

Values of carbonate and organic carbon from the 52 sample sites are shown as weight percent in table 5. Surface distribution of carbonate is uniformly low and shows little variation (0.04% to 0.22%) throughout the Navarin Basin area (Fig. 15). The total range in carbonate values is small from 0.03% to 0.57%. Some changes were observed down a few cores (Fig. 16); however, in the majority of cores the carbonate percentages were uniformly low.

Organic carbon values in contrast with carbonate values showed greater variance, averaging 0.83% for the entire area and ranging from 0.26% to 1.56%. Figure 17 shows the distribution of organic carbon in surface sediments for the Navarin Basin. Salient features include high organic carbon values on the northwest continental shelf and low values on the southeast continental shelf. In addition, an arcuate band of low percentages of organic carbon content exists parallel to the continental slope at depths of less than 1600 m. Some of the lowest organic carbon values are found at the heads of the largest submarine canyons (Navarinsky and Zhemchug). Comparisons of shelf and slope areas (Table 6) shows that organic carbon in Navarin Basin is concentrated at the base of the continental slope and on the continental shelf west of St. Matthew Island (Fig. 17).

Variation of organic carbon with depth in the cores can be seen in figures 16 and 18. There is a general trend towards lower organic content with depth in those cores collected in water depths greater than 1600 m; however, there are no consistent trends with depth in cores collected on the shelf and upper slope.

DISCUSSION

The consistently low carbonate values show the relative lack of calcareous organisms in the Navarin Basin area. Similar results were obtained to the southeast of the study area by Gardner and others (1980), and to the north of the study area by Knebel (1972). Sporadic increases in carbonate, both at the surface and down core, probably represents the concentrated remains of calcareous organisms.

The primary source of carbon in the Bering Sea is organic carbon (Lisitsyn, 1966). Two sources for this organic carbon are terrestrial and marine. Terrestrial organics are carried to sea via rivers and marine phytoplankton produce organics at sea.

Once organics are in the sea they are influenced by several factors, the most important of which are distance of transport, rate of sedimentation, and grain size. Organic particles are destroyed in transport over large distances; the more prolonged their stay in the water, the higher their degree of decomposition (Lisitsyn, 1959). One exception worth noting is the relatively stable bitumens; however Bordovskiy (1964) has estimated their concentration to be 0.05% or less for organic carbons in the Bering Sea. The rate of sedimentation also affects the concentration of organic carbon; dissolution of organic matter is related to its duration of exposure, so the sooner the organic matter is buried the slower the rate of decay (Lisitsyn, 1972). Finally, in fine grained sediments organic matter is absorbed, and thus preserved, by clays. This negative correlation between organic carbon and grain size has been observed by many scientists (eg., Trask, 1932; Gardner and others, 1980).

The contribution of organic matter from the three largest rivers that enter the Bering Sea, the Anadyr, Kuskokwim, and Yukon, is estimated to be less than 1% of the total organic matter in the Bering Sea (Lisitsyn, 1966).

In addition, these rivers are over 400 km away; these two factors seem to preclude terrestrial sources as significant contributors of organics to the study area.

Most organic carbon in the Bering Sea probably is related to intense diatom blooms that occur in the spring (Lisitsyn, 1966). These blooms are closely related to ice retreat, supply of nutrients from upwelling, spring river runoff, and general turbidity of the seas due to spring storms (Lisitsyn, 1966). Diatoms are significant contributors to sediments at the base of the slope and some northwest shelf regions of the Navarin Basin study area (Karl and others, this report). Comparison of sediment composition to organic carbon distribution shows a postive correlation between areas of diatom concentration and areas of high organic carbon content.

Winnowing and redistribution of sediments by currents can play an important role in the distribution of organic carbon. Relatively low organic carbon values are associated with coarse sediments where currents have winnowed out the fine fractions that contain organic carbon (Gershanovich, 1962). Comparison of sand/mud ratios (Fig. 11, Karl and others, this report) and organic carbon (Fig. 17) shows that the negative correlation of organic carbon and grain size holds for the Navarin Basin province. Where currents predominate, as along the shelf break and at the heads of the submarine canyons, sand content increases with a concommitant reduction in organic carbon. Conversely at the base of the slope where slumped sediment accumulates, where currents are relatively weak, and where muds predominate, the organic carbon content is high. Depletion of organics at the top of the continental margin and accumulation of organics at its' base is normal for continental margins according to Bordovskiy (1965).

Variations of organic carbon percentages on the continental shelf, although not easily understood, are probably due to a variety of factors. The general patchiness may be due in part to differential consumption of the organic matter by the benthic fauna. Low values of organic carbon on the southeast shelf between St. Paul Island and St. Matthew Island (Fig. 17) are consistent with a coarser particle size that perhaps results from a more hydrodynamically active shelf. Alternately, the shelf west of St. Matthews Island has some of the highest organic carbon values found in this study. Correlation of organic carbon (Figs. 17) with particle size of sediments (Fig. 11; Karl and others, this report) shows that the high organic content is accompanied, as would be expected, by fine grained sediments. Both these pieces of evidence seem to indicate an area of little water movement. Indeed Muench and others (1976), have suggested just such an area. Sources for the organics could be diatom blooms transported across the shelf from upwelling along the continental margin. A seasonal cover of ice probably protects this area from the winnowing action of intense winter storms.

CONCLUSIONS

The data for the Navarin Basin province seem to indicate normal trends for an arctic continental margin with a somewhat anomalous area on the shelf west of St. Matthew Island. Carbonate contents are low and in most cases insignificant. Most organic carbon is probably supplied by diatoms and deposited close to their source. Some of the highest organic carbon percentages were found in sediments from the base of the continental slope. Organic carbon is depleted at shallower depths along the slope. Grain size shows a negative correlation with organic carbon especially on the shelf. The fine grained sediments of the northwest shelf have a higher organic carbon content than the southeast shelf which has low organic carbon possibly due to fines having been removed by winnowing of currents.

REFERENCES CITED

Bordovskiy, O. K., 1965, Accumulation of organic matter in bottom sediments: Marine Geology, vol. 3, p. 33-82.

Bordovskiy, O. K., 1969, Organic matter of Recent sediments of the Caspian Sea: Oceanology, vol. 9, p. 799-807.

Bush, P. R., 1970, A rapid method for the determination of carbonate carbon and organic carbon: Chemical Geology, vol. 6, p. 59-62.

Dow, Wallace G. and Pearson, Daniel B., 1975, Organic matter in Gulf Coast Sediments: 7th Offshore Technology Conference, Houston, Tex., Paper Number OTC 2343.

Gardner, James V., Dean, Walter E., and Vallier, Tracy L., 1980, Sedimentology and geochemistry of surface sediments, outer continental shelf, southern Bering Sea: Marine Geology, v. 35, p. 299-329.

Gershenovich, D. E., 1962, New data on the recent deposits of the Bering Sea: All-Union Scientific Research Institute of Marine Fisheries and Oceanography - Proceedings Vol. XLVI, (Translated by Hulbert Verwey, 1963), p. 128-164.

Kinder, T. H., and Coachman, L. K., 1975, The Bering Slope Current System: Journal of Physical Oceanography, vol. 5, No. 2, p. 231-244.

Kinder, T. H., and Schumacher, J. D., in press, Circulation over the continental shelf of the southeastern Bering Sea: The Bering Sea shelf, oceanography and resources, D. W. Hood (Ed.), Dept. of Commerce, N.O.A.A.

Knebel, Harley J., 1972, Holocene sedimentary framework of the east-central Bering Sea Continental Shelf: Ph.D. Thesis, University of Washington, Seattle, 186 p.

Lisitsyn, A. P., 1959, Bottom sediments of the Bering Sea: in Bezrukov, P. L., (Ed.), Geographical description of the Bering Sea, (Translated by Israel Program for Scientific Translations, available from Office of Technical Services, U. S. Dept. of Commerce, 1964), 188 p.

Lisitsyn, A. P., 1966, Recent sedimentation in the Bering Sea (in Russian): Inst. Okeanol. Akad. Nauk U.S.S.R., (Translated by Israel Program for Scientific Translations, available from U. S. Dept. Commerce, Clearinghouse for Fed. Sci. and Tech. Info., 1969), 614 p.

Lisitsyn, A. P., 1972, Sedimentation in the world ocean: Society of Economic Paleontologists and Mineralogists-Special Publication No. 17, 171 p.

Muench, R. D., and Ahlnas, K., 1976, Ice movement and distribution in the Bering Sea from March to June 1974: Journal of Geophysical Research, vol. 81, No. 24, p. 4467-4476.

Trask, P. D., 1932, Origin and environments of source sediment of petroleum, Gulf Pub. Co., Houston, Tx., 323 p.

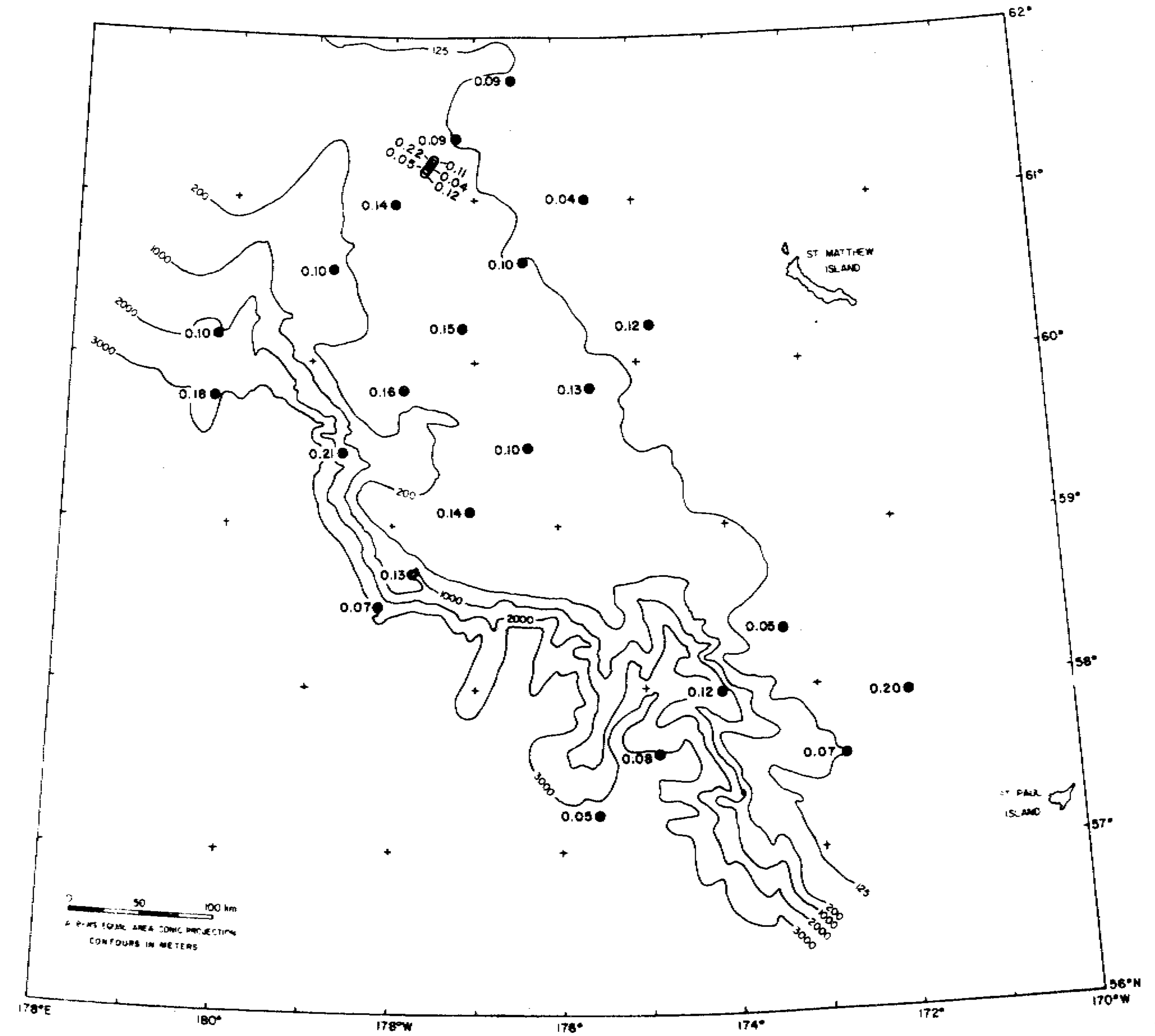

Figure 15. Surface distribution of carbonate carbon (weight percent).

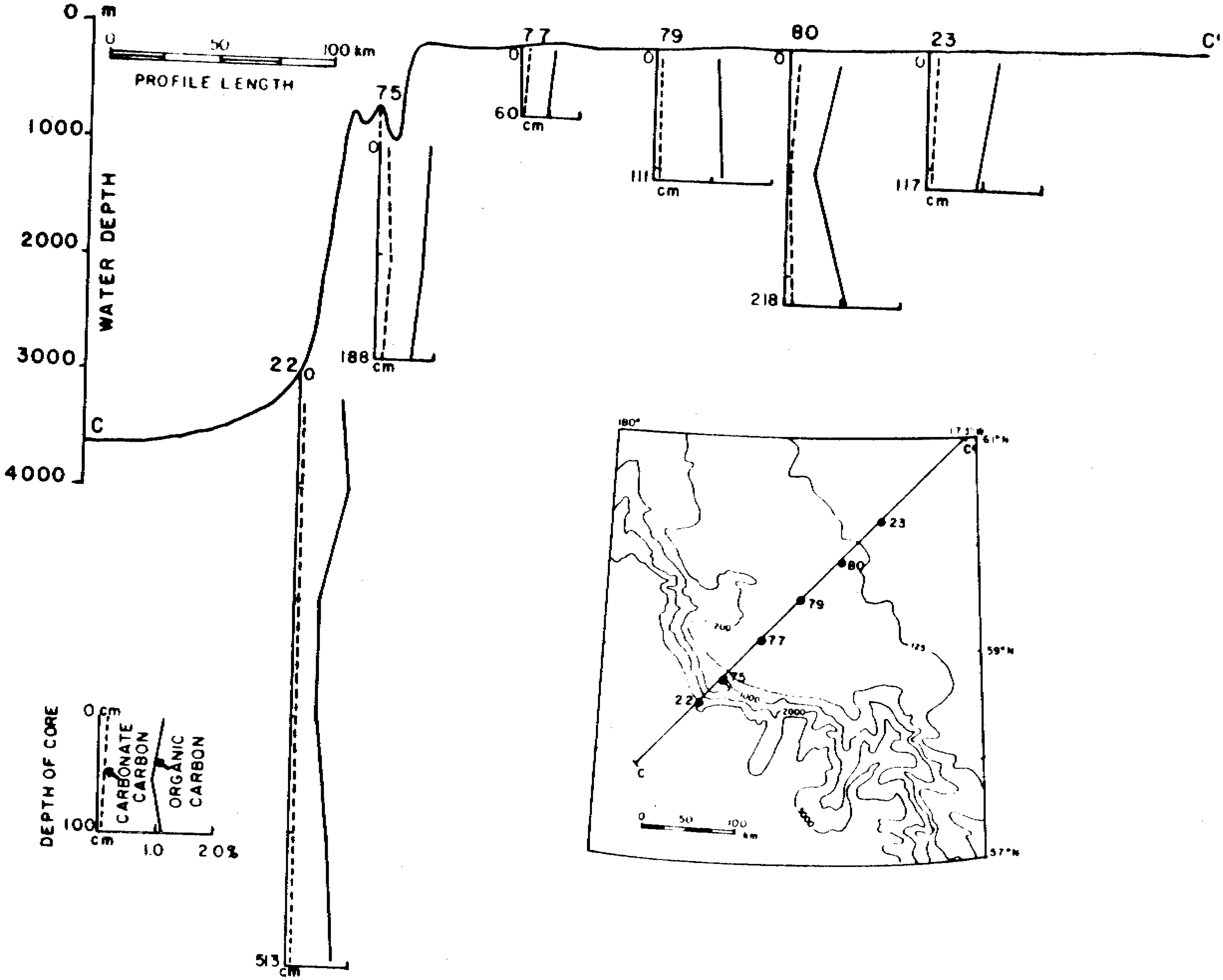

Figure 16. Down core variations of carbonate (dashed line) and organic carbon (solid line) across the Navarin Basin province.

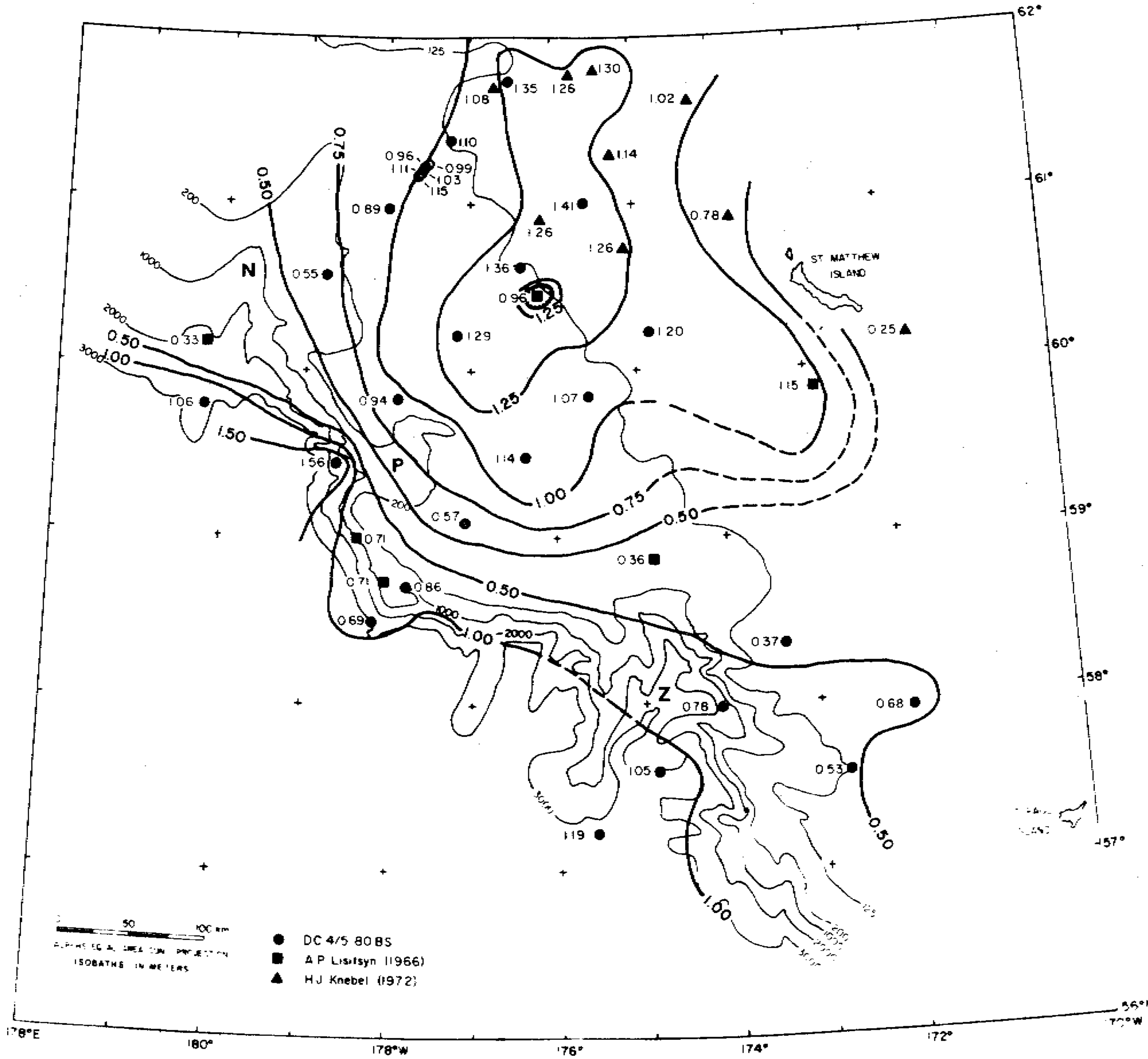

Figure 17. Contour map of weight percents of organic carbon in surface sediments from Navarin Basin province. Contour interval 0.25% on shelf and 0.50% on slope. Letters N, P, Z locate Navarinsky, Pervenets, and Zhemchug Canyons.

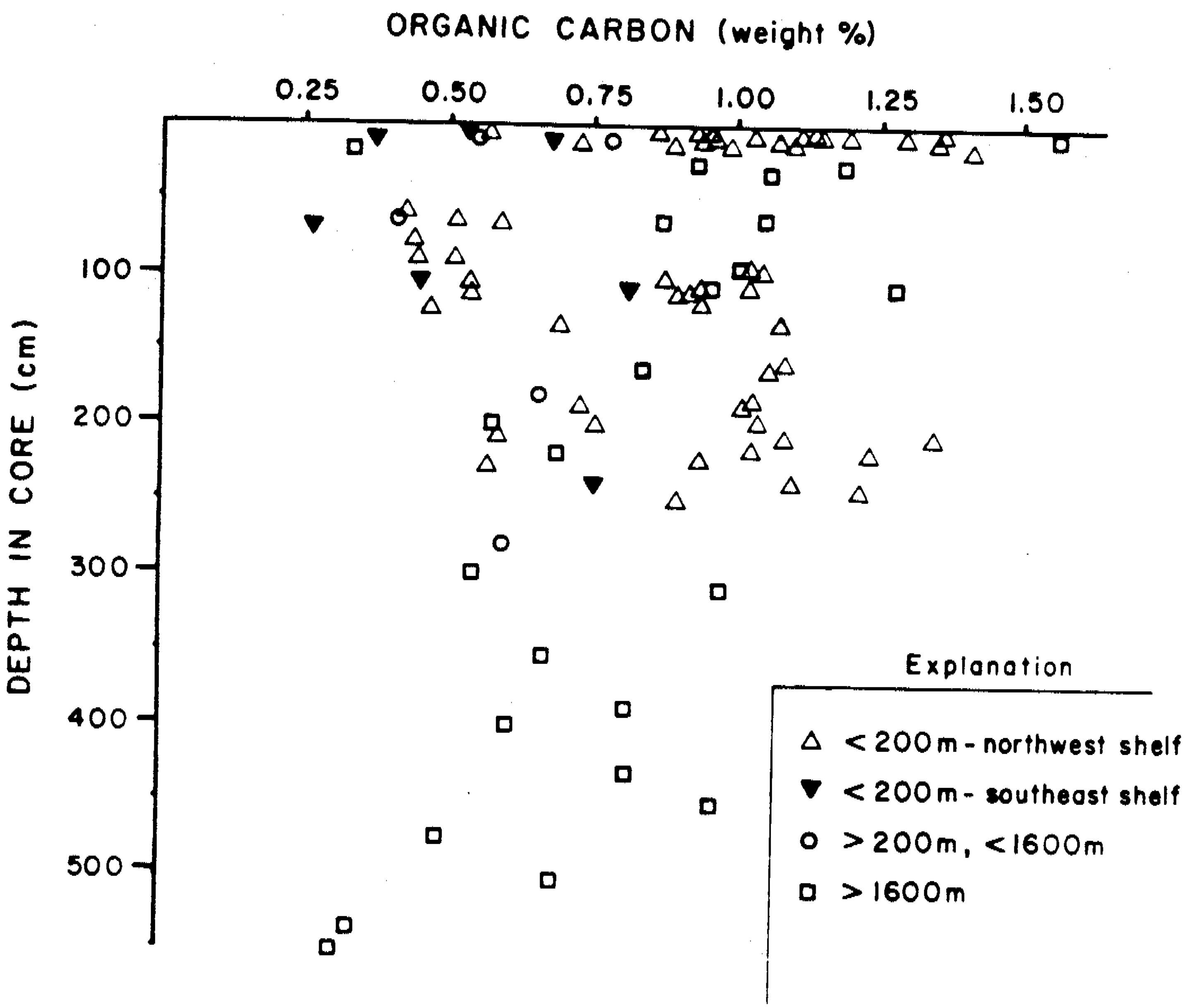

Figure 18. Variation in percent organic carbon with depth in core.

Table 5. Weight percents of organic carbon and carbonate carbon in Navarin Basin Province sediment.

DC 4/5 - 80BS cruise data

Core Number	Depth in core (cm)	Depth of Water (m)	Organic Carbon (%)	Carbonate Carbon (%)
22	28-30	2842	0.93	0.70
	98-100		1.01	0.06
	200-202		0.58	0.06
	300-302		0.55	0.07
	400-402		0.61	0.06
	503-513*		0.69	0.07
23	8-10	110	1.20	0.12
	115-117		0.90	0.06
28	225-227	150	0.94	0.28
32	13-15	150	0.73	0.11
	227-237		0.57	0.11
34	270-280*	210	0.60	0.08
36	18-20	1924	0.33	0.10
	66-68		0.87	0.18
	220-222		0.69	0.17
	354-356		0.67	0.22
	475-477		0.49	0.34
	535-537		0.34	0.38
	539-549*		0.31	0.25
37	35-37	2856	1.06	0.18
	110-112		0.96	0.12
	310-312		0.98	0.23
	441-450*		0.97	0.21
39	0-10**	229	0.44	0.13
40	10-12	230	0.55	0.10
	58-65*		0.41	0.14
41	14-15	148	0.89	0.14
	81-90*		0.51	0.17

* Core catcher
** Grab sample

Table 5. Weight percents of organic carbon and carbonate carbon in Navarin Basin Province sediment. (cont'd)

DC 4/5 - 80BS cruise Data

Core Number	Depth in core (cm)	Depth of Water (m)	Organic Carbon (%)	Carbonate Carbon (%
42	7-8	141	1.15	0.12
	97-98		1.03	0.03
	204-210*		1.09	0.13
43	5-7	148	1.11	0.05
	120-122		0.94	0.07
	246-256*		0.90	0.19
44	8-10	138	1.03	0.04
	112-114		0.94	0.15
	200-210*		0.59	0.02
45	8-10	137	0.96	0.22
	106-116*		0.54	0.14
46	14-15	134	0.99	0.11
	79-80		0.44	0.12
	127-137*	134	0.70	0.20
47	5-7		0.93	0.11
	84-94*		0.45	0.21
48	14-15	124	1.10	0.09
	192-202*		0.76	0.08
49	12-14	108	1.35	0.09
	160-162		1.09	0.13
	232-242*		1.10	0.13
60	17-19	106	1.41	0.04
	134-135		1.08	0.04
	165-167		1.06	0.57
	205-215*		1.35	0.06
61	240-250*	125	1.22	0.13
62	5-7	125	1.36	0.10
	100-102		1.05	0.13
	200-202		1.04	0.17
	214-224*		1.24	0.03

Table 5. Weight percents of organic carbon and carbonate carbon in Navarin Basin Province sediment (cont'd)

DC 4/5 - 80BS cruise Data

Core Number	Depth in core (cm)	Depth of Water (m)	Organic Carbon (%)	Carbonate Carbon (%)
63	8-10	150	1.29	0.15
	115-117		0.92	0.10
	184-194*		1.02	0.16
64	10-11	147	0.94	0.16
	99-109*		0.54	0.09
65	0-2		1.56	0.21
	110-112		1.28	0.14
74	178-188*	920	1.03	0.22
75	5-7		0.86	0.22
	105-107		0.88	0.22
	174-188*		0.73	0.15
76	60-70*	147	0.59	0.05
77	5-7	147	0.57	0.14
	54-64*		0.43	0.05
78	58-68*	147	0.51	0.11
79	5-6	136	1.14	0.10
	101-111*		1.03	0.10
80	11-13	128	1.07	0.13
	125-126		0.47	0.02
	211-221*		1.03	0.16
82	0-10**	105	0.95	0.11
83	12-15	105	0.68	0.20
	112-114		0.81	0.05
	235-241*		0.76	0.05
84	3-5	119	0.53	0.07
	97-107*		0.45	0.02
95	0-10[1]	117	0.39	0.08
96	11-13	116	0.37	0.05
	67-73*		0.26	0.05
98	10-12	1610	0.78	0.12

Table 5. Weight percents of organic carbon and carbonate carbon in Navarin Basin Province sediment. (cont'd)

DC 4/5 - 80BS cruise data

Core Number	Depth in core (cm)	Depth of Water (m)	Organic Carbon (%)	Carbonate Carbon (%)
	171-182*		0.66	0.07
	165-167		0.84	0.06
	408-431*		0.82	0.08
100	28-30	3232	1.19	0.05
	382-392		0.82	0.11

* Core catcher
** Grab sample

Data from H. Knebel (1972)

Core Number	Depth in Core (cm)	Depth of Water (m)	Organic Carbon (%)	Carbonate Carbon (%)
42-140-GR297	0-20	--	1.0	0
42-144-GR301	0-20	--	1.14	0
42-147-GR308	0-20	--	1.08	0
42-149-PC313	0-17	--	1.26	0
42-150-GR314	0-20	--	1.30	0
51-011-GR030	0-20	--	1.26	0
51-109-GR208	0-20	--	0.25	0

Data from A. P. Lizitsyn (1966)

Li-1	Top	--	1.15	--
Li-2	Top	--	0.96	--
Li-3	Top	--	0.33	--
Li-4	Top	--	0.71	--
Li-5	Top	--	0.92	--

Table 6. Organic carbon averages from selected areas in Navarin Basin province (Ave. for DC 4/5-80BS samples)

Location	Number of samples	Organic Carbon (%)		
		Maximum	Minimum	Average
Northwest shelf	56	1.41	0.57	0.89
Southeast shelf	7	0.68	0.37	0.55
200 - 1600 m	5	0.78	0.41	0.60
1600 m	24	1.56	0.69	0.81

SEAFLOOR GEOLOGIC HAZARDS

Paul R. Carlson and Herman A. Karl

INTRODUCTION

Potential geologic hazards in the Navarin Basin province include faulting and earthquakes; seafloor instability due to submarine landslides, sediment transport and erosion, and subsidence or blowouts resulting from disturbance of gas-charged sediment; volcanic activity; and ice. Seafloor instability probably poses the greatest seafloor hazard. The purpose of this chapter is to present preliminary maps and brief discussions of the potential geologic hazards in the study area.

FAULTING AND SEISMICITY

The limited seismic coverage in the Navarin Basin province restricts the interpretation of length, orientation, and age of the faults. The distribution of the faults is shown in figure 19; however, the wide spacing of the tracklines ($\sim$ 30 km) makes correlation from line to line extremely uncertain. Thus, until more seismic lines are available, the only correlation that we have attempted is to connect those points that represent the bounding faults on a graben that is oriented in a northwest-southeast direction (Fig. 19). This graben is about 5 km wide and has been mapped over a distance of nearly 240 km. The maximum apparent relief of this structure (Fig. 20) is about 50 m, resulting from a series of offsets on each side of the down-thrown block. Throw of the individual faults varies from about 10 to 20 m. The graben is buried beneath 130 m of sediment over the depressed block and about 80 m of sediment over the adjacent flat-lying strata. The faults located on lines oriented perpendicular to the long axis of Navarin basin greatly outnumber those on lines that parallel the basin, suggesting a northwest-southeast trend of the faults. This trend is parallel to the basin and to the shelf-break. The majority of these faults occur on the continental slope and outer most shelf.

Many of the faults shown on Figure 19 are mapped from high-resolution seismic-reflection records that have resolution of 1-3 meters; however, none of the faults mapped to date show offset of the Holocene seafloor. Although the ages of the faults are unknown, C^{14} dates of sediment in the southern part of the area indicate accumulation rates of the upper six meters of sediment to be about 25 cm/10^3 yrs. (Askren, 1972). Therefore faults that reach to within three meters of the seafloor may cut sediment as young as 12,000 yrs. B.P. and are considered active.

According to Cooper and others (1976), Marlow and others (1976), and Scholl and others (1975), subduction of the Kula plate beneath the Bering Sea margin apparently ceased in late Mesozoic or early Tertiary and subduction of the Pacific plate shifted to the Aleutian Trench. This transfer tectonically deactivated the Bering Sea margin. The lack of modern seismicity is readily seen on the maps of Alaska earthquake epicenters published by Meyers (1976).

Only six earthquakes have been reported from the Navarin Basin province for the time period prior to 1974, and all were less than magnitude six. These data may be somewhat misleading because of the wide spacing and limited number of seismograph stations in western Alaska.

SEAFLOOR INSTABILITY

Within the broad category of seafloor instability, we have included discussions of three major types; submarine landslides, sediment transport and erosion, and gas-charged sediment.

Submarine Landslides

Submarine landslide is used as an all inclusive term for a variety of slope movements. The preliminary nature of our study makes it impractical at this time to attempt to classify each of the areas of slope movement according to type of movement and type of material.

The continental margin of the Navarin Basin province is incised by three large submarine canyons and it is in association with these canyons that many of the submarine slides have been found (Fig. 21). We have not correlated slide masses from line to line because of the wide spacing between tracklines. None of the slides begin in water shallower than 200 m, several begin below 400 m, and one appears to begin at a depth of greater than 1200 m. The length of the zone affected by down-slope movement is at least 50 km and some of these zones appear to be 25 km wide. Some landslides may affect the upper 200-300 m of the sediment column (Fig. 22). Gravity cores (2-5 m) were collected from a few of the slide masses. These cores recovered a variety of sediment types that range from pebbly mud to sandy mud to very soft, probably oversaturated mud. Preliminary evaluation of the seismic profiles crossing the outer continental shelf and slope suggest that the slope movements vary according to Varnes' (1979) classification from slumps to debris slides to earth flows. The most likely triggering mechanisms of the submarine landslides are agitation of presumed underconsolidated sediment by storm waves, internal waves or tsunamis. Other less likely causes of sliding in this region are prolonged ground shaking during earthquakes, overloading and excessive steepening by erosion and/or rapid sediment accumulation, and buildup of excessive pore-water pressures in underconsolidated clayey sediments due to rapid sedimentation or increase in concentration of bubble-phase gas in the sediment.

Sediment Transport and Erosion

Large Bedforms

Large sediment waves have been found at the heads of Zhemchug, Pervenets, and Navarinsky Submarine Canyons (Fig. 23). The sediment waves in each area are similar. Those at the head of Navarinsky Canyon have been studied in greatest detail. These large bedforms occur on a substrate of silty very fine sand within a 600 to 700 km^2 area between the 215 and 450 m isobaths. These bedforms strike approximately north-south, have an average wavelength of about 600 m, and have an average height of about 8 m and a maximum height about 15 m (Fig. 24). Both symmetrical and asymmetrical waves have been observed. The bedforms are not only expressed on the surface, but also are remarkably well defined in the subsurface. The stratigraphic unit containing the sediment waves developed over a flat-lying reflector and attains a maximum thickness of about 120 m in the sediment wave field. In a few places the bedforms are covered by a thin layer of apparently younger sediment. One such locality occurs at the head of Pervenets Canyon, where the buried sediment waves are part of an intricate stratigraphic complex lying below a unit of parallel bedded reflectors (Fig. 25). The parallel bedded unit is generally about 20 m thick, but ranges in thickness from less than 5 m to about 110 m.

We do not know if these bedforms are relict or if some of the bedforms are presently active, nor are we certain if they indicate continuous sedimentation or discrete episodes of activity and non-activity. If these features are active, they, as well as the processes responsible for them, could represent sea-floor hazards.

Surface Waves

Currents generated by surface waves probably are a more significant factor in the transport of silt and larger-size particles on the open slope and shelf of Navarin Basin than, for example, tidal currents or the mean circulation. Bottom currents have not been measured in the lease sale area, nor are there good observations of surface waves. However, some surface wave data has been compiled in areas adjacent to and including a portion of the eastern boundary of the lease sale area (Brower and others, 1977).

Storms, and consequently storm-generated waves, are strongest and most frequent during the fall and winter (Lisitsyn, 1966; Brower and others, 1977). Waves as high as 15 m with possible periods of 9-11 seconds have been observed just to the east of the lease area (Browers and others, 1977). Waves with these heights and periods do not generate currents of sufficient strength near the bottom to erode sediments over a large portion of the shelf. Assuming a threshold value of 10 cm/sec for fine sand (Komar and others, 1972), an 11 sec, 15-m high wave generates currents strong enough to erode only fine sand and smaller grains in water shallower than 125 m. A wave 10-m high with a 15 second period, however, produces near-bottom currents greater than 10 cm/sec in water as deep as 200 m. Extreme waves, empirically estimated to be as large as 42.5 m high, can occur statistically on the average once every 100 years in the Navarin area (Brower and others, 1977). These data indicate that storm waves are a potential hazard in the Navarin Basin area.

Gas-charged sediment

Gas-charged sediment has reduced strength and bearing capacity compared to the strength of gas-free sediment (Nelson and others, 1978; Whelan and others, 1976). An increase in the concentration of gas results in an increase of excess pore pressure and a decrease in sediment stability until failure occurs. Failure of the sediment poses a potential hazard to seafloor exploitation because drilling into gas-charged sediment, disruption of the sediment by cyclic loading, or spontaneous over-pressurization may cause a sudden release of gas leading to failure of pipelines or platforms (U.S. Geological Survey, 1977).

The numerous areas of gas-charged sediment mapped in Navarin Basin (Fig. 26) are identified on the high-resolution seismic reflection profiles by acoustic anomalies such as displaced reflectors, and "wipe out" zones (Fig. 27). These anomalies are prevalent in the upper 50 to 100 m of sediment. Often these shallow anomalies coincide closely with well-developed "bright spots" that show up deeper in the section on multi-channel or medium-resolution single-channel profiles.

Gravity cores collected throughout the basin province were analyzed for hydrocarbons (methane through butanes) (Vogel and Kvenvolden, this report). All of the cores sampled contained hydrocarbon gases, but none showed significant amounts of thermogenic hydrocarbons. Three cores, two from the shelf and one from the slope, contained concentrations of methane and ethane 5 to and 10 to 20 times higher, respectively, than background values (Vogel and others, 1981). These cores also contained ratios of ethane to ethene and methane to ethane and propane that marginally suggest the presence of some thermogenic hydrocarbons. A possible explanation for the low concentrations of hydrocarbons is the short length of the cores (<6m; most of the cores collected on the shelf were <2 m long).

VOLCANIC ACTIVITY

Although no evidence of active volcanism exists in the Navarin Basin province, the volcanically active Alaska Peninsula and Aleutian Islands mark the southern border of the Bering Sea (Fig. 28). Coats (1950) lists 25 active volcanoes in the Aleutian Islands and 11 on the Alaska Peninsula. Quaternary volcanism on the Pribiloff Islands, is located less than 500 km southeast of Navarin Basin. Volcanic hazards are associated with eruption of lava and ash and the accompanying earthquakes, and the possible generation of large seismic sea waves.

Eruptions from large andesitic cones like those found on the Aleutians and the Alaska Peninsula are explosive and can spread pyroclastic material over large areas. Eruptions from basaltic volcanoes like those on the Pribilof Islands are less explosive and would have local effects.

About 21 km of ash, was erupted in Alaska in 1912 by Katmai volcano when ash was carried over distances of 2000 km or more. Ash was deposited 180 km from the volcano with a density of about 45 g/cm (Lisitsyn, 1966). According to historical data, individual ash deposits in the Bering Sea region extend 200 to 2000 km from the source. We have found minor amounts of volcanic glass in Navarin cores (see Karl and others, this report).

ICE

We have estimated ice conditions in Navarin Basin province by synthesizing data reported in Lisitsyn (1966), McRoy and Goering (1974), and Brower et al. (1977). The proposed lease area is ice-free from June through October. Migratory pack ice begins to encroach upon the northern part of the lease area in November. The pack ice is fully developed by March or April at which time the extreme southern limit of the ice edge extends over most of the lease area (Fig. 28). Ice concentrations begin to decrease in April and the ice edge continues to retreat northward through May. First year ice in the southern portion of the Bering Sea ranges in thickness from 30-71 cm, whereas ice further north can attain a thickness of 1-2 m in unstressed floes (Lisitsyn, 1966). The southern limit and concentration of the pack ice varies from year to year depending upon weather conditions--some years migratory pack ice may not affect the lease area, but in other years concentrations of ice may completely cover it.

REFERENCES CITED

Askren, D. R., 1972, Holocene stratigraphic framework southern Bering Sea continental shelf: MS Thesis, Univ. of Washington, 104 p.

Brower, W. A., Jr., Searby, H. W., Wise, J. L., Diaz, H. F., and Prechtel, A. S., 1977, Climatic atlas of the outer continental shelf waters and coastal regions of Alaska, vol. II, Bering Sea, NOAA OCSEAP Final Report-RU 347, 443 pp.

Coats, R. R., 1950, Volcanic activity in the Aleutian arc: U.S. Geol. Survey Bull. 974-B, p. 35-47.

Cooper, A. K., Scholl, D. W., and Marlow, M. S., 1976, Plate tectonic model for the evolution of the Bering Sea basin: Geol. Soc. Amer. Bull., v. 87, p. 1119-1126.

Komar, P. A., Neudeck, R. H., and Kulm, L. D., 1972, Observation and significance of deep-water oscillatory ripple marks on the Oregon continental shelf: in D. J. P. Swift, D. B., Duane, and O. H. Pilkey, eds., Shelf sediment transport: process and pattern, Dowden, Hutchinson and Ross, Inc., Stroudsbourg, Pa., P. 601-619.

Lisitsyn, A. P., 1966, Recent sedimentation in the Bering Sea (in Russian): Inst. Okeanol. Ahoc. Nauk USSR, (translated by Israel Program for Scientific Translation, available from U. S. Dept. Commerce, Clearinghouse for Fed. Sci. and Tech. Info. 1969, 614 pp.).

Marlow, M. S., Scholl, D. W., Cooper, A. K., and Buffington, E. C., 1976, Structure and evolution of Bering Sea shelf south of St. Lawrence Island: American Association of Petroleum Geologists Bulletin, v. 60, p. 161-183.

McRoy, C. P. and Goering J. J., 1974, The influence of ice on the primary productivity of the Bering Sea: in D. W. Hood and E. J. Kelley, eds., Oceanography of the Bering Sea with emphasis on renewable resources, Univ. of Alaska, Fairbanks, Alaska, p. 403-419.

Meyers, H., 1979, A historical summary of earthquake epicenters in and near Alaska: N.O.A.A. Tech. Memorandum EDS NGSDC-1, 80 p.

Nelson, Hans, Kvenvolden, K. A., and Clukey, E. C., 1978, Thermogenic gases in near-surface sediments of Norton Sound, Alaska: In, Proceedings of the 1978 Offshore Technology Society, p. 2623-2633.

Scholl, D. W., Buffington, E. C., and Marlow, M. S., 1975, Plate tectonics and the structural evolution of the Aleutian-Bering Sea region: in R. B. Forbes, ed., Contributions to the geology of the Bering Sea basin and adjacent regions: Geological Society of America Special Paper 151, p. 1-32.

U. S. Geological Survey, 1977, An investigation of Pennzoil's blow-out and loss of platform: U. S. Geological Survey unpublished administrative report, 22 p.

Varnes, D. J., 1978, Slope movement types and processes in: R. L. Schuster and R. J. Krizek, eds., Landslides, analysis and control, Natl. Acad. of Sciences, Wash. D. C., p. 11-33.

Vogel, T. M., Kvenvolden, K. A., Carlson, P. R., and Karl, H. A., 1981, Geochemical prospecting for hydrocarbons in the Navarin Basin province: American Association of Petroleum Geologists Bulletin, v. 64, no. 4.

Webster, B. D., 1979, Ice edge probabilities for the eastern Bering Sea: N.O.A.A. Technical Memorandum NWS AR-26, 20 p.

Whelan, T., Coleman, J. M., Roberts, H. H., and Suhayda, J. N., 1976, The occurrence of methane in recent deltaic sediments and its effect on soil stability: Bull. of the International Association of Engineering Geology, No. 14, p. 55-64.

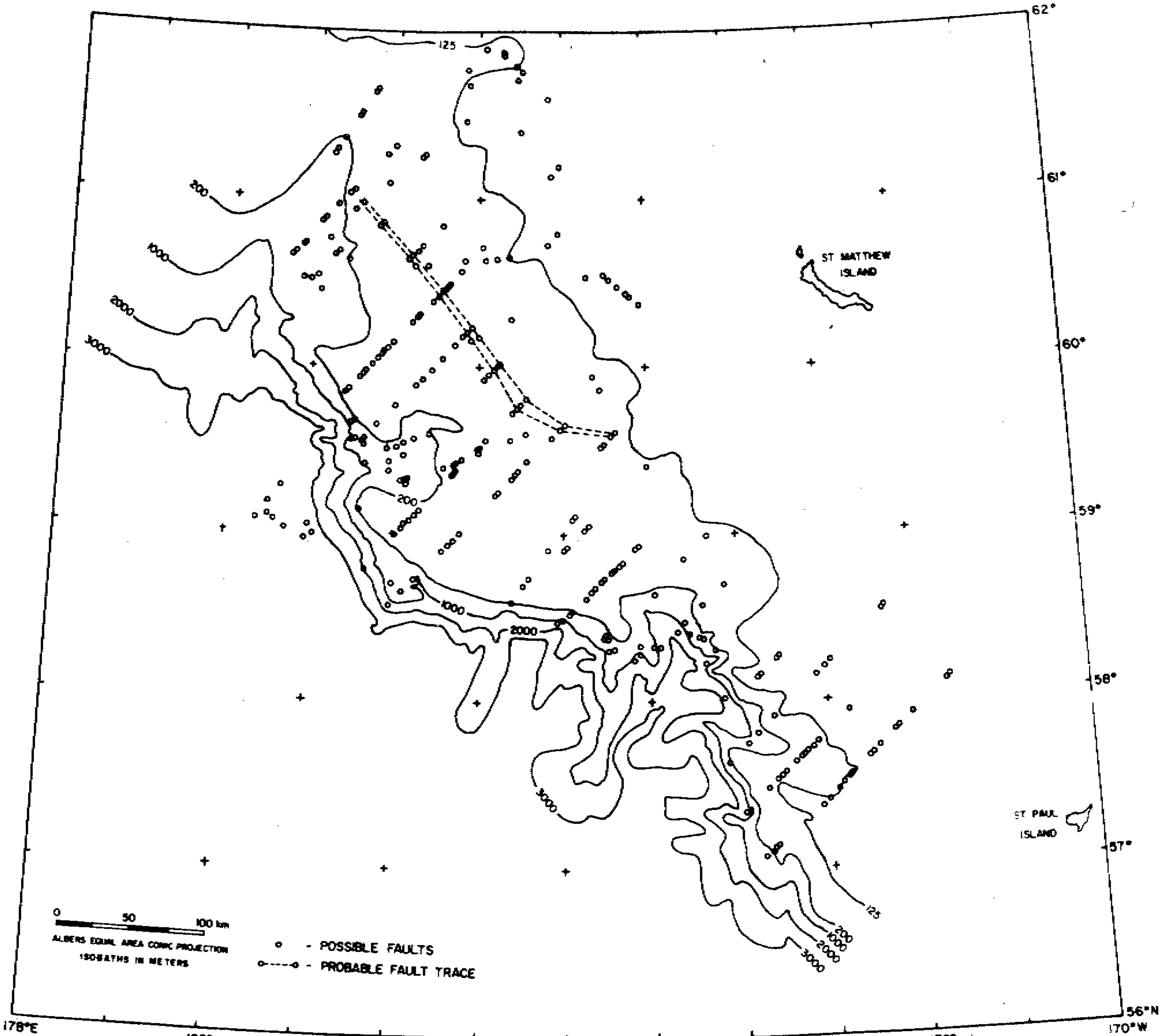

Figure 19. Preliminary map of faults in Navarin Basin province.

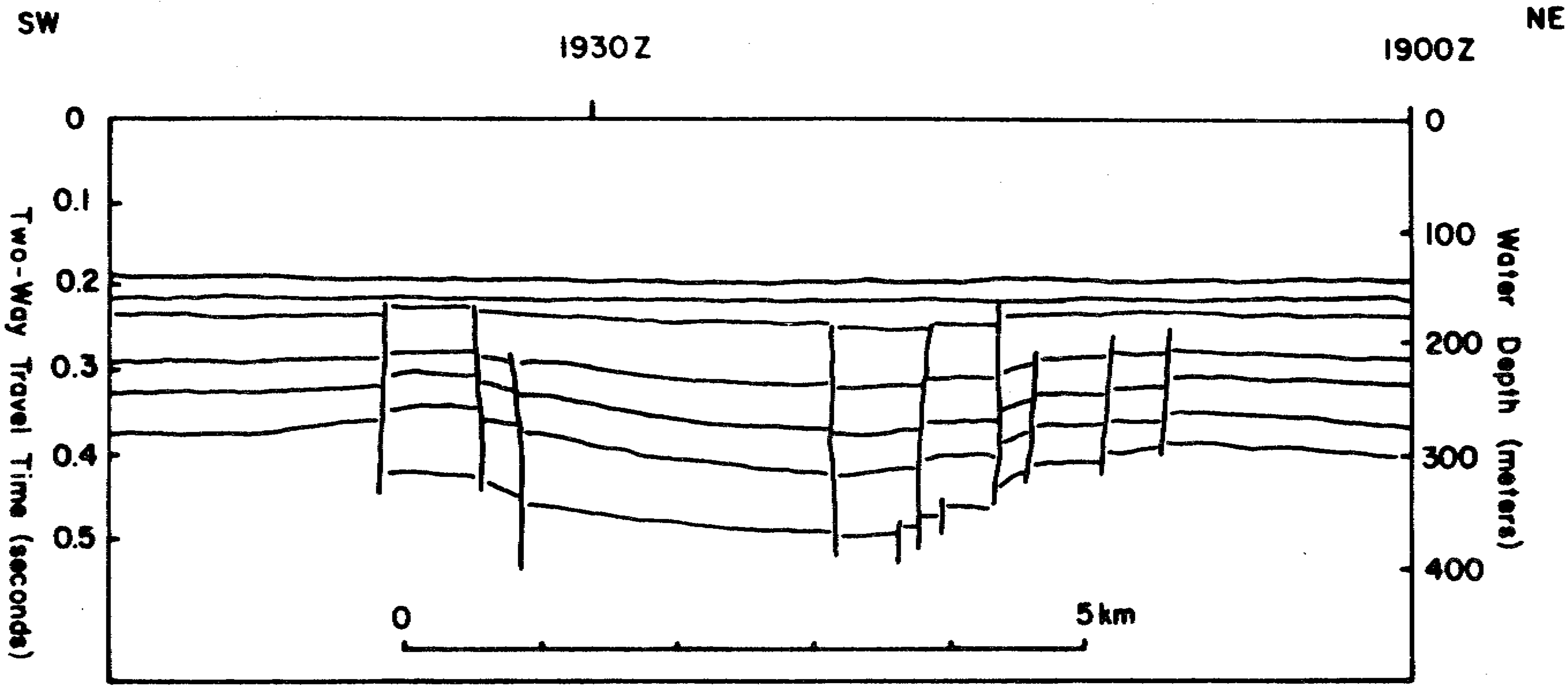

Figure 20. Interpretive line drawing of seismic-reflection profile (2-40 in^3 air guns) across graben in Navarin Basin province (see Fig. 21). Line 42, cruise DC5-80-BS/NB. Vertical exaggeration ~ 8.5 x.

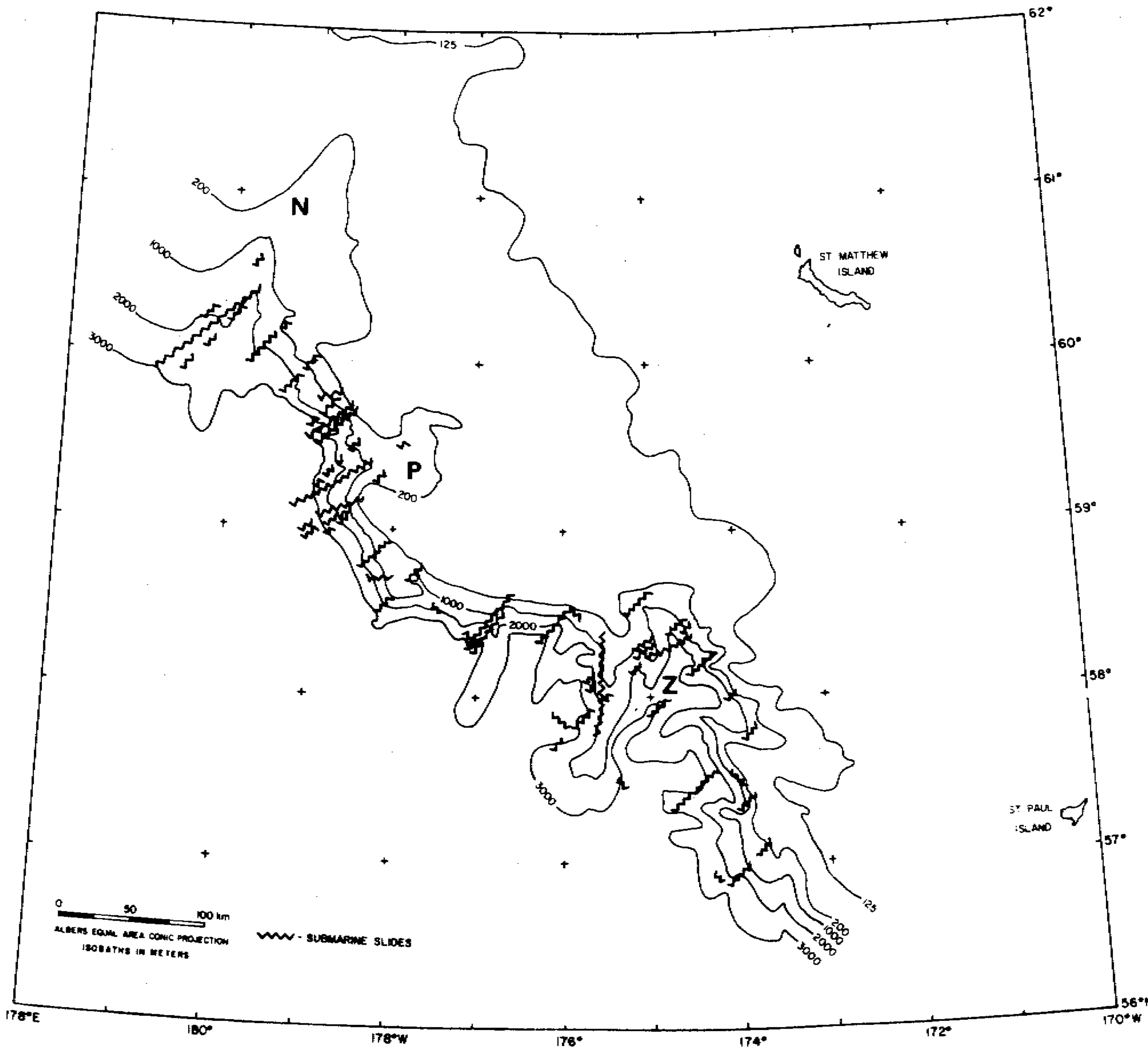

Figure 21. Preliminary map of areas of submarine landslides in Navarin Basin province. Letters N, P, Z locate Navarinsky, Pervenets, and Zhemchug Canyons.

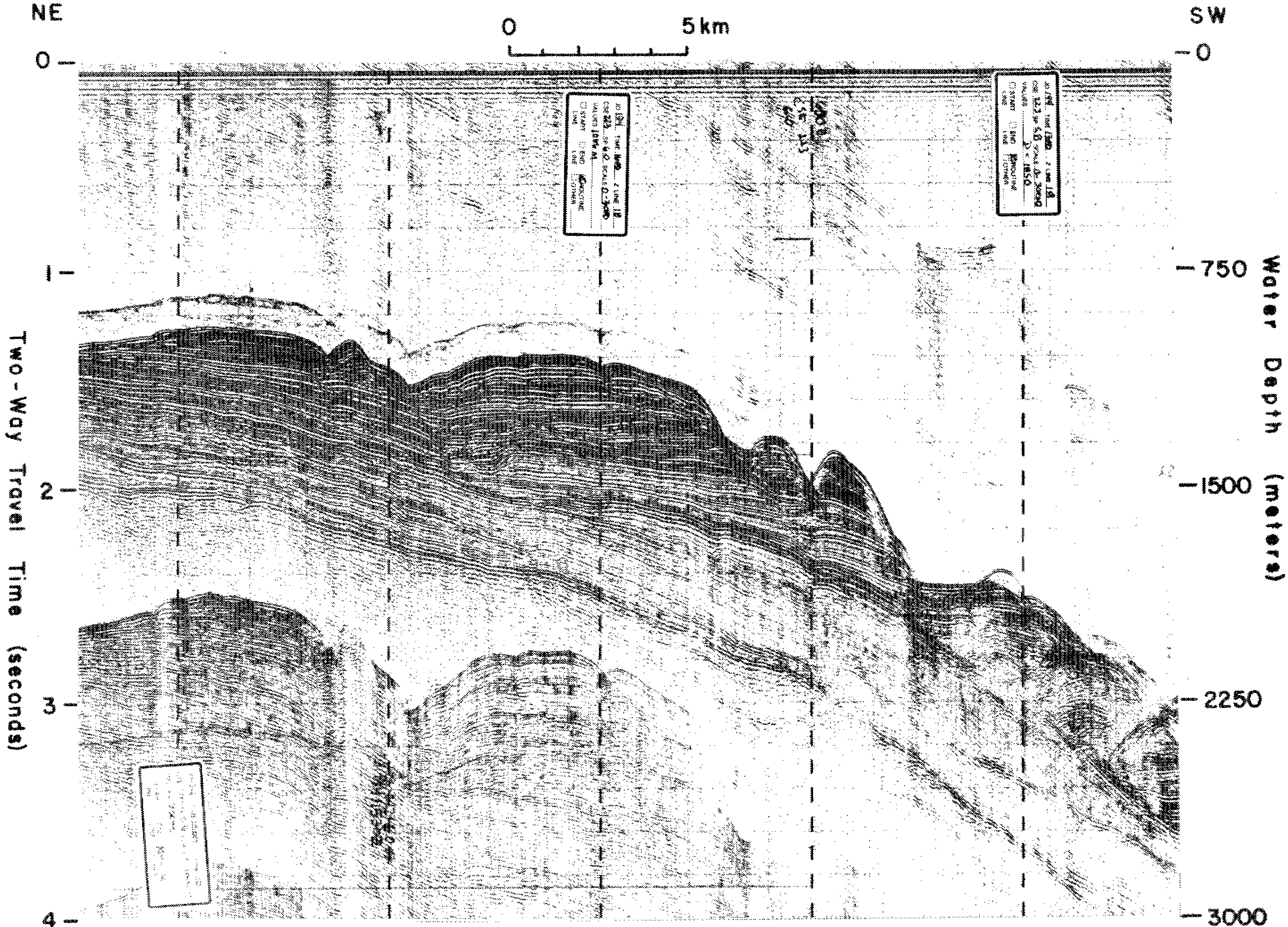

Figure 22. Seismic-reflection profile (2-40 in^3 air guns) showing slumping in Navarinsky Canyon. Note the slumps, the buried channel (∿ 1545 Z), and the associated cut and fill structures. Line 18, cruise DC4-80-BS/NB. Vertical exaggeration ∿ 10 x.

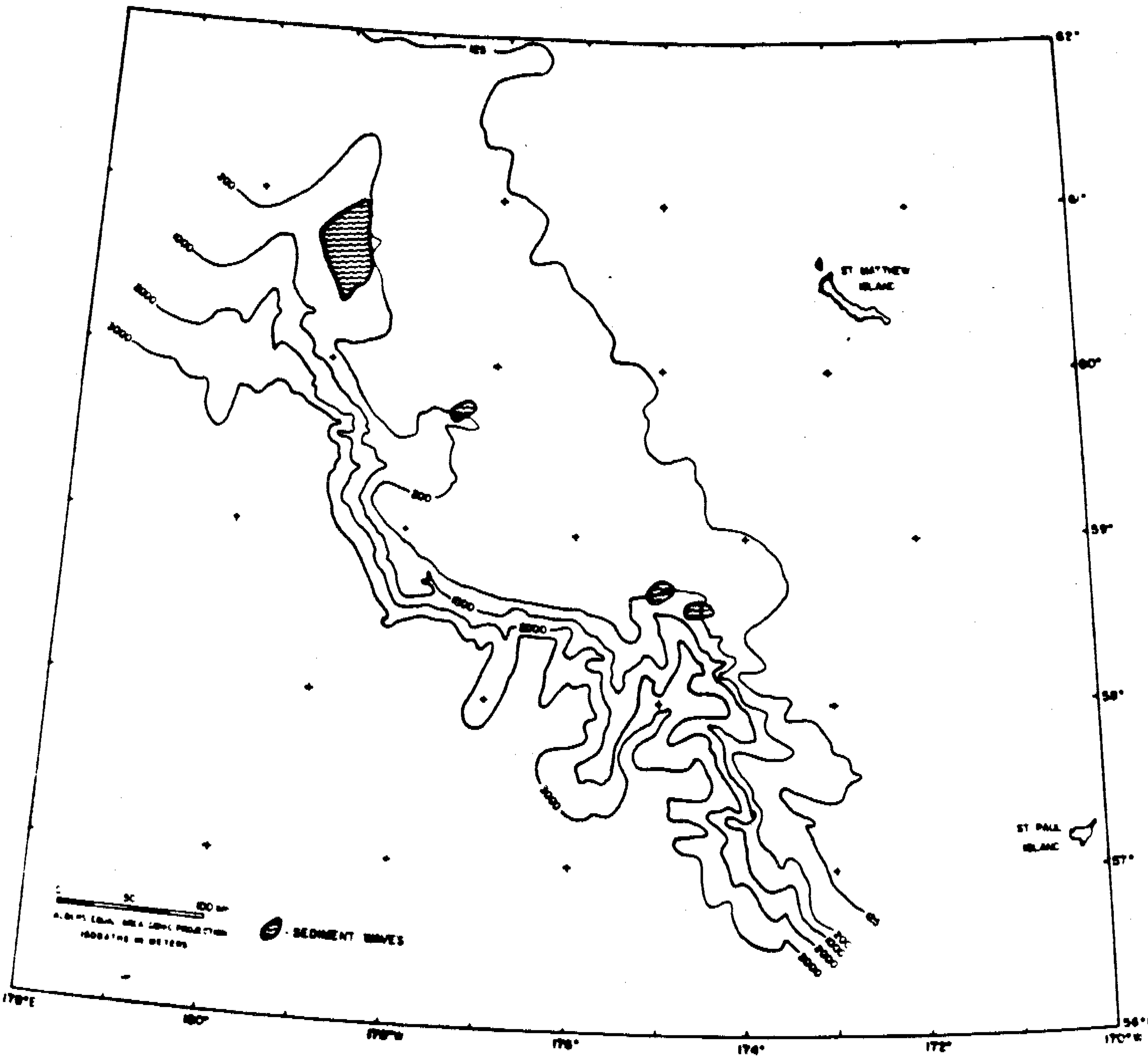

Figure 23. Preliminary map of areas of sediment waves in Navarin Basin province. Letters N, P, Z locate Navarinsky, Pervenets, and Zhemchug Canyons.

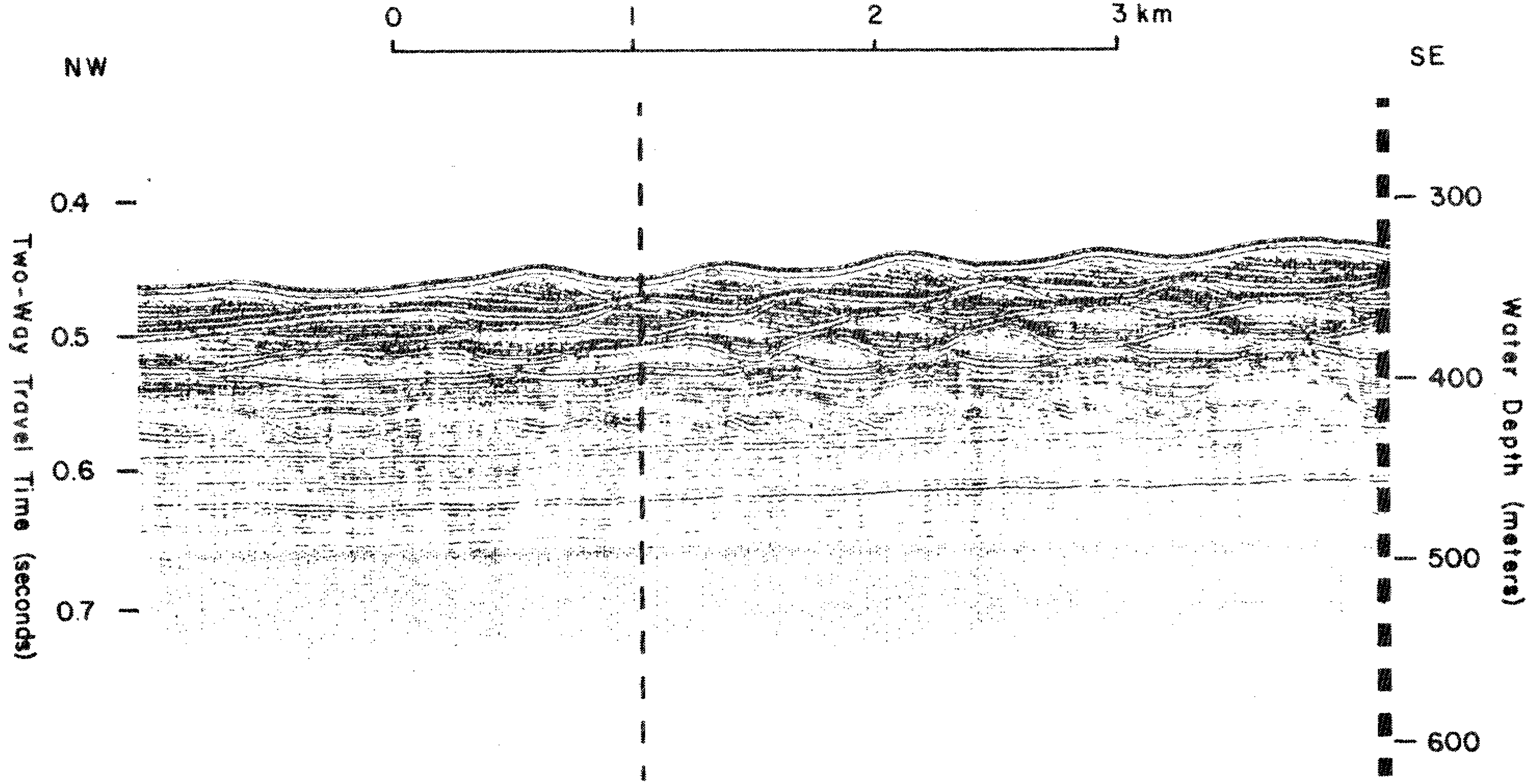

Figure 24. Seismic-reflection profile (1000J minisparker) showing sediment waves at head of Navarinsky Canyon. Line 12, DC4-80-BS/NB. Vertical exaggeration ∿ 7.5 x.

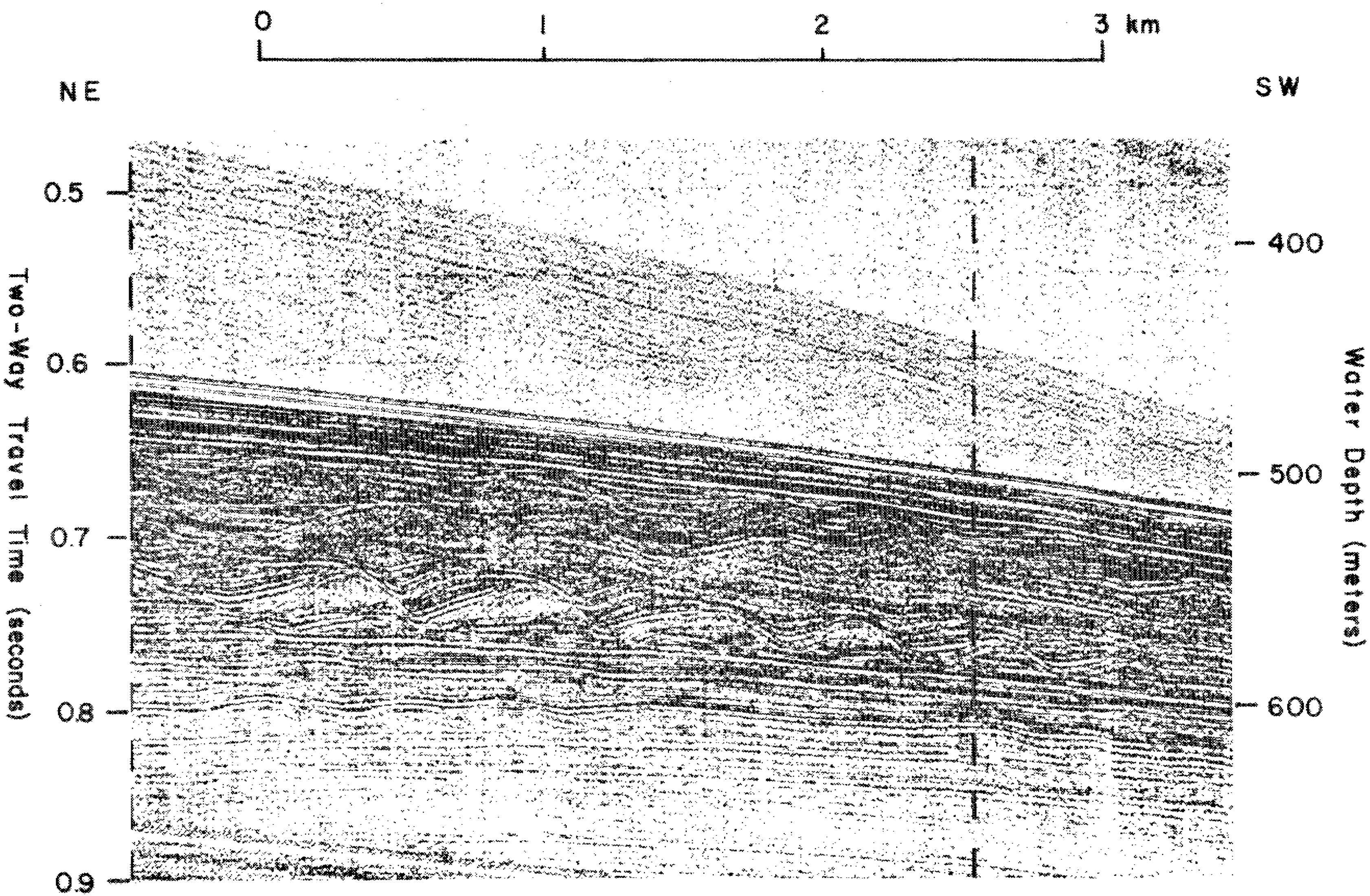

Figure 25. Seismic-reflection profile (1000J minisparker) showing sediment waves covered by about 20 m of parallel-bedded sediment at head of Pervenets Canyon. Line 43, DC5-80-BS/NB. Vertical exaggeration ~ 8.5 x.

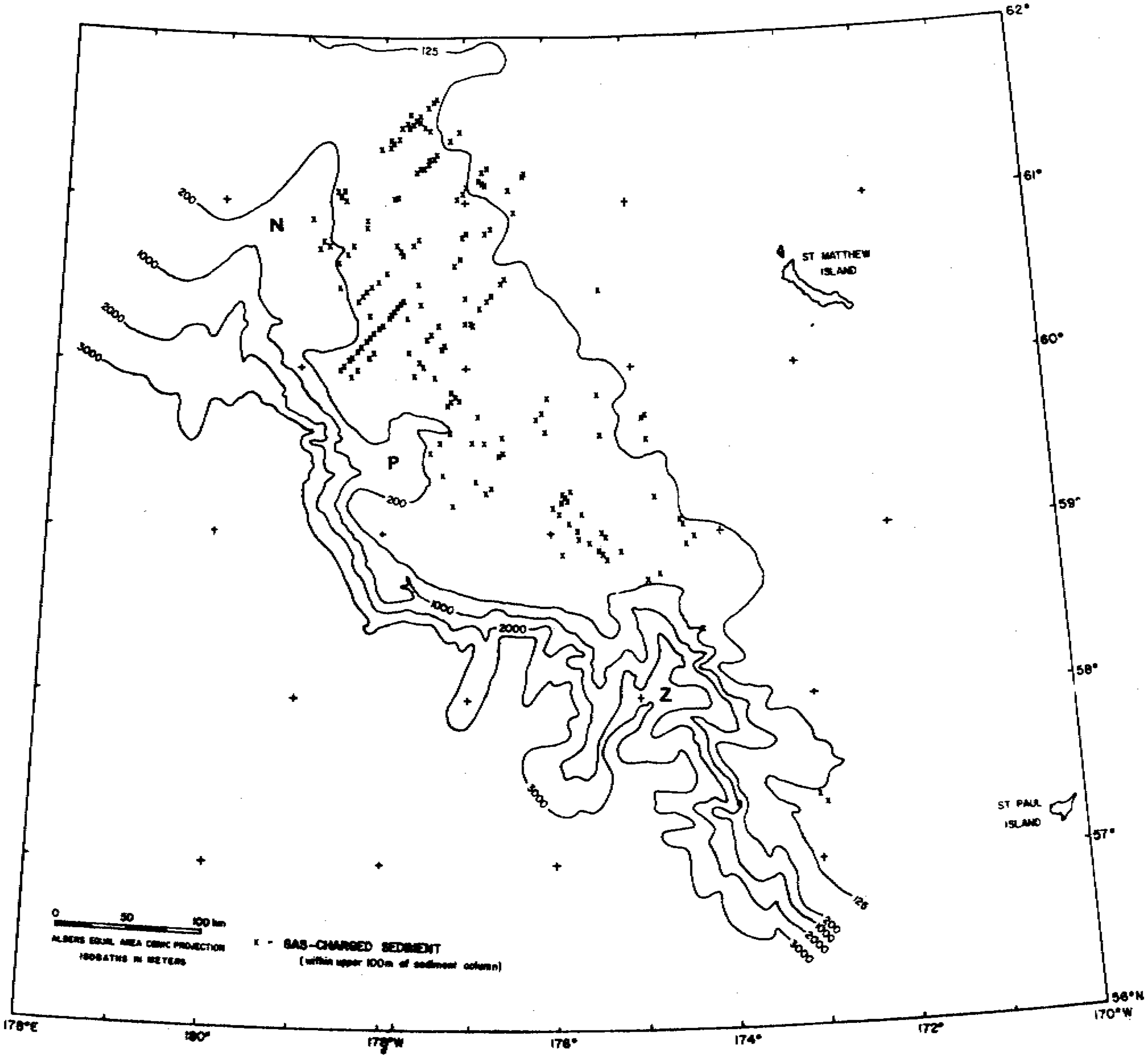

Figure 26. Preliminary map of areas of gas-charged sediment in Navarin Basin province.

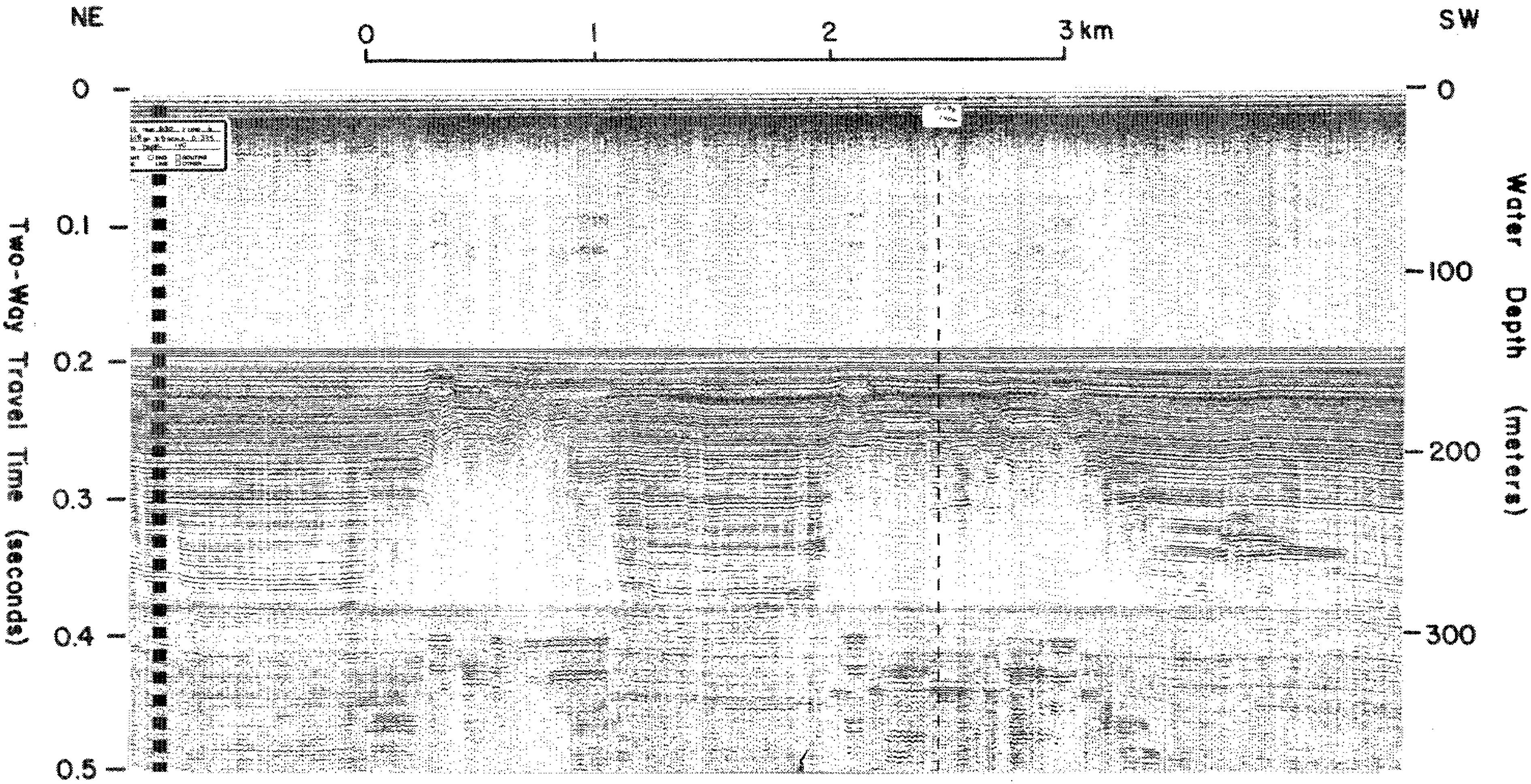

Figure 27. Seismic-reflection profile (500J minisparker) from northern part of Navarin Basin province showing acoustic anomalies interpreted to be caused by gas-charged sediment. Line 6, DC4-80-BS/NB. Vertical exaggeration ∿ 7.5 x.

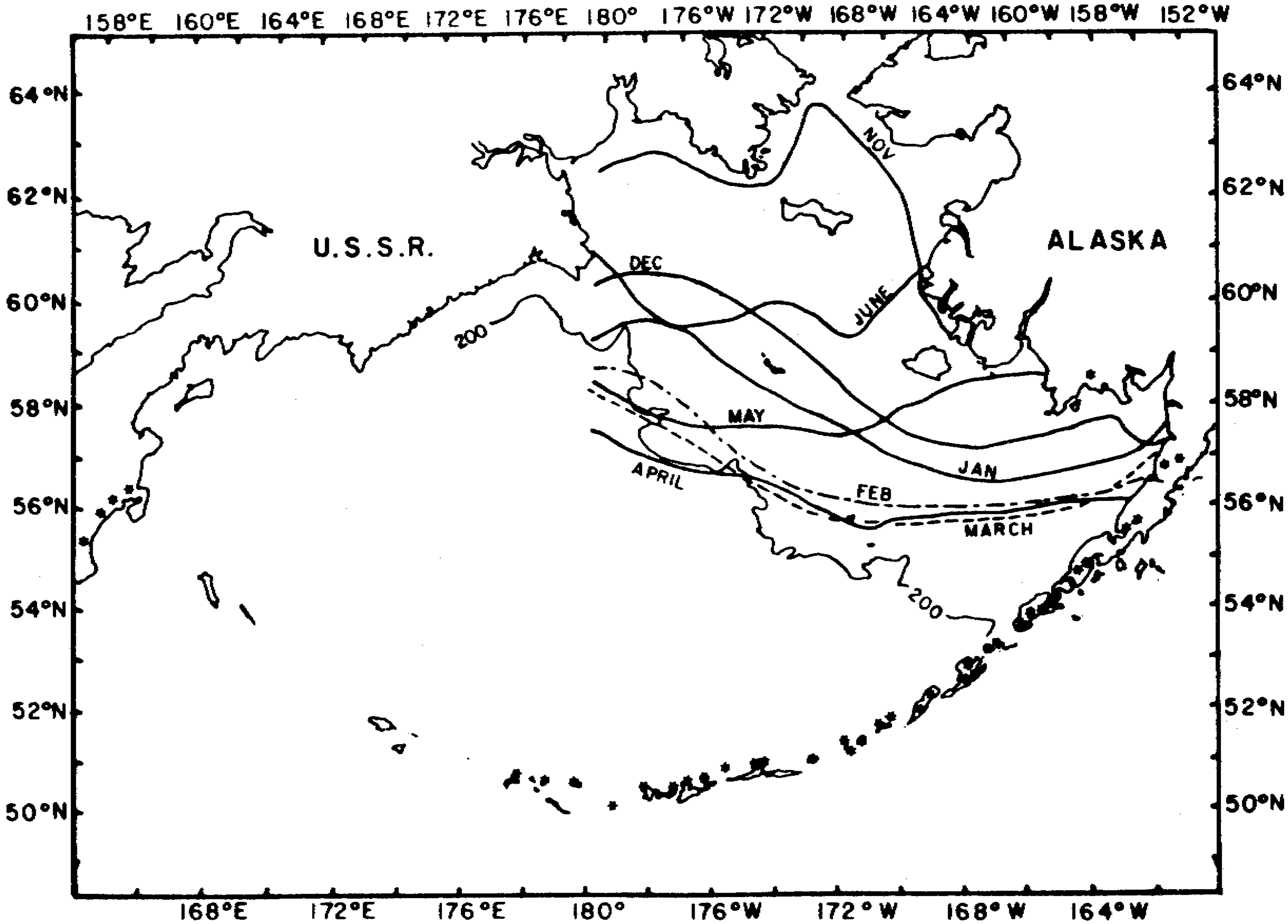

Figure 28. Location map of active volcanoes (*) (after Coates, 1950) and lines of average monthly ice-front positions (after Webster, 1979). The ice positions are for the 15th of each month and are estimated to have a 50% probability.

GEOTECHNICAL PROPERTIES OF NAVARIN BASIN SEDIMENT

Brian D. Edwards

INTRODUCTION

Cores from 68 stations have been tested to define geotechnical variables useful in describing regional changes in Navarin Basin sediment properties. The term geotechnical is applied in this study to quantitative physical characteristics of the sediment that are useful in assesssing sedimentary processes of engineering importance. Basic properties of geotechnical importance include strength and compressibility characteristics. Additional "index" variables that are known to correlate with or affect these more fundamental properties include water content, grain density, Atterberg limits (i.e. plastic and liquid limits), grain size distribution and composition of sediment.

Shipboard Techniques

A suite of 68 gravity cores was collected for stratigraphic and sedimentologic analysis. At 7 stations, replicate cores were collected and preserved in refrigeration for subsequent triaxial and consolidation testing. Shipboard testing was limited to strength measurements and subsampling for water content.

Cores were cut into multiple sections by use of a rotary knife blade cutter. Core sections designated for stratigraphic and sedimentologic analyses were then split longitudinally using a specially designed cutting system and a wire saw. Although sample disturbance is aggrevated by such longitudinal splitting, this procedure allows more frequent downcore testing while maintaining sample integrity for other analyses (e.g., X-ray radiography, photography, and textural analysis).

Strength measurements were made using a motorized Wykeham-Farrance miniature vane shear device. Tests were made at 20 cm intervals on the stratigraphic cores using a four-bladed 1/2 inch vane which was inserted into the cores so the top of the vane was buried by an amount equivalent to blade height. Torque was applied to the vane by either a torque cell that rotates the vane directly, or by a connected spring. Rotation rate of the torque cell and the top of the calibrated spring was a constant 90° per minute. When the spring system was used, torsion was measured and correlated directly with torque applied at the vane. Because of the spring's flexibility, rotation rate at the vane changed throughout the test. The method of torque measurement (spring vs torque cell) and the core state (split vs unsplit) appeared to have little impact on the general trend of the shear strength versus depth variation (Fig. 29). Vane shearing strength (S_v), is calculated from peak torque by assuming that the sediment builds a peak shearing resistance everywhere along a right-circular cylinder inscribed around the vane. This term (S_v) is commonly equated with the undrained shear strength of the sediment (S_u).

Water content and bulk density subsamples were obtained from the location of the vane test immediately following strength testing. These samples were taken with a small tube sampler and stored in sealed sample bottles for subsequent weighing and drying at the shorebased laboratory.

Replicate cores collected for more sophisticated geotechnical testing laboratory were sectioned as described above, but were not split longitudinally. Vane shear tests were conducted at the top of each unsplit core section and water content subsamples were taken at those sites. End caps were sealed on both ends of each core section. Cores were then wrapped in cheesecloth, sealed with a non-shrinking, microcrystalline wax, labelled, and stored vertically in refrigeration. The replicate cores were shipped by refrigerated air transport from Kodiak, Alaska, to storage facilities at the U.S. Geological Survey laboratory in Palo Alto, California. These cores were subsequently shipped to the commercial testing laboratory. At all times, the cores were kept in refrigeration and handled vertically.

RESULTS

Distribution of Peak Shear Strength

The areal distribution of peak undrained shear strength (S_v) at a subbottom depth of one m is shown in Figure 30. The study area can be divided physiographically into three zones: (1) shelf, (2) shelf break and uppermost slope, and (3) slope. Shelf sediment (< 200 m) typically has a peak vane shear strength (S_v) that ranges between 10 and 15 kPa (1 psi=6.9 kPa). An elongate zone of weaker sediment (<10 kPa) extends onto the central shelf from the north and reflects the presence of a tongue of fine-grained, higher water content sediment (see Karl and others, this report; Fig. 11). A zone of stronger sediment (>15 kPa) exists to the southeast although station control is too sparse to allow definition. Shear strengths in the region of the shelf break (lined area) are not shown because high sand content allows pore-water drainage during testing which compromises measured S_v values, and/or insufficient sample was recovered to warrant testing. Peak shear strength typically decreases downslope, ranging from 11 kPa near the shelf break to 3 kPa, on the abyssal floor. However, anomalously strong sediment was encountered at two stations in 3000 m of water at about 58°30'N, 178°30'W (Cores G22 and G73). Here, shear strengths are between 19 and 39 kPa.

Water Content Distribution

Sediment at a 1 m subbottom depth on the shelf has a water content that ranges between 40 and 110% by dry weight (Fig. 31). An elongate zone of water contents greater than 100% is seen in the north-central part of the shelf. This zone is coincident with the area of anomalously low peak undrained shear strength. Water content of shelf sediment gradually decreases to the southeast, with the exception of two stations that have water contents greater than 50%.

Sediment from the shelf edge and uppermost slope typically has a low water content (<50%) which correlates with increased sand percentages. Water content increases down slope and reaches a maximum (>300%; Core G 13) to the southeast in the vicinity of Zhemchug Canyon.

Consolidation State

Near-surface sediment from Navarin Basin is lightly to moderately overconsolidated (OCR: 3-4) except on the shelf where overconsolidation ratios as high as 22 are observed (Table 7). The cause of the observed overconsolidation is uncertain. Sediment on the shelf is subjected to a number of loads capable of inducing this overconsolidation state (e.g., creep, erosion of overlying material, cyclic loading, cementation, ice loading, and subaerial exposure at low sea level stands). At present, we have insufficient data to evaluate these mechanisms.

SUMMARY OF FINDINGS

An inverse correlation exists between peak undrained shear strength (S_v) and water content of Navarin Basin sediment. At a 1 m subbottom depth, a tongue of relatively weak (< 10 kPa), high water content (> 100%), fine-grained sediment extends onto the central shelf from the north. To the southeast, near the head of Zhemchug Canyon, shear strengths are anomalously high (> 15 kPa). Vane shear strengths at the shelf edge are of low reliability because of the coarse-grained texture and are not reported. Strength of the fine-grained, high water content sediment on the slope typically decreases with water depth from a high of 11 kPa near the shelf break to a low of 3 kPa at the base of the slope. Two stations of very high shear strength (19 and 39 kPa) were found at the base of the slope between Zhemchug and Pervenets Canyons.

Preliminary consolidation data indicates that the shelf sediment is lightly to heavily overconsolidated (OCR's ranging from 3 to 22 at a subbottom depth of 1 m). At present, we have insufficient data to interpret the cause of overconsolidation. It is apparent that the central shelf is more heavily overconsolidated than adjacent areas.

TABLE 7. Overconsolidation Ratios (OCR's) of near-surface sediment

Core	σ_{vm}' (kPa)	σ_v' (kPa)	OCR	Physiographic Province
G31	20	6.8	3	Shelf
G34	28	7.0	4	Canyon
G61	27	4.5	6	Shelf
G74	25	9.2	3	Slope
G78*	95	4.3	22	Shelf
G97	30	5.0	6	Canyon
G111	60	6.5	9	Shelf

*values 1 m subbottom depth except G78 which was determined at 58 cm.

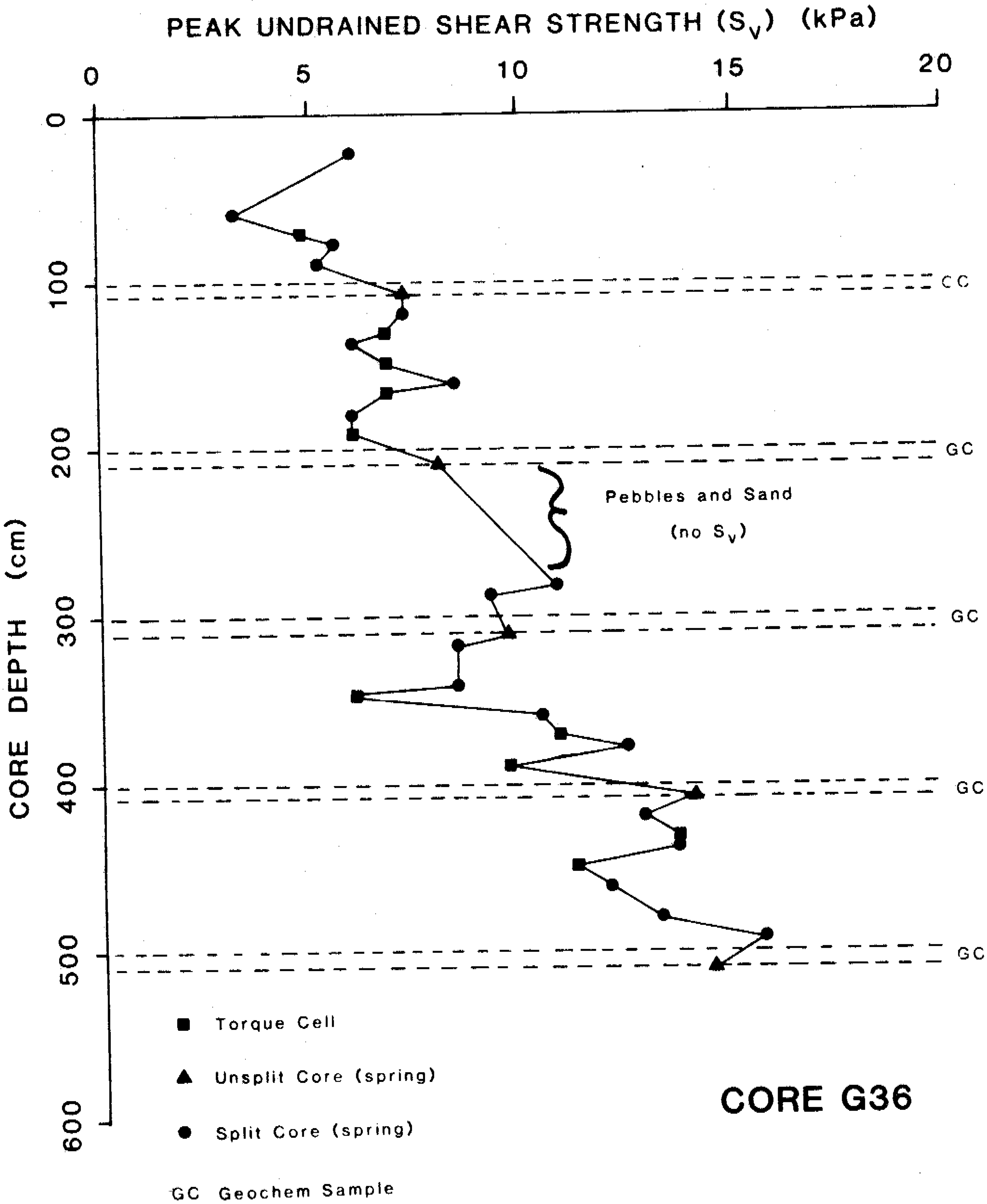

Figure 29. Peak undrained shear strength (S_v) versus core depth for core G36. Note the general increase in S_v with subbottom depth and the good correlation between strength determinations by the various methods used.

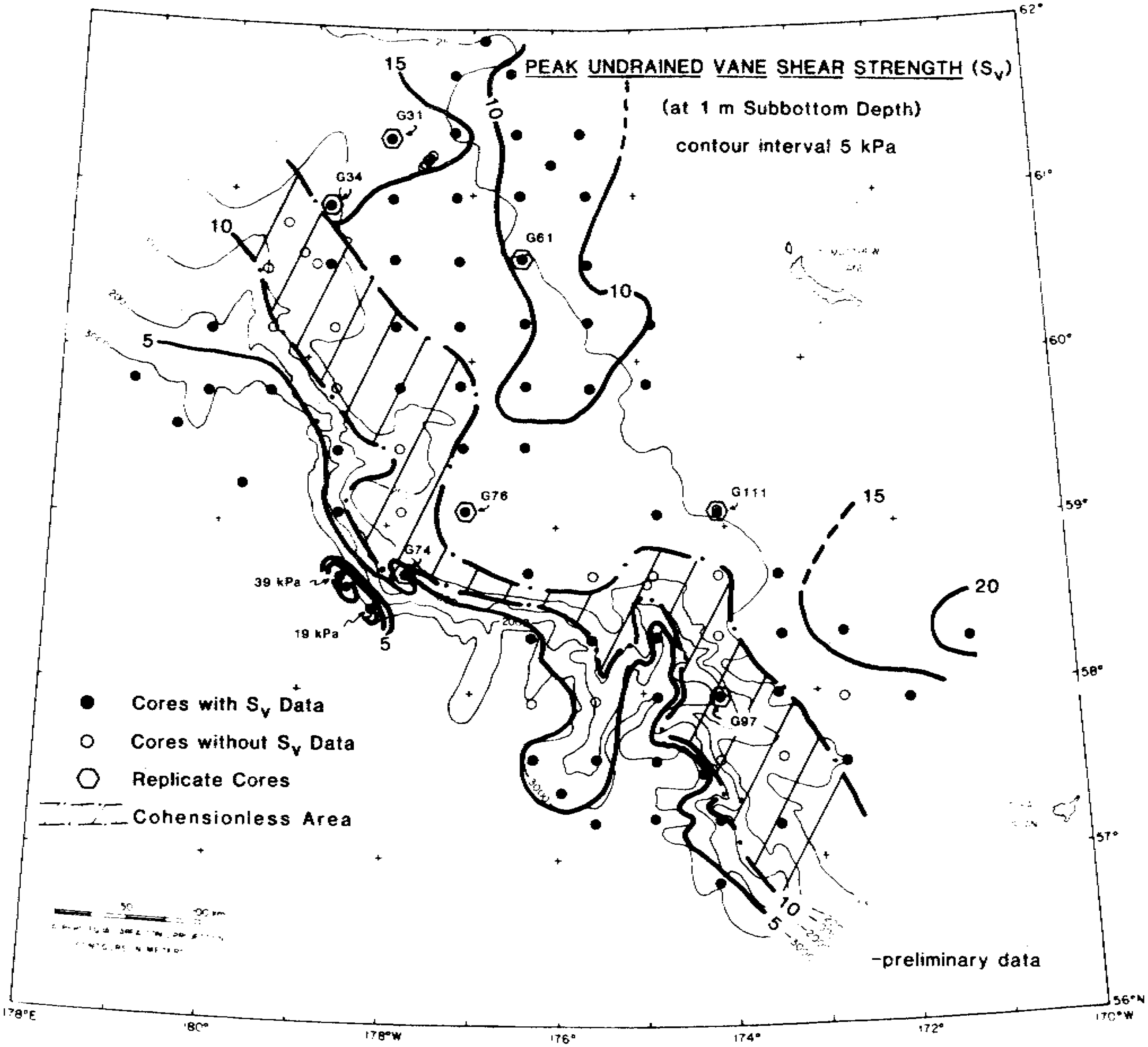

Figure 30. Areal distribution of peak undrained vane shear strength (S_v) at 1 m subbottom depth.

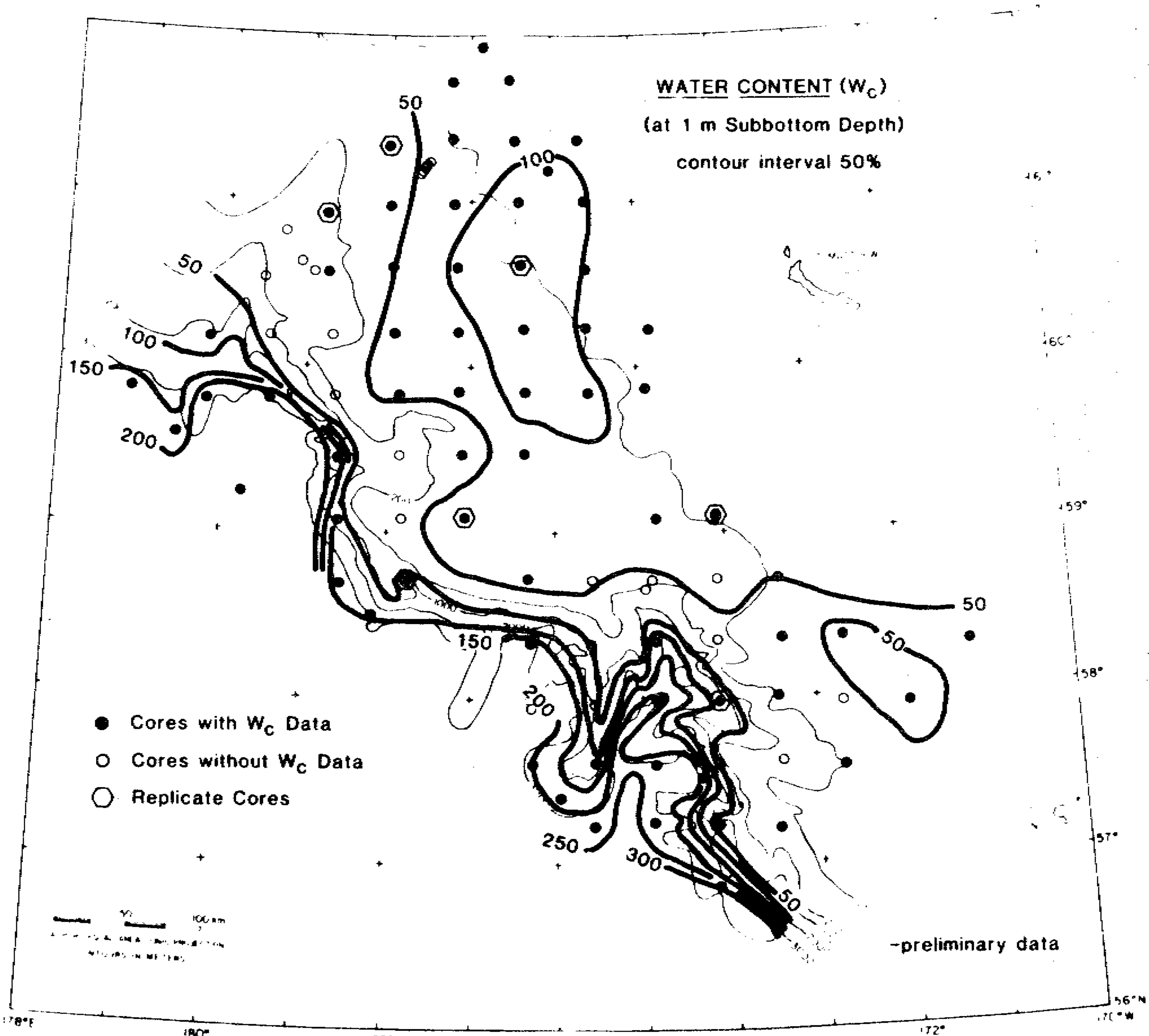

Figure 31. Areal distribution of salt-corrected water content at a 1 m subbottom depth.

HYDROCARBON GASES IN NAVARIN BASIN PROVINCE SEDIMENTS

Timothy M. Vogel and Keith A. Kvenvolden

INTRODUCTION

The first occurrence of hydrocarbon gases in marine sediments was described by Emery and Hoggan (1958) who noted these gases in the surface sediments of the Santa Barbara Basin offshore southern California. They reported concentrations of methane (C_1), ethane (C_2), propane (C_3), butanes (C_4), pentanes (C_5), and hexanes (C_6). However, since 1958 the majority of the geochemical studies devoted to gases in marine sediments have centered on the distribution and origin of methane, which is usually several orders of magnitude greater in concentration than the C_2-C_4 hydrocarbons (Reeburgh, 1969; Whelan, 1974; Martens and Berner, 1974; Claypool and Kaplan, 1974; Oremland, 1975; and Kosiur and Warford, 1979). In recent years, methods have been developed that measure the hydrocarbons C_2-C_4 at the 1 ppb level. For example, Bernard and others (1978) reported the concentrations of C_1-C_3 in sediment from the slope and shelf of the Gulf of Mexico. Whelan (1979) observed C_1-C_7 hydrocarbon gases in Deep Sea Drilling Project cores over 1000 m in length, and Whelan and others (1980) reported the occurrence of C_1-C_7 hydrocarbons in surface sediment of Walvis Bay, offshore South Africa. Kvenvolden and others (1979) reported the occurrence of C_1-C_4 hydrocarbons in sediment from Norton Sound, Alaska, and Kvenvolden and Redden (1980) observed C_1-C_4 hydrocarbon gases in sediment from the shelf, slope, and basin of the Bering Sea. Recently, models have been developed that characterize the hydrocarbon gases found in seeps in the marine environment, Bernard and others (1977) suggested the use of the ratio C_1/C_2+C_3 to help characterize the source of the hydrocarbon gases in submarine seeps. A C_1/C_2+C_3 ratio greater than 1000 is indicative of biogenic gas and a ratio less than 50 is suggestive of thermogenic gas. Cline and Holmes (1977) discussed the usefulness of the ratio $C_2/C_{2=}$. If the ratio is significantly greater than one, the hydrocarbon gas is possibly thermogenic, and if the ratio is less than one the gas is possibly biogenic. Kvenvolden and Redden (1980) cautioned that in areas where gas concentrations are low (non-seep areas), interpretation of sources of gases based on the ratio C_1/C_2+C_3 can be equivocal. The same can be said when the ratio $C_2/C_{2=}$ is used to interpret sources of gases.

This study considers the hydrocarbon gases C_1, C_2, C_3, ethene ($C_{2=}$), propene ($C_{3=}$), isobutane (i-C_4) and normal butane (n-C_4), detected by semi-quantitative analysis of sediment recovered from the Navarin Basin province in the Bering Sea. Interpretation based upon existing models and statistical evaluation of the data are presented to provide a general view of the region.

METHODS AND MATERIALS

Analytical procedures used in this work have been previously described (Kvenvolden and Redden, 1980). Cores were cut into 10-cm lengths at various intervals (usually 100-110, 200-210 cm, etc. sediment depths). Sediment from each of these 10-cm sections was placed in an unlined can (0.95 liters) that had two septa-covered holes on the side near the top. Each can was filled with distilled and degassed water. The can was sealed with a lid after a headspace was established by removing 100 ml of water. The headspace was purged with helium through the septa. The cans were then shaken for 10 minutes to equilibrate the hydrocarbon gases in the sediment with the helium headspace. A sample of the headspace of about one-half the cans was withdrawn through a septa by a gas-tight syringe. This syringe was sealed by a valve in the syringe and stored for shore-based studies. The cans of sediment were inverted, frozen, and shipped back to the shore-based laboratory where gases in both syringes and the cans were analyzed by gas chromatography using flame ionization and thermal conductivity detectors. The cans of sediment were brought to room temperature and shaken for five minutes before portions of their headspaces were analyzed. Calculations of the gas concentrations were determined by computer comparison of the integrated area of each hydrocarbon with the integrated area of a hydrocarbon standard. Partition coefficients were calculated by repeatedly purging the headspace of some of the cans, re-equilibrating the gases by shaking the cans again, and analyzing a portion of the resulting headspace gas mixture. The partition coefficient (P.C.) is derived from the following equations:

$$\text{P.C.} = \frac{\text{amount in gas phase } (G_1)}{\text{total amount in can } (T_1)} = \frac{\text{new amount in gas phase after purge } (G_2)}{\text{new total in can after purge } (T_2)}$$

$$T_2 = T_1 - G_2, \text{ so P.C.} = 1 - \frac{G_2}{G_1}, \text{ or generally P.C.} = 1 - \sqrt[n]{\frac{G_n}{G_1}} \text{ where } n = \# \text{ of times}$$

For a discussion of the theory see Drozd and Novak (1979). Concentrations of the hydrocarbons are reported in nl of gas/liter of wet sediment (nl/l), except for methane, which is reported in ul of methane/liter of wet sediment (ul/l). The analytical detection limit is 1 nl of gas/liter of wet sediment. Partition coefficients used are 0.7 for C_1, and 0.5 for C_2-C_4. The partition coefficients were rounded to the nearest 0.1. Error determined from repeat analysis, duplicate cores at the same station and analytical variation is <20%.

RESULTS

Hydrocarbon gases (C_1-C_4) were observed to a subbottom depth of 520 cm in the sediments of the Navarin Basin province (Table 8). The locations of the coring sites are shown in Figure 32. Methane (C_1), was the most abundant gas, often present in concentrations several orders of magnitude larger than the other hydrocarbon gases. C_1 ranged from 2 to over 850 ul/l. The geographic distribution of C_1 at the 100-110 cm and the 200-210 cm sediment depths are shown in Figures 33 and 34, respectively. In six cores (22, 36, 37, 70, 74 and 97), anomalously high C_1 concentrations were observed. These concentrations are outside the 85% confidence interval, which is based upon the concentrations of all the samples, assuming a lognormal distribution.

Ethane (C_2) is the second most abundant hydrocarbon gas measured in the Navarin Basin province sediment. The distribution of propane (C_3) generally follows the same trend as ethane (C_2), but is less abundant. C_2 ranged from trace amounts to approximately 1500 nl/l, whereas C_3 ranged from trace amounts to about 200 nl/l. Geographic distribution of these gases at the sediment depths of 100-110 cm and 200-210 cm are shown in Figures 35-38.

The alkenes, ethene ($C_{2=}$) and propene ($C_{3=}$), are generally lower in concentration than C_2 and C_3, respectively, and the alkenes usually decrease with depth. The gas-tight syringes used for sampling contained significant amounts of $C_{3=}$, resulting from outgassing of C_3 = from the teflon plunger. No other hydrocarbon gases were outgassed in significant amounts.

Concentrations of isobutane (i-C_4) and normal butane (n-C_4) are lower than the concentrations of the lighter hydrocarbons C_1-C_3. The concentrations of i-C_4 and n-C_4 are often below the detection limit of 1 nl/l, and range to a maximum concentration of 272 and 36 nl/l, respectively. The C_5-C_7 hydrocarbons are measured as a single back-flush peak on the gas chromatogram. These hydrocarbons were seldom detected and are generally low in concentration (less than 100 nl/l). Occasionally, the C_5-C_7 concentration reached 400 nl/l. Carbon dioxide was qualitatively estimated and its concentration varied little from a mean of 2 ml/l of wet sediment. For all the samples analyzed, the C_1/C_2+C_3 ratio ranged from less than 10 to over 2000, averaging 248. The $C_2/C_{2=}$ ratio ranged from 0.2 to 198, averaging 12.

Six cores (22, 36, 37, 70, 74, and 97) have anomalous C_1 concentrations; four of these (22, 36, 37 and 74) have anomalous ethane concentrations. Three of these four cores (22, 36, and 37) have anomalous propane concentrations. The C_1/C_2+C_3 ratio in core 37 is 721, whereas the ratio in cores 22 and 36 are 70 and 60, respectively. A profile of the distribution of hydrocarbons C_1-C_3, C_1/C_2+C_3 and $C_2/C_{2=}$ ratios with depth in core 36 are shown in Figure 39. For comparison, a profile of gas concentrations with depth in core 100, in which all the gas concentrations are within the 85% confidence interval based upon a lognormal distribution, is shown in Figure 40.

DISCUSSION

Sediment in Navarin Basin province contains mixtures of gases that can be classified into four types based on the relative abundances of the hydrocarbon gases present. These four types are defined in Table 9. The first and most abundant type (Type I) has low concentrations of all the hydrocarbon gases. The typical distribution with depth of Type I gas mixture is shown on Figure 40. Type I is defined as the environmental baseline for Navarin Basin province sediment. Twenty-nine stations have Type I gas at some depth in the sediment (see Table 8).

The second type of gas (Type II) has anomalously high concentrations of C_1 and just baseline concentrations of the other hydrocarbon gases. Five cores (49, 63, 68, 102, and 105) have Type II gas. The Type II gas mixture is characterized by high C_1/C_2+C_3 ratio (greater than 450) and a low $C_2/C_{2=}$ ratio (less than two).

The third type of gas (Type III) has above-baseline concentrations of C_1 and always has anomalously high concentrations of C_2 and C_3. Eight cores (22, 25, 36, 37, 70, 71, 74, and 97) have Type III gas. The C_1/C_2+C_3 ratio ranges from 56 in core 36 to 721 in core 37. The $C_2/C_{2=}$ ratio ranges from 6 in core 71 to 198 in core 22.

The fourth type of gas (Type IV) has high concentrations of at least one of the alkanes C_2-C_4. In the Navarin Basin sediments, Type IV gas is characterized by the presence of measureable quantities of i-C_4 and n-C_4. Two major groups exist within Type IV; the first group, (cores 26, 31, 41, 42, 43, 45, 50, 59, and 105) only has anomalous concentrations of C_3; the second, group, (cores 52, 54, 63, 66, 68, 73, 97, 101, and 107) has various anomalies in the C_1-C_3 hydrocarbon range. The C_1/ C_2+C_3 ratio ranges from as low as 16 to over 800 and the $C_2/C_{2=}$ ratio ranges from less than one to over 24.

In Type I gas, interpretations based on the C_1/C_2+ C_3 and $C_2/C_{2=}$ ratios are inconclusive because the concentrations of the hydrocarbon gases are too low for these ratios to indicate whether the gases are derived from a biogenic or thermogenic source (Kvenvolden and Redden, 1980). Although C_1 alone is often considered to be a biogenic gas, the alkanes C_2 and C_3 are often considered to be thermogenic gases. However, in open-ocean sediment isolated from any apparent thermogenic source, traces of C_2 and C_3 are found, and evidence exists that suggests that these traces can be produced by biological processes (Davis and Squires, 1954; Kvenvolden and Redden, 1980; Whelan and others, 1980; Vogel and others, 1980; Oremland and others, 1980).

Type II gas has anomalous C_1 concentrations, probably derived from microbiological activity in the surface sediment. The high concentration of C_1 in anoxic sediments resulting from microbial activity is well documented (Barnes and Goldberg, 1976; Kosiur and Warford, 1979; and Martens and Berner, 1974). The less reducing sediment of the open marine environment has biogenic C_1 present in lesser amounts (Bernard and others, 1978; Kvenvolden and Redden, 1980; Kvenvolden and others, 1981). The microbial processes that produce C_1 in both types of sediment are probably similar.

Type III gas has the molecular distribution of hydrocarbons most similar to the distribution that would suggest a thermogenic source. However, i-C_4 and n-C_4 are generally not present in anomalous concentrations in Type III. Some cores (22, 25, 36, and 74) have C_1/C_2+C_3 ratios less than 80 and $C_2/C_{2=}$ ratios greater than one. However, only cores 22 and 36 have extremely high concentrations of all three alkanes C_1-C_3. Core 36 also has detectable i-C_4 and n-C_4 at depth in the sediment. If the observed gas was from a thermogenic source at depth in the sediment, the hydrocarbon gases should increase with depth similar to core 36 (Fig. 39).

Type IV gas has a large variability in the concentrations of the hydrocarbon gases, causing conclusions to be equivocal. Type IV may be interpreted to be a mixture of thermogenic and biogenic gases. The high methane concentration could possibly be caused by the mixing of large amounts of biogenic C_1 in the surface sediments with the C_1 diffusing up from a thermogenic source. The large amounts of C_2 and C_3 seem to possibly require a thermogenic source for production. For example, if a natural gas deposit existed at depth, C_1-C_3 hydrocarbon gases would possibly diffuse upward into the surface sediment, mixing with the biogenic gas produced by microbes at the surface.

A gas mixture that has only high C_3 could be caused either by error in determining the propane concentration or by a physical or chemical process (like diffusion) reducing the concentration of the other gases.

The alkenes $C_{2=}$ and $C_{3=}$ are present in all the gas types in some quantity. These alkenes have been produced in the laboratory (Davies and Squires, 1954); $C_{2=}$ is produced in soils by bacteria (Primrose and Dilworth, 1976) and $C_{2=}$ and $C_{3=}$ have been observed in non-thermogenic gases in the southern Bering Sea (Kvenvolden and Redden, 1980) and in San Francisco Bay (Vogel and others, 1980). The processes that produce the alkanes probably differ from the biological processes that produce the alkenes. All cores (31, 54, 59, 63, 66, and 107) that have anomalous $C_{2=}$ and $C_{3=}$ concentrations, have Type IV gas. This further confuses any interpretation of the source for Type IV gas. Obviously, the high alkene concentrations imply a significant biological input to the gas detected in the surface sediments.

Cores 42-45 were taken above an acoustic anomaly that ranges to within 25 meters of the sediment surface (see Fig. 27, Carlson and Karl, this report). The gas concentrations did not show a correlation with the acoustic anomaly, possibly because either the anomaly is not due to gas-charged sediment or the gas is stopped from reaching the surface by some impenetrable sediment layer.

CONCLUSIONS

Our results show that hydrocarbon gases are common in near-surface sediment of the Navarin Basin province. Generally, the concentrations of gases are low relative to earlier observations made on sediment from Norton Sound (Kvenvolden and others, 1981). The concentrations of methane in Norton Sound, were high enough to affect the stability of the sediment and thus pose a possible geologic hazard. Measured concentrations of gases in sediment from the Navarin Basin province are much smaller; thus, we are less certain of the degree of hazard. The composition of hydrocarbon gases is variable over the province. Most of the observed gas mixtures can be attributed to microbiological activity. No significant anomalies were observed, although the gas from sediment samples from core 36 suggest that some thermogenic gas may be present. No correlation was observed between gas concentrations measured in the surficial sediment and the occurrence of an acoustic anomaly that is attributed by Carlson and Karl (this report) to possible high gas concentrations at depths of about 25 meters.

REFERENCES CITED

Barnes, R. O. and Goldberg, E. D., 1976, Methane production and consumption in anoxic marine sediments: Geology, v. 4, p. 297-300.

Bernard, B. B., Brooks, J. M., and Sackett, W. M., 1977, A geochemical model for characterization of hydrocarbon gas sources in marine sediments: Proc. 9th Offshore Tech. Conf., 1, p. 435-438.

Bernard, B. B., Brooks, J. M., and Sackett, W. M., 1978, Light hydrocarbons in recent Texas continental shelf and slope sediments: Jour. Geophys. Res., 83, p. 4053-4061.

Claypool, G. E. and Kaplan, I. R., 1974, The origin and distribution of methane in marine sediments: In Natural Gases in Marine Sediments, Kaplan, I. R., ed., Plenum, New York, p. 99-139.

Cline, J. D., and Holmes, M. L., 1977, Submarine seepage of natural gas in Norton Sound, Alaska: Science, no. 198, p. 1149-1153.

Davis, J. B. and Squires, R. M., 1954, Detection of microbially produced gaseous hydrocarbons other than methane: Science, no. 119, p. 381-382.

Drozd, J. and Novak, J., 1979, Headspace gas analysis by gas chromatography: Jour. Chromatogr., vol. 165, p. 141-165.

Emery, K. O. and Hoggan, D., 1958, Gases in marine sediments: Am. Assoc. Petrol. Geol. Bull., no. 42, p. 2174-2188.

Kosiur, D. R., and Warford, A. L., 1979, Methane production and oxidation in Santa Barbara Basin sediments: Estuarine and Coastal Marine Science, v. 8, p. 379-385.

Kvenvolden, K. A., Nelson, C. H., Thor, D. R., Larsen, M. C., Redden, G. D., Rapp, J. B., and DesMarais, D. J., 1979a, Biogenic and thermogenic gas in gas-charged sediment of Norton Sound, Alaska: Proc. 11th Offshore Tech. Conf. 1, p. 479-486.

Kvenvolden, K. A. and Redden, G. D., 1980, Hydrocarbon gas in sediment from the shelf, slope, and basin of the Bering Sea: Geochim. Cosmochim. Acta, vol. 44, p. 1145-1150.

Kvenvolden, K. A., Redden, G. D., Thor, D. R., Nelson, C. H., 1981, Hydrocarbon gases in near-surface sediment of the Northern Bering Sea. In: The Eastern Bering Sea Shelf: Oceanography and Resources, vol. 1, Ed. Hood D. W. and Calder, J. A., Gov't Print. Off.

Martens, C. S., and Berner, R. A., 1974, Methane production in the interstitial waters of sulfate-depleted marine sediments: Science, 185, p. 1167-1169.

Oremland, R. S., 1975, Methane production in shallow-water, tropical marine sediments: Appl. Microbiol., no. 30, p. 602-608.

Oremland, R. S., Culbertson, C. and Kvenvolden, K. A., 1980, Microbial formation of ethylene and ethane in anoxic estuarine sediments: Abs. Ann. Meeting Amer. Soc. Microbiol., no. 118, p. 104.

Primrose, S. B. and Dilworth, M. J., 1976, Ethylene production by bacteria: Jour. General Microbiology, no. 93, p. 177-181.

Reeburgh, W. S., 1969, Observations of gases in Chesapeake Bay sediments: Limnol. Oceanog., no. 14, p. 368-375.

Vogel, T. M., Kvenvolden, K. A., and Oremland, R. S., 1980, Hydrocarbon gases in surface sediments of San Francisco Bay, California: Abs. Ann. Meet. Pac. Div. Amer. Assoc. Advancement Sci., p. 33.

Whelan, T., 1974, Methane, carbon dioxide and dissolved sulfide from interstitial water of coastal marsh sediments: Estuarine and Coastal Marine Science, no. 2, p. 407-415.

Whelan, J. K., 1979, C_1 to C_7 hydrocarbons from IPOD holes 397 and 397A: Initial Reports Deep Sea Drilling Project, 47, part 1, p. 531-539.

Whelan, J. K., Hunt, J. M., and Berman, J., 1980, Volatile C_1-C_7 organic compounds in surface sediments from Walvis Bay: Geochim. Cosmochim. Acta, no. 44, p. 1767-1785.

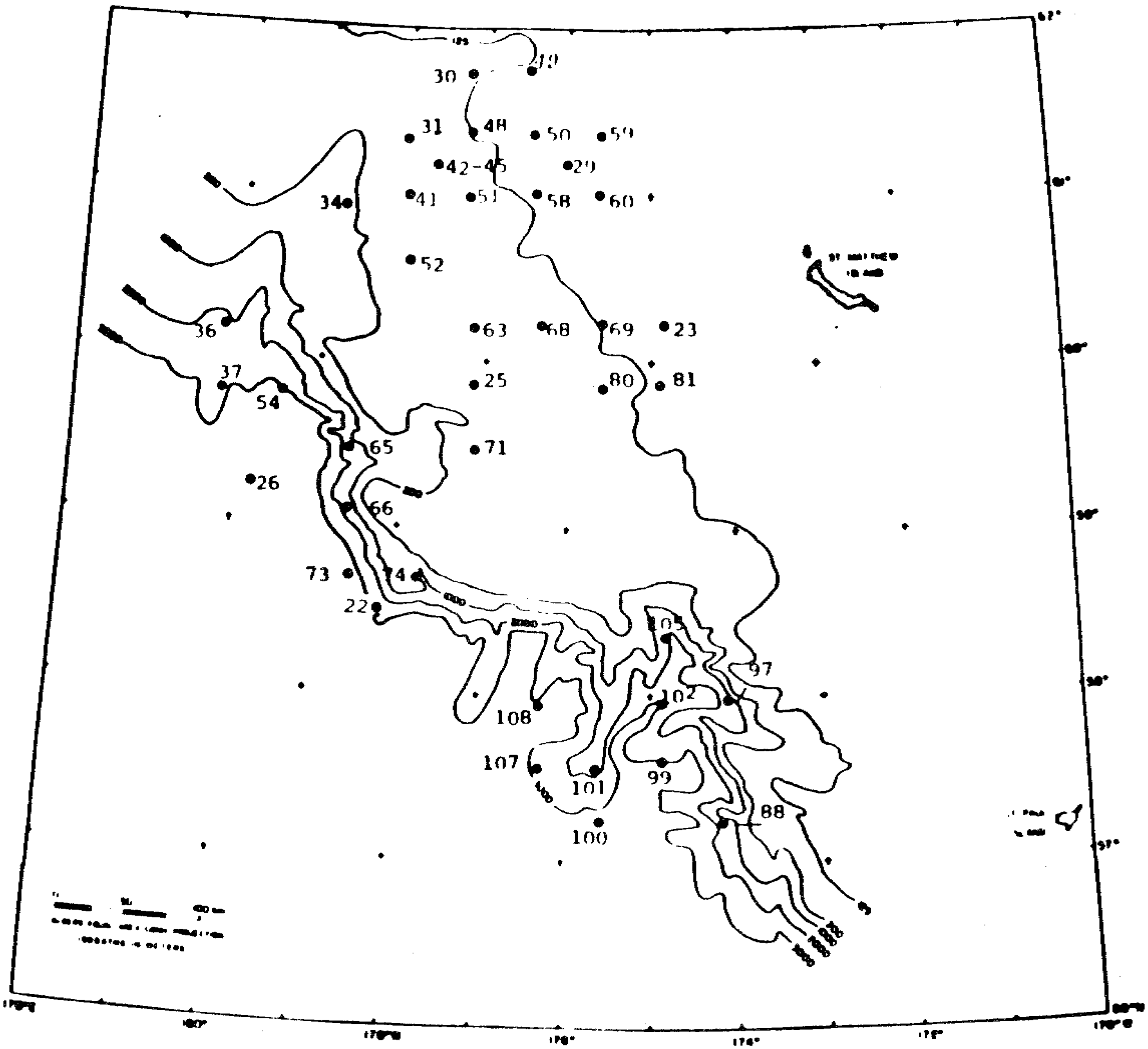

Figure 32. Map of core locations in the Navarin Basin province.

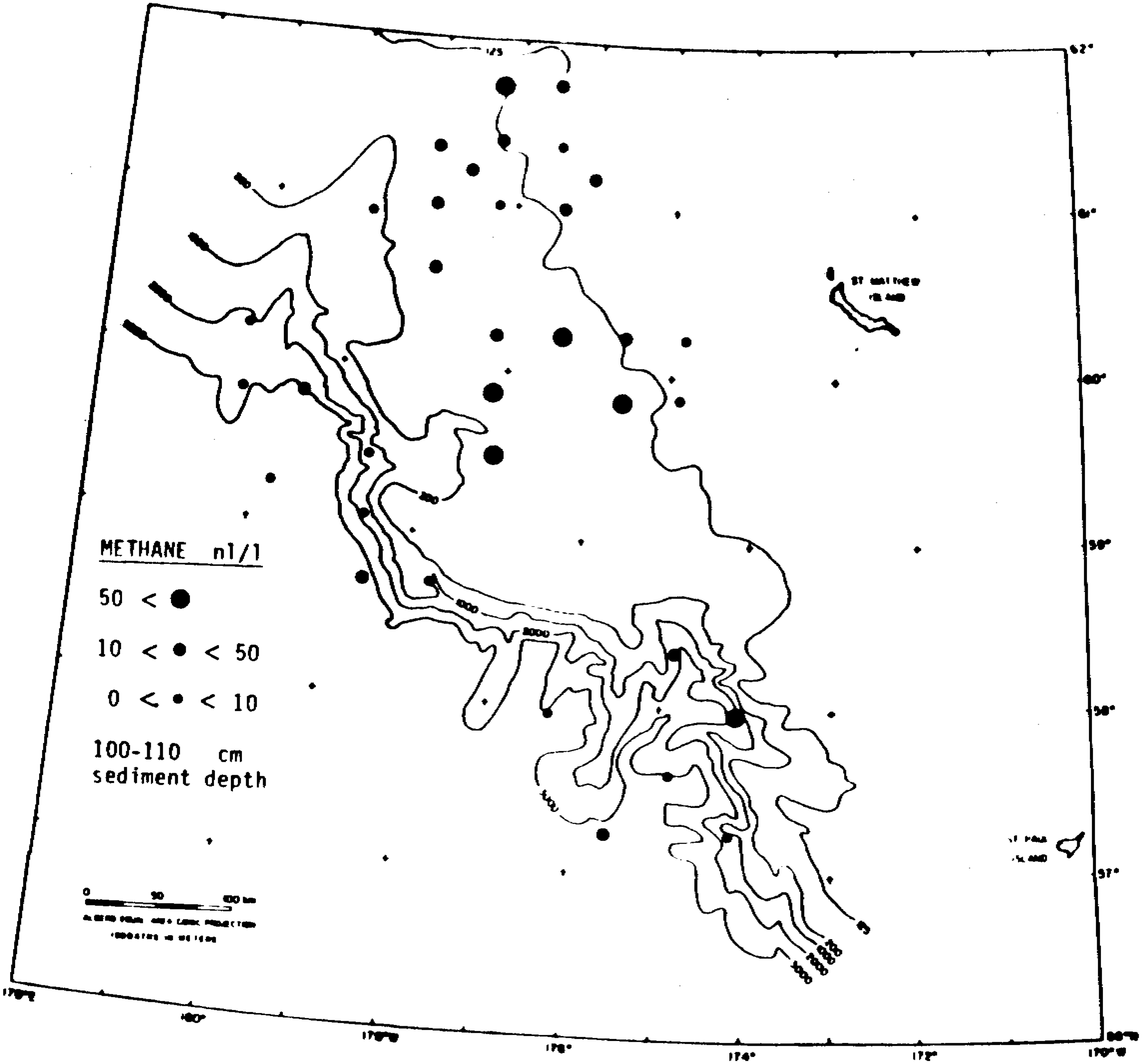

Figure 33. Distribution of methane at 100-110 cm sediment depth; reported in μl/liter of wet sediment.

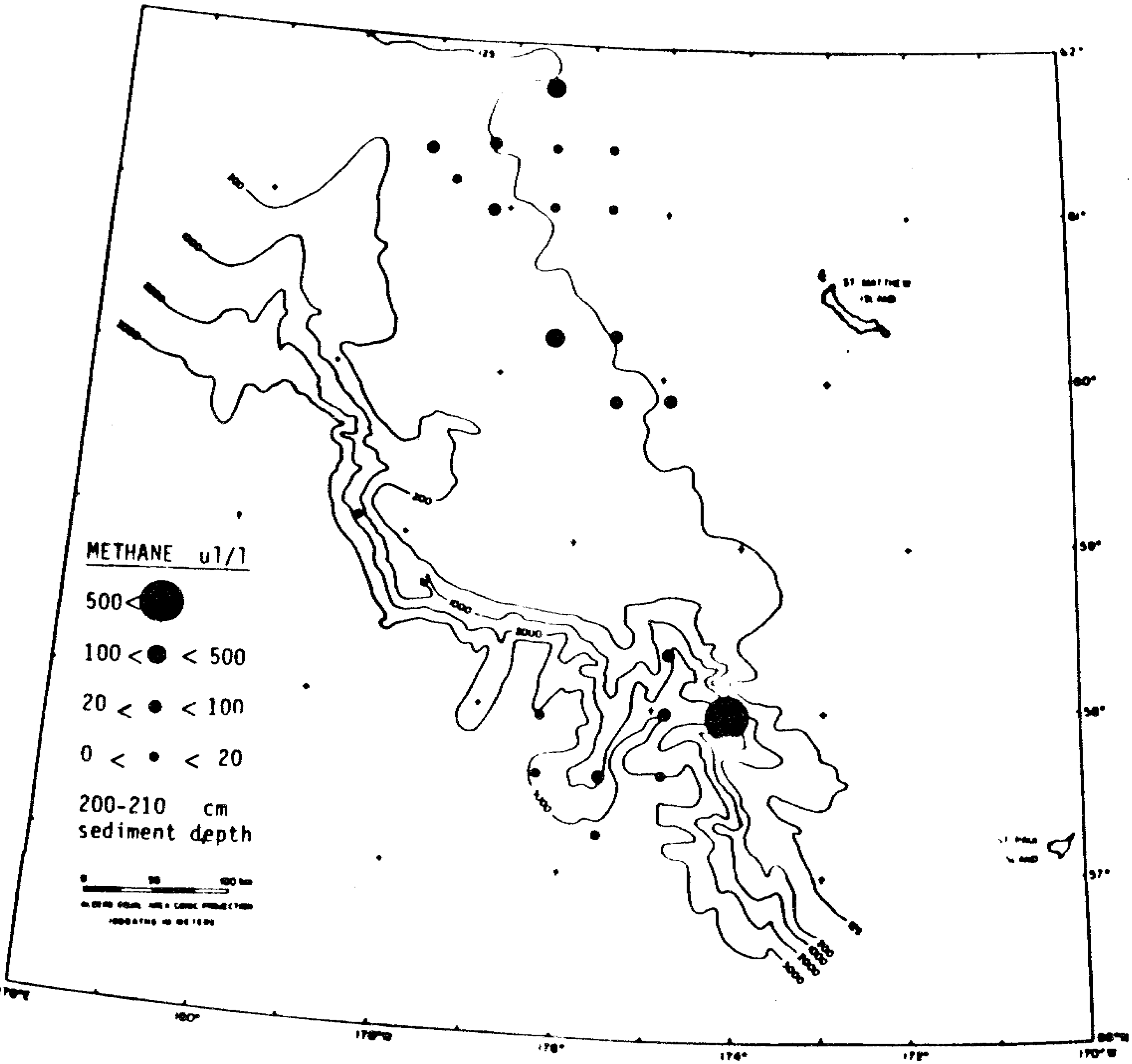

Figure 34. Distribution of methane at 200-210 cm sediment depth; reported in µl/liter of wet sediment.

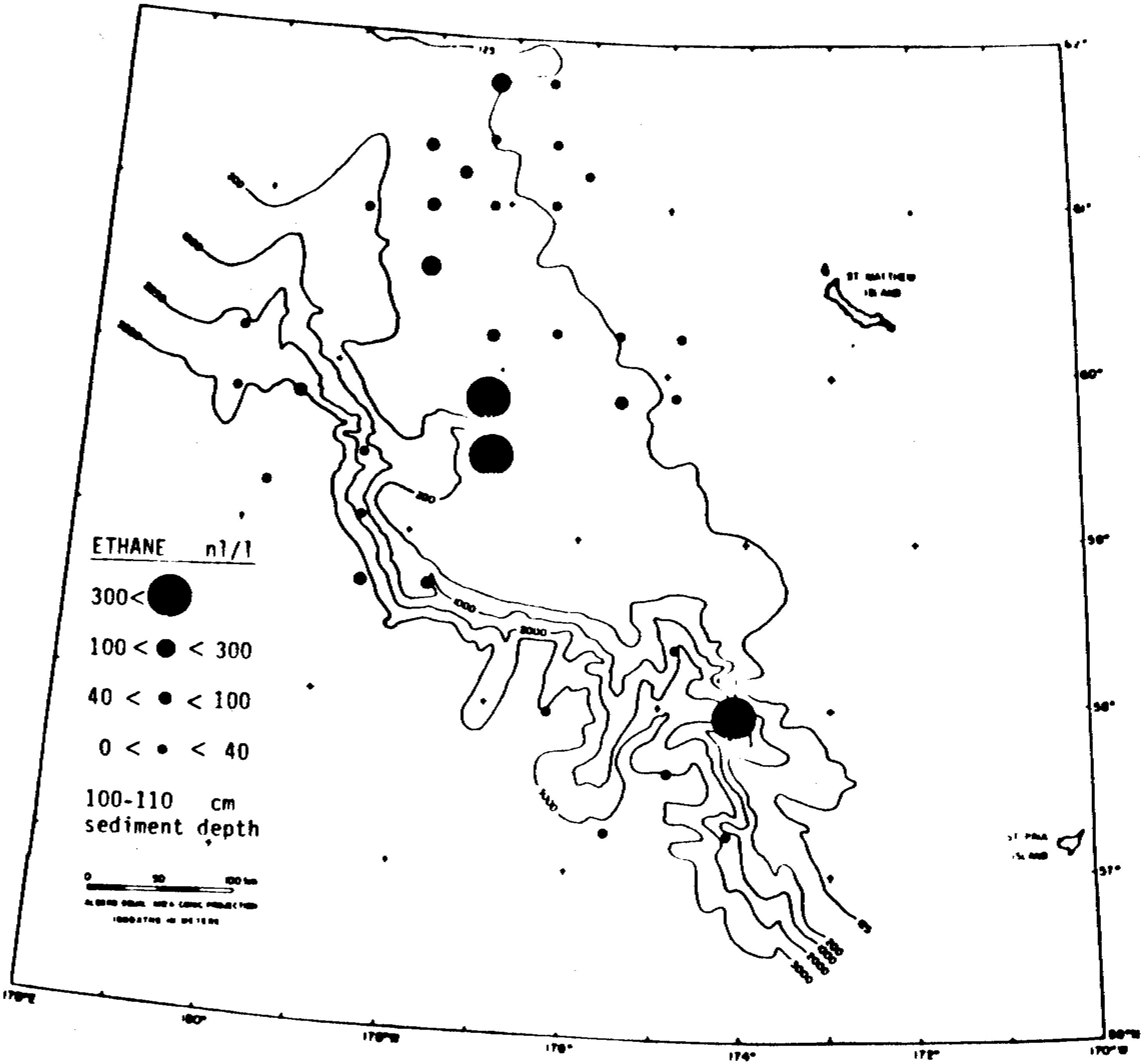

Figure 35. Distribution of ethane at 100-110 cm sediment depth; reported in nl/liter of wet sediment.

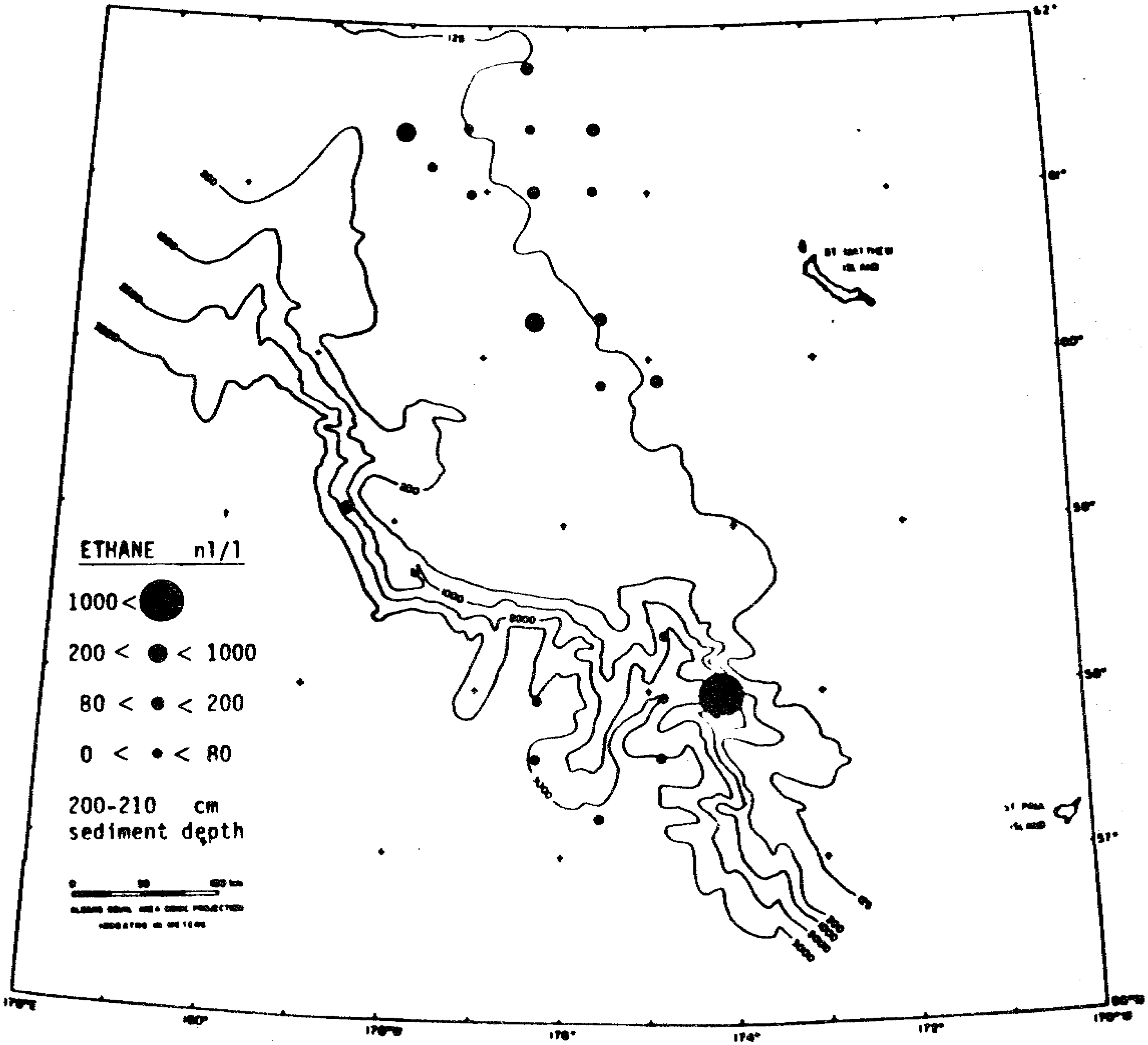

Figure 36. Distribution of ethane at 200-210 cm sediment depth; reported in nl/liter of wet sediment.

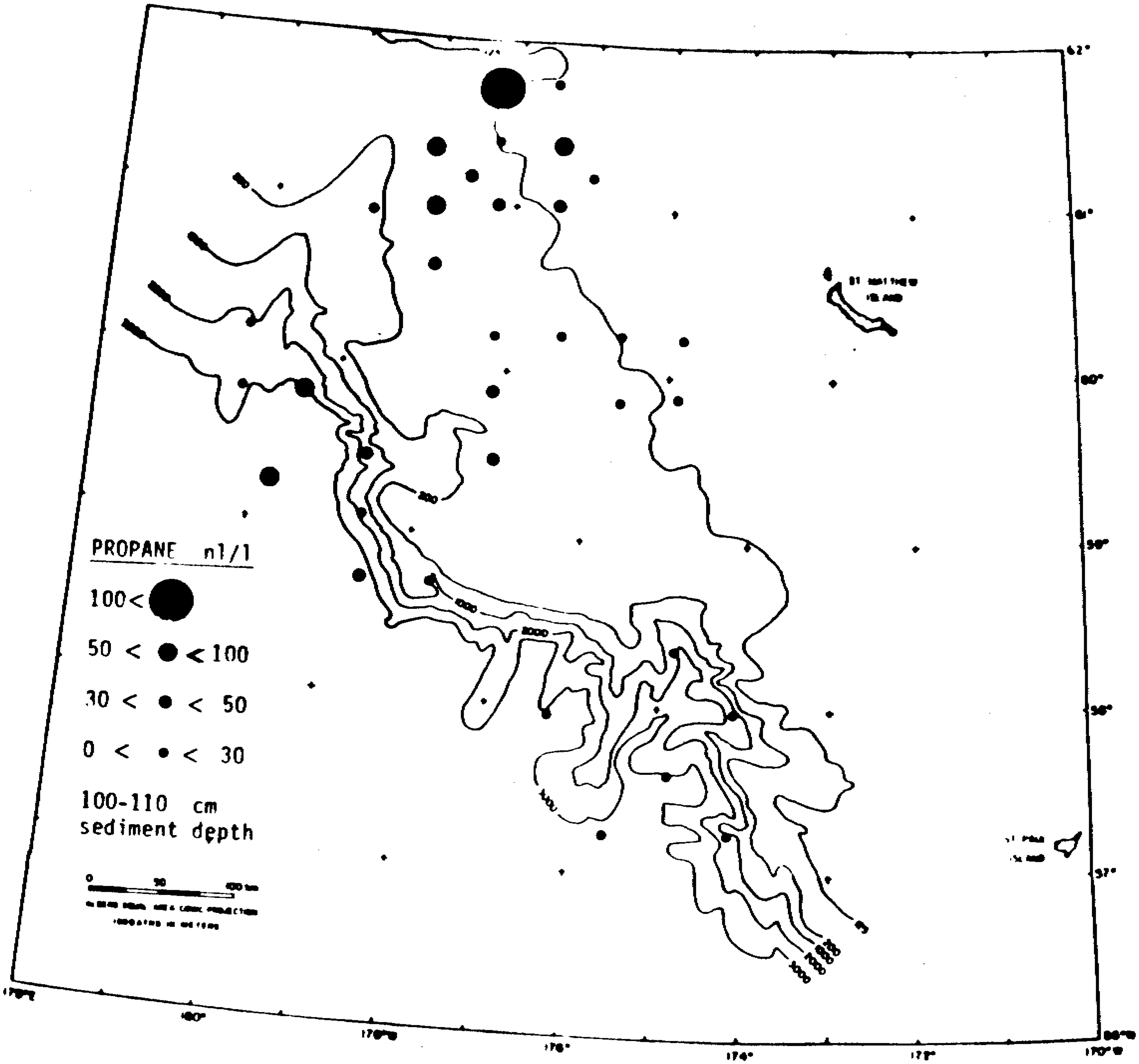

Figure 37. Distribution of propane at 100-110 cm sediment depth; reported in nl/liter of wet sediment.

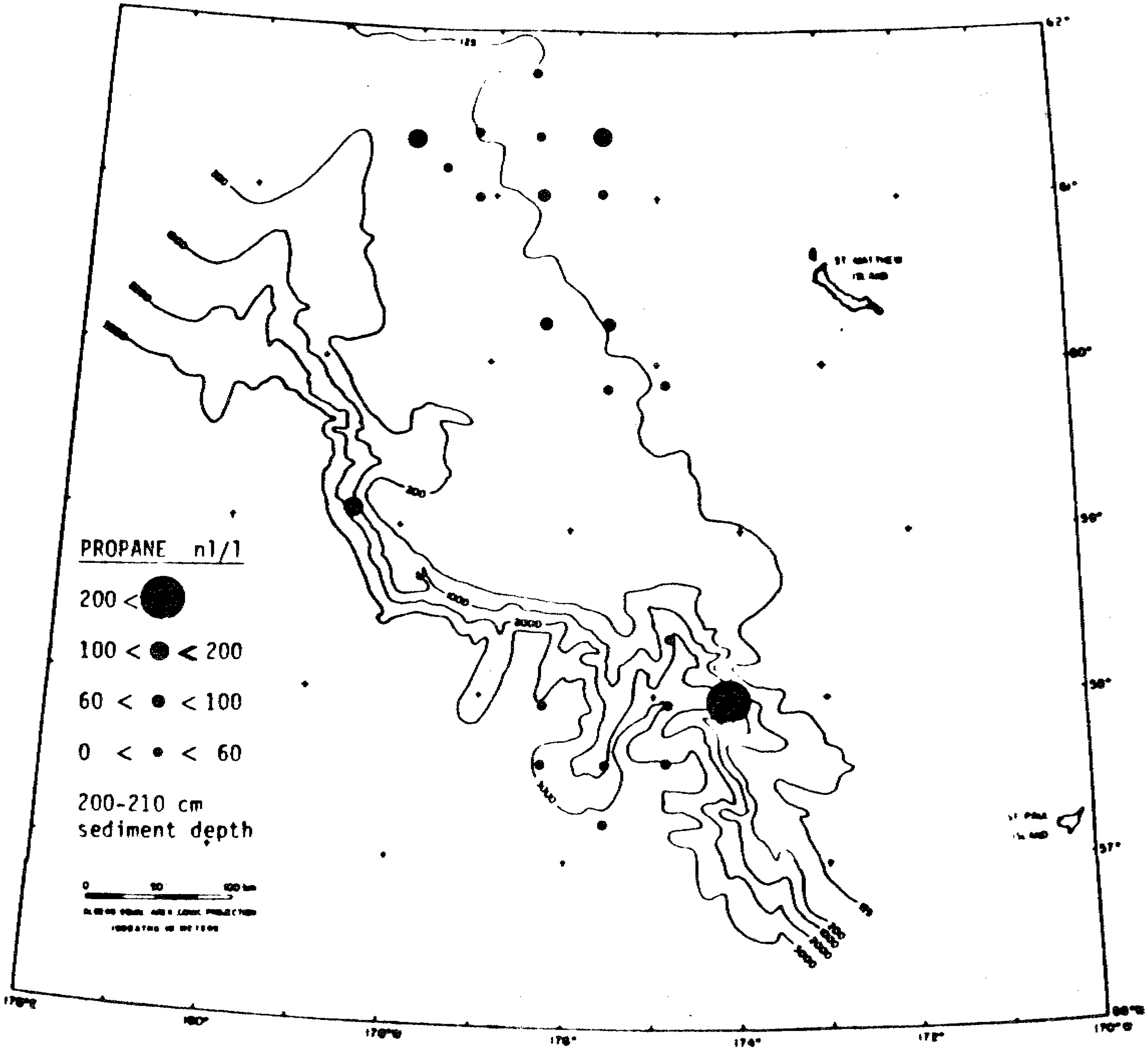

Figure 38. Distribution of propane at 200-210 cm sediment depth; reported in nl/liter of wet sediment.

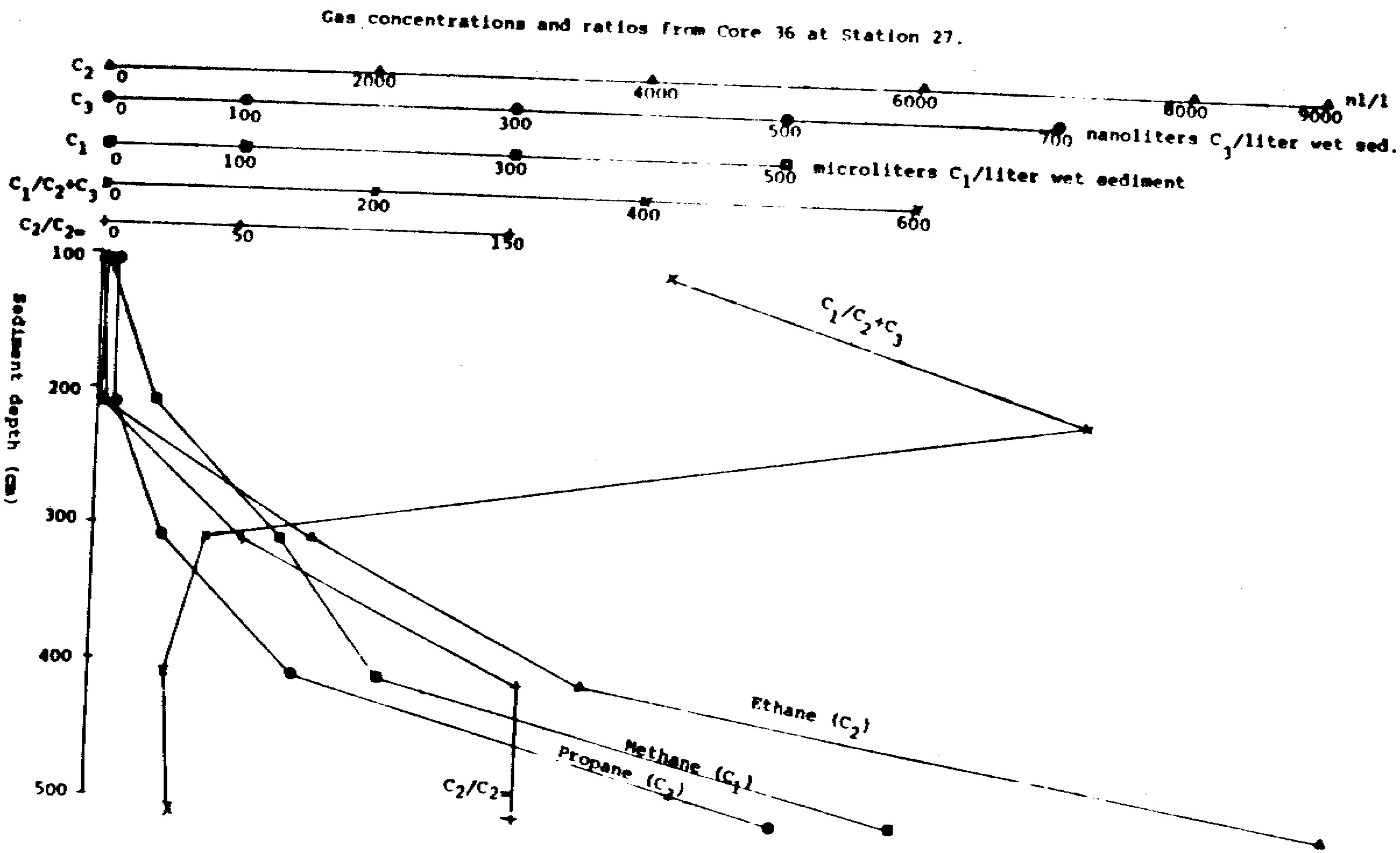

Figure 39. Graph of C_1-C_3 concentrations and C_1/C_2+C_3 and $C_2/C_{2=}$ ratios with depth in core 36.

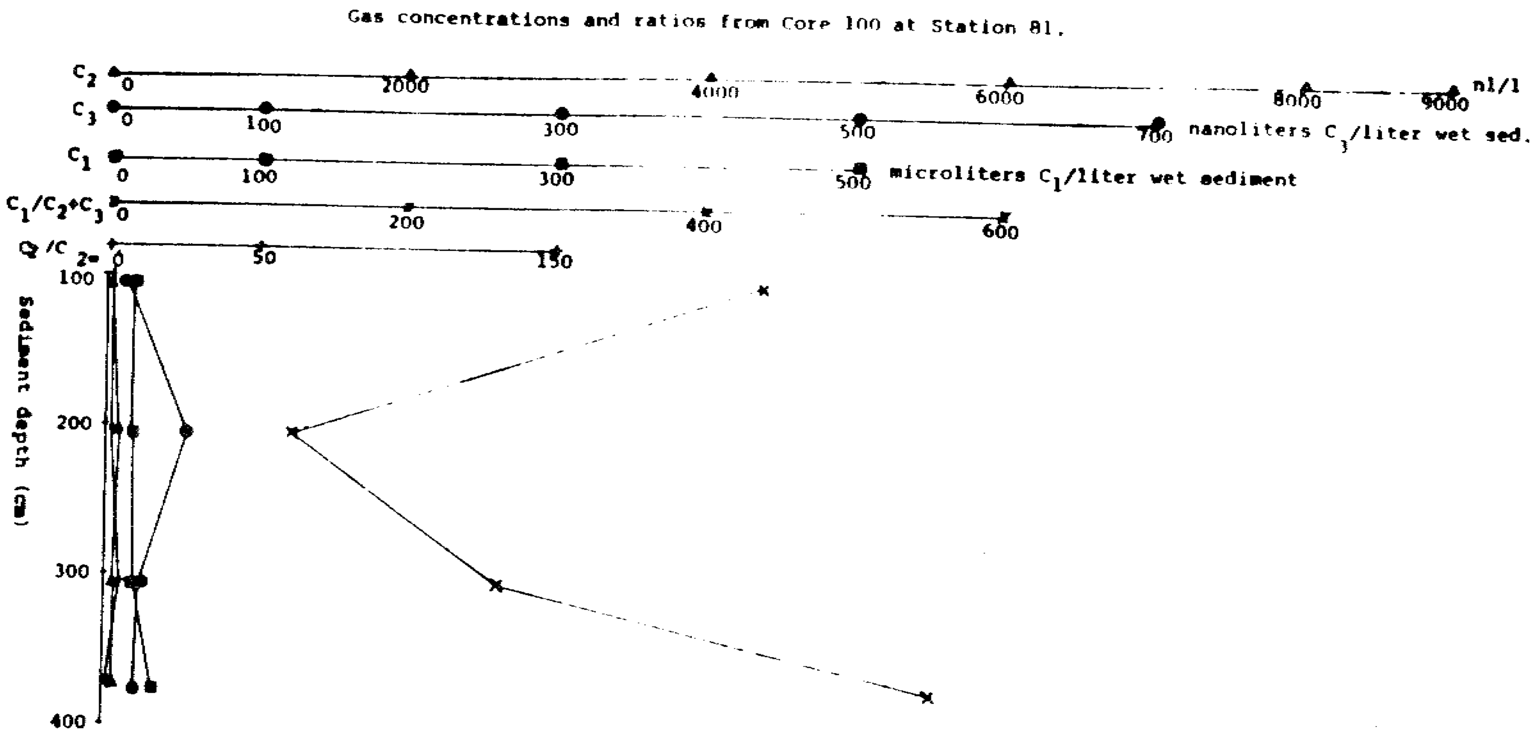

Figure 40. Graph of C_1–C_3 concentrations and C_1/C_2+C_3 and $C_2/C_{2=}$ ratios with depth in core 100. A typical type I hydrocarbon distribution.

Table 8. Hydrocarbon Gas (C_1-C_{5+}) Concentrations and Ratios from Sediment Samples from the Navarin Basin Province

Sample No. and Interval in cm	Water Depth (m)	Sta. No.	C_1 ul/l wet sed.	C_2 nl/l sed.	$C_{2:1}$	C_3	$C_{3:1}$	i-C_4	n-C_4	C_{5+}	$\frac{C_1}{C_2+C_3}$	$\frac{C_2}{C_{2:1}}$	$\frac{C_3}{C_{3:1}}$	$\frac{C_2}{C_3}$	Location Latitude	Location Longitude	Gas Type
G22 493-503	2842	16	620	8500	40	200	n.d.	10	0	0	70	200	-	40	58°29.8'	178°09.6'	III
G23 100-110	110	17	7	20	20	10	n.d.	0	0	0	190	1.2	-	2	60°14.5'	174°48.7'	I
G25 100-110	140	19	90	840	30	50	n.d.	0	6	70	100	30	-	20	59°50.8'	177°06.8'	III
G25 191-201	140	19	0	20	0	60	n.d.	0	0	20	10	-	-	0.3	59°50.8'	177°06.8'	I
G26 100-110	3373	20	7	30	20	50	n.d.	0	8	40	90	1.4	-	0.6	59°13.8'	179°43.9'	IV
G29 100-110	109	22	10	30	20	10	n.d.	0	0	0	270	1.2	-	3	61°11.4'	176°01.2'	I
G30 87-97	120	23	80	160	60	100	n.d.	6	20	20	290	3	-	2	61°43.8'	177°14.0'	III
G31 100-110	150	24	20	40	40	60	n.d.	6	8	310	170	1.0	-	0.7	61°19.9'	178°01.0'	IV
G31 200-210	150	24	30	330	160	150	120	10	8	0	70	2.0	1.3	2	61°19.9'	178°01.0'	IV
G34 100-110	210	25	7	30	30	20	n.d.	0	0	110	150	1.0	-	1.1	60°55.3'	178°46.9'	I
G34 270-280	210	25	10	60	50	20	114	0	0	0	160	1.1	0.2	3	60°55.3'	178°46.9'	I
G36 100-110	1924	27	7	6	8	10	n.d.	0	0	80	420	0.7	-	0.5	60°09.0'	179°49.0'	I
G36 200-210	1924	27	40	50	20	10	n.d.	0	0	50	730	2.0	-	5	60°09.0'	179°49.0'	I
G36 300-310	1924	27	140	1600	30	50	n.d.	0	0	30	80	50	-	32	60°09.0'	179°49.0'	III
G36 400-410	1924	27	210	3600	20	150	n.d.	0	10	30	60	160	-	24	60°09.0'	179°49.0'	III
G36 500-510	1924	27	600	9100	60	500	n.d.	8	10	440	60	160	-	18	60°09.0'	179°49.0'	III
G37 100-110	2856	28	2	0	0	0	n.d.	0	0	60	-	-	-	-	59°26.3'	179°48.3'	I
G37 431-441	2856	28	1900	1700	90	1000	0	270	20	60	700	20		2	59°26.3'	179°48.3'	III
G41 71-81	148	31	20	60	70	50	n.d.	10	10	210	130	0.9	-	1.2	60°58.3'	177°59.3'	IV
G42 100-110	141	32	20	40	40	50	n.d.	6	0	160	180	1.1	-	0.9	61°09.8'	177°37.9'	IV
G42 194-204	141	32	20	50	30	30	130	0	0	0	200	1.4	0.3	1.4	61°09.8'	177°37.9'	I
G43 100-110	148	33	10	20	30	50	n.d.	0	0	150	871	0.6	-	0.3	61°10.9'	177°36.1'	IV
G43 236-246	148	33	20	40	10	50	80	0	0	0	220	4	0.6	0.9	61°10.9'	177°36.1'	I
G44 100-110	138	34	7	20	20	0	n.d.	0	0	210	370	1.1	-		60°11.9'	177°34.2'	I
G44 190-200	138	34	10	50	60	50	120	0	0	0	100	0.8	0.5	0.9	60°11.9'	177°34.2'	I
G45 96-106	137	35	2	10	20	130	n.d.	0	0	160	20	0.7	-	0.1	61°13.1'	177°32.3'	IV
G47 74-84	134	36	1	30	0	0	n.d.	0	0	120	40		-		61°14.4'	177°30.5'	I
G48 100-110	124	37	10	30	30	20	n.d.	0	0	60	290	1.1	-	2	61°22.3'	177°13.9'	I
G48 182-192	124	37	20	50	30	30	70	0	0	0	280	1.4	0.4	2	61°22.3'	177°13.9'	I
G49 100-110		38	30	30	10	20	n.d.	0	0	50	550	2	-	2			
G49 222-232		38	100	150	30	40	80	0	0	0	530	5	0.5	4			II
G50 101-111	110	39	6	20	6	50	n.d.	0	0	120	80	3	-	0.3	61°22.3'	176°25.2'	IV
G50 208-218	110	39	10	50	20	30	50	0	0	0	150	2	0.6	2	61°22.3'	176°25.2'	I

Table 8. (Continued)

Sample No. and Interval in cm.	Water Depth (m)	Sta. No.	C_1 ul/l wet. sed.	C_2 nl/l sed.	$C_{2:1}$	C_3	$C_{3:1}$	$i\text{-}C_4$	$n\text{-}C_4$	C_{5+}	$\frac{C_1}{C_2 + C_3}$	$\frac{C_2}{C_{2:1}}$	$\frac{C_3}{C_{3:1}}$	$\frac{C_2}{C_3}$	Location Latitude	Location Longitude	Gas Type
G51 100-110	123	40	9	10	10	40	n.d.	0	0	20	160	1.1	-	0.2	60°59.2'	177°12.2'	IV
G51 207-217	123	40	30	60	30	30	80	0	0	0	300	2	0.4	2	60°59.2'	177°12.2'	I
G52 100-110	159	41	20	160	20	30	n.d.	4	0	20	100	10	-	5	60°35.6'	177°57.4'	IV
G52 167-177	159	41	80	1200	20	20	50	0	0	0	60	67	0.5	50	60°35.6'	177°57.4'	IV
G54 100-110	2929	43	20	50	50	60	n.d.	10	10	150	230	0.9	-	0.8	59°47.2'	179°25.2'	IV
G54 283-293	2929	43	60	970	130	140	40	8	10	0	60	7	4	7	59°47.2'	179°25.2'	IV
G58 100-110	118	46	10	10	20	40	n.d.	0	0	0	200	0.6	-	0.3	60°59.9'	176°24.4'	I
G58 221-231	118	46	20	80	60	60	70	0	0	0	140	1.4	0.8	1.4	60°59.9'	176°24.4'	I
G59 210-220	99	47	6	120	260	160	80	10	30	0	20	0.5	2	0.8	61°22.4'	175°39.3'	IV
G60 100-110	106	48	3	10	10	10	n.d.	0	0	0	150	1.0	-	1.0	61°00.1'	175°35.7'	I
G60 195-205	106	48	10	60	70	30	90	0	0	0	130	0.8	0.4	2	61°00.1'	175°35.7'	I
G61 100-110	125	49	1	0	0	0	n.d.	0	0	0	-	-	-	-	60°36.8'	176°23.4'	I
G61 230-240	125	49	40	90	80	60	90	0	6	0	290	1.1	0.7	2	60°36.8'	176°23.4'	I
G63 100-110	150	50	40	50	30	30	n.d.	6	6	0	470	2	-	2	60°12.7'	177°08.8'	II
G63 174-184	150	50	60	220	300	100	130	0	0	0	190	0.7	0.8	2	60°12.7'	177°08.8'	IV
G65 100-110	1609	52	3	30	40	40	n.d.	0	0	0	40	0.8	-	0.9	59°26.4'	178°35.9'	IV
G65 171-181	1609	52	40	90	60	30	130	0	0	0	350	2	0.2	4	59°26.4'	178°35.9'	I
G66 100-110	1336	53	3	20	20	20	n.d.	0	0	0	70	1.3	-	1.2	58°3.9'	178°34.7'	I
G66 200-210			4	140	170	110	120	10	0	0	20	0.9	0.9	1.4			IV
G66 300-310			4	130	130	90	90	0	10	0	20	1.0	1.0	1.4			IV
G66 400-410			8	140	30	40	70	0	0	0	40	6	0.7	3			IV
G66 520-530	1336	53	8	190	20	170	90	8	0	0	20	12	2.0	1.1	58°3.9'	178°34.7'	IV
G68 100-110	132	56	90	30	30	10	n.d.	0	0	0	2000	1.0	-	3	60°13.8'	176°20.9'	II
G68 149-159	132	56	90	110	50	40	100	0	0	0	590	2.0	0.5	2	60°13.8'	176°20.9'	IV
G69 100-110	117	58	10	10	10	20	n.d.	0	0	0	330	0.8	-	0.5	60°14.2'	175°35.5'	I
G69 193-203	117	58	40	110	60	70	130	0	0	0	230	1.7	0.6	2	60°14.2'	175°35.5'	IV
G70 198-208	142	59	160	380	30	70	150	10	0	0	360	13	0.5	6	59°51.3'	176°20.5'	III
G71 95-105	151	60	50	330	50	40	n.d.	4	8	0	140	6	-	9	59°28.0'	177°05.6'	III
G73 100-110	3170	62	20	90	50	40	n.d.	6	8	170	140	2.0	-	3	58°40.9'	178°32.2'	IV
G74 100-110	950	63	5	50	40	30	n.d.	8	8	0	60	1.3	-	2	58°42.3'	177°47.2'	I
G74 168-178	950	63	260	3000	30	60	240	0	0	0	80	110	0.3	50	58°42.3'	177°47.2'	III
G80 110-120	128	66	50	70	20	30	90	0	0	0	440	3	0.3	3	59°51.2'	175°34.3'	I
G81 100-110	117	67	5	10	0	10	n.d.	0	0	0	280	-	-	1.0	59°52.4'	174°52.8'	I
G81 199-209	117	67	30	100	30	50	140	0	0	0	180	3	0.4	2	59°52.4'	174°52.8'	I
G83 225-235	105	68	7	40	50	40	120	8	0	0	90	0.9	0.4	1.1	57°56.1'	171°56.7'	I

Table 8. (Continued)

Sample No. and Interval in cm.	Water Depth (m)	Sta. No.	C_1 ul/l wet sed.	C_2 nl/l sed.	$C_{2:1}$	C_3	$C_{3:1}$	$i\text{-}C_4$	$n\text{-}C_4$	C_{5+}	$\frac{C_1}{C_2 + C_3}$	$\frac{C_2}{C_{2:1}}$	$\frac{C_3}{C_{3:1}}$	$\frac{C_2}{C_3}$	Location Latitude	Location Longitude	Gas Type
G88 100-110	1252	72	2	10	30	10	n.d.	0	0	40	90	0.4	-	1.0	57°13.7'	174°09.8'	I
G97 100-110	1570	79	70	380	20	30	n.d.	0	0	180	180	25	-	15	57°58.6'	174°07.1'	IV
G97 192-202	1570	79	860	1360	40	220	110	30	10	0	550	35	2	6	57°58.6'	174°07.1'	III
G99 100-110	3075	80	8	20	30	10	n.d.	0	0	10	270	0.7	-	1.3	57°35.7'	174°52.5'	I
G99 200-210	3075	80	10	20	10	20	20	0	0	0	270	2	0.8	1.4	57°35.7'	174°52.5'	I
G99 300-310	3075	80	10	30	20	20	40	0	0	0	250	1.3	0.4	1.5	57°35.7'	174°52.5'	I
G99 398-408	3075	80	9	40	30	30	90	0	0	0	140	1.4	0.3	1.5	57°35.7'	174°52.5'	I
G100 100-110	3232	81	20	20	30	10	n.d.	0	0	120	440	0.7	-	1.4	57°13.5'	175°34.0'	I
G100 200-210	3232	81	20	80	40	50	70	6	10	0	120	2	0.8	1.4	57°13.5'	175°34.0'	I
G100 300-310	3232	81	20	50	10	20	30	0	0	0	260	4	0.7	2	57°13.5'	175°34.0'	I
G100 372-382	3232	81	30	40	30	20	90	0	0	0	550	1.3	0.2	2	57°13.5'	175°34.0'	I
G101 207-217	2155	82	20	90	20	30	60	0	0	0	170	4	0.4	3	57°36.5'	175°34.2'	I
G101 309-319	2155	82	50	230	30	40	100	0	0	0	180	9	0.4	6	57°36.5'	175°34.2'	IV
G102 211-221	2960	83	70	60	30	30	60	0	0	0	860	2	0.5	2	57°58.5'	174°51.4'	II
G105 100-110	2050	86	30	40	40	20	n.d.	0	10	90	540	0.9	-	2	58°20.9'	174°50.3'	II
G105 200-210	2050	86	40	70	40	30	90	0	0	0	410	2	0.3	3	58°20.9'	174°50.3'	I
G105 300-310	2050	86	50	160	130	120	140	0	20	8	170	1.2	0.8	1.4	58°20.9'	174°50.3'	IV
G107 100-110	2750	88	10	230	490	190	230	30	30	20	20	0.5	0.8	1.2	57°36.3'	176°16.5'	IV
G107 200-210	2750	88	20	200	660	200	230	20	40	30	20	0.3	0.9	1.0	57°36.3'	176°16.5'	IV
G108 100-110	3253	89	4	20	90	10	n.d.	0	0	120	120	0.2	-	2	57°57.1'	176°17.7'	I
G108 200-210	3253	89	10	30	40	40	90	0	0	0	190	0.9	0.5	0.8	57°57.1'	176°17.7'	I
G108 300-310	3253	89	20	90	70	70	90	0	0	0	100	1.3	0.8	1.3	57°57.1'	176°17.7'	I
G109 100-110	610	90	6	70	40	60	90	0	0	0	50	2	0.6	1.3	58°20.9'	175°33.8'	I

n.d.= not determined

Table 9. CLASSIFICATION OF SEDIMENT GAS TYPES

	TYPE I	TYPE II	TYPE III	TYPE IV
METHANE	LOW	HIGH	HIGH	VARIABLE
ETHANE	LOW	LOW	HIGH	VARIABLE
PROPANE	LOW	LOW	HIGH	VARIABLE
ETHENE	LOW	VARIABLE	LOW	LOW
PROPENE	LOW	VARIABLE	LOW	LOW
ISOBUTANE	LOW	LOW	LOW	LOW
N-BUTANE	LOW	LOW	LOW	LOW
C_1/C_2+C_3	VARIABLE	HIGH	LOW	VARIABLE
$C_2/C_{2=}$	LOW	LOW	HIGH	VARIABLE

DIATOMS FROM LATE QUATERNARY SEDIMENTS FROM THE NAVARIN BASIN PROVINCE

Jack G. Baldauf

INTRODUCTION

Diatoms are difficult to use as biostratigraphic indicators because no extinctions or first occurrences exist younger than 0.26 m.y., therefore, it is necessary to use fluctuations in abundance of commonly occurring species, such as Denticulopsis seminae and Nitzschia oceanica, to identify the glacial and interglacial stages of the late Quaternary and the probable Holocene/Pleistocene boundary.

METHODS AND PROCEDURE

Strewn slides of unproccesed sediment were prepared for each sample. Near top and bottom samples of each core were scanned at 500 x for age-related species. Samples from 30 core tops were used to establish the modern ecological distribution and samples taken at 15 cm intervals down two cores were used for down-core studies (Fig. 41). Strewn slides were examined in detail at 1,250 x, and the first 300 specimens encountered were tabulated to determine the abundance of individual species within each sample.

The quality of preservation for each sample was based on the absence and presence of selected diatoms. Fine, delicate species such as Thalassiosira hyalina, Thalassiothrix longessima, and Pseudopodosira elegans, were used to determine well preserved samples, whereas the presence of only heavily-silicified forms such as Coscinodiscus marginatus, C. radiatus and Rhizosolenia hebatata forma. hebatata, suggest poor preservation.

RESULTS

Cores recovered from this region were examined and all except Core 106 contain late Quaternary diatoms. Core 106 is assigned to the Denticulopsis seminae var. fossilis - D. kamtschatica Zone of Barron (1980) and is equivalent in age to the early late Pliocene. Occurrence of Pliocene sediments within this core is not surprising, because the core is located on the continental slope where down-slope transport may be a common phenomenon.

Table 10 shows the occurrences of species encountered during the examination of the surface samples. The assemblages composed of planktic and tychopelagic species (See Plate 1), represent the Arctoboreal and North Boreal diatom complexes of Jouse (1971). The abundance of individual taxa remains fairly constant throughout the study area, with the exception of Denticulopsis seminae and Nitzschia oceanica. These two species alternate in their dominance of the two identified assemblages. D. seminae comprises 22 to 40 percent of the assemblage in areas where water depths are greater than 2800 m (Fig. 42). This abundance rapidly decreases to 10 to 20 percent near the shelf break at approximately 200 m water depth, and only to 1 to 10 percent in sediment from water depths less than 200 m. This distribution pattern agrees well with the pattern described by Sancetta (in press) for the entire Bering Sea. Nitzschia oceanica is the other common diatom species within the Navarin Basin surface sediment. This species is abundant in sediment from the shallow shelf in the northwestern portion of the study area where it composes approximately 25 percent of the assemblage (Fig. 43). The abundance of N. oceanica gradually decreases southward, across the continental slope to the deeper regions where it comprises 7-15 percent of the assemblage. This pattern of abundance is consistent with previous studies by Jouse (1962, 1967), Hasle (1965), and Kozlova and Mukhina (1967) and Sancetta (in press) who all found N. oceanica to be common in the Arctic coastal waters as well as in coastal regions of the Bering Sea. In addition, Gran (1904), Homer and Alexander (1972), and Sancetta (in press) concluded that N. oceanica is associated with ice-covered areas where ice exists for a period of at least six months.

The boundary between dominance of the floras by N. oceanica and D. seminae in surface samples closely coincides with the shelf break (Fig. 44). The southern zone, dominated by D. seminae, is confined to the Aleutian basin region, whereas the shelf zone is dominated by N. oceanica, and corresponds to the extent of ice distribution in the Bering Sea (Park and others, 1974).

The present day distribution of diatoms within surface sediments of Navarin Basin provides a foundation for ecological interpretations of diatom assemblages from stratigraphic samples. All intervals examined from Cores 13 and 26 contain diatoms of the late Quaternary Denticulopsis seminae Zone of Barron (1980). The stratigraphic assemblages are similar to those of surface samples and are dominated by D. seminae or N. oceanica with an occasionally common occurrence of Thalassiosira gravida (Fig. 45). However, in Core 26, at the intervals 231 cm and 300 cm, rare specimens of Rhizosolenia curvirostris and Thalassiosira nidulus occur, that suggest the sediment is slightly older. Well-preserved diatoms of the D. Seminae Zone exist below these two intervals, which suggests that specimens within the intervals of 231 cm and 300 cm are reworked.

Sediments in the upper 232 cm of Core 13 located in 2962 m of water are dominated by D. seminae. Denticulopsis seminae composes approximately 25 percent of the assemblage in this interval and is similar to the abundance within the surface samples. The abundance of D. seminae sharply decreases at 232 cm as the abundances of N. oceanica and T. gravida increase. This dominance of N. oceanica and T. gravida continues to the base of the core at 290 cm.

A similar pattern exists in the top 230 cm of core 26 taken in 3377 m of water. The remaining samples in core 26 show a brief increase, at 250 cm in the number of D. seminae and a decrease in the abundance of N. oceanica and T. gravida prior to the overall domination of N. oceanica and T. gravida. Minor fluctuations in the three taxa exist within the upper 227 cm but may in part result from downslope transport from Navarinsky and Pervenets Canyons, which have submarine fans that intersect near the location of core 26.

The distribution of N. oceanica in surface samples suggest this species represents a cold-water form associated with ice, whereas the distribution of

D. seminae suggests it represents a true oceanic form associated with cool waters. It is therefore possible to use this pattern to interpret the stratigraphic occurrences of dominant N. oceanica over D. seminae in cores 13 and 26 as a record of the last glacial event in the Bering Sea. Consequently, the Holocene/Pleistocene boundary may be placed immediately above the interval.

The abundance of Thalassiosira gravida, which mimics the abundance of N. oceanica throughout the core, supports this conclusion. T. gravida is a coarse, well-silicified species associated with conditions on the shelf and upper slope. Lowered sea level during a glacial stage exposes broad areas of the continental shelf to erosion and results in increased downslope transport of sediments. Concentrations of frustules of T. gravida occur at 231 cm in core 13, and 227 cm in core 26 and can be interpreted to correlate with a marine regression. The lithology of the cores lends further support to the interpreted glacial/interglacial transition. Both cores are predominately mud; however, in core 13, from 227 to 237 cm, and in core 26, from 223 to 230 cm, an interval of pebbles, gravels and shell fragments occurs. These coarse grain layers probably represent lag deposits. The top of these intervals occur exactly where the reversal of the diatom species takes place.

If the change-over in dominance of D. seminae and N. oceanica is assumed to represent the end of the last glacial event at about 11,000 years ago, then an average sedimentation rate of 22 cm/10^3 years is found in cores 13 and 26. This average sedimentation rate agrees with those calculated by Knebel and others (1974), who reported an approximate accumulation rate of 34 cm/10^3 years based on radio-carbon data.

To determine whether the D. seminae-N. oceanica reversal is a local event restricted to the immediate area, or if it can be reproduced in other areas of the Bering Sea, samples at 10 cm intervals were taken from a gravity core S3-77 6G1) recovered from the Aleutian Basin (Gardner, et al., in press). Diatom abundance data from these samples are also shown in Figure 45. The results from core 6G1 are similar to those obtained from cores 13 and 26 but suggest a lower sedimentation rate. The abundance of D. seminae in the upper 25 cm of 6G1 is 25 to 30 percent, followed down-core by a dominance of N. oceanica. A brief increase at approximately 60 cm occurs in D. seminae, a feature that also occurs in core 26. If the Holocene/ Pleistocene boundary is placed at 25 cm, this gives an average sedimentation rate of 2.25 cm/1000 years. The brief increase of D. seminae at 60 cm would reflect a warming trend that occurred about 25,000 y BP preceded by glacial conditions at about 29,000 y.BP.

CONCLUSION

Diatoms can be used to recognize glacial and interglacial events in late Quaternary sediments and allow recognition of the Holocene/Pleistocene boundary.

Cores within the study area are characterized by an assemblage dominated by D. seminae and relatively minor numbers of N. oceanica and T. gravida in the upper section of the cores. This is followed down core by an interval where D. seminae abruptly decreases in abundance and is replaced by N. oceanica and T. gravida. This reversal is interpreted to define the Holocene/Pleistocene boundary at 11,000 y BP.

ACKNOWLEDGEMENTS

Paul Carlson and Herman Karl directed the surface and subsurface sampling within the Navarin Basin. Special thanks are given to John Barron for providing valuable assistance throughout the study, and to Kristin McDougall, John Barron and Jim Gardner for reviewing the manuscript.

REFERENCES CITED

Barron, J. A. 1980, Lower Miocene to Quaternary diatom fiostratigraphy of Leg 57, off northeastern Japan, Deep Sea Drilling Project; in Honza, E. and others, Initial Reports of the Deep Sea Drilling Project Volume LVI, LVII, Washington (U.S. Goverrment Printing Office). pp. 641-685.

Gardner, J. V., Dean, W. E., Klise, D. L., and Baldauf, J. G., in press, A climate-related oxidizing event in deep-sea sediment from the Bering Sea: Quaternary Research.

Gran, H. H., 1904, Diatomaceae from the ice-floes and plankton of the Arctic Ocean. In: F. Hansen (Editor), The Norwegian North Polar Expedition 1893-1896, IV: 1-74.

Hasle, G. R., 1965, Nitzchia and Fragilariopsis species studies in the light and electron microscopes. III The genus Fragilariopsis. Skrift. Norske videns.-Atkad. Oslo., Math.-Natur. Kl. 21 (n.s.): 1-47.

Horner, R. A. and Alexander, V., 1972, Algal populations in Arctic sea-ice: An investigatir of heterotrophy. Limnology and Oceanography 17:454-458.

Jouse, A. P., 1962. (Stratigraphic and Paleogeographic Investigations in the North-west Part of the Pacific Ocean). In Russian. Oceanol. Inst., Akad. Nauk, SSR, Moscow. 258 pp.

Jouse, A. P.,1967, Diatom floras and the history of Okhotsk and Bering Seas. In: D. Hopkins (Editor), The Bering Land Bridge. Standford University Press, Standford, California. pp. 369-372.

Jouse, A. P.,1971, Diatoms in Pleistocene sediments from the northern Pacific Ocean. In: Riedel, W. R. and Funnell B. M. (Eds.) The Micropaleontology of Oceans, Cambridge Univ. Press, Oxford. 407-421.

Knebel, H., Creager, J., and Echols, R., 1974, Holocene sedimentary framework, east-central Bering Sea continental shelf., in Herman, E. (ed.) Marine geology and oceanography of the Arctic Seas, Springer-Verlas, New York 1974, pp. 157-172.

Kozlova, O. G. and Mukhina, V. V., 1967, Diatoms and silicoflagellates in suspension and floor sediments of the Pacific Ocean: Internat. Geol. Rev. 9:1322-1342.

Lisitsyn, A. P., 1966, Recent sedimentation in the Bering Sea: Israel Program Sci. Transl., Jerusalem. Washington, D. C.: U.S. Department of Commerce, National Science Foundation, 614 pp.

Park, P. K., Gordon, L. I., and S. Alvarez-Borrego, 1974, Carbon dioxide systems of the Bering Sea In: D. W. Hood and E. J. Kelley (Editors) Oceanography of the Bering Sea, Institute of Marine Sciences, University of Alaska, Fairbanks, pp. 107-148.

Sancetta, C. (In press), Taxonomy and distribution of diatom in surface sediments of the Bering and Okhotsk Seas.

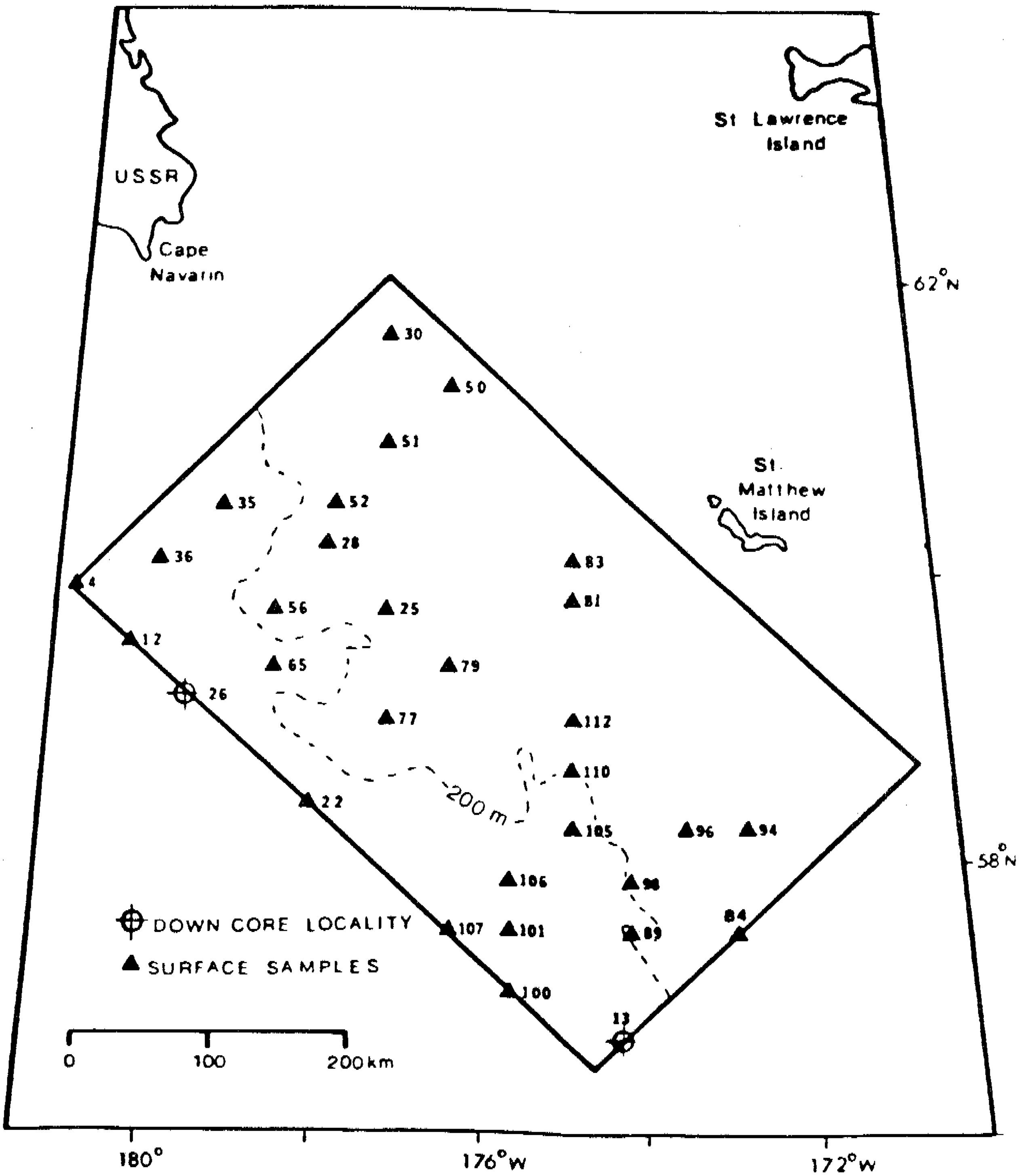

Figure 41. Location of surface samples and cores used for studies.

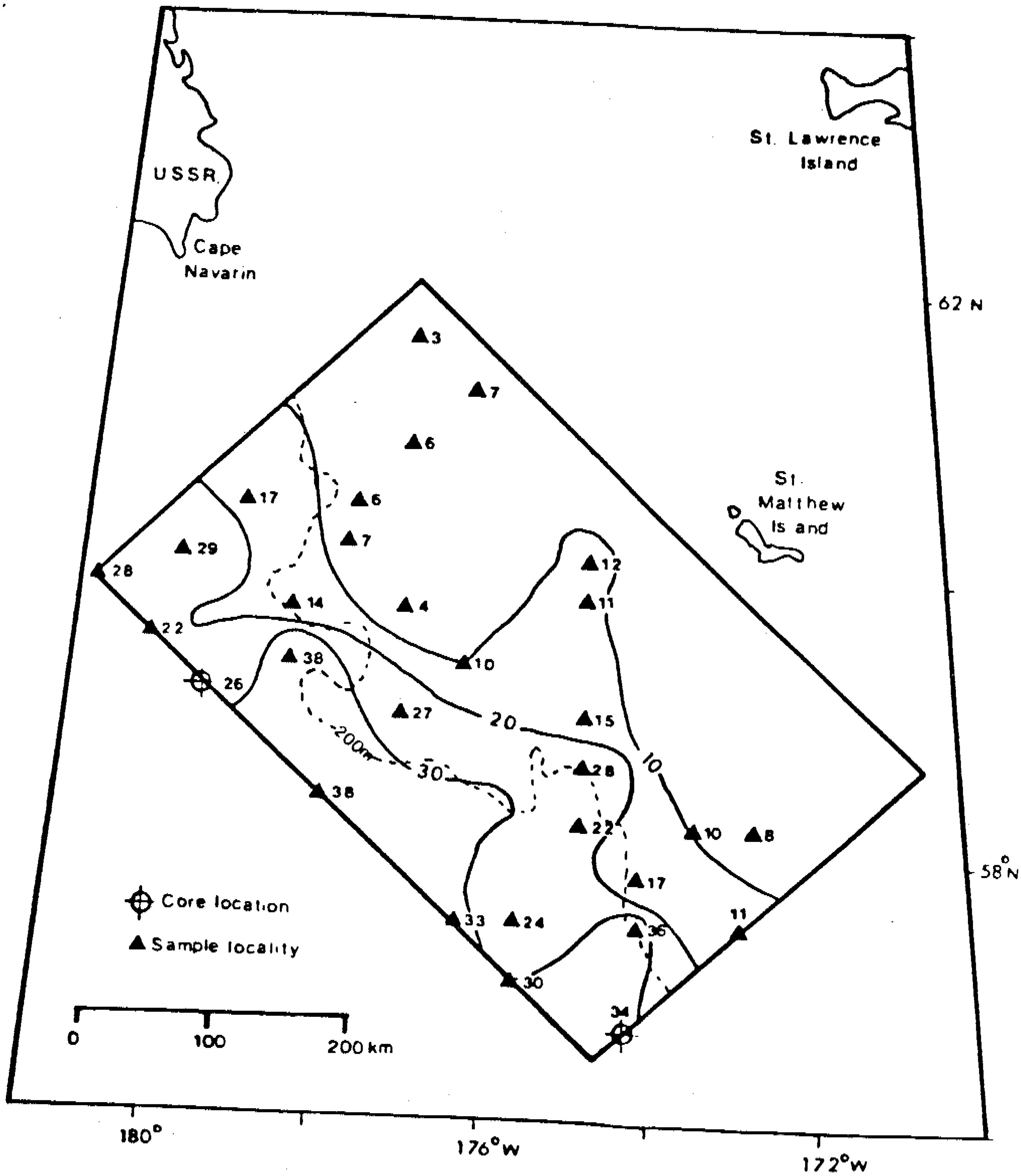

Figure 42. Distribution of Denticulopsis seminae in the surface sediments. Contours represent values of 10, 20 and 30 percent.

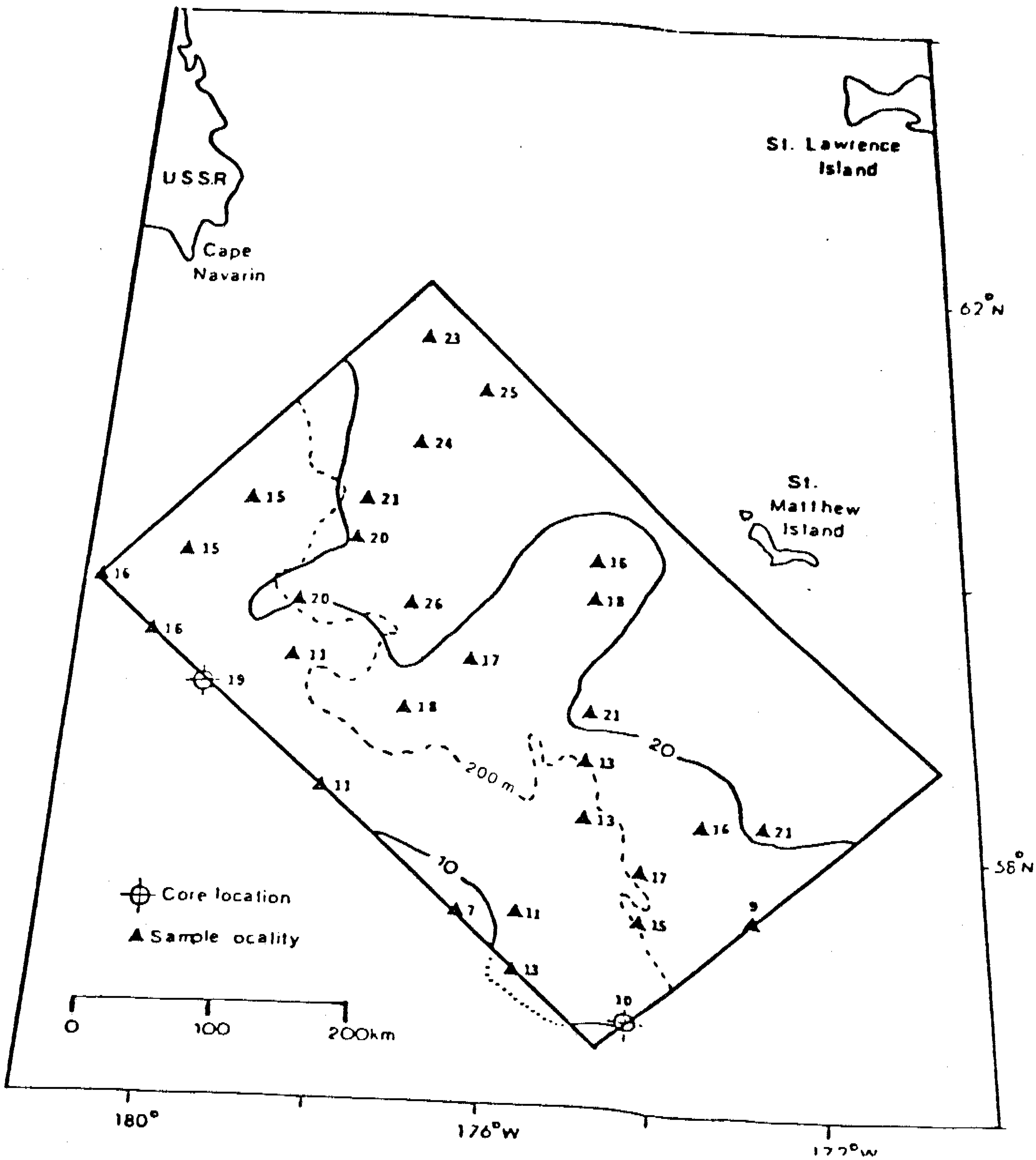

Figure 43. Distribution of Nitzschia oceanica in the surface sediments. Contours represent values of 10, 20, and 30 percent.

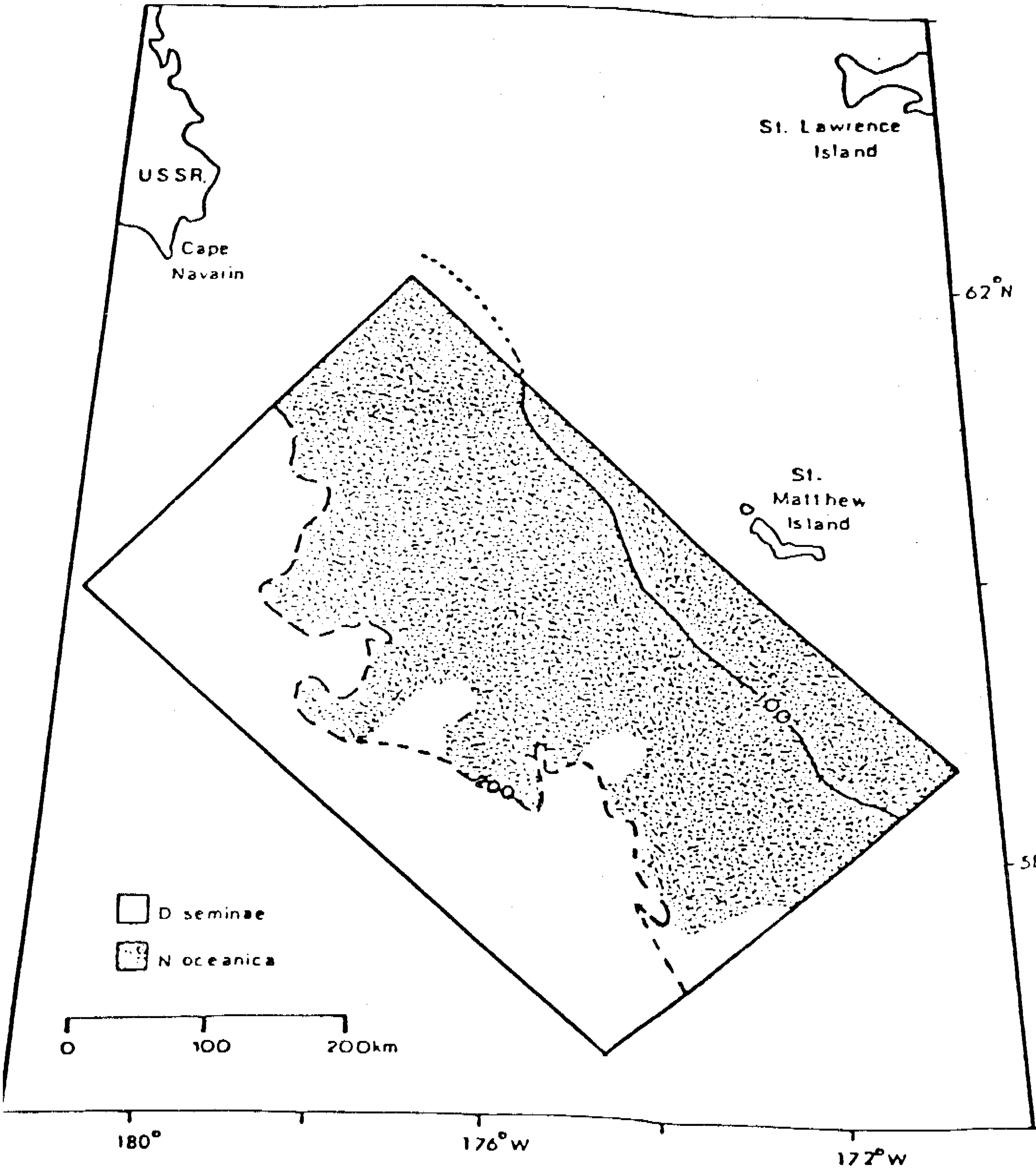

Figure 44. Area within the Navarin Basin, that is dominated by D. seminae or N. oceanica in the sediments. Contours represent depths of 100 and 200 meters. The 200 meters contour is the shelf-slope boundary.

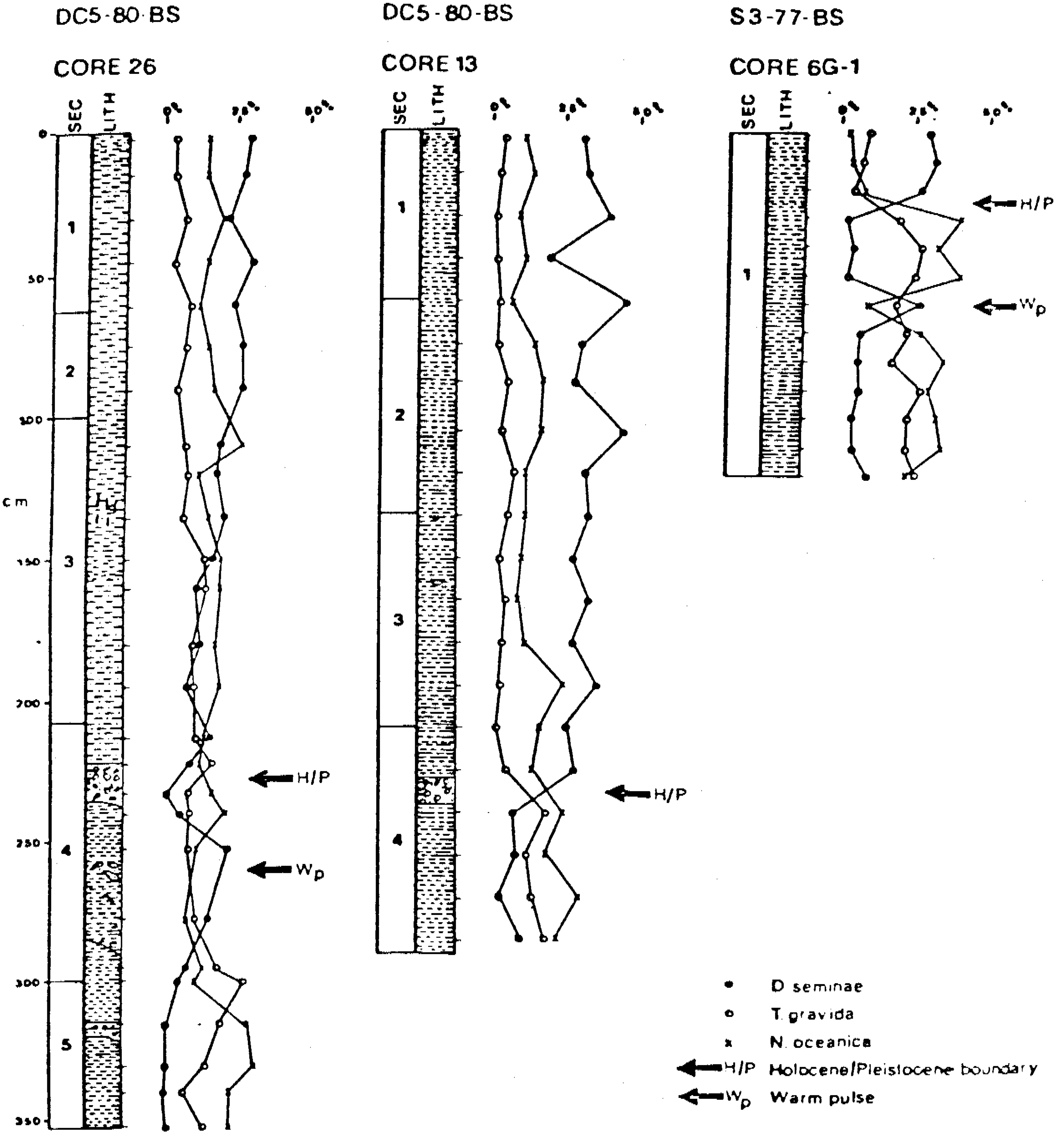

Figure 45. Down core abundance of Denticulopsis seminae, Nitzschia oceanica, and Thalassiosira gravida.

PLATE 1

Figures 1. Thalassiosira trifulata Fryxell
Sample 26-1, 75 cm; 28 μ m in diameter

2. Thalassiosira gravida Cleve
Sample 13-2, 135 cm; 25 μ m in diameter

3. Asteromphalus robustus Castracane
Sample 22-1, 2-3 cm; 56 μ m in diameter

4. Thalassiosira nordenskioldii Cleve
Sample 26-1, 75 cm; 22 μ m in diameter

5. Bacteria fragilis Gran
Sample 83-1, 0-2 cm; 20 m in diameter

6. Coscinodiscus lacustris Grunow
Sample 13-4, 79 μ m in diameter

7. Pseudopodosira elegans Sheshukova-Poretskaya
Sample 26-1, 75 cm; 17 μ m in diameter

8. Thalassiosira oestrupii
Sample 26-1, 75 cm; 8 μ m in diameter

9. Porosira glacialis (Grunow) Jørgensen
Sample 28-1, 0-2 cm4 48 μ m in diameter

10. Navicula sp. 2.
Sample 28-1, 0-2 cm; 48 μ m in length

11. Rhizosolenia hebatata f. hiemalis (Bailey) Gran
Sample 13-3, 165 cm; 84 μ m in length

12. Nitzchia oceanica (Cleve) Hasle
Sample 22-1, 2-3 cm; 28 μ m in length

13. Denticulopsis seminae (Semina) Simonsen
Sample 22-1, 2-3 cm; 34 μ m in length

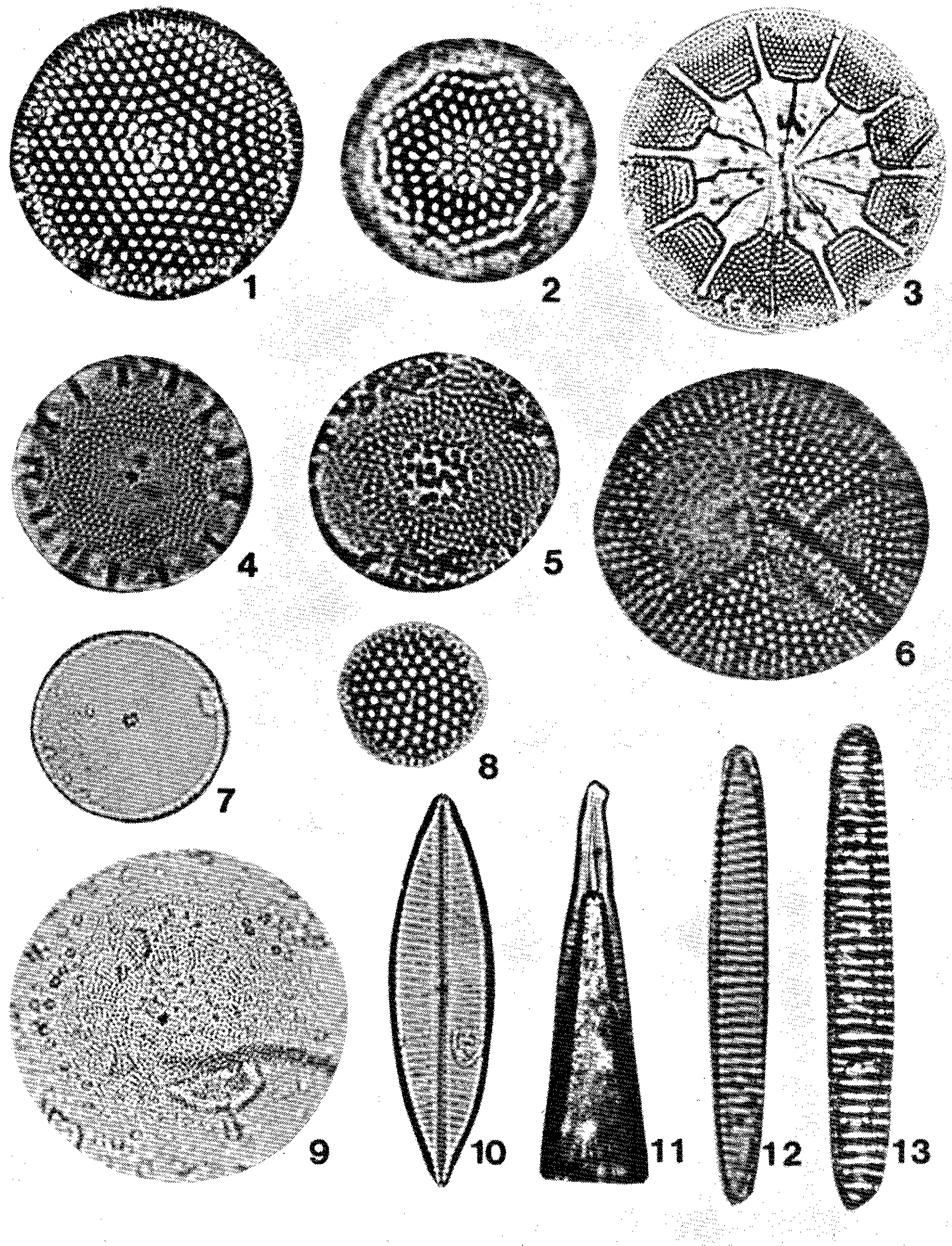
1
2
3
4
5
6
7
8
9
10
11
12
13

SPECIES \ SAMPLE	4	12	13	22	25	26	28	30	35	36	50	51	52	56	65
Actinocyclus curvatulus	-	-	0.3	-	0.6	-	-	-	-	-	-	-	0.6	1.0	-
A. divisus	0.6	0.6	0.3	0.3	1.6	0.3	2.6	0.3	1.0	0.6	1.0	1.0	0.3	1.6	-
A. ochotensis	-	-	-	1.0	-	-	-	0.6	0.6	-	-	-	1.0	1.6	-
Actinoptychus undulatus	-	-	-	-	0.6	-	0.3	-	-	-	0.6	-	-	-	0.3
A. vulgaris	-	0.3	-	0.3	-	-	-	-	-	0.3	-	-	-	-	-
Asteromphalus robustus	-	0.6	-	-	-	-	-	-	0.6	-	-	-	-	-	-
Bacteriosira fragilis	6.0	6.6	2.6	3.0	4.3	4.3	7.3	7.3	3.3	6.0	9.3	9.0	10.6	7.0	3.0
Biddulphia aurita	3.0	1.6	2.6	1.0	1.0	2.0	1.0	1.6	2.3	1.3	2.0	1.3	1.6	1.3	0.3
Coscinodiscus lacustris	-	-	-	0.3	-	-	-	0.3	-	-	0.6	-	-	-	-
C. marginatus	0.6	2.0	0.3	0.6	-	1.6	1.0	0.3	1.3	0.3	-	0.3	1.6	1.3	2.3
C. oculus-iridis	1.0	1.3	1.3	0.3	-	1.3	0.6	0.3	1.3	1.3	0.6	1.6	0.6	0.3	2.6
C. stellaris	-	-	-	-	-	-	-	-	-	-	-	-	-	-	-
C. tabularis	0.3	0.3	-	-	-	0.6	-	-	0.3	-	0.3	0.6	0.3	-	-
Denticulopsis seminae	28.0	27.0	31.3	38.3	4.0	26.0	7.3	3.0	17.0	29.0	7.0	6.3	6.0	14.3	33.0
Melosira clavigera	-	-	-	-	1.6	-	-	-	0.6	-	-	-	0.6	0.3	-
M. sulcata	1.0	1.0	0.6	2.0	7.6	1.0	2.6	5.3	3.3	2.6	3.6	5.3	3.6	4.3	1.6
Navicula sp. 1.	0.3	0.3	-	0.3	2.0	0.6	5.0	4.3	1.6	0.6	3.3	2.6	2.3	0.3	1.0
Navicula sp. 2.	-	0.3	0.3	0.3	1.0	-	0.6	-	1.3	1.6	0.6	1.3	0.6	0.6	0.6
Navicula sp. 3.	0.3	0.3	-	-	-	-	-	-	0.6	0.3	0.3	0.3	1.0	0.3	-
Nitzschia cylindrus	4.0	3.0	3.6	3.1	9.0	5.6	10.6	13.6	10.0	7.0	9.0	10.3	10.6	8.3	7.3
N. oceanica	16.3	10.6	9.6	11.0	26.3	19.0	19.3	36.0	18.6	15.0	25.6	24.3	20.6	20.3	11.3
Pleurosigma sp.	-	-	-	0.3	-	-	0.6	-	-	0.3	-	0.3	-	-	-
Porosira glacialis	1.0	2.0	1.3	1.6	2.3	3.0	4.6	2.6	3.6	3.6	2.1	1.3	6.0	3.3	4.0
Pseudopodosira elegans	1.3	3.0	-	1.3	1.3	0.6	0.6	-	0.6	-	-	1.0	-	2.6	-
Rhaphoneis sachalinensis	-	-	-	0.3	0.6	-	-	-	1.0	0.3	-	0.3	-	-	0.3
R. surirella	-	0.3	-	-	1.3	-	-	1.3	2.3	-	0.6	-	0.3	-	0.3
Rhizosolenia hebatata	2.6	3.0	4.6	3.0	1.6	3.3	1.6	0.3	2.0	1.6	0.3	1.6	2.6	2.3	2.3
R. styliformis	1.3	2.3	-	1.0	0.3	-	-	0.6	0.3	0.3	0.3	1.3	1.6	0.6	2.6
Stephanopyxis turris	-	-	-	-	-	0.6	-	-	0.3	-	-	-	-	-	0.3
Thalassionema nitzschioides	-	-	1.6	1.0	3.6	0.3	2.0	2.6	2.6	1.0	1.3	0.6	3.0	2.6	2.0
Thalassiosira decipiens	2.3	3.3	2.0	2.1	1.3	2.6	2.6	1.6	2.6	1.0	3.3	2.3	2.6	3.3	2.0
T. gravida	7.3	6.6	2.3	3.0	3.6	2.3	4.6	8.6	1.6	4.3	10.0	12.3	3.0	2.6	2.6
T. hyalina	10.0	8.0	11.0	5.6	5.6	7.6	8.6	0.6	6.6	5.0	7.0	5.0	5.0	6.0	5.3
T. leptopus	1.0	-	0.3	-	0.6	-	0.3	0.3	0.3	-	0.3	1.0	0.6	0.3	-
T. nordenskioldii	3.0	-	6.0	5.6	3.6	4.6	8.0	4.6	1.6	6.3	4.1	3.6	5.3	4.3	4.0
T. oestrupii	-	1.3	2.0	2.0	-	1.3	2.0	-	2.6	2.6	-	1.0	-	2.6	0.3
T. trifulta	6.6	8.3	10.0	7.3	4.6	10.3	3.3	2.1	5.3	6.0	3.3	2.3	3.0	3.3	5.3
T. undulosa	-	1.6	1.0	1.6	0.6	1.6	-	-	0.6	1.3	0.6	0.6	1.0	1.6	1.3
Thalassiothrix longissima	1.0	0.6	3.0	1.6	1.0	1.6	1.0	0.6	1.6	0.3	0.3	-	0.6	1.0	0.3

Table 10. Abundance (in percent) of species encountered during the examination of the surface sediments.

SPECIES \ SAMPLE	77	79	81	83	84	89	94	96	98	100	101	105	107	110	112
Actinocyclus curvatulus	-	-	-	-	0.6	0.3	-	1.0	0.3	-	0.6	0.6	-	-	-
A. divisus	0.6	0.6	2.0	2.3	2.3	1.0	0.6	0.6	-	1.0	1.0	1.0	3.0	2.0	2.3
A. ochotensis	-	-	-	-	1.0	1.0	0.6	2.0	0.3	-	1.0	1.0	-	0.6	0.6
Actinoptychus undulatus	-	0.3	0.3	0.6	-	-	0.6	1.0	-	-	-	0.3	-	-	-
A. vulgaris	-	-	-	-	-	-	-	-	-	-	-	-	-	-	-
Asteromphalus robustus	-	-	-	-	-	-	-	-	-	0.6	-	-	-	-	-
Bacteriosira fragilis	7.6	7.0	7.3	6.0	5.3	3.0	7.0	6.0	4.3	4.3	3.6	4.6	4.3	6.6	5.6
Biddulphia aurita	1.3	0.6	1.0	1.6	2.3	2.3	1.3	1.3	1.0	0.3	2.3	2.0	1.6	3.3	0.6
Coscinodiscus lacustris	-	0.3	0.3	-	-	-	-	-	-	-	-	0.3	-	-	0.3
C. marginatus	0.3	2.0	1.0	1.3	1.3	1.6	0.3	0.6	1.3	1.6	0.6	0.6	1.6	-	1.0
C. oculus-iridis	-	0.6	0.6	0.3	1.6	2.0	1.0	1.0	1.0	0.6	1.3	1.3	1.3	0.6	0.6
C. stellaris	-	-	-	-	0.3	0.3	-	-	-	-	-	-	-	-	-
C. tabularis	-	-	-	-	-	0.6	-	-	0.3	1.3	-	1.0	-	-	0.3
Denticulopsis seminae	27.6	10.0	10.6	13.0	11.3	37.0	9.6	10.3	17.6	28.0	24.0	22.3	33.3	15.0	14.6
Melosira clavigera	-	0.3	-	3.0	1.6	-	2.6	0.6	0.6	-	-	1.0	-	0.1	0.3
M. sulcata	2.3	5.0	11.6	14.0	7.6	2.3	9.3	5.3	4.0	2.0	2.6	6.0	1.0	3.6	10.0
Navicula sp. 1.	0.3	1.6	2.3	0.3	1.3	0.3	1.0	3.0	1.6	1.0	0.3	2.0	-	-	-
Navicula sp. 2.	-	0.6	-	0.3	1.0	0.6	0.3	-	1.3	-	-	-	-	-	-
Navicula sp. 3.	-	0.3	1.0	1.0	-	0.3	-	0.3	0.3	-	-	0.3	-	-	-
Nitzschia cylindrus	6.6	9.3	6.0	6.6	7.6	1.0	8.0	9.6	9.3	3.0	3.0	6.6	4.6	5.6	4.3
N. oceanica	16.6	16.6	17.6	15.3	9.0	5.6	21.0	15.6	17.6	13.0	11.0	13.0	7.0	21.0	21.6
Pleurosigma sp.	-	0.6	-	0.3	-	-	-	-	-	0.3	-	-	-	-	-
Porosira glacialis	1.3	3.3	1.3	3.3	4.0	2.6	4.0	3.3	3.6	2.0	2.6	1.6	4.0	1.6	2.0
Pseudopodosira elegans	2.0	1.0	0.6	0.3	1.0	-	2.6	-	-	1.0	1.6	0.6	0.6	1.0	0.6
Rhaphoneis sachalinensis	0.3	1.3	0.3	0.6	-	-	0.3	0.3	-	-	-	-	-	-	-
R. surirella	-	-	-	-	2.0	-	2.0	1.3	2.0	-	0.3	0.6	-	-	1.6
Rhizosolenia hebatata	2.3	3.0	2.0	0.3	1.3	2.3	2.3	0.6	2.3	2.6	5.3	1.3	3.0	1.3	2.3
R. styliformis	1.6	1.3	0.3	1.3	2.3	2.0	1.6	0.6	2.0	3.3	1.6	2.0	0.6	0.6	0.3
Stephanopyxis turris	-	-	-	-	-	-	-	-	-	-	0.3	-	-	-	-
Thalassionema nitzschioides	0.6	1.6	-	2.6	4.6	4.0	2.3	4.0	3.0	0.6	3.0	3.3	1.6	0.6	4.0
Thalassiosira decipiens	3.3	4.3	2.3	3.3	3.6	1.6	1.3	2.6	3.0	3.0	1.0	2.0	2.3	1.2	2.3
T. gravida	5.6	6.3	10.0	7.0	1.0	2.3	3.6	4.3	1.3	2.6	4.0	3.3	4.3	5.3	3.0
T. hyalina	3.0	5.3	5.0	3.6	4.0	6.3	2.6	4.0	7.6	7.6	5.3	7.0	7.3	4.6	6.0
T. leptopus	-	-	0.3	-	0.3	-	0.3	-	0.3	0.3	-	0.6	0.6	-	-
T. nordenskioldii	6.0	4.6	4.6	1.6	5.3	4.0	3.0	5.6	1.6	6.6	6.0	4.3	3.6	3.3	5.6
T. oestrupii	2.0	2.0	1.3	2.3	2.6	1.0	1.0	1.6	0.6	1.0	0.3	1.3	2.6	0.6	0.6
T. trifulta	7.3	6.6	5.6	6.0	8.3	10.3	5.0	6.0	6.0	7.3	17.0	6.3	8.3	2.6	4.3
T. undulosa	0.6	1.3	0.3	-	0.6	0.3	0.6	1.3	0.6	0.6	0.3	1.6	1.6	0.6	1.3
Thalassiothrix longissima	-	-	-	1.0	0.6	1.3	1.0	1.0	0.6	1.6	0.6	1.3	1.0	0.3	0.6

Table 10. Abundance (in percent) of species encountered during the examination of the surface sediments. (cont'd)

PRELIMINARY REPORT ON BENTHIC FORAMINIFERS FROM NAVARIN BASIN PROVINCE, BERING SEA, ALASKA

Paula J. Quinterno

INTRODUCTION

Previous studies of benthic foraminifers in the Bering Sea are mostly confined to areas to the north and west (Saidova, 1967; Lisitsyn, 1966) and to shallow-water areas to the east and northeast of the study area. (Anderson, 1963; Knebel and others, 1974) of the study area. The distribution of benthic foraminifers in the present study area was determined in 49 subsamples from water depths of 91m to 3420 m. Fourteen of these subsamples are from core tops or grab samples (Fig. 46), and 33 are from various depths within the cores. The goals of this study are to determine the distribution of benthic foraminifers in surface sediment and to record stratigraphic changes of the fauna with depth.

METHODS

Five of the 14 surface samples were preserved in 70% ethyl alcohol and stained with Rose Bengal shortly after they were collected. Rose Bengal stains protoplasm a deep pink, thereby distinguishing living foraminifers from dead specimens. This method is not without error; for example, foreign organic material such as bacteria or worms on or within the tests, may take the stain and be mistaken for foraminiferal protoplasm. Also, if the tests are thick or amber-colored, the stain is difficult to see.

The sampling techniques used to collect the cores in this study disturbed the upper few centimeters of sediment. Just before the sampler hits bottom, it creates a shock wave that scatters some of the surface sediment. All gravity cores collected on this cruise were turned horizontally to remove the liner in order to facilitate handling on deck. If the upper section of a core consisted of water-saturated sediment, some of the slurry was lost and some probably mixed with sediment deeper in the core. Because foraminifers live in the upper few centimeters of sediment, it is not likely that a representative sample of the living population was obtained. Therefore, results of live studies are approximations.

Samples (both preserved and unpreserved) were processed by washing over a 62 μm mesh sieve to remove silt and clay. Preserved samples were air dried to prevent protoplasm from shrinking; unpreserved samples were dried in an oven. In samples with abundant terrigenous material, foraminifers were concentrated by floating in carbon tetrachloride. A microsplitter was used to obtain a representative split of approximately 300 benthic foraminifers, but the actual number of benthic foraminifers in the splits ranged from 3 to 2860. Foraminifers were mounted on cardboard slides, identified, and the percentage of each species in the assemblage was calculated (Table 11).

DISTRIBUTION OF FORAMINIFERS

Forty-five calcareous and 20 agglutinated benthic species have been identified in the samples examined (Table 11).

Calcareous Species

The maximum water depth at which calcareous benthic foraminifers have been found in the Bering Sea is 3500 m; agglutinated species occur from shallow depths to depths greater than 3500 (Saidova, 1967).

Calcareous benthic foraminifers are present in all but 4 of the samples (Table 11). The exceptions are a G-14 (2-3 cm) from 91 m water depth, which contains all agglutinated specimens; G-6 (19-20 cm and 80-81 cm) from a water depth of 113 m -- both intervals are barren of calcareous and agglutinated specimens; and G-106 (55-58 cm) from 1785-m water depth which contains several fragments of poorly-preserved large, agglutinated forms tentatively identified as *Hyperammina* and *Rhabdammina*.

Calcareous benthic foraminifers in the samples studied are well- to poorly-preserved (Plates 2A and 2B). Both abrasion during transport and dissolution seem to affect preservation. Although *Elphidium* tests look robust, broken specimens are common. Dissolution also affects this genus; in some surface samples the entire calcareous test has been dissolved, leaving only the amber-colored organic inner lining (Plate 2B). Calcareous specimens in G-13 (240 cm) and G-12 (582-584 cm) show definite signs of dissolution. Tests are dull and grainy and features are obscure. These samples are from water depths of 2962 and 3164 m, respectively.

Agglutinated Species

Previous studies in the Bering Sea have reported the highest percentages of agglutinated foraminifers at water depths of less than 200 meters and also at depths greater than 2500 m (Anderson, 1963 and Saidova, 1967). This trend was not observed in the present study. Percentages varied from high to low at all water depths. There is, however, a definite decrease in the percentage of agglutinated foraminifers with depth in the cores (Figs. 47, 48, and 49; Table 11). This decrease could be attributed to poor preservability; the organic cement binding the grains together may be destroyed after the tests are buried, or to present conditions which provide a more-favorable habitat for agglutinated forms and less favorable for calcareous forms than did past conditions.

The large, agglutinated foraminifers, *Hyperammina* and *Rhabdammina*, in core G-106 (55-58 cm) differ from the agglutinated specimens near the top of this core (5-8 cm) and from those of all other samples analyzed (Table 11). The fauna at 55-58 cm resembles the faunas found in Bering Sea dredge samples which were dated as possibly early Tertiary (Robert Arnal, personal communication). Although age-diagnostic foraminifers are absent from G-106 (55-58 cm), the general character of the fauna and the lithology (well-consolidated mud with shale fragments) suggests a pre-Quaternary age.

Down-core Studies

All the benthic foraminifer species found in these cores have representatives that are still living today, so evolutionary extinctions cannot be used here for stratigraphic interpretation. Fluctuating abundances of certain species, however, may be useful for deciphering Quaternary history.

Elphidium is generally considered to be restricted to the shelf, yet high percentages of this genus occur in 3 cores from water depths greater than 1900 m (Figs. 47, 48, 49). These occurences may indicate a change in environmental conditions at the time of deposition. Percentages of Elphidium in G-13 increase from less than 5% in the intervals examined above 227 cm to 35% and 22% at 230-231 cm and 235-236 cm, respectively. A decrease to 8% or less occurs below 240 cm (Fig. 47). Elphidium reaches a maximum of 74% at 330 cm in G-26 and a maximum of 20% at 325 cm in G-36 (Figs. 48 and 49). These maxima are associated with sediment consisting of sands and gravelly sands. This coarse sediment is overlain by diatom ooze in G-13 and G-26 which extends from the core top down to 220 cm. Diatom ooze is the dominant sediment type in surface samples from the continental slope of the Navarin Basin province (Karl and others, this report). Coarse sediment on the slope may have been displaced from shelf depths. Lowering of sea level during Pleistocene glaciation caused much of the flat shelf to be exposed. Shallow-water faunas could have been easily transported downslope or ice rafted into the deep-water environment. Furthermore, cores 36, 26, and 13 are located near the mouths of Navarinsky, Pervenets, and Zhemchug Canyons, respectively (Fig. 46); where downslope sediment transport would have been facilitated.

Baldauf (this report) concludes that fluctuating abundances of the diatoms D. seminae, N. oceanica, and T. gravida can be used to identify the Holocene/Pleistocene boundary in cores G-13 and G-26 (Figs. 50 and 51). He states that N. oceanica is a cold-water species associated with ice, whereas D. seminae is a true oceanic species associated with cool waters. The change in dominance from D. seminae to N. oceanica marks the transition from glacial to interglacial conditions that occurred about 11,000 years ago. The maximum abundance of Elphidium in G-13 occurs at Baldauf's proposed Holocene/Pleistocene boundary (Fig. 50). Although Elphidium does not show a peak at 220 cm in G-26 (the proposed Holocene/Pleistocene boundary), the peak at 330 cm correlates with another decrease of D. seminae (Fig. 51).

Faunas from Low-Oxygen Environments

Low diversity, high abundance benthic foraminiferal assemblages are typical in sediments where the dissolved oxygen content of the overlying water is less than 1 ml/l. A few species of the genera Bolivina, Buliminella, Fursenkoina, and Globobulimina often dominate the fauna.

Benthic foraminiferal faunas at 2 depth intervals in G-66 are similar to the low-oxygen faunas described by Douglas and Heitman (1979) from the southern California borderland and by Ingle and Keller (1980) from the eastern Pacific margin. Frequency percentages of the most abundant species from 2 depth intervals in G-66 are presented in Table 12.

Table 12. Percentages of benthic foraminifers from 2 intervals in G-66

Core 66 (1336 m deep)	380-382 cm	385-387 cm
Buliminella tenuata	45%	52%
Bolivina pacifica	25	25
Fursenkoina spp.	23	6
Globobulimina auriculata	4	4

The 380-382-cm interval of G-66 is a dark greenish gray and olive gray laminated mud. The sand-size fraction is approximately 90% foraminifers, dominated by the few species shown in Table 12. Previous studies have shown that laminated sediments are common where dissolved oxygen content of the overlying water is less than 1ml/l; these conditions are unfavorable for most scavenging macro-invertebrates, so there are few organisms to disturb the sediment. Although the fauna at 385-387 cm in G-66 is similar to the fauna at 380-382 cm (Table 12), the sediment is very different. The lower interval (385-387 cm) is coarse material made up largely of volcanic ash. The sediment below 390 cm changes abruptly to mud (similar to sediment at 380-382 cm), but the fauna does not change significantly. The coarse layer is probably an air-borne volcanic ash deposit, and if found in other cores in the Navarin Basin province, could be a useful stratigraphic marker.

Live Species

Rose Bengal stain was used to recognize live foraminifers in 5 surface samples, and the percentage of each species in the live fauna was calculated. The composition of the live and dead species in surface samples G-59, G-32, S-110, and G-40 are similar for each station. This is not the case at G-26 (Tables 11 and 13). Eighteen species were present in G-26, but only 6 of these species (33%) were represented by both live and dead specimens. *Elphidium*, a genus usually restricted to shelf depths, made up 8% of the total fauna (Table 11) in G-26 (3373 m. water depth). All specimens of *Elphidium* were dead and poorly preserved. Displacement, possibly by downslope transport in Pervenets Canyon, could account for the discrepancy between living and dead species in core G-26.

Table 13. Similarity of live and dead species

Sample no.	Total no. of species	No. of species represented by both live and dead	% of species in common
G-59	18	14	78
G-32	26	23	88
S-110	32	24	75
G-40	27	20	74
G-26	18	6	33

ACKNOWLEDGMENTS

I wish to thank Carol Hirozawa, Michael Mullen, and Susan Vath for their help in preparing the samples for this study and Robert Arnal, Joyce Blueford, Paul Carlson, and Herman Karl for critically reviewing an earlier version of the manuscript.

REFERENCES

Anderson, G. J., 1963, Distribution patterns of Recent foraminifera of the Bering Sea: Micropaleontology, v. 9, no. 3, p. 305-317.

Douglas, R. G. and Heitman, H. L., 1979, Slope and basin benthic foraminifera of the California borderland: SEPM Special Publ. no. 27, p. 231-246.

Ingle, J. C. and Keller, G., 1980, Benthic foraminiferal bio-facies of the eastern Pacific margin between 40° S and 32° N, in Field, M. E., and others (eds.), Quaternary Depositional Environments of the Pacific Coast: Pacific Coast Paleogeography Symposium 4, Los Angeles, Soc. Econ. Paleo. and Mineralogists, p. 341-355.

Knebel, H. J., Creager, J. S., and Echols, R. J., 1974, Holocene sedimentary framework, east-central Bering Sea continental shelf, in Herman, Y. (ed.), Marine Geology and Oceanography of the Arctic Seas: New York, Springer-Verlag, p. 157-172.

Lisitsyn, A. P., 1966, Recent sedimentation in the Bering Sea in Russian): Inst. Okeanol. Akad. Nauk. USSR, (translated by Israel Program Sci. Transl., Jerusalem, Washington, D.C., U.S. Dept. Commerce, National Sci. Foundation, 614 p.

Saidova, Kh. M., 1967, Depth changes in Bering Sea during the Upper Quaternary, as indicated by benthonic foraminifera, in Hopkins, D. (ed.), The Bering Land Bridge: Stanford Univ. Press, p. 364-368.

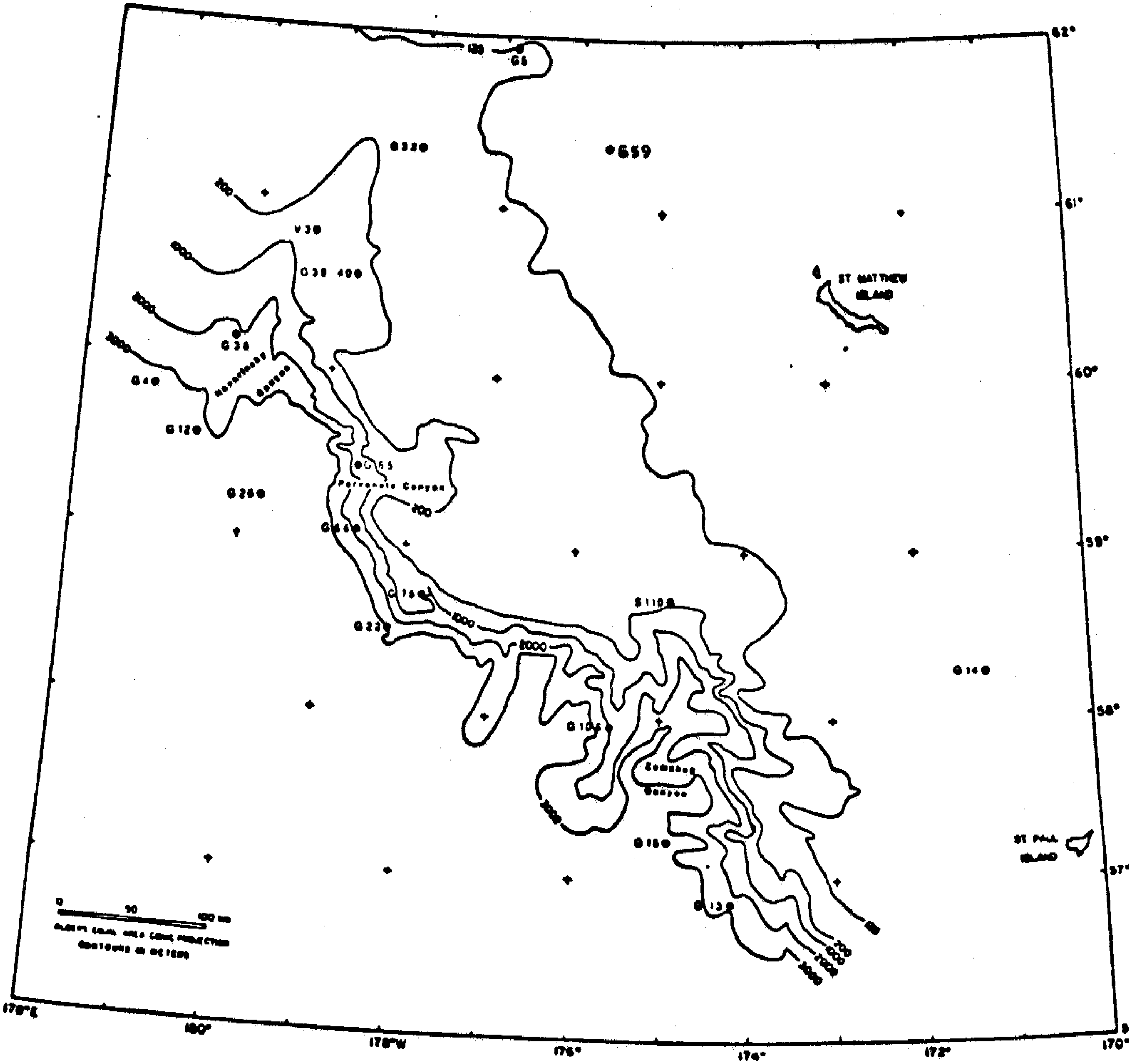

Figure 46. Sample locations

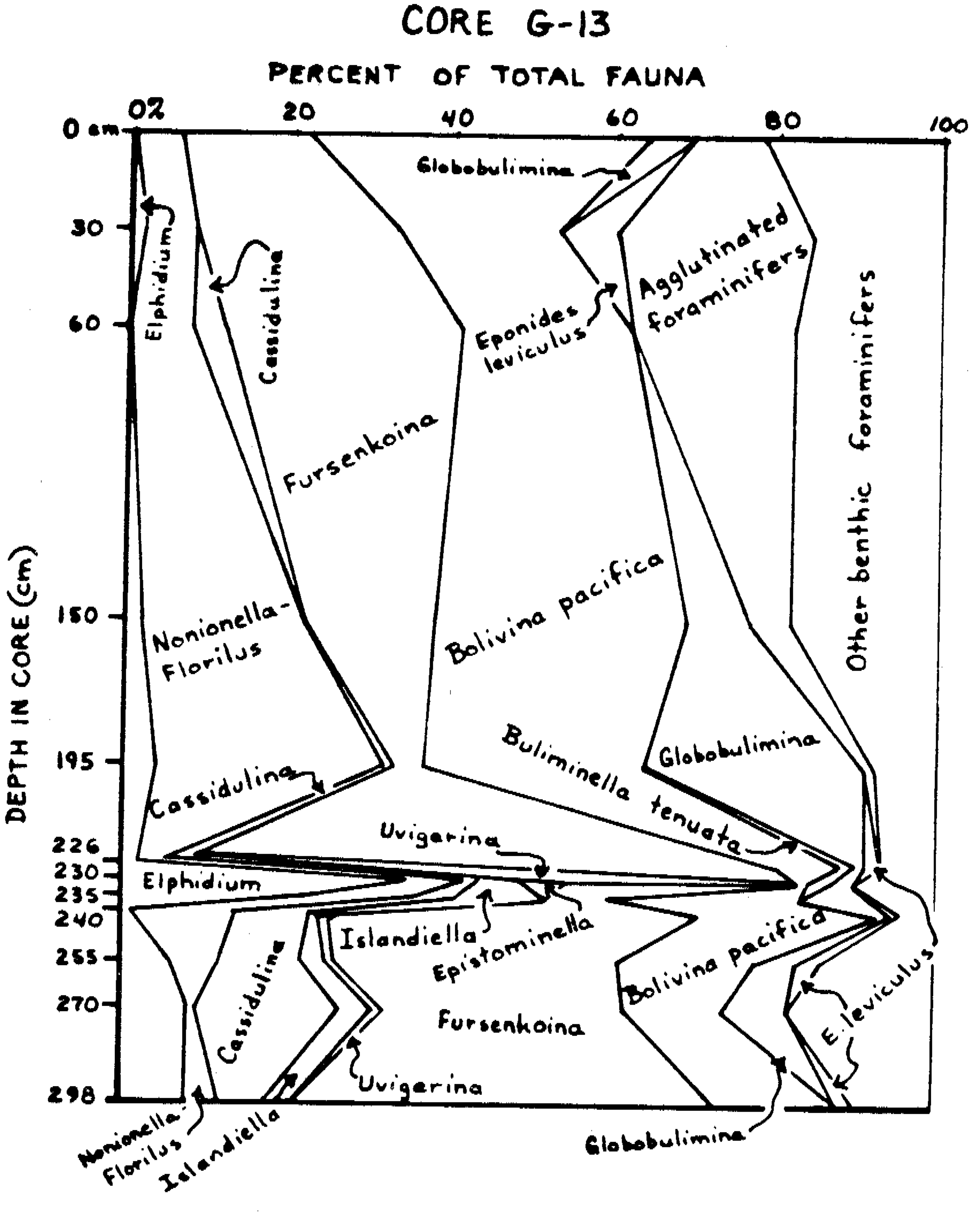

Figure 47 Distribution of benthic foraminifers with depth in Core G-13.

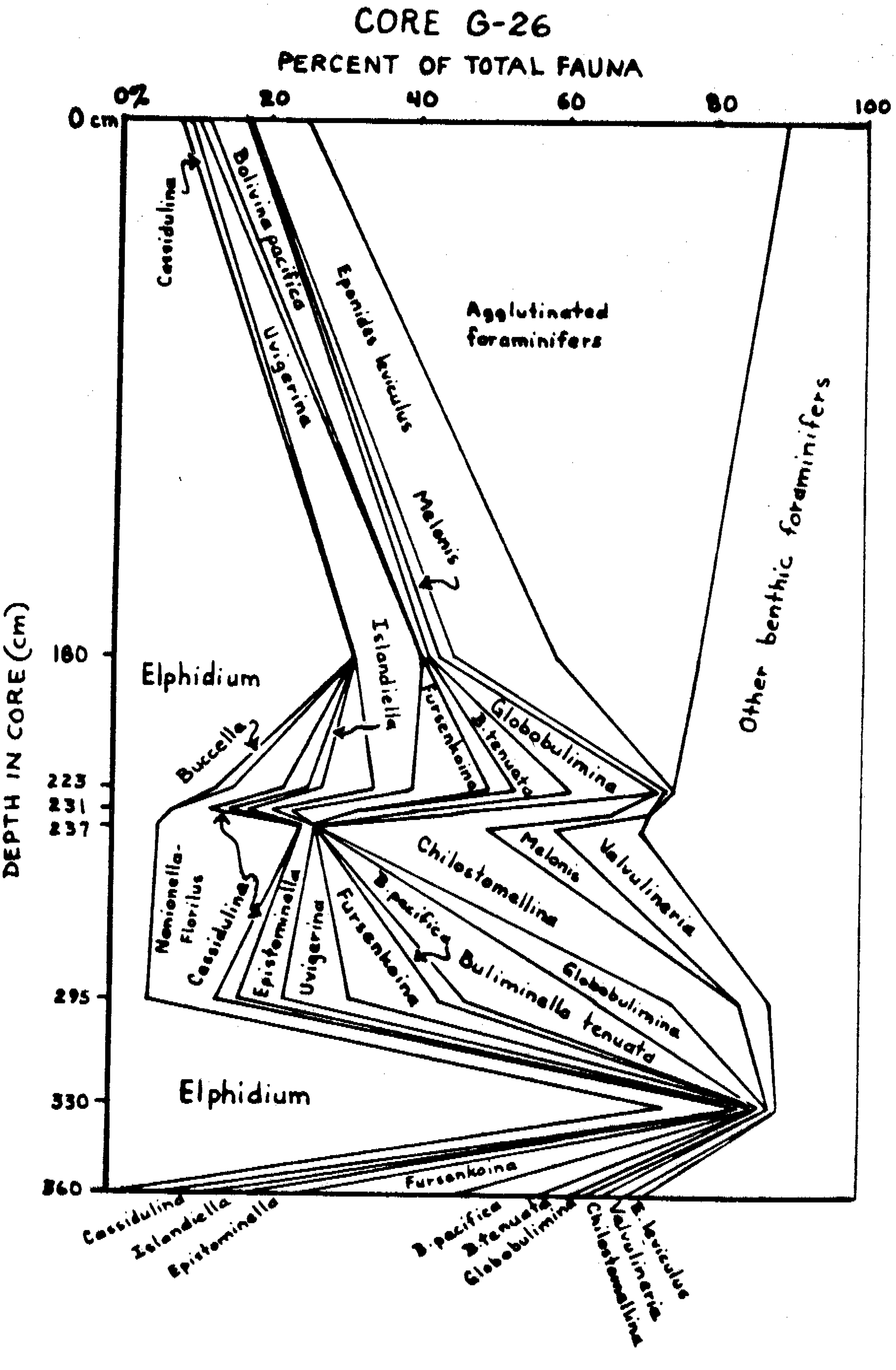

Figure 48. Distribution of benthic foraminifers with depths in Core G-26.

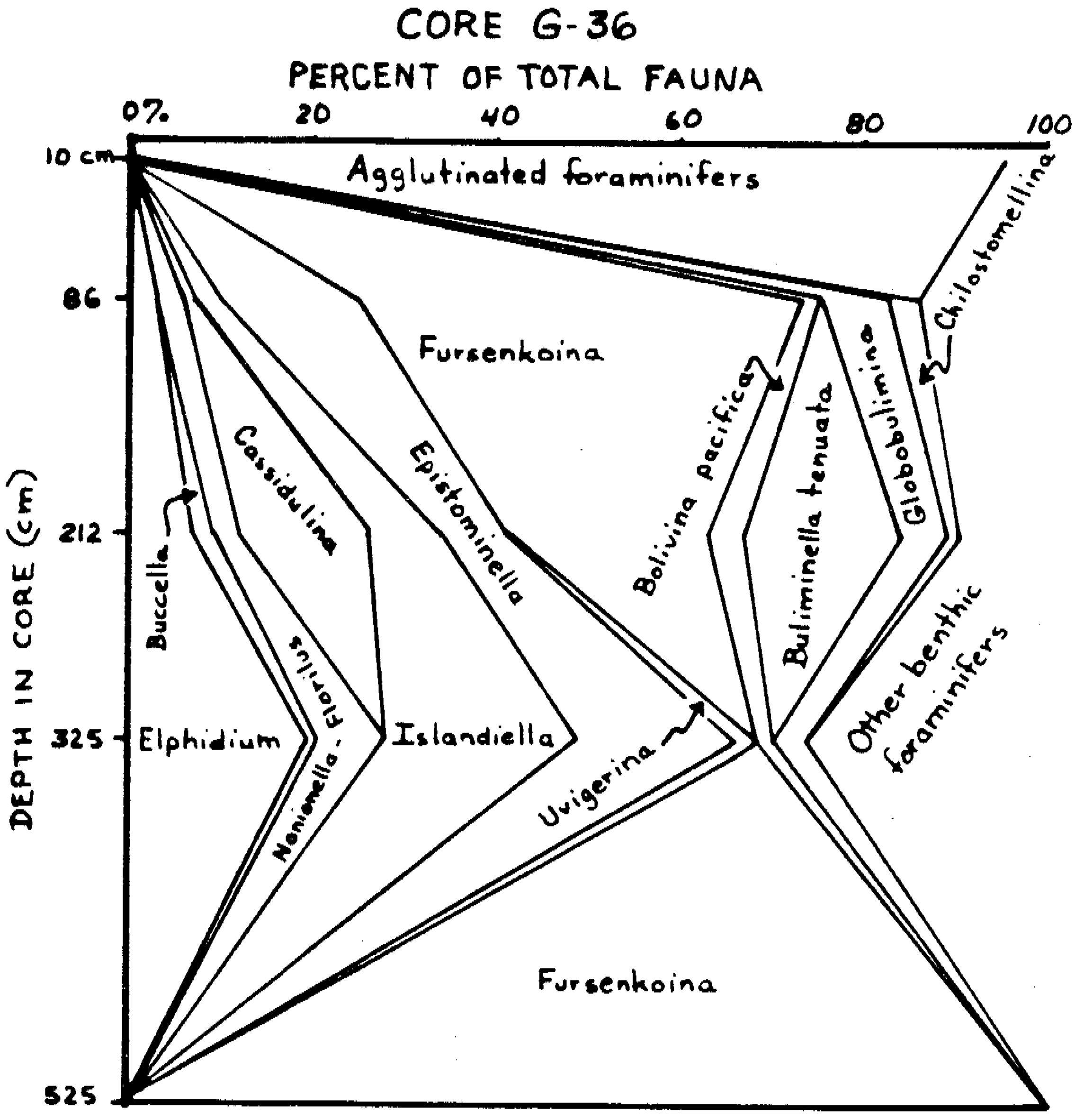

Figure 49. Distribution of benthic foraminifers with depth in Core G-36.

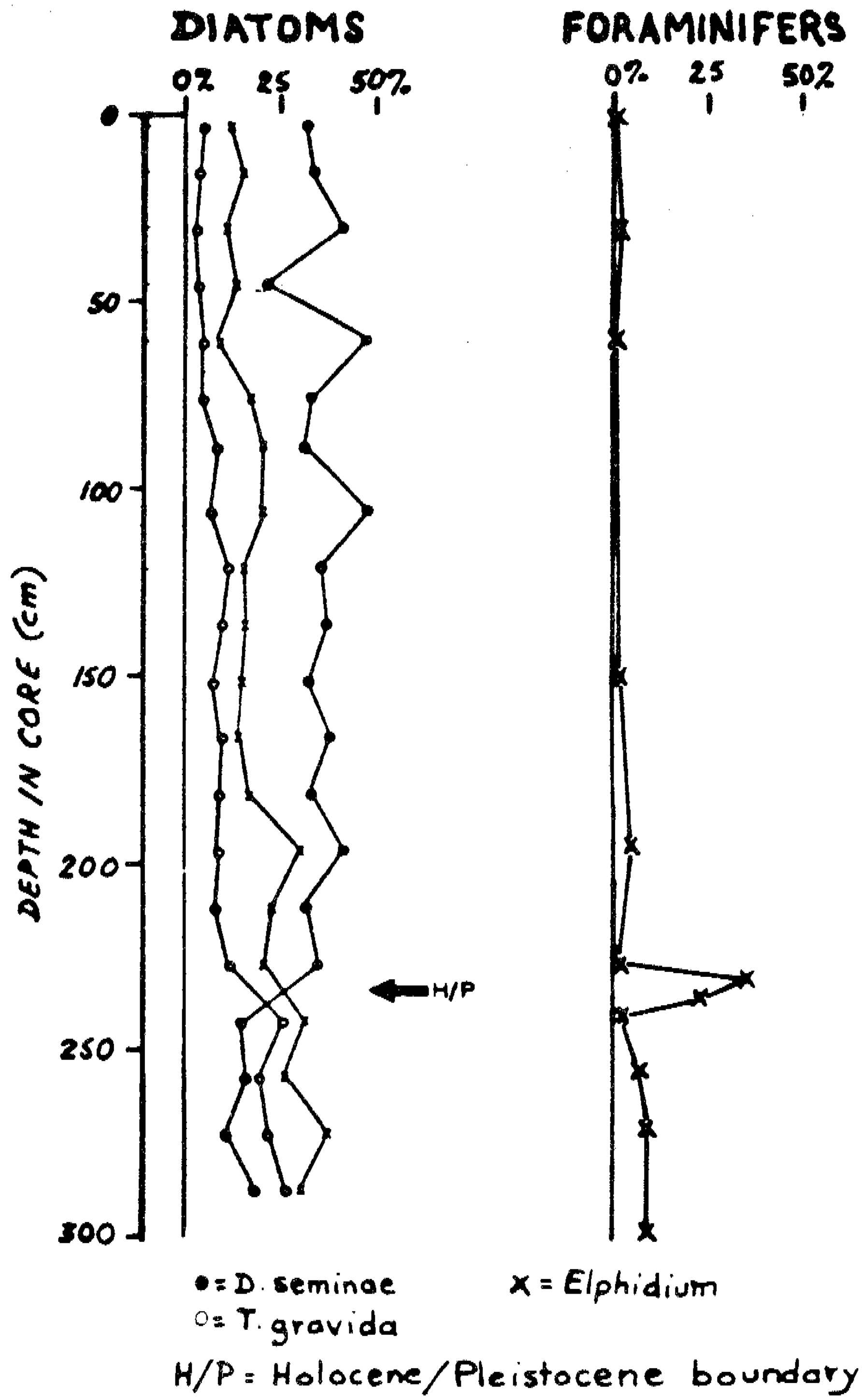

Figure 50. Downcore distributions of diatoms and foraminifers in Core G-13.

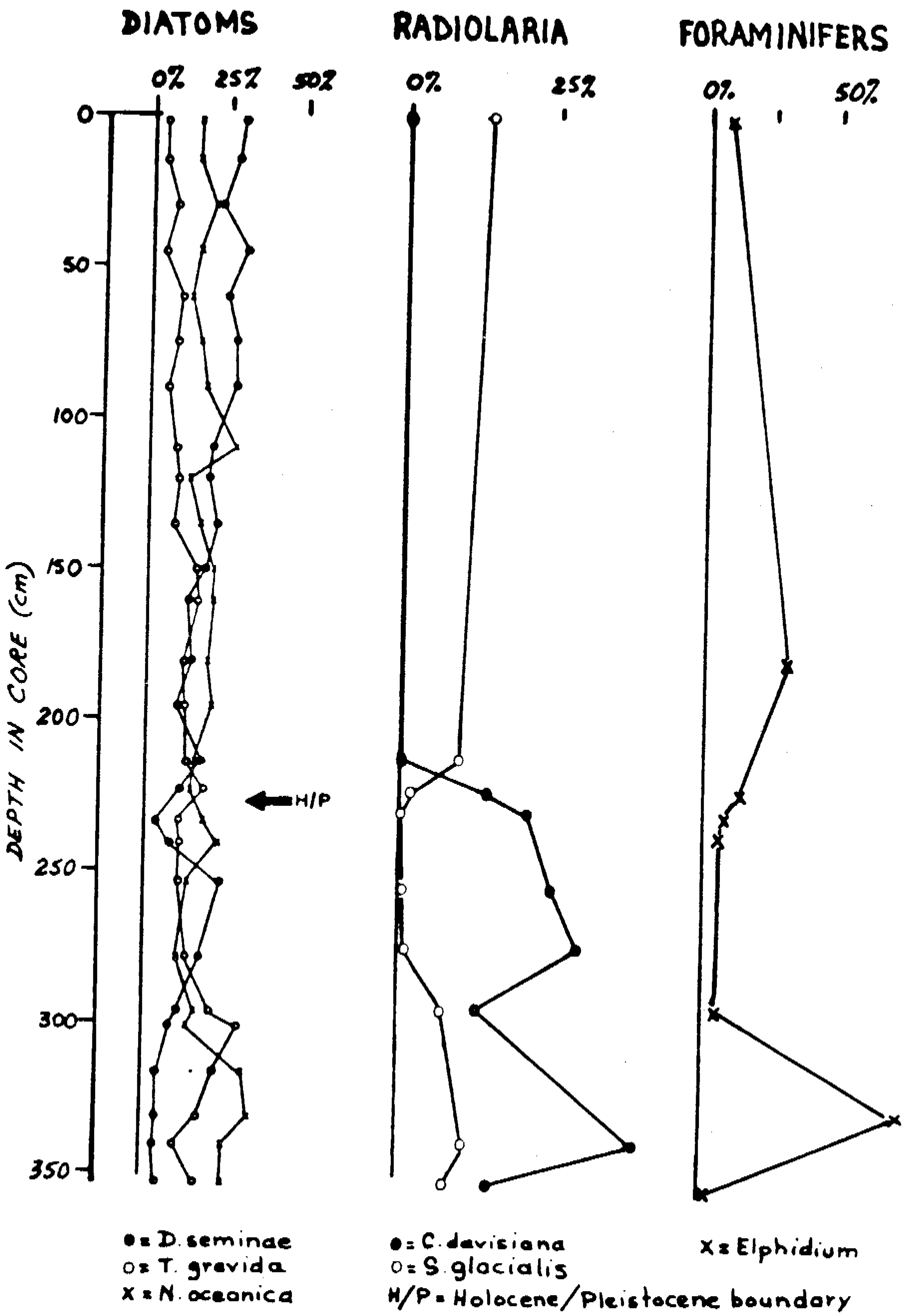

Figure 51. Downcore distributions of diatoms, radiolarians, and foraminifers in Core G-26.

PLATE 2

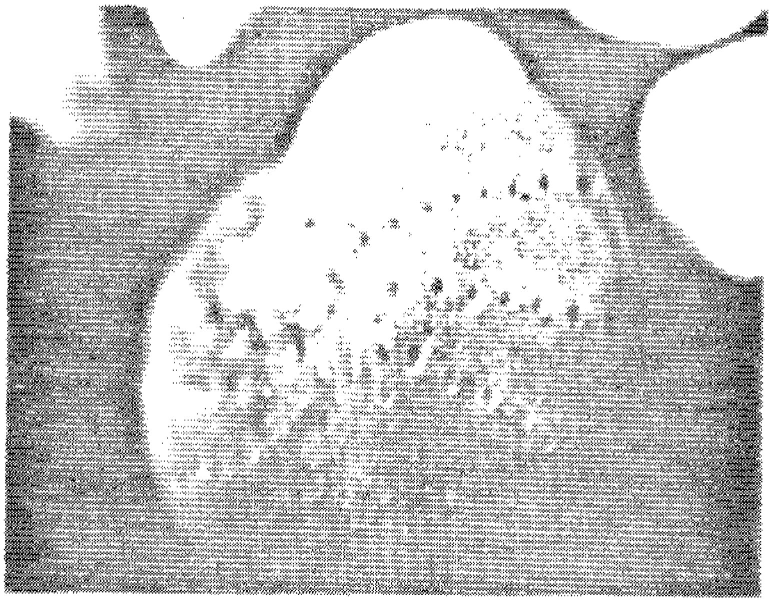

A. Well-preserved _Elphidium sp._ from S-110 (X60)

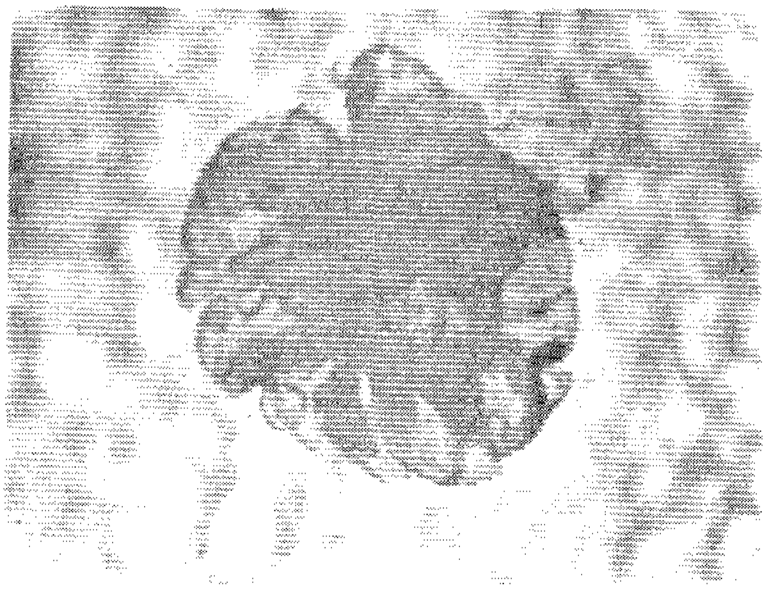

B. Organic inner lining of _Elphidium sp._ from G-54, 0-2cm (X100)

CORE NUMBER AND DEPTH IN CORE / SPECIES	G-14 2-3cm	G-59 0-2cm	G-6 19-20cm	80-81cm	G-32 0-2cm	S-110	G-39	G-40 0-2cm	V-3	G-75 10-12cm	G-66 380cm	385cm	G-65 181cm	G-106 5-8cm	55-58cm	G-36 10-12 cm	86-88cm	212-214cm	315-317cm	525-527cm	G-22 2-3cm
WATER DEPTH (m)	91	99	113		150	164	220	220	524	951	1336		1609	1785		1924					2842
Adercotryma glomeratum*	X	X(2)			9(14)	11(15)	3	12(16)	4							2					
Alveolophragmium crassimargo*					2(2)	1(3)		6(10)													
Ammoscalaria tennuimargo*																86					
Ammotium cassis*	X	X(2)			X																
Bathysiphon sp*																					
Bigenerina sp*	35	37(10)			2(3)	1(1)		X(1)	X												
Bolivina decussata					X(1)		1		7								1	X	1		
Bolivina pacifica		X			2(4)			2(5)	X	1	25	25	8				2	4	2		42
Bolivina seminuda																					
Bolivina striatula										6											
Bolivina spp						(X)															
Buccella spp		1(1)			4(6)	3(1)	3	X(1)	1				X				X	2	1		
Bulimina spp																					
Buliminella elegantissima			Z	Z					X												
Buliminella tenuata											45	52						17			
Cassidulina californica			ш	ш		1(1)	X									2					
Cassidulina limbata																			X		
Cassidulina sp		4(8)	α	α	4(6)	4(5)	4	1(3)	1	2		1	10				1	14			
Cassidulinoides sp												X	X					X			
Chilostomella sp			α	α												1					
Chilostomellina fimbriata											1		6				4	1			4
Cibicides sp			<	<		(X)			1								X	X			
Cribrostomoides scitulus*	4																				
Cyclammina cancellata*			■	▲												4					
Dentalina sp							X														
Eggerella advena*	35	2(2)			17(12)	7(3)	15	20(10)	13												
Elphidium clavatum var.		15(8)			7(6)	1	X		1	6	X		26				3	7	20		1
Elphidium frigidum						1(1)															
Epistominella pacifica									21	2	X	3					12	X	18		
Epistominella vitrea					10(9)	16(24)	17	7(6)	24		X		1				3	7			
Eponides leviculus						2(3)	1	1	1			1	X					X			
Eponides spp																					19
Fissurina spp		X(X)				X(X)			X									X	X		2
Florilus labradoricus		X(X)			2(2)	2		(2)	4	7	X	2	19				3	3	7		
Fursenkoina spp		22(43)			3(2)		X	5(8)	1		23	6	16				48	22		100	11
Globobulimina auriculata					1(2)				X	3	4	4	2	14			8	5	4		
Gyroidina spp																					
Haplophragmoides bradyi*					X	1(1)		1(1)	X							5					

Table II Relative frequency percentages of benthic foraminifers from the Navarin Basin province
X = less than 1%. * = agglutinated species
Data for "live" species is shown in parentheses

WATER DEPTH (m)	91	99	113		150	164	220	220	524	951	1336		1609	1785		1924					2042
CORE NUMBER	G-14	G-59	G-6		G-32	S-110	G-39	G-40	V-3	G-75	G-66		G-65	G-106		G-36					G-22
DEPTH IN CORE / SPECIES	2-3cm	0-2cm	19-20cm	80-81cm	0-2cm			0-2cm		10-12cm	380cm	385cm	181cm	5-8cm	55-58cm	10-12cm	86-88cm	212-214cm	325-327cm	526-527cm	2-3cm
Haplophragmoides columbiense *		5				x (x)			x												
Hyperammina sp (fragments=F)*															F						
Islandiella spp					8 (1)	x (x)	2	1 (x)									3	8	21		
Karreriella sp.*																					
Lagena spp					x (x)	x	x	x	x	x		x	1				x	x	x		
Melonis pompilioides																					
Nonionella pulchella																					
Nonionella turgida digitata							x	3 (5)	7			1	3				x	x			5
Nonionella spp																		x			
Pelosina variabilis*			N	N												1					
Protelphidium orbiculare								x										x			
Pseudononion auricula			E	E		1 (2)	2	2 (4)	x				3				5	2	x		
Pullenia salisburyi						x (x)		x (x)													
Pyrgo spp			R	R																	
Quinqueloculina spp									x												
Recurvoides spp *		3 (4)	R	R	2 (3)	1 (2)	1	x (1)	x												
Reophax spp *	x	1 (3)			5 (8)	3 (3)	1	(1)	x	x						65					5
Rhabdammina sp (fragments=F)*			A	A											F						
Spiroplectammina biformis*	16	7 (2)	B	B	13 (7)	5 (1)	3	13 (6)	5					28				x			
Textularia sp *	2	5 (6)			6 (6)	8 (3)	2	8 (3)						28							5
Trifarina angulosa					3 (3)	20 (17)	32	(10)	2	1			x								
Triloculina trihedra																	x	x	x		
Trochammina spp.*	6				x (x)	2 (3)			1					14		2					2
Uvigerina (costate)					1 (x)	5 (4)	9	1 (2)	1	69		4	2					x	2		
Uvigerina (smooth)																		x	x		1
Uvigerina (hispid)																					
Valvulineria sp										2		1							x		
other calcareous species						x							1				4	3	3		1
other agglutinated species		(3)			x (1)	1 (2)		x (1)	1					14							
Percent agglutinated	98	55	0	0	56	41	25	60	24	0	0	0	0	84		94	0	0	0	0	11
NUMBER OF BENTHIC SPECIMENS COUNTED — TOTAL	628	1747	0	0	681	1441	309	591	2860	211	679	325	370	7	Fragments	89	568	666	360	3	74
(LIVE)		(727)			(292)	(537)		(238)													

Table 11 (continued)

CORE NUMBER AND DEPTH IN CORE / SPECIES	G-13 0-2cm	30cm	60cm	150cm	195cm	226-227cm	230-231cm	235-236cm	240cm	255cm	270cm	298-299cm	G-12 582-584cm	B-4 0-2cm	8-9cm	296cm	G-26 0-2cm	180cm	223-225cm	231-232cm	237cm	295-300cm	330cm	360cm	G-15 50-100cm	195-196cm
WATER DEPTH(m)	2962												3164	3222			3373								3420	
Adercotryma glomeratum*		2															16(10)									
Alveolophragmium crassimargo*																	1(3)									
Ammoscalaria tennuimargo*																		1								
Ammotium cassis*																										
Bathysiphon sp*									x																	
Bigenerina sp*																	1									
Bolivina decussata						x					x	x														x
Bolivina pacifica	42	20	21	31	27	8	1	23	22	17	12	15	6	42			5	1	4			3		11		1
Bolivina seminuda	3			5	7														1	1						1
Bolivina striatula																										4
Bolivina spp							3		1	1			29						1					2		
Buccella spp						X			x	x	x	x							2			x	1			1
Bulimina spp																			x							x
Buliminella elegantissima								2		1									x			x		1		
Buliminella tenuata						2	3	x					13						7	7		18		4		8
Cassidulina californica																			3	1						x
Cassidulina limbata																			x	1						
Cassidulina sp			4	x	1	5	2	5	9	10	18	6	x				1(3)		3	1		3		3	9	4
Cassidulinoides sp							3						x			3			1	2		x	1	2		1
Chilostomella sp				1															3			1				x
Chilostomellina fimbriata					1				x			x	17							21	21	9		2		1
Cibicides sp								X				X	X				1	7	X	9	6		7	1		1
Cribrostomoides scitulus*																										
Cyclammina cancellata*																										
Dentalina sp												x							x							x
Eggerella advena*		9	12	2	1									2				1								
Elphidium clavatum var.		2		2	4	1	36	22	1	6	8	8	8	15	50	x	8	32	14	8	6	5	74	2	64	16
Elphidium frigidum																										
Epistominella pacifica						1	6	X											5	3		5		2		10
Epistominella vitrea						1			1	1		x	1						2		2	1	1	4		4
Eponides leviculus		7				2			1	3		2				26	8(3)	14	1					2		x
Eponides spp				x				2		3	7		3	2	17	1		2	1		9		1			
Fissurina spp											x	1						3	x				3	2		
Florilus labradoricus	3	2		9	20	x	7	4			1	1	4	5					7	5	11	8	10	2	27	8
Fursenkoina spp	16	25	29	16	4	68	1	8	45	34	30	52	8	2			1		10	9		12		21		3
Globobulimina auriculata	5			8	27	1	3	8	1	5	8		1	5	17	11		1	12	6		10	1	2		9
Gyroidina spp																		1	x			1		x		x
Haplophragmoides bradyi*																										

Table 11 (continued)

SPECIES \ CORE NUMBER AND DEPTH IN CORE	G-13 0-2cm	30 cm	60 cm	150 cm	195 cm	226-227cm	230-231cm	235-236cm	240 cm	255 cm	270 cm	290-291cm	G-12 582-584 cm	G-4 0-2 cm	8-9 cm	296cm	G-26 0-2cm	100cm	220-225 cm	231-232 cm	257 cm	295-300 cm	330 cm	360cm	G-15 50-100 cm	195-196 cm
WATER DEPTH (m)	2962												3164	3282			3373								3420	
Haplophragmoides columbiense*				1																						
Hyperammina sp.*																										
Islandiella spp.							5	11	1	3	4	3							2	1		1		2		3
Karreriella sp.*																		1								x
Lagena spp						x	x	x	x		x	x	x						x	1	2	x		x		x
Melonis pompilioides											x							2	1	5	9	x				x
Nonionella pulchella																										
Nonionella turgida digitata	3		8	11	8	1		10	13	6		3									8	1		1		x
Nonionella spp	4					2													x					2		
Pelosina variabilis*																										
Protelphidium orbiculare																			x							
Pseudononion auricula	3								x	1		2					1					x				
Pullenia salisburyi																			x							
Pyrgo spp																	1			2						
Quinqueloculina spp									x								1			3		x		1		
Recurvoides spp.*																										
Reophax spp.*	3	4		1										8			34(71)	10								
Rhabdammina sp.*																										
Spiroplectammina biformis*	6	4															2									
Textularia sp.*				x										8				6								
Trifarina angulosa																			x	1		x				x
Triloculina trihedra	3			1							x	x						1	x		2			2		
Trochammina spp.*		2	8	1										2			11(7)									
Uvigerina (costate)						1	27												5	2		8				14
Uvigerina (smooth)									1	1	1	x	3	5	17	45	1	9	1			1	1	x		2
Uvigerina (hispid)											x									1						
Valvulineria sp							1						2			13			x		11	4	1	3		1
other calcareous species	15	13	17	9		5		x	3	7	4	1	1	2			4	5	2	11	12	4		27		
other agglutinated species		2																								
Percent agglutinated	9	24	20	5	1	0	0	0	x	0	0	0	0	20	0	0	65	19	0	0	0	0	0	0	0	0
NUMBER OF BENTHIC SPECIMENS COUNTED — TOTAL	38	44	24	225	90	402	662	183	396	321	177	368	489	40	6	233	153	87	493	102	53	567	120	290	11	868
NUMBER OF BENTHIC SPECIMENS COUNTED — (LIVE)																	(38)									

Table 11 (continued).

RADIOLARIA FROM THE NAVARIN BASIN PROVINCE, BERING SEA

Joyce R. Blueford

INTRODUCTION

Although several biostratigraphic studies describe radiolarian faunas in the North Pacific (Hays, 1970; Nigrini, 1970; Sachs, 1973; Kling, 1971 and 1973; Ling, 1970; Robertson, 1975; and Kruglikova, 1976 and 1977), The only comprehensive study of the radiolarian fauna from surface sediments from the Bering Sea is by Ling and others (1970). Many north Pacific species are not found in the Bering Sea. Radiolarians from the surface layer in the Sea of Okhotsk (Kruglikova, 1975) are similar to those analyzed for this report.

The purpose of this preliminary survey of radiolaria is threefold. First, it establishes what species are present in the upper 600 cm of the sediment; secondly, it suggests useful species for stratigraphy; and thirdly, it suggests areas of further studies that may yield useful stratigraphic and environmental information.

METHODS

It was concluded after a preliminary scan of prepared foraminiferal samples that samples from cores collected in water depths deeper than 200 m contained the most abundant and diverse radiolaria fauna. Therefore, a concentrated effort was made on deep water cores as shown in Figure 52. Samples were taken from the top and bottom of most of the cores. Some cores, such as 12, 26, 109, and 115, were sampled at intermediate levels as well.

Samples were washed through a 52 mm mesh sieve. Because carbonate and organic contents were low, the usual method of adding HCl and hydrogen peroxide was not used. Radiolaria from samples that contain a high percentage of diatoms were concentrated by first drying the sample, then putting half of the sample on a watch glass, then pouring it into another watchglass. The first watchglass is wiped clean and the process is repeated about 4 or 5 times. Diatoms tend to adhere to the watchglass that does not have the bulk of the sample because of static electricity. Radiolaria are concentrated in the sample and strewn slides are then made. The entire slide was scanned in an effort to look at the total assemblage.

RESULTS

The radiolarian fauna of the Bering Sea is different from that of the North Pacific in being more diverse with endemic arctoboreal and cosmopolitan species (Kruglikova, 1977). The Navarin Basin province assemblage is similar to the assemblage in surface sediment throughout the Bering Sea (Ling and others, 1970) and the Sea of Okhotsk (Kruglikova, 1975). This may be due in part to oceanographic current and water mass patterns.

Seventy different species were identified from Navarin Basin province cores (Table 14). Their abundance as a group in samples collected from the slope and rise is second only to diatoms. The following species are found to be most abundant in this area (in decreasing order): *Stylochlamidium venustum*

(Bailey), Spongotrochus glacialis Popofsky group, Cycladophora (?) cornuta (Bailey), Cycladophora davisiana Ehrenberg, Stylodictya aculeata Jorgensen, Acanthodesmiidae gen. et. sp. indet. A, Lithelius sp., Stylatractus pyriformis (Bailey)? emend Kruglikova, Dictyophimus gracilipes Bailey, Prunopyle antarctica Dreyer, Acanthodesmia micropora (Popofsky), Arachnocorys (?) dubius Dogiel and Stylodictya validispina Jorgensen. Table 15 shows the abundance of all species counted in this study.

The occurrence of Lychnocanoma grande in some samples (Table 15) is noteworthy in that this species has been shown in studies of Pacific Ocean cores to be stratigraphically significant (see e.g., Robertsen, 1975; Kruglikova, 1976). Not enough samples have been examined, however, to determine the significance of L. grande in the Navarin cores.

REFERENCES CITED

Casey, R. Price, A. and Swift, C., 1972, Radiolarian definition and paleoecology of the late Miocene to E. Pliocene in S. California: in Proceedings of the Pacific Coast Miocene Biostratigraphic Symposium S.E.P.M., p. 226-238.

Cleve, P. T., 1899, Plankton collected by the Swedish Expedition to Spitzbergen in 1898: Swedish Acad. Sci., Bandel 32, No. 3.

Dogiel, V. A. and V. V. Reshnetnyak, 1952, Material on radiolarians of the northwestern part of the Pacific Ocean: Invest. Far East Seas USSR, publication III.

Hays, J. D., 1970, Stratigraphy and evolutionary trends of radiolaria in north Pacific deep sea sediments: GSA Memoir 126, p. 185-218.

Hays, J. D., 1971, Faunal extinctions and reversals of the earth's magnetic field: GSA v. 82, p. 2433-2447.

Hulsemann, Kunigunde, 1963, Radiolarions in plankton from the Arctic drifting station T-3: Arctic Ins. of N.A. Tech. Paper No. 13, p. 5-43.

Jorgensen, E., 1905, The protist plankton and the diatoms in bottom samples: Bergens Mus. Skrifter, no. 7, p. 49-151, pls. 6-18.

Kling, S., 1971, Radiolaria: Leg 6 DSDP; in Fisher, A. G., Heezen, B. C., and others, Initial Reports Deep Sea Drilling Project, v. 6, Washington, D.C., p. 1069-1096.

Kling, S., 1973, Radiolaria from east north Pacific, DSDP Leg 18: in Kulm, L. D., von Huene, R., and others, 1973, Initial Reports Deep Sea Drilling Project, v. 18, Washington D.C., p. 617-641.

Kruglikova, S. B., 1975, Radiolarians in the surface layer of the sediments of the Okhotsk Sea. Oceanology, v. XV, Acad. of Sciences USSR.

Kruglikova, S. B., 1976, Radiolarians in the upper Pleistocene sediments of the boreal and northern subtropical zones of the Pacific Ocean: Oceanology, v. XVI, Acad. of Sci. USSR.

Kruglikova, S. B., 1977, Peculiarities of the distribution of radiolarians in the sediments of the boreal and subtropical zones of the Pacific Ocean in the Pleistocene: Oceanology, v. XVII, Acad. of Sci. USSR.

Ling, H. Y., 1973, Radiolaria: Leg 19, Deep Sea Drilling Project: in Creager, J. S., Scholl, D. W., and others, Initial Reports Deep Sea Drilling Project, v. 19, Washington, D.C., p. 777-797.

Ling, H. Y., and others, 1970, Polysystine radiolaria from Bering Sea surface sediments: in Proceedings of II Plankt. Conference, Rome, p. 705-729.

Nigrini, C., 1970, Radiolarian assemblages in the north Pacific and their application to a study of Quaternary sediments in core V20-130: GSA Memoir, 126, p. 139-183.

Nigrini, C. and Moore, T., 1979, A guide to modern radiolaria, Cushman Foundation Sp. Publ. No. 16, p. 212.

Petrushevskaya, M. G., 1967, Antarctic spumelline and nasselline radiolarians: Issled. Fauny Morei 4 (12) Rez. biol. Issled., Sov. Antarkt. Eksped. 1955-1958, 3, p. 5-186.

Reshetnyak, V. V., 1966, Deep Water Phaeodaria Radiolaria of the northwest Pacific Ocean, Akad. of Sci. USSR, Ins. of Zoology, no. 94.

Riedel, W. R., 1958, Radiolaria in Antarctic sediments, Rept. BANZ Antarctic Research Exped., ser. B, v. 6, pt. 10, p. 217-255.

Robertson, J., 1975, Glacial to interglacial oceanographic changes in the northwest PAcific, including a continuous record of the last 400,000 yrs., Ph.D. dissertation, Columbia University, New York, p. 326.

Sachs, H. M., 1973, Late Pleistocene history of the north Pacific: evidence from a quantitative study of radiolaria in core V21-173: Quaternary Research 3, p. 89-98.

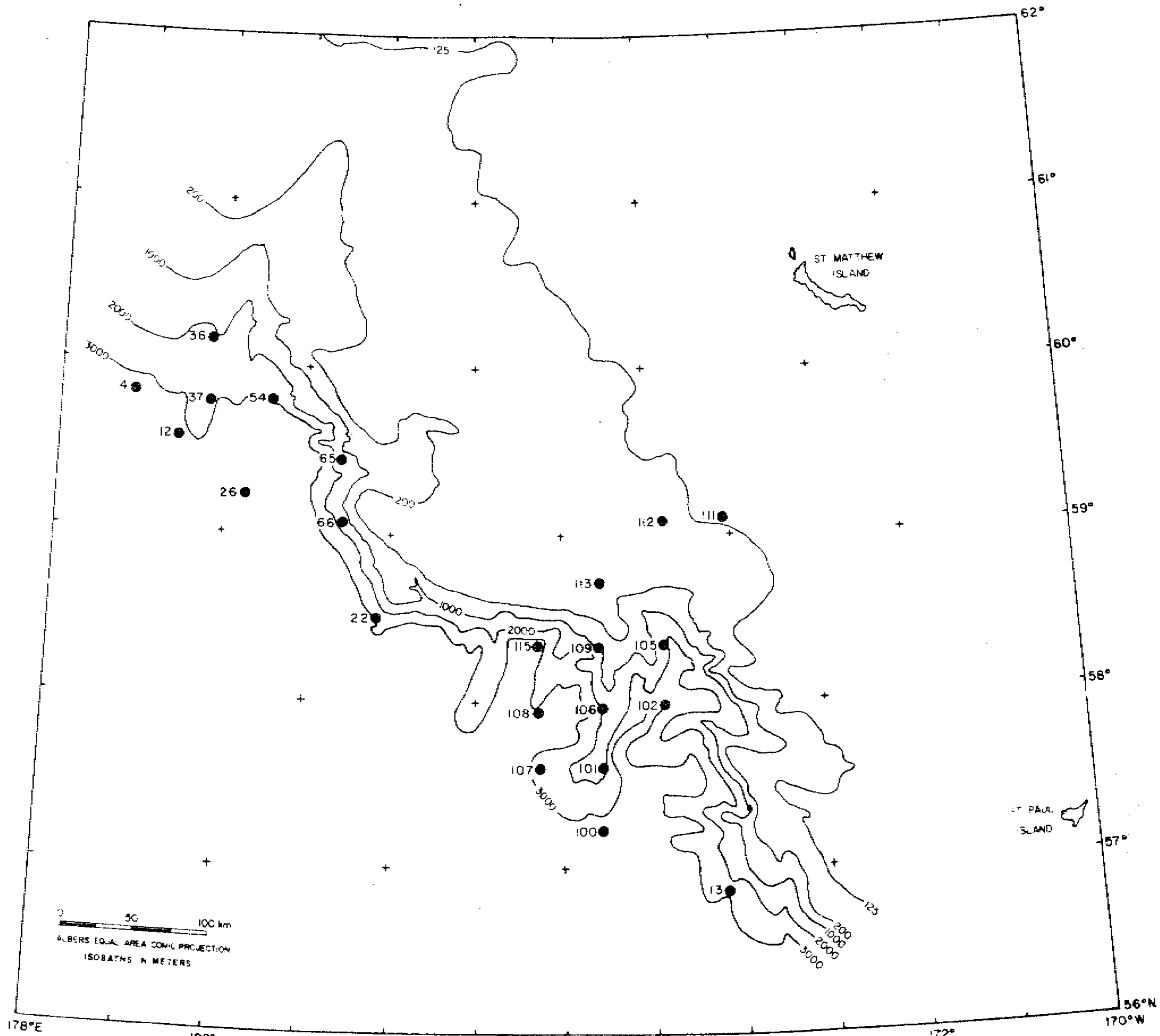

Figure 52. Location map of cores analysed for radiolarians.

Table 14. LIST OF RADIOLARIAN SPECIES FOUND IN NAVARIN BASIN

Species Name	Taxonomic Reference	Percentage of samples in which species occur (62 total samples)
*1,2Acanthodesmia micropora (Popofsky)	Kruglikova, 1975	63
*1,Acanthodesmiidae gen. et.sp. indet A	Kling, 1973	81
Acanthodesmiidae gen. et.sp. indet B		44
Acanthosphaera sp. indet.		2
*1,2,Arachnocorys dubius Dogiel	Dogiel, 1952	58
Artostrobiidae sp. indet.		3
Artostrobus annulatus (Bailey)	Ling et al., 1970	8
Botryocampe inflata (Bailey)	Kruglikova, 1974	32
Botryostrobus auritus (Ehrenberg)	Nigrini and Moore, 1978	40
Carposphaera sp. indet. A		55
Carposphaera sp. indet. B		27
Carposphaera sp. indet. C		37
Carposphaera sp. indet. D		16
Cenosphaera cristata Haeckel	Riedel, 1958	35
Cenosphaera sp. indet. A		23
Cenosphaera sp. indet. B		6
Cornutella profunda Ehrenberg	Casey, 1972	32
Cromyechinus borealis (Cleve)	Hulseman, 1963	2
*2,Crytopera laguncula Haeckel	Haeckel, 1887	42
*1,2,Cycladophora ? cornuta (Bailey)	Kruglikova, 1974	82
*1,2,Cycladophora davisiana Ehrenberg	Ling et al., 1970	76
Dictyocephalus papillosus (Ehrenberg)	Riedel, 1958	37
*1,Dictyophimus gracilipes Bailey	Petrushevskaya, 1967	74
*2,Dictyophimus hirundo (Haeckel group)	Nigrini and Moore, 1978	45
Dictyophimus sp. indet.		13
Diploplegma banzare Riedel	Riedel, 1958	29
Echinomma delicatulum (Dogiel)	Kruglikova, 1975	42
Echinomma sp. indet.		5
Eucecryphalus histricosus Hulseman	Hulseman, 1963	15
Eucyrtidium hexagonatum Haeckel	Nigrini and Moore, 1978	11
Euphysetta elegans Bogert	Reshetnyak, 1966	5
Helisoma sp. indet.		47
Lipmanella dictyoceras (Haeckel)	Kling, 1973	2
Lirella mela (Cleve)		2
*1,Lithelius? sp.	Petrushevskaya, 1967	32
*2,Lithomitra arachnea (Ehrenberg)	Ling, 1970	29
*2,Lychnocanoma grande Campbell	Casey, 1972	35
Peridium minutum Cleve	Cleve, 1899	11
Peridium sp. indet.		11
Peripyramis circumtexta Haeckel	CAsey, 1972	55
Phaeodaria gen. et. sp. indet. A		2
Phaeodaria gen. et. sp. indet. B		11
Plagoniidae gen. et. sp. indet.		15

Plectacantha oikiskos Jorgensen	Jorgensen, 1905	13
Polysolenia arktios Nigrini	Nigrini, 1970	18
Polysolenia sp. indet.		8
*1,2,Prunopyle antarctica Dreyer	Riedel, 1958	68
Pterocanium korotnevi (Dogiel)	Nigrini and Moore, 1978	58
Pterocanium sp. indet.		2
*2,Pterocorys hirundo Haeckel	Kruglikova, 1974	56
Rhizoplegma boreale (Cleve)	Ling et al., 1970	47
Saccospyris robustus Kruglikova	Kruglikova, 1974	2
Sethoconus ? tabulatus (Ehrenberg)	Petrushevskaya, 1967	2
*2,Siphocame aquilonaris (Bailey)	Ling et al., 1970	37
*1,Spongotrochus glacialis Popofsky	Nigrini and Moore, 1978	74
Spongurus pylomaticus Riedel	Kruglikova, 1974	44
Spongurus sp.	Ling et al., 1970	31
*2,Stylacontarium acquilonium (Hays)	Hays, 1971	55
*1,Stylatractus pyriformis (Bailey)	Kruglikova, 1974	61
Stylatractus univerus	Hays, 1971	6
*1,2,Stylochlamidium venustum (Bailey)	Kruglikova, 1974	90
*1,2,Stylodictya aculeata Jorgensen	Nigrini and Moore, 1978	76
*1,Stylodictya validispina Jorgensen	Kruglikova, 1974	58
Tetraphormis enneastrum (Haeckel)	Hulseman, 1963	3
Theoperidae gen. et. sp. indet. A		6
Theoperidae gen. et. sp. indet. B		29
Theoperidae gen. et. sp. indet. C		5
Tholospyris borealis (Bailey)	Kruglikova, 1974	34
*2,Tholospyris spinosus Kruglikova	Kruglikova, 1974	56
Triceraspyris antarctica (Haecker)	Casey, 1972	6

* Detailed information given in Table 15a and 15b.
1. Species that are abundant.
2. Possible stratigraphic or environmental indicators.

species \ depth in cent-cm	4-0	4-295	12-0	12-68	12-140	12-210	12-340	12-410	12-480	12-567	13-0	13-285	22-30	22-156	22-148	26-0	26-212	26-223	26-231	26-255	26-275	26-295	26-340	26-CC	36-50	36-530	36-CC	37-30	37-CC	54-18	54-CC	65-0
Acanthodesma micropora	x	2	1	1	3	3	0	2	4	4	2	3	2	x	1	2	x	2	0	8	2	3	2	2	0	0	1	0	2	1	2	0
Acanthodesmidae sp. indet. A	5	4	5	4	6	x	2	2	2	4	x	4	x	2	1	3	4	5	3	8	2	x	0	5	0	9	1	0	0	2	2	0
Arachnocorys dubius	2	x	0	x	x	x	x	x	0	0	14	0	3	x	0	2	4	0	3	0	1	1	x	0	0	0	0	2	2	3	1	0
Crytopera laguncula	x	0	0	0	1	2	2	1	x	x	0	x	1	0	0	x	2	0	0	8	x	x	2	x	0	0	1	0	0	0	0	0
Cycladophora ? cornuta	4	5	5	4	11	11	27	29	55	27	8	20	3	2	17	5	9	12	18	17	14	15	11	8	0	23	23	6	26	6	34	3
Cycladophora davisiana	x	26	2	x	1	26	22	24	12	19	x	5	x	x	38	0	x	14	21	25	28	13	39	15	7	14	25	2	22	0	24	0
Dictyophimus gracilipes	2	2	5	2	5	2	2	2	x	1	10	7	4	2	x	6	7	2	6	0	3	2	2	x	4	0	1	6	6	15	6	2
Dictyophimus hirundo	1	0	0	1	2	x	x	1	x	x	2	2	1	0	0	0	0	2	0	0	1	0	0	0	0	0	0	0	0	0	x	3
Lithelius ? sp.	3	4	2	2	3	x	3	1	x	3	6	12	x	0	3	2	7	5	12	17	7	9	6	2	4	14	3	5	3	5	2	3
Lithomitra arachnea	2	0	x	1	x	0	0	2	2	1	1	0	x	0	7	x	0	2	6	0	1	1	2	x	0	5	0	0	0	0	x	0
Lychnocanoma grande	0	0	x	0	x	0	x	x	0	0	0	7	x	0	0	x	0	18	3	0	5	8	2	9	32	5	8	0	0	0	x	0
Prunopyle antarctica	5	5	5	4	1	4	3	10	5	8	x	3	3	12	5	4	4	3	5	0	x	7	6	9	0	0	4	6	3	3	5	0
Pterocorys hirundo	x	0	x	0	1	0	2	1	3	2	0	2	1	0	x	0	2	2	3	0	x	x	0	5	7	0	0	2	5	1	x	0
Siphocampe aquilonaris	3	8	2	3	x	0	0	0	0	0	x	0	7	2	4	2	3	0	0	0	3	3	0	x	0	0	0	0	0	1	0	0
Spongotrochus glacialis	10	9	13	10	10	6	5	6	3	7	13	6	10	14	9	14	8	2	0	0	1	7	6	4	4	0	4	15	2	11	4	44
Stylacontarium acquilonium	0	x	3	2	x	0	2	x	x	1	2	0	2	5	0	0	x	2	0	0	x	x	0	2	0	0	4	6	0	0	0	0
Stylatractus pyriformis	2	4	4	3	11	4	4	2	0	4	8	5	3	3	0	8	8	0	0	8	3	1	0	1	0	0	4	8	0	8	0	0
Stylochlamidium venustum	21	11	33	35	14	9	11	2	2	4	12	4	18	35	1	25	21	2	0	0	1	4	2	4	14	0	5	22	8	20	6	32
Stylodictya aculeata	5	4	2	3	2	18	2	9	6	10	2	7	3	0	2	x	4	0	0	0	3	7	7	6	4	9	8	2	2	1	5	2
Stylodictya validispina	2	x	x	x	0	x	x	2	x	1	1	2	x	0	0	3	2	0	0	0	x	x	x	x	0	0	0	3	2	1	x	0
Tholospyris spinosus	2	1	1	3	x	x	x	0	0	0	x	x	9	3	3	7	x	2	5	0	x	1	0	x	4	5	3	2	2	2	0	3
other species	31	15	22	22	29	15	13	4	8	4	21	11	22	28	9	17	15	31	19	9	25	18	11	28	20	16	4	15	15	19	14	8
total species counted	385	310	163	368	383	197	196	201	640	328	212	218	176	197	182	201	297	8	20	12	235	149	182	635	28	32	77	65	183	147	254	50

Table 15a. Abundance, shown in % of total assemblage of cores 4 to 65. Species used are those identified in table 1 as either abundant or potientially stratigraphically significant. (x = less than 1%)

species / depth in [illegible]	64-15	64-cc	100-21	100-cc	101-1	101-cc	102-30	102-cc	105-0	105-cc	106-15	106-28	106-43	107-30	107-cc	108-56	108-113	108-cc	109-5	109-126	109-232	109-cc	111-cc	112-0	112-cc	113	115-6	115-224	115-244	115-cc
Acanthodesma micropora	0	6	0	4	0	2	0	8	0	0	2	2	0	3	5	0	0	3	0	0	0	0	0	0	0	0	1	2	1	2
Acanthodesmidae sp. indet. A	9	4	5	6	6	5	4	1	6	5	4	9	0	2	2	3	5	3	6	0	0	0	0	0	0	0	2	5	2	8
Arachnocorys dubius	0	0	10	x	2	1	14	[illegible]	6	10	2	5	0	x	0	0	x	x	0	0	0	0	0	0	0	0	4	x	1	x
Crytopera laguncula	0	1	0	x	0	x	0	0	0	0	0	0	0	0	2	0	x	2	0	0	0	0	0	0	0	0	x	0	2	2
Cycladophora ? cornuta	6	31	7	25	2	22	4	4	0	0	2	2	0	2	34	0	x	24	0	14	0	0	0	0	0	0	8	9	55	55
Cycladophora davisiana	17	8	5	7	x	16	0	1	12	6	0	17	6	x	11	2	0	14	0	29	0	0	0	0	0	0	0	3	13	14
Dictyophimus gracilipes	2	14	12	8	8	x	0	5	0	0	4	12	0	5	5	0	x	x	0	0	0	0	0	0	0	0	4	2	2	2
Dictyophimus hirundo	x	1	2	x	1	0	0	x	0	0	0	0	0	x	2	x	x	1	0	0	0	0	0	0	0	9	x	1	2	2
Lithelius ? sp.	x	10	2	5	1	8	0	2	0	14	6	5	6	3	8	3	4	1	0	0	26	0	0	0	0	0	4	7	1	2
Lithomitra arachnea	0	0	0	2	0	0	0	1	0	0	0	5	13	0	1	0	x	x	0	0	0	0	0	0	0	0	0	0	2	x
Lychnocanoma grande	0	8	0	x	x	0	4	0	0	0	0	2	0	0	0	0	0	0	0	9	0	0	0	0	0	0	0	0	x	x
Prunopyle antarctica	6	0	2	4	3	10	4	x	0	0	0	0	0	3	3	2	2	14	0	0	0	0	0	0	0	0	4	3	8	8
Pterocorys hirundo	0	3	0	2	2	1	0	0	0	0	4	0	0	x	2	x	x	3	0	0	0	0	0	0	0	0	0	x	x	x
Siphocampe aquilonaris	x	0	0	0	0	0	4	2	0	0	0	0	0	2	0	2	5	0	2	0	0	0	0	0	0	0	x	1	0	0
Spongotrochus glacialis	17	1	10	7	22	5	7	9	29	14	17	14	6	16	1	18	13	7	29	14	25	0	75	85	52	46	11	15	6	3
Stylacontarium acquilonium	2	0	0	x	x	0	11	x	6	0	4	0	0	2	1	5	6	1	0	0	0	0	0	0	0	0	x	3	x	x
Stylatractus pyriformis	0	0	0	3	3	x	7	3	0	0	2	0	0	2	5	x	1	x	0	0	0	0	0	0	0	0	6	8	3	4
Stylochlamidium venustum	28	10	25	8	31	7	26	15	35	29	24	0	0	40	3	49	47	3	55	14	0	0	17	10	[illegible]	27	35	20	3	6
Stylodictya aculeata	4	4	0	4	4	3	0	3	0	6	4	0	6	x	5	2	x	13	0	9	0	0	8	0	0	0	x	2	8	9
Stylodictya validispina	0	0	0	x	1	2	0	1	0	0	2	0	0	x	4	2	2	4	0	0	0	0	0	0	0	0	4	4	1	3
Tholospyris spinosus	x	1	0	x	4	x	0	0	0	5	0	0	6	2	0	x	2	0	0	0	0	0	0	0	0	9	5	2	2	0
other species	9	16	20	21	13	13	16	20	11	10	19	23	57	18	13	12	13	7	8	11	50	0	0	5	9	10	12	7	8	7
total species counted	108	[illegible]	[illegible]	[illegible]	[illegible]	[illegible]	[illegible]	170	17	21	[illegible]	[illegible]	[illegible]	205	188	131	329	237	[illegible]	21	[illegible]	0	12	20	23	11	146	337	380	789

Table 15b. Abundance, shown in 5 of total assemblage of cores 4 to 65. Species used are those identified in table 1 as either abundant or potientially stratigraphically significant. (x = less than 1%)

A PRELIMINARY REPORT ON AMINO ACID DIAGENESIS IN FOSSIL MOLLUSKS RECOVERED FROM THE NAVARIN BASIN PROVINCE, BERING SEA

David J. Blunt and Keith A. Kvenvolden

INTRODUCTION

Fossil mollusks were recovered in marine sediments from the Navarin Basin province, Bering Sea. The relative age of the fossil mollusks can be calculated from the amount of amino acid diagenesis that has occurred within the fossil shell since the organism's death. Correlation and geochronology of marine sedimentary deposits can be accomplished using the diagenesis of amino acids in mollusk shells. Reviews and recent advances using this method can be found in Hare and others (1980).

Theory

Individual amino acids that are no longer being biologically reproduced in the protein of the shell matrix undergo a stereochemical change from the L-enantiomer (living optical configuration having a mirror image) to the D-enantiomeric configuration during hydrolysis. The process of interconversion is called racemization. Over time, a mixture of L- and D-amino acids results. The kinetics of racemization can be expressed as a reversible first-order reaction:

$$\text{L - amino acid} \underset{k_D}{\overset{k_L}{\rightleftharpoons}} \text{D - amino acid}$$

where k_L and k_D are the respective reaction rate constants for the L- and D-amino acid enantiomers. The integrated rate expression for the racemization reaction as derived by Bada and Schroeder (1972) is:

$$\ln\left(\frac{1 + D/L}{1 - D/L}\right) - \ln\left(\frac{1 + D/L}{1 - D/L}\right)_{t=o} = 2kt \qquad (1)$$

where k is the racemization rate constant, D/L is the ratio of D- and L- amino acid enantiomers, and t is time. The logarithmic term at t=o is evaluated by measuring the D/L ratios in modern specimens.

MATERIALS AND METHODS

Samples

Gravity cores selected for this study were recovered in the northern Navarin Basin province (Fig. 52). Bottom water temperatures in the region are about 2° C, but they are related to the hydrographic regime in some complex fashion (Herman Karl, personal communication).

Fossil mollusks selected for amino acid analysis are reported in Table 16 together with gravity core numbers and subbottom depths. Of the ten gravity cores selected for this study, only in cores 42 and 44 were samples recovered from more than one depth interval. Seven articulated samples were recovered.

Methodology

The procedures used to extract and quantitate amino acid residues in the total amino acid fraction (both free and bound) in mollusk shell are fully described in Kvenvolden and others (1981). Briefly, about 0.2 g of shell material is hydrolyzed in 6 N HCL for 20 hours at 110° C. The hydrolysate is then dried and redissolved in a pH 1 norleucine standard. The mixture is applied to DOWEX 50 W x 8 (H^+) cation exchange resin. Amino acids are eluted with 2N NH_4OH. The eluate is subsequently split; half is quantitated by automatic ion-exchange chromatography and half is derivatized as a penta-fluoropropionyl-amino acid-(+)-2 butyl ester and analyzed for amino acid D/L ratios by gas chromatography.

RESULTS

Amino acid compositions in twelve mollusks recovered in sediments from the Navarin Basin province are reported in residues per 10^3 (Table 17). Relative differences in amino acid composition between each species can be detected by this method of presentation. For example, the specimens of Nuculana have relative concentrations of about 200 for aspartic acid, proline and glycine, whereas the specimens of Macoma have relative concentrations that are about 25-50% lower for the same three amino acids. Mya truncata, Yoldia myalis, Clinocardium nuttallii and Cyclocardia crebricostata also show relative differences in their amino acid compositions. Total amino acid concentrations are quite variable and range from 22.7 micro-moles per gram of shell (um/g) in Cyclocardia crebricostata to 6.12 um/g in Mya truncata.

Amino acid D/L ratios for aspartic acid, alanine, glutamic acid, phenylalanine, proline, leucine, and valine are reported for each specimen (Table 18). The highest D/L ratio was consistently measured in aspartic acid and the lowest D/L ratio was consistently measured in valine. The highest aspartic acid D/L ratio was measured to be 0.379 in Nuculana radiata (core no. 26, 227 cm), and the lowest was measured to be 0.071 in Macoma sp. (core no. 6, 10 cm). The highest valine D/L ratio was measured to be 0.056 in Yoldia myalis (core no. 42, 60 cm), and the lowest valine D/L ratio was measured to be 0.027 in Macoma sp. (core no. 6, 10 cm). The D/L ratios of alanine, glutamic acid, phenylalanine, proline, and leucine in all samples were measured to be between the limits of aspartic acid and valine (0.379-0.027).

DISCUSSION

Correlation and Geochronology

Relative correlation and geochronology of sediments from Navarin Basin province using amino acid diagenesis in fossil mollusks is possible, providing the shells have not been reworked. Shells that were living in situ probably have not been disarticulated, and seven articulated samples were recovered at five different stations (see Table 16). All of the specimens of *Nuculana* are articulated. These samples provide a means of relative geochronology and correlation. Clearly from Table 18 the amino acid D/L ratios in *N. radiata* from core no. 26 are higher than the amino acid D/L ratios in *N. radiata* from core no. 50. Both of these samples were recovered from about the same subbottom depth interval which indicates that different sedimentation rates, erosion and/or non-deposition has occurred in these cores. Samples of *Macoma* are more likely to have been reworked as is suggested by their disarticulated state (with the exception of core no. 44). However, the D/L ratios of *Macoma obliqua* and *Macoma brota* recovered from subbottom depths of 200 cm in core 44 and 217 cm in core 62 respectively are distinctly greater than the D/L ratios in the two *Macoma sp.* samples recovered from subbottom depths of only 10 cm in core 6 and 13 cm in core 59. This is an expected result for samples recovered *in situ*.

Isoleucine and leucine are two amino acids that are commonly used for correlation and geochronology in fossil mollusk shells (for example, see Mitterer, 1974; Wehmiller and others, 1977; Kvenvolden and others, 1979; and Miller and others, 1979). Aspartic acid and glutamic acid have also been used in correlation and geochronology of fossil estuarine deposits (Kvenvolden and others, 1979). Only leucine will be applied in this preliminary report.

Application of amino acid geochronology is possible providing the factors that affect leucine racemization in each sample have been properly assessed. Leucine geochronology should include three major factors: 1) applicability of linear racemization kinetics; 2) assessment of *in situ* temperature history and 3) species effects on racemization kinetics. Linear racemization kinetics using equation 1 can be applied in this study because the highest leucine D/L ratio measured is only 0.116 and it has been reported that non-linear kinetics occur in mollusks at leucine D/L ratios greater than $\sim$ 0.3 (Wehmiller and Belknap, 1978). The *in situ* temperature history is perhaps the most difficult factor to assess, and the present bottom water temperature of $\sim 2°$ C will be tentatively used for calculations. Species effects on leucine racemization kinetics are apparent when samples having the same time and temperature history are compared. Species effects between *Nuculana*, *Macoma*, and *Clinocardium* will be discussed in the following section.

Leucine Calibration

Specimens of *Nuculana*, *Macoma*, *Clinocardium* and *Mya* all of which have been measured for leucine D/L ratios and have been recovered from radiocarbon dated localities, are reported on Table 19. Temperature histories are based on long-term climatological records for the region. Temperature histories of $\sim 10°$ C have been estimated for samples from the Puget Lowland (see Miller and Hare, 1980; Kvenvolden and others, 1981). The *Mya truncata* from Anchorage is estimated to have a temperature history of $\sim 2°$ C (Miller and Hare, 1980). Differences in leucine D/L ratios between *Nuculana*, *Macoma* and *Clinocardium* are small and the leucine D/L ratios are probably too low to distinguish species characteristics for these samples with this limited comparison. These samples have the same magnitude of D/L ratio as the Navarin Basin province samples.

However, the leucine D/L ratio for Mya truncata is about 50% lower than others of about the same age. This difference is a result of its lower (~ 2° C) temperature history. This illustrates a necessity for proper assessment of temperature history.

The leucine racemization rate constant used in equation 1 must reflect the diagenetic temperature history that the sample has experienced. The variables of time and temperature recorded in Navarin Basin province sediment need further study. A preliminary estimate of a leucine rate constant usable in the Navarin Basin province can be calculated from the Washington and Alaskan localities that have been radiocarbon-dated and have temperature histories that can be calculated. Leucine racemization rate constants can be calculated using the Arrhenius relationship:

$$\ln\left(\frac{k_2}{k_1}\right) = \frac{Ea}{R} \frac{(T_2 - T_1)}{(T_2 T_1)} \qquad (2)$$

where k_2 and k_1 are the leucine racemization rate constants; the leucine racemization activation energy (Ea) is assumed to be 29.4 kcal/mole for all samples; the gas constant R is 1.987; and T_2 and T_1 are the respective estimated temperature histories in degrees Kelvin for each sample.

Leucine rate constants from Table 19 can be calibrated by the method of Bada and Protsch (1973) using equation 1. These calibrated rate constants and calculated temperatures can be applied to equation 2 and a leucine rate constant at 2° C can be calculated for Nuculana, Macoma, and Clinocardium. The leucine racemization rate constant calculated at 2° C for each species is: Nuculana, $(1.73 \pm 0.23) \times 10^{-6}$; Macoma, $(1.78 \pm 0.09) \times 10^{-6}$; and Clinocardium, 1.45×10^{-6}. Leucine rate constant determined for Macoma and Clinocardium are tentatively applied to Yoldia and Cyclocardia. Since the calibrated Mya truncata already has a temperature history of 2° C, the calibrated rate constant of 2.31×10^{-6} will be used in calculations.

Age and Accumulation Rates

The calibrated leucine rate constants at 2° C and the measured leucine D/L ratios from fossil mollusks in the Navarin Basin province results in ages from equation 1 that range from 5,600 years in core 59 to 53,000 years in core 26 (Table 20). It must be restated that the present lack of a local in situ temperature calibration site within the Navarin Basin province prohibits these ages as being considered "absolute". For example, an average temperature history of about 6° C for bottom water temperatures will reduce the calculated ages by as much as 50 percent. It is encouraging to note that the ages determined from two depth intervals in cores 42 and 44 are in the correct geochronological order. The oldest age of 53,000 years is calculated from an articulated Nuculana from core 26. The radiolarian Lychnocanum grande which may have become extinct about 35,000 to 40,000 years ago (Joyce Blueford, personal communication) occurs with the Nuculana in core 26. However, diatom assemblages of this antiquity are not present in core 26 (Jack Baldauf, personal communication). The articulated Nuculana in core 26 may have been reworked perhaps from submarine slumping.

The preliminary age calculations can be used to evaluate minimum accumulation rates in cores collected on the shelf, slope, and basin in the Navarin Basin province. Sample reworking, erosion and/or non-deposition of sediment will result in minimum accumulation rates being calculated. Minimum average accumulation rates range from 0.6 to 16 cm/10^3 years (Table 20). Aveerage accumulation rates along the shelf are quite variable and range from 0.6 cm/10^3 years in core 28 to as high as 16 cm/10^3 years in core 50. The paucity of microfauna in core 28 may be attributed to dilution of microfauna by rapid accumulationn (Paula Quinterno, personal communication). The contrasting slower accumulation rate using amino acid geochronology in core 28 suggests that the top of the core has undergone erosion or that the non-articulated Cyclocardia has been reworked and redeposited during conditions of rapid accumulation. The average minimum accumulation rate above the 200 m contour in the northern Navarin Basin province is about 7 cm/10^3 years, using amino acid geochronology.

Core 66, collected in 1336 m of water, has a minimum average sedimentation rate of 1.4 cm/10^3 years. This apparent accumulation rate is low, perhaps from erosion and/or non-deposition above the articulated Yoldia myalis located at a subbottom depth of 60 cm. Core 26, collected in 3337 m of water, is calculated to have a minimum average accumulation rate of 4.3 cm/10^3 years.

SUMMARY

Fossil mollusks recovered from sediments in Navarin Basin province were analyzed for amino acid content and stereochemistry. Concentrations of individual amino acids reported in residues per 10^3 characterize species of Nuculana, Macoma, Clinocardium, Yoldia, Cyclocardia and Mya. Amino acid D/L ratios show variable extents of racemization between the limits of valine and aspartic acid. Geochronology using leucine racemization is limited, mainly due to the lack of in situ temperature history and local calibration samples. Tentative amino acid geochronology based on an average temperature history of 2° C results in age estimations which range from 5,600 years to 53,000 years. Minimum average accumulation rates on the shelf range from 0.6 to 16 cm/10^3 years and average about 7 cm/10^3 years. The interpretation of accumulation rates using fossil mollusks must take into account sample reworking and sediment erosion and/or non-deposition.

REFERENCES CITED

Bada, J. L. and Schroeder, R. A., 1972, Racemization of isoleucine in calcareous marine sediments: kinetics and mechanism: Earth and Planet. Sci. Lett., v. 15, p. 223-231.

Bada, J. L. and Protsch, R., 1973, Racemization reaction of aspartic acid and its use in dating fossil bones: Proc. Nat. Acad. Sci., v. 70, p. 1331-1334.

Hare, P. E., Hoering, T. C., and K. King, Jr., 1980, Biogeochemistry of Amino Acids: New York, Wiley, 558 p.

Kvenvolden, K. A., Blunt, D. J., and H. E. Clifton, 1979, Amino acid racemization in Quaternary shell deposits at Willapa Bay, Washington: Geochim. Cosmochim. Acta, v. 43, p. 1505-1520.

Kvenvolden, K. A., Blunt, D. J., McMenamin, M. A., and S. E. Strahan, 1981, Geochemistry of amino acids in shells of the bivalve mollusk Saxidomus: In Proc. of the Ninth Internatl. Meeting on Organic Geochem., in press.

Miller, G. H., Hollin, J. T., and J. T. Andrews, 1979, Aminostratigraphy of U.K. Pleistocene deposits: Nature, v. 281, p. 539-543.

Miller, G. H. and P. E. Hare, 1980, Amino acid geochronology: Integrity of the carbonate matrix and potential of molluscan fossils: In Hare, P. E., Hoering, T. C., and K. King, Jr., eds., Biogeochemistry of Amino Acids: New York, Wiley, 558 p.

Mitterer, R. M., 1974, Pleistocene stratigraphy in southern Florida based on amino acid diagenesis in fossil Mercenaria: Geology, v. 2, p. 425-428.

Wehmiller, J. F. and D. F. Belknap, 1978, Alternative kinetic models for the interpretation of amino acid enantiomeric ratios in Pleistocene mollusks: examples from California, Washington and Florida: Quat. Res., v. 9, p. 330-348.

Wehmiller, J. F., Lajoie, K. R., Kvenvolden, K. A., Peterson, E., Belknap, D. F., Kennedy, G. L., Addicott, W. O., Vedder, J. G., and R. W. Wright, 1977, Correlation and chronology of Pacific coast marine terrace deposits of continental United States by fossil amino acid stereochemistry - technique evaluation, relative ages, kinetic model ages and geologic implications: U.S. Geol. Surv. Open-file Report 77-680, 197 p.

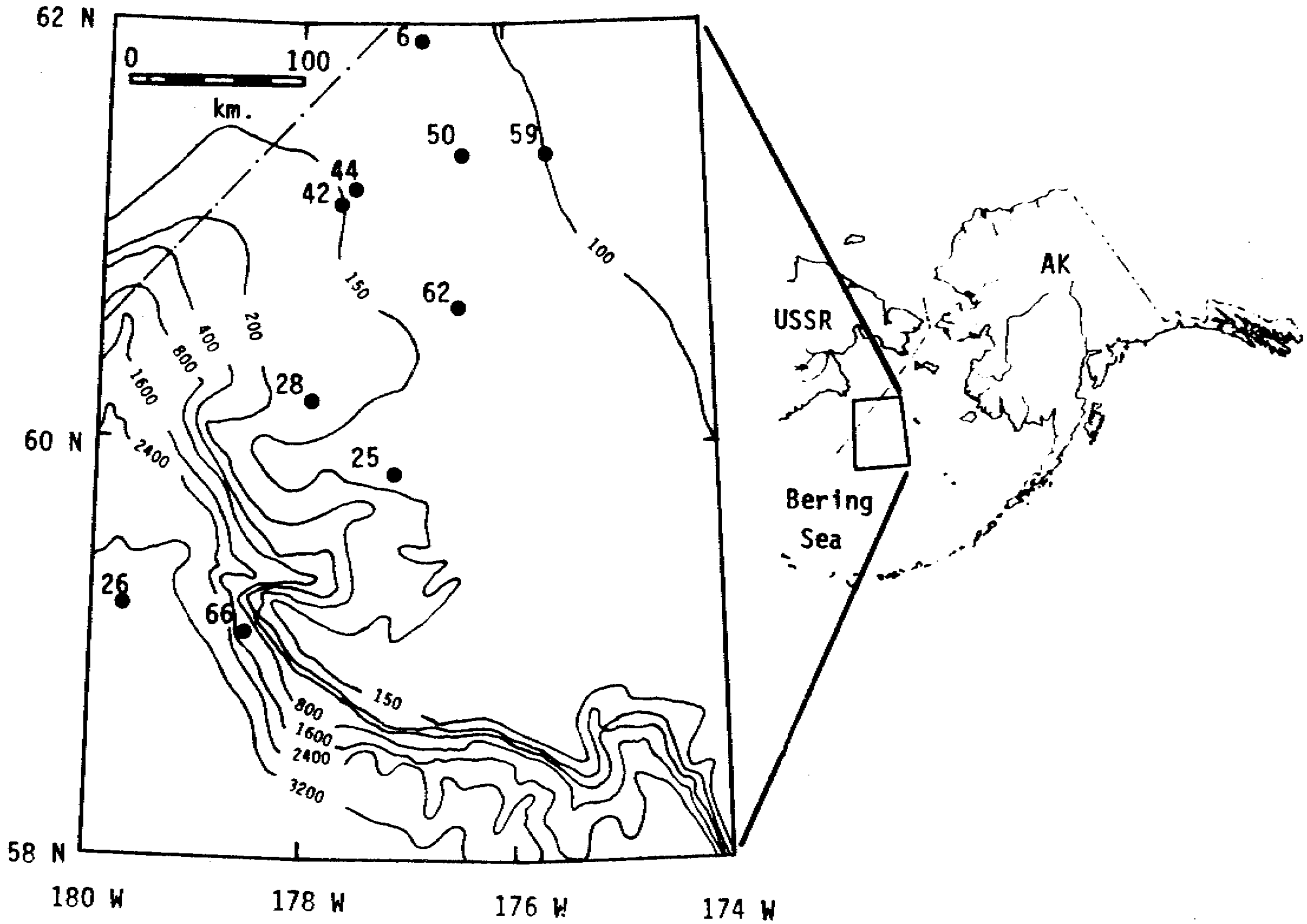

Figure 53. Location of gravity cores in the northern Navarin Basin province where fossil mollusks were studied. Bathymetry is in meters.

Table 16. **Sample Identification and Subbottom Depths in Gravity Cores Recovered in the Navarin Basin Province, Bering Sea**

Station No.	Gravity Core No.	Subbottom Depth cm	Sample
3	6	10	*Macoma* sp. (not art.)
19	25	173	*Mya truncata* (not art.)
20	26	223-230	*Nuculana radiata* (art.)
21	28	8	*Cyclocardia crebricostata* (not art.)
32	42	97	*Clinocardium nuttallii* (art.)
32	42	170	*Nuculana fossa* (art.)
34	44	125	*Nuculana fossa* (art.
34	44	200-206	*Macoma cf. M. obliqua* (art.)
39	50	219-230	*Nuculana radiata* (art.)
47	59	13-14	*Macoma* sp. (not art.)
49	62	214-220	*Macoma brota* (not art.)
53	66	60	*Yoldia myalis* (art.)

1. Specimens identified by L. Marincovich, USGS, Menlo Park

2. (not art.)= sample not articulated; (art.)= sample articulated

Table 17. Amino Acid Residues/10^3 in Molluscan Fauna Recovered in the Navarin Basin Province

Sample	Nuculana	Nuculana	Nuculana	Nuculana	Macoma	Macoma	Macoma	Macoma	Mya	Yoldia	Clinocardium	Cyclocardia
Core No.	26	50	42	44	44	62	6	59	25	66	42	28
Subbottom Depth cm.	∿ 227	∿ 225	170	125	∿ 203	∿ 217	10	∿ 14	173	60	97	8
Aspartic acid	198	197	207	220	145	147	109	114	289	226	241	96
Threonine	46	46	48	45	58	54	52	60	50	40	46	33
Serine	46	56	54	48	68	77	66	81	53	58	53	50
Glutamic acid	63	65	65	67	109	113	78	84	70	103	67	46
Proline	255	199	217	215	141	117	150	143	100	114	125	56
Glycine	186	196	183	162	166	156	226	188	175	194	205	414
Alanine	58	60	67	58	97	93	87	105	83	86	48	56
Valine	63	56	58	56	49	53	48	46	45	64	58	30
Methionine	12	14	7	7	15	16	28	34	8	12	23	7
Isoleucine	17	13	14	14	20	28	26	21	19	24	26	18
Leucine	24	21	22	25	45	48	39	46	27	33	30	29
Tyrosine	22	24	21	29	25	24	26	19	17	26	27	61
Phenylalanine	7	5	6	6	21	23	18	16	7	9	10	32
Histidine	13	10	4	3	10	14	15	10	6	NR	NR	17
Lysine	35	31	28	30	27	31	29	27	47	NR	41	47
Arginine	7	8	7	14	3	5	3	4	6	11	< 1	7
Total Concentration (um/g)	8.54	13.7	14.8	18.6	8.06	9.41	16.7	8.72	6.12	12.2	11.8	22.7

Table 18. Amino Acid D/L Ratios in Molluscan Fauna Recovered in the Navarin Basin Province

Sample	Nuculana	Nuculana	Nuculana	Nuculana	Macoma	Macoma	Macoma	Macoma	Mya	Yoldia	Clinocardium	Cyclocardia
Core No.	26	50	42	44	44	62	6	59	25	66	42	28
Subbottom Depth cm.	∿ 227	∿ 225	170	125	∿ 203	∿ 217	10	∿ 14	173	60	97	8
Aspartic acid	0.379	0.233	0.300	0.241	0.227	0.206	0.071	0.075	0.213	0.299	0.206	0.099
Alanine	.164	.084	.115	.091	.093	.073	.035	.038	.096	.127	.074	.048
Glutamic acid	.136	.080	.097	.076	.090	.073	.042	.047	.080	.089	.073	.060
Phenylalanine	.160	.102	.124	.106	.106	.086	.038	.058	NR	.103	.093	.050
Proline	.122	.058	.074	.063	.104	.081	.034	.034	.109	.158	.067	.045
Leucine	.116	.049	.073	.053	.074	.058	.036	.035	.061	.102	.060	.046
Valine	.040	.030	.037	.031	.046	.037	.027	.022	.04	.056	.043	.041

Table 19. Calibration Localities Used for Age Calculation by Leucine Racemization

Sample	Sample/ Locality No[1]	Leucine D/L	^{14}C Age	k_{leu}[2] $(x10^{-6})$	T[3]	Location[4]
<u>Nuculana</u> <u>fossa</u>	80-37	0.105	11,640±275 (W-940)	6.89	∿ 10	Cedarville, WA
<u>Nuculana</u> <u>fossa</u>	80-24	.142	13,010±170 (UW-32)	9.07	∿ 10	Penn Cove, WA
<u>Macoma</u> <u>calcarea</u>	80-37	.125	11,640±275 (W-940)	8.63	∿ 10	Cedarville, WA
<u>Macoma</u> <u>sp</u>.	80-24	.126	13,010±170 (UW-32)	7.82	∿ 10	Penn Cove, WA
<u>Clinocardium</u> <u>nuttallii</u>	79-3	.112	13,010±170 (UW-32)	6.72	∿ 10	Penn Cove, WA
<u>Mya</u> <u>truncata</u>	77-MTA-1 (m1552)	.055	13,000±	2.31	∿ 2	Bootlegger Cove, Anchorage, AK

[1] Samples from the Puget Lowland, Washington, collected with D. Easterbrook, Western Washington University. Alaskan <u>Mya</u> received as an interlaboratory calibration sample, 1977, with G. Miller, INSTAAR, University of Colorado

[2] For all calculations a leucine $D/L_{t=o}$ of 0.025 was used

[3] Average diagenetic temperature estimated from long-term temperature records

[4] Washington radiocarbon dated localities can be found in Easterbrook, 1969. Alaskan locality reported in Miller and Hopkins, 1980

Table 20. Leucine Racemization Age and Sedimentation Rate in Cores from the Navarin Basin Province, Bering Sea

Gravity Core No.	Subbottom Depth cm.	Estimated Sample[1] Age 2^{C}	Minimum[2] Sedimentation Rate (cm $x10^{-3}$yr)	Reworked[3] Sample
6	10	6,200±300	1.6	(?)
25	173	16,000	10	(?)
26	223-230	53,000±6,000	4.3	(?)
28	8	14,000±	0.6	(?)
42	97	24,000	4	-
42	170	28,000±3,000	6.1	-
44	125	16,000±2,000	7.8	-
44	200-206	28,000±2,000	7.3	-
50	219-230	14,000±2,000	16	-
59	13-14	5,600±300	2.4	(?)
62	214-220	19,000±1,000	11	(?)
66	60	43,000±2,000	1.4	-

[1]Error reported is from the calibrated rate constant. An increase of 4^{C} in average temperature history will decrease the calculated age by as much as 50%

[2]Assuming constant sedimentation and sediment surface is at time zero

[3]Disarticulated samples possibly reworked

U. S. DEPARTMENT OF COMMERCE
NATIONAL OCEANIC AND ATMOSPHERIC ADMINISTRATION

NOS OMS32xJ (OCSEAP)
P.O. Box 1808
Juneau, Alaska 99802

OFFICIAL BUSINESS
PENALTY FOR PRIVATE USE, $300

POSTAGE AND FEES PAID
U.S. DEPARTMENT OF COMMERCE
COM-210

PRINTED MATTER

CLASS OF POSTAL SERVICE

U.S. MAIL

NOAA FORM 61-32A (11-77)
See NDM 61-50 for Class of Postal Service